Cimarron Corporation

References for Cimarron Corporation Bioremediation Project in Burial Area #1

Prepared by:
Jim Harrington
630 Plaza Drive, Suite 200
Highlands Ranch, CO 80129
720.344.3843
Jmharrington@arcadis-us.com

ARCADIS

Infrastructure, buildings, environment, communications

CIMARRON CORPORATION LETTER OF TRANSMITTAL

DATE : 8/06/2003

TO:

U.S. Nuclear Regulatory Commission
Document Control Desk
Washington, D.C. 20555

FROM: **Quality Assurance Coordinator**
Cimarron Corporation
P.O. BOX 315
Crescent, OK 73028

☐ First Class Mail ☐ Internal ☐ Overnight–UPS
☑ Overnight–Fed Ex ☐ UniShippers ☐ Second Day Air–UPS
☐ Second Day–Fed Ex ☐ Other _____

COPY NO.	DATE	DESCRIPTION
1	*August, 2003*	*Information on Immobilization of Uranium In Groundwater*

These are transmitted as checked below:

☐ For Approval ☐ Approved as submitted ■ For your use
☐ As requested ☐ Returned for corrections ☐ Return ____ corrected prints
☐ Disapproved ☐ For review and comment ☐ Controlled copy

REMARKS: The above item(s) is for your use. Please sign and return transmittal letter.

NOTE:

SIGNATURE: La Donna Smith

ACKNOWLEDGMENT OF RECEIPT **PLEASE RETURN ONE SIGNED COPY TO SENDER**

I HAVE RECEIVED THE DOCUMENTS IDENTIFIED ABOVE AND THE PRIOR REVISIONS OF THESE HAVE BEEN DESTROYED N/A VOIDED N/A

PRINTED NAME OF RECIPIENT: _____

SIGNATURE OF RECIPIENT: _____

DATE RECEIVED: _____

If enclosures are not noted, kindly notify Cimarron Corporation at once.

CIMARRON CORPORATION

P.O. BOX 315 • CRESCENT, OK 73028

August 5, 2003

Mr. Kenneth Kalman
Low-Level Waste & Decommissioning Projects Branch
Division of Waste Management
Office of Nuclear Materials Safety & Safeguards
U. S. Nuclear Regulatory Commission
Washington, D.C. 20555

Re: Docket No. 70-925; License No. SNM-928
Information on Immobilization of Uranium in Groundwater

Dear Mr. Kalman:

Cimarron Corporation (Cimarron) is providing the attached information to NRC for evaluation of our plans to immobilize uranium in groundwater at the Cimarron facility. This information was provided to NRC by ARCADIS informally in April, 2003.

This information consists of a summary section, in which Mr. Harrington (ARCADIS) explains how the content of each paper fits in with the technology Cimarron proposes to use to remediate groundwater in Burial Area #1. Each referenced paper is included behind tabs bearing the author's name.

Cimarron plans to submit a work plan for the remediation of groundwater in Burial Area #1, most likely as an addendum to the NRC-approved site Decommissioning Plan, in the near future. That work plan will reference a number of these papers, which we trust will aid you in your review. If you have questions or comments, please call me at **405-282-5680** (Cimarron) or **918-223-2522** (Cushing).

Sincerely,

Jeff Lux
Manager, Planning and Regulatory Compliance

xc: D. Blair Spitzberg, NRC Region IV
Saba Tahmassebi, DEQ

NM5501

ARCADIS
Infrastructure, buildings, environment, communications

ARCADIS G&M, Inc.
630 Plaza Drive
Suite 200
Highlands Ranch
Colorado 80129
Tel 720 344 3500
Fax 720 344 3535
www.arcadis-us.com

Reference List

Abdeouas, A., W. Lutze, W. Gong, E. Nuttall, B. Strietelmeier, and B. Travis. 2000. Biological reduction of uranium in groundwater and subsurface soil. Science of the Total Environment, 25: 21-35.

This paper documents the benefits of excess iron sulfide formation on uranium stability. They show that with sufficient excess of iron sulfide that uranium is stable even in groundwater that contains saturated dissolved oxygen.

Abdelouas, A., W. Lutze, and H. Nuttall. 1998. Chemical reations of uranium in ground water at a mill tailings site. Journal of Contaminant Hydrology, 34:343-361.

This paper documents the uranium conditions that are the baseline chemistry conditions for all of the Abdelouas papers. These papers are important because they show what might be observed if a column study were to be run for Cimarron. Column studies have been performed in this case, in several cases by ARCADIS (for NFS, for Sweetwater, and for Fernald) and they all show the same general trend that the Abdelouas papers show.

Abdelouas, A., W. Lutze, and H. Nuttall. 1999. Oxidative dissolution of uraninite precipitated on Navajo sandstone. Journal of Contaminant Hydrology, 36:353-375.

This paper documents that mackinawite (the primary iron sulfide initially formed by sulfate reducing bacteria) provides uranium stability. They show that uranium less than 4 µg/L (3 pCi/L) is maintained if sufficient mackinawite is formed.

Abdelouas, A., Y. Lu, W. Lutze, E. Nuttall. 1988. Reduction of U(VI) to U(IV) by indigenous bacteria in contaminated ground water. Journal of Contaminant Hydrology 35: 217-233.

This paper shows that bacteria directly reduce uranium and sulfate separately, that uranium is precipitated to concentrations less than 1 µg/L by bacteria, and that this

reaction is rapid in soil columns.

Casas, I., J. De Pablo, J. Gimenez, M. Torrero, J. Bruno, E. Cera, R. Finch, and R. Ewing. 1998. The role of pe, pH, and carbonate on the solubility of UO_2 and uraninite under nominally reducing conditions. Geochimica et Cosmochimica Acta, ***62***, 2223-2231.

This paper shows that the solubility of uraninite, the uranium mineral formed by bacteria in the bioremediation process, is very low (log K_{sp} = -8.5). This solubility is consistent with the low concentrations of dissolved uranium measured in our treatment experience and in the work performed by Abdelouas and others.

Chang, Y., A. Peacock, P. Long, J. Stephen, J. McKinley, S. Macnaughton, A. Hussain, A. Saxton, and D. White. 2001.Diversity and Characterization of Sulfate-Reducing Bacteria in Groundwater at a Uranium Mill Tailings Site. Applied and Environmental Microbiology, 67: 3149-3160.

This paper shows that naturally occurring sulfate reducing bacteria are commonly found in subsurface environments contaminated with uranium. While a wide variety of different strains were identified, the activity of the bacteria to reduce sulfate and reduce uranium was widespread.

Ferris, F., R. Hallberg, B. Lyhven, and K. Pedersen. 2000. Retention of strontium, cesium, lead and uranium by bacterial iron oxides from a subterranean environment. Applied Geochemistry, 15: 1035-1042.

This paper documents strong sorption of uranium on bacterial iron oxides formed in a subterranean environment. These same iron oxides would be formed at the interface of oxygen-containing water and the iron sulfides in the groundwater at Cimarron after the bioremediation process has been implemented. As the oxygen in the water consumes the iron sulfides formed in the ARCADIS bioremediation process, fresh iron oxides will form, and these iron oxides have a very strong affinity for uranium.

Fruchter, J.S., C.R. Cole, M.D. Williams, V.R. Vermeul, J.E. Amonette, J.E. Szecsody, J.D. Istok, M.D. Humphrey. 2000. Creation of Subsurface Permeable Treatment Zone for Aqueous Chrome Contamination Using In Situ Redox Manipulation. GWMR Spring 2002:66-77.

This paper documents the transformation of ferric iron oxides in situ into reduced iron minerals by creating reducing conditions in situ. They also show that this process continues to scavenge dissolved oxygen for many years when a sufficient amount of iron is deposited in situ. They apply this process to chromium remediation (where chromium has some analogous properties to uranium).

Giammar, Daniel E., and Janet G. Hering. 2001. Time Scales for Sorption – Desorption and Surface Precipitation of Uranyl on Goethite. Evironmental Science Technology.

This paper shows removal of oxidized uranium on goethite is a rapid reaction, achieving equilibrium in most cases in minutes to hours. This is important for the Cimarron aquifer, where goethite is likely to form at the redox front where groundwater that contains oxygen reacts with the iron sulfides ARCADIS creates in the aquifer during the bioremediation process. Goethite is another iron mineral that shows sorptive capacity for uranium.

Harrington, James M., In situ treatment of metals in mine workings and materials. 2002. Tailings and Mine Waste 251-261

This paper documents a variety of instances where the ARCADIS process was implemented for remediation of metals in situ. Several case studies are presented showing stabilization of metals can be achieved in full scale implementation of reducing conditions by injection of organic carbon. This paper also identifies the factors that affect the permanence of treatment in an in situ treatment system.

Hartog, N., J. Griffioen, P. Van Bergen, and C. Van Der Weijden. 2001. Determining the reactivity of reduced components in Dutch aquifer

sediments. Impacts of Human Activity on Groundwater Dynamics, Publication no 269.

This paper is an example of how iron sulfides and organic matter are a redox buffer in situations where oxidizing solutions are infiltrating into reduced aquifer materials. It is an example of how mass balances can be obtained by comparing bulk concentrations of these reduced materials with oxidizing inputs from infiltrating groundwater to predict long-term aquifer removal of oxygen and nitrate.

Lack, J., S. Chaudhuri, S. Kelly, K. Kemner, S. O'Connor, and J. Coates. 2002. Immobilization of Radionuclides and Heavy Metals through Anaerobic Bio-oxidation of Fe (II). Applied and Environmental Microbiology, 68: 2704-2710.

This paper documents the removal of uranium in groundwater by the in situ formation of ferric iron. This is part of the long-term stability process at Cimarron, where ferric iron oxides will be formed as groundwater that contains oxygen is infiltrating into the zone with uranium and iron sulfides. Particularly note the last paragraph in the paper: "selective anaerobic bio-oxidation of Fe(II) added to the environment may be an effective means of capping off and completing the attenuation of heavy metals and radionuclides in a reducing environment, allowing the system to revert to an oxic state while preventing remobilization of previously reduced and immobilized heavy metals and radionuclides."

Leventhal, J and E. Santos. 1981. Relative importance of organic carbon and sulfide sulfur in a Wyoming roll-type uranium deposit. Open File Report (US Geological Survey) 81-580.

This paper provides results from a study of a naturally-occurring uranium ore body that shows that iron sulfide is the primary mechanism maintaining uranium in a stable form in a subsurface environment.

Lovley, D., E. Phillips, Y. Gorby, and E. Landa. 1991. Microbial reduction of uranium. Nature, 350, 413-416.

This paper is the first paper to document that uranium can be reduced and precipitated by microorganisms, and suggests that this could form the basis of a bioremediation process.

Martin, T., and H. Kempton. 2000. In Situ Stabilization of Metal-Contaminated Groundwater by Hydrous Ferric Oxide: An Experimental and Modeling Investigation. Environmental Science and Technology, 34, 3229-3234.

This is another paper that documents that iron oxides formed in place can provide an efficient process to scavenge metals from groundwater. This paper is an elegant description of why these oxides, formed along a flow path in groundwater, are likely to be more efficient in situ than can even be demonstrated in column studies.

Moyes, Lesley, N., Richard H. Parkman, John M. Charnock, David J, Vaughn, Francis R. Livens, Colin R. Hughes, and Anna Braithwaite. Uranium uptake from aqueous solution by interaction with goethite, lepidocrocite, muscovite, and mackinawite: An X-ray absorption spectroscopy study. Environmental Science Technology 2002. 34, 1062-1068.

This paper documents the very strong sorptive capacity of mackinawite (iron sulfide) for uranium, and why this mineral is so much stronger than even iron oxides (such as goethite) for uranium removal.

Patterson, Ronald R., and S. Fendorf. Reduction of Hexavalent Chromium by Amorphous Iron Sulfide. Environmental Science Technology. 1997 37, 2039-2044.

This paper documents how amorphous iron sulfide (the form initially formed during sulfate reduction) is a very reactive mineral, reacting with and reducing dissolved metals (in this case, chromium) to insoluble forms. It is a good paper discussing the usefulness of iron sulfide as a reactive mineral in remediation systems for metals.

Pauwels, H., W. Kloppmann, J. Foucher, A. Martelat, and V. Fritsche. 1998. Field tracer test for denitrification in a pyrite-bearing schist aquifer. Applied Geochemistry, 13: 767-778.

This is another paper that shows the usefulness of even very old iron sulfides for rapidly reacting with nitrate and oxygen to support reduction of these oxygen sources. This process forms the basis for why ARCADIS proposes to use iron sulfides to maintain an aquifer in a reduced form for 1000s of years.

Spear, J., L. Figueroa, and B. Honeyman. 2000. Modeling Reduction of U (VI) under Variable Sulfate Concentrations by Sulfate-Reducing Bacteria. Applied and Environmental Microbiology, 66: 3711-3721.

This paper documents why sulfate reducing bacteria are a logical bacterial group for uranium bioremediation. The capacity of these bacteria to reduce uranium even when sulfate concentrations are very high means that uranium will be reduced in an aquifer even if large quantities of sulfate are also being injected to create an iron sulfide matrix.

Wersin, Paul, M. F. Hochella Jr., P. Persson, G. Redden, J. O. Leckie, and D. W. Harris. Interaction between aqueous uranium (VI) and sulfide minerals: Spectroscopic evidence for sorption and reduction. Geochimica et Cosmochimica Aeta, 1994. Vol. No. 58 13, pp 2829-2843.

This paper shows that iron sulfides are reactive with dissolved uranium, reducing the uranium to insoluble forms and creating stable and insoluble uranium minerals. This is important for preventing any mobility of uranium downgradient of the zone where oxygen might initially make uranium soluble. The downgradient IRZ containing high concentrations of iron sulfide will thereby act as a removal mechanism for any uranium mobilized upgradient.

ELSEVIER

The Science of the Total Environment 250 (2000) 21–35

the Science of the Total Environment

www.elsevier.com/locate/scitotenv

Biological reduction of uranium in groundwater and subsurface soil

Abdesselam Abdelouas[a,*], Werner Lutze[b], Weiliang Gong[a], Eric H. Nuttall[b], Betty A. Strietelmeier[c], Bryan J. Travis[d]

[a] *Advanced Materials Laboratory, Center for Radioactive Waste Management, 1001 University Blvd., SE-Suite 201, Albuquerque, NM 87106, USA*

[b] *Department of Chemical and Nuclear Engineering, University of New Mexico, Albuquerque, NM 87131, USA*

[c] *Los Alamos National Laboratory, Chemical Sciences and Technology Division, MS J514, Los Alamos, NM 87544, USA*

[d] *Los Alamos National Laboratory, Earth and Environmental Sciences Division, MS F665, Los Alamos, NM 87545, USA*

Received 15 June 1999; accepted 5 December 1999

Abstract

Biological reduction of uranium is one of the techniques currently studied for in situ remediation of groundwater and subsurface soil. We investigated U(VI) reduction in groundwaters and soils of different origin to verify the presence of bacteria capable of U(VI) reduction. The groundwaters originated from mill tailings sites with U concentrations as high as 50 mg/l, and from other sites where uranium is not a contaminant, but was added in the laboratory to reach concentrations up to 11 mg/l. All waters contained nitrate and sulfate. After oxygen and nitrate reduction, U(VI) was reduced by sulfate-reducing bacteria, whose growth was stimulated by ethanol and tri*meta*phosphate. Uranium precipitated as hydrated uraninite ($UO_2 \cdot xH_2O$). In the course of reduction of U(VI), Mn(IV) and Fe(III) from the soil were reduced as well. During uraninite precipitation a comparatively large mass of iron sulfides formed and served as a redox buffer. If the excess of iron sulfide is large enough, uraninite will not be oxidized by oxygenated groundwater. We show that bacteria capable of reducing U(VI) to U(IV) are ubiquitous in nature. The uranium reducers are primarily sulfate reducers and are stimulated by adding nutrients to the groundwater.

Keywords: Uranium; Bioremediation; Groundwater; Uraninite; Iron sulfide; Indigenous bacteria; Speciation; Redox buffer

* Corresponding author. Tel.: +1-505-272-7271; fax: +1-505-272-7304.
E-mail address: badria@unm.edu (A. Abdelouas)

0048-9697/00/$ - see front matter
PII: S0048-9697(99)00549-5

1. Introduction

Biological reduction of uranium has been proposed as a technique for uranium removal from groundwaters via reductive precipitation (Kauffman et al., 1986; Francis et al., 1991, 1994; Lovley et al., 1991, 1993; Gorby and Lovley, 1992; Lovley and Phillips, 1992a,b; Barnes and Cochran, 1993; Lovley, 1995; Phillips et al., 1995; Barton et al., 1996; Uhrie et al., 1996; Tucker et al., 1996, 1998a,b; Hard et al., 1997; Ganesh et al., 1997; Abdelouas et al., 1998a, 1999a,b). These authors showed that aqueous uranium can be reduced by a variety of microorganisms including iron- and sulfate-reducing bacteria and in some cases by denitrifying bacteria. The product of uranium reduction is uraninite, UO_2, a highly insoluble mineral under reducing conditions (Langmuir, 1978; Parks and Pohl, 1988). In nature, reduction of U(VI) in anoxic marine sediments is the most important sink of dissolved uranium (e.g. Cochran et al., 1986; Klinkhammer and Palmer, 1991). Reduction of U(VI) in the subsurface environment lead to the formation of uranium ore deposits (Jensen, 1958; Hosteler and Garrels, 1962; Taylor, 1979; Maynard, 1983). Uraninite and pitchblende, both nominally UO_2, are the principal ore minerals in many ore deposits (Rich et al., 1977; Kimberley, 1979). Natural uraninite is fairly stable over geological time. For instance, 2 billion-year-old uranium ore deposits are known in Oklo (Gabon) (Gauthier-Lafaye and Weber, 1989; Gauthier-Lafaye et al., 1989, 1996, 1997; Nagy et al., 1991; Bros et al., 1993). The stability of uraninite at the Oklo deposits was sustained by the presence of siderite ($FeCO_3$), pyrite (FeS_2) and organic matter in the form of bitumen, which consumed the oxygen supplied by infiltrating groundwater (Blanc, 1995; Janeczek, 1999). Abdelouas et al. (1999a) reported that oxidation of biologically reduced uranium increased with increasing ratio of dissolved oxygen/uraninite. In the present work we study the effect of iron sulfide/uraninite ratio on U(IV) oxidation.

A recent study (Quinton et al., 1997) showed that among the groundwater cleanup technologies — pump and treat, permeable reactive barrier with zero-valent iron granular filings, and a biobarrier, intrinsic or engineered in situ bioremediation — the latter is the most cost-effective. In situ bioremediation consists of the activation of indigenous microbial populations to degrade or precipitate the contaminants (National Research Council, 1994). A conventional technique such as 'pump and treat' may not be adequate for uranium removal because pumping the water may change the uranium speciation followed by sorption of uranium on the host rock (Abdelouas et al., 1998b). With in situ bioremediation both soluble and sorbed U(VI) can be reduced and immobilized by bacteria. To date in situ biological remediation of uranium has not been demonstrated in the field. In natural aquifers mixed cultures of nitrate-, metal- and sulfate-reducing bacteria are likely to be present (Hodgkinson, 1987; Ghiorse, 1997; Nealson and Stahl, 1997; Bachofen et al., 1998). In the presence of carbon, nitrogen and phosphorus sources and adequate respective electron acceptors, these bacteria will be stimulated in the following order: denitrifying bacteria, metal-reducing bacteria, and finally sulfate-reducing bacteria (Nealson and Stahl, 1997; Lu, 1998; Abdelouas et al., 1998a).

Several laboratory studies have been devoted to the enzymatic reduction of uranium under a variety of conditions relevant to ex situ treatments of waste streams from radionuclide processing facilities (e.g. Macaskie, 1991; Ganesh et al., 1997). These studies used pure strains of bacteria (e.g. desulfovibrio species) to elucidate the impact of inorganic (e.g. nitrate, sulfate, bicarbonate) and organic (e.g. acetate, malonate, oxalate, citrate) ions on uranium removal from waste waters. Only a few studies focused on uranium reduction with mixed cultures of bacteria in groundwaters (Barton et al., 1996; Ganesh et al., 1997; Abdelouas et al., 1998a). In the case of in situ bioremediation the presence of mixed-culture of bacteria is a prerequisite for uranium reduction.

The objective of this study is to determine whether bacteria capable of uranium reduction are encountered in groundwaters and soils from different locations, and whether they can be easily activated.

2. Experimental

2.1. Groundwater and soil

Groundwaters and soils were collected in autoclaved 1-l plastic containers and in 160-ml serum bottles placed in a nitrogen flushed glove box in the field. Temperature, pH, dissolved oxygen were measured either in situ using a YSI-6920 probe (YSI, OH, USA) or using samples in the glove box after the well had been pumped extensively. The bottles with the groundwater and soil were kept under argon atmosphere to avoid oxidation of samples in a refrigerator at 4°C without additives. Water and soil samples were used within the first week following their collection to conduct experiments of biological reduction of uranium. In the past we found that long storage of groundwater resulted in a significant decrease of the number of viable bacteria including denitrifying and sulfate-reducing bacteria (Lu, 1998). Furthermore, prolonged storage of groundwater can also affect its geochemistry such as calcium carbonate precipitation and change in pH (Abdelouas et al., 1998b).

Groundwater compositions are given in Table 1. One groundwater sample (well #926) originated from the mill tailings site near Tuba City, AZ (USA), four groundwater samples (GW1–GW4) came from mining and tailing site in Germany, two groundwater samples (NMW1 and NMW2) from the mill tailings site in Grants, NM (USA), one groundwater sample from a dairy site in Bernalillo, NM (USA), and one groundwater from a former farm site in Albuquerque, NM (USA). Uranium(VI) concentrations ranged between 0.25 and 50 mg/l, sulfate concentrations between 0.105 and 17.9 g/l, and nitrate concentrations between 0.0085 and 1.2 g/l. All groundwaters showed a pH near neutral except those collected from the mill tailings site near Grants. NM (pH = 10). In this water the alkaline leaching process used to extract uranium from the rock lead to strong enrichment of the groundwater with carbonate (1.3×10^{-1} M), which may inhibit uranium biological reduction (Phillips et al., 1995).

2.2. Groundwater amendment

Addition of amendment to the system groundwater/soil was required to activate indigenous bacteria. In the experiments where only organic carbon or phosphorus sources were added to the groundwater and soil, uranium was not reduced. This observation suggested that neither carbon nor phosphorus in groundwater and soil were available to the indigenous bacteria. As a result groundwater amendment with organic carbon and

Table 1
Chemical composition of unamended groundwaters from various locations (mg/l)

	Location of uranium mill tailings sites							Dairy site Bernalillo NM (USA)	Farm site Albuquerque NM (USA)
	Tuba City AZ (USA) Well #926	Germany				Grants NM (USA)			
		GW1	GW2	GW3	GW4	NMW1	NMW2		
U(VI)	0.25	0.9	0.77	1.76	3.60	50.0	50.0	3.7[a]	1–11[a]
SO_4^{2-}	1830	457	6300	17 952	14 942	11 353	12 421	234	105
Total Fe	0.05	3.5	2.0	< 0.5	2.0	0.6	1.3	< 0.05	0.03
Total Mn	0.02	0.4	0.06	2.6	0.15	0.1	0.1	0.04	0.05
NO_3^-	1220	52.8	29.0	134	125	8.5	33.5	240	450
Dissolved oxygen	3.1	6.1	6.2	6.2	6.3	6.5	6.4	5.7	4.8
pH	6.6	7.6	7.6	7.7	7.8	10.0	9.9	6.8	7.3
Water level (feet)	40	7	7	7	7	100	100	70	16

[a]Uranium was added to the groundwater in the laboratory.

phosphorus sources was required to stimulate bacterial growth. In previous work (Abdelouas et al., 1998a; Lu, 1998; Lu et al., 1999), the authors tested enzymatic uranium reduction in groundwater using several organic carbons (acetate, methanol, glucose, lactate, ethanol) and phosphorus (*ortho*- and *meta*phosphate) sources and found that ethanol (C_2H_5OH) and sodium tri*meta*phosphate (TMP), $Na_3P_3O_9$, yielded the highest rates of growth of bacteria and uranium reduction. Benner et al. (1997) showed that ethanol is a suitable carbon source for the growth of a mixed-culture of sulfate reducing bacteria to remove zinc from groundwater in an ex situ treatment plant. In the present work, we used ethanol and TMP to amend the groundwater. No pH-buffers or reducing agents were added. The groundwater was amended with the minimum amount of chemicals necessary. The less chemicals added to the groundwater, the lower the overall costs of the remediation and the better the quality of the groundwater at the end of the process.

For denitrification, an ethanol/nitrate ratio was established slightly higher than the stoichiometric one of 5:12 [Eq. (1)].

$$12NO_3^- + 5C_2H_5OH + 2H^+ = 6N_2 + 10HCO_3^- + 11H_2O \quad (1)$$

For uranium and sulfate reduction, the ethanol/sulfate ratio was 2:3 [Eq. (2)] for the groundwaters with low sulfate concentration.

$$3SO_4^{2-} + 2C_2H_5OH = 4HCO_3^- + 3HS^- + H^+ + 2H_2O \quad (2)$$

To the groundwaters with high sulfate concentrations just enough ethanol was added to reduce 3–5 mM SO_4^{2-} together with uranium, which resulted in addition of 2–3.3 mM of ethanol to 100 ml of groundwater. During the reduction of 3–5 mM SO_4^{2-} in groundwater, U(VI) at a concentration of 1–10 mg/l was entirely reduced. Furthermore, for water with high uranium concentration (mill tailings site in Grants) more ethanol was added according to Eq. (3).

$$6UO_2(CO_3)_2^{2-} + C_2H_5OH + 5H_2O = 6UO_2 + 14HCO_3^- + 2H^+ \quad (3)$$

TMP was added to the groundwater to reach a final concentration of PO_4^{2-} of 20 mg/l, which yielded the highest rate of sulfate and uranium reduction. Eqs. (1)–(3) neglect biomass formation, but a small fraction of the carbon will be incorporated into bacterial biosynthesis.

2.3. Batch experiments

Stock solutions of 0.5 M ethanol and 7×10^{-2} M of TMP were prepared and transferred into serum bottles. The bottles were then purged with argon to remove oxygen and autoclaved at 120°C for 25 min.

The experiments were conducted in serum bottles shortly after sample collection. For each experiment 100 ml of groundwater and 8 g of soil were used. The bottles were sealed with a butyl rubber stopper in an aseptic environment in a glove box, crimped with an aluminum seal, and were removed from the glove box. A syringe needle was introduced through the stopper to purge the groundwater with argon to establish an anaerobic environment. The reaction progress was monitored by collecting aliquots of 2 ml using a sterile 3-ml syringe for chemical analysis. The reaction progress was indicated by precipitation of black compounds, presumably iron sulfides and uraninite. At the end of the reaction the final volume of water was between 80 and 90 ml. Control experiments were conducted to distinguish between biotic and abiotic reduction of U(VI). In these experiments the microorganisms were killed by heat before addition of amendments.

Groundwater with low sulfate concentration was doped with sulfate $FeSO_4 \cdot 7H_2O$ or Na_2SO_4 (1 g/l sulfate) to determine the impact of sulfate concentration on uranium reduction and dissolution/oxidation, and to obtain enough iron sulfide for identification. Precipitation of iron sulfide can help protect uraninite from dissolution/oxidation by flowing oxygenated groundwater following in situ bioremediation. To groundwater from the

Tuba City mill tailings site uranyl nitrate $[UO_2(NO_3)_2 \cdot 6H_2O]$, was added to obtain enough uraninite for identification.

In some experiments sulfate-reducing bacteria were cultivated in batch experiments using untreated groundwater/soil by adding ethanol and TMP. The growth of sulfate-reducing bacteria was indicated by the reduction of sulfate and formation of H_2S and iron sulfide. Aliquots of the cultures (5–10 ml) were added to some experiments to enhance reduction of uranium.

In the experiments with variable molar ratio of uraninite/iron sulfide, the bioremediated water was replaced by uncontaminated naturally oxygenated groundwater from the Tuba City site. The reoxidation of uraninite and iron sulfide was determined by measuring U(VI) and sulfate in solution.

2.4. Analytical procedures

Prior to analysis, groundwaters were passed

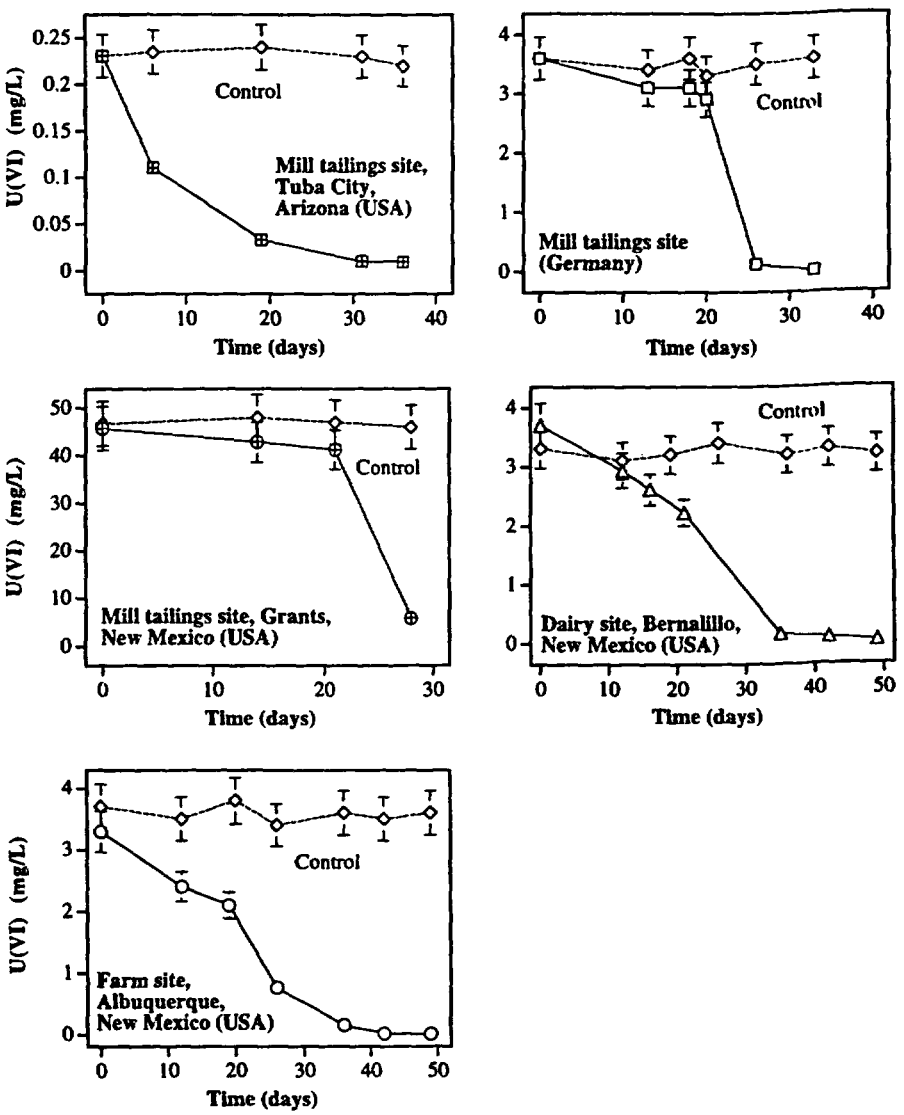

Fig. 1. Reduction of uranium in groundwaters amended with ethanol and trimetaphosphate at 24°C.

through a nylon Acrodisc syringe filter with a 0.2-μm pore size to remove biomass and mineral particles from the soil. Uranium was analyzed using a laser fluorescence analyzer (Scintrex UA-3) with a detection limit of 0.5 μg/l and a precision of ±15%. The uranium analyzer detects only hexavalent uranium. Nitrate and sulfate were measured by ion chromatography using a Dionex (DX-500) ion chromatograph with a precision of ±5%. Iron and manganese were measured by atomic absorption spectroscopy with a precision of ±5%. The solid phases containing reduced uranium and iron were identified using a Jeol JEM-2000 FX transmission electron microscope. Ethanol content was not measured.

3. Results and discussions

3.1. Uranium reduction in groundwater and soil

The activity of indigenous bacteria was observed by the production of gas, which increased the pressure in the serum bottles, and by the formation of dark precipitates, presumably iron sulfide and uraninite. The results of uranium reduction in groundwaters are plotted in Fig. 1. In all but the experiments with the groundwater from the mill tailings site (Grants, NM), uranium concentration decreased to a level below the United States groundwater protection standard (44 μg/l) (Federal Register, 1995). At 24°C, the uranium reduction was complete typically within 5 weeks (Fig. 1). In the experiments using the groundwater from the mill tailings at Grants, the uranium concentration decreased by 90% within 4 weeks to reach a final concentration of 5 mg/l. Control experiments with autoclaved groundwater and soil did not show any uranium reduction, suggesting that the reduction of uranium is microbially-mediated. Reduction of uranium by sulfide is possible, but this process is relatively slow. In fact, Abdelouas et al. (1998a) showed that the presence of carbonate and bicarbonate in groundwater inhibits uranium reduction by sulfide. Carbonate and bi-carbonate are common anions in groundwaters (Langmuir, 1997), and are produced by oxidation of organic carbon by bacteria [Eqs. (1)–(3)].

The chemical composition of groundwater at the end of uranium reduction is given in Table 2. Despite the production of H^+ during the reduction of sulfate and uranium, there was no significant change in pH, which underlines the strong buffering capacity of the soil (e.g. Read et al., 1993). Most of the sulfate was reduced to sulfide (S^{2-}) in groundwater with low initial sulfate concentration (GW1, dairy site, farm site). The experiments with high initial sulfate concentration (Tuba city, GW2, GW3, GW4, NMW1, NMW2)

Table 2
Chemical composition of bioremediated groundwaters from various locations (mg/l)

	Location of uranium mill tailings sites							Dairy site Bernalillo NM (USA) –	Farm site Albuquerque NM (USA) –
	Tuba City AZ (USA) Well #926	Germany				Grants NM (USA)			
		GW1	GW2	GW3	GW4	NMW1	NMW2		
U(VI)	0.014	0.004	0.001	0.001	0.001	5.0[a]	4.5[a]	0.001	0.002
SO_4^{2-}	1250	7.7	3657	16 409	10 709	8770	8000	0.5	1.6
Total Fe	0.59	12.6	5.0	1.0	12.6	2.2	18.1	3.5	4.4
Total Mn	0.76	18	22.0	48.0	6.4	0.3	0.1	2.2	1.2
NO_3^-	< 0.1	< 0.1	< 0.1	< 0.1	< 0.1	< 0.1	< 0.1	< 0.1	< 0.1
Dissolved oxygen	< 0.1	< 0.1	< 0.1	< 0.1	< 0.1	< 0.1	< 0.1	< 0.1	< 0.1
pH	6.8	7.3	7.5	7.9	7.6	9.8	9.7	6.7	7.2

[a]The high carbonate concentrations in these solutions (1.3×10^{-1} M) lead to formation of U(VI)-carbonato complexes stable under reducing conditions (Brookins, 1988), which inhibited the complete reduction of U(VI).

showed only partial reduction of sulfate. The reduction of sulfate confirms the activity of sulfate-reducing bacteria. A fraction of Fe(III) and Mn(IV) from the soil was reduced to Fe(II) and Mn(II), respectively. Iron(II) and Mn(II) in solution can be oxidized by dissolved oxygen and precipitated as oxyhydroxides. These are not considered a health hazard (Seelig et al., 1992).

We conducted thermodynamic calculations using the EQ3NR code (Wolery, 1992) to determine the uranium speciation in groundwater and to identify the mineral phases likely to precipitate. As input data, the chemical composition of the waters measured at the end of uranium reduction was used (Table 2). The carbonate concentration was derived from Eqs. (1) and (2). Two E_H values were used, $E_H = -100$ and -300 mV, which are reached at the end of denitrification (Abdelouas et al., 1998a) and under sulfate reducing conditions (Odom and Singleton, 1993), respectively. Hydrogen sulfide concentration was estimated as the difference between the final and initial sulfate concentrations. The results of uranium speciation calculations and saturation index calculations (log Q/K; Q = ion activity product, K = equilibrium constant) of selected minerals are given in Tables 3 and 4, respectively. At near neutral pH, an $E_H = -100$ mV, and relatively low bicarbonate concentration (< 0.05 mM HCO_3^-), uranium speciation is dominated by the species $U(OH)_4(aq)$ and some U(VI)-carbonato complexes (Table 3). The groundwaters are saturated with respect to uraninite and iron sulfides such as pyrite (FeS_2) and pyrrhotite ($Fe_{1-x}S$) (Table 4). Experimentally, mackinawite ($FeS_{0.9}$) and some pyrite and pyrrhotite were identified as the main iron sulfide compounds. Mackinawite does not exist in the EQ3NR code's data base. Mackinawite is a *meta*stable phase and will ultimately be converted to the more stable pyrite (Pósfai et al., 1998). For an E_H of -300 mV, the only uranium species present in solution is $U(OH)_4(aq)$ and uraninite and iron sulfide saturation indices increased, making these phases likely to precipitate. For groundwater from the mill tailings site at Grants, uranium is complexed with carbonate even at $E_H = -300$ mV (Table 3). For an $E_H = -100$ mV, the solution is highly undersaturated with respect to uraninite (log $Q/K = -6.6$), but saturated with respect pyrite and rhodochrosite ($MnCO_3$) (Table 4). Precipitation of rhodochrosite in groundwater from the mill tailings site at Grants, but not in the rest of groundwaters, is possible because of the high pH and

Table 3
Calculated uranium speciation in groundwaters at 24°C[a]

	$E_H = -100$ mV	$E_H = -300$ mV
Mill tailings, Tuba City, AZ (USA), groundwater well #926	73% $U(OH)_4(aq)$ 21% $UO_2(CO_3)_3^{4-}$ 6% $UO_2(CO_3)^{2-}$	100% $U(OH)_4(aq)$
Mill tailings, Germany, groundwater (GW1)	81% $U(OH)_4(aq)$ 12% $UO_2(CO_3)_3^{4-}$ 7% $UO_2(CO_3)^{2-}$	100% $U(OH)_4(aq)$
Mill tailings, Grants, NM (USA), groundwater (NMW1)	100% $UO_2(CO_3)_3^{4-}$	100% $UO_2(CO_3)_3^{4-}$
Dairy site, Bernalillo, NM (USA)	100% $U(OH)_4(aq)$	100% $U(OH)_4(aq)$
Farm site, Albuquerque, NM (USA)	65% $U(OH)_4(aq)$ 40% $UO_2(CO_3)_3^{4-}$ 2% $UO_2(CO_3)^{2-}$	100% $U(OH)_4(aq)$

[a]The composition of the water used in calculations with EQ3NR code is that measured at the end of uranium reduction (Table 2).

Table 4
Saturation indices (log Q/K) of groundwaters at 24°C for U(IV) and Mn(II) phases and iron sulfides[a]

	Uraninite	$UO_{2.25}$	Pyrite (FeS_2)	Pyrrhotite ($Fe_{1-x}S$)	Rhodochrosite ($MnCO_3$)
Mill tailings, Tuba City, AZ (USA), groundwater well #926	+4.9	+2.0	+16.3	+2.9	< −10
Mill tailings, Germany, groundwater (GW1)	+5.3	+3.9	+17.9	+2.4	−4.6
Mill tailings, Grants, NM (USA) groundwater (NMW1)	−6.6 +2.6[b]	−6.3 +0.6[b]	+14.7 +20.3[b]	−0.9 +6.8[b]	+0.9 +0.9[b]
Dairy site, Bernalillo, NM (USA)	+6.2	+4.4	+18.1	+2.0	−1.3
Farm site, Albuquerque, NM (USA)	+5.9	+4.5	+18.1	+2.1	−0.4

[a]The composition of the water used in calculations with EQ3NR code is that measured at the end of uranium reduction (Table 2): $E_H = -100$ mV.
[b]$E_H = -300$ mV.

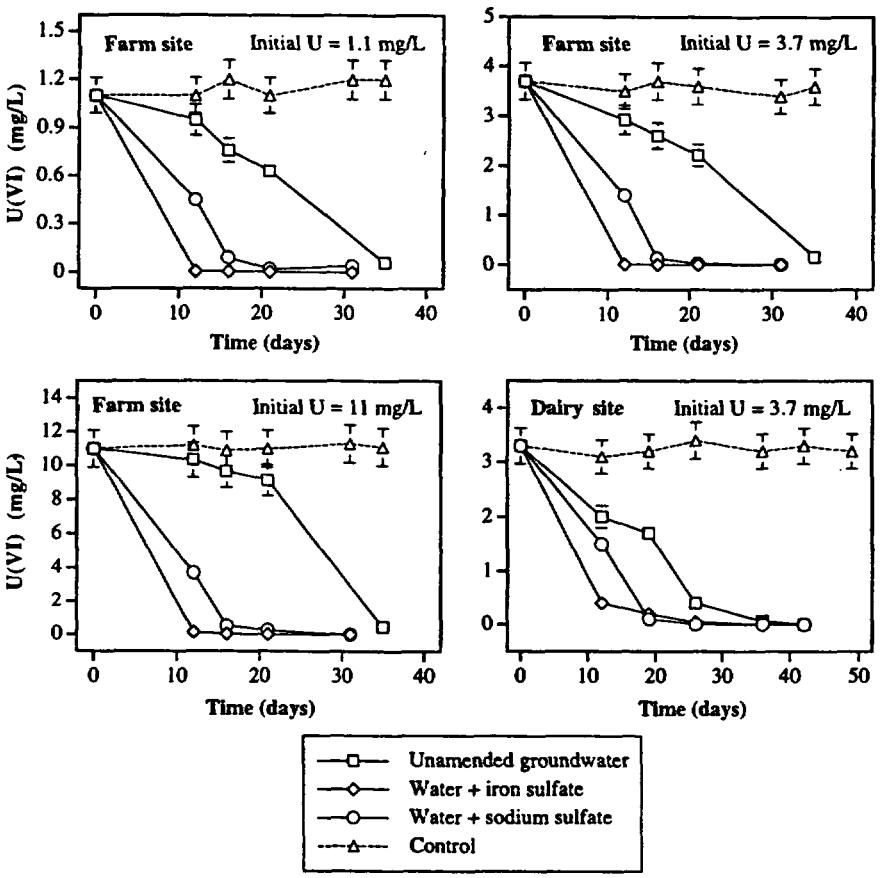

Fig. 2. Effect of sulfate addition on uranium reduction in groundwaters. Iron or sodium sulfate were added to reach a final sulfate concentration of approximately 1 g/l. The initial sulfate concentration in the farm and dairy site groundwaters are 105 and 234 mg/l, respectively.

carbonate concentration in this water (Table 1). However, for an $E_H = -300$ mV the solution is highly super-saturated with respect to uraninite (log $Q/K = +2.6$). The competition between uranium complexation and reduction is the most likely cause of incomplete reduction of uranium. This result is in agreement with findings by Phillips et al. (1995) who showed that a carbonate concentration of 100 mM inhibited the enzymatic reduction of uranium, while a carbonate concentration of 33 mM had no effect. The presence of sulfide prevents formation of siderite, $FeCO_3$.

3.2. Effect of sulfate concentration on uranium reduction in groundwater / soil

To test the effect of sulfate concentration on U(VI) reduction, sodium or iron sulfate were added to the groundwaters with low sulfate concentrations. After addition of iron sulfate to the water, a yellowish precipitate of Fe(III) hydroxide formed. Results of uranium reduction with/without addition of sulfate are given in Fig. 2. Control experiments using autoclaved groundwater and soil show no reduction of uranium. Reduction of uranium took longer in groundwaters with low sulfate concentration and uranium concentrations between 1.1 and 11 mg/l. Uranium reduction was complete within 5 weeks. Experiments with high sulfate concentration took 12 days (farm site, water + iron sulfate) to 21 days (farm and dairy sites, water + sodium sulfate) to completely reduce uranium. The abundance of sulfate in solution as an electron acceptor for sulfate-reducing bacteria stimulated the growth of these bacteria and enhanced uranium reduction. Uranium(VI) was removed faster in the experiment with iron sulfate than with sodium sulfate probably because of its partial sorption onto the newly formed Fe(III) hydroxides. At the end of the experiment, all the U(VI) sorbed was reduced because all the Fe(III) hydroxide was reduced to form Fe(II) sulfides.

In some experiments iron sulfate was added to reach sulfate concentrations of 0.9, 0.7, 0.5, and 0.3 g/l to determine the concentration of sulfate necessary to yield a high reduction rate of uranium. The results are plotted in Fig. 3. The uranium reduction is slower in water containing 0.5 and 0.3 g/l than in water with sulfate concentrations of 0.7 and 0.9 g/l. In the experiments with low sulfate concentration (≤ 0.5 g/l) uranium was totally reduced within 36 days, while in water with sulfate concentration ≥ 0.7 g/l uranium was reduced within 21 days. Comparing the results in Fig. 3 with those in Fig. 2, we can say that the increase in sulfate concentration in groundwater (farm site) from the initial concentration of 105 mg/l to 0.5 g/l did not affect the reduction rate of uranium. In these experiments, uranium was reduced roughly within 5 weeks. However, for a sulfate concentration ≥ 0.5 g/l uranium reduction was fast. Finally, it took only 12 days to reduce uranium in water completely with 1.1 g/l sulfate.

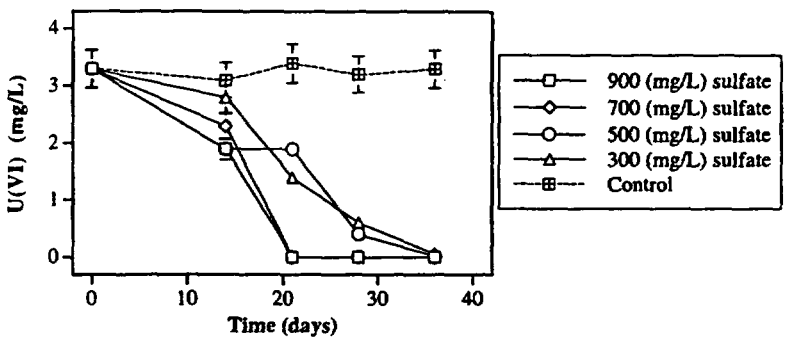

Fig. 3. Effect of sulfate concentration on uranium reduction in groundwater from the farm site.

3.3. Effect of soil treatment on uranium reduction in groundwater / soil

We conducted experiments with groundwater and untreated soil (contains viable bacteria) or autoclaved soil (does not contain viable bacteria). The water and soil samples originated from the mill tailings site in Germany. The results are given in Fig. 4. Control experiments using autoclaved groundwater and soil show no reduction of uranium. Fig. 4 shows that regardless of the composition of the water. uranium was reduced within 13 days in the experiment with untreated soil and groundwater, while it took almost 5 weeks to reduce uranium completely in the experiments with autoclaved soil samples but with untreated water. Inoculation of the samples containing autoclaved soil and untreated water (Fig. 4, square) with cultivated bacteria from the experiments with untreated soil and groundwater (Fig. 4, circle) at day 13 increased the rate of reduction of uranium as can be seen in Fig. 4 (diamond). This result shows that mixed-culture containing indigenous sulfate-reducing bacteria can be grown in batch experiments using groundwater/soil from the contaminated site and can be used to promote uranium reduction, if necessary. In the experiments with untreated soil (Fig. 4, circle), the abundance of viable bacteria in the soil led to a rapid growth of sulfate-reducing bacteria that reduced uranium. In the experiments with autoclaved soil, only the groundwater contained bacteria, resulting in smaller initial populations of bacteria. These results suggest that in situ reduc-

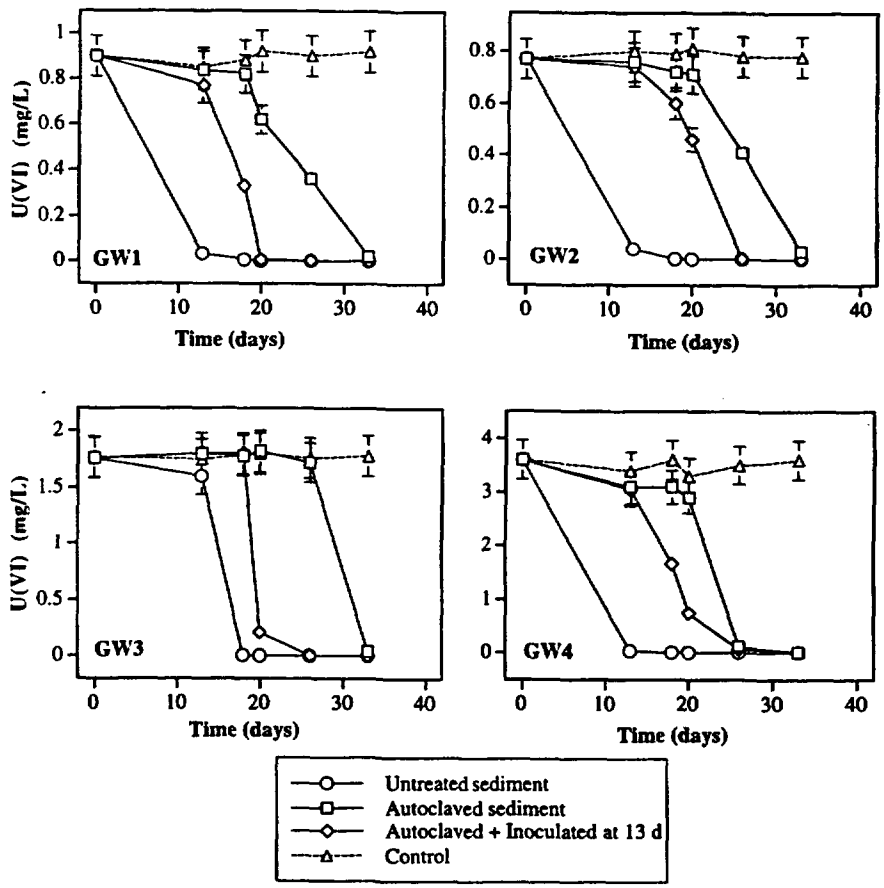

Fig. 4. Effect of soil treatment on uranium reduction in groundwaters from the mill tailings site in Germany.

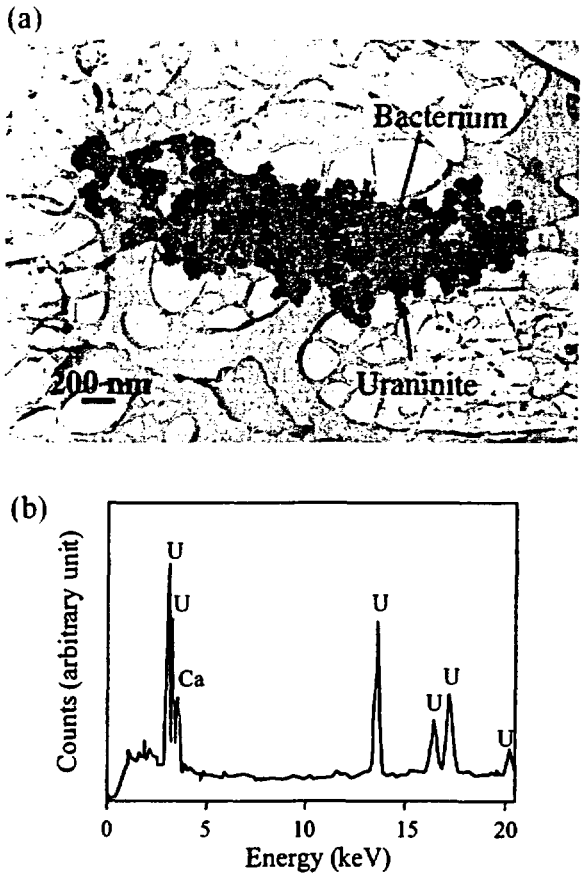

Fig. 5. (a) Bacterium with uraninite particles (mill tailings site, Tuba city); and (b) chemical microanalysis spectrum of uraninite.

tion of uranium by sulfate-reducing bacteria is likely to be faster than in the laboratory because of the high ratio soil/water, providing a high initial concentration of bacteria. In a previous study on in situ biological denitrification, it was found that the in situ reduction of nitrate in groundwater/soil was fast and complete within 5 days, while it took up to 15 days in the laboratory using batch experiments (Deng, 1998; Abdelouas et al., 1999c).

3.4. Importance of iron sulfide formation during in situ bioremediation of uranium

An example of uraninite that precipitated from the Tuba city groundwater after enzymatic reduction of uranium is given in Fig. 5a. Uraninite particles are attached to a bacterium. An example of chemical microanalysis spectrum of a uraninite particle is shown in Fig. 5b. Mackinawite, and some pyrite and pyrrhotite were encountered in the experiments. Fig. 6a,b and Fig. 7a,b show mackinawite and pyrite, formed by reduction of Fe(III) to Fe(II) and SO_4^{2-} to S^0 and S^{2-}, and their chemical microanalysis spectra. The results of the thermodynamic calculations in Table 4 are in agreement with the experimental findings.

It is important to consider uraninite reoxidation in the case of in situ bioremediation. The remediated groundwater will be replaced eventu-

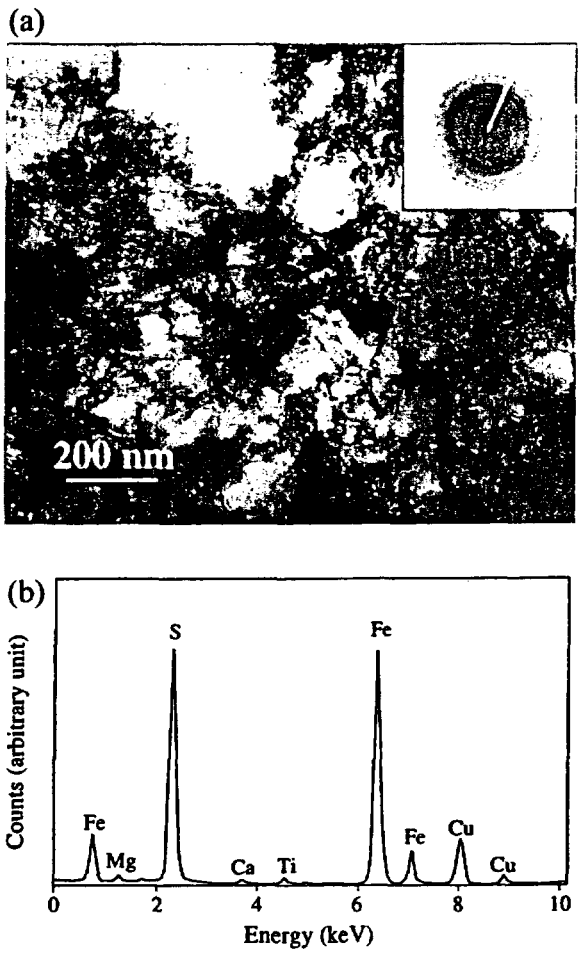

Fig. 6. (a) Mackinawite particles, electron diffraction pattern; and (b) chemical microanalysis spectrum of mackinawite (farm site).

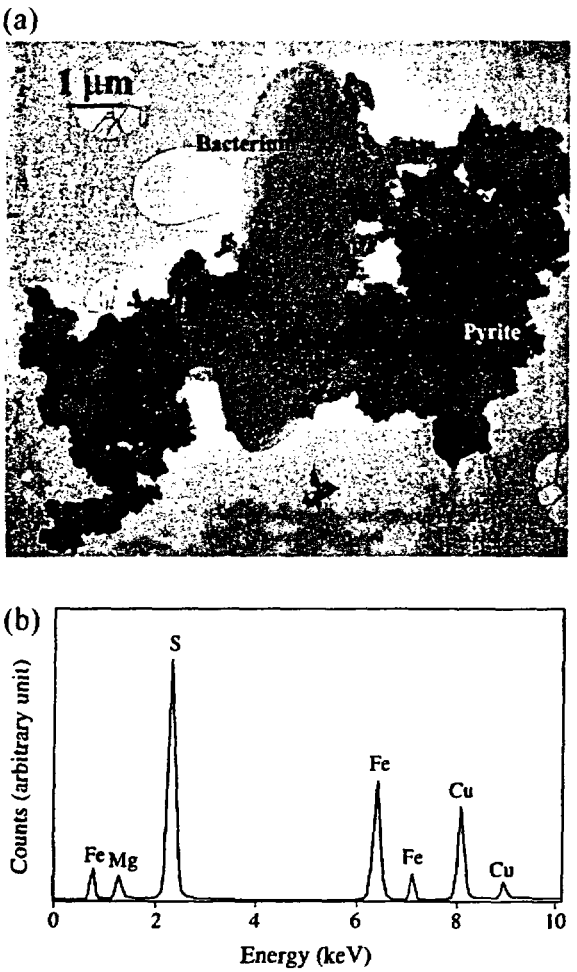

Fig. 7. (a) Bacterium with pyrite particles; and (b) chemical microanalysis of pyrite (mill tailings site, Germany).

ally by uncontaminated water containing oxygen, and uraninite could be reoxidized. We conducted batch and soil column experiments with the groundwater and soil from the mill tailings site at Tuba City and the biologically precipitated uraninite was leached with oxygen-rich uncontaminated groundwater from the same site (Abdelouas et al., 1999a). In the batch experiments we kept a constant molar ratio $UO_2/FeS_{0.9} = 1.5 \times 10^{-3}$ but we varied the oxygen supply between 7 and 58 µM. We found that the amount of oxidized uraninite increased with increasing amounts of oxygen supplied. While most of the oxygen (> 90%) was consumed by mackinawite oxidation, a small fraction of the oxygen (< 0.1%) was used to oxidize uraninite; the rest of the oxygen was consumed by oxidation of biomass. In the column experiments, the concentration of uranium in solution (outlet of the column) was on the order of a few µg/l, typically 4 µg/l, and did not change with time in the presence of mackinawite and dissolved oxygen. Again, it was found that most of the oxygen was consumed by makinawite oxidation. By using the inventory of uraninite and mackinawite in the column and the concentration of oxidized uranium and sulfide in the groundwater leaving the column, we calculated that before total oxidation of mackinawite all uraninite is expected to oxidize at a very slow rate. Hence, the large amount of iron sulfide (roughly 4.5 mM) in the column compared to that of uraninite (roughly 10^{-4} mM) protected uraninite from rapid oxidation and prevented the increase of U(VI) concentration above 44 µg/l, the groundwater protection standard in the United States. The preferential oxidation of mackinawite relative to uraninite was expected because the redox intensity $p\varepsilon^\circ$ of SO_4^{2-} reduction, $p\varepsilon^\circ = -3.75$ (Stumm and Morgan, 1981), is lower than that of U(VI), $p\varepsilon^\circ = +4.9$ (Abdelouas et al., 1998a). Rhodochrosite is not expected to protect uraninite from reoxidation because the redox intensity of Mn(IV), $p\varepsilon^\circ = +8.9$ (Stumm and Morgan, 1981), is higher than that of U(VI).

To study the effect of $UO_2/FeS_{0.9}$ on uraninite dissolution we conducted batch experiments where the oxygen concentration was kept constant at 0.4×10^{-2} mM and the molar ratio $UO_2/FeS_{0.9}$ was varied between 6.1×10^{-3} and 1.4×10^{-3} by varying the initial concentration of $FeSO_4 \cdot 7H_2O$ of the groundwater. The results are given in Fig. 8, which shows that U(IV) is oxidized to U(VI) whose concentration reaches a maximum in all experiments and decreases to below 20 µg/l after 23 days. Fig. 8 shows that the maximum concentration of U(VI) reached in each experiment increased with increasing the ratio $UO_2/FeS_{0.9}$. In other words, the more iron sulfide present, the higher the stability of uraninite. The slow decrease of U(VI) concentration over time is probably due to reduction and reprecipita-

tion of uraninite because, after consumption of oxygen, the redox intensity of the solution is determined by H_2S/HS^-.

Iron(III) compounds are ubiquitous in soils and sediments and their concentration is usually much higher than the small amount of precipitated uraninite. Iron(III) oxides and hydroxides are found in concentrations of a few percent depending on the origin of the soil (Langmuir, 1997). Sulfate concentrations are also often quite high. The median concentration of sulfate in uncontaminated groundwaters is 30 mg/l (Turekian, 1977). Sulfate concentrations in acid-mine waters, tailings waters, and waste waters, the contaminated sites for potential application of bioremediation technologies, can exceed 30 g/l (Langmuir, 1997). Thus, much more mackinawite and other iron sulfides are formed than uraninite. It has been shown that mackinawite can protect uraninite for hundreds of years (Abdelouas et al., 1999a) using an acceleration test. In the case of iron-poor soil and sulfate-poor groundwater, the addition of iron sulfate to the groundwater would help precipitate enough iron sulfide to protect uraninite from oxidation. at least to the extent necessary to keep the uranium concentration below 44 μg/l.

4. Summary and conclusion

Bacteria capable of reducing uranium can be found in groundwaters with different chemical composition. The uranium reducers are primarily sulfate-reducers and can be stimulated by addition of nutrients to groundwaters with high concentrations of sulfate. Ethanol together with tri*meta*phosphate yielded the highest rates of sulfate and uranium reduction. The uranium-reducers can also be stimulated in groundwater with low sulfate concentration. Addition of iron sulfate may be necessary in iron- and sulfate-poor groundwater/soil systems to precipitate enough iron sulfide to protect uraninite from reoxidation in oxygenated groundwaters.

The present results suggest that in situ bioremediation may find application to remediate uranium contaminated sites. An engineered process of U in situ bioremediation relies on two critical issues: (1) the presence of bacteria capable of reducing uranium; and (2) mixing of the contaminated water with the necessary additives to stimulate bacterial growth. For the first issue. the present work suggests that uranium reducers are ubiquitous in nature. The second issue is strictly technical and there are many solutions to this problem.

Though significant progress was made with U bioremediation, demonstration of the technology in the field is necessary to confirm the laboratory results. We conducted a small in situ experiment to test our technology and to study the mixing process, but only for biological denitrification of nitrate-contaminated groundwater at a site in Albuquerque, NM (USA). Nitrate was reduced to nitrogen within 5 days (Abdelouas et al., 1999c).

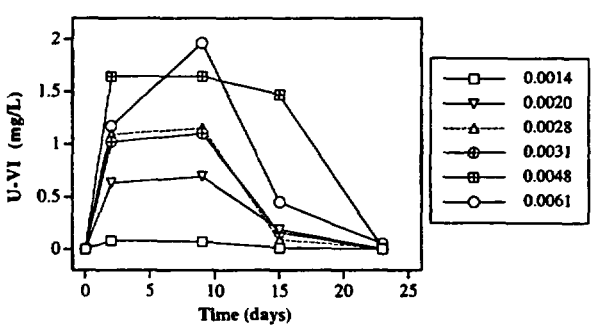

Fig. 8. Uraninite oxidation in oxygen-rich uncontaminated groundwater. Numbers in legend correspond to the uraninite/mackinawite molar ratio.

References

Abdelouas A, Lu Y, Lutze W, Nuttall HE. Reduction of U(IV) to U(IV) by indigenous bacteria in contaminated ground water. J Contam Hydrol 1998a;35:217–233.

Abdelouas A, Lutze W, Nuttall HE. Chemical reactions of uranium in ground water at a mill tailings site. J Contam Hydrol 1998b;34:343–361.

Abdelouas A, Lutze W, Nuttall HE. Oxidative dissolution of uraninite precipitated on Navajo sandstone. J Contam Hydrol 1999a;36:353–375.

Abdelouas A, Lutze W, Nuttall HE. Uranium contamination in the subsurface: characterization and remediation. In: Burns PC, Finch R, editors. Uranium: mineralogy, geochemistry and the environment. Reviews in mineralogy, vol. 38, 1999b:433–473.

Abdelouas A. Deng L, Nuttall HE, Lutze W, Fritz B, Crovisier

JL. In situ biological denitrification of groundwater. C R Acad Sci 1999c;328:161–166.

Bachofen R. Ferloni P, Flynn I. Microorganisms in the subsurface. Microbiol Res 1998;153:1–22.

Barnes CE. Cochran JK. Uranium geochemistry in estuarine sediments: controls on removal and release processes. Geochim Cosmochim Acta 1993;57:555–569.

Barton LL. Choudhury K, Thomson BM, Steenhoudt K, Groffman AR. Bacterial reduction of soluble uranium: the first step of in situ immobilization of uranium. Radioac Waste Manag Environ Restor 1996;20:141–151.

Benner SG. Blowes DW, Ptacek CJ. A full-scale porous reactive wall for prevention of acid mine drainage. Goundwater Monitoring Remediation 1997;17:99–107.

Blanc PL. Acquirements of the natural analogy programme. Oklo natural analogue for a radioactive waste repository. Final Report IPSN/CEA. Fontenay-aux-Roses, France, 1995.

Brookins DG. Eh-pH diagrams for Geochemistry. Berlin: Springer-Verlag, 1988.

Bros R. Turpin L, Gauthier-Lafaye F, Holliger P, Stille P. Occurrence of naturally enriched U-235: Implications for plutonium behaviour in natural environments. Geochim Cosmochim Acta 1993;57:1351–1356.

Cochran JK. Carey AE, Sholkovitz ER, Surprenant LD. The geochemistry of uranium and thorium in coastal marine sediments and sediment pore waters. Geochim Cosmochim Acta 1986:50:663–680.

Deng L. In situ biological denitrification of groundwater. M.S. dissertation, The University of New Mexico, 1998.

Federal Register. Environmental Protection Agency (EPA), CFR 40 Part 192, groundwater standards for remedial actions at inactive uranium processing sites. Table 1, November 1995:2866.

Francis AJ. Dodge CJ, Gillow JB, Cline JE. Microbial transformations of uranium in wastes. Radiochim Acta 1991; 52:311–316.

Francis AJ. Dodge CJ, Lu F, Halada GP, Clayton CR. XPS and XANES studies of uranium reduction by *Colstridium* sp. Eviron Sci Technol 1994;28:636–639.

Ganesh R. Robinson KG. Reed G, Sayler GS. Reduction of hexavalent uranium from organic complexes by sulfate- and iron-reducing bacteria. Appl Environ Microbiol 1997;3: 4385–4391.

Gauthier-Lafaye F, Weber F. The Francevillian (lower proterozoic) uranium ore-deposits of Gabon. Econ Geol 1989:84:2267–2285.

Gauthier-Lafaye F, Weber F, Ohmoto H. Natural fission reactors of Oklo. Econ Geol 1989;84:2286–2295.

Gauthier-Lafaye F, Holliger P, Blanc PL. Natural fission reactors in the Franceville basin, Gabon: a review of the conditions and results of a critical event in a geological system. Geochim Cosmochim Acta 1996;60:4831–4852.

Gauthier-Lafaye F, Blanc PL, Bruno J et al. The last natural nuclear-fission reactor. Nature 1997;387:337.

Ghiorse WC. Subterranean life. Science 1997;275:789–790.

Gorby YA, Lovley DR. Enzymatic uranium precipitation. Eviron Sci Technol 1992;6:205–207.

Hard BC, Friedrich S, Babel W. Bioremediation of acid-mine water using facultatively methylotrophic metal-tolerant sulfate-reducing bacteria. Microbiol Res 1997;152:65–73.

Hodgkinson DP. The NIREX safety assessment research program on near-field effects in cementitious repositories. Radioactive Waste Managem Nuclear Fuel Cycle 1987; 9:272–291.

Hosteler PB, Garrels RM. Transportation and precipitation of uranium and vanadium at low temperatures with special reference to sandstone-type uranium. Econ Geol 1962; 57:137–167.

Janeczek J. Mineralogy and geochemistry of natural fission reactors in Gabon. In: Burns PC, Finch R, editors. Uranium: mineralogy, geochemistry and the environment. Reviews in mineralogy, vol. 38, 1999:312–392.

Jensen ML. Sulfur isotopes and the origin of sandstone-type uranium deposits. Econ Geol 1958;53:598–616.

Kauffman JW, Laughlin WC, Baldwin RA. Microbiological treatment of uranium mine waters. Eviron Sci Technol 1986;20:243–248.

Kimberley MM. Uranium deposits, their mineralogy and origin. Mineral Assoc Canada, Univ. Toronto Press, 1979.

Klinkhammer GP, Palmer MR. Uranium in the oceans: where it goes and why? Geochim Cosmochim Acta 1991;55: 1799–1806.

Langmuir D. Aqueous environmental geochemistry. Prentice-Hall Inc. Upper Saddle River, NJ, 1997.

Langmuir D. Uranium solution-mineral equilibria at low temperatures with applications to sedimentary ore deposits. Geochim Cosmochim Acta 1978;42:547–569.

Lovley DR. Bioremediation of organic and metal contaminants with dissimilatory metal reduction. J Ind Microbiol 1995;14:85–93.

Lovley DR, Phillips EJP. Bioremediation of uranium contamination with enzymatic uranium reduction. Eviron Sci Technol 1992a;26:2228–2234.

Lovley DR, Phillips EJP. Reductiom of uranium by desulfovibrio desulfuricans. Eviron Sci Technol 1992b;58: 850–856.

Lovley DR, Phillips EJP, Gorby YA, Landa ER. Biological reduction of uranium. Nature 1991;350:413–416.

Lovley DR, Roden EE, Phillips EJP, Woodward JC. Enzymatic iron and uranium reduction by sulfate-reducing bacteria. Mar Geol 1993;113:41–53.

Lu Y, Nuttall HE, Lutze W, Abdelouas A. Biological removal of nitrate and uranium from contaminated groundwater. J Hazard Mater 1999:in press.

Lu Y. Sequential bioremediation of nitrate and uranium in contaminated groundwater. Ph.D. dissertation, The University of New Mexico, 1998.

Macaskie LE. The application of biotechnology to the treatment of wastes produced from the nuclear fuel cycle: biodegradation and bioaccumulation as a means of treating radionuclide-contaminated streams. CRC Crit Rev Biotechnol 1991;11:41–112.

Maynard JB. Geochemistry of sedimentary ore deposits. New York: Springer-Verlag, 1983.

Nagy B, Gauthier-Lafaye F, Holliger P et al. Organic-matter and containment of uranium and fissiongenic isotopes at the Oklo natural reactors. Nature 1991;354:472–475.

National Research Council. 1994. Alternatives for ground water cleanup. Washington, DC: National Academy Press. 1994.

Nealson KH, Stahl DA. Microorganisms and biogeochemical cycles: what can we learn from layered microbial communities? In: Banfield JF, Nealson KH, editors. Geomicrobiology: interactions between microbes and minerals. Reviews in Mineralogy, vol. 35, 1997:5–34.

Odom JM, Singleton R. The sulfate-reducing bacteria: contemporary perspectives. New York: Springer-Verlag, 1993.

Parks GA, Pohl DC. Hydrothermal solubility of uraninite. Geochim Cosmochim Acta 1988;52:863–875.

Phillips EJP, Landa ER, Lovley DR. Remediation of uranium contaminated soils with bicarbonate extraction and microbial U(VI) reduction. J Ind Micrbiol 1995;14:203–207.

Pósfai M, Buseck PR, Bazylinski DA, Frankel RB. Reaction sequence of iron sulfide minerals in bacteria and their use as biomarkers. Science 1998;280:880–883.

Quinton GE, Buchanan RJ, Ellis DE, Shoemaker SH. A method to compare groundwater cleanup technologies. Remediation, Autumn 1997:7–16.

Read D, Lawless TA, Sims RJ, Butter CR. Uranium migration through intact sandstone cores. J Contam Hydrol 1993; 13:277–289.

Rich A, Holland HD, Petersen U. Hydrothermal uranium deposits. New York: Elsevier, 1977.

Seelig B, Derickson R, Bergsrud F. Iron and manganese removal. In: Treatment Systems for Houshold Water Supplies series. AG-FO-5940, 1–5. Minnesota Extension Service, University of Minnesota, 1992.

Stumm W, Morgan JJ. Aquatic chemistry. New York: John Wiley & Sons, 1981.

Taylor GH. Biogeochemistry of uranium minerals. In: Trudinger PA, Swaine DJ, editors. Biogeochemical cycling of mineral-forming elements. New York: Elsevier, 1979: 485–514.

Tucker MD, Barton LL, Thomson BM. Kinetic coefficients for simultaneous reduction of sulfate and uranium by desulfovibrio desulfuricans. Appl Microbiol Biotechnol 1996; 46:74–77.

Tucker MD, Barton LL, Thomson BM. Removal of U and Mo from water by immobilized desulfovibrio desulfuricans in column reactors. Biotechnol Bioeng 1998a;60:88–96.

Tucker MD, Barton LL, Thomson BM. Reduction of Cr, Mo, Se and U by desulfovibrio desulfuricans immobilized in polyacrylamide gels. J Ind Microbiol Biotechnol 1998b;20: 13–19.

Turekian KK. The fate of metals in the oceans. Geochim Cosmochim Acta 1977;41:1139–1144.

Uhrie JL, Drever JI, Colberg PJS, Nesbitt CC. In situ immobilization of heavy metals associated with uranium leach mines by bacterial sulfate reduction. Hydrometallurgy 1996;43:231–239.

Wolery TJ. EQ3NR, a computer program for Geochemical aqueous speciation solubility calculations: theoretical manual. User's guide and the related documentation (Version 7.0): UCRL-MA-110662-PT-IV. Lawrence Livermore National Laboratory, Livermore, CA, USA, 1992.

ELSEVIER

Journal of Contaminant Hydrology 34 (1998) 343–361

JOURNAL OF
Contaminant
Hydrology

Chemical reactions of uranium in ground water at a mill tailings site

A. Abdelouas [a,*], W. Lutze [b], E. Nuttall [b]

[a] *University of New Mexico, Center for Radioactive Waste Management, 1001 University Blvd., SE-Suite 201, Albuquerque, NM 87106, USA*

[b] *University of New Mexico, Department of Chemical and Nuclear Engineering, Albuquerque, NM 87131, USA*

Received 3 October 1997; revised 18 June 1998; accepted 18 June 1998

Abstract

We studied soil and ground water samples from the tailings disposal site near Tuba City, AZ, located on Navajo sandstone, in terms of uranium adsorption and precipitation. The uranium concentration is up to 1 mg/l, 20 times the maximum concentration for ground water protection in the United States. The concentration of bicarbonate (HCO_3^-) in the ground water increased from $\leq 7 \times 10^{-4}$ M, the background concentration, to 7×10^{-3} M. Negatively charged uranium carbonate complexes prevail at high carbonate concentrations and uranium is not adsorbed on the negatively charged mineral surfaces. Leaching experiments using contaminated and uncontaminated sandstone and 1 N HCl show that adsorption of uranium from the ground water is negligible. Batch adsorption experiments with the sandstone and ground water at 16°C, the in situ ground water temperature, show that uranium is not adsorbed, in agreement with the results of the leaching experiments. Adsorption of uranium at 16°C is observed when the contaminated ground water is diluted with carbonate-free water. The observed increase in pH from 6.7 to 7.3 after dilution is too small to affect adsorption of uranium on the sandstone. Storage of undiluted ground water to 24°C, the temperature in the laboratory, causes coprecipitation of uranium with aragonite and calcite. Our study provides knowledge of the on-site uranium chemistry that can be used to select the optimum ground water remediation strategy. We discuss our results in terms of ground

* Corresponding author. Advanced Materials Laboratory, Center for Radioactive Waste Management, 1001 University Blvd., SE-Suite 201, Albuquerque, NM 87106, USA. Tel.: +1-505-272-7271; fax: +1-505-272-7304; e-mail: badria@unm.edu

0169-7722/98/$ - see front matter
PII: S0169-7722(98)00097-7

water remediation strategies such as pump and treat, in situ bioremediation, steam injection, and natural flushing.

Keywords: Adsorption; Complexation; Coprecipitation; Ground water; Sandstone; Uranium

1. Introduction

Interest in migration of uranium through geological media increased in the Western United States after numerous sites were identified with elevated concentrations of this element in ground water as a result of past or on-going mining and milling activities. For example, there are 24 sites in the Western United States where uranium ore was processed and where mill tailings were left behind. In 1978, Federal law (UMTRCA, 1978) assigned the U.S. Department of Energy responsibility for remediating these sites.

We analyzed soil and ground water samples from one of these sites, the tailings disposal site near Tuba City, AZ, located on Navajo sandstone. From 1956 to 1966, a uranium ore processing mill operated on this site. Over that decade 800,000 tons of uranium ore were concentrated by means of acid and alkaline leach processes. Mill tailings were deposited in three contiguous piles at the site. Water used in processing was discharged to unlined tailings and evaporation ponds (Anon., 1993, 1994). It is estimated that 1.3×10^6 m^3 of water contaminated with tailings metals migrated into the ground water. Large quantities of sulfate and nitrate are present in the ground water at this site, and the concentration of uranium is up to 20 times the maximum concentration for ground water protection (Federal Register, 1995). Surface remediation was completed in 1990 by stabilizing about 1.4×10^6 m^3 of tailings in an engineered disposal cell covering 50 acres.

Fig. 1 shows the location of wells in the vicinity of the tailings pile and gives analytical data for uranium, sulfate, nitrate, pH, dissolved oxygen (DO), and total dissolved solids (TDS) in the ground water. All wells are screened (12 m) and are located in the same stratigraphic interval. The data indicate the horizontal extension of the plume. The flow direction of the ground water is also indicated. Well #911 is located north of the pile and represents the composition of the uncontaminated ground water. Ground water at the site is a minimum of 12 m below ground surface. A 12-m saturated zone is estimated to be contaminated. The plume of contaminated water spread approximately 500 m downgradient of the disposal. The ground water is moving at a rate of 3 m to 60 m per year. The average plume migration rate is 15 m per year.

The arid climate makes the supply of surface water rare and highly variable and ground water is an important resource in the area. In the immediate vicinity of the site, land use is limited to grazing. No exposure pathway has been identified that could pose a risk to human health or to other life forms, but a pathway could exist, if contaminated ground water were to reach the seep area further downstream, feeding the Monkopi wash whose water is used for irrigation.

The objective of our work is to know whether uranium released from the mill tailings into the ground water is adsorbed on the Navajo sandstone within the contaminated area of 50 acres, precipitated with newly formed minerals, or free to migrate with the ground water. Knowledge of the on-site uranium chemistry is the basis for the selection of a

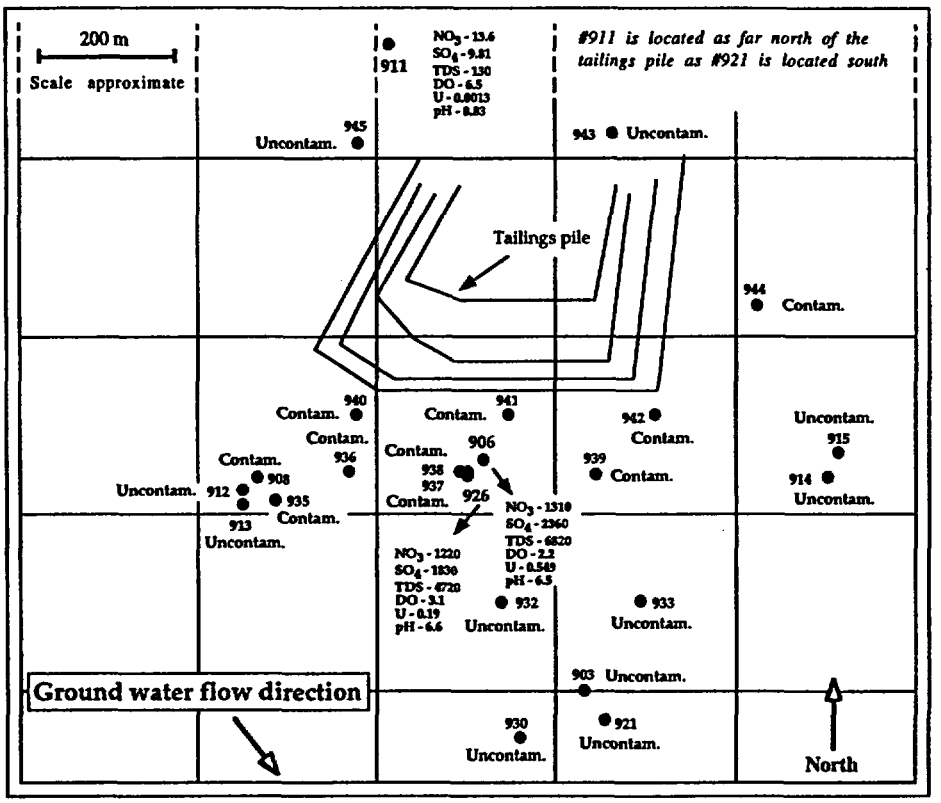

Fig. 1. Concentrations in mg/l of contaminants (nitrate, sulfate, and uranium), dissolved oxygen (DO) and total dissolved solids (TDS) in ground water at Tuba City site. Wells are identified by number; their locations are indicated by black dots.

remediation strategy, such as ex situ (e.g., pump and treat) or in situ (e.g., bioremediation) treatment. To be effective, pump and treat relies on extraction of uranium with the water and on fast desorption kinetics, if contaminants are adsorbed on the host rock. With in situ bioremediation soluble U–VI species are precipitated as insoluble UO_2 (uraninite). In situ bioremediation is less sensitive to adsorption because bacteria are ubiquitous in ground water and in soil and are capable to reduce either soluble or adsorbed contaminants (Abdelouas et al., 1998).

Several studies (Berry et al., 1988; Read et al., 1993; Sims et al., 1996) report high adsorption of uranium on geological material such as sandstone or clays. Uranium speciation in solution depends on pH, e.g., Bond et al. (1991). Carbonate complexes are negatively charged and are known to decrease uranium adsorption (Hsi and Langmuir, 1985; Koß, 1988; Bond et al., 1991; Zielinsky et al., 1995; Duff and Amrhein, 1996; Duff et al., 1997).

Adsorption of uranium on calcite, quartz, and orthoclase was studied by Dran et al. (1988). These authors interpreted the decrease of uranium in solution by precipitation of

insoluble mixed $Ca^{2+} - UO_2^{2+}$ hydrated carbonates on calcite and incorporation into amorphous hydrosilicates on the surface of the silicate minerals.

Read et al. (1993) and Sims et al. (1996) studied uranium migration through sandstone cores. They concluded that aqueous uranium species have a strong affinity for sandstone components such as quartz and iron oxides and hydroxides. These authors interpreted uranium adsorption as a surface complexation process of positively charged uranium species, e.g., UO_2OH^+ and $(UO_2)^{2+}$ on negatively charged surface sites, in particular FeO^-. The carbonate concentration was too low to affect uranium speciation in this study.

We used two methods to study the behavior of uranium in the Navajo sandstone: (1) acid leaching (Clauer et al., 1993) of the sandstone to determine the fractions of uranium present in sandstone before contamination (primary uranium) and of uranium incorporated into sandstone from the mill tailings leachates (secondary uranium); (2) the batch technique (Berry et al., 1988, 1991) to study uranium adsorption kinetics and equilibrium. New uranium bearing mineral phases were studied by electron microscopy, complemented by thermodynamic calculations based on the composition of the contaminated ground water.

2. Characterization of Navajo sandstone and ground water

2.1. Sandstone

The Navajo sandstone is a pure and well sorted eolian quartz sand of Middle Jurassic age and was sampled at the tailings disposal site near Tuba City in northeastern Arizona (USA). A stratigraphic study of the Navajo sandstone was published by Peterson and Pipiringos (1979). Samples were taken from drilled cores in the ground water saturated zone. Two types of sandstone samples were selected for this study: one from the area of highest contamination (well #906, Fig. 1), and one from an uncontaminated area nearby (well #911, Fig. 1). Quartz is the dominant phase. Microcline is present but strongly altered. Clay minerals such as smectite and illite form a coating, ≤ 10 μm thick, on the quartz grains. Scanning electron microscope (SEM) images in conjunction with energy dispersive X-ray (EDX) analyses show occasionally calcium, probably as calcite, enriched in the clay coating. Iron oxide rims are observed on the quartz under the optical microscope, imparting an orange–brown hue. Given the high concentrations of calcium and carbonate in the contaminated ground water (Table 1), calcium carbonate (e.g., aragonite and calcite) could have formed on the sample from well #906, coprecipitating uranium. No differences in the phase composition of the two samples were found.

Atomic absorption and inductively-coupled plasma atomic emission spectrometry (ICP-AES) analyses were used to analyze chemical composition of the sandstone after digestion of the whole rock in nitric acid. Sand samples were crushed, mixed with lithium tetraborate and melted at 1000°C. The resulting glass was totally dissolved in nitric acid for analysis. Uranium was determined by ICP mass spectrometry. The pristine sandstone and that in contact with the contaminated ground water were analyzed for 45

Table 1
Chemical composition of ground water (mg/l)

	Well #906	Well #926	Well #911
U	0.55	0.19	0.0013
Alkalinity ($CaCO_3$)	710	572	66
Ca	784	681	20.5
Mg	354	329	4.31
Na	621	172	10.8
K	9.4	3.0	3.68
Sr	7.89	7.04	0.60
Fe	< 0.03	0.05	< 0.03
NO_3	1310	1220	13.6
SO_4	2360	1830	9.81
PO_4	0.31	< 0.1	< 0.1
Cl	363	88.4	7.12
TDS	6820	4720	130
Temperature (°C)	16.3	16.8	17.2
Dissolved oxygen (mg/l)	2.2	3.1	6.5
pH	6.5	6.6	8.8
U.S. ground water standards (mg/l)*			
U	0.044		
NO_3^-	44		

*Federal Register (1995).

trace elements. Average trace element concentrations were on the order of 1 mg/kg. Table 2 lists the concentrations of the trace elements U and Zr. The presence of a relatively high concentration of Zr may indicate the presence of zircon. Zircon is an accessory mineral in Navajo sandstone (Jennison, 1980; Uygur, 1980). This mineral is a host for primary uranium. Table 2 shows that there is no significant difference in analytical data obtained for the Navajo sandstone samples from the contaminated (well #906) and uncontaminated (well #911) area.

The fraction of Fe presumably present as hematite and oxyhydroxide was determined by selective leaching of the sandstone grains in a mixture of hydroxylamine-hydrochloride and acetic acid and analyzing the leachate. For a variety of samples from the contaminated and uncontaminated area (wells #906, 911, 932, 937, and 940; Fig. 1), the results for Fe_2O_3 ranged between 0.024 and 0.086 weight percent with an average of 0.040 wt.% (Table 3). Samples of the sandstone were heated to 1000°C for 1 h to determine their weight loss.

The uranium concentration in the sandstone was measured in samples from 5 different locations (wells #906, 911, 932, 937, and 940; Fig. 1). The average concentration is 0.47 mg/kg. The concentration of uranium in the two samples from the contaminated well #906 and the uncontaminated well #911 are 0.56 mg/kg and 0.55 mg/kg, respectively. The analytical error of the uranium analyses does not exceed ±10%. Hence, there is no significant variation in the uranium concentration of the

Table 2
Chemical composition of Navajo sandstone after digestion of the rock sample in nitric acid

% Weight	Untreated		Leached with 1 N HCl	
	Well #906	Well #911	Well #906	Well #911
SiO_2	95.7	94.0	98.2	95.6
Al_2O_3	1.3	1.9	1.1	2.4
MgO	0.17	0.22	0.10	0.21
CaO	< 0.2	< 0.2	< 0.2	< 0.2
Fe_2O_3	< 0.1	< 0.1	< 0.1	< 0.1
TiO_2	< 0.02	0.05	0.02	0.09
MnO	0.019	0.007	0.001	0.005
Na_2O	< 0.05	0.06	< 0.05	0.07
K_2O	0.98	1.24	0.66	1.19
P_2O_5	< 0.1	< 0.1	< 0.1	< 0.1
Weight loss at 1000°C for 1 h	0.50	0.66	0.34	0.61
Total	*98.67*	*98.08*	*100.44*	*100.49*
(mg/kg)				
U	0.56	0.55	0.38	0.34
Zr	30	84	19	58

sandstone between locations. Using the value of 0.47 mg/kg of sandstone, we calculated a primary uranium inventory of 3000 kg in the sandstone within the entire contaminated volume of water or plume. The volume of the plume water is about 6×10^5 m^3, based on a measured porosity of the sandstone of 24%. Using an average concentration of 0.5 mg/l, the plume inventory was estimated to be about 300 kg of uranium dissolved in the ground water. Furthermore, Table 3 shows that there is no relationship between the uranium and iron content in the sandstone. Uranium and iron concentrations do not vary significantly from one sample to another, suggesting that the use of sandstone from different wells in adsorption experiments would provide similar results.

2.2. Ground water

Ground water was collected from monitoring wells #906 and 926 (Table 1), located within the plume, and from well #911 (Table 1), located outside the plume. Samples of

Table 3
Concentration of uranium and iron given in mg/kg of sandstone from different wells (see Fig. 1)

Wells # and sandstone color	U	Fe_2O_3
906 (white)	0.56	438
911 (reddish)	0.55	455
932 (white)	0.39	492
937 (white + red spots)	0.45	861
940 (reddish)	0.43	240

Total iron expressed as Fe_2O_3.

contaminated and uncontaminated ground water were analyzed by Core Laboratories. In the field, water was pumped directly into sterilized plastic bottles placed in a nitrogen flushed glove box. The average in situ water temperature was 16°C without significant seasonal variation. The concentration of dissolved oxygen, 2.2 mg/l and 3.1 mg/l for wells #906 and 926, respectively, and 7.0 mg/l (well #911), was measured by lowering a YSI 5739 field probe into the water in the wells after pumping for a while. The pH was measured in the glove box and was 6.5 and 6.6 for wells #906 and 926, respectively, and 8.8 (well #911). In the laboratory, the water was stored at 4°C. During storage the pH of the water did not change. The water in wells #906 and 926 are contaminated with alkaline and alkaline earth metal nitrates and sulfates. The alkalinity, expressed as dissolved $CaCO_3$, is an order of magnitude above background concentration (well #911). The concentration of uranium exceeds U.S. standards for maximum concentrations for ground water protection (Federal Register, 1995). The uranium concentration in the plume is up to a factor of 1000 higher than the background concentration. Dissolved oxygen levels indicate oxidizing conditions; pH values are lower in the plume than in the surrounding water (Fig. 1).

3. Uranium leaching and adsorption experiments

3.1. Uranium leaching

Sandstone samples from the contaminated (well #906) and uncontaminated (well #911) area were investigated in terms of leachable uranium. One gram of dry sandstone sampled in situ was crushed gently in a mortar to minimize generation of fresh surfaces and was then leached, without sieving, for 15 min at room temperature in 50 cm^3 of 1 N HCl. The average size of the crushed sandstone was 100 μm measured by a light scattering Coulter instrument LS230. All experiments were conducted in duplicate. Before leaching, each sample was heated at 110°C to eliminate adsorbed moisture. Following cooling, the samples were held at 24°C for 30 min, then weighed and leached. Leachates and solids were separated by centrifugation at 4000 revolution per minute. Polypropylene centrifuge tubes and caps were used. The residues were washed with deionized water, centrifuged again, and dried at 110°C, followed by observation under the SEM and chemical analysis.

Some of the sandstone samples, 1 g each, from wells #906 and #911 previously leached with 1 N HCl were leached in 20 cm^3 of 0.04 M hydroxylamine hydrochloride in 25% by volume of acetic acid to dissolve and measure the amount of iron presumably present as hematite and oxyhydroxide. Since iron hydroxides and iron oxides are preferred adsorption substrates for uranium (Hsi and Langmuir, 1985; Brown et al., 1991), we analyzed the solution for uranium as well. The experiments were carried out in duplicate for 10 h at 96°C with occasional agitation, following the sequential extraction method described by Tessier et al. (1979). Observations of the leached material under an SEM showed the iron coating to be completely dissolved.

Table 4
Results of uranium adsorption experiments with Navajo sandstone and ground water from well #906 at 16°C

Initial concentration of uranium/mg/l	Final concentration of uranium/mg/l		Rock/water (1 g in 10 cm^3)	R_D/cm^3 g^{-1}	
	Teflon	Glass		Teflon	Glass
Sol. 1: 2.10	2.10	2.1	1:10	0	0
Sol. 2: 0.59	0.58	0.56	1:10	<1	<1
Sol. 3: 0.37	0.37	0.37	1:10	0	0

3.2. Uranium adsorption

Sandstone samples from well #906 were prepared in the same way as for the leaching experiments. One gram of crushed sandstone and 10 cm^3 of solution were used to obtain a water to sandstone mass ratio of 10:1. Ground water from wells #906 and 926 were used. Four solutions from well #906 with different concentrations of uranium (Tables 4 and 5) were prepared by either adding uranium as $UO_2(NO_3)_2$, or by diluting the ground water with deionized water. In order to simulate the effect of natural dilution of contaminated ground water, water samples from well #926 were diluted 2, 5, 7, and 10 times with carbonate-free deionized water before conducting adsorption experiments; the pH was measured before and at the end of these experiments (Table 6). The sandstone/water mixture was equilibrated, waiting for either adsorption or desorption to be complete, as indicated by constant concentration of uranium in solution. Experiments were carried out in triplicate in test tubes shaked at room temperature (24°C) or at 16°C in a Lindberg/Blue M water shaker bath. A blank, containing uranium-rich solution without sandstone, was run in parallel to detect adsorption or precipitation on the walls of the tubes. No control experiments with regard to bacterial growth in the ground water were conducted. The low concentration of organic carbon (3 mg/l) and lack of phosphate make bacterial growth unlikely and insignificant. After equilibration, the uranium concentrations in solution were measured again. Uranium concentrations in the ground water were analyzed by laser florescence, using the commercial Scintrex UA-3 Uranium Analyzer. The detection limit of this instrument is 0.05 μg/l and the precision is ±15% at 1 μg/l and above. Before uranium measurement, fluran, a complexing agent provided by the Scintrex, was added to complex U(VI) to increase light absorption by uranium in its hexavalent state. At the end of the experiments, the sandstone was

Table 5
Results of uranium adsorption experiments with Navajo sandstone and ground water from well #906 at 24°C

Initial concentration of uranium/mg/l	Final concentration of uranium/mg/l	Rock/water (1 g in 10 cm^3)	R_D/cm^3 g^{-1}
Sol. 1: 2.1	1.92	1:10	1
Sol. 2: 0.57	0.39	1:10	5
Sol. 3: 0.31	0.30	1:10	<1
Sol. 4: 0.05	0.012	1:10	32

Table 6
Results of uranium adsorption experiments with Navajo sandstone and ground water from well #926 at 16°C

Initial concentration of uranium/mg/l	Initial pH	Final concentration of uranium/mg/l	Final pH	Rock/water (1 g in 10 cm^3)	R_D/cm^3 g^{-1}
Sol. 1: 0.19	6.6	0.19	6.7	1:10	0
Sol. 1*: 0.19	6.6	0.02	7.4	1:10	85*
Sol. 2: 0.095	7.5	0.089	7.5	1:10	<1
Sol. 3: 0.039	7.5	0.027	7.6	1:10	5
Sol. 4: 0.027	7.5	0.006	7.6	1:10	31
Sol. 5: 0.019	7.6	0.002	7.7	1:10	63

*Experiment conducted at 24°C without sandstone. In this experiment aragonite precipitated on the plastic bottle wall.

studied with a Hitachi S-450 scanning electron microscope equipped with a Tracor TN 2000 X-ray microanalyzer to detect changes of the phase assemblage, e.g., precipitation of carbonates or uranium minerals.

4. Results

4.1. Uranium leaching

The results of the leaching experiments with the sandstone are shown in Table 2, columns 4 and 5. After leaching with 1 N HCl, the uranium concentration in the sandstone was lowered by 32% (well #906) and 38% (well #911), respectively. The difference between 32% and 38% is not significant, taking our experimental errors into account. The leached fraction of uranium is assumed to be bonded on clay minerals, iron oxide, and probably on carbonates. The residual uranium appears to be strongly bonded in other accessory minerals. The results in Table 2 neither give evidence for adsorption of uranium on the sandstone from the contaminated ground water, nor can the contrary be concluded in light of the scattering of uranium concentrations in the sandstone (Section 2) and the errors of the leaching experiments.

Table 2 shows that 0.18 mg/kg (well #906) and 0.21 mg U/kg (well #911) were leached by 1 N HCl from the sandstone. The two solutions with the selectively dissolved iron each contained 0.04 mg U/kg of sandstone. This corresponds to $\approx$ 20% of the overall leachable uranium. The remaining 80% of the leachable uranium are attributed other constituents of the sandstone, mainly clay and carbonates.

4.2. Uranium adsorption

The results of the adsorption experiments in water from well #906 are given in the form of R_D values in Table 4 ($T = 16$°C) and Table 5 ($T = 24$°C). The results of the experiments with water from well #926 are given in Table 6. R_D values are defined as in Berry et al. (1988) as $R_D = V/M \times (C_o - C)/C$, where R_D is the distribution ratio,

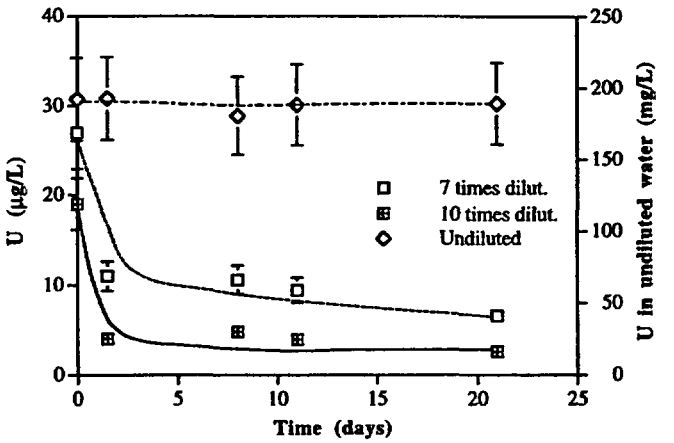

Fig. 2. Uranium adsorption on sandstone from well #926 in diluted ground water at 16°C.

V is the volume of solution, M is the mass of solid, C_0 is the initial and C the equilibrium concentration of uranium.

At 16°C, no change of the initial concentration of uranium was noticed in undiluted water from wells #906 and 926. However, the uranium concentration in the highly diluted water from both wells decreased significantly after only 1 day (Fig. 2). The depletion of uranium can be explained by adsorption on the sandstone. There was no pH change in the experiments with water from well #926 at 16°C.

The results of the experiments with water from well #906 at 24°C are listed in Table 5. These results, in particular those with solution 2, are quite different compared with those at 16°C. At 24°C, uranium concentration decreased with time even in the slightly diluted samples. However, as with ground water from well #926, the ten fold diluted sample shows a high decrease of uranium concentration in solution due presumably to its adsorption on the sand particles.

5. Discussion

5.1. Uranium adsorption and speciation

At 16°C the results obtained using ground waters with different composition (wells #906 and 926) show that uranium is not adsorbed on the Navajo sandstone from the contaminated ground water (Tables 4 and 6), though its uranium concentration is up to 500 times higher than in the uncontaminated ground water. The sandstone has been in contact with the contaminated water for over 30 years. There is also no detectable change in the phase assemblage of the sandstone or in the concentration of 45 trace elements. However, significant adsorption of uranium is observed when the contaminated ground water is diluted seven to ten times (Tables 5 and 6). As shown in Table 6, dilution of ground water from well #926 did not cause a drastic change in pH to

enhance significantly the uranium sorption on the sandstone. In fact Hsi and Langmuir (1985) showed that the maximum adsorption of uranyl on iron oxides and oxyhydroxides occurs between pH = 6 and 7. This suggests that, in our experiments, adsorption depends mainly on carbonate concentration in solution and perhaps on the decrease of ionic strength due to dilution with carbonate-free deionized water.

Hsi and Langmuir (1985), Koß (1988), and Bond et al. (1991) observed decreasing adsorption of uranium on sandstone and iron hydroxides with increasing carbonate concentration in solution. Hsi and Langmuir (1985) studied the adsorption of uranium on amorphous iron-hydroxide, goethite, and hematite. For hematite, the authors showed that an increase of the carbonate concentration in solution from zero to 10^{-3} M decreases the adsorption of uranium substantially.

The leachates from the mill tailings increased the total concentration of bicarbonate (HCO_3^-) in the ground water from $\leq 7 \times 10^{-4}$ M to 7×10^{-3} M. Obviously, adsorption of uranium on the Navajo sandstone is negligible at this high bicarbonate concentration but is significant in the highly diluted ground water. This suggests that uranium is present in solution as negatively charged carbonate complexes. We measured the zeta-potential of the sandstone surface in the ground water and found a value of -12 mV. Hence, the negatively charged uranium species cannot be adsorbed.

Koß (1988) found that the fraction of adsorbed uranium in sandy sediments decreased from nearly 100% to 5% when the concentration of HCO_3^- increased from 0.25×10^{-3} M to 6×10^{-3} M at pH = 7.2 and $T = 20°C$. The initial uranium concentration was $c_i = 0.24$ mg/l (10^{-6} M). We find no adsorption at 7×10^{-3} M HCO_3^- at pH = 6.46, $T = 24°C$ and $c_i \geq 0.57$ mg/l ($\approx 2 \times 10^{-6}$ M).

Bond et al. (1991) showed that an increase in uranium(VI)–carbonato-complex concentrations in solution results in a decrease in R_D; (water:rock ratio of 5:1 and 50:1, $c_i \geq 0.24$ mg/l (10^{-6} M)). These experimental variables are also close to those used in our experiments. Our results in Tables 4 and 6 support the findings of Bond et al. (1991).

We conducted speciation calculations with the composition of the undiluted and diluted ground water from well #906 using the EQ3NR code (Wolery, 1992). The data base used to calculate uranium speciation was taken from Grenthe et al. (1992). Our results are shown in Table 7. According to these calculations, more than 98% of the uranium in the undiluted ground water is complexed as carbonates. The uranium species are: $UO_2(CO_3)_2^{2-}$, $UO_2(CO_3)_3^{4-}$, and UO_2CO_3. The neutral species $UO_2(OH)_2(aq)$ can dissociate and provides positively charged uranium species such as UO_2^{++} and $UO_2(OH)^+$ that can be adsorbed on the negatively charged sandstone surface. However, the concentration of this species (1%) is too low to yield a measurable amount of adsorbed uranium.

In the ten times diluted ground water from wells #906 and 926, the concentration of $UO_2(OH)_2(aq)$ is increased by a factor of 17 and 30 compared to that in the undiluted ground water. Adsorption of the $UO_2(OH)^+$ species on the sandstone leads to further dissociation of the neutral species and to measurable quantities of adsorbed uranium, in agreement with the experimental results (Fig. 2). The figure shows that adsorption is fairly rapid. A final concentration in solution of 2 μg/l is reached within few days at 16°C.

Table 7
Uranium speciation of ground water plume (Well #906) and other solutions

Bicarbonate concentration (M)	pH	Aqueous uranium species (Ground water from well #906) in percent	pH	Aqueous uranium species (Portland cement equilibrated water) in percent
7×10^{-3}	6.46	56.1 $UO_2(CO_3)_2^{--}$ 38.1 $UO_2(CO_3)_3^{----}$ 4.1 $UO_2(CO_3)(aq)$ 1.0 $UO_2(OH)_2$ (aq) (This work)	8.0	89.2 $UO_2(CO_3)_3^{----}$ 10.7 $UO_2(CO_3)_2^{--}$ (Recalculated from the data of Berry et al., 1991)
7×10^{-4}	7.3	52.6 $UO_2(CO_3)_2^{--}$ 31.1 $UO_2(OH)_2(aq)$ 5.0 $UO_2(CO_3)_3^{----}$ 6.5 $(UO_2)_2CO_3(OH)_3^-$ 3.8 $UO_2(CO_3)(aq)$ 0.9 $UO_2(OH)_3^-$ (This work)		
10^{-4}			8.0	71.0 $UO_2(CO_3)_2^{--}$ 9.4 $UO_2(OH)_2(aq)$ 8.9 $UO_2(CO_3)(aq)$ 6.4 $UO_2(CO_3)_3^{----}$ 4.3 UO_2OH^+ (Berry et al., 1991)

Berry et al. (1991) studied adsorption of uranium on sandstone using a bicarbonate concentration of $HCO_3^- = 10^{-4}$ M. Their uranium speciation is shown in Table 7 for pH = 8 as calculated by Bond et al. (1991). The results show that there are $UO_2(OH)_2(aq)$ (9.4%) and $UO_2(OH)^+$ (4.3%) species in solution. $UO_2(OH)_2(aq)$ constitutes the source of positively charged uranium species that explains their high R_D values for uranium. Recalculating Berry et al.'s speciation data for $HCO_3^- = 7 \times 10^{-3}$ M, Table 7 shows that no adsorption of uranium would be expected, because negatively charged uranium carbonate complexes would be dominant in solution. Remaining differences in the uranium speciation when comparing the recalculated data to ours are mainly due to the different pH values.

Read et al. (1993) showed that aqueous uranium species were adsorbed on Clashach sandstone from Elgin district in northeast Scotland, particularly on its iron hydroxide component. The iron hydroxide phase is expected to be the one with the highest adsorption capacity relative to other minor phases. The iron phase in our sandstone contains about 1/4 of the primary uranium. This fraction is the same for sandstone from well #906 (contaminated) and #911 (clean). Unfortunately, Read et al. (1993) do not give values for their carbonate concentrations. Their speciation calculations at pH $\approx$ 5.6 show that there are positively charged uranium species that can be adsorbed, such as UO_2OH^+ and UO_2^{++}. In the ground water from the Tuba City site, these species are practically absent.

5.2. Uranium coprecipitation

The observed decrease in the uranium concentration in the undiluted ground water at 24°C (solutions 1 and 2 in Table 5) may be due to coprecipitation with secondary phases. After completion of the adsorption experiments, we examined the sandstone/solution mixtures for precipitates that might contain uranium. In solutions 1 and 2 (Table 5) a white precipitate was found (Fig. 3). Though, the concentration of the white precipitate was too low to be identified by X-ray diffraction, EDX analyses showed the presence of calcium and, occasionally, sulfur. A precipitate of the same morphology was found in stock solutions from wells #906 and 926 (5 gallons) stored at 24°C (Fig. 4). The precipitate was separated by filtration, dried and weighed. The dry precipitate was analyzed by X-ray diffraction and identified as aragonite and some calcite (Fig. 5). No sulfate-bearing mineral, such as gypsum ($CaSO_4 \times 2H_2O$) was detected. The high salt contents of the water favored the precipitation of aragonite rather than calcite. Aragonite was dissolved in 1 N HCl, the solution was analyzed for uranium and a concentration of 0.4 g/kg of aragonite was found. We conclude that the decrease of uranium concentration in undiluted ground water from wells #906 and 926 during storage at 24°C is due to coprecipitation with aragonite. As expected, ground water stored in the refrigerator (4°C) did not show any precipitates.

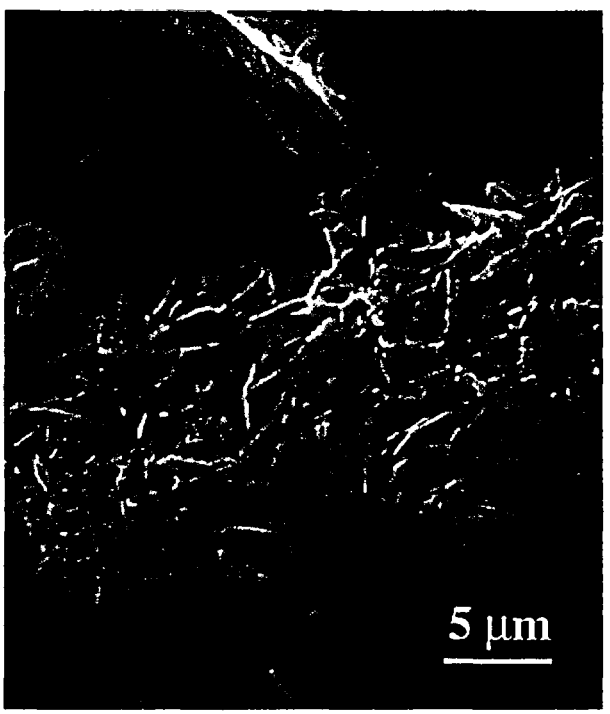

Fig. 3. Aragonite precipitated during uranium adsorption on sandstone from well #906 at 24°C (SEM micrograph).

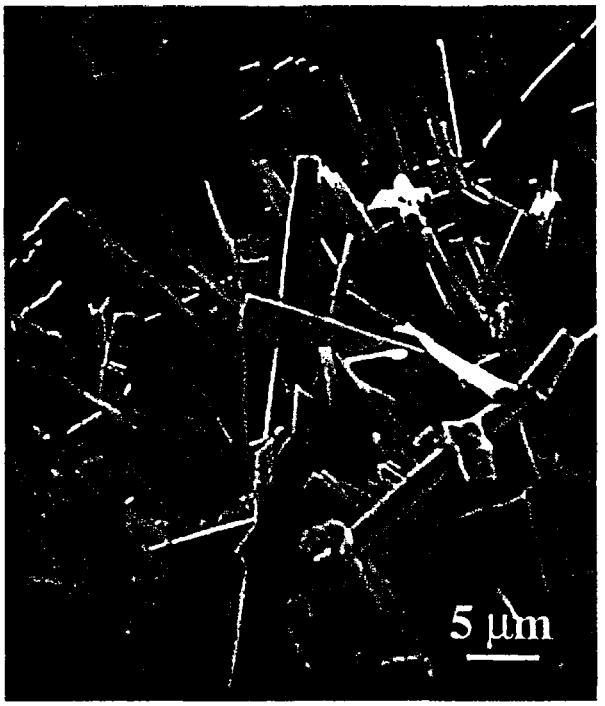

Fig. 4. Aragonite containing 0.4 mg/g uranium, precipitated from well #906 ground water stored at 24°C (SEM micrograph).

Precipitation of aragonite at 24°C occurred because the solubility of aragonite decreases with increasing temperature and pH. We conducted an experiment at 24°C with ground water from well #926 without soil (Table 6). A white precipitate,

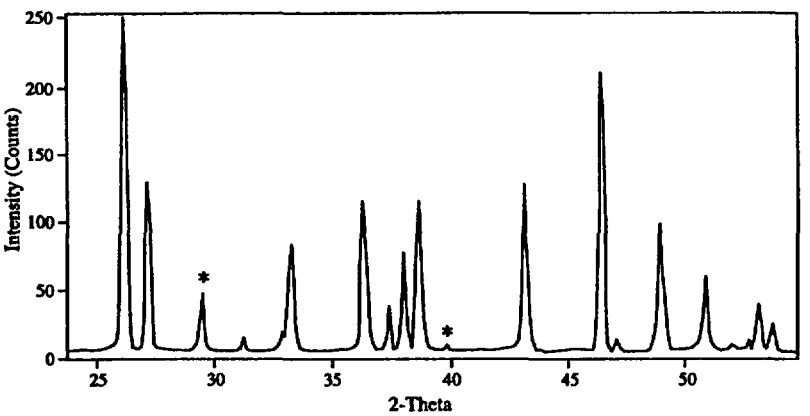

Fig. 5. X-ray diffraction pattern of aragonite shown in Fig. 4. All reflections belong to aragonite except those with (*), which belong to calcite.

Table 8
Saturation index (log Q/K) of solid uranium phases in ground water from well #926 at 24°C

Mineral	log Q/K
β-$UO_2(OH)_2$	−3.3
UO_2CO_3	−4.0
UO_2HPO_4	−6.9
$UO_2HPO_4 \times 4H_2O$	−6.6
α-UO_3	−7.0
β-UO_3	−6.7
γ-UO_3	−6.0
α-$UO_3 \times 0.9H_2O$	−3.4
$UO_3 \times 2H_2O$	−3.2

presumably aragonite, formed on the plastic bottle wall after few days. In this experiment the final uranium concentration was 0.02 mg/l; the final pH = 7.4. The saturation index log Q/K (Q = ion activity product, K = equilibrium constant) of aragonite, calculated with the help of the EQ3NR code, increased from −0.3 at 16°C (pH = 6.6) to 0.7 at 24°C (pH = 7.4), a value high enough to indicate supersaturation of the solution with respect to aragonite. The saturation index of calcite increased from −0.2 at 16°C to 0.8 at 24°C. Calculations of saturation indices for uranium compounds showed that none of the compounds contained in the data base of the code were close to saturation. Phases with calculated log $Q/K > -10$ are listed in Table 8.

Fig. 6 shows that the decrease of calcium concentration in the ground water, which is proportional to the amount of aragonite formed causes increasing removal of uranium from solution. With the measured concentration of 0.4 g/kg of uranium in the aragonite and assuming that all calcium removed from solution precipitates as aragonite, we calculated the amount of uranium precipitated as shown in Fig. 7. As seen, there is qualitative agreement between the calculated and measured values. The measured

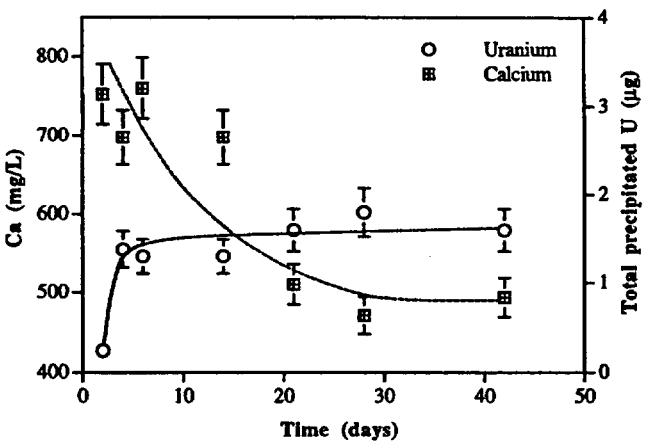

Fig. 6. Calcium concentration in solution and amount of uranium precipitated as a function of time at 24°C. Experiment using solution with 0.57 mg/l U.

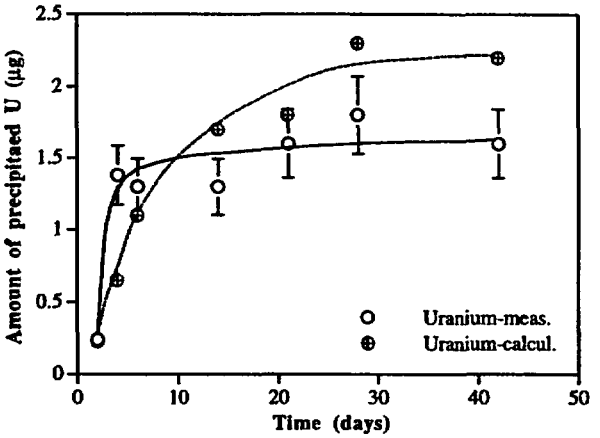

Fig. 7. Amount of precipitated uranium derived from solution concentrations (meas.) at 24°C and from the amount of precipitated calcite containing 0.4 mg/kg of uranium (calcul.). Experiment using solution with 0.57 mg/l U.

amounts of precipitated uranium for the 28 and 42 day experiments are lower than those calculated from the amount of aragonite formed, suggesting that some of the precipitated calcium is sequestered in another phase, e.g., gypsum.

In light of the discussion of coprecipitation we can interpret R_D values reported in Table 5 (well #906) as follow: we find that the same decrease in uranium concentration takes place in solution 1 and 2 (180 µg/l of uranium removed). The R_D values are 1 and 5, respectively. The solutions are undiluted ground water. Here, the R_D values relate to uranium coprecipitated with aragonite. Solution 3 is diluted. No aragonite precipitated. Here the R_D value relates adsorption. Solutions 3 has been diluted by a factor of 2, obviously not enough to yield enough positively charged uranium species to measure an effect. Dilution by a factor of 10 (solution 4) yields a sufficient concentration of positively charged uranium species to measure adsorption ($R_D = 32$ cm^3 g^{-1}). The effect of dilution is further elucidated in Table 6 at 16°C (well #926), showing that adsorption increases with increasing dilution.

Calcium carbonate formation and coprecipitation of uranium have not been considered by other authors. For example, Berry et al. (1991) studied uranium adsorption on sandstone in water equilibrated with Portland cement. Using the authors' data, we

Table 9
Saturation index (log Q/K) of the ground water (well #926) for calcite compared to data from the literature

	Initial pH	Final pH	T (°C)	log Q/K calcite	Saturation	log Q/K aragonite	Saturation
This work	6.6	6.7	16	−0.2	Saturated	−0.3	Not Saturated
This work	6.6	7.4	24	+0.8	Supersaturated	+0.7	Supersaturated
Berry et al. (1991)	9.0	n.r.	20	+0.5	Supersaturated	+0.3	Supersaturated
Koß (1988)	7.2	n.r.	20	0	Saturated	−0.2	Saturated

calculated a saturation index of 0.3 for aragonite and 0.5 for calcite for his experiments at pH = 9. The solution was also supersaturated with respect $CaUO_4$ (log $Q/K = 2.9$). Koß (1988) studied uranium adsorption on sandstone from Gorleben in Northern Germany where a repository for radioactive waste is being constructed. Calcium carbonate and other uranium-bearing minerals were not mentioned. Our calculations with his data yielded a saturation index for aragonite of -0.2 and 0 for calcite (Table 9).

5.3. Practical aspects

The effect of dilution on uranium speciation and of temperature on aragonite formation can be used to evaluate remediation strategies. Ex situ remediation by pumping the contaminated ground water to the surface to remove uranium would be accompanied by dilution in situ with uncontaminated ground water. The result would be that uranium adsorption on the sandstone increases, leaving a fraction of uranium in the ground. This fraction is difficult to quantify.

Storage of ground water on the surface prior to uranium removal, especially in the hot summers with temperatures up to 40°C, can result in the formation of a radioactive precipitate, aragonite/calcite, that may require special treatment.

In situ technologies, such as in situ bioremediation, where water is pumped and immediately reinjected together with organic nutrients to stimulate bacterial activity, do not cause dilution or temperature changes. Uranium in carbonate complexes can be reduced quickly (Phillips et al., 1995; Abdelouas et al., 1998).

Some strategies (Technology Catalogue, 1995) suggest injection of steam as part of the remediation process. In situ heating of the ground water at Tuba City with steam would lead to precipitation of aragonite and perhaps to sufficient removal of uranium from the ground water. In fact, the adsorption experiment using ground water from well #926 at 24°C shows that precipitation of aragonite/calcite reduced significantly the uranium concentration from 0.19 mg/l to 0.02 mg/l within 40 days (Table 6). A concentration of 0.02 mg/l is 2 times below the maximum concentration for ground water protection in the U.S.

Natural flushing is a very slow process at Tuba City and appears to be incompatible with legal requirements, if suggested as a remediation strategy. However, the result of natural flushing would be that most of the uranium in the plume, an estimated 300 kg, will eventually be adsorbed on the sandstone. The carbonate concentration would decrease by one order of magnitude to the natural background. These are the conditions of the experiment with diluted ground water from well #926 conducted at the in situ temperature of 16°C. Adsorption would yield depletion of uranium in the water to about 2 μg/l, which is one order of magnitude below the maximum concentration for ground water protection in the U.S. and close enough to the background concentration of 1.4 μg/l, leaving most of the uranium in the ground.

6. Conclusions

Adsorption and/or coprecipitation of uranium on sandstone is strongly affected by composition, temperature, and pH of the aqueous phase. In order to generate a data base

applicable to a specific site, experiments must be conducted with ground water from the site and at the in situ water temperature. We have shown that conditions may prevail on site where adsorption of uranium on sandstone is negligible whereas in the laboratory artifacts are produced, such as calcium carbonate precipitation, that can lead to ambiguous interpretations of uranium adsorption data.

Understanding the effects of the contaminants from uranium mill tailings on the speciation of uranium in the ground water can help to select the optimum remediation strategy. Ex situ technologies will affect the speciation and may increase the temperature of the ground water. This may lead to adsorption of uranium on the Navajo sandstone and to coprecipitation of uranium with calcium carbonate. If this is undesirable, in situ technologies, such as in situ bioremediation, may be preferable because temperature effects and changes in the uranium speciation can be avoided.

Acknowledgements

The authors are grateful to R. Rouault and J. Samuel for chemical analyses of our sandstone samples at Centre de Géochimie de la Surface, CNRS, and to Dr. J.-L. Crovisier (Strasbourg, France) for facilitating the process. We also thank Dr. K. Semhi for providing information on the leaching experiments.

References

Abdelouas, A., Yongming, L., Nuttall, E., Lutze, W., 1998. Reduction of U(VI) to U(IV) by indigenous bacteria in contaminated ground water. J. Contam. Hydrol., in press.

Anon., 1993. Programmatic Environmental Impact Statement for the Uranium Mill Tailings Remedial Action Water Project, DOE/EIS-0198, Oct. 1993.

Anon., 1994. Site Observational Work Plan for the UMTRA Project at Tuba City, AZ, DOE/AL/62350-160.

Berry, J.A., Bond, K.A., Ferguson, D.R., Pilkington, N.J., 1991. Experimental studies of the effects of organic materials on the sorption of uranium and plutonium. Radiochim. Acta 52/53, 201–209.

Berry, J.A., Bourke, P.J., Coates, H.A., Green, A., Jefferies, N.L., Littleboy, A.K., Hooper, A.J., 1988. Sorption of radionuclides on sandstones and mudstones. Radiochim. Acta 44/45, 135–144.

Bond, K.A., Cross, J.E., Ewart, F.T., 1991. Thermodynamic modelling of the effect of organic complexants on sorption behaviour. Radiochim. Acta 52/53, 433–437.

Brown, P.L., Haworth, A., Sharland, S.M., Tweed, C.J., 1991. Modelling studies of the sorption of radionuclides in the far field of a nuclear waste repository. Radiochim. Acta 52/53, 439–443.

Clauer, N., Chaudhuri, S., Kralik, M., Bonnot-Courtois, C., 1993. Effects of experimental leaching on Rb–Sr and K–Ar isotopic systems and REE contents of diagenetic illite. Chem. Geol. 103, 1–16.

Dran, J.C., Della Mea, G., Paccagnella, A., Petit, J.C., Menager, M.T., 1988. Sorption of actinides analogues on granite minerals studied by MeV ion beam techniques. Radiochim. Acta 44/45, 299–304.

Duff, M.C., Amrhein, C., 1996. Uranium(VI) adsorption on goethite and soil in carbonate solutions. Soil Sci. Soc. Am. J. 60, 1393–1400.

Duff, M.C., Amrhein, C., Bertsch, P.M., Hunter, D.B., 1997. The chemistry of uranium in evaporation pond sediment in the San Joaquim Valley, CA, USA, using X-ray fluorescence and XANES techniques. Geochim. Cosmochim. Acta 61, 73–81.

Federal Register, 1995. Environmental Protection Agency (EPA), CFR 40 Part 192, Groundwater Standards for Remedial Actions at Inactive Uranium Processing Sites, Table 1, November, 1995, p. 2866.

Grenthe, I., Fuger, J., Lemire, R.J., Muller, A.B., Nguyen-Trung, C., Wanner, H. (Eds.), 1992. Chemical Thermodynamics of Uranium. Elsevier, New York.

Hsi, C.-K.D., Langmuir, D., 1985. Adsorption of uranyl onto ferric oxyhydroxides: application of the surface complexation site-binding model. Geochim. Cosmochim. Acta 49, 1931–1941.

Jennison, M.J., 1980. Zircon Ages and Feldspar Mineralogy of the Navajo Sandstone. Master's Thesis, University of Utah, Salt Lake City, UT.

Koß, V., 1988. Modeling of uranium(VI) sorption and speciation in a natural sediment-groundwater system. Radiochim. Acta 44/45, 403–406.

Peterson, F., Pipiringos, G.N., 1979. Stratigraphic relations of the Navajo Sandstone to middle Jurassic formations, Southern Utah and Northern Arizona. U.S. Geol. Survey Prof. Paper 1035-B, 43 pp.

Phillips, E.J.P., Landa, E.R., Lovley, D.R., 1995. Remediation of uranium contaminated soils with bicarbonate extraction and microbial U(VI) reduction. J. Indust. Microbiol. 14, 203–207.

Read, D., Lawless, T.A., Sims, R.J., Butter, K.R., 1993. Uranium migration through intact sandstone cores. J. Contam. Hydrol. 13, 277–289.

Sims, R., Lawless, T.A., Alexander, J.L., Bennett, D.G., Read, D., 1996. Uranium migration through intact sandstone: effect of pollutant concentration and the reversibility of uptake. J. Contam. Hydrol. 21, 215–228.

Technology Catalogue, 1995. US Department of Energy, Office of Environmental Management, Office of Technology Development, DOE/EM-0235, April 1995.

Tessier, A., Campbell, P.G.C., Bisson, M., 1979. Sequential extraction procedure for the speciation of particulate trace metals. Anal. Chem. 51 (7), 844–851.

UMTRCA, 1978. Uranium Mill tailings Radiation Control Act, enacted by American Congress on November 8, 1978, Public Law 95-604.

Wolery, T.J., 1992. EQ3NR, A computer program for geochemical aqueous speciation-solubility calculations: Theoretical Manual, User's Guide and Related Documentation (version 7.0): UCRL-MA-110662-PT-IV, Lawrence Livermore National Laboratory, Livermore, CA.

Uygur, K., 1980. Hydraulic and petrographic characteristics of the Navajo Sandstone in southern Utah. Master's Thesis, Univ. of Utah, Salt Lake City, UT.

Zielinsky, R.A., Asher-Bolinder, S., Meir, A.L., 1995. Uraniferous waters of the Arkansas River Valley, CO, USA: a function of geology and land use. Appl. Geochem. 10, 133–144.

ELSEVIER

Journal of Contaminant Hydrology 36 (1999) 353–375

JOURNAL OF
Contaminant
Hydrology

Oxidative dissolution of uraninite precipitated on Navajo sandstone

A. Abdelouas [a,*], W. Lutze [b], H.E. Nuttall [b]

[a] *Advanced Materials Laboratory, Center for Radioactive Waste Management, University of New Mexico, 1001 University Blvd., SE-Suite 201, Albuquerque, NM 87106, USA*

[b] *Department of Chemical and Nuclear Engineering, University of New Mexico, Albuquerque, NM 87131, USA*

Received 9 December 1997; revised 7 October 1998; accepted 23 October 1998

Abstract

Column and batch experiments were conducted with sandstone and ground water samples to investigate oxidation of uraninite precipitated by microbially mediated reduction of U(VI), a contaminant in ground water beneath a uranium mill tailings site near Tuba City, AZ, USA. Uraninite precipitated together with mackinawite ($FeS_{0.9}$) because Fe(III) from the sandstone and sulfate, another contaminant in the water were reduced together with U(VI). After completion of U(VI) reduction, experiments were conducted to find out whether uraninite is protected by mackinawite against reoxidation. Uncontaminated ground water from the same site, containing 7 mg/l of dissolved oxygen, was passed through the columns or mixed with sandstone in batch experiments. The results showed that small masses of uraninite, 0.1 μg/g of sandstone, are protected by mackinawite from reoxidation. Uraninite masses on the order of 0.1 μg/g correspond to U(VI) concentrations of 0.5 mg/l, typically encountered in uranium contaminated ground waters. Mackinawite is an effective buffer and is formed in sufficient quantity to provide long-term protection of uraninite. Uranium concentrations in ground water passed through the columns are too low (4 μg/l) to distinguish between dissolution and oxidative dissolution of uraninite. However, batch experiments showed that uraninite oxidation takes place.

Keywords: Uraninite; Uranium; In situ bioremediation; Ground water; Mackinawite; Navajo sandstone; Redox buffer

* Corresponding author. Tel.: +1-505-272-7271; fax: +1-505-272-7304; e-mail: badria@unm.edu

0169-7722/99/$ - see front matter
PII: S0169-7722(98)00151-X

1. Introduction

In 1991, Lovley et al. reported that microorganisms such as *Shewanella putrefaciens* catalyze the reduction of U(VI) to U(IV). The observation was confirmed and further researched by various authors (Francis et al., 1991, 1994; Lovley et al., 1991, 1993; Gorby and Lovley, 1992; Lovley and Phillips, 1992a,b; Barnes and Cochran, 1993; Lovley, 1995; Phillips et al., 1995; Barton et al., 1996; Tucker et al., 1996; Nuttall et al., 1997; Abdelouas et al., 1998a).

Though application of U(VI) reduction to remove uranium from contaminated ground water had been suggested previously (e.g., Tucker et al., 1996), Abdelouas et al. (1998a) were the first to investigate this possibility in more detail. We conducted respective experiments in the laboratory with ground water and Navajo sandstone (host rock) from a uranium mill tailings site at Tuba City, AZ. The ground water was contaminated with uranium, nitrate, and sulfate. After amending water samples with ethanol and sodium trimetaphosphate, nitrate reduction to nitrogen gas was mediated by *Pseudomonas aeruginosa* and *P. stutzeri*. U(VI) was reduced to U(IV) and SO_4^{2-} to S^{2-} with the help of *S. putrefaciens*. U(IV) precipitated as uraninite (UO_2). The uranium concentration decreased from 250 μg/l to 0.1 μg/l. The ground water protection standard in the United States is 44 μg/l (Federal Register, 1995). Fe(III) from the sandstone was also reduced and iron sulfide (mackinawite) precipitated. All reduction reactions were mediated by indigenous bacteria (Abdelouas et al., 1998a).

Our results suggested that ground water could be decontaminated with respect to uranium, using in situ reduction of U(VI) to U(IV). Quinton et al. (1997) conducted comparative cost estimates for various ground water remediation technologies and showed that in situ methods are economically most attractive and more compatible with the environment than others.

We designed a technology for implementation at Tuba City (Nuttall et al., 1996; Abdelouas et al., 1998b). A schematic sketch is shown in Fig. 1. Water would be

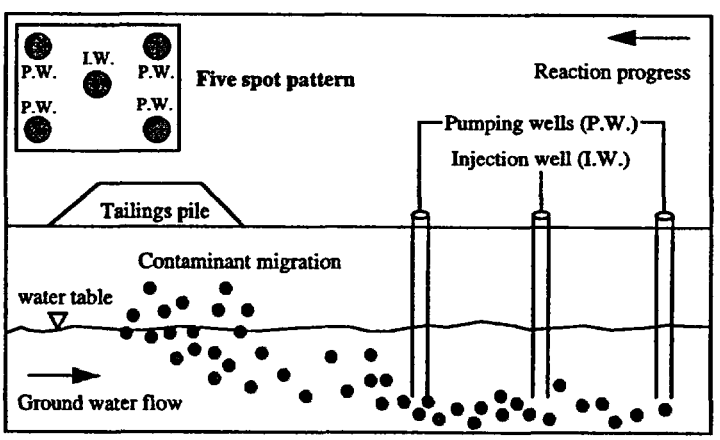

Fig. 1. Five spot pattern for in situ biological remediation.

pumped from peripheral wells, amended with nutrients for indigenous bacteria and injected in a center well. Pumping would be continued until nutrients are detected in the peripheral wells. The well configuration can be repeated, covering the entire area of the plume from the forefront to the source.

A remediation process that relies on in situ immobilization of uranium by reduction and precipitation would only work if the rates of oxidation and dissolution of the precipitate are slow enough to assure long-term stability of uraninite. Reoxidation need not to be avoided completely, but must be slow enough to maintain uranium concentrations in the ground water between the natural background ($\approx$ 1 μg/l at Tuba City) and the ground water protection standard of 44 μg/l. In the field, ground water is flowing and the remediated water will be replaced by oxygenated ground water. It is well known that uraninite can be oxidized fairly readily under oxic conditions (Finch and Ewing, 1992; Isobe et al., 1992; Yanase et al., 1995).

The objective of this study is to investigate the stability of uraninite precipitated by indigenous bacteria when the precipitate comes into contact with naturally oxygenated ground water from the Tuba City area.

2. Summary of previous work

Work reported here is a continuation of research and results published earlier. Therefore, we give a brief summary of the characteristics of the ground water and the host rock (Navajo sandstone) used and results on which the present work is based. More details on experimental procedures and results can be found in two previous papers (Abdelouas et al., 1998a,c).

2.1. Ground water

Contaminated ground water was collected from wells No. 926, located within the plume, and No. 948 located outside the plume (Table 1) at the Tuba City mill tailings site. The water was pumped into sterilized plastic bottles placed in a nitrogen flushed glove box. The average water temperature in situ is 16°C. In the laboratory, the water was stored at 4°C. All experiments with the water were performed at 16°C and/or 24°C.

The concentration of dissolved oxygen in situ was 7 mg/l in the uncontaminated and 3.1 mg/l in the contaminated water. The pH was 6.6 in well No. 926 and 7.7 in well No. 948. As a result of alkaline leaching of the ore, HCO_3^- seeped into the ground water and increased its concentration to $HCO_3^- = 7 \times 10^{-3}$ M, a factor of 10 above natural background. The uranium concentration in the plume is up to a factor of 10^3 higher than the background concentration ($\approx$ 1 μg/l).

2.1.1. Uranium speciation and adsorption

Detailed results on uranium adsorption have been published by Abdelouas et al. (1998c). Batch experiments using crushed sandstone and contaminated ground water (weight ratio 1:10) at 16°C showed that uranium is not adsorbed on the sandstone particles. Thermodynamic calculations using the EQ3NR code (Wolery, 1992) showed

Table 1
Chemical composition of the groundwater (mg/l)

	Contaminated mg/l (well 926)	Uncontaminated mg/l (well 948)
U (μg/l)	250	1.4
Ca	681	28.2
NO_3	1220	11.85
SO_4	1830	9.56
Cl	88.4	6.9
Na	172	14
K	3.0	1.8
Sr	7.04	0.65
TOC	4.0	5.0
Alkalinity ($CaCO_3$)	572	88
Temperature (°C) (in situ)	16.8	17.1
Dissolved oxygen (in situ)	3.1	7.0
pH (in glove box)	6.6	7.7
TDS	4720	130
U.S. ground water protection standards[a]		
U	44 μg/l	
NO_3	44 mg/l	

[a]Federal Register, 1995.

that 94% of the uranium is complexed as $UO_2(CO_3)_2^{2-}$ and $UO_2(CO_3)_3^{4-}$. The zeta-potential of the sandstone surface in the ground water was −12 mV. Uranium from the tailings is in solution and readily accessible by bacteria.

2.1.2. Uranium coprecipitation

An increase of ground water temperature from 16°C to 24°C, the temperature in the laboratory, led to slow formation of aragonite ($CaCO_3$). Uranium coprecipitated with aragonite (0.4 gU/kg aragonite). The uranium concentration in the ground water decreased by 40% within six months. This is an important result to the extent that calcium carbonate may precipitate during the biochemical reactions when organic compounds are oxidized to CO_2 (Abdelouas et al., 1998c).

2.2. Sandstone

2.2.1. Description

Host rock, Navajo sandstone, was also collected on site. The porosity ranges between 24% and 28%. Sandstone mineralogy is dominated by quartz, with some microcline often heavily corroded to clays. Quartz is coated with a layer of clays and iron oxides, presumably hematite and iron oxyhydroxides. Clays consist of a mixture of illite and smectite with potassium as the interlayer cation.

2.2.2. Adsorption of uranium

The average concentration of uranium in five sandstone samples from inside and outside the contaminated area was determined to be 0.47 mg/kg. It is well known that

iron oxides and oxyhydoxides can adsorb uranium species (Hsi and Langmuir, 1985; Sato et al., 1997). As iron oxides are present in the sandstone, uranium could have been adsorbed or coprecipitated when the contamination of the ground water took place. Sandstone samples from inside and outside the contaminated area were leached in a mixture of hydroxylamine-hydrochloride and acetic acid to dissolve the iron selectively. The leachates were analyzed for iron and uranium. The Fe content in five sandstone samples was calculated from the analytical data and ranged between 168 mg/kg and 602 mg/kg with an average of 348 mg/kg. The respective uranium content was about 0.04 mg/kg independent of location. Leaching sandstone samples from the same sources in 1 N HCl yielded an average uranium content of 0.2 mg/kg for all samples because other uranium sources such as clay and carbonates were leached. The remaining uranium is believed to be associated with minerals insoluble in HCl, e.g., zircon. None of the measured data showed significant differences between contaminated and uncontaminated samples. We concluded that adsorption of uranium on the sandstone is insignificant (Abdelouas et al., 1998c).

2.3. Microbially mediated uranium reduction

After amendment of the ground water with ethanol and trimetaphosphate dissolved oxygen and nitrate were reduced, catalyzed by the indigenous bacteria *P. aeruginosa* and *P. stutzeri*. The chemical reactions were accompanied by consumption of H^+ and the pH increased to pH = 8, Eq. (1):

$$12NO_3^- + 5C_2H_5OH + 2H^+ \rightarrow 6N_2 + 10HCO_3^- + 11H_2O \quad (1)$$

Some aragonite precipitated. During denitrification the U(VI) concentration decreased by about 50% due to coprecipitation with aragonite and adsorption on biomass (Nuttall et al., 1996). The concentration of cells was on the order of 10^8 to 10^9 cells/ml. The redox potential decreased to $-70\ \text{mV} < E_H < -100\ \text{mV}$. Once anoxic conditions were established, U(VI), Fe(III) and SO_4^{2-} were reduced simultaneously, catalyzed by *S. putrefaciens*. U(VI) reduction is shown by Eq. (2):

$$6UO_2(CO_3)_2^{2-} + C_2H_5OH + 5H_2O \rightarrow 6UO_2(S) + 14HCO_3^- + 2H^+ \quad (2)$$

3. Experimental work

In this study we conducted column and batch experiments with Navajo sandstone, contaminated and uncontaminated ground water at 16°C and 24°C. All samples contained the indigenous bacteria *P. aeruginosa* and *P. stutzeri* and *S. putrefaciens*. Whenever oxygen contamination of the experimental system (columns or serum bottles) had to be excluded, the respective manipulations were conducted in an argon flushed glove box, maintaining a slight overpressure inside.

3.1. Column experiments

Plexiglas tubes, 5 cm wide, 20 cm long, were used to construct columns. Sandstone was packed in the columns following a procedure described by Siegel et al. (1994) to ensure homogeneous packing. The sand was washed in hydrogen peroxide following a procedure by Kunze and Dixon (1989) to remove relic organic matter. End plates with feed through were tied to the Plexiglas tubes. Long stainless steel screws and bolts, outside the columns, connected the two endplates holding them in place. An example of a column experiment is given in Fig. 2. The column was washed with 10 pore volumes of deoxygenated, deionized water. Then three pore volumes of amended ground water were passed through the column to ensure that only ground water remained in the column. Three columns were prepared for this study: two with a low and one with a high uranium inventory. Data for the columns are given in Table 2. Uranium reduction was effected as described in Section 2.3. It was known from previous work that the experiments would take several weeks for the uranium concentration to decrease to 1 μg/l. Therefore, the column was sampled only once or twice to confirm completion of the reaction. With the help of a syringe a few milliliters of water were extracted through a seal and analyzed.

After uranium reduction the liquid in the column was replaced by uncontaminated, naturally oxygenated ground water from the site. The oxygen concentration was 7 mg/l. Replacement took place at a flow rate of 7 ml/h in column 1 and 100 ml/h in columns 2 and 3. U(VI), SO_4^{2-}, and NO_3^- concentrations were measured in the water leaving the

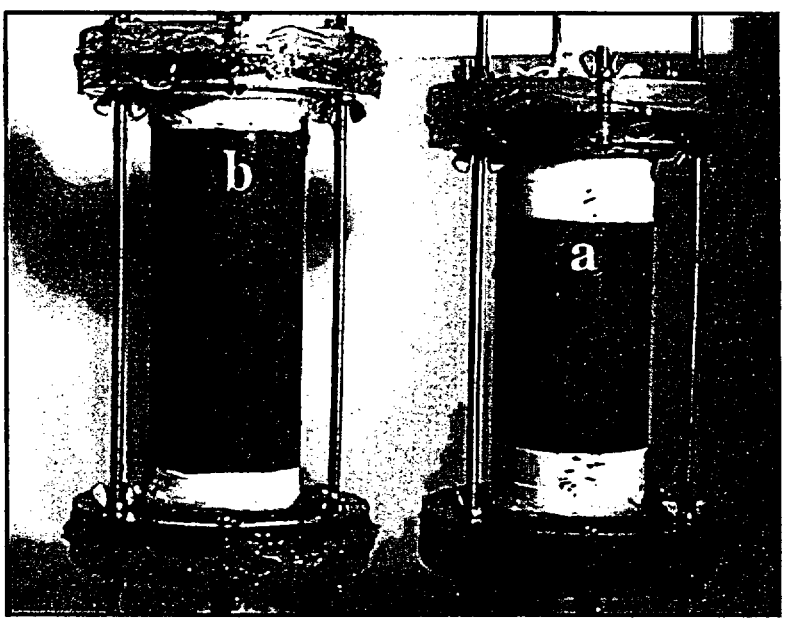

Fig. 2. Sandstone column before (a) and after (b) reduction of U(VI); black spots are iron sulfide (mackinawite).

Table 2
Data for experiments with sandstone columns

Column no.	Leaching flow rate (ml/h)	Pore volume (ml)	Amount of bioprecipitated U (mg)	Fraction of U leached and detached
1	7	129	0.026	0.18
2	100	129	0.026	0.24
3	100	180	43	0.43

column. A total of 35 pore volumes of water were pumped through column 1 and 15 pore volumes through columns 2 and 3.

3.2. Batch experiments

Batch experiments were conducted to quantify the consumption of oxygen introduced with the uncontaminated ground water. The mass of oxygen supplied to 1 g of sandstone was varied between $0.7 \cdot 10^{-2}$ and $5.8 \cdot 10^{-2}$ mmole (Table 3). In the column experiments the ground water to sandstone ratio was 0.15 by mass, assuming a porosity of 30% and a density of the sandstone of 2.1 g/cm^3. Ground water (0.15 ml) with a concentration of dissolved oxygen of 7 mg/l in contact with 1 g of sandstone contains $6.5 \cdot 10^{-5}$ mmole of oxygen. Therefore, the oxygen supplied to 1 g of sandstone was 108 to 880 times larger than in the column experiments, based on the supply of one pore volume of uncontaminated ground water.

In the course of the uranium reduction experiment (see Section 2.3), the color of the sand changed from red to black from the precipitation of uraninite and iron sulfide. The sandstone was separated from the solution under anoxic conditions. The sandstone was then oxidized in sterilized serum bottles. After introducing uncontaminated ground water the bottles were sealed with a butyl rubber stopper in an aseptic environment and crimped with an aluminum seal. A mass of 1 g of sand and various volumes (16, 33, 66, and 132 ml) of water were used in the oxidation experiments. By using different volumes of water, the same mass of sand was exposed to different masses of oxygen. Data for the batch experiments are given in Table 3. In some experiments, deionized water was added to the sand to determine whether carbonate has an effect on the rate and the quantity of uraninite dissolved. As seen in Table 1, the uncontaminated ground water contains less carbonate than the contaminated water. Uraninite oxidation was monitored by sampling the bottles using a sterilized 3 ml syringe and analyzing for U(VI) after filtration. SO_4^{2-} and NO_3^- were also measured.

Some batch experiment were conducted with contaminated ground water but without sandstone (Table 1), to produce freshly precipitated uraninite and iron sulfide and its oxidation products for crystal structure analysis by electron diffraction. Uranyl nitrate was added to increase the U(VI) concentration by a factor of 10^3 to 250 mg/l to obtain enough uraninite for further experimentation. Ferrous sulfate was added to produce an Fe(II) concentration of 500 mg/l. After denitrification, reduction of uranium was enhanced by adding *S. putrefaciens* to the solution. After completion of the experiment,

Table 3
Data for batch experiments (1 g of sandstone was used in each experiment)

Volume of solution (ml)	Dissolved oxygen (mmole)	Dissolved carbonate (mmole)	Mass of uranium per gram of sand (small mass of UO_2) (mmole)	Mass of uranium per gram of sand (large mass of UO_2) (mmole)
132	$5.8 \cdot 10^{-2}$	$1.2 \cdot 10^{-1}$	$1.3 \cdot 10^{-5}$	$1.2 \cdot 10^{-2}$
66	$2.9 \cdot 10^{-2}$	$5.8 \cdot 10^{-2}$	–	$1.2 \cdot 10^{-2}$
33	$1.4 \cdot 10^{-2}$	$2.9 \cdot 10^{-2}$	$1.3 \cdot 10^{-5}$	$1.2 \cdot 10^{-2}$
16	$0.7 \cdot 10^{-2}$	$1.4 \cdot 10^{-2}$	$1.3 \cdot 10^{-5}$	$1.2 \cdot 10^{-2}$
132 DI water[a]	$5.8 \cdot 10^{-2}$	–	$1.3 \cdot 10^{-5}$	$1.2 \cdot 10^{-2}$

[a] DI = deionized water.

the black precipitate sampled and placed into a transmission electron microscope within a few minutes to minimize access of oxygen to the sample.

3.3. Analytical procedures

Analyses of uraninite and iron sulfide were conducted with the help of a JEM-2000FX transmission electron microscope (TEM) and a Noran TN-5500 EDX element analyzer. The microscope was operated at 200 keV.

Prior to analysis, all solutions were filtered through a Nylon Acrodisc syringe filter (0.2 μm pore size; Gelman Science). A Scintrex UA-3 uranium analyzer was used to measure U(VI) in solution. This laser-induced fluorescence instrument allows the detection of uranium concentrations as low as 0.5 μg/l with a precision of ±15% at 1 μg/l. Sulfate and nitrate were measured by ion chromatography (IC Dionex DX 500) with an estimated error of ±5%. The detection limit was 0.1 mg/l.

4. Results and discussion

4.1. Identification of uraninite and mackinawite

The dark precipitate recovered after 90 days from the batch experiment with an initial uranium concentration of 250 mg/l is shown Fig. 3 together with its electron diffraction pattern. The pattern matches that of uraninite and shows that the precipitate is poorly

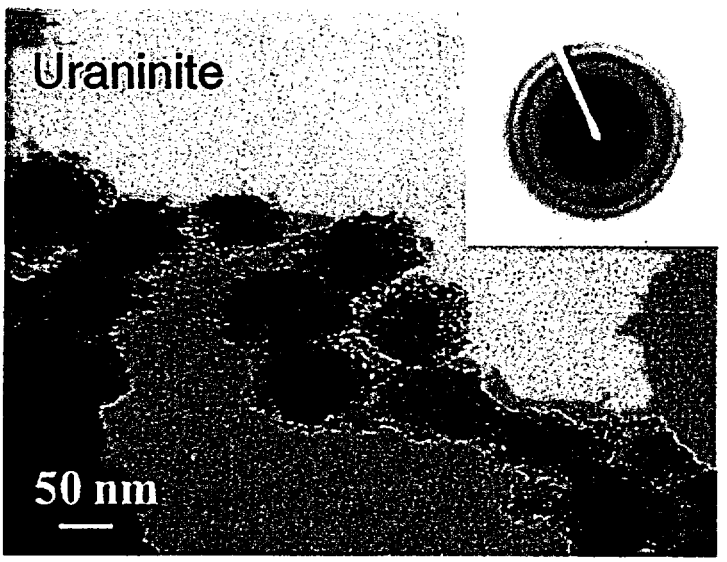

Fig. 3. Uraninite particles and electron diffraction pattern.

crystallized. The uraninite particles are about 50 nm in size but form agglomerates of a few hundred nanometers in size. Detection of uraninite in column experiments was not possible because the inventory was too small and because a comparatively large mass of iron sulfide was produced making separation impossible. Fig. 4 shows the decrease of U(VI) and SO_4^{2-} concentrations in the aqueous phase of the batch experiment.

The black precipitate recovered from the batch experiment with the high ferrous sulfate concentration is shown in Fig. 5. Electron diffraction and chemical microanalyses data show that the precipitate is mackinawite ($FeS_{0.9}$). This result is in agreement with the finding of McNeil and Little (1990) who showed that mackinawite formed when sulfate reducing bacteria mediate reduction of sulfate in the presence of iron compounds. Mackinawite is also known to be a precursor of pyrite in sedimentary and hydrothermal systems (Davison, 1991).

Beside uraninite and mackinawite, bacterial growth formed a significant amount of organic matter which remains in the form of dead bacteria after termination of the experiments. This biomass constitutes a redox buffer that may consume dissolved oxygen and, together with mackinawite, protect the precipitated uraninite against oxidation and dissolution. This hypothesis is based on observations in natural uranium ore deposits. As an example, the well-studied uranium deposit at Oklo (Gabon), located in sandstone, is buffered by two iron minerals, siderite ($FeCO_3$) and ferrihydrite ($Fe(OH)_3$) controlling the Fe^{2+}/Fe^{3+} ratio and maintaining reducing conditions though oxygenated ground water infiltrates the ore body (Blanc, 1995). Organic matter, now converted to graphite, was also present. Cross et al. (1991) and Dewynne et al. (1993) studied the oxidation–reduction reactions occurring in a uranium mine at Poços de Caldas in Brazil and found that pyrite (FeS_2) oxidation consumes most of the oxygen of surface water that penetrates into the mine.

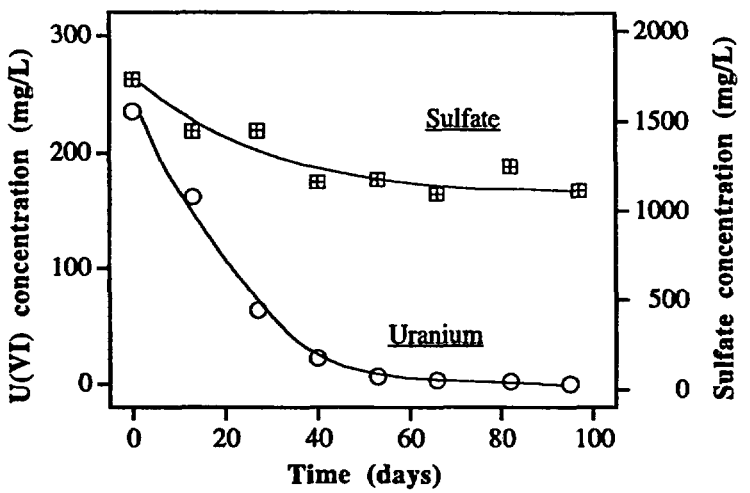

Fig. 4. Decrease of U(VI) and sulfate concentrations in ground water during microbially mediated reduction at 24°C.

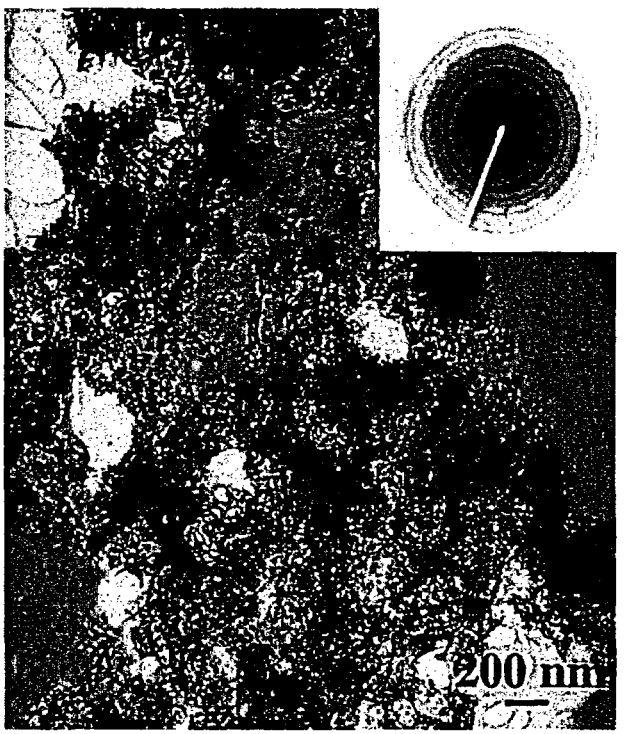

Fig. 5. Mackinawite particles and electron diffraction pattern.

4.2. Release of uranium from sandstone columns

Fig. 2b shows a sandstone column after completion of a microbially mediated uranium reduction experiment. Column (a) shows the sand before the experiment. The black spots on column (b) are mackinawite. Initially, the sandstone contained some 250 mg of iron oxides available for reduction and precipitation of mackinawite in the column. Though the fraction of reduced and precipitated iron was not measured, it is estimated to be large compared with the 26 μg of uraninite precipitated. When uncontaminated ground water was passed through the column, the black spots became smaller.

great observation!

4.2.1. Columns 1 and 2

4.2.1.1. Release of uranium. The results of the two leaching experiments with uncontaminated ground water are shown in Fig. 6 and in Table 2. The figure shows the uranium concentration in the leachate as function of the number of pore volumes passed through the column. One pore volume corresponds to 129 ml. After one pore volume, the U(VI) concentration in column 1 decreased to about 1.4 μg/l. This is a result of washing out and diluting the number of bacteria not adhering to the sand particles. It was shown in

?

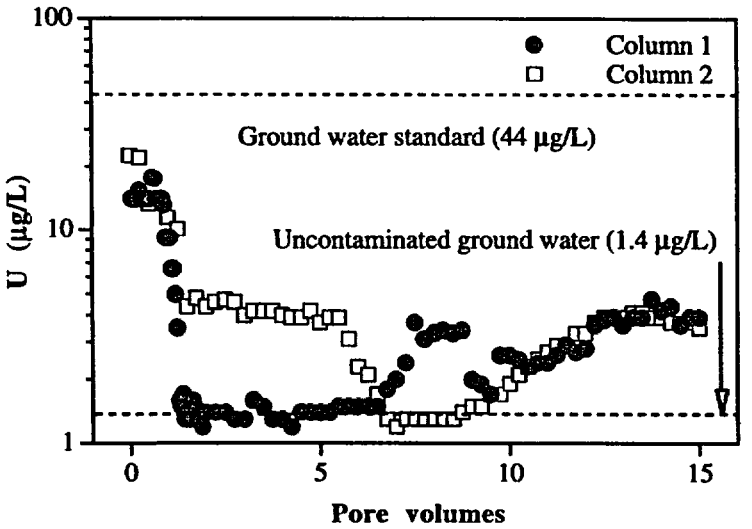

Fig. 6. Leaching of uraninite from sandstone columns with uncontaminated ground water (DO = 7 mg/l). Column 1 (leaching rate = 7 ml/h), column 2 (leaching rate = 100 ml/h). U(IV) inventory in the column is 26 µg.

previous work that uraninite particles adhere to the surface of bacteria and to some extent to the sand particles (Abdelouas et al., 1998a). The uraninite released is oxidized as soon as the water sample is exposed to air and prepared for uranium analysis. If the oxygen introduced with the first pore volume had oxidized uranium, the U(VI) concentration would have increased instead of decreasing. The sulfate concentration was found to increase as a result of oxidation of mackinawite. Between 2 and 15 pore volumes the concentration of uranium fluctuated between not detectable and 2.6 µg/l, after subtraction of the natural uranium concentration in the uncontaminated ground water. There was no significant dependence of the uranium concentration on the rate at which the uncontaminated water was passed through the column. The velocity of the ground water at Tuba City is 15 m/year. Fifteen pore volumes translate to a time of 450 years in the field. As the total inventory of uraninite on the column is only 26 µg, the fraction of uranium leached from the column corresponds to roughly 20% (Table 2). Uraninite has a solubility of 10^{-8} to 10^{-9} mole/l at pH = 7 (Langmuir, 1978; Parks and Pohl, 1988). If this compound controls the concentration of U(IV) in solution, one would expect values between 0.3 and 3 µg/l, in good agreement with what was measured. As a result, there was no indication of oxidation of U(IV) to U(VI) by oxygen introduced with the uncontaminated ground water. It is the oxidation of mackinawite to sulfate that consumes the oxygen and protects uraninite.

Leaching of column 1 with an additional 20 pore volumes of uncontaminated ground water showed that the U(VI) concentration fluctuated between background concentration and 3 µg/l (Fig. 7). This result suggests that uraninite is protected over a long period of time in the field.

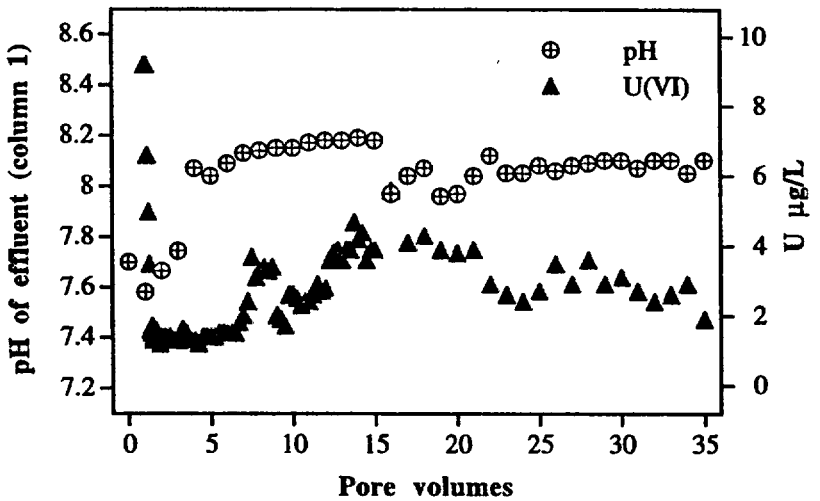

Fig. 7. U(VI) concentrations and pH in uncontaminated water leaving column 1. The leaching rate was 7 ml/h and U(IV) inventory in the column is 26 µg.

4.2.1.2. Oxidation of mackinawite. Fig. 8 (upper curve) shows the increase of the sulfate concentration of the uncontaminated ground water leaving column 1. We observe a steady state sulfate concentration of 21 mg/l after 10 pore volumes. The uncontaminated ground water entering the column contained 9.6 mg/l. Relating the net steady

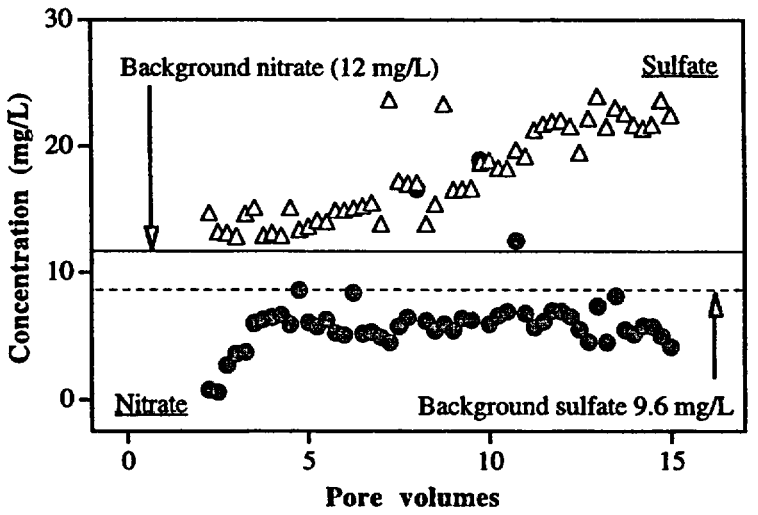

Fig. 8. Leaching of mackinawite from a sandstone column with uncontaminated ground water. A fraction of nitrate was reduced by denitrifying bacteria.

state concentration of 10.5 mg/l to the oxygen concentration in the ground water (7 mg/l) yields that oxygen is consumed by mackinawite oxidation as shown in Eq. (3):

$$FeS + 9/4O_2 + 3/2H_2O \rightarrow SO_4^{2-} + FeOOH + 2H^+ \quad (3)$$

4.2.1.3. Nitrate reduction. Fig. 8 (lower curve) shows a steady state nitrate concentration of about 7 mg/l in the water leaving the column, compared with 12 mg/l, the concentration of nitrate in the uncontaminated ground water entering the column. This indicates that denitrifying bacteria are still alive. For thermodynamic reasons, microbially mediated reduction of nitrate is preceded by oxygen reduction (Stumm and Morgan, 1981). Thus, observation of ongoing denitrification indicates that dissolved oxygen is removed with the help of bacteria. This process competes with sulfide oxidation and supports maintenance of reducing conditions in the column.

4.2.1.4. Iron oxyhydroxide formation. In the presence of oxygenated water mackinawite was oxidized to goethite (FeOOH) as shown by Eq. (3). Goethite was identified by TEM (Fig. 9). If uraninite is oxidized in the column, U(VI) species could be adsorbed on goethite (Hsi and Langmuir, 1985). However, the speciation of U(VI) in the ground water from well No. 948 (Table 1) is such that 77% of the uranium is in the form of

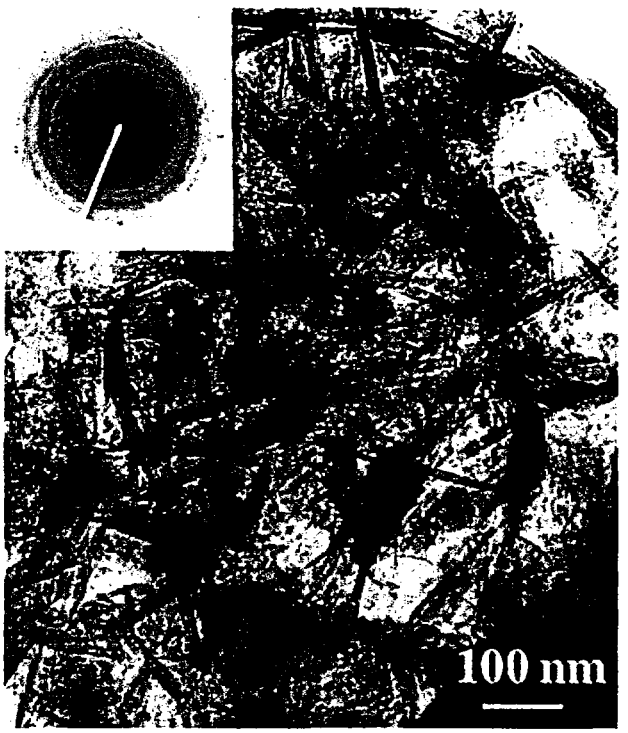

Fig. 9. Goethite particles and electron diffraction pattern.

negatively charged carbonate complexes not adsorbed on goethite and soil (Hsi and Langmuir, 1985; Duff and Amrhein, 1996). The rest of U(VI) species are neutral carbonate and hydroxo complexes, as calculated with the help of the EQ3NR code (Wolery, 1992). U(VI) carbonate complexes are stable under slightly reducing conditions (Brookins, 1988) as they are expected to prevail during mackinawite oxidation and microbially mediated denitrification.

4.2.1.5. Evolution of pH in the effluent. The pH was measured in the effluent of column 1 to study the effect of mackinawite oxidation (Eq. (3)) on ground water acidification. In fact, sulfides, in particular pyrite oxidation is known to cause acidification of uranium mill tailings waters, thereby enhancing the leaching of heavy metals such as Cd, As, Ce and Hg (Al-Hachimi, 1992; Al-Hachimi et al., 1994, 1996). The results of pH measurements in the effluent of column 1 are plotted in Fig. 7. The pH of water leaving the column varies between $7.7 \leq pH \leq 8.0$. The variation is insignificant given an experimental error of ± 0.1 pH unit. The result is not in agreement with the expected acidification according to Eq. (3). The discrepancy could be explained by dissolution of aragonite (Eq. (4)), precipitated during denitrification:

$$CaCO_3 + H^+ \rightarrow Ca^{2+} + HCO_3^- \quad (4)$$

Furthermore, the clay coating on the sand particles can contribute to stabilize the pH by buffering excess acidity through ion-exchange between protons and interlayer cations (Read et al., 1993). These authors used HCl to leach the Clashach sandstone, whose mineralogy and chemical composition are similar to that of Navajo sandstone. Read et al. (1993) showed that more than 50 pore volumes of 0.1 N HCl were needed to reach pH 1 in the effluent, demonstrating the strong buffering capacity of the sandstone.

4.2.2. Column 3

The results of the leaching experiment are shown in Fig. 10 and Table 2. On column 3 the uraninite inventory was over a factor of 10^3 higher than on columns 1 and 2. The first injected pore volume washed out the uraninite adhering to suspended bacteria. The experiment with the higher concentration revealed that detachment of bacteria and uraninite from the sandstone surfaces is slow, even at a flow rate of 100 ml/h, but not negligible. Detachment was inferred from sedimentation of bacteria and uraninite in the bottles used to collect the effluent. Both bacteria and uraninite were found in sediment samples under the TEM. The transport of bacteria and uraninite in ground water is facilitated by the small particle size (50 nm to a few microns), relative to the average pore size of > 50 μm in the column.

Concentrations of uranium in the effluent water of column 3 exceed the U.S. ground water protection standard by 2 orders of magnitude. Detachment of bacteria is significant enough to transport 43% of the uraninite out of the column after 15 pore volumes. Detachment of bacteria and high uranium concentrations in the effluent suggest that an in situ application of bacterially catalyzed uranium reduction does not provide sufficiently low concentrations in order to remediate ground water. Generally, the concentration of uranium in contaminated ground water is on the order of 1 mg/l or less. Hence,

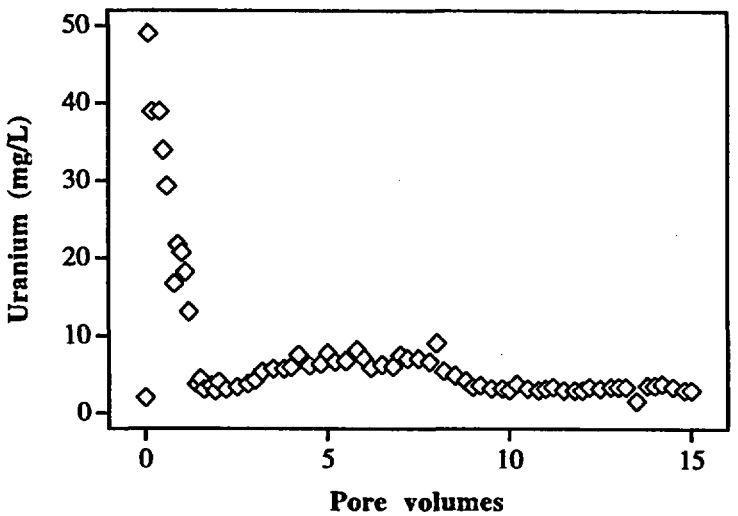

Fig. 10. Leaching of uraninite from a sandstone column with uncontaminated ground water (DO = 7 mg/l); leaching rate = 100 ml/h. U(IV) inventory in the column is 43 mg.

the results obtained with columns 1 and 2, are satisfactory and support application of in situ bioremediation of uranium in ground water.

4.3. Release of uranium in batch experiments

4.3.1. Sandstone with low uraninite inventory

The results of the oxidation experiments in ground water with $0.7 \cdot 10^{-2}$ to $5.8 \cdot 10^{-2}$ mmole of oxygen and $1.3 \cdot 10^{-5}$ mmole of uraninite (Table 3), are shown in Fig. 11a,b. Uraninite oxidation was determined by measuring the U(VI) concentration in the aqueous phase. The water was filtered through 0.2 μm filter right after sampling to prevent oxidation of uraninite in the sample to be analyzed for U(VI). In the experiment with 16 ml of water the final U(VI) concentration exceeded 30 μg/l suggesting that uraninite was oxidized. Fig. 11a shows that the fraction of uraninite oxidized increases with increasing volume of uncontaminated groundwater (dissolved oxygen). Oxidation was fast and there was no increase of the fraction of oxidized uraninite with time, except for the largest volume (132 ml). In all experiments, enough oxygen was supplied (Table 3) to oxidize uraninite quantitatively. However, total oxidation was not observed. Instead, the maximum mass of oxidized uraninite was proportional to the mass of oxygen supplied (Fig. 11b). An empirical linear relationship between the fraction of oxidized uraninite and the oxygen supply was obtained: $F = (7.386 \times Q) + 0.017$; where F is the fraction of oxidized uraninite and Q is the mass of oxygen supplied (mmole).

We tested whether this relationship holds for the column experiment where the water to sand ratio was 0.15 by mass, corresponding to an oxygen mass of $6.5 \cdot 10^{-3}$ mmole. Using this oxygen mass in the equation above, yields a fraction of oxidized uraninite of 0.0175. By multiplying this value by the total mass of U(IV) precipitated in the column

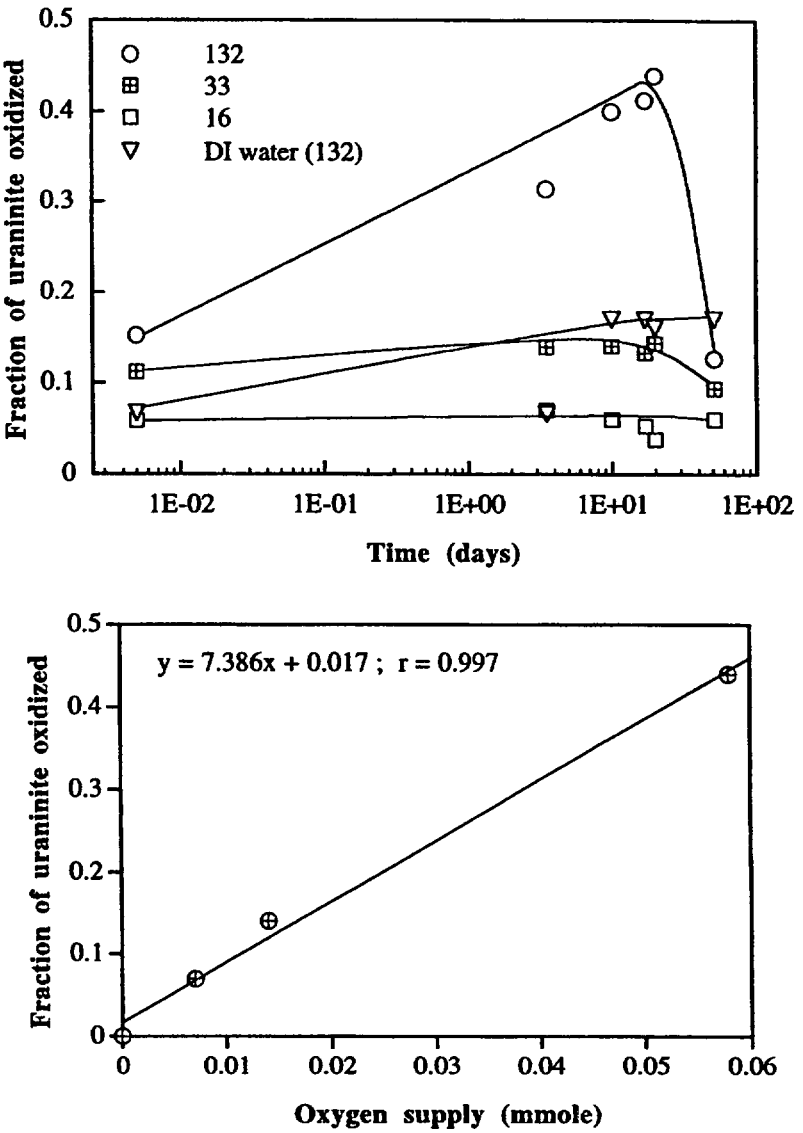

Fig. 11. (a) Leaching of precipitated uraninite (batch experiments). Numbers in legend correspond to the solution:sand ratio. One gram of sand contains 3.1 μg U(IV). (b) Fraction of uranium inventory oxidized as a function of oxygen supplied by ground water.

(26 μg), the mass of oxidized uranium expected in one pore volume (129 ml) is 0.45 μg, which corresponds to a concentration of $0.45 \times (1000/129) = 3.5$ μg/l. Adding 1.4 μg/l, the natural uranium concentration in the ground water (Table 1), yields a total concentration of uranium of 4.9 μg/l in the water leaving columns 1 and 2. Given the uncertainties of the thermodynamic data for the solubility of UO_2 in water, given in

Section 4.2, it is not possible to discuss our measured uranium concentration of about 4 μg/l (Fig. 6) in terms of oxidation of U(IV) to U(VI) or dissolution of U(IV) or both. Nevertheless the concentration of uranium in the remediated ground water is a factor of ten below the ground water protection standard in the U.S.

4.3.2. Sandstone with a high inventory of uraninite

The results of the oxidation experiments in ground water with $0.7 \cdot 10^{-2}$ to $5.8 \cdot 10^{-2}$ mmole of oxygen and $1.2 \cdot 10^{-2}$ mmole of uraninite (Table 3) are shown in Fig. 12a,b. The uranium concentration was between 1 and 7 mg/l suggesting that uraninite was oxidized. Fig. 12a shows that the fraction of uraninite oxidized increased with increasing volume of uncontaminated groundwater (dissolved oxygen). As with the preceding experiments, oxidation was fast initially but it took several days until the maximum fraction of oxidized uraninite was attained, except when there was much less oxygen ($0.7 \cdot 10^{-5}$ mole) than uraninite. Again, total oxidation of uraninite was not observed and the maximum mass of oxidized uraninite was proportional to the mass of oxygen supplied (Fig. 12b).

4.4. Quantification of oxygen consumption

An oxygen mass balance between supply, O_T(mg), and consumption was calculated from the oxidation of mackinawite (Eq. (3)), X(mg); oxidation of uraninite (Eq. (5)), Y(mg); reduction of oxygen by bacteria and oxidation of biomass, Z(mg). $Z = O_T - X - Y$.

$$UO_2 + 1/2O_2 + 2HCO_3^- \rightarrow UO_2(CO_3)_2^{2-} + H_2O \quad (5)$$

The fractions of oxygen consumed in these reactions are shown in Table 4. In batch experiments with a small mass of uraninite, over 90% of the oxygen was consumed by oxidation of mackinawite, less than 1% by oxidation of uraninite. The rest was attributed to oxidation of biomass and the activity of denitrifying bacteria. The strong protective function of mackinawite vis-a-vis uraninite is evidenced by the numbers in the table. For experiments with the higher mass of uranium (Table 4), the fraction of oxygen consumed by uraninite oxidation is higher than in the experiments with less uranium (discussion in the next section).

The preferential oxidation of mackinawite relative to U(IV) was expected because the redox intensity of SO_4^{2-} reduction, $p\varepsilon^\circ = -3.75$ (Stumm and Morgan, 1981), is lower than that of U(VI), $p\varepsilon^\circ = +4.9$ (Abdelouas et al., 1998a). Oxidation of uraninite in the presence of mackinawite occurred for kinetic reasons. Oxygen is provided to these minerals faster than it is consumed by mackinawite oxidation.

4.5. Effect of carbonate on uraninite dissolution

The results in Fig. 11a and Fig. 12a include those from two experiments with deionized water and a water to sandstone mass ratio of 132. The same ratio was used in two experiments with uncontaminated ground water. The concentration of dissolved oxygen was the same (7 mg/l) in both waters. This means that the same mass of

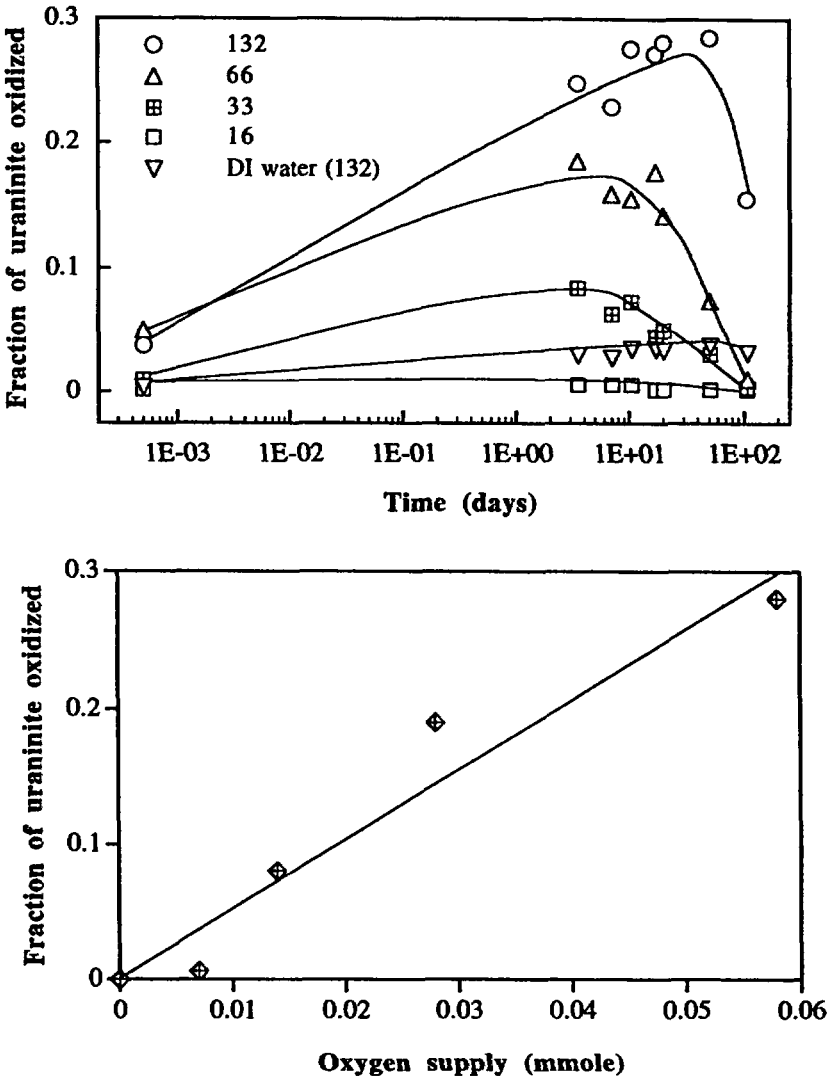

Fig. 12. (a) Leaching of precipitated uraninite (batch experiments). Numbers in legend correspond to the solution:sand ratio. One gram of sand contains 2.9 mg U(IV). (b) Fraction of uranium inventory oxidized as a function of oxygen supplied by ground water.

uraninite should have been oxidized. Apparently, much less uraninite was oxidized in deionized water. The difference could be explained by assuming that the carbonate concentration has an effect on the rate at which secondary minerals precipitate from deionized and from uncontaminated ground water.

The deionized water is practically free of carbonate. Speciation calculations for the uncontaminated ground water using the EQ3NR code (Wolery, 1992) showed that

Table 4
Oxygen consumption by mackinawite, uraninite, denitrifiers and biomass (batch experiments with 1 g of sandstone)

Volume of water (ml)	$1.3 \cdot 10^{-5}$ mmole U(IV); fraction of oxygen consumed by			$1.2 \cdot 10^{-2}$ mmole U(IV); fraction of oxygen consumed by		
	Uraninite	Denitrifiers, biomass	Mackinawite	Uraninite	Denitrifiers, biomass	Mackinawite
132	< 0.01	0.07	0.92	0.04	0.05	0.91
66	–	–	–	0.04	0.03	0.93
33	< 0.01	0.03	0.96	0.07	0.01	0.92
16	< 0.01	0.05	0.94	< 0.01	–	0.99
132 DI water[b]	< 0.01	–	> 0.99	< 0.01[a]	–	0.74

[a] Total fraction of oxygen consumed by uraninite oxidation could be 0.26. The value of < 0.01 is based on U(VI) concentration in solution. The difference is probably due to precipitation of schoepite and $CaUO_4$ (see text).
[b] DI = deionized water.

uranium is expected to be present mostly as soluble uranium carbonate complexes: $(UO_2)_2(CO_3)_2^{2-}$ (61%) and $UO_2(CO_3)_3^{3-}$ (11%) at pH = 7.7 after 20 days (experiment with low uranium inventory). The remaining 23% consist of $UO_2(OH)_2$(aq). A decrease from 45% after 20 days to 13% after 51 days of the fraction of uraninite oxidized (Fig. 11a) was measured. This could be explained by slower formation of U-rich minerals with complexed then with uncomplexed uranium. In the experiment with the high uraninite inventory (Fig. 12a), the apparent decrease of the fraction of uraninite oxidized from 29% after 20 days to 16% after 51 days can be explained by precipitation of schoepite ($UO_3 \cdot 2H_2O$) and $CaUO_4$ as suggested by calculations with EQ3NR.

5. Conclusions

Our experiments show that small masses of uraninite, 0.1 μg/g of host rock (sandstone), precipitated by microbially mediated reduction of U(VI), are protected from oxidation in ground water in the presence of iron sulfide, mackinawite ($FeS_{0.9}$). The precursor of mackinawite, an Fe(III) oxide coating on the sandstone, is present in abundance and enough mackinawite formed to provide long-term protection of the uraninite precipitate. Fe(III) is reduced together with uranium. The source of sulfide is provided by biocatalyzed reduction of sulfate. Sulfate may be present in ground water naturally, or as a contaminant, or can be added upon amendment of the water when stimulating the biocatalytical reactions.

Uranium concentrations in ground water passed through sandstone columns in the laboratory are too low (4 μg/l) to distinguish between simple dissolution of uraninite and oxidative dissolution. However, batch experiments gave evidence of oxidative dissolution of uraninite. Reoxidation is insignificant in the presence of mackinawite, if the inventory of uraninite on the sandstone is sufficiently small. This is the case when the initial uranium concentration in the ground water is on the order of a few milligrams per liter or less. If another microbially mediated process, e.g., denitrification, precedes uranium reduction, enough biomass may be present to enhance the buffer capacity for oxygen in the system. However, if uraninite precipitates from ground water with a much higher initial uranium concentration, e.g., 240 mg/l, detachment of bacteria from the sandstone surface and transport of uraninite particles becomes significant, and residual uranium concentrations exceed the ground water protection standards.

Data obtained in the present study are site specific (the mill tailings site at Tuba City). However, Fe(III) minerals in the host rock and sulfate in the aqueous phase are frequently encountered in ground water contaminated with uranium. This suggests that mackinawite formation can be expected and in situ bioremediation of uranium may work at many sites, given that bacteria capable of reducing uranium, iron, and sulfate are ubiquitous in nature (Abdelouas et al., 1998d).

Acknowledgements

We thank Dr. Weiliang Gong for his help with the transmission electron microscope work. We thank Neil Butt for sandstone sample and column preparation.

References

Abdelouas, A., Lu, Y., Nuttall, E., Lutze, W., 1998a. Reduction of U(VI) to U(IV) by indigenous bacteria in contaminated ground water. J. Contam. Hydrol. 35, 217–233.

Abdelouas, A., Nuttall, H.E., Lutze, W., Lu, Y., 1998b. In situ removal of uranium from ground water. In: Proceedings of the Tailings and Mine Waste '98. Balkema, Rotterdam, pp. 669–677.

Abdelouas, A., Lutze, W., Nuttall, E., 1998c. Chemical reactions of uranium in ground water at a mill tailings site. J. Contam. Hydrol. 34, 343–361.

Abdelouas, A., Lutze, W., Nuttall, E., Gong, W., Fritz, B., 1998d. Enzymatic reduction of U(VI) in groundwaters. Journal of the French Academy of Sciences (submitted).

Al-Hachimi, A., 1992. Uranium tailings disposal: review of current technology. Int. J. Environ. Studies 42, 53–62.

Al-Hachimi, A., Evans, G.J., Cox, B., 1994. Leachability of hazardous elements from uranium tailings. Int. J. Environ. Studies 46, 59–68.

Al-Hachimi, A., Evans, G.J., Cox, B., 1996. Aspects of the permanent storage of uranium tailings. Water Air Soil Pollut. 88, 83–92.

Barnes, C.E., Cochran, J.K., 1993. Uranium geochemistry in estuarine sediments: controls on removal and release processes. Geochim. Cosmochim. Acta 57, 555–569.

Barton, L.L., Choudhury, K., Thomson, B.M., Steenhoudt, K., Groffman, A.R., 1996. Bacterial reduction of soluble uranium: the first step of in situ immobilization of uranium. Radio. Waste Manag. Environ. Restor. 20, 141–151.

Blanc, P.L., 1995. Acquirements of the natural analogy programme. Oklo, natural analogue for a radioactive waste repository. Final Report, IPSN/CEA, Fontenay-aux-Roses Cedex, France.

Brookins, D., 1988. Eh–pH diagrams for geochemistry, Springer-Verlag, 175 pp.

Cross, J.E., Haworth, A., Neretnieks, I., Sharland, S.M., Tweed, C.J., 1991. Modelling of redox front and uranium movement in a uranium mine at Poços de Caldas. Radiochim. Acta 52/53, 445–451.

Davison, W., 1991. The solubility of iron sulphides in synthetic and natural waters at ambient temperature. Aqua. Sci. 53, 309–329.

Dewynne, J.N., Fowler, A.C., Hagan, P.S., 1993. Multiple reaction fronts in the oxidation–reduction of iron-rich uranium ores. SIAM J. Appl. Math. 53, 971–989.

Duff, M.C., Amrhein, C., 1996. Uranium (VI) adsorption on goethite and soil in carbonate solutions. Soil Sci. Soc. Am. J. 60, 1393–1400.

Federal Register, 1995. Environmental Protection Agency (EPA), CFR 40 Part 192, Groundwater Standards for Remedial Actions at Inactive Uranium Processing Sites, Table 1, November 1995, p. 2866.

Finch, R.J., Ewing, R.C., 1992. The corrosion of uraninite under oxidizing conditions. J. Nucl. Mater. 190, 133–156.

Francis, A.J., Dodge, C.J., Gillow, J.B., Cline, J.E., 1991. Microbial transformations of uranium in wastes. Radiochim. Acta 52/53, 311–316.

Francis, A.J., Dodge, C.J., Lu, F., Halada, G.P., Clayton, C.R., 1994. XPS and XANES studies of uranium reduction by *Clostridium* sp. Environ. Sci. Technol. 28, 636–639.

Gorby, Y.A., Lovley, D.R., 1992. Enzymatic uranium precipitation. Environ. Sci. Technol. 26, 205–207.

Hsi, C.K.D., Langmuir, D., 1985. Adsorption of uranyl onto ferric oxyhydroxides: application of the surface complexation site-binding model. Geochim. Cosmochim. Acta 49, 1931–1941.

Isobe, H., Murakami, T., Ewing, R.C., 1992. Alteration of uranium minerals in the Koongarra deposit. J. Nucl. Mater. 190, 174–187.

Kunze, G.W., Dixon, J.B., 1989. Pretreatment for mineralogical analysis. In: Kulte, A. (Ed.), Methods of Soil Analysis: Part 1. Physical and Mineralogical Methods, 2nd edn., pp. 91–100.

Langmuir, D., 1978. Uranium solution–mineral equilibria at low temperatures with applications to sedimentary ore deposits. Geochim. Cosmochim. Acta 42, 547–569.

Lovley, D.R., 1995. Microbial reduction of iron, manganese, and other metals. In: Donald, L., Sparks, L. (Eds.), Advances in Agronomy. Vol. 54, Academic Press, New York, pp. 175–231.

Lovley, D.R., Phillips, E.J.P., 1992a. Reduction of uranium by *Desulfovibrio desulfuricans*. Appl. Environ. Microbiol. 58, 850–856.

Lovley, D.R., Phillips, E.J.P., 1992b. Bioremediation of uranium contamination with enzymatic uranium reduction. Environ. Sci. Technol. 26, 2228–2234.

Lovley, D.R., Phillips, E.J.P., Gorby, Y.A., Landa, E.R., 1991. Microbial reduction of uranium. Nature 350, 413–415.

Lovley, D.R., Roden, E.E., Phillips, E.J.P., Woodward, J.C., 1993. Enzymatic iron and uranium reduction by sulfate-reducing bacteria. Marine Geol. 113, 41–53.

McNeil, M.B., Little, B.J., 1990. Mackinawite formation during microbial corrosion. Corrosion 46, 599.

Nuttall, E., Lutze, W., Barton, L., Choudhury, K., 1996. Preliminary screening results for in situ bioremediation at an UMTRA site. Waste Management '96, Session 45, paper 6, Tucsan, February, 1996.

Nuttall, H.E., Lutze, W., Barton, L.L., Wolfram, J., 1997. In situ bioremediation of contaminated ground water at an UMTRA site. International Symposium In Situ and On Site Bioreclamation, New Orleans, Louisiana, April 28–May 1. Proceedings Vol. 1, pp. 435–440.

Parks, G.A., Pohl, D.C., 1988. Hydrothermal solubility of uraninite. Geochim. Cosmochim. Acta 52, 863–875.

Phillips, E.J.P., Landa, E., Lovley, D.R., 1995. Remediation of uranium contaminated soils with bicarbonate extraction and microbial U(VI) reduction. J. Industr. Microbiol. 14, 203–207.

Quinton, G.E., Buchanan, R.J., Ellis, D.E., Shoemaker, S.H., 1997. A method to compare groundwater cleanup technologies. Remediation, Autumn, pp. 7–16.

Read, D., Lawless, T.A., Sims, R.J., Butter, K.R., 1993. Uranium migration through intact sandstone cores. J. Contam. Hydrol. 13, 277–289.

Sato, T., Murakami, T., Yanase, N., Isobe, H., Payne, T., Airey, P.L., 1997. Iron nodules scavenging uranium from groundwater. Environ. Sci. Technol. 31, 2854–2858.

Siegel, M.D., Ward, D.B., Bryan, C.R., Cheng, W.C., 1994. Characterization of materials for a reactive transport model validation experiment. Int. Rep. Sandia National Labs., SAND 94-0189.

Stumm, W., Morgan, J.J., 1981. Aquatic Chemistry, Wiley, New York, pp. 453–461.

Tucker, M., Barton, L.L., Thomson, B.M., 1996. Kinetic coefficients for simultaneous reduction of sulfate and uranium by *Desulfovibrio desulfuricans*. Appl. Microbiol. Biotechnol. 46, 74–77.

Wolery, T.J., 1992. EQ3NR, A computer program for geochemical aqueous speciation-solubility calculations: theoretical manual, user's guide, and related documentation (version 7.0): UCRL-MA-110662-PT-IV. Lawrence Livermore National Laboratory, Livermore, CA.

Yanase, N., Payne, T., Sekine, K., 1995. Groundwater geochemistry in the Koongarra ore deposit, Australia (I): implications for uranium migration. Geochem. J. 29, 1–29.

ELSEVIER

Journal of Contaminant Hydrology 35 (1998) 217–233

JOURNAL OF
Contaminant
Hydrology

Reduction of U(VI) to U(IV) by indigenous bacteria in contaminated ground water

A. Abdelouas [a,*], Yongming Lu [a], W. Lutze [b], H.E. Nuttall [b]

[a] *Advanced Materials Laboratory, University of New Mexico, Center for Radioactive Waste Management, 1001 University Blvd., SE-Suite 201, Albuquerque, NM 87106, USA*

[b] *University of New Mexico, Department of Chemical and Nuclear Engineering, Albuquerque, NM 87131, USA*

Abstract

We report on bio-catalyzed reduction and immobilization of U(VI) species (0.25 mg/l to 235 mg/l) in ground water in the presence of high concentrations of nitrate, sulfate and carbonate. We studied ground water from the uranium mill tailings site near Tuba City, Arizona (USA). Experiments with the ground water were conducted in the presence of the Navajo sandstone host rock. Uranium in solution is complexed by carbonate. Two indigenous denitrifying bacteria were identified *Pseudomonas aeruginosa* and *P. stutzeri*, and one sulfate reducing bacterium, *Shewanella putrefaciens*, also known as Fe(III)-reducer. *S. putrefaciens* can use U(VI) as an electron acceptor, instead of Fe(III). Ethanol was used as the organic carbon source. Microbially mediated reactions are sequential in the order of decreasing redox intensity. Metabolic reduction of nitrate to gaseous species (N_2, N_2O) was complete within 1 week at 16°C. The sulfate concentration remained constant. Some of the U(VI) coprecipitated with aragonite/calcite or was adsorbed on biomass during denitrification. Subsequently, the enzymatically catalyzed reduction of U(VI) to U(IV) was complete within 3 weeks but was accompanied by reduction of sulfate to sulfide. U(IV) precipitated as a uraninite solid solution (U, Ca)O_2, adhering to the bacteria. The final concentration in solution was ≤ 1 μg/l. U(VI) was not reduced by sulfide. Complexation of U(VI) by carbonate made its reduction by sulfide even slower than in pure water. The bio-catalyzed reaction is the faster process under the conditions given by the composition of the ground water.

Keywords: Biosorption; Calcite; Coprecipitation; Denitrification; Ground water; Navajo sandstone; Speciation; Uraninite; Uranium bioremediation

* Corresponding author. Tel.: +1-505-272-7271; fax: +1-505-272-7304; e-mail: badria@unm.edu

0169-7722/98/$ - see front matter
PII: S0169-7722(98)00134-X

1. Introduction

A variety of reduction and oxidation reactions can be combined to result in exergonic processes mediated by heterotrophic bacteria. As these bacteria are widely distributed in nature and nearly always found in water and soils, microbial mediation is frequently used to remove pollutants from soil and water. The focus has been on converting organic pollutants into inorganic non-toxic compounds (Rittmann et al., 1994). Inorganic species such as nitrate and radioactive elements, e.g., uranium, are receiving increasing attention (Knowles, 1982; Gorby and Lovley, 1992).

In the case of uranium heterotrophic bacteria catalyze the reduction of U(VI) to U(IV) enzymatically, if specific E_H and pH conditions are met. Uranium precipitates as uraninite, UO_2 (Lovley et al., 1991; Gorby and Lovley, 1992; Lovley and Phillips, 1992a,b; Lovley et al., 1993a,b; Francis et al., 1994; Lovley, 1995a,b; Phillips et al., 1995; Barton et al., 1996; Tucker et al., 1996).

The first microorganisms found to catalyze reduction of U(VI) were the dissimilatory bacteria, *Geobacter metallireducens* and *Shewanella putrefaciens*, both known as 'Fe-reducing' bacteria (Lovley, 1995a). These organisms can use U(VI) as an electron acceptor, instead of Fe(III) (Lovley et al., 1991). These authors found that both organisms grow in the presence of high concentrations of uranium (8 mM), at rates comparable to those observed with Fe(III). The experiments were conducted in a closed system using pure cultures. Various 'sulfate-reducing' bacteria, *Desulfovibrio* species, including *D. desulfuricans*, *D. vulgaris*, and *D. baculatum*, are able to reduce U(VI) to U(IV) as well (Lovley and Phillips, 1992a; Lovley et al., 1993a,b). Several authors showed that the reduction of U(VI) is an enzymatically catalyzed reaction, regardless of the experimental conditions, e.g., type of bacteria, composition of growth medium, uranium concentration, and incubation temperature (Lovley and Phillips, 1992a; Lovley et al., 1993a,b). These authors showed also that HS^-, used in their experiments to establish reducing conditions, reacts only slowly with U(VI) compared with the bio-catalyzed reaction, at near neutral pH and near room temperature. Application of the process to precipitate uranium in situ from contaminated ground water was proposed in several of the referenced publications.

The objective of our work is to study the removal and immobilization of small amounts of soluble uranium species from ground water in the presence of high concentrations of nitrate, sulfate and carbonate. Large volumes of such waters have been encountered at milling sites where uraniferous minerals were leached and process waters and tailings were deposited in unlined structures (DOE, 1994).

2. Chemical reactions

In an aqueous multi-component system microbially mediated reactions are sequential in the order of decreasing redox intensity. The reducible constituents in the ground water and in the host rock need to be specified to identify possible redox reactions and to determine the conditions for reduction of U(VI). We studied the contaminated ground water and the host rock at the mill tailings site near Tuba City, Arizona (USA).

The sequence of reduction reactions in the order of decreasing redox intensity at pH = 7 is (Stumm and Morgan, 1981; 459 pp.):

$$1/4\,O_2(g) + H^+ + e = 1/2\,H_2O \qquad +13.75(p\varepsilon^\circ(\text{Water})) \tag{1}$$

$$1/5\,NO_3^- + 6/5\,H^+ + e = 1/10\,N_2(g) + 3/5\,H_2O \qquad +12.65(p\varepsilon^\circ(\text{Water})) \tag{2}$$

$$1/2\,MnO_2 + 1/2\,HCO_3^-(10^{-3}) + 3/2H^+ + e = 1/2\,MnCO_3(s) + H_2O \qquad +8.9(p\varepsilon^\circ(\text{Water})) \tag{3}$$

$$1/2\,UO_2(CO_3)_2^{2-} + H^+ + e = 1/2\,UO_2(s) + HCO_3^-(10^{-3}) \qquad +4.9(p\varepsilon^\circ(\text{Water})) \tag{4}$$

$$FeOOH(s) + HCO_3^-(10^{-3}) + 2\,H^+ + e = FeCO_3(s) + 2\,H_2O \qquad -0.8(p\varepsilon^\circ(\text{Water})) \tag{5}$$

$$1/8\,SO_4^{2-} + 9/8\,H^+ + e = 1/8\,HS^- + 1/2\,H_2O \qquad -3.75(p\varepsilon^\circ(\text{Water})) \tag{6}$$

Oxygen, nitrate, uranium and sulfate are contained in the ground water, manganese and iron are minor constituents of the host rock (Navajo sandstone).

Reaction (4) was not reported by Stumm and Morgan (1981) and was added by calculating the respective redox intensity for a carbonate concentration of 10^{-3} M, using thermodynamic data from (Grenthe et al., 1992). At $[HCO_3^-] = 10^{-3}$ M and pH = 7, $UO(CO_3)_2^{2-}$ is the main species (37%), calculated by EQ3NR (Wolery, 1992).

Reduction reactions and their rates are affected by the choice of an electron donor, i.e., an organic compound, and the type and quantity of bacteria present. Many organic compounds have been reported in the literature (Lovley and Phillips, 1986, 1988; Lovley, 1995a; Barton et al., 1996), including methanol, ethanol, acetate, glucose, and lactate. All of them work with our system, but we report on ethanol only because it yielded the highest reaction rates. Ethanol is oxidized as follows:

$$1/12\,C_2H_5OH + 1/4\,H_2O = 1/6\,CO_2 + H^+ + e \tag{7}$$

3. Experimental

3.1. Sandstone

The geological formation at Tuba City is Navajo sandstone of Middle Jurassic age. A stratigraphic study of the Navajo sandstone was published by Peterson and Pipiringos (1979). Samples were taken from drilled cores in the ground water saturated zone and from the surface. The samples consist of well sorted and fine to medium grained quartzose sandstone. Microcline is present but strongly altered. Clay minerals and iron oxide form a coating on quartz. A micrograph of the as sampled sandstone is shown in Fig. 1a. Quantitative chemical composition of the sandstone was obtained by atomic absorption and inductively-coupled plasma (ICP) atomic emission spectrometry. Ura-

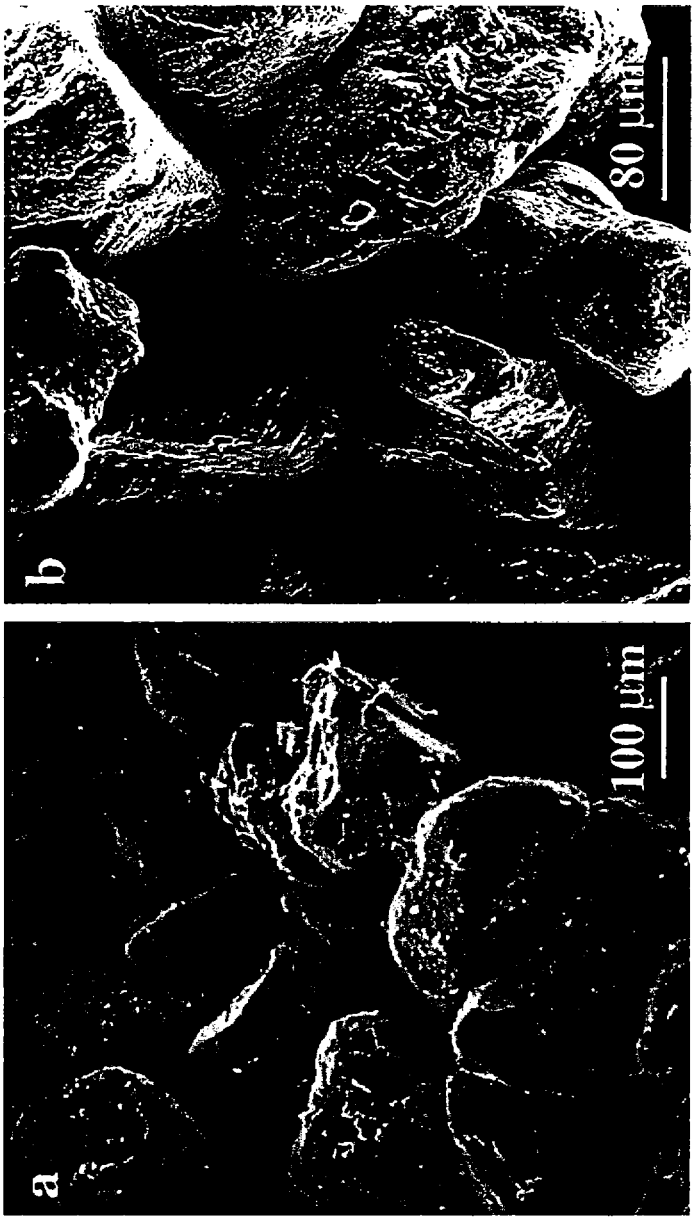

Fig. 1. SEM photographs of Navajo sandstone before (a) and after (b) bioremediation.

Table 1
Chemical composition of Navajo sandstone (average and standard deviation of six samples)

	%
SiO_2	95.18 ± 0.82
Al_2O_3	1.82 ± 0.44
MgO	0.23 ± 0.05
CaO	< 0.2
Fe_2O_3	0.05 ± 0.01
TiO_2	0.05 ± 0.01
MnO	0.05 ± 0.003
Na_2O	0.06 ± 0.01
K_2O	1.09 ± 0.22
P_2O_5	< 0.1
Loss	0.66 ± 0.13
Total	99.12 ± 0.72
	mg/kg
U	0.44 ± 0.08

nium was determined by ICP mass spectrometry. Results are given in Table 1. The Fe_2O_3 content of the sandstone ranged between 0.024 and 0.086 wt.% with an average of 0.040 wt.%. The average concentration of primary uranium in the sandstone is 0.44 mg/kg. There was no significant difference in the uranium content between samples in contact with contaminated or uncontaminated ground water.

3.2. Ground water

3.2.1. Water composition

Ground water was collected from monitoring well #926 (Table 2), located within the area of contaminated ground water, and from well #948 (Table 2), located outside the plume. Water was pumped directly into plastic bottles placed in a nitrogen flushed glove box in the field. The in situ water temperature was 16°C, the concentration of dissolved oxygen 3.1 mg/l (#926) and 7.0 mg/l (#948), measured by lowering a YSI 5739 field probe (YSI, OH, USA) into the water in the wells after pumping for a while. The pH was measured in the glove box and was 6.6 (#926) and 7.7 (#948). In the laboratory, the water was stored at 4°C. The water was analyzed by Core Laboratories. Results are given in Table 2. The salt content is high (4.7 g/l). Nitrate and sulfate are the major anions. In water from well #926, the uranium concentration exceeds US ground water protection standards more than 5 times and nitrate 28 times (Table 2). The high alkalinity of the contaminated water, expressed in terms of $CaCO_3$, results from leaching of the ore with Na_2CO_3. Dissolved oxygen concentrations indicate oxidizing conditions.

3.2.2. Uranium speciation and adsorption

Batch experiments with crushed sandstone and contaminated ground water showed that uranium is not adsorbed on the sand particles. Thermodynamic calculations using the EQ3NR code (Wolery, 1992) showed that more than 98% of the uranium is

Table 2
Chemical composition of ground water (mg/l)

	Well #926	Well #948
U	0.250	0.0014
Alkalinity ($CaCO_3$)	572	88
Ca	681	28.2
Mg	329	6.2
Na	172	14
K	3.0	1.8
Sr	7.04	0.65
Fe	0.05	0.34
Mo	0.01	0.01
NO_3	1220	11.85
SO_4	1830	9.56
Cl	88.4	6.9
TOC	4.0	5.0
TDS	4720	130
Temperature (°C)	16.8	17.1
Dissolved oxygen	3.1	7.0
pH	6.63	7.70
US ground water protection standards[a] (mg/l)		
U	0.044	
NO_3	44	

[a] Federal Register (1995).

complexed as $UO_2(CO_3)_2^{2-}$, $UO_2(CO_3)_3^{4-}$, and some UO_2CO_3. We measured the zeta-potential of the sandstone surface in the ground water and found a value of −12 mV. The negatively charged uranium species cannot be adsorbed on negatively charged surfaces. Uranium from the tailings is in solution and is readily accessible to bacteria.

3.2.3. *Uranium coprecipitation*

At 16°C, the water is saturated with $CaCO_3$. Aragonite precipitates when the temperature is increased and uranium is coprecipitated. The process is slow. At 24°C, the uranium concentration decreased by 40% after 6 months and its concentration in the mixture aragonite/calcite was 0.4 g/kg (Abdelouas et al., 1998). Walker et al. (1989) studied biodenitrification of waste waters from a uranium refinery and reported that calcite precipitated and plugged their fluidized bed reactor. Calcite precipitated because organic matter was oxidized to CO_2 during denitrification. This is an important finding and is taken into consideration in this work. Coprecipitation of uranium was not studied by Walker et al. (1989).

3.3. *Indigenous bacteria*

Cultures grown during oxidation–reduction experiments were analyzed by Microbe Inotech Laboratories (Saint Louis, MO, USA). The most probable number method (MPN) was used to count nitrate and sulfate reducing microorganisms. The U.S.G.S.

method B-0430-85 (1988) was used to determine the MPN of nitrate reducing bacteria. The US Environmental Protection Agency (EPA) standard method 9240 D.H. (E.P.A. Standard Method 9240, 1992) was used to determine the MPN of sulfate reducing bacteria. Following isolation, the strains were incubated and processed by standard GC-FAME method 1. The processed strains were examined against both the Aerobe (TSBA [rev. 3.90]) and Clinical Aerobe (CLIN [rev. 3.90]) GC-FAME data bases supplied by Midi Microbes (Newark, DE, USA). [1] Two denitrifying bacteria were identified *Pseudomonas aeruginosa* and *P. stutzeri*, and one sulfate reducing bacterium, *S. putrefaciens*. *S. putrefaciens* is reported by Lovley (1995a) to catalyze reduction of U(VI) in the presence of H_2. The initial concentration of sulfate reducing bacteria in the ground water was very low (1 cell/100 ml) compared to that of denitrifiers (450 cells/100 ml) (L.L. Barton, personal communication).

3.4. Amendment

Ethanol (reaction 7) was used as a carbon source. Phosphorus was added because its concentration (< 0.1 mg/l) was found to be too low to sustain growth of bacteria. Sodium trimetaphosphate (TMP), $Na_3P_3O_9$, was used. Readily soluble phosphates were not useful because calcium phosphate precipitated. The concentration of TMP was varied between 0 and 100 mg/l and 20 mg/l was selected for all experiments because it yielded the highest rates of denitrification and sulfate reduction.

3.5. Batch experiments

Numerous experiments were conducted in serum bottles to identify the best amendments (organic carbon compound and phosphorus source) in terms of high yield and fast reaction. Contaminated ground water from well #926 and sand were used in the batch experiments. Sand sampled from the surface was washed before use following the procedure by Kunze and Dixon (1989). This procedure was applied to remove relic organic carbon compounds. Serum bottles (160 ml) with 8 g of desegregated Navajo sandstone were autoclaved at 120°C for 25 min. Then 100 ml of ground water were added. A few drops of a 0.2% resazurin solution were added as a redox potential indicator. Resazurin is colorless at $E_H < -100$ mV and, depending on pH, pink or blue under more oxidizing conditions. The bottles were sealed with a butyl rubber stopper in an aseptic environment in a glove box. A syringe needle was introduced through the stopper to purge the ground water with argon. In this way an anaerobic environment was maintained. To keep the argon gas sterile, a gas filter with 0.2 μm pore size was used. Finally, the bottles were crimped with an aluminum seal. The bottles were then kept at 16°C and 24°C, respectively, for the duration of the experiments.

[1] GC-FAME databases. Aerobes (TSBA [rev. 3.90]) and Clinical Aerobe (CLIN [rev. 3.90]) GC-FAME databases. Midi Microbio, 125 Sandy Drive, Newark, DE 19711, USA.

3.6. Column experiments

The optimum experimental conditions determined by the batch experiments were applied to column experiments. Plexiglas tubes, 5 cm wide, 20 cm long, were used to construct columns. Sand was packed in the columns following a procedure described by Siegel et al. (1994) to ensure homogeneous packing inside the columns. End plates with feed-throughs were tied to the Plexiglas tubes. Long stainless steel screws and bolts, outside the columns, connected the two endplates holding them in place. Argon was flushed through the columns for 2 h to remove oxygen, followed by ten pore volumes of deoxygenated deionized water to ensure complete saturation. The pore volume of each column was determined by weighing it dry and water saturated. A porosity of about 30% was obtained, close to that of sandstone cores (24 to 28%). Introduction of ground water into the column and maintenance of anaerobic conditions was effected by a procedure illustrated in Fig. 2. Water was pumped into the column and replaced by argon in the reservoir, the effluent was collected in an argon filled serum bottle. Between sampling, the column was sealed with wax to prevent penetration of oxygen.

Some batch and column experiments were executed by adding uranyl nitrate, $(UO_2(NO_3)_2 \cdot 6H_2O)$, e.g., to produce enough UO_2 for analytical detection and structure analysis. In other experiments, $Na_2S \cdot 9H_2O$ was added to determine whether a significant amount of uranium is reduced by sulfide. This determination is necessary because of the high sulfate concentration in the ground water and simultaneous

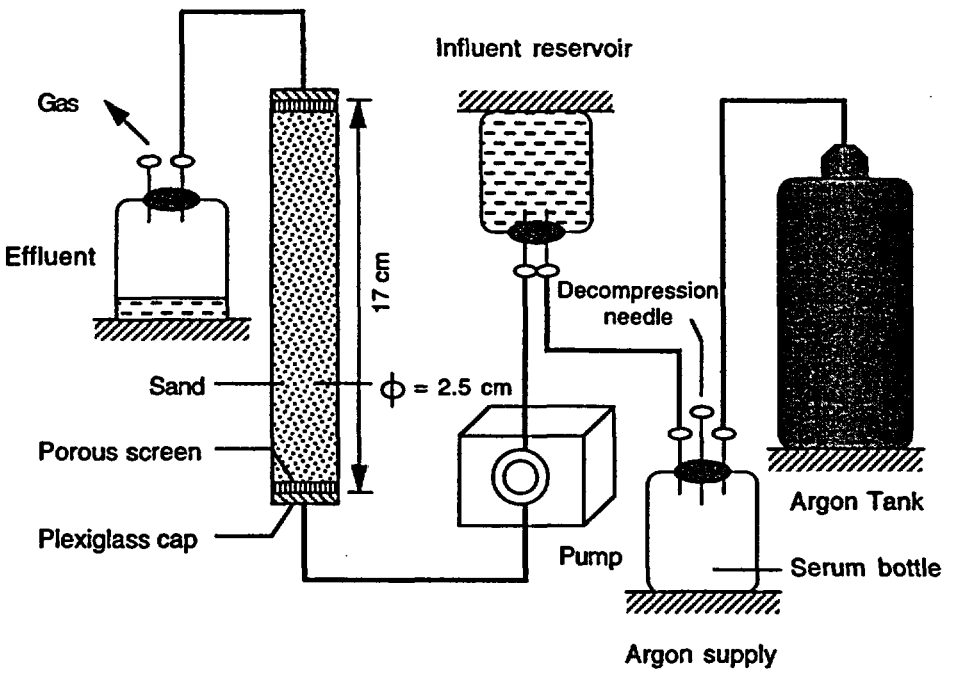

Fig. 2. Schematic diagram of the column system.

reduction of uranium and sulfate (reactions 4 and 6, Section 2). Experiments were conducted to test whether uranium precipitates as uranium phosphate. The ground water was sterilized at 120°C. Ethanol and TMP were added and the concentrations of uranium, nitrate and sulfate were measured over 2 months.

3.7. Analytical procedures

After completion of batch and soil column experiments sandstone samples were taken and deposited on a sample holder to detect uraninite using a JEM-2000FX transmission electron microscope and a Noran TN-5500 EDX element analyzer. The microscope was operated at 200 keV. Electron diffraction analysis was conducted to identify uraninite by its crystal structure. Analysis by environmental scanning electron microscopy (Electro-Scan) was performed to avoid complete drying of the samples and to visualize bacteria. The instrument was operated at ≤ 20 keV. Measurements of nitrate, nitrite, and sulfate were conducted using ion chromatography (IC Dionex DX 500). Before measurement, solutions was filtered through a Nylon Acrodisc syringe filter (0.2 μm pore size; Gelman Science) to remove biomass. A Laser fluorescence uranium analyzer (Scintrex UA-3) was used to measure U(VI) concentrations selectively in solution on the order of microgram/liter with a precision of $\pm 15\%$.

4. Results and discussion

4.1. Denitrification

At 16°C and 24°C biological denitrification in column experiments (reactions 2 and 7, Section 2) was complete within 10 and 3 days, respectively. The nitrate concentration decreased from 1.2 g/l to below the detection limit of the ion chromatograph (0.1 mg/l). The results for 24°C are shown in Fig. 3. Nitrate reduction was followed by an

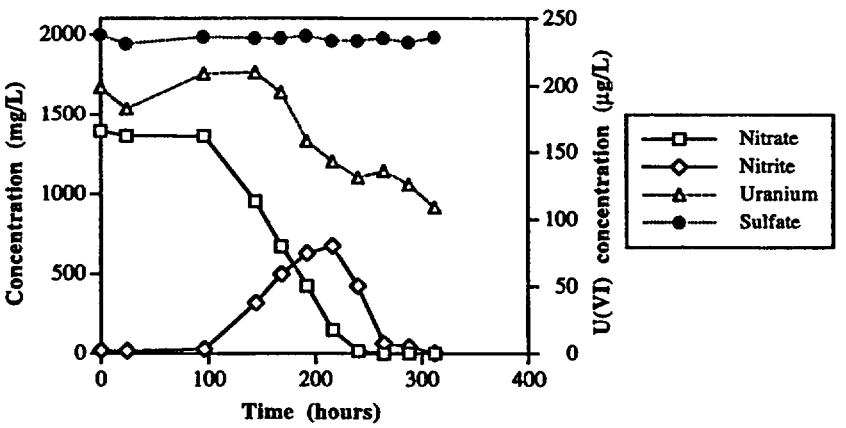

Fig. 3. Denitrification at 24°C using contaminated ground water from the Tuba City site amended with ethanol and trimetaphosphate.

accumulation of nitrite. This phenomenon is due to a higher reduction rate of NO_3^- to NO_2^- than NO_2^- to N_2O and N_2 (Betlach and Tiedje, 1981; Green et al., 1994). The accumulated nitrite is reduced to nitrogen, indicated by the generation of bubbles in the serum bottles.

pH changes were almost insignificant: after amendment with ethanol and TMP pH = 8.6 ± 0.1 was measured. The lowest value in the course of denitrification was pH = 8.2 ± 0.1 and the final value was pH = 8.4 ± 0.1. A much stronger decrease was calculated (pH ≈ 3.2 at 24°C and 3.3 at 16°C) based on the intermediate formation of nitrite and its relatively slow further reduction (Fig. 3). This should lead to a transient accumulation of H^+ in solution:

$$1/2\,NO_3^- + 1/12\,C_2H_5OH = 1/2\,NO_2^- + 1/6\,HCO_3^- + 1/6\,H^+ + 1/12\,H_2O \quad (8)$$

$$1/2\,NO_2^- + 1/8\,C_2H_5OH + 1/4\,H^+ = 1/4\,N_2 + 1/4\,HCO_3^- + 3/8\,H_2O \quad (9)$$

However, the acidity produced by these reactions is buffered (Read et al., 1993) by ion exchange of H^+ with K^+ and Ca^{2+} in the clay. The production of CO_2 during ethanol oxidation lead to precipitation of aragonite/calcite from the $CaCO_3$-saturated ground water at 16°C. A mixture of aragonite/calcite was detected in the sandstone after denitrification.

The sulfate concentration remained constant during denitrification, in agreement with the sequential nature of the process. A decrease in E_H to < -100 mV during denitrification was indicated by resazurin's color change from blue, via pink to colorless at the end of denitrification. In addition, the E_H was measured electrochemically and a value of -70 to -100 mV was obtained.

There is fairly large scattering of the uranium concentration data during nitrate reduction. However, the decrease in the uranium concentration from an initial value of 199 μg/l to 109 μg/l (Fig. 3) at the end of denitrification is significant. Nuttall et al. (1996) showed that this decrease is due to adsorption of uranium on denitrifying bacteria. Additionally, uranium may have been coprecipitated with aragonite/calcite (Section 3.2). During denitrification the calcium concentration in the ground water decreased by 66%.

Experiments with sterilized ground water and TMP in serum bottles showed that the concentrations of uranium, nitrate and sulfate did not change (Fig. 4). There was no precipitation of uranium phosphate.

4.2. Reduction of uranium at low concentration (0.25 mg / l U)

At the end of our denitrification experiments the redox potential in the columns had decreased to ≤ -100 mV. Under this condition sulfate reducing bacteria can be grown (Pfennig et al., 1981; Postgate, 1984). In the presence of sulfate, uranium and sulfate reduction are expected to take place at the same time. To activate *S. putrefaciens*, we added more ethanol to reach a molar ratio of ethanol/sulfate of 2/3 according to reaction 10:

$$3\,SO_4^{2-} + 2\,C_2H_5OH = 4\,HCO_3^- + 3\,HS^- + H^+ + 2\,H_2O \quad (10)$$

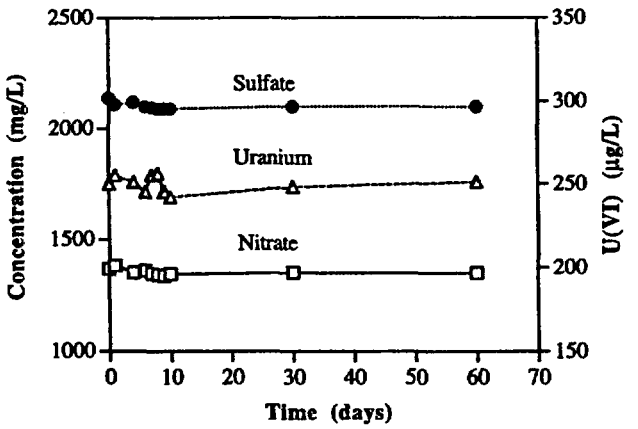

Fig. 4. U(VI), nitrate and sulfate concentrations in ground water amended with ethanol and trimetaphosphate. The indigenous bacteria were heat-killed.

No additional TMP was added, assuming that the microorganisms would use residual phosphate in solution or phosphate from dead denitrifiers. After 2 weeks at 24°C, sulfate reduction was detected by the smell of H_2S and by black spots on the sand containing Fe and S, presumably FeS. The U(VI) concentration in the effluent of the column had decreased to 14 µg/l after 21 days and 0.5 µg/l after 2 months. The concentration of uranium in the uncontaminated ground water is about 1 µg/l. The chemical composition of ground water from well #926 after denitrification and partial reduction of sulfate in a column experiment is given in Table 3, column 3. The concentration of Ca was measured before and after sulfate reduction and was constant, indicating that no aragonite/calcite precipitated. We conclude that uranium was reduced in the course of

Table 3
Chemical composition of contaminated ground water before and after bioremediation (mg/l)

	Well #926, before bioremediation	Well #926, after bioremediation
NO_3	1220	< 0.1
SO_4	1830	1250
U	0.250	0.014
Cd	0.005	0.005
Ca	681	234[a]
Fe	0.05	0.59
Pb	0.05	0.05
Mg	329	264
Mn	0.02	0.76
Mo	0.05	0.05
Se	0.1	0.1
Sr	7.04	3.47

[a]Reached after denitrification and remained constant during reduction of uranium.

sulfate reduction. Table 3 shows that the sulfate concentration decreased by 600 mg/l, indicating that an equivalent concentration of sulfide was produced. Thermodynamically, U(VI) is not stable in the presence of sulfide (HS^-) and should be reduced to U(IV). Therefore, we examined the possibility that uranium was reduced by sulfide and not by the catalytic activity of bacteria. Experiments in serum bottles were conducted at 24°C using ground water with a U(VI) concentration of 250 μg/l to which sodium sulfide was added. The sulfide concentration was varied between 0 and 20 mM. The results are shown in Fig. 5. For sodium sulfide concentrations between 0 mM (control) and 2 mM, there was no correlation with the amount of uranium removed. In all experiments the U(VI) concentration decreased by 35% to 50% after 62 days. Removal of uranium was entirely due to precipitation of aragonite/calcite. Experiments with 10 mM and 20 mM sodium sulfide showed fast removal of U(VI) initially, 75% within the first 3 h (Fig. 5), reaching 98% only after 108 days. Results in Fig. 6 show U(VI) removal at 24°C in the presence of sulfate reducers. The maximum concentration of sulfide generated in this experiment was 4 mM. The rate of U(VI) removal was slower in the beginning but 99% of U(VI) were removed after 36 days. There is no similarity with the respective curves in Fig. 5. In the experiments with 10 and 20 mM sodium sulfide the pH was 10 and the solution was supersaturated with respect to $Mg(OH)_2$ and saponite type clays, in addition to aragonite/calcite. The precipitate from these solutions was analyzed and a saponite-type clay was detected under the electron microscope by conducting energy dispersive X-ray and electron diffraction analyses. The zeta potential of the precipitate was found to be +10 mV. Adsorption of negatively charged U(VI)-carbonato complexes on these particles may explain why U(VI) removal is higher initially than with lower sodium sulfide concentrations.

We conclude that reduction of uranium is mediated by enzymatic activity of sulfate reducing bacteria. Competing reactions are either too slow or too inefficient to explain depletion of uranium to concentrations of 1 μg/l.

Experiments in serum bottles showed that the rate of uranium reduction is slower at 16°C than at 24°C. Results are shown in Fig. 6. The U(VI) concentration decreased from

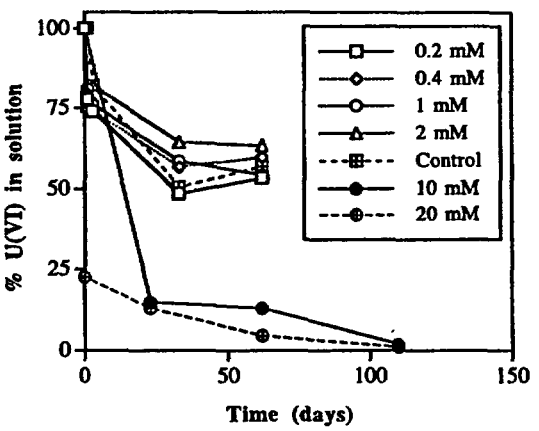

Fig. 5. U(VI) removal from the ground water containing sodium sulfide.

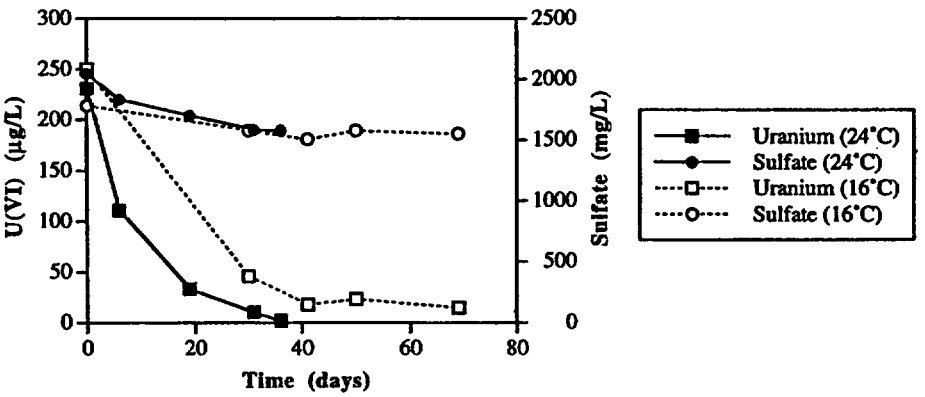

Fig. 6. U(VI) reduction at 16 and 24°C using contaminated ground water from the Tuba City site amended with ethanol and trimetaphosphate.

231 to 1.8 µg/l in 36 days at 24°C and from 250 to 15 µg/l in 69 days at 16°C. Compared to Lovley's results (Lovley et al., 1991) our uranium reduction process is slow. Their reduction rates lead, e.g., to removal of 1.4 g/l of uranium in 1 day. This difference can be explained by the lower initial concentration of sulfate reducing bacteria (on the order of 1 cell/100 ml) in the ground water and by the lower temperatures in our experiments. Lovley et al. inoculated high concentrations of cultured cells (10^8–10^9 cells/100 ml) and incubated them at 30–35°C.

4.3. Reduction of uranium at high concentrations (27–235 mg / l U)

Series of experiments were conducted to test whether uranium can also be reduced enzymatically at high concentrations. After denitrification of the ground water in serum bottles, uranyl nitrate was added together with 5 ml of a stock containing sulfate reducing bacteria to accelerate the uranium reduction. These bacteria originate from the Tuba City ground water but were grown in a separate experiment by adding ethanol and TMP to the contaminated ground water and sand. Initial uranium concentrations varied between 27 mg/l and 235 mg/l and were two to three orders of magnitude higher than in the Tuba City ground water. Uranium concentrations then decreased as a function of time and a dark precipitate formed. The solutions were filtered and the precipitate was separated. To determine the contribution of adsorption of uranium on biomass (dead denitrifiers) to the removal of uranium from solution, a control experiment was conducted without adding sulfate reducers and ethanol. Biosorption was a concern because a lot of biomass ($7 \cdot 10^8$ cells/ml) produced during denitrification.

Fig. 7a shows that uranium is removed from solution by enzymatic reduction, independent of its initial concentration. Final concentrations of U(VI) after 90 days ranged between 0.1 mg/l and 0.2 mg/l. The control experiment [119 mg/l U(VI)] shows the uranium concentration in absence of sulfate reducers and ethanol. The concentration fluctuated in the course of the experiment and a net decrease of 33% was

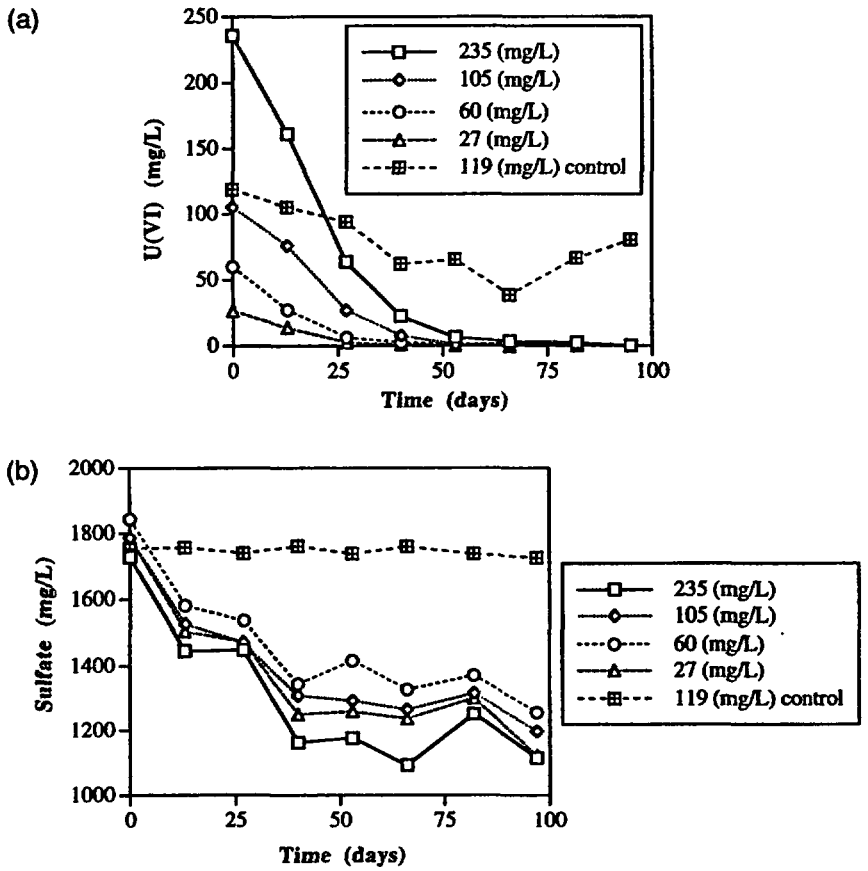

Fig. 7. (a) U(VI) reduction at 24°C in ground water amended with ethanol and trimetaphosphate. U(VI) concentrations were artificially increased by adding uranyl nitrate. (b) Sulfate reduction at 24°C in ground water amended with ethanol and trimetaphosphate. Numbers in legend are initial U(VI) concentrations in solution.

measured after 90 days. This decrease is attributed to biosorption. No dark precipitate was detected and no aragonite/calcite precipitated. Fig. 7b shows the decrease in sulfate concentration observed along with the decrease in the uranium concentration. There was no reduction of sulfate in the control experiment.

4.4. Identification of uraninite

The dark precipitate formed during the experiments with high U(VI) concentration (Section 4.3) was studied by transmission electron microscopy. Fig. 8 shows a bacterium with dark spots on its surface. The spots were analyzed with the help of the EDS microanalyzer attached to the transmission electron microscope. Uranium, calcium and oxygen were found. Electron diffraction analysis showed that the spots are a poorly

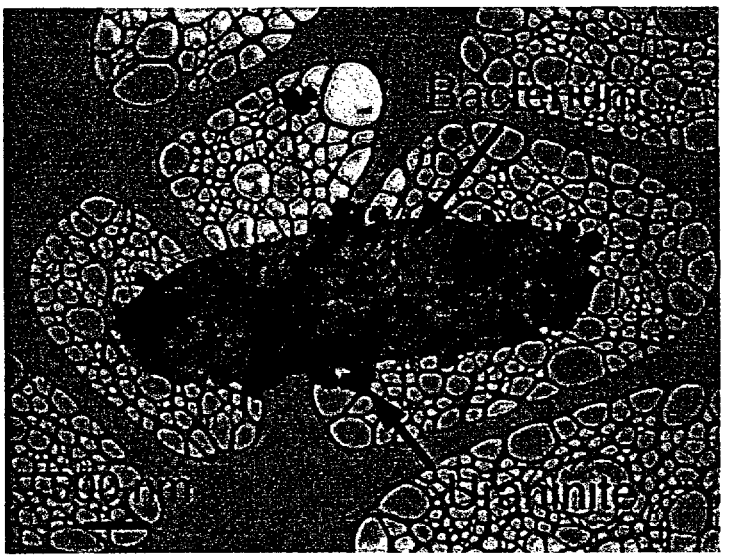

Fig. 8. Bacterium with uraninite particles.

crystallized solid solution of $(U,Ca)O_2$. The d spacings of the Ca-bearing uraninite match those of pure uraninite (Table 4). The presence of calcium in uraninite is not surprising. Natural uraninite usually contains calcium (Janeczek and Ewing, 1992). The ionic radius of Ca (0.112 nm) is close to that of U(IV) (0.10 nm).

4.5. Porosity of the sandstone after production of biomass

After termination of the denitrification/uranium reduction experiments sandstone samples were taken from the column and observed under the ESEM. Fig. 1b shows that there is no evidence of plugging of pores with biomass or aragonite/calcite. The hydrological properties of the sandstone are not deteriorated by enhanced bacterial activity in the ground water. This finding is important, if a microbially catalyzed process were applied for in situ ground water remediation at the Tuba City site. An in situ bioremediation process relies on sufficient conductivity and mixing in the host rock.

Table 4
Comparison of d spacings of Ca-rich uraninite bioprecipitated in ground water from well #926 with the JCPDS data of uraninite

hkl	d spacings of Ca-uraninite (nm)	JCPDS[a] d spacings of UO_2	Difference, %
111	0.311	0.316	1.6
200	0.275	0.274	0.4
220	0.195	0.193	1.0
311	0.163	0.165	1.2

[a]International Center for Diffraction Data, 1979.

5. Conclusions

This study shows that uranium (0.25 to 235 mg/l) can be removed from ground water contaminated with large amounts of nitrate, sulfate and carbonate using bio-catalyzed reactions. After complete denitrification, uranium is reduced to U(IV) and precipitates as uraninite. Simultaneous reduction of a fraction of sulfate to sulfide is observed. Some Mn(IV) and Fe(III) from the sandstone are reduced as well. Enzymatic reduction of uranium was proven unambiguously after all other reactions of uranium in the ground water host rock system were described and understood.

The ground water from the uranium mill tailings site near Tuba City contains the bacteria necessary to catalyze reactions with its contaminants after amendment. The reaction rates can be controlled by the choice of the organic compound to stimulate bacterial growth. Our results provide a basis for the design of an in situ bioremediation process at Tuba City, using indigenous bacteria. The results emphasize the importance of experiments closely simulating the specific conditions of the site to evaluate the potential of bioremediation. The fact that useful bacteria are ubiquitous makes it worthwhile to study other sites with uranium contaminated ground water.

Acknowledgements

The authors thank Dr. Weiliang Gong for TEM work and Neil Butt for sand and column preparation. This work was financially supported by the US. Department of Energy under contract PR 04-94AL633805.507.

References

Abdelouas, A., Lutze, W., Nuttall, H.E., 1998. Chemical reactions of uranium in ground water at a mill tailings site. J. Contam. Hydrol., in press.

Barton, L.L., Choudhury, K., Thomson, B.M., Steenhoudt, K., Groffman, A.R., 1996. Bacterial reduction of soluble uranium: the first step of in situ immobilization of uranium. Radio. Waste. Manage. Environ. Restor. 20, 141–151.

Betlach, M.R., Tiedje, J.M., 1981. Kinetic explanation for accumulation of nitrite, nitric oxide, and nitrous oxide during bacterial denitrification. Appl. Environ. Microbiol. 42, 11074–11084.

DOE, 1994. Site observational work plan for the UMTRA Project at Tuba City, AZ, DOE/AL/62350-160.

E.P.A. Standard Method 9240, 1992. Standard Method for the examination of water and waste water. American Public Health Association (Ed.), 1015 15th Street NW, Washington, DC 20005, 9/73–9/82.

Federal Register, 1995. Environmental Protection Agency (EPA), CFR 40 Part 192, Groundwater Standards for Remedial Actions at Inactive Uranium Processing Sites, Table 1, p. 2866, November, 1995.

Francis, A.J., Dodge, C.J., Lu, F., Halada, G.P., Clayton, C.R., 1994. XPS and XANES studies of uranium reduction by *Clostridium* sp. Environ. Sci. Technol. 28, 636–639.

Gorby, Y.A., Lovley, D.R., 1992. Enzymatic uranium precipitation. Environ. Sci. Technol. 26, 205–207.

Green, M., Shnitzer, M., Tarre, S., Bogdan, B., Shelf, G., Sorden, C.J., 1994. Fluidized bed reactor operation for ground water denitrification. Wat. Sci. Technol. 29, 509–515.

Grenthe, I., Fuger, J., Lemire, R.J., Muller, A.B., Nguyen-Trung, C., Wanner, H., 1992. Chemical thermodynamics of uranium. Elsevier Science Publishing, New York.

Janeczek, J., Ewing, R.C., 1992. Structural formula of uraninite. J. Nucl. Mater. 190, 128–132.

Knowles, R., 1982. Denitrification. Microbiol. Rev. 46, 43–70.
Kunze, G.W., Dixon, J.B., 1989. Pretreatment for mineralogical analysis. In: Kulte, A. (Ed.), Methods of Soil Analysis, Part 1. Physical and Mineralogical Methods, 2nd edn., pp. 91–100.
Lovley, D.R., 1995a. Microbial reduction of iron, manganese, and other metals. In: Donald, L., Sparks, L. (Eds.), Advances in Agronomy, 54. Academic Press, New York, pp. 175–231.
Lovley, D.R., 1995b. Bioremediation of organic and metal contaminants with dissimilatory metal reduction. J. Ind. Microbiol. 14, 85–93.
Lovley, D.R., Phillips, E.J.P., 1986. Organic matter mineralization with reduction of ferric iron in anaerobic sediments. Appl. Environ. Microbiol. 51, 683–689.
Lovley, D.R., Phillips, E.J.P., 1988. Novel mode of microbial energy metabolism: organic carbon oxidation coupled to dissimilatory reduction of iron or manganese. Appl. Environ. Microbiol. 54, 1472–1480.
Lovley, D.R., Phillips, E.J.P., 1992a. Reduction of uranium by *Desulfovibrio desulfuricans*. Appl. Environ. Microbiol. 58, 850–856.
Lovley, D.R., Phillips, E.J.P., 1992b. Bioremediation of uranium contamination with enzymatic uranium reduction. Environ. Sci. Technol. 26, 2228–2234.
Lovley, D.R., Phillips, E.J.P., Gorby, Y.A., Landa, E.R., 1991. Microbial reduction of uranium. Nature 350, 413–415.
Lovley, D.R., Giovannoni, S.J., White, D.C., Champine, J.E., Phillips, J.E., Gorby, Y.A., Goodwin, S., 1993a. *Geobacter metallireducens* gen. nov. sp. nov., a microorganism capable of coupling the complete oxidation of organic compounds to the reduction of iron and other matals. Arch. Microbiol. 159, 336–344.
Lovley, D.R., Roden, E.E., Phillips, E.J.P., Woodward, J.C., 1993b. Enzymatic iron and uranium reduction by sulfate-reducing bacteria. Marine Geol. 113, 41–53.
Nuttall, E., Lutze, W., Barton, L., Choudhury, K., 1996. Preliminary screening results for in situ bioremediation at an UMTRA site, Waste Management '96, Session 45, paper 6, Tucsan, February, 1996.
Peterson, F., Pipiringos, G.N., 1979. Stratigraphic relations of the Navajo sandstone to middle Jurassic formations, Southern Utah and Northern Arizona. U.S. Geol. Survey Prof. Paper 1035-B, 43 pp.
Pfennig, N., Widdel, F., Trüper, H.G., 1981. The dissimilatory sulfate-reducing bacteria. In: Starr, M.P., Stolp, H., Trüper, H.G., Balows, A., Schlegel, H.G. (Eds.), The Prokaryotes, Vol. 1. Springer-Verlag, Heidelberg, pp. 926–940.
Phillips, E.J.P., Landa, E., Lovley, D.R., 1995. Remediation of uranium contaminated soils with bicarbonate extraction and microbial U(VI) reduction. J. Ind. Microbiol. 14, 203–207.
Postgate, J.R., 1984. The Sulfate-Reducing Bacteria, 2nd edn. Cambridge University Press, Cambridge, UK, 208 pp.
Read, D., Lawless, T.A., Sims, R.J., Butter, K.R., 1993. Uranium migration through intact sandstone cores. J. Contam. Hydrol. 13, 277–289.
Rittmann, B.E., Seagren, E., Wrenn, B.A., Valocchi, A.J., Ray, C., Raskin, L., 1994. In Situ Bioremediation, 2nd edn. Noyes Publishers, NJ, USA.
Siegel, M.D., Ward, D.B., Bryan, C.R., Cheng, W.C., 1994. Characterization of materials for a reactive transport model validation experiment. Int. Rep. Sandia National Labs., SAND 94-0189.
Stumm, W., Morgan, J.J., 1981. Aquatic Chemistry. Wiley, New York, pp. 453–461.
Tucker, M., Barton, L.L., Thomson, B.M., 1996. Kinetic coefficients for simultaneous reduction of sulfate and uranium by *Desulfovibrio desulfuricans*. Appl. Microbiol. Biotechnol. 46, 74–77.
U.S.G.S. (United States Geological Survey) method B-0430-85, 1988. MPN of nitrate reducing bacteria, parameter and code, denitrifying bacteria (MPN), 31856. University of Texas, Austin, TX, USA, Bureau of Economic Geology.
Walker, J.F., Helfrich, M.V., Donaldson, T.L., 1989. Biodenitrification of uranium refinery wastewaters. Environ. Progress 8, 97–101.
Wolery, T.J., 1992. EQ3NR, A computer program for geochmical aqueous speciation-solubility calculations. Theoretical Manual, User's Guide, and Related Documentation, version 7.0. UCRL-MA-110662-PT-IV, Lawrence Livermore National Laboratory, Livermore, CA.

Pergamon

Geochimica et Cosmochimica Acta, Vol. 62, No. 13, pp. 2223–2231, 1998

0016-7037/98 $19.00 + .00

PII S0016-7037(98)00140-9

The role of pe, pH, and carbonate on the solubility of UO_2 and uraninite under nominally reducing conditions

IGNASI CASAS,[1] JOAN DE PABLO,[1] JAVIER GIMÉNEZ,[1] M. ELENA TORRERO,[1] JORDI BRUNO,[2] ESTHER CERA,[2] ROBERT J. FINCH,[3,*] and RODNEY C. EWING[3,†]

[1]Department of Chemical Engineering, Polytechnic University of Catalunya, Barcelona 08028, Spain
[2]QuantiSci SL, Parc Tecnològic del Vallès, Cerdanyola 08290, Spain
[3]Department of Earth and Planetary Sciences, University of New Mexico, Albuquerque, New Mexico 87131, USA

(*Received August* 14, 1997; *accepted in revised form March* 26, 1998)

Abstract—Experimental data obtained from uranium dioxide solubility studies as a function of pH and under nominally reducing conditions in a 0.008 mol dm^{-3} perchlorate medium and in a 1 mol dm^{-3} chloride solution are presented. The solubility of extensively characterized uraninite samples from Cigar Lake (Canada), Jachymov (Czech Republic), and Oklo (Gabon) was determined in a solution matching the composition of a groundwater associated with granitic terrain. The redox potential of the test solution was monitored throughout the experimental period.

The results obtained were modeled using aqueous formation constants compiled by the NEA, using stability constants corrected to appropriate ionic strengths. The solubility curves have been adjusted by calculating the value of K_{s4} ($UO_{2(s)} + 2H_2O \Leftrightarrow U(OH)_{4(aq)}$) that gave the best fit with the experimental data. For a low temperature synthetic UO_2, a value of $\log K_{s4}$ of -7.3 was determined, while for uraninites the best fit was obtained with a value of $\log K_{s4}$ of -8.5. A wide range of published UO_2 solubilities can be reproduced by the available database, where experimental conditions were adequately defined in the original experiments.

A lower value of the solubility product of the uranium dioxide phase defined as fuel in the SKB uranium database provides reasonable solubilities for a wide span of experimental results at near to neutral pH. Based on the modeling and using the $\beta_{1,4}$ for the U(IV)-OH complexation given by Grenthe et al. (1992a), a $\log K_{s0}$ ($UO_2(s) + 4H^+ \Leftrightarrow U^{4+} + 2H_2O$) value of -2.3 ± 0.2 is proposed.

Differences in solubility between natural and synthetic samples are attributed to the presence of carbonate in the experiments performed with uraninites, while differences in solubility observed among the natural samples can be correlated to radiation effects at atomic scale. *Copyright © 1998 Elsevier Science Ltd*

1. INTRODUCTION

The cycling of U in natural water systems has received considerable attention since the seminal paper by Hostetler and Garrels (1962); however, the focus of interest has shifted from uranium exploration to the transport and fate of uranium in groundwaters related to the disposal of high-level nuclear waste. Much of the recent work has been to provide thermodynamic data identified as needed by Langmuir (1978) and recently a compilation of selected thermodynamic data has been published by Grenthe et al. (1992a). Additionally, much work has been undertaken in order to determine the thermodynamic and kinetic properties of uraninites (UO_{2+x}). International projects at Poços de Caldas in Brazil, Cigar Lake in Canada and Oklo in Gabon (Miller et al., 1994) have investigated different U ore deposits in order to understand the key hydrogeochemical parameters that determine the mobility of U and other trace metals.

In light of these new data and recent experimental work, it is appropriate to review the transport and precipitation of U in natural waters, particularly with attention to a key variable in the U system: the redox potential. In spite of the controversy associated with the use of redox potentials in natural systems (see Grenthe et al., 1992b, for discussion), U behavior is clearly determined by the oxic/anoxic conditions of natural water systems.

This work presents a series of laboratory experiments which establish the dependence of the solubility of UO_2 on the key variables of pH, pe, and carbonate content. These results are interpreted in light of published selected thermodynamic databases for U (Bruno and Puigdomènech, 1989; Grenthe et al., 1992a). Furthermore, we apply the derived thermodynamic model to UO_2 solubility data obtained from dissolution studies of natural uraninite samples from selected sites: Cigar Lake (Canada), Oklo (Gabon), and Jachymov (Czech Republic). We propose a thermodynamic model for the behavior of U in anoxic environments that is tested against experimental data extracted from the literature.

2. EXPERIMENTAL

2.1. Solid Phases

2.1.1. Uranium dioxide

The solid phase used in the experiments was an unirradiated powdered synthetic uranium dioxide sample suplied by ENUSA (Empresa Nacional del Uranio S.A.), with a particle size ranging between 10 and 50 μm. X-ray powder diffraction (XRD) analysis showed the bulk of the sample to correspond to a stoichiometry of $UO_{2.01}$.

**Present address:* Argonne National Laboratory, Argonne, Illinois 60439-4837, USA.

†*Present address:* Department of Nuclear Engineering and Radiological Sciences, University of Michigan, Ann Arbor, Michigan 48109, USA.

Table 1. Main minerals identified in the uraninite samples.

Mineral	Vol % (est.)		
	Cigar Lake	Jachymov	Oklo
uraninite	45-55	85-90	90-95
"illite"(Al-rich)	30-35		<5
"chlorite"(Fe-rich)	20		<5
calcite		10-15	<5
antigorite (?)	<5		
galena	<5		<5
chalcopyrite	<5		
kaolinite (?)			<5
organic material			<5
quartz			<5
coffinite (?)	?	?	?
pyrite (?)	?		

2.1.2. *Uraninite*

Three uraninite samples were used in the experiments and characterized by a variety of analytical methods that include optical microscopy, XRD, electron microprobe analysis (EMPA), conventional and environmental scanning electron microscopy (SEM and ESEM) with energy dispersive x-ray spectroscopic analysis (EDS), back scattering electron imaging (BSEI), and transmission electron microscopy (TEM). This characterization was performed in both leached and unleached samples (see Casas et al., 1994) showing an uraninite composition described as (U^{+4}, U^{+6}, Pb, Ca, Y, REE) O_{2+x}. The samples came from Cigar Lake (Canada), Jachymov (Czech Republic), and Oklo (Gabon), and they were supplied by AECL (CS615-B2), Harvard Museum (HM 86537), and Los Alamos National Lab. (ORZ-9-005), respectively. In Table 1 a summary of the minerals identified in each sample is presented. For a more complete description of the sample see Casas et al. (1994).

2.2. Test Solutions

Experiments were made at 25°C in three different ionic media: sodium perchlorate, sodium chloride (using powdered UO_2 in both cases), and a synthetic water with the composition of a typical groundwater in a granitic environment (experiments with uraninite samples).

Table 2. Total uranium in solution for the dissolution of UO_2 in $8 \cdot 10^{-3}$ mol dm^{-3} sodium perchlorate.

pH	pe	log [U]
1.56	0.39	-3.87
2.15	1.25	-4.04
2.18	1.22	-4.03
2.81	0.59	-4.62
2.83	1.35	-4.30
2.99	0.49	-4.86
3.35		-5.34
3.57		-5.52
3.66		-5.87
3.80		-5.40
3.84	-0.98	-5.19
3.95	1.72	-6.38
4.17	2.08	-6.28
5.33	0.95	-7.20
6.30		-7.50
6.71	-2.79	-7.18
7.80		-7.20
9.41	-1.33	-7.10

2.2.1. *Sodium perchlorate*

Solutions were prepared from sodium perchlorate Merck® p.a., used directly as supplied and doubly distilled water. The sodium perchlorate concentration was 0.008 mol dm^{-3} to simulate a noncomplexing medium of low ionic strength.

2.2.2. *Sodium chloride*

NaCl solutions were prepared from sodium chloride Merck® p.a., used directly as supplied, and doubly distilled water. A sodium chloride concentration of 1 mol dm^{-3} was used as an approach to the conditions expected in high ionic strength media.

2.2.3. *Synthetic granitic groundwater*

A synthetic groundwater (GW) test solution was prepared to simulate the composition of a groundwater in equilibrium with granite (Sandino et al., 1991). The solution is representative of a complexing medium of low ionic strength, as found in a granitic environment.

2.3. Experimental Procedure

Prior to the experiments, the solid phases were pretreated by immersion in diluted perchloric acid for 24 h in order to eliminate fines, oxidized phases, or, in general, more reactive phases. Afterwards, the solids were washed several times with doubly distilled water to eliminate the excess acid and, finally, transferred to the vessel with the test solution. In all these steps reducing conditions were maintained by hydrogen bubbling in the presence of a palladium catalyst.

Test solutions were continuously purged with hydrogen. The gas used was nominally 99.999% pure. The only exception was for the experiments performed with uraninites in the synthetic granitic groundwater, where mixtures of hydrogen and carbon dioxide (1%) were used. In all cases, the gas stream was initially bubbled through a solution of Cr(II) in contact with a Zn/Hg amalgam in order to avoid any possibility of introducing oxidants into the system. In the experimental vessel, hydrogen gas and a palladium black catalyst were used to ensure reducing experimental conditions.

Once the solid was introduced into the experimental vessel, samples were taken and analyzed at various times until constant total U concentrations (±5%, the error range of the U analysis for the levels determined) as well as pH readings (±0.1) were reached. At this point, equilibrium was assumed, the pH was shifted to a new value, and the procedure restarted. To shift the pH of the test solution to more acidic values, either perchloric or hydrochloric acid was used, depending on the ionic medium. A carbonate-free diluted solution of sodium hydroxide was used to increase the pH. Samples were immediately filtered through a 0.22μm MILLIPORE®. The analyses were usually completed in few hours after sampling. When this was not possible and the sample had to be stored before analysis, the solution was acidified by adding a small volume of concentrated nitric acid.

2.3. Analysis

The pH of the solutions was monitored by means of a calibrated, combined-glass electrode. The redox potentials were measured with a platinum electrode. The measurements were made against the silver/silver chloride and KCl saturated reference of the combined glass electrode. Under the experimental conditions of this work the measured Pt-electrode potential is likely to correspond to a mixed potential because it will also respond to pH. However, it seems to give a reasonably good indication of the redox state of the system (see Results section).

Uranium was determined using the Scintrex® UA-3. Analytical problems may arise in the experiments performed in chloride media because this anion interferes with the fluorimetric method. However, the relatively high U concentrations in these experiments allowed them to be diluted prior to analysis, so that the chloride values were below

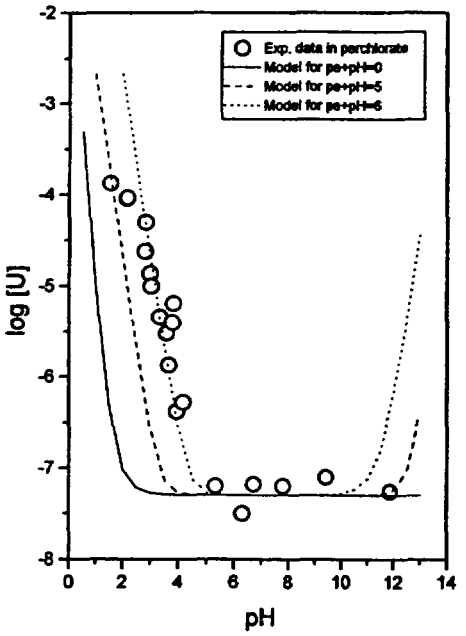

Fig. 1. Experimental solubilities as total uranium concentrations in solution for the dissolution of uranium dioxide in 8×10^{-3} mol dm^{-3} sodium perchlorate test solution. Solid line corresponds to the calculated solubility.

the level where interferences may affect determinations (de Pablo et al., 1992).

3. RESULTS AND DATA TREATMENT

3.1. Uranium Dioxide Solubility in Perchlorate Medium

The results are given in Table 2 and Fig. 1. They are presented as the logarithm of the solubility (given as the total concentration of U in solution) as a function of pH. The redox potential measurements are given for most sampled solutions.

Hydroxo-complexes of U(IV) and U(VI) are the predominant aqueous complexes under these experimental conditions. Formation constants given in the recent NEA compilation (Grenthe et al., 1992a) were used throughout this paper. Formation constants at different ionic strengths were calculated (see Table 3) using the Specific Interaction Theory (SIT) method (Grenthe et al., 1992a). The activity coefficients for this correction were also taken from Grenthe et al. (1992a) (for the uranyl-hydroxo complexes (1,4) and (2,1) the activity coefficients were not available, and the calculations were not made; however, these two complexes are not significant under the experimental conditions).

Predominance diagrams show the possibility of coexistence of an U(IV) solid phase with U(VI) aqueous complexes, in case where strictly reducing conditions are not achieved (Fig. 2a and 2b). For this reason, the solubility model must include all the U(IV) and U(VI) species calculated for different values of oxygen fugacities (identified in our case to oxygen partial pressures: P_{O2}). Considering the water-oxygen equilibrium reaction:

$$O_2(g) + 4H^+ + 4e^- \Leftrightarrow 2H_2O \qquad (1)$$

Table 3. Thermodynamic constants for uranium at 25°C from Grenthe et al. (1992a), except solid phases marked with an asterisk, from Bruno and Puigdomènech (1989). All aqueous species formation and solid dissolution reactions are related to U^{4+}.

Aqueous species	log β (I=0)	log β (I=8 mM)	log β (I=1 M)
UO_2^{2+}	-9.04	-9.36	-10.85
UOH^{3+}	-0.54	-0.78	-1.76
$U(OH)_2^{2+}$	-2.36	-2.76	-4.18
$U(OH)_3^+$	-3.93	-4.17	-6.08
$U(OH)_{4(aq)}$	-5.13	-5.61	-7.30
UO_2OH^+	-14.24	-14.64	-16.06
$UO_2(OH)_{2(aq)}$	≤-19.34	≤-19.90	≤-22.35
$UO_2(OH)_3^-$	-28.78	-29.1	-30.40
$UO_2(OH)_4^{2-}$	-42.04		
$(UO_2)_2OH^{3+}$	-20.78		
$(UO_2)_2(OH)_2^{2+}$	-23.7	-24.42	-27.74
$(UO_2)_3(OH)_4^{2+}$	-39.02	-40.15	-44.87
$(UO_2)_3(OH)_5^+$	-42.67	-43.88	-49.36
$(UO_2)_3(OH)_7^-$	-58.12	-57.00	-64.94
$(UO_2)_4(OH)_7^+$	-58.06	-59.66	-66.75
$UO_2CO_{3(aq)}$	0.64	0.00	
$UO_2(CO_3)_2^{2-}$	7.90	7.26	
$UO_2(CO_3)_3^{4-}$	12.56	12.24	
$U(CO_3)_4^{4-}$	35.12		
$U(CO_3)_5^{6-}$	34.00		
UCl^{3+}	1.72	1.40	0.38
UO_2Cl^+	-8.87	-9.35	-10.45
$UO_2Cl_{2(aq)}$	-10.14	-10.70	-12.47
Solid phases	**log K_{s0} (I=0)**	**log K_{s0} (I=8mM)**	**log K_{s0} (I=1M)**
$UO_{2(c)}$	-4.85		
$UO_{2(fuel)}$ (*)	-1.60	-1.12	0.57
$UO_{2(am)}$ (*)	0.50		
$U_3O_{7(c,\beta)}$	1.29		
$U_4O_{9(c)}$	-4.11		
$UO_2(OH)_{2(c,\beta)}$	13.97		
$UO_{3(c,\gamma)}$	16.74		

with an equilibrium constant defined as:

$$K = \frac{a_{H_2O}^2}{P_{O_2} \cdot \{H^+\}^4 \cdot \{e^-\}} = 10^{83.12} \qquad (2)$$

the following relationship is obtained:

$$\log P_{O2} = 4(pH + pe) - \log K + 2\log a_{H2O} \qquad (3)$$

In this way, two main experimental variables are required to define the solubility: pH and pe. Calculations were made for different constant oxygen partial pressures by using a simplified form of Eqn. 3:

$$pe + pH = n \qquad (4)$$

being n a constant term which takes, in our case, any value

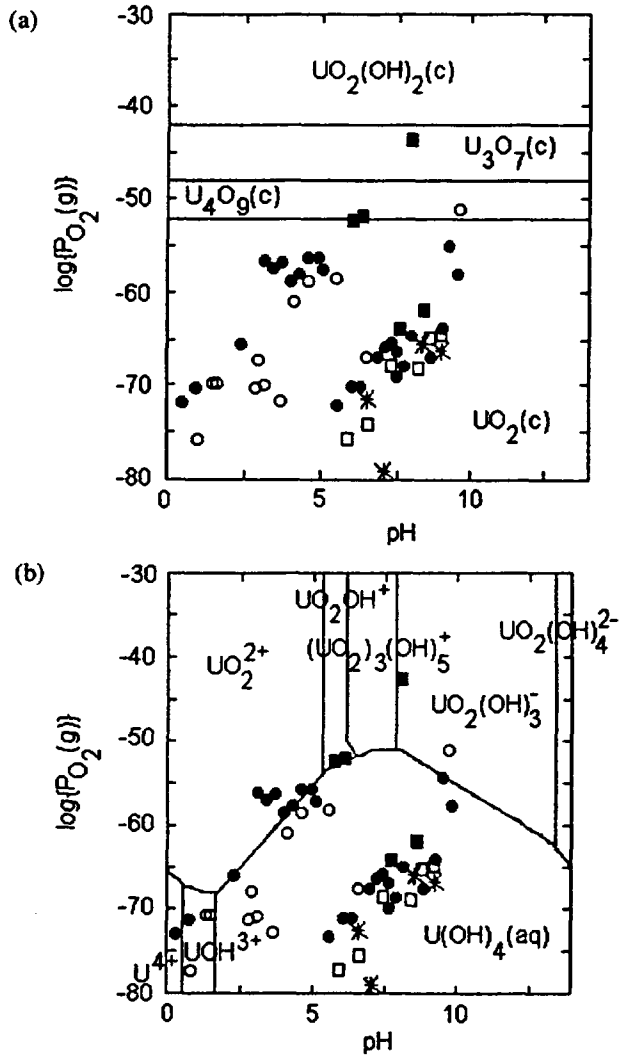

Fig. 2. Predominance diagrams of uranium as a function of logarithm of oxygen partial pressure and pH: (a) Predominant solid phases; (b) Predominant aqueous species. Experimental pe (corrected to log P_{O2})-pH measurements of the experiments: perchlorate (open dots), chloride (full dots), Cigar Lake (open squares), Jachymov (full squares), and Oklo (stars).

between 0 (water/hydrogen equilibrium, log $P_{O2} \cong -83$) and 7.3 (UO_2:U_4O_9 transition, log $P_{O2} \cong -54$), to fall within the stability range of UO_2.

The solubility curves calculated are presented in Fig.1. In addition, the best fit was determined by varying the value of K_{s4}, which is obtained by a combination of K_{s0} and $\beta_{1,4}$. In this way, errors that may arise from the uncertainties on the values of these two constants are circumvented. The relative credit that can be give to the values of these two constants are clearly expressed in the database compilation used (Grenthe et al., 1992). A similar approach has recently been used by Shock et al. (1997) when deriving U thermodynamic properties at high temperature and pressure.

As the value of n is augmented (Fig. 1), an important increase of the calculated total U concentration in solution is observed at both acidic and alkaline pH, due to the predominance of uranyl ion and uranyl-hydroxo complexes in solution, respectively. At neutral pH values the solubility is not significantly affected in the range of values of n used. This is due to the high stability of the fourth hydroxo complex of U(IV), predominant in this pH range.

The logarithm of K_{s4} which gives the best fit to the data (Fig. 1) is −7.3, with a value of n of 6. The experimentally measured pH and pe pairs give a range of values for n of 4.5 ± 1.5. The experimental results show a large scatter, but with a fairly good agreement with the theoretically determined value of n (see Fig. 1). This comparison provides confidence in the use of Eqn. 4, which stresses the important role of the redox potential in the solubility of UO_2(s).

Table 4. Total uranium concentration (mol dm^{-3}) in solution for the dissolution of UO_2 in 1 mol dm^{-3} sodium chloride.

pH	pe	log [U]
1.06	1.62	-3.73
1.54	1.93	-3.80
2.27	2.38	-3.68
2.70	3.80	-3.64
2.73	3.70	-3.63
3.10	3.63	-3.60
3.32	2.52	-3.77
3.84	2.40	-3.97
4.23	2.21	-4.67
4.69	1.84	-5.54
4.81	1.34	-4.56
5.34	-2.62	-5.41
5.90	-2.84	-6.00
6.30	-3.23	-6.99
6.84	-2.92	-7.14
7.05	-2.76	-6.95
7.09	-2.60	-7.26
7.14	-3.84	-6.52
7.17	-2.92	-7.36
7.49	-3.80	-6.89
7.67	-2.91	-6.67
8.10	-4.02	-7.36
8.29	-3.41	-6.62
9.07	-1.86	-7.03
9.19	-3.11	-6.72

3.2. Uranium Dioxide Solubility in Chloride Medium

The results are given in Table 4 and Fig. 3. A plateau of solubility values is evident for pH values lower than 4. For the rest of the pH range, the data are comparable to those obtained in perchlorate medium.

In this case the modeling included, in addition to the hydroxo complexes, the U(IV and VI)-chloride complexes:

$$UCl^{+3}, UO_2Cl^+, UO_2Cl_2(aq) \quad (5)$$

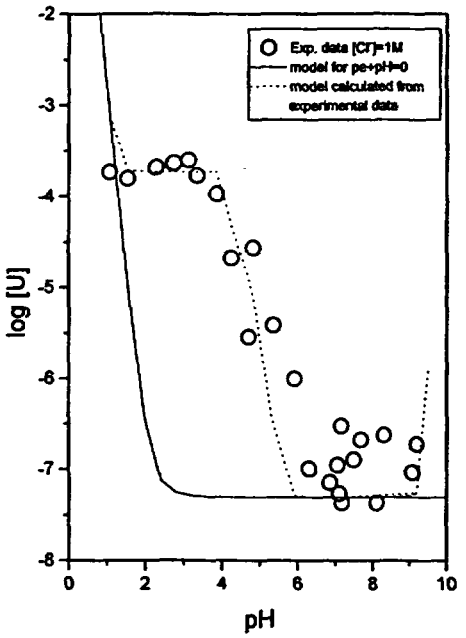

Fig. 3. Experimental solubilities as total uranium concentrations in solution for the dissolution of uranium dioxide in 1 mol dm−3 sodium chloride test solution. Solid line corresponds to the calculated solubility.

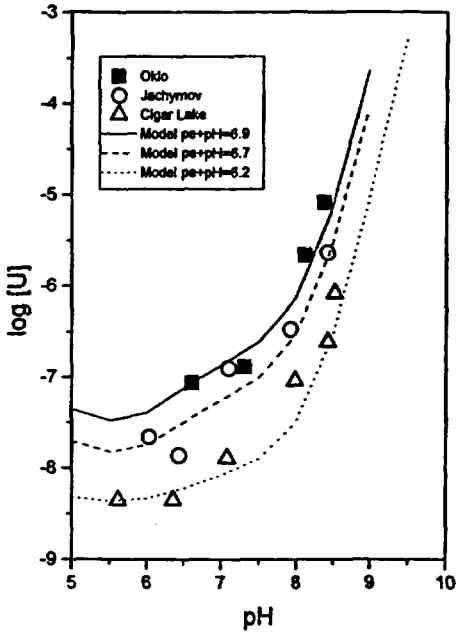

Fig. 4. Experimental solubilities as total uranium concentration in solution for the three experiments of dissolution of uraninite samples. Solid lines correspond to the calculated solubilities.

The formation constants were corrected to 1 mol dm^{-3} (see Table 3), using the specific interaction theory (SIT). Owing to the unique character of the solubility plateau, the calculations were made using as input the experimental pH-pe pairs. Also, we used the same value of K_{s4}, optimized in the previous section, corrected to the corresponding ionic strength. The model obtained is shown as a dashed line in Fig. 3 and compared with the model calculated for a pe + pH value of zero, shown as a solid line.

A fairly good agreement was found between calculated and experimental data. In addition, the solubility plateau was clearly reproduced for pH's lower than 4. The experimental pe values of this pH range appear to follow the potential of the equilibrium between U(VI) and U(IV) aqueous species (see Fig. 2b) within the fairly large uncertainty of the Eh measurements. This is somewhat surprising due to the low concentration levels of the aqueous species. At this point we can only speculate about the redox buffering role of the active UO_{2+x} surface, which could be similar to the one posed by mixed oxide phases like Fe_2O_3 (White, 1990).

3.3. Uraninite Solubility in Synthetic Granitic Groundwater

The results obtained are presented in Fig. 4 and Table 5. The experimental values of (pH + pe) pairs for the three experiments were (3 ± 1), (7 ± 2) and (3 ± 1) for Cigar Lake, Jachymov, and Oklo, respectively.

The modeling exercise included in this case also the U(VI)-carbonato-complexes because U(IV)-carbonato complexes will never be significant under the experimental conditions (Grenthe et al., 1992a). The equilibrium constants used were those corrected at 0.008 mol dm^{-3}, close to the ionic strength of the synthetic granitic groundwater. Initially, we used the same value of K_{s4} as in the previous analysis. However, the best fits were obtained with a value of log K_{s4} of −8.5 and n (pe + pH) values that ranged from 6.2 to 6.9 depending on the sample (Fig. 4).

3.4. Comparison to Previous Work

The model used in this study was compared to previous data for the dissolution of uranium dioxide under nominally reducing conditions (Gayer and Leider, 1957; Galkin and Stepanov, 1961; Tremaine et al., 1981; Ryan and Rai, 1983; Rai et al., 1990). These data are presented in Fig. 5. The theoretical solubilities shown in the figure have been calculated using the same K_{s4} values determined in our experiments with UO_2 ($\log K_{s4} = -7.3$) and with uraninites ($\log K_{s4} = -8.5$), and the best fit has been obtained by calculating the solubilities for different values of n. In the absence of measured redox potentials in these studies, it is not possible to choose the best model.

3.4.1. Crystalline uranium dioxide

The data corresponding to the work of Parks and Pohl (1988) are presented in Fig. 6. These solubility measurements were

Table 5. Total uranium concentrations (mol dm^{-3}) from natural uraninites dissolution in synthetic granitic groundwater.

CIGAR LAKE			JACHIMOV			OKLO		
pH	pe	log [U]	pH	pe	log [U]	pH	pe	log [U]
5.61	-3.84	-8.30	6.03	1.40	-7.66	6.61	-3.63	-7.06
6.36	-4.09	-7.94	6.44	1.30	-7.86	7.31	-6.52	-6.88
7.06	-3.57	-7.89	7.10	-2.65	-6.90	8.12	-3.65	-5.66
7.98	-4.24	-7.04	7.92	-2.20	-6.47	8.39	-4.36	-5.08
8.43	-3.72	-6.60	8.43	1.40	-5.73			
8.53	-3.60	-6.08						

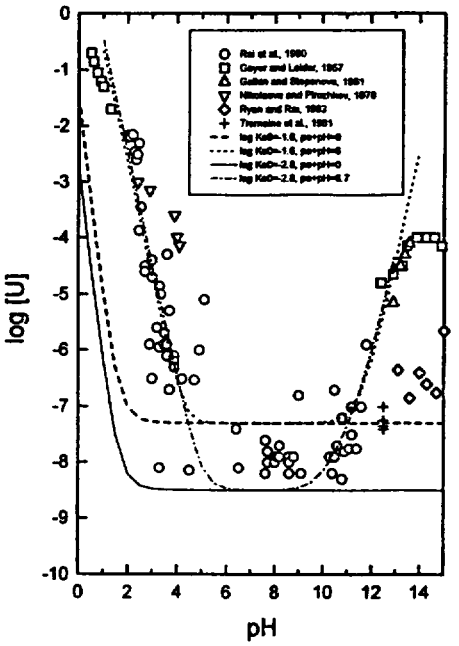

Fig. 5. Uranium dioxide solubility data obtained under nominally reducing conditions, corresponding to values extracted from the literature as given in the figure legend.

made between 25 and 300°C. Their U levels are the lowest reported. From pH 4 up to 10, U concentrations are below $10^{-9.5}$ mol dm^{-3} and are readily fitted assuming the K_{s0} and the $\beta_{1,4}$ proposed by the NEA, as indicated by the solid line in Fig. 6. From those values a log K_{s4} of −9.8 is calculated. Also, these experimental data more closely follow the NEA model under reducing conditions. There is a slight discrepancy at acidic pH values, although the more noticeable disagreement

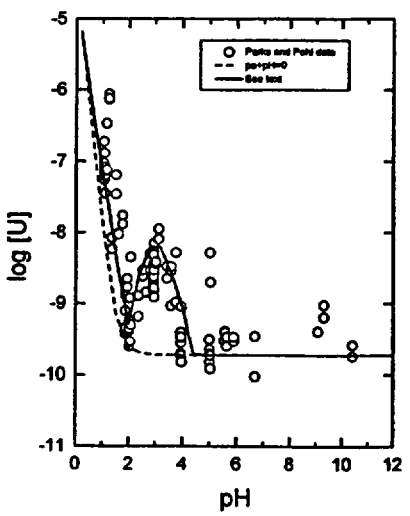

Fig. 6. Parks and Pohl uranium dioxide solubility data obtained under reducing conditions. Dashed line corresponds to UO2 solubility calculated under strict reducing conditions. Solid line is calculated with pe-pH pairs of values following the pairs corresponding to the equilibrium between U(IV) and U(VI).

occurs at pH 3, with a solubility peak that cannot be explained by the different hydroxo-complexes that may be formed. The possibility of U(IV)-fluoride complexation was postulated as an explanation of this abnormal behavior of the system. However, the effect is too large, and the authors themselves expressed skepticism at this explanation. Oxidation of the U in solution is a possible explanation.

As compared to previous models, we note that for (pe + pH) = 6, the increase of solubility occurs at the pH where Parks and Pohl (1988) observed the peak of solubility. This pH corresponds to the one at which aqueous U(VI) attains its largest predominance area (see Fig. 2b). In addition, the solubilities determined by Parks and Pohl (1988) at pH values lower than three are larger than predicted with the NEA model. As a modeling exercise, we used a set of redox potentials following the same trend as obtained in our experiments (see Fig. 2) to calculate the solubility curve which is presented in Fig. 6 as a solid line. The experimental peak in solubility obtained by Parks and Pohl (1988) at pH = 3 is reproduced by these calculations. The calculations also show that slight variations of pe at this pH lead to important differences in solubilities, which could as well account for the large range of U concentrations found by Parks and Pohl (1988) around this pH.

4. DISCUSSION

4.1. Natural Systems

The interpretation of our experimental results can be applied to observations made in natural systems. We concentrate on a widely studied and well characterized system, the natural U deposit located in Cigar Lake, Canada.

The Cigar Lake system has been extensively studied as a natural analogue of a spent nuclear fuel repository. The U ore is located at 450 m depth, and careful characterization of the site has demonstrated that Eh values as low as −243 mV can be measured in the ore zone (Cramer and Smellie, 1994). This measurement corresponds to a pe value of −4.11 and taking into account the corresponding measured pH of 7.37, we obtain: pH + pe = 3.26.

This redox potential, accurately measured, corresponds to the least oxidized zone of the deposit and corresponds to a reducing natural environment. However, the above result shows the possibility of limited oxidation of the aqueous U(IV) species. In fact, the field determinations are close to the values measured in this study in the dissolution experiment of uraninite from Cigar Lake. Hence, the mobilization of U in reducing environments can occur by only slight changes on the surrounding conditions, even if the solid phase is chiefly in its reduced form.

4.2. Uranium Dioxide Crystallinity

The issue of the different degrees of solubility assigned to solid phases with different degrees of crystallinity has not yet been resolved. Two principal solid phases may define the experimental solubilities under reducing conditions. Assuming the solubility reaction is written in the form

$$UO_2(s) + 4\,H^+ \Leftrightarrow U^{4+} + 2\,H_2O \qquad (6)$$

their solubility products are:

$$\log K_{s0}(UO_2cr) = -4.85$$

$$\log K_{s0}(UO_2f) = -1.6$$

The first is applied to a well crystallized uranium dioxide (Grenthe et al., 1992a), while the second was the solubility of synthesized uranium dioxide or actual spent nuclear fuel (Bruno and Puigdomènech, 1989).

Amorphous UO_2 solid has a solubility product of $\log K_{s0}$ (UO_2am) = 0.5 (Grenthe et al. 1992a). However, there are discrepancies in the identification and solubility of this phase. Rai et al. (1990) used an amorphous uranium dioxide and presented an XRD diffractogram that showed broad diffraction maxima, characteristic of a poorly crystalline solid. However, their solubility measurements give values comparable to those obtained in this study for highly crystalline solids, which were also checked by XRD analysis for the degree of crystallinity (Aguilar et al., 1991).

A close examination of the overall dissolution process may clarify these discrepancies. Bruno et al. (1991) studied the kinetics of dissolution of uranium dioxide using a solid phase identical to the powdered sample used in the present work. The overall dissolution reaction showed a rapid and relatively large initial release of U, that after few hours decreased until equilibrium, or steady-state, was reached (after approximately 2 weeks). These data were interpreted as the dissolution of an oxidized surface phase, releasing U(VI) into solution. Owing to the hydrogen and the Pd catalyst, this U is reduced to U(IV) that subsequently reprecipitates. This freshly formed phase will determine the final solubility. The degree of crystallinity of this layer is difficult to determine although it will likely correspond to a less crystalline phase than that of the bulk sample. This would explain the agreement between our determinations and those of Rai et al. (1990). Such a mechanism explains the U concentrations generally attained at neutral pH values of 10^{-7} -10^{-8} mol dm^{-3} in different studies of solids obtained from different sources, including from spent nuclear fuel (Forsyth and Werme, 1992).

The mechanism of dissolution was carefully studied in chloride medium following the change in composition of the solid surface by means of x-ray photoelectron spectroscopy (XPS) observations at various stages of the dissolution process (Torrero et al., 1991). In general, the aqueous U concentrations showed the same initial rapid release and subsequent precipitation. The XPS data, on the other hand, allow evaluation of the average U(VI)/U(IV) ratios in a surface layer of approximately 50–100 Angstrom thickness. These determinations showed the presence of an oxidized overlayer that was dissolved during the first stage of the experiment, leading to a less oxidized solid surface. These observations provide some confidence in the proposed mechanism and stress the possibility of a common phase being responsible for the measured solubilities. This raises the issue of the amorphous uranium dioxide in the NEA database with a solubility product of 0.5. This solid phase gives, at neutral pH values, solubilities as high as $3 \cdot 10^{-5}$ mol dm^{-3} (Bruno et al., 1987). Based on the more recent results presented in this work, we doubt that the appropriate redox conditions were successfully maintained in the solubility experiments from which this solubility product was derived. At this point, we consider the reevaluation of the solubility product of the so-called uranium dioxide fuel based on the U concentrations measured in this study.

A modeling exercise was made with all the data presented in this work, including the results taken in the literature shown in Fig. 5 (Gayer and Leider, 1957; Galkin and Stepanov, 1961; Tremaine et al., 1981; Ryan and Rai, 1983; Rai et al., 1990). From the best fit obtained for the model and using the $\beta_{1,4}$ formation constant for the fourth U(IV)-OH complex given by Grenthe et al. (1992a), a logarithm of the solubility product of -2.3 ± 0.2 is proposed. A value close to this can also be obtained by a different approach. The possible effect of grain size on solubility is given by the following equation (Stumm and Morgan, 1981):

$$\log K_{s0} = \log K_{s0(S=0)} + [(2/3) \cdot \gamma/(2.3 \cdot R \cdot T)] \cdot S \quad (7)$$

where S is the molar surface area and γ is the surface free energy. A value of $\gamma = 2.1$ (± 0.2) J m^{-2} was used (Bruno, 1989). We also measured BET specific surface areas of the different solids under study. Substituting these measured surface areas in Eqn. 7 no significant difference of the $\log K_{s0}$ was obtained. However, as said above, the formation of an amorphous or microcrystalline solid surface can be assumed from the reaction mechanism. For that reason, we performed a BET measurement of a micro-crystalline UO_2 (as showed by broad peaks in its XRD pattern). A molar surface area of 9000 (± 20) m^2 mol^{-1} was determined. With this value, and using $\log K_{s0(S=0)} = -4.85$, a $\log K_{s0}$ of -2.7 ± 0.2 was obtained, in fairly good agreement with the one determined by the model. In the experiments performed with uraninites, in which the model used the logarithm of K_{s0} of -4.85, we must consider the presence of carbonate in the test solution used in these experiments. The formation of strong U(VI)-carbonate complexes stabilizes U(VI) in solution and prevents its subsequent reduction and precipitation. XPS studies have shown that in the presence of carbonate in solution, the composition of the solid surface layer is close to stoichiometric UO_2, while under similar experimental conditions but in the absence of carbonate, the final solid surface showed different degrees of U oxidation (Bruno et al., 1995).

The final subject of discussion considers the differences in uraninite solubilities. In the experimental results we observed the highest solubilities using the Oklo sample, which were approximately 1 order of magnitude higher than those obtained with the sample of Cigar Lake (Fig. 4). These differences may be discussed as follows: although UO_2 and uraninite are both considered to be highly radiation resistant (hence UO_2 is used as a nuclear fuel) and remain crystalline despite high radiation doses (Johnson and Shoesmith, 1988; Janeczek et al., 1996), there are well documented radiation effects at the atomic scale, such as the increase of the unit cell parameter (Weber, 1981, 1984; Janeczek and Ewing, 1991; Matzke and Wang, 1996) and an increase in the release of recoil nuclei from disordered regions of the structure (Eyal and Fleischer, 1985; Vance and Gascoyne, 1987). Natural uraninites experience very high radiation doses due to alpha-decay of radionuclides in the decay chains of U and Th. The natural samples from Cigar Lake, Jachymov, and Oklo are very old, and the doses (in displacements per atom) are calculated to be 750, 200, and >1000 dpa, respectively. Although the uraninites remain crystalline due to

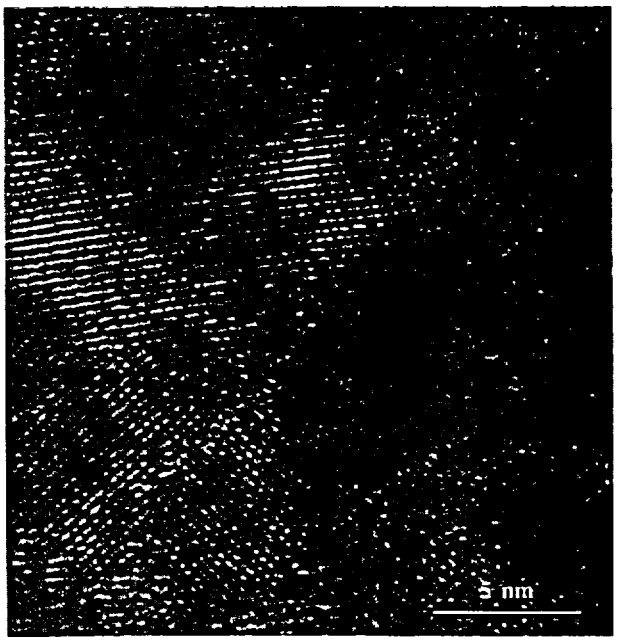

Fig. 7. HRTEM micrograph of uraninite from the border of the natural fission reactor zone 10 (SF29: 91.67 m) at Oklo in Gabon. The image shows that the uraninite grain consists of up to approximately 10nm large nanocrystals with large angle grain boundaries. The nanocrystalline aggregate also contains amorphous regions with inclusions of <1 nm large crystallites as observed in the lower left corner of the image (Micrograph courtesy of Keld Alstrup Jensen).

relatively rapid annealing of radiation-induced defects (Eyal and Fleischer, 1985), there are clear effects on the microstructure (Fig. 7). The highly damaged uraninite consists of domains with low angle grain boundaries or even distinct crystallites with high angle grain boundaries. Isolated areas of amorphous material may form at the grain boundaries, and there may be chemical segregation (e.g., Pb) along the grain boundaries (Janeczek and Ewing, 1995). Additionally, helium bubbles form in the structure due to the alpha particles. All of these features may lead to increased solubility of the Oklo sample as compared to Cigar Lake uraninite.

5. CONCLUSIONS

Uranium dioxide solubilities have been experimentally determined under nominally reducing conditions in a dilute perchlorate medium and in highly concentrated chloride solutions, as an analogue of the ionic strength of groundwaters encountered in granitic and saline environments, respectively. The key experimental variables, pe and pH, have been monitored throughout the experiment. In another series of experiments, the solubilities of three natural uraninites from Cigar Lake (Canada), Jachymov (Czech Republic), and Oklo (Gabon) were determined under the same conditions in a test solution matching the composition of a groundwater in equilibrium with granitic bedrock.

In all cases, measured solubilities were larger than expected for strictly reducing conditions, according to the U databases used (Grenthe et al., 1992a; Bruno and Puigdomènech, 1989), corrected to the corresponding ionic media. In chloride medium, a plateau of solubilities was determined for pH values lower than 4. The increase in solubility under alkaline pH values was much larger for the experiments performed with uraninites in a synthetic granitic groundwater.

The experimentally measured redox potentials have shown that although U may be maintained in its reduced form in the solid phase, it can be at least partially oxidized in the aqueous phase, resulting in the increased solubilities observed. By using the experimental pe values, the solubilities can be approximately reproduced in all media. In chloride media, even the plateau of solubility obtained was reproduced by the introduction of the experimentally determined pe data into the calculations. The experiments performed in the synthetic groundwater have shown that the increase of solubilities at alkaline pH values is probably due to complex formation between the U (VI) formed and the carbonate present in the test solution. The experiments performed with the uraninite samples were better reproduced by using a $\log K_{s4}$ value of -8.5. For the remaining experiments (using uranium dioxide), the best agreement between calculated and measured U concentrations was obtained by using a more soluble phase, with a $\log K_{s4}$ value of -7.3. Experimental solubilities in the literature determined under nominally reducing conditions can also be reproduced with the available databases by considering a partial oxidation of U in the aqueous phase.

A lower value of the solubility product of the uranium dioxide fuel phase (Bruno and Puigdomènech, 1989) gives more representative solubilities for a wide span of experimental results at near neutral pH (both for the results obtained in this work and previous studies). From the modeling exercise, a tentative logarithm of the solubility product (K_{s0}) of -2.3 ± 0.2 is proposed.

Differences in solubility between natural and synthetic samples are attributed to the presence of carbonate in the experiments performed with uraninites, while differences in solubility observed between the natural samples can be correlated to radiation effects at atomic scale.

Acknowledgments—We are indebted to C. Francis of the Harvard Museum, D. Curtis of Los Alamos National Laboratory, and P. Sargent of Atomic Energy of Canada, Ltd. for the uraninite samples. X. Alcober and F. García are acknowledged for the XRD and the XPS determinations, respectively, of the UO_2 samples. We are grateful to S. Rao for his generous help with the ESEM analysis, performed at the Dept. of Civil Engineering, at the University of New Mexico. We also thank M. Spilde for assistance with EMPA and SEM and M. Miller for help with XRD, which was performed at the Dept. of Earth and Planetary Sciences at the UNM. The final manuscript has been improved by the suggestions of Dr. I. Grenthe, Dr. W. Nesbitt, and another anonymous reviewer. The experimental work was financially supported by ENRESA and SKB (Spanish and Swedish Nuclear Fuel and Waste Management Companies, respectively).

REFERENCES

Aguilar M., Casas I., de Pablo J., Giménez J., and Torrero M. E. (1991) Preliminary solubility studies of uranium dioxide under the conditions expected in a saline repository. ENRESA Tech. Rept. 03/91.

Bruno J., Casas I., Lagerman B., and Muñoz M. (1987) The determination of the solubility of amorphous UO_2 (s) and the mononuclear hydrolysis constants of uranium (IV) at 25°C. *Mat. Res. Soc. Symp. Proc.* **84**, 153–161.

Bruno J. (1989) A reinterpretation of the solubility product of solid uranium (IV) dioxide. *Acta Chem. Scand.* **43**, 99–100.

Bruno J. and Puigdomènech I. (1989) Validation of the SKBU1 uranium thermodynamic database for its use in geochemical calculations with EQ3/6. *Mat. Res. Soc. Symp. Proc.* **127**, 887–896.

Bruno J., Casas I., and Puigdomènech I. (1991) The kinetics of dissolution of UO_2 under reducing conditions and the influence of an oxidized surface layer (UO_{2+x}): Application of a continuous flow-through reactor. *Geochim. Cosmochim. Acta* **55**, 647–658.

Bruno J., Casas I., Cera E., de Pablo J., Giménez, J., and Torrero M. E. (1995) Uranium (IV) dioxide and SIMFUEL as chemical analogues of nuclear spent fuel matrix dissolution. A comparison of dissolution results in a standard NaCl/$NaHCO_3$ solution. *Mat. Res. Soc. Symp. Proc.* **353**, 601–608.

Casas I., Bruno J., Cera E., Finch R. J., and Ewing R. C. (1994) Kinetics and thermodynamic studies of uranium minerals. Assessment of the long-term evolution of spent nuclear fuel. Report SKB TR 94-16.

Cramer J. J. and Smellie J. A. T. (1994) Final Report of the AECL/SKB Cigar Lake Analog Study. Report AECL-10851, COG-93-147, SKB TR 94-04, pp. 157–160.

De Pablo J., Duro L., Giménez J., Havel J., Torrero M. E., and Casas I. (1992) Fluorimetric determination of traces of uranium (VI) in brines and iron (III) oxides using separation on an activated silica gel column. *Anal. Chim. Acta* **264**, 115–119.

Eyal Y. and Fleischer R. L. (1985) Preferential leaching and the age of radiation damage from alpha decay in minerals. *Geochim. Cosmochim. Acta* **49**, 1155–1164.

Forsyth R. S. and Werme L. O. (1992) Spent fuel corrosion and dissolution. *J. Nucl. Mat.* **190**, 3–19.

Galkin N. P. and Stepanov M. A. (1961) Solubility of uranium (IV) hydroxide in sodium hydroxide. *Sov. J. Atom. Energy* **8**, 231–233.

Gayer K. H. and Leider H. (1957) The solubility of uranium (IV) hydroxide in solutions of sodium hydroxide and perchloric acid at 25°C. *Canadian J. Chem.* **35**, 5–7.

Grenthe I. et al. (1992a) *Chemical Thermodynamics of Uranium.* Elsevier.

Grenthe I., Stumm W., Laaksuharju M., Nilsson A. C., and Wikberg P. (1992b) Redox potentials and redox reactions in deep groundwater systems. *Chem. Geol.* **98**, 131–150.

Hostetler P. B. and Garrels R. M. (1962) Transportation and precipitation of uranium and vanadium at low temperatures, with special reference to sandstone-type uranium deposits. *Econ. Geol.* **57**, 137–167

Janeczek J. and Ewing R. C. (1991) X-ray powder diffraction study of annealed uraninite. *J. Nucl. Mat.* **185**, 66–77.

Janeczek J. and Ewing R. C. (1995) Mechanisms of lead release from uraninite in the natural fission reactors in Gabon. *Geochim. Cosmochim. Acta* **59**, 1917–1931.

Janeczek J., Ewing R. C., Oversby V. M., and Werme L. O. (1996) Uraninite and UO_2 in spent nuclear fuel: a comparison. *J. Nucl. Mat.* **238**, 121–130.

Johnson L. H. and Shoesmith D. W. (1988) Spent Fuel. In *Radioactive Waste Forms for the Future* (ed. W. Lutze and R. C. Ewing), pp. 635–698. North-Holland.

Langmuir D. (1978) Uranium solution mineral equilibria at low temperatures with application to sedimentary ore deposits. *Geochim. Cosmochim. Acta* **42**, 547–569.

Matzke Hj. and Wang L. M. (1996) High-resolution transmission electron microscopy of ion irradiated uranium oxide. *J. Nucl. Mat.* **231**, 155–158.

Miller W., Alexander R., Chapman N., McKinley I., and Smellie J. (1994) *Natural Analogue Studies in the Geological Disposal of Radioactive Wastes.* Elsevier.

Parks G. A. and Pohl D. C. (1988) Hydrothermal solubility of uraninite. *Geochim. Cosmochim. Acta* **52**, 863–875.

Rai D., Felmy A. R., and Ryan J. L. (1990) Uranium (IV) hydrolysis constants and solubility product of $UO_2 \cdot x\ H_2O$ (am). *Inorg. Chem.* **29**, 260–264.

Ryan J. L. and Rai D. (1983) The solubility of uranium (IV) hydrous oxide in sodium hydroxide solutions under reducing conditions. *Polyhedron* **2**, 947–952.

Sandino A., Casas I., Ollila K., and Bruno J. (1991) SIMFUEL dissolution studies in granitic groundwater at 25°C. *Mat. Res. Soc. Symp. Proc.* **212**, 221–228.

Shock E. L., Sassani D. C., and Betz H. (1997) Uranium in geologic fluids: estimates of standard partial molal properties, oxidation potentials and hydrolysis constants at high temperature and pressures. *Geochim. Cosmochim. Acta* **61**, 4245–66

Stumm W. and Morgan J. J. (1981) Solubility of fine particles. In *Aquatic Chemistry*, 2nd ed., pp. 295–299. Wiley.

Torrero M. E., Casas I., Aguilar M., de Pablo J., Giménez J., and Bruno J. (1991). The solubility of unirradiated UO_2 in both perchlorate and chloride test solutions. Influence of the ionic medium. *Mat. Res. Soc. Symp. Proc.* **212**, 229–234.

Tremaine P. R., Chen J. D., Wallace G. J., and Boivin W. A. (1981) Solubility of uranium (IV) oxide in alkaline aqueous solutions to 300°C. *J. Soln. Chem.* **10**, 221–230.

Vance E. R. and Gascoyne M. (1987) Isotopic disequilibrium effects in leaching of natural uraninite and thorianite. *Geochim. Cosmochim. Acta* **51**, 2593–2594.

Weber W. J. (1981) Ingrowth of lattice defects in alpha irradiated UO_2 single crystals. *J. Nucl. Mat.* **98**, 206–215.

Weber W. J. (1984) Alpha-irradiation damage in CeO_2, UO_2, and PuO_2. *Radiation Effects* **83**, 145–156.

White A. F. (1990) Heterogeneous Electrochemical Reactions Associated with Oxidation of Ferrous Oxide and Silicate Surfaces. In *Mineral Water Interface Geochemistry* (ed. M. F. Hochella and A. F. White); Rev. Mineral. **23**.

APPLIED AND ENVIRONMENTAL MICROBIOLOGY, July 2001, p. 3149–3160 Vol. 67, No. 7
0099-2240/01/$04.00+0 DOI: 10.1128/AEM.67.7.3149–3160.2001

Diversity and Characterization of Sulfate-Reducing Bacteria in Groundwater at a Uranium Mill Tailings Site

YUN-JUAN CHANG,[1] AARON D. PEACOCK,[1] PHILIP E. LONG,[2] JOHN R. STEPHEN,[3] JAMES P. McKINLEY,[2] SARAH J. MACNAUGHTON,[4] A. K. M. ANWAR HUSSAIN,[1] ARNOLD M. SAXTON,[5] AND DAVID C. WHITE[1]*

Center for Biomarker Analysis[1] and Department of Animal Science,[5] The University of Tennessee, Knoxville, Tennessee 37932-2575; Environmental Technology, Pacific Northwest National Laboratory, Richland, Washington 99352[2]; and Crop and Weed Science, Horticulture Research International, Wellesbourne, Warwick CV35 9EF,[3] and AEA Technology Environment, Abingdon, OX 14 3BD,[4] United Kingdom

Received 5 February 2001/Accepted 26 March 2001

Microbially mediated reduction and immobilization of U(VI) to U(IV) plays a role in both natural attenuation and accelerated bioremediation of uranium-contaminated sites. To realize bioremediation potential and accurately predict natural attenuation, it is important to first understand the microbial diversity of such sites. In this paper, the distribution of sulfate-reducing bacteria (SRB) in contaminated groundwater associated with a uranium mill tailings disposal site at Shiprock, N.Mex., was investigated. Two culture-independent analyses were employed: sequencing of clone libraries of PCR-amplified dissimilatory sulfite reductase (DSR) gene fragments and phospholipid fatty acid (PLFA) biomarker analysis. A remarkable diversity among the DSR sequences was revealed, including sequences from δ-Proteobacteria, gram-positive organisms, and the *Nitrospira* division. PLFA analysis detected at least 52 different mid-chain-branched saturate PLFA and included a high proportion of 10me16:0. *Desulfotomaculum* and *Desulfotomaculum*-like sequences were the most dominant DSR genes detected. Those belonging to SRB within δ-Proteobacteria were mainly recovered from low-uranium (≤302 ppb) samples. One *Desulfotomaculum*-like sequence cluster overwhelmingly dominated high-U (>1,500 ppb) sites. Logistic regression showed a significant influence of uranium concentration over the dominance of this cluster of sequences ($P = 0.0001$). This strong association indicates that *Desulfotomaculum* has remarkable tolerance and adaptation to high levels of uranium and suggests the organism's possible involvement in natural attenuation of uranium. The in situ activity level of *Desulfotomaculum* in uranium-contaminated environments and its comparison to the activities of other SRB and other functional groups should be an important area for future research.

Microbially mediated reduction of redox-sensitive metals offers the potential to remediate metal-contaminated groundwater in situ. Sulfate-reducing bacteria (SRB) are important members of microbial communities involved in such metal reduction and occur in a variety of environments, including oil- and gas-bearing formations, soils, and domestic, industrial, and mining wastewaters (39). Although traditionally considered obligate anaerobes, observations of sulfate reduction occurring in the aerobic environment reported in the last 15 years have demonstrated a much larger ecological range of the SRB than previously thought (5, 6, 13). The dissimilatory sulfate-reducing bacteria in particular are environmentally ubiquitous, are found over an extensive range of pH and salt concentrations, and exhibit a superior ability to reduce and accumulate metals (16, 30, 53). Additionally they can tolerate a variety of heavy metals and dissolved sulfide. Some of these organisms can use U(VI) as a terminal electron acceptor, reducing the toxic and soluble U(VI) to insoluble U(IV), and also generate insoluble uranium sulfides in the presence of H_2S.

Uranium has no known biological function and is toxic to cells at low concentrations: 20 to 40 times more toxic than copper or nickel (20). The toxicity of uranium is primarily derived from its chemical properties rather than from its radioactivity (12). It has been reported that bacteria capable of reducing U(VI) to U(IV) are ubiquitous in nature (1, 2). The uranium reducers are also primarily sulfate reducers, and their growth can be stimulated by adding nutrients to the groundwater (1).

It has been well documented that *Desulfovibrio* species can reduce the soluble oxidized form of uranium, U(VI), to insoluble U(IV) (22, 23). A recent study demonstrated that a *Desulfotomaculum* strain isolated from heavy metal-contaminated sediment can grow with U(VI) as the sole electron acceptor (44). Overall the SRB play an important role in uranium geochemistry and may be a useful tool for removing uranium from contaminated environments by using ex situ treatments and stabilizing uranium in situ. However, little is known about the diversity of these bacteria, both in terms of community structure (the different SRB present in a single environmental community at a specific site) and community composition (the numbers or percentages of different SRB at a particular site). There is also little information available on variations in the SRB community structure and composition in response to changing environmental conditions.

The objective of this research is to establish the diversity of SRB at a heavy metal-contaminated site in relation to geochemical measurements, particularly uranium concentration.

* Corresponding author. Mailing address: Center for Biomarker Analysis, The University of Tennessee, 10515 Research Dr., Suite 300, Knoxville, TN 37932-2575. Phone: (865) 974-8001. Fax: (865) 974-8027. E-mail: Milipids@aol.com

This work is part of a broader effort to study the dominant terminal electron accepting processes and biotransformation occurring in the subsurface at such sites. The Shiprock site was chosen because of its wide range of uranium concentrations in groundwater and a wide range of cocontaminant concentrations, particularly sulfate and nitrate. The site has been subject to uranium contamination since the 1950s, providing a significant length of time for microbial communities to adapt to elevated levels of uranium. Groundwater samples with a range of contaminant concentrations were used as the means of accessing and interpreting the subsurface microbial communities. Two culture-independent analyses were used. (i) The first was a molecular method based on PCR, restriction enzyme digestion, and sequence analysis of dissimilatory sulfite reductase (DSR) gene fragments (17, 29, 49), which provided detailed information on the major taxonomic groups of sulfate-reducers present in these samples. The presence of *Desulfovibrio* sp. (δ-Proteobacteria) was also directly assessed by specific PCR targeting the NiFe hydrogenase indicative of this genus (48, 50). (ii) The second method, signature lipid analysis, was used to quantify viable sulfate/metal reducers by measuring mid-chain branched saturates and branched monounsaturates in the community phospholipid fatty acids (PLFA) (51, 52). These techniques taken together and compared to measured groundwater geochemical parameters provide new information on SRB diversity. As similar studies are conducted at other sites, we anticipate insight into community structure and composition that will enable effective in situ bioremediation of uranium-contaminated sites.

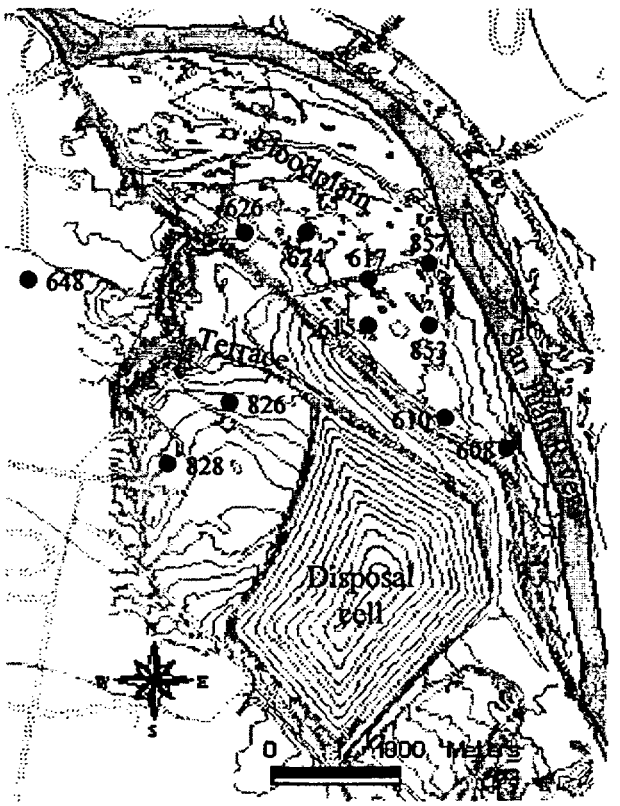

FIG. 1. Map of the UMTRA Shiprock mill tailing site.

MATERIALS AND METHODS

Site description. The U.S. Department of Energy is responsible for uranium mill tailings under the Uranium Mill Tailings Radiation Control Act of 1978. The Shiprock UMTRA site is on Navajo Nation land in San Juan County, N.Mex., located adjacent to and partly within the town of Shiprock, along the south side of the San Juan River on an elevated terrace about 21 m above the river (samples 828 and 826; Fig. 1). Bob Lee Wash flows northward on the terrace along the west side of the site and flows down onto the floodplain of the river. This wash would contain flowing water ephemerally, but the lower 200 m of the wash receives a constant discharge of about 230 liters min^{-1} from a potable-water artesian well (well 648). This water has created wetlands within Bob Lee Wash and at the mouth of the wash, where it discharges onto the river's floodplain (proximal to wells 608, 610, 615, 617, 624, 626, 853, and 857; Fig. 1). Several drainage ditches in the floodplain contain water year-round (7). An uncontaminated control sample was taken from well 648 (Fig. 1).

The Shiprock disposal cell is on unconsolidated alluvial terrace deposits underlain by Mancos Shale. Groundwater occurs at the contact between the terrace alluvium and the upper portion of the Mancos Shale, where it has been weathered. Uranium contamination occurs in the alluvium and upper Mancos Shale on the terrace and in the floodplain alluvium. The contaminated groundwater in the terrace alluvium and upper Mancos Shale beneath the site and in the floodplain alluvium along the river have exceeded the maximum concentration limits established by the Environmental Protection Agency EPA for nitrate and uranium. The volume of contaminated groundwater is estimated to be 610,000 m^3 (160 million gallons).

Sample collection. Prior to sample collection, all glassware used was washed in a 10% (vol/vol) Micro cleaning solution (VWR Scientific), rinsed 10 times in tap water, and then rinsed 10 times in deionized water. The glassware was then heated at 450°C for 4 h in a muffle furnace prior to use. All groundwater samples were collected in March 1999 with a downhole peristaltic or impeller pump. A minimum of 3 well volumes was purged from the well before sampling. Between sampling events, the pump and associated tubing were decontaminated with a dilute detergent and rinsed with deionized water. Samples (2 to 4 liters each) were filtered through sterile (methanol rinsed) Anodisc filters (Whatman International, Ltd., Maidstone, England), 47 mm diameter, 0.2 μm pore size. Filters were stored in muffle-sterilized glass petri dishes, preserved on dry ice, and shipped overnight to the University of Tennessee, Knoxville. The filtration method was designed to ensure that all suspended particles, including both sediment grains (with microorganisms attached) and individual microorganisms, are retained for analysis. A significant proportion of the microbial populations analyzed likely is attached to sediment particles.

Measurement of relevant geochemical properties. Sulfate and sulfide were determined as components of a suite of anions analyzed by ion chromatography (Dionex Model DX-300; AS-4a column, chemical suppression, and conductivity detection) according to McKinley et al. (28). Samples were quantified against commercial standards that ranged from 0.1 to 100 mg $liter^{-1}$. Uranium (U(VI)) concentrations were determined with a kinetic phosphorescence analyzer (model KPA-11, Chemchek Instruments, Inc.) according to McKinley et al. (27). The detection limit was 0.3 μg of uranium $liter^{-1}$. Quantitation was against NIST-traceable standards over the standard concentration range of 0.25 μg of uranium $liter^{-1}$ to 50 μg of uranium $liter^{-1}$ in 11 steps. Samples were treated only by the addition of a phosphorescent complexant and were run in batch using an autosampler. When necessary, samples were diluted and rerun so that raw results fell within the standard concentration range and yielded acceptable counting statistics. A full suite of standards was run at the beginning and end of each analytical sample set as an internal check on accuracy and precision. Dissolved oxygen (DO) was measured with a flow cell during well purging. Stable (invariant) DO values typically occurred prior to completion of well purging; the minimum observed concentration was taken as the in situ value. The pH was measured by electrode against commercial standards.

Lipid analysis. All solvents used were of GC grade (Fisher Scientific, Pittsburgh, Pa.). Glassware was washed in 10% (vol/vol) micro cleaner solution (VWR Scientific), rinsed 10 times in tap water and 5 times in deionized water, and then heated for 4 h in a muffle furnace at 450°C. Lipids were extracted from filters by the modified procedure of Bligh and Dyer (52). Total lipid fractions were then fractionated into glyco-, neutral, and polar lipids (14). The phospholipid-containing polar lipid was then subjected to a mild alkaline methanolysis, transesterifying the fatty acids into methyl esters (FAME) and recovered with hexane (14). The PLFA were separated, quantified, and identified by GC-MS

TABLE 1. Geochemical measurements of Shiprock groundwater

Well	Concn of:					pH	Temp (°C)
	U(VI) (ppb)	DO (mg liter^{-1})	Nitrate (mg liter^{-1})	Sulfate (mg liter^{-1})	Sulfide (μg ml^{-1})		
826	2,848	0.41	148	13,396	0.0027	6.53	15.5
615	2,458	0.54	3,907	13,539	0.0027	6.84	10.9
608	2,089	0.31	2,688	11,715	0.0026	6.75	8.4
610	1,687	0.48	3,090	9,772	0.0014	7.06	9.6
624	1,205	0.18	189	8,673	0.0004	7.04	14.0
617	544	0.32	793	5,579	0.0024	7.00	11.5
828	343	3.05	168	3,294	0.0059	6.89	13.0
857	302	0.23	<1	3,529	0.0088	7.08	13.3
853	227	0.24	<1	2,021	0.0048	7.12	12.5
626	90	0.21	1	2,831	0.0027	7.31	9.4
648	0	0.00	<1	2,000	0.0202	8.0	30.0

(37). Fatty acids were identified by relative retention times, comparison with authentic standards (Matreya, Inc.) and by mass spectra (collected at an electron energy of 70 mV) (38). Fatty acid nomenclature is in the form of "A:Bω C," where "A" designates the total number of carbons, "B" designates the number of double bonds, and "C" designates the distance of the closest unsaturation from the aliphatic end of the molecule. The suffixes "c" for *cis* and "t" for *trans* refer to geometric isomers. The prefixes "i," "a," and "me" refer to iso and anteiso methyl branching and mid-chain methyl branching, respectively. Cyclopropyl rings are indicated by "cy" (18).

DNA extraction and PCR from pure cultures and filters. Pure cultures of the following *Desulfotomaculum* strains were kindly provided by David Boone, Portland State University; *D. acetoxidans* strain DSM771 (type strain), *D. aeronauticum* strain 9, *D. luciae* strain SLT, *D. nigrificans* strain Delft 74T, *D. orientis* strain DSM765 (type strain), *D. putei* strain TH-12. *Desulfovibrio desulfuricans* (ATCC 29577) was purchased from the American Type Culture Collection. The organisms were grown anaerobically to mid-log phase in MS enrichment medium (pH 7) (http://caddis.esr.pdx.edu/smccw/; for *Desulfovibrio desulfuricans*, ATCC medium 1250 was used as recommended), and nucleic acids were extracted from cell pellets by a bead-beating procedure (41). Anodisk filters were broken into shards by hand with solvent-sterilized forceps and placed into 2-ml screw-cap microcentrifuge tubes. DNA was extracted directly from filters by mechanical disruption as described above. PCR amplifications were performed with two sets of primers, one targeting the [NiFe] hydrogenase of *Desulfovibrio* sp. as described by Wawer et al. (50). The second employed general SRB-specific primers targeting the DSR gene (dsr1F, 5′-ACSCACTGGAAGCACG-3′; dsr4R, 5′-GTGTAGCAGTTACCGCA-3′) described by Wagner et al. (49). Briefly, thermocycling for DSR consisted of 30 cycles of 94°C for 45 s, 54°C for 30 s, and 68°C for 90s (10 min on final cycle) with 1.25 U of Expand HF polymerase (Boehringer, Indianapolis, Ind.) and 10 pmol each of the primers in a total volume of 25 μl to produce a ca. 1.9-kb DNA fragment encoding most of the α- and β- subunits of the gene (49). Thermocycling was performed with a "Robocycler" PCR block (Stratagene, La Jolla, Calif.). For the hydrogenase gene, a touchdown PCR from 66°C to 55°C (50) was performed to reduce the formation of spurious byproducts. The primer targets the [NiFe] hydrogenase gene, which encodes an enzyme playing an important role in hydrogen metabolism of SRB (47) and in dissimilatory metal reduction by SRB (24, 25). This enzyme is present in all *Desulfovibrio* species (48), with a PCR product length around 450 bp using the primer described above.

Cloning and restriction digestion. PCR products of the DSR gene fragment were gel purified and extracted with a Gene-Clean kit (BIO-101, Vista, Calif.). Purified fragments were cloned using the vector PCR2.1 TOPO and *Escherichia coli* TOP10F′ competent cells according to the manufacturer's instructions (Invitrogen, Carlsbad, Calif.). From each of those 11 libraries, 21 to 34 white colonies were randomly selected and the cloned inserts were reamplified with the vector primers M13 reverse and T7 (30 cycles of 94°C for30 s, 55°C for 30 s, and 72°C for 90 s). A portion (5 μl) of the resulting amplification product was digested at 37°C with the restriction endonuclease *Msp*I according to the manufacturer's instructions (Boehringer) and analyzed by separation of fragments on a 2% agarose TAE gel.

Sequence analysis. Representative plasmids from each digestion pattern were selected for sequencing. Clones with *Msp*I digestion patterns that appeared more than once were sequenced from both the 3′ and 5′ ends of each insert with vector primers M13 reverse/T7, while those with unique *Msp*I digestion patterns were sequenced with the DSR1F primer to obtain a partial α-subunit sequence of the gene. The M13 reverse/T7 amplification product was gel purified, extracted with a Gene Clean kit (BIO-101), and subjected to sequencing on an Applied Biosystems automated sequencer (model 310) with Prism Big-Dye terminators. The sequences were assembled and aligned by using D. G. Gilbert's SeqPup sequence alignment editor, version 0.6 (available from the author at ftp.bio.indiana.edu). Sequence identification was performed by use of the BLASTN facility of the National Center for Biotechnology Information (http://www.ncbi.nlm.nih.gov/BLAST/). Phylogenetic trees were constructed by the neighbor-joining method, with the ARB software environment (42). Cloned sequences were screened for possible chimeric origin by independent neighbor-joining analysis of the 5′ and 3′ halves of sequences within an alignment of all published DSR sequences, including DSR sequences from pure cultures generated in this study. Sequences from pure cultures were derived from direct analysis of amplification products from genomic DNA templates.

Statistical analysis. Pearson r linear correlations between geochemical variables were performed using the basic stats module of Statistica, version 5.1 for Windows (Statsoft, Inc., Tulsa, Okla.). Logistic regression was used to test whether concentrations of environmental chemicals could explain occurrence frequencies for specific clades of DSR sequences, where sufficient samples for statistical analysis were detected (SAS Institute, version 8.1, Cary, N.C.).

Nucleotide sequence accession number. Partial cloned DSR sequences recovered from Shiprock groundwater samples were submitted to GenBank under accession no. AY015500 to AY015569 (α-subunits) and AY015582 to AY015615 (β-subunits). Partial DSR sequences recovered from cultured reference strains were submitted as AY015493 to AY015495 and AY015496 to AY015499 for the α-subunits and AY015577 to AY015581 for the β-subunits.

RESULTS

Physical and chemical characteristics of UMTRA groundwater wells. Samples collected on the terrace (wells 828 and 826) were collected from the top 3.0 m of the water table, averaging a minimal depth of 4.9 m below the ground surface. Samples collected on the floodplain (wells 608, 610, 615, 617, 624, 626, 853, and 857) were taken from the top 1.3 m of the water table, averaging a minimal depth of 2.1 m below the ground surface. The pH measured at all groundwater sites was nearly neutral and ranged from 6.53 to 7.12, except that for the control well 648, which was slightly alkaline (pH 7.8 to 8.0). (See Fig. 1 for well locations and Table 1 for geochemical data.) Well 648 is an artesian well with the water produced from the Morrison Formation (Jurassic age) through perforated casing from a depth of approximately 450 to 540 m. Well 648 was also warmer (30°C) than other wells (from 8.4°C to 15.5°C), due to its source depth.

The highest uranium concentration (2,848 ppb) was in well 826, and the highest sulfate concentration (13,539 mg liter^{-1})

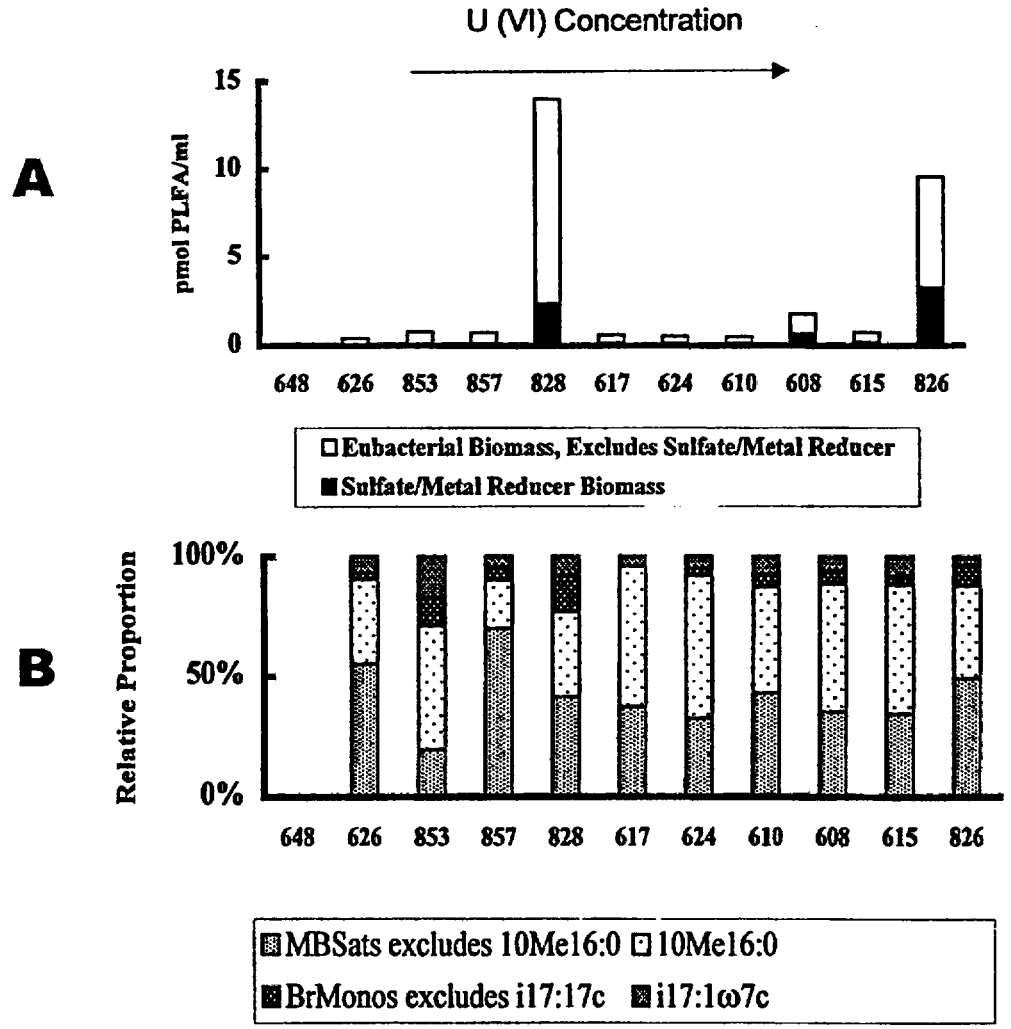

FIG. 2. PLFA profile of UMTRA Shiprock groundwater samples. (A) Community abundance as measured by total bacterial biomass level. ■, SRB-metal reducer biomass measured as picomoles per milliliter of mid-chain branched saturates (MBSats) and branched monounsaturates (BrMonos). □, the remaining bacterial biomass measured as total PLFA, with normal saturates over 18 carbons in length, polynoics (eukaryote PLFA), SRB-metal reducer PLFA, and trace quantities of PLFA of unknown structure excluded. (B) Community composition as categorized via SRB-metal reducer PLFA structural group.

was in well 615. Pearson r linear correlation analysis showed a significant correlation between the concentrations of uranium and sulfate ($R = 0.98$, $P < 0.05$).

PLFA profile of SRB. PLFA biomarkers indicative of bacterial sulfate reducers have been identified in previous studies. The lipid marker Br17:1 (especially i17:1ω7) has been associated with *Desulfovibrio* (11, 46, 50, 51); 10me16:0 and 17:1 (especially 17:1ω6) were recognized as a major fatty acid component for *Desulfobacter* (10, 11) and *Desulfobulbus* (32), respectively. These biomarkers were determined for a small subset of isolates and may not be present in, or exclusive to, all members of the groups they are reported to represent. Within the genus *Desulfotomaculum*, fatty acid composition was only determined for strains of *D. acetoxidans*, *D. orientis*, *D. ruminis*, and *D. nigrificans* (19, 31). Unclassified components were predominant in all four of the species mentioned above, except for *D. acetoxidans*; other major fatty acids were i17:0, i15:0, 10me16:0, and i17:1ω7, etc. (19, 31).

The highest biomass detected in groundwater samples was from well 828 (14.00 pmol ml^{-1}), and the lowest was from well 648 (0.02 pmol ml^{-1}) (Fig. 2A). In order to determine bacterial biomass, PLFA generally taken to be indicative of eukaryotes (normal saturates over 18 carbons in length, polynoics) and the trace quantities of PLFA of unknown structure were excluded. PLFA analysis showed that all samples contained biomarkers for SRB and metal-reducing bacteria (specifically 10me16:0). Of these, 10me16:0 comprised >10% of thePLFA of the SRB and metal-reducing bacteria. Well 853 has the highest proportion of i17:1ω7c PLFA (16.77%) compared with the other wells (3.53 to 8.00% of SRB and metal-reducing bacterial PLFA) (Fig. 2B).

Based on PLFA analysis, these samples most likely contain

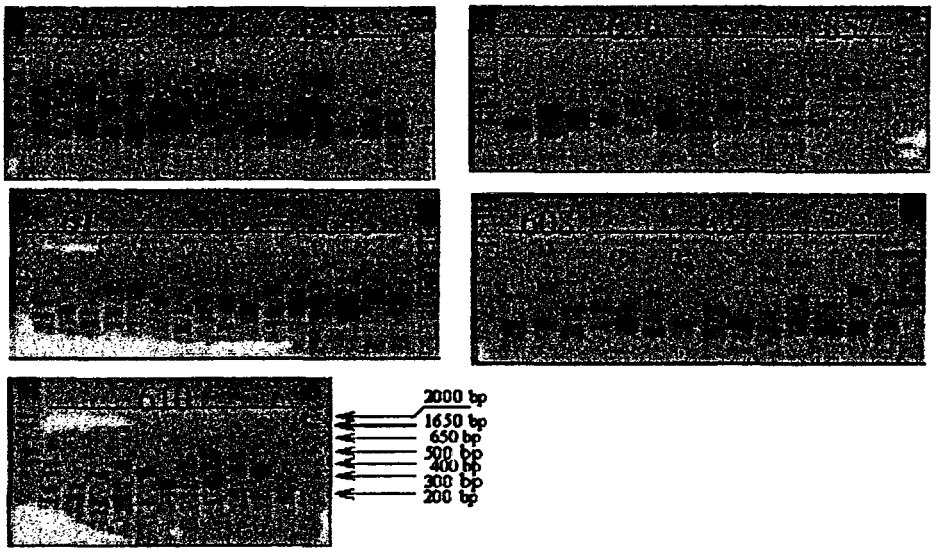

FIG. 3. Restriction digestion analysis of DSR clones with *Msp*I. Cloned DSR gene fragments were amplified from the cloning vector by using primers directed at the T7 and M13 reverse RNA polymerase binding sites, producing a fragment with approximately 70 bp of vector sequence on each end. The vector sequence contained no *Msp*I recognition sites. Products were digested with a twofold excess of *Msp*I for 1 h at 37°C, analyzed by electrophoresis on a 2% agarose gel with TAE buffer, and visualized by ethidium bromide fluorescence.

complex SRB microbial communities with a wide range of biomass content. Community complexity was estimated from the number of different mid-chain branched saturates detected (in this case over 52), nearly half of them with unknown branch structures.

DNA extraction and PCR amplification of DSR genes, [NiFe] Hydrogenase genes. Genomic DNA was extracted from a total of 13 samples with uranium concentrations varying from 0 to 2848 ppb. Genes encoding DSR were successfully detected from 11 sites. The amplicons were approximately the size generated in control amplifications of the dissimilatory sulfite reductase gene of *D. vulgaris* (1.9 kb). For [NiFe] hydrogenase gene amplification, only sample 853 produced a positive band of the expected size as the control organism *Desulfovibrio desulfuricans* (about 450 bp).

Clone library characterization. A clone library of DSR PCR products from each sample well was used to explore the diversity of DSR genes of the bacteria from this contaminated groundwater. A total of 305 clones were assembled into 70 clone families based on *Msp*I restriction fragment banding patterns (Fig. 3). Some samples yielded as many as 11 different types of digestion patterns (e.g., well 610), while others were less diverse and produced 3 different restriction patterns (e.g., wells 857 and 608). Identical sequences were recognized between different samples mostly from floodplain wells 610, 615, 608, 624, 626, and 617.

Phylogenetic analysis of Shiprock DSR genes. The α-subunits of recovered DSR gene fragments and of a variety of cultured *Desulfotomaculum* strains were sequenced. On average, 500 nucleotides were determined. For the groundwater clones, the sequence of representatives for each library and restriction pattern (total, 70 clones) was determined. Potential chimeric artifacts (one artifact) and non-DSR sequences (five sequences) were recognized in some of the clone library and were excluded from further analysis. In order to obtain an accurate description of the phylogenetic relationships of the SRB population in these groundwaters, we included in our analysis most environmental DSR clone sequences available from the database, as well as the newly characterized sequences of pure SRB reference cultures. Neighbor-joining analysis revealed the presence of eight well-resolved lineages of DSR sequences, designated clusters A to H (Fig. 4). Clusters F and G were further subdivided into 5 and 11 subclusters, respectively, most of which are well separated by similarity values between 70 and 85% (Fig. 4). Within subclusters, the similarity values were greater than 90%. The *Desulfotomaculum* pure culture sequences showed a division of the available organisms into two clusters, with group 1 containing *D. thermocistern, D. luciae*, and *D. acetoxydans* (in cluster E) and group 2 containing *D. aeronauticum, D. putei, D. nigrificans*, and *D. ruminis* (in cluster G-9).

Cluster A. Cluster A contained all available DSR α-subunit sequences from cultured *Desulfovibrio* (δ-subclass of the class Proteobacteria) strains and one clone recovered from well 853, in which both uranium contamination and and the sulfate concentration were relatively low.

Cluster B. The cluster B sequence also contained sequences derived from δ-subclass Proteobacteria, *Desulfobacter latus, Desulfonema limicola, Desulfococcus multivorans*, and *Desulfobotulus sapovorans.* A single clone recovered from well 626 grouped with these strains. This site was a low-uranium sample, in which sulfate was measured at 2,831 mg liter^{-1}.

Cluster C. Cluster C contains no cultured representatives. It is comprised of three unique sequences, from high-uranium to medium-uranium samples from wells 624 and 828. They are closely related to an environmental DSR clone (accession no. AF179329) (29) generated from a microbial mat at Solar Lake and are peripherally related to the genus *Desulfobulbus*.

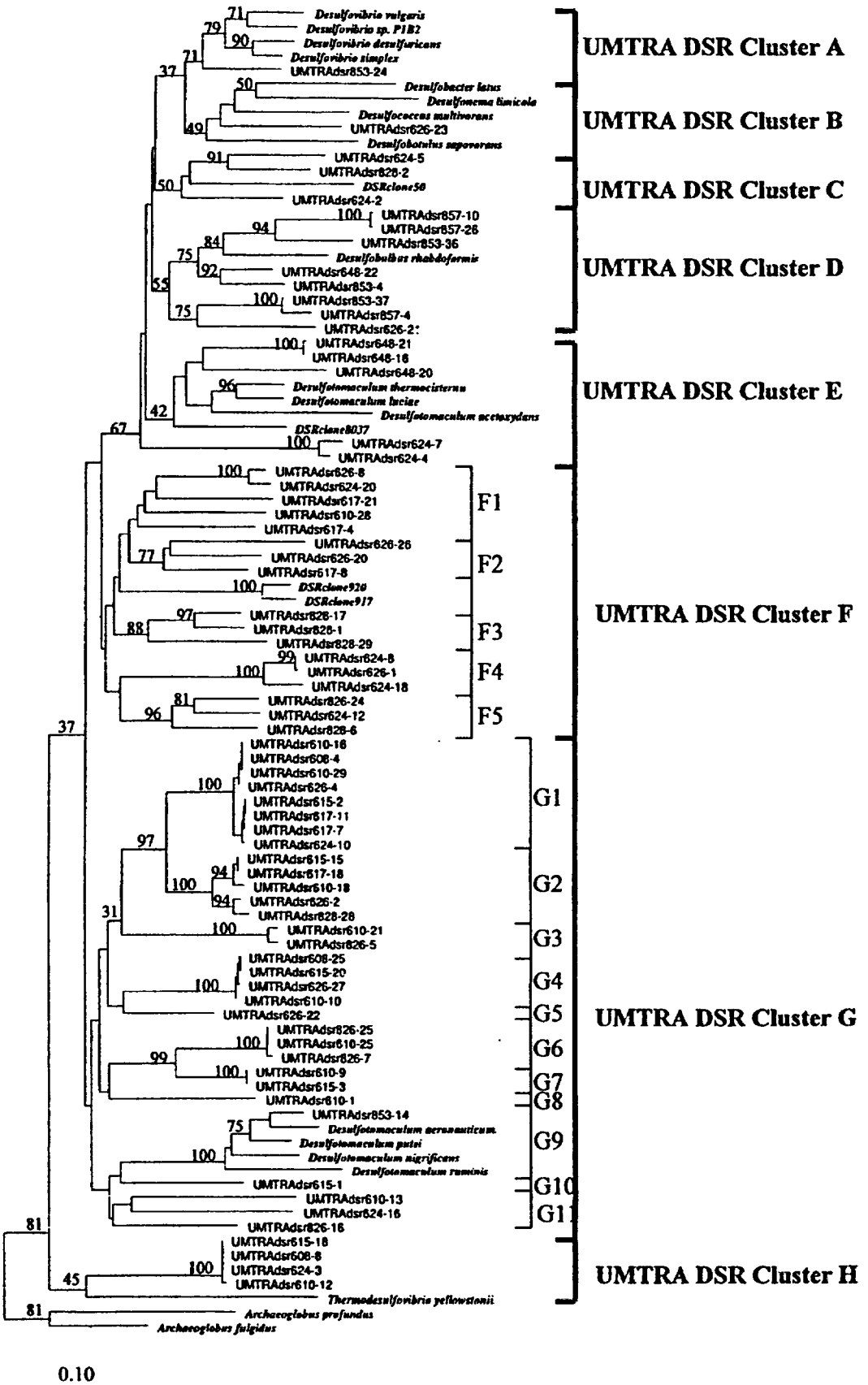
Desulfovibrio vulgaris
Desulfovibrio sp. P1B2
Desulfovibrio desulfuricans
Desulfovibrio simplex
UMTRAdsr853-24
Desulfobacter latus
Desulfonema limicola
Desulfococcus multivorans
UMTRAdsr626-23
Desulfobotulus sapovorans
UMTRAdsr624-5
UMTRAdsr828-2
DSRclone50
UMTRAdsr624-2
UMTRAdsr857-10
UMTRAdsr857-28
UMTRAdsr853-36
Desulfobulbus rhabdoformis
UMTRAdsr648-22
UMTRAdsr853-4
UMTRAdsr853-37
UMTRAdsr857-4
UMTRAdsr626-2
UMTRAdsr648-21
UMTRAdsr648-16
UMTRAdsr648-20
Desulfotomaculum thermocisternum
Desulfotomaculum luciae
Desulfotomaculum acetoxydans
DSRclone8037
UMTRAdsr624-7
UMTRAdsr624-4
UMTRAdsr826-8
UMTRAdsr624-20
UMTRAdsr617-21
UMTRAdsr610-28
UMTRAdsr617-4
UMTRAdsr626-26
UMTRAdsr626-20
UMTRAdsr617-8
DSRclone926
DSRclone917
UMTRAdsr828-17
UMTRAdsr828-1
UMTRAdsr828-29
UMTRAdsr624-8
UMTRAdsr626-1
UMTRAdsr624-18
UMTRAdsr826-24
UMTRAdsr624-12
UMTRAdsr828-6
UMTRAdsr610-16
UMTRAdsr608-4
UMTRAdsr610-29
UMTRAdsr626-4
UMTRAdsr615-2
UMTRAdsr617-11
UMTRAdsr617-7
UMTRAdsr624-10
UMTRAdsr615-15
UMTRAdsr617-18
UMTRAdsr610-18
UMTRAdsr626-2
UMTRAdsr828-28
UMTRAdsr610-21
UMTRAdsr626-5
UMTRAdsr608-25
UMTRAdsr615-20
UMTRAdsr626-27
UMTRAdsr610-10
UMTRAdsr626-22
UMTRAdsr826-25
UMTRAdsr610-25
UMTRAdsr826-7
UMTRAdsr610-9
UMTRAdsr615-3
UMTRAdsr610-1
UMTRAdsr853-14
Desulfotomaculum aeronauticum
Desulfotomaculum putei
Desulfotomaculum nigrificans
Desulfotomaculum ruminis
UMTRAdsr615-1
UMTRAdsr610-13
UMTRAdsr624-16
UMTRAdsr826-16
UMTRAdsr615-18
UMTRAdsr608-8
UMTRAdsr624-3
UMTRAdsr610-12
Thermodesulfovibrio yellowstonii
Archaeoglobus profundus
Archaeoglobus fulgidus
F1
F2
F3
F4
F5
G1
G2
G3
G4
G5
G6
G7
G8
G9
G10
G11
UMTRA DSR Cluster A
UMTRA DSR Cluster B
UMTRA DSR Cluster C
UMTRA DSR Cluster D
UMTRA DSR Cluster E
UMTRA DSR Cluster F
UMTRA DSR Cluster G
UMTRA DSR Cluster H
0.10

Cluster D. Cluster D contains the DSR α-subunit sequence of *Desulfobulbus rhabdoformis*, a δ-proteobacterium. Eight clones, all from low-uranium samples, fell into this group.

Cluster E. Cluster E contained the three cultured strains, *D. thermocistern*, *D. luciae*, and *D. acetoxydans*, referred to here as *Desulfotomaculum* group 1. Three clone sequences fell into this group; all had been recovered from well 648. Another two clones, generated from well 624 are loosely associated with this group. Although this group does not appear monophyletic, based on DSR α-subunit sequencing, phylogenetic analysis of the DSR β-subunits encoded in these clones showed that they branch together (Fig. 5A).

Cluster F. Cluster F contains no DSR α-subunit sequences from cultured organisms. This was the second most abundant group of clone sequences recovered (17 in total). Ten of them were recovered from high-uranium samples, 4 of them are from low-uranium well 626, and 3 are from well 828 (medium uranium). Although not closely related to any available pure culture sequences, this cluster showed close relationship with two DSR clones recovered from the Solar Lake microbial mat (DSR clone 917 and 920, accession no. AF179334 and AF179339) (29). Each subcluster contains three to five distinct sequences, except subcluster F4, which contained only closely related sequences.

Cluster G. Cluster G includes the *Desulfotomaculum* strains designated as group 2. This is the largest single cluster of cloned sequences, all but one of which was associated basally with *Desulfotomaculum* group 2. Among 31 clones in this cluster, 25 originated from high-uranium samples. The remaining six clones were recovered from medium- to low-uranium wells, including the single sequence within *Desulfotomaculum* group 2 (well 853). The remaining four sequences were recovered from well 626. The phylogenetic depths of the individual subclusters are different: subclusters G1, G2, G3, G4, G6, and G7 contain clones sharing 95 to 100% sequence similarity, and subclusters G9 and G11 contain sequences that are more deeply diverged. Subclusters G5, G8, and G10 are represented by single clones.

Cluster H. Cluster H is defined by four clone sequences, all generated from high-uranium samples, and shows a relationship to *Thermodesulfovibrio yellowstonii*, in the *Nitrospira* group.

Population structure in relation to uranium concentration. Of the sequenced clones, 40% grouped with lineage G, which includes the gram-positive, thermophilic *Desulfotomaculum* species *D. nigrificans*, *D. putei*, *D. aeronauticum*, and *D. ruminis*. Sequences recovered from high-uranium (>1,500 ppb) samples were dominated by this lineage, although cluster F and the less frequently recovered cluster H were also detected. DSR α-subunit sequences recovered from low-uranium (≤302 ppb) samples were more diverse, including representatives of clusters A, B, D, E, F, and G (Fig. 6A). Figure 6B shows the distribution of different DSR sequences detected among different sample wells. Cluster D, belonging to the δ-Proteobacteria, was recovered exclusively from low-uranium (≤302 ppb) samples. Together with sequences closely related to *Desulfotomaculum* group 1, they constitute the recovered SRB community of well 648, which had the lowest uranium concentration. Notably, sequences related to δ-Proteobacteria and *Desulfotomaculum* group 1 were not recovered from high-uranium samples. Lineage G dominated in all high-uranium samples. Cluster H, related to *Thermodesulfovibrio yellowstonii*, was recovered from samples 615, 608, 610, and 624, in which the uranium concentration is relatively high (1,205 to 2,458 ppb of uranium).

Logistic regression suggested a significant association between sequence cluster G and uranium concentration (slope = 0.00111, $P = 0.0005$; Table 2). With only 11 samples, many combinations of chemical concentrations were not observed, creating difficulty in separating the influences of the various chemical constituents. With that caution, however, important relationships between chemical concentrations were found in cluster F, but not for cluster G, although the overall model was significant ($P = 0.0007$, full model). DO had the largest effect, as measured by the slope. A model with only uranium showed that as uranium increased from 0 to 3,000 ppb, clade G frequencies were predicted to increase from 18.5% to 90% (Table 2).

DISCUSSION

Genetic diversity and metabolic activity. Until now, the abundance and diversity of SRB have been analyzed mostly through cultivation techniques and through hybridizations with rRNA-targeted oligonucleotide probes (8, 9, 15, 21, 26, 34–36). 16S ribosomal DNA (rDNA) sequences are currently popular as a useful criterion for the definition of taxa at several levels. However, 16S rRNA sequences by themselves provide no information about potential physiological differences between closely related bacteria. Here we present a field-scale study using an alternative PCR-based approach, targeting the dissimilatory sulfite reductase gene along with the [NiFe] hydrogenase gene. Although it is well established that PCR-based methods in microbial ecology have intrinsic biases (33, 43), these biases can be assumed to be equal for each of the groundwater samples described here. Furthermore, as a com-

FIG. 4. Neighbor-joining analysis of DSR α-subunit fragments selected from clone libraries as frequently occurring *Msp*I digestion patterns. Sequences prefixed "UMTRAdsr" were generated during this study. The prefix is followed by the sample well number, which is followed by the clone number. Clones were selected from libraries on the basis of *Msp*I patterns to provide a preliminary survey of the most commonly recovered DSR gene sequences from each sample. Nucleotide sequence accession numbers are given in parentheses for the following organisms: *Desulfobulbus rhabdoformis* (AJ250473), *Desulfovibrio desulfuricans* (AJ289157), *Desulfococcus multivorans* (AJ277107), *Desulfotomaculum thermocisternum* (F074396), *Archaeoglobus profundus* (AF071499), *Thermodesulfovibrio yellowstonii* (U58122), *Desulfobotulus sapovorans* (U58120), *Desulfovibrio* sp. strain P1B2 (U58116), *Desulfotomaculum ruminis* (U58118), *Desulfococcus multivorans* (U58126), *Desulfonema limicola* (U58128), *Desulfobacter latus* (U58124), *Desulfovibrio vulgaris* (U16723), *Archaeoglobus fulgidus* (M95624), and *Desulfovibrio simplex* (U78738). Gene sequences from *Desulfotomaculum luciae*, *D. acetoxidans*, *D. putei*, *D. aeronauticum*, *D. nigrificans*, *and Desulfovibrio desulfuricans* were generated in this study under accession no. AY015493 to AY015499. The numbers on the tree refer to bootstrap values on 100 replicates; only values above 30 are given. Scale bar represents 10% estimated change.

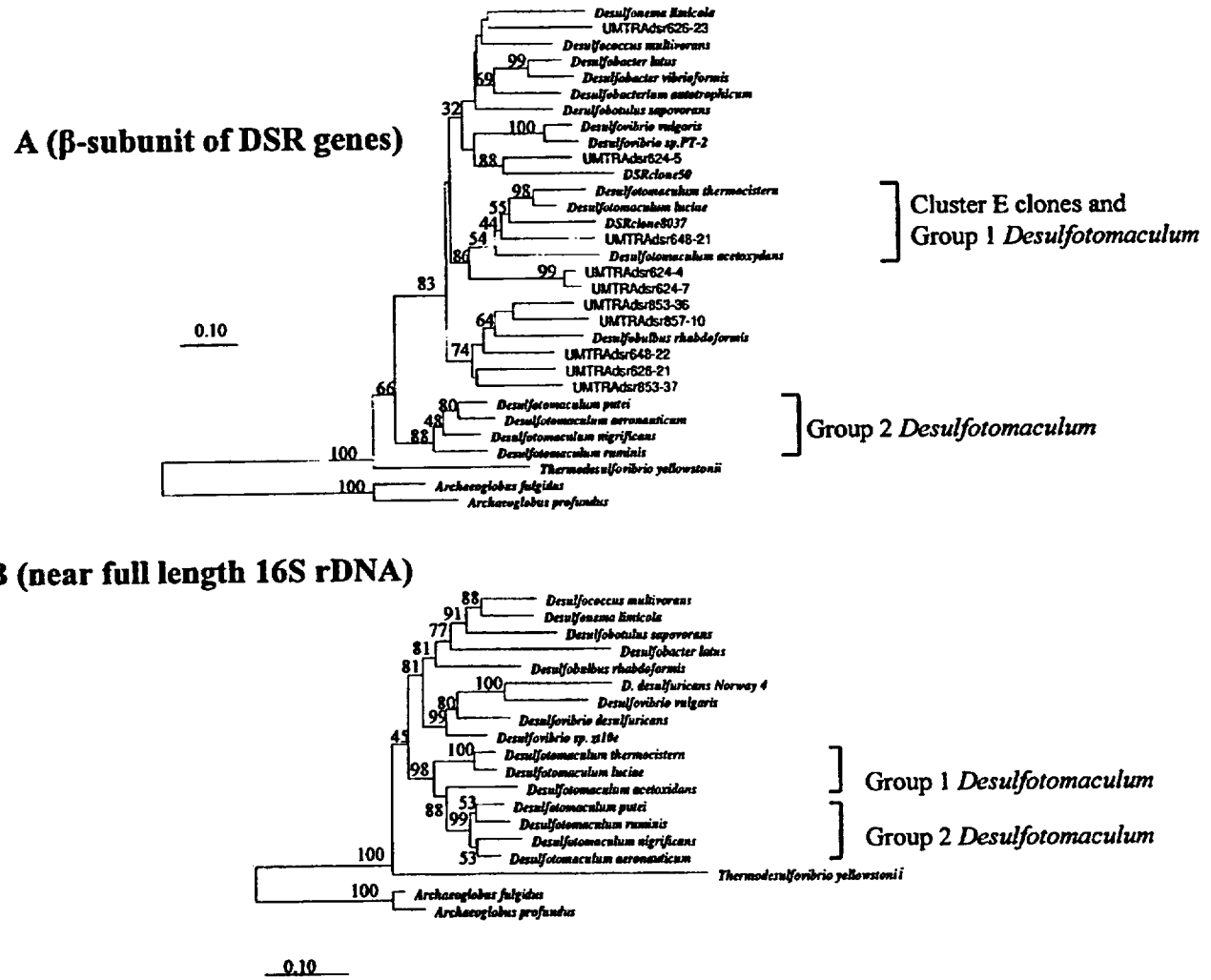

FIG. 5. (A) Neighbor-joining analysis of some DSR β-subunit sequences from UMTRA Shiprock site clones and reference pure culture organisms. Sequences prefixed "UMTRAdsr" were generated during this study. Nucleotide sequence accession numbers are given in parentheses for the following organisms: *Desulfobulbus rhabdoformis* (AJ250473), *Desulfococcus multivorans* (U58127), *Desulfotomaculum thermocisternum* (AF074396), *Archaeoglobus profundus* (AF071499), *Thermodesulfovibrio yellowstonii* (U58123), *Desulfobotulus sapovorans* (U58121), *Desulfovibrio* sp. strain PT-2. (U58115), *Desulfotomaculum ruminis* (U58119), *Desulfonema limicola* (U58129), *Desulfobacter latus* (U58125), *Desulfovibrio vulgaris* (U16723), *Archaeoglobus fulgidus* (M95624), *Desulfobacter vibrioformis* (AJ250472), *Desulfobacterium autotrophicum* (Y15478), DSR clone 50 (AF179329), and DSR clone 8037 (AF179336). Gene sequences from *Desulfotomaculum luciae*, *D. acetoxidans*, *D. putei*, *D. aeronauticum*, and *D. nigrificans* were generated in this study under accession no. AY015577 to AY015581. (B) Neighbor-joining analysis of near full-length 16S rDNA from pure cultures. Nucleotide sequence accession numbers are given in parentheses for the following organisms: *Desulfotomaculum ruminis* (Y11572), *D. putei* strain SMCCW 459 (AF053929), *D. aeronauticum* (X98407), *D. acetoxidans* (Y11566), *D. thermocisternum* (U33455), *D. nigrificans* (X62176), *D. luciae* (AF069293), *Desulfococcus multivorans* ATCC 33890 (M34405), *Desulfonema limicola* (U45990), *Desulfobacter latus* (M34414), *Desulfobotulus sapovorans* (M34402), *Desulfovibrio vulgaris* (M34399), *D. desulfuricans* (AF098671), *Archaeoglobus profundus*. (AF272841), *Desulfovibrio* sp. strain zt10e (AF109469), *Archaeoglobus fulgidus* (Y00275), and *D. desulfuricans* sp. strain Norway 4 (M37312). The numbers on the trees refer to bootstrap values on 100 replicates; only values above 30 are given. The scale bar represents 10% estimated change.

plement to this molecular diversity study, analysis of PLFA biomarkers for SRB groups provides quantitative confirmation of the presence of viable SRB.

Based on near full-length 16S rDNA sequence analysis, *Desulfotomaculum* spp. form a distinct cluster of related sequences (Fig. 5B). Comparison of partial α- and β-subunit DSR gene sequences revealed a greater genetic diversity, as expected, but suggested a similar grouping of *Desulfotomaculum* strains (Fig. 4 and 5A): i.e., a division of the *Desulfotomaculum* genus into at least two clusters, which we have designated as groups 1 and 2. This is consistent with recent findings about SRB taxonomy described by Stackebrandt et al. (40) and Hristova et al. (15).

*Msp*I restriction enzyme digestion analysis revealed substantial diversity of the DSR gene sequence. A total of 70 DSR sequences (61 of them unique) were identified, and all were affiliated with the bacterial domain. Comparison of phylogenetic trees constructed with different portions of the DSR

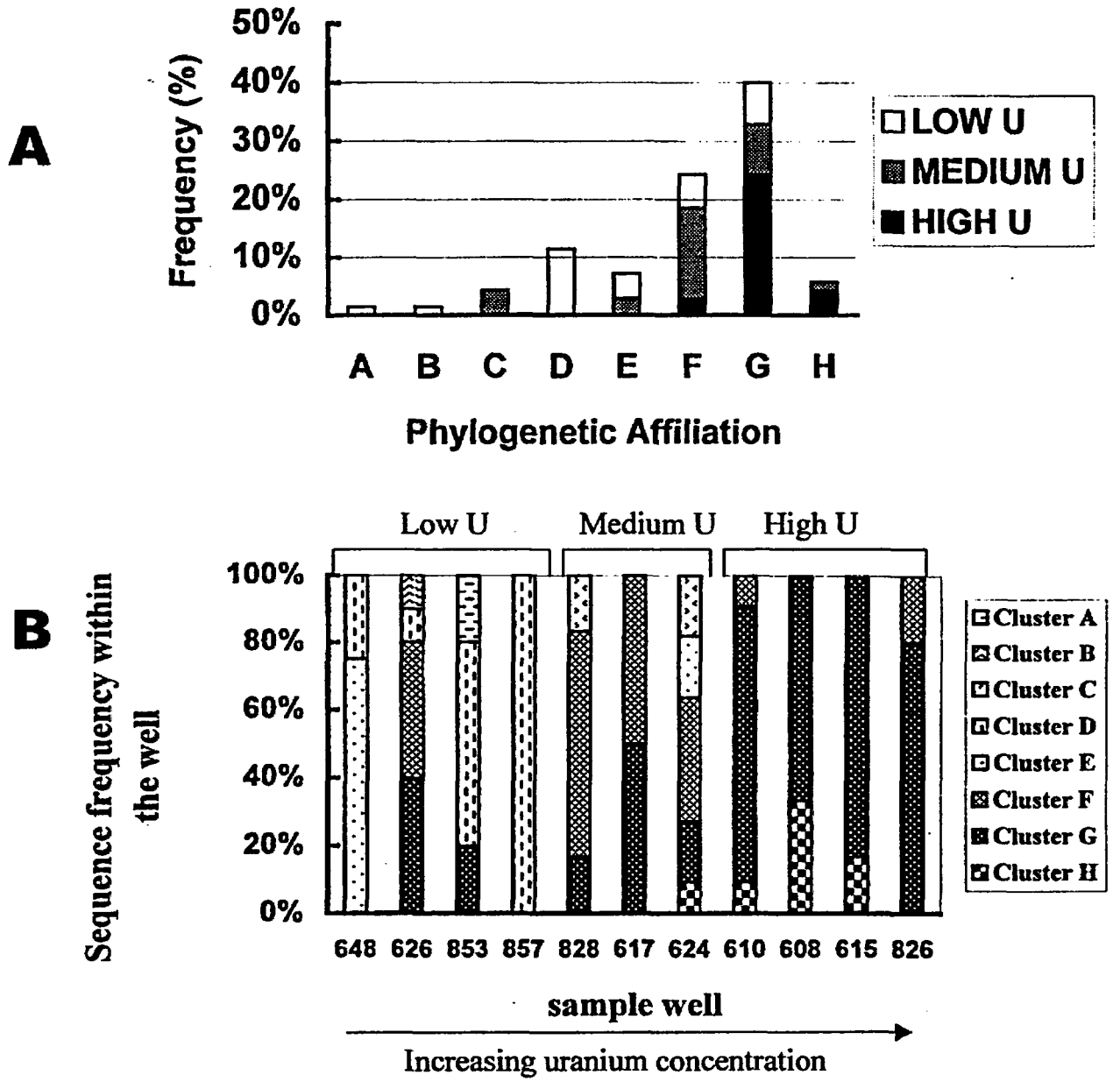

FIG. 6. (A) Sequence distribution for 70 DSR clone sequences (α-subunit) obtained from high-uranium [samples 610, 608, 615, and 826; U(VI) from 2,847.5 to 1,687 ppb], medium-uranium (samples 624, 617, and 828; U(VI) from 1,205 to 342.7 ppb), and low-uranium samples (857, 853, 626, and 648; U(VI) from 301 to 0.001 ppb). (B) SRB population structure in different sample wells as measured by DSR sequences recovered and their affiliation with different cluster of SRB.

genes revealed, in general, consistent topologies for both α- and β-subunits of DSR, although slight variance was observed (Fig. 4 and 5A). Eight well-resolved lineages of DSR sequences are represented by the cloned sequences (A to H, Fig. 4). Some sequence differences within the subclusters (Fig. 4) involved only several base changes. It is entirely possible that this microheterogeneity may reflect PCR point errors. The finding of the same partial DSR sequences in different gene libraries suggests that most of the differences are real. The [NiFe] hydrogenase *Desulfovibrio*-specific PCR detected positive amplification only from well 853, and *Desulfovibrio*-like DSR fragments were indeed recovered from only this well. The PLFA profile of well 853 also showed highest proportion of i17:1ω7, a biomarker associated with *Desulfovibrio* spp. (11). The consistent occurrence of *Desulfovibrio*-like signals in well 853 may be significant, since it is a location at the Shiprock site, where active microbial reduction of U(VI) may be responsible for low uranium concentrations in groundwater (D. Elias, D.

TABLE 2. Parameter estimates from two logistic regression models used to explain Cluster F and G frequencies in relation to selected geochemical measurements

Parameter[a]	Cluster F		Cluster G	
	Estimate	$P >$ Chi square	Estimate	$P >$ Chi square
Full model				
Intercept	−3.6181	0.009	−0.6515	0.554
Sulfate	0.000969	0.038	−0.00029	0.453
DO	0.8999	0.015	−0.1827	0.647
Uranium	−0.00416	0.047	0.00183	0.258
Nitrate	−0.00066	0.088	0.000532	0.049
Model with U(VI) as sole variable				
Intercept	−0.5934	0.1421	−1.4794	0.0008
Uranium	−0.00055	0.1086	0.00111	0.0005

[a] P values of the full model are 0.0074 for cluster F and 0.0007 for cluster G. The P values of the model with U(VI) as the sole variable are 0.0902 for cluster F and 0.0001 for cluster G.

Wong, J. Senko, P. E. Long, J. P. McKinley, J. M. Suflita, and L. R. Krumholz, EOS, Trans. Am. Geophys. Union Fall Meet., vol. 81, no. 48, p. F214, 2000).

Since DNA recovered from environmental samples may be derived in part from dead or inactive cells, the recovery of DSR sequences alone does not provide direct evidence for an active sulfate-respiring population. However, a significant amount of lipids known to be markers for sulfate or metal reducers were found in 10 samples (all except background well 648) tested, which supported the presence of a viable SRB microbiota in this groundwater environment. An unusually high number of distinct mid-chain branched saturates (more than 50, constituting 7 to 25% of total bacteria biomass) suggested a diverse SRB community as well as a high relative abundance within the domain *Bacteria*.

Dominance of *Desulfotomaculum* and *Desulfotomaculum*-like sequences. As dissimilatory SRB, the genus *Desulfotomaculum* and *Desulfovibrio* spp. were reported to exhibit a superior ability, over assimilatory organisms, to extract large amounts of metals from culture media (16). Tolerance and adaptation to heavy metals by *Desulfovibrio* and *Desulfotomaculum* strains of different origins have been investigated in enrichment cultures under a range of sulfate concentrations (4).This study revealed an overwhelming dominance of *Desulfotomaculum* and *Desulfotomaculum*-like sequences, particularly in those wells with high uranium (> 1,500 ppb) concentration. As many as 50 different DSR sequences associated with the genus *Desulfotomaculum* were recovered. The majority of them form subclusters representing sequences basal to the established *Desulfotomaculum* genus and are, as yet, to be characterized.

Previous work indicates that the abundance of *Desulfotomaculum* spp. in various environments is probably related to sulfate availability and exposure to adverse environmental conditions, such as regular exposure to oxygen (53). This study suggests that at the Shiprock site, uranium contamination is another factor influencing the *Desulfotomaculum* population. To test this hypothesis, we used logistic regression, a statistical technique that is widely used in medical research, but is rarely used in microbial ecology (3, 45). It is a variation of ordinary regression, useful when the observed outcome variable represents the occurrence or nonoccurrence of some outcome event (such as the occurrence or nonoccurrence of sequence cluster G or F). It produces a formula that predicts the probability of the occurrence as a function of the independent variables (such as uranium concentration, DO, and sulfate and nitrate concentration). Logistic regression predicted an increase in the frequency of the presence of cluster G from 18.5% to 90% as the uranium concentration increased from 0 to 3,000 ppb, clearly suggesting that this genus holds a selective advantage over other SRB populations at high U(VI) concentrations. The present work is the first report of *Desulfotomaculum* dominance among SRB in a mesophilic natural environment setting. *Desulfotomaculum* strains isolated from thermophilic environments have been reported more often than those from mesophilic environments; however, this frequency may be attributable to intensified research of extreme environments rather than to a preference of most *Desulfotomaculum* spp. for thermophilic conditions. While the correlation of *Desulfotomaculum* with uranium concentration is clear, we cannot entirely rule out the possibility of another factor related to uranium contamination. However, a full suite of groundwater geochemical parameters, including total organic carbon, were analyzed and included in a preliminary statistical analysis, and no parameters other than uranium and sulfate showed a strong correlation. Since sulfate is present in concentrations ranging from 2 to 3 orders of magnitude greater than that of uranium, sulfate clearly plays the dominant role in *Desulfotomaculum* metabolism. However, the more significant statistical linkage between *Desulfotomaculum* and uranium concentration suggests a competitive advantage for *Desulfotomaculum* conferred by the presence of uranium. This competitive advantage may result from uranium tolerance or from the ability of *Desulfotomaculum* to use U(VI) as a terminal electron acceptor or both.

Conclusions. This study demonstrates a remarkable diversity of DSR sequences associated with bacteria from the δ-*Proteobacteria*, gram-positive, and *Nitrospira* divisions. Since strains with different functional genomic fingerprints also differ considerably in their physiological capabilities, this result suggests strongly that the high diversity detected at the Shiprock site is very likely of ecological significance. These data also showed that the genus *Desulfotomaculum* and *Desulfotomaculum*-like organisms dominated the SRB population of this uranium-contaminated environment. The overall level of SRB

activity relative to those of other functional metabolic groups and the specific role that *Desulfotomaculum* may play in uranium reduction are not addressed by this study, nor is the role of sulfate. However, the strong association between DSR cluster G and uranium concentration indicates that *Desulfotomaculum* has remarkable tolerance and adaptation to high levels of uranium. In addition to confirming the results of this study at other sites, future research might well focus on the in situ activity level of *Desulfotomaculum* relative to uranium concentration and relative to those of other SRB and other functional groups. *Desulfotomaculum* apparently could play a role in both intrinsic and accelerated bioremediation of U(VI)-contaminated environments. For accelerated bioremediation of U(VI), it may be important to either suppress *Desulfotomaculum* to avoid production of toxic H_2S and allow iron reducers to reduce U(VI) or to stimulate *Desulfotomaculum* to intentionally produce insoluble sulfide minerals such as FeS_2 to stabilize U(IV) precipitates. Either case will require advances in understanding of SRB in uranium-contaminated environments.

ACKNOWLEDGMENTS

This work was supported by the U.S. Department of Energy, Office of Science, grant no. DE-FC02-96ER62278 to D. C. White as part of the Assessment Component of the Natural and Accelerated Bioremediation Research Program (NABIR), administered by Anna Palmisano. Support for sample collection and geochemistry was also provided by NABIR to the Pacific Northwest National Laboratory. D. C. White also received support from National Science Foundation grant DEB-9814813. The cooperation of the Navajo Tribal Nation and the U.S. Department of Energy, Uranium Mill Tailings Remedial Action (UMTRA) Program is gratefully acknowledged. Pacific Northwest National Laboratory is operated by Battelle Memorial Institute for the U.S. Department of Energy.

Don Metzler, Craig Goodknight, Stan Morrison, and Mark Kautsky of the UMTRA Program were particularly helpful in the successful conduct of fieldwork to obtain samples critical to this research. We are grateful to David Boone (Portland State University, Portland, Oreg.), who helped this project by kindly providing pure culture strains of SRB.

REFERENCES

1. **Abdelouas, A., W. Lutze, W. Gong, E. H. Nuttall, B. A. Strietelmeier, and B. J. Travis.** 2000. Biological reduction of uranium in groundwater and subsurface soil. Sci. Total Environ. **250**:21–35.
2. **Abdelouas, A., W. Leutz, and E. H., Nuttall.** 1999. Uranium contamination in the subsurface: characterization and remediation, p. 433–473. *In* P. C. Burns and R. Finch (ed.), Uranium: mineralogy, geochemistry, and the environment. Reviews in mineralogy, vol. 38. Mineralogical Society of America, Washington, D.C.
3. **Agresti, A.** 1996 An introduction to categorical data analysis. John Wiley and Sons, Inc., New York, N.Y.
4. **Brecklinghaus, J., W. Schwartz, and R. Naveke.** 1981. Geomicrobiological studies. XIV. Heavy metal tolerance of desulfurizing bacteria under various ecological conditions. Z. Allg. Mikrobiol. **21**:65–76.
5. **Canfield, D. E., and D. J. DeMarias.** 1991. Aerobic sulfate reduction in microbial mats. Science **251**:1471–1473.
6. **Cypionka, H.** 2000. Oxygen respiration by *Desulfovibrio* species. Annu. Rev. Microbiol. **54**:827–848.
7. **Department of Energy.** 2000. Final site observational work plan for the Shiprock, New Mexico, UMTRA Project site. GJO-2000-169-TAR, MAC-GWSHP 1:1. Rev 2. U.S. Department of Energy, Grand Junction, Colo.
8. **Devereux, R., and D. Stahl.** 1993. Phylogeny of sulfate-reducing bacteria and a perspective for analyzing their natural communities, p. 131–160. *In* J. M. Odom and R. Singleton, Jr. (ed.), The sulfate-reducing bacteria: contemporary perspectives. Springer, Berlin, Germany.
9. **Devereux, R., M. R. Winfrey, J. Winfrey, and D. A. Stahl.** 1996. Depth profile of sulfate-reducing bacterial ribosomal RNA and mercury methylation in an estuarine sediment. FEMS Microbiol. Ecol. **20**:23–31.
10. **Dowling, N. J. E., F. Widdle, and D. C. White.** 1986. Phospholipid ester-linked fatty acid biomarkers of acetate-oxidizing sulfate-reducers and other sulfide-forming bacteria. J. Gen. Microbiol. **132**:1815–1826.
11. **Edlund, A., P. D. Nichols, R. Roffey, and D. C. White.** 1985. Extractable and lipopolysaccharide fatty acid and hydroxy fatty acid profiles from *Desulfovibrio* species. J. Lipid Res. **26**:982–988.
12. **Ehrlich, H. L.** 1996. Geomicrobiology. Marcel Dekker, New York, N.Y.
13. **Fründ, C., and Y. Cohen.** 1992. Diurnal cycles of sulfate reduction under oxic conditions in cyanobacterial mats. Appl. Environ. Microbiol. **58**:70–77.
14. **Guckert, J. B., C. P. Antworth, P. D. Nichols, and D. C. White.** 1985. Phospholipid ester-linked fatty acid profiles as reproducible assays for changes in prokaryotic community structure of estuarine sediments. FEMS Microbiol. Ecol. **31**:147–158.
15. **Hristova, K. R., M. Mau, D. Zheng, R. I. Aminov, R. I. Mackie, H. R. Gaskins, and L. Raskin.** 2000. *Desulfotomaculum* genus- and subgenus-specific 16S rRNA hybridization probes for environmental studies. Environ. Microbiol. **2**:143–159.
16. **Jones, H. E., P. A. Trudinger, L. A. Chambers, and N. A. Pyliotis.** 1976. Metal accumulation by bacteria with particular reference to dissimilatory sulphate-reducing bacteria. Z. Allg. Mikrobiol. **16**:425–435.
17. **Karkhoff-Schweizer, R. R., D. P. W. Huber, and G. Voordouw.** 1995. Conservation of the genes for dissimilatory sulfite reductase from *Desulfovibrio vulgaris* and *Archaeoglobus fulgidus* allows their detection by PCR. Appl. Environ. Microbiol. **61**:290–296.
18. **Kates, M.** 1986. Techniques in lipidology: isolation, analysis and identification of lipids, 2nd ed. Elsevier Press, Amsterdam, The Netherlands.
19. **Kohring, L. L., D. B. Ringelberg, R. Devereux, D. A. Stahl, M. W. Mittelman, and D. C. White.** 1994. Comparison of phylogenetic relationships based on phospholipid fatty acid profiles and ribosomal RNA sequence similarities among dissimilatory sulfate-reducing bacteria. FEMS Microbiol. Lett. **119**: 303–308.
20. **LeDuc, L. G., G. D. Feroni, and J. T. Trevors.** 1997. Resistance to heavy metals in different strains of Thiobacillus ferooxidans. World J. Microbiol. Biotechnol. **13**:453–455.
21. **Llobet-Brossa, E., R. Rosello-Mora, and R. Amann.** 1998. Microbial community composition of Wadden Sea sediments as revealed by fluorescence in situ hybridization. Appl Environ. Microbiol. **64**:2691–2696.
22. **Lovley, D. R., and E. J. P. Phillips.** 1992. Reduction of uranium by *Desulfovibrio desulfuricans*. Appl. Environ. Microbiol. **58**:850–856.
23. **Lovley, D. R.** 1993. Dissimilatory metal reduction. Annu. Rev. Microbiol. **47**:263–290.
24. **Lovley, D. R., E. E. Roden, E. J. P. Phillips, and J. C. Woodward.** 1993. Enzymatic iron and uranium reduction by sulfate-reducing bacteria. Mar. Geol. **113**:41–53.
25. **Lovley, D. R., P. K. Widman, J. C. Woodward, and E. J. P. Phillips.** 1993. Reduction of uranium by cytochrome c_3 of *Desulfovibrio vulgaris*. Appl. Environ. Microbiol. **59**:3572–3576.
26. **Manz, W., M. Eisenbrecher, T. R. Neu, and U. Szewzyk.** 1998. Abundance and spatial organization of Gram-negative sulfate-reducing bacteria in activated sludge investigated by *in situ* probing with specific 16S rRNA targeted oligonucleotides. FEMS Microbiol. Ecol. **25**:43–61.
27. **McKinley, J. P., J. M. Zachara, S. C. Smith, and G. D. Turner.** 1995. The influence of uranyl hydrolysis and multiple site-binding reactions on adsorption of U(VI) to montmorillonite. Clays Clay Minerals **43**:586–598.
28. **McKinley, J. P., T. O. Stevens, J. K. Fredrickson, J. M. Zachara, F. S. Colwell, K. B. Wagnon, S. C. Smith, S. A. Rawson, and B. N. Bjornstad.** 1997. Biogeochemistry of anaerobic lacustrine and paleosol sediments within an aerobic unconfined aquifer. Geomicrobiol. J. **14**:23–39.
29. **Minz, D., J. L. Flax, S. J. Green, G. Muyzer, Y. Cohen, M. Wagner, B. E. Rittmann, and D. A. Stahl.** 1999. Diversity of sulfate-reducing bacteria in oxic and anoxic regions of a microbial mat characterized by comparative analysis of dissimilatory sulfite reductase genes. Appl. Environ. Microbiol. **65**:4666–4671.
30. **Odom, J. M.** 1993. Industrial and environmental activities of sulfate-reducing bacteria, p. 189–210. *In* J. M. Odom and R. Singelton, Jr. (ed.), The sulfate-reducing bacteria: contemporary perspectives. Springer-Verlag, Inc., New York, N.Y.
31. **O'Leary, W. M., and S. G. Wilkinson.** 1988. *In*: Microbial lipids vol.1, edited by C. Ratledge and S.G. Wilkinson, Academic Press, Harcourt Brace Jovanovich, Publishers, p172–173.
32. **Parkes, R. J., and A. G. Calder.** 1985. The cellular fatty acids of three strains of *Desulfobulbus*, a propionate-utilizing sulfate-reducing bacterium. FEMS Microbiol. Ecol. **31**:361–363.
33. **Polz, M. F., and C. M. Cavanaugh.** 1998. Bias in template-to-product ratios in multitemplate PCR. Appl. Environ. Microbiol. **64**:3724–3730.
34. **Rabus, R., M. Fukui, H. Wilkes, and F. Widdle.** 1996. Degradative capacities and 16S rRNA-targeted whole-cell hybridization of sulfate-reducing bacteria in an anaerobic enrichment culture utilizing alkylbenzenes from crude oil. Appl. Environ. Microbiol **62**:3605–3613.
35. **Ramsing, N. B., M. Kühl, and B. B. Jørgensen.** 1993. Distribution of sulfate-reducing bacteria, O_2 and H_2S in photosynthetic biofilms determined by oligonucleotide probes and microelectrode. Appl. Environ. Microbiol **59**: 3840–3849.
36. **Ramsing, N. B., H. Fossing, T. Ferdelman, F. Anderson, and B. Thamdrup.**

1996. Distribution of bacterial populations in a stratified fjord (Mariager Fjord, Denmark) quantified by in situ hybridization and related to chemical gradients in the water column. Appl. Environ. Microbiol 62:1391–1404.
37. **Ringelberg, D. B., G. T. Townsend, K. A. DeWeerd, J. M. Sulita, and D. C. White.** 1994. Detection of the anaerobic dechlorinating microorganism *Desulfomonile tiedjei* in environmental matrices by its signature lipopolysaccharide branch-long-chain hydroxy fatty acids. FEMS Microbiol. Ecol. 14:9–18.
38. **Ringelberg, D. B., J. D. Davis, G. A. Smith, S. M. Pfiffner, P. D. Nichols, J. S. Nickels, J. M. Henson, J. T. Wilson, M. Yates, D. H. Kampbell, H. W. Read, T. T. Stocksdale, and D. C. White.** 1989. Validation of signature polar lipid fatty acid biomarkers for alkane-utilizing bacteria in soils and subsurface aquifer materials. FEMS Microbiol. Ecol. 62:39–50.
39. **Singleton, R., Jr.** 1993. The sulfate-reducing bacteria: an overview, p. 1–20. *In* J.M. Odom and R. Singleton, Jr. (ed.), The sulfate-reducing bacteria: contemporary perspectives. Springer Verlag, Inc., New York, N.Y.
40. **Stackebrandt, E., C. Sproer, F. A. Rainey, J. Burghardt, O. Pauker, and H. Hippe.** 1997. Phylogenetic analysis of the genus *Desulfotomaculum*: evidence for the misclassification of *Desulfotomaculum guttoideum* and description of *Desulfotomaculum orientis* as *Desulfosporosinus orientis* gen. nov., comb. nov. Int. J. Syst. Bacteriol. 47:1134–1139.
41. **Stephen, J. R., Y. J. Chang, S. J. Macnaughton, G. A. Kowalchuk, K. T. Leung, C. A. Flemming, and D. C. White.** 1999. Effect of toxic metals on indigenous soil β-subgroup proteobacterium ammonia oxidizer community structure and protection against toxicity by inoculated metal-resistant bacteria. Appl. Environ. Microbiol. 65:95–101.
42. **Strunk, O., and W. Ludwig.** 1996. ARB: a software environment for sequence data. Technische Universität München, Munich, Germany.
43. **Suzuki, M.; M. S. Rappé, and S. J. Giovannoni.** 1998. Kinetic bias in estimates of coastal picoplankton community structure obtained by measurements of small-subunit rRNA gene PCR amplicon length heterogeneity. Appl. Environ. Microbiol. 64:4522–4529.
44. **Tebo, B. M., and A. Y. Obraztsova.** 1998. Sulfate-reducing bacterium grows with Cr(VI), U(VI), Mn(IV), and Fe (III) as electron acceptors. FEMS Microbiol. Lett. 162:193–198.
45. **Trexler, J. C., and J. Travis.** 1993. Nontraditional regression analysis. Ecology 74:1629–1637.
46. **Vainshtein, M., H. Hippe, and R. M. Kroppenstedt.** 1992. Cellular fatty acid composition of *Desulfovibrio* species and its use in classification of sulfate-reducing bacteria. Syst. Appl. Microbiol. 15:554–566.
47. **Voordouw, G.** 1990. Hydrogenase genes in *Desulfovibrio*, p. 37–51. *In* J. P. Belaich, M. Bruschi, and J. L. Garcia (ed.), Microbiology and biochemistry of strict anaerobes involved in interspecies hydrogen transfer. Plenum, New York, N.Y.
48. **Voordouw, G., V. Niviere, F. G. Ferris, P. M. Fedorak, and D. W. S. Westlake.** 1990. Distribution of hydrogenase genes in *Desulfovibrio* spp. and their use in identification of species from the oil field environment. Appl. Environ. Microbiol. 56:3748–3754.
49. **Wagner, M., A. J. Roger, J. L. Flax, G. A. Brusseau, and D. A. Stahl.** 1998. Phylogeny of dissimilatory sulfite reductase supports an early origin of sulfate respiration. J. Bacteriol. 180:2975–2982.
50. **Wawer, C., M. S. M. Jetten, and G. Muyzer.** 1995. Genetic diversity and expression of the [NiFe] hydrogenase large-subunit gene of *Desulfovibrio* spp. in environmental samples. Appl. Environ. Microbiol. 63:4360–4369.
51. **White, D. C., K. Leung, S. J. Macnaughton, C. Flemming, M. Wimpee, and G. Davis.** 1997. Lipid/DNA biomarker analysis for assessment of in situ bioremediation effectiveness, p. 319–324. *In* B. C. Alleman and A. Leeson (ed.), *In situ* and on-site bioremediation, vol. 5. Battelle Press, Columbus, Ohio.
52. **White, D. C., W. M. Davis, J. S. Nickels, J. D. King, and R. J. Bobbie.** 1979. Determination of the sedimentary microbial biomass by extractable lipid phosphate. Oecologia 40:51–62.
53. **Widdle, F.** 1988. Microbiology and ecology of sulfate- and sulfur-reducing bacteria, p.469–585. *In* A. J. B. Zebnder (ed.), Biology of anaerobic microorganisms. John Wiley and Sons, Inc., New York, N.Y.

PERGAMON

Applied Geochemistry 15 (2000) 1035–1042

Applied Geochemistry

www.elsevier.com/locate/apgeochem

Retention of strontium, cesium, lead and uranium by bacterial iron oxides from a subterranean environment

F.G. Ferris[a,*], R.O. Hallberg[b], B. Lyvén[c], K. Pedersen[d]

[a]*Department of Geology, University of Toronto, 22 Russell Street, Toronto, Ont., Canada M5S 3B1*
[b]*Department of Geology and Geochemistry, Stockholm University, S-106 91 Stockholm, Sweden*
[c]*Department of Analytical and Marine Chemistry, Chalmers University, S-412 96 Göteborg, Sweden*
[d]*Department of Cell and Molecular Biology, Microbiology Section, University of Göteborg, Box 462, S-405 30 Göteborg, Sweden*

Received 4 May 1999; accepted 18 August 1999
Editorial handling by R. Fuge

Abstract

Bacteriogenic Fe oxides (BIOS) and groundwater samples were collected 195 m underground at the Strässa Mine in central Sweden. Ferrous iron oxidizing bacteria, including stalked *Gallionella ferruginea* and filamenous *Leptothrix* sp., were prominent in the BIOS samples. The BIOS samples were found to contain only poorly ordered (amorphous) hydrous ferric oxide, as determined by X-ray diffraction. Inductively coupled plasma mass spectroscopy revealed hydroxylamine-reducible Fe and Mn oxide contents that ranged from 55 to 85% on a dry weight basis. Concentrations of Sr, Cs, Pb and U in filtered groundwater ranged from 0.002 to 1.8 μM. Solid phase concentrations of these heavy metals in the BIOS spanned the 0.04–2.23 mmol/kg range. Distribution coefficients (K_d values), calculated as the ratio between BIOS and dissolved heavy metal concentrations, revealed solid phase enrichments that, depending on the heavy metal and Fe oxide content of the sample, extended from $10^{3.0}$ to $10^{4.7}$. At the same time, however, a strong inverse linear relationship was found between $\log K_d$ values and the corresponding mass fraction of reducible oxide in the samples, implying that metal uptake was strongly influenced by the relative proportion of bacterial organic matter in the composite solids. Based on the metal accumulation properties of the BIOS, an important role can be inferred for intermixed Fe oxides and bacterial organic matter in the transport and fate of dissolved metals in groundwater systems.

1. Introduction

Because of their reactive surface properties and ubiquitous distribution in unconsolidated sediments and in hydraulically conductive fracture zones in low permeability bodies of rock, hydrous Fe oxides are considered to be dominant sorbents controlling the dispersion of dissolved metals in groundwater systems (Stumm and Morgan, 1996). This widely held view extends from a large body of experimental laboratory work conducted with synthetic or highly purified crystalline Fe oxides (Dzombak and Morel, 1990). Natural Fe oxides, however, are usually poorly ordered and often contain significant amounts of organic matter, including intact as well as partly degraded bacterial cells (Ferris et al., 1989; Filella et al., 1993; Fortin et al., 1993; Konhauser, 1997). These organic materials,

* Corresponding author. Fax: +1-416-978-3938.
E-mail address: ferris@quartz.geology.utoronto.ca (F.G. Ferris).

0883-2927/00/$ - see front matter
PII: S0883-2927(99)00093-1

including the bacteria, are also known to be highly reactive and effectively comprise a separate sorbent phase for dissolved metals. The intermixing of Fe oxides and organic materials thus produces complex multiple sorbent solids that, depending on their composition, exhibit unique and highly variable metal retention properties (Warren and Zimmerman, 1994a; Ingri and Widerlund, 1994; Tessier et al., 1996).

The precipitation and accumulation of Fe oxides in association with bacterial cells is common in aqueous environments where high concentrations of Fe(III) are produced by either chemical oxidation or bacterial oxidation of Fe(II) (Ferris et al., 1989; Fortin et al., 1993; Konhauser and Ferris, 1996). Significant concentrations of dissolved metals are sorbed and retained by these bacteriogenic Fe oxides (BIOS) (Ferris et al., 1989; Nelson et al., 1995). Moreover, the extent of metal partitioning in BIOS precipitates is enhanced by increasing amounts of bacterial cell organic matter (Ferris et al., 1999). While these effects must extend fundamentally from different sorption affinities between the intermixed Fe oxides and bacterial cell-derived organic matter, an exact account of how changes in metal retention properties relate quantitatively to BIOS composition remains to be established. In this investigation, the Sr, Cs, Pb and U retention properties of BIOS from a hard rock groundwater environment are shown to vary systematically as a function of the relative proportions of oxides and bacterial cell-derived organic matter.

2. Methodology

2.1. Sample collection

Samples of bacteriogenic Fe oxides (BIOS) and water were obtained from two different locations 195 m underground at the now inactive Strässa Fe ore mine in central Sweden (Sundblad, 1994). The first set of samples were collected at mine survey point FP353 (site A) and the second set of samples were collected 50 m further into the tunnel (site B). Throughout the mine, Fe oxides precipitate on tunnel walls where groundwater discharges from hydraulically conductive fractures and in drainage ditches on the tunnel floor. From other microbiological studies in mine environments, the formation of these Fe oxide precipitates can be attributed principally to extensive growth of Fe(II)-oxidizing, bacteria such as *Gallionella ferruginea* and *Leptothrix* sp. (Pedersen and Karlsson, 1995; Pedersen, 1997).

At each site, BIOS precipitates were recovered from both the tunnel wall (samples A1 and B1) and drainage ditch (samples A2 and B2) using sterile plastic spatulas. The samples were placed directly into 200 ml polypropylene tubes. After the precipitates had settled by gravity to the bottom of the tubes (approximately 2–5 min), excess water was decanted to accommodate additional sample collection. This procedure was continued with each sample until at least 30 ml of solid material was accumulated. The BIOS samples collected from the tunnel wall were an orange–brown color, whereas those recovered from the drainage ditch were gray–brown (sample A2) and bright orange (sample B2), respectively. Water samples collected at each of the two sites were filtered through 0.22 μm filters into 200 ml polypropylene tubes and acidified to a final concentration of 2 vol% HNO_3. All of the sample tubes were sealed with screw caps and stored at 4°C in a refrigerator for chemical analyses.

2.2. Chemical and mineralogical analyses

Standard suspensions of the BIOS (ca. 3–30 mg dry weight per ml) were prepared by concentrating and washing samples twice in deionized double distilled water (DDW) by centrifugation at 10,000 × *g* for 15 min. For measurement of total metal concentrations, 0.5 ml of the standard suspensions were digested at 65°C for 24 h in 8.0 ml (final volume) of 32.5% HNO_3. To determine the distribution of metals between reducible oxide and residual solid fractions of the samples, 0.5 ml of the standard suspensions were reacted for 6 h at 65°C in 8.0 ml (final volume) of 0.04 M $NH_2OH.HCl$ in 25 vol% acetic acid, then filtered through 0.22 μm filters (Landström and Tullborg, 1995).

Metal concentrations of the BIOS and water samples were determined using a VG-PQ 1 plasma source mass spectrometer (ICP-MS) equipped with a Babbington V-groove nebulizer. A Gilson 222 autosampler was employed with a sample uptake rate of 0.9 ml/min and dwell times of 0.1 sec for each analyzed element. Between samples the system was rinsed for 30 sec with 1.0 % HNO_3. For C analyses, 0.5 ml of the BIOS standard suspensions were dispensed into small Al cups and then dried at 65°C for 48 h. The weights of the samples were determined on a Cahn high precision balance before C contents were measured with a Carlo Erba Model 1106 elemental analyzer. To evaluate the mineralogy and crystallinity of the BIOS precipitates, samples were dried at 65°C and analyzed with an INEL XRG 3000 X-ray diffractometer using a curved position sensitive detector and Cu Kα radiation (Institute for Energy Technology, Kjeller, Norway).

The structure of hydrated BIOS precipitates was examined using an environmental scanning electron microscope (ESEM). Whole mounts were prepared by placing small droplets of standard suspensions on Al

stubs. These were mounted on a cold stage and imaged at 2.0°C in a Philips XL30 ESEM equipped with a field emission gun and EDAX energy dispersive X-ray (EDX) spectrometer. The instrument was operated in the wet imaging mode (i.e. 100% relative humidity) at 2.9 torr and 20 kV.

3. Results

The Fe(II)-oxidizing bacteria *Leptothrix* sp. and *G. ferruginea*, were easily discerned using the ESEM in whole mounts of the BIOS samples (Fig. 1). Fine-grained mineral precipitates were commonly intermixed among helical twisted stalks of *G. ferruginea* and the filamentous sheaths of *Leptothrix* sp. These precipitates generated strong peaks for Fe in EDX spectra (data not shown) and typically exhibited a granular morphology that emerged from the aggregation of individual crystallites approximately 10–20 nm in diameter. Bulk powder X-ray diffraction did not yield any peaks indicative of crystalline material implying that the mineral grains analyzed by EDX spectroscopy were poorly ordered fine-grained hydrous Fe(III) oxides and also that the samples were substantially free of rock fragments or other mineral debris.

The major element composition of the BIOS was dominated principally by reducible oxide Fe (Table 1), which comprised 41.8–81.6 % of the solid mass as hydrous Fe(III) oxide, $Fe(OH)_3$ (Table 2). Significant amounts of Mn were also present in a reducible oxide phase, accounting for up to 13.4% of the solid mass as MnO_2, contributing presumably to some of the color variations between samples. Calcium concentrations, which approached those of Mn, were removed completely by the hydroxylamine extraction. This is taken normally to infer an association with a reducible oxide phase, either as a sorbed or coprecipitated species, although dissolution of small amounts of Ca CO_3 in response to the acidic extraction procedure cannot be entirely ruled out. Measured Na and Al concentrations were considerably lower (Table 1). Partial recovery of Na in the reducible oxide fraction of samples A2 and B2 and of Al in sample B2, suggest that the drainage ditch BIOS contained minute amounts of detrital clay minerals. In contrast, C analyses indicated that the bulk of the residual mass in the samples was derived

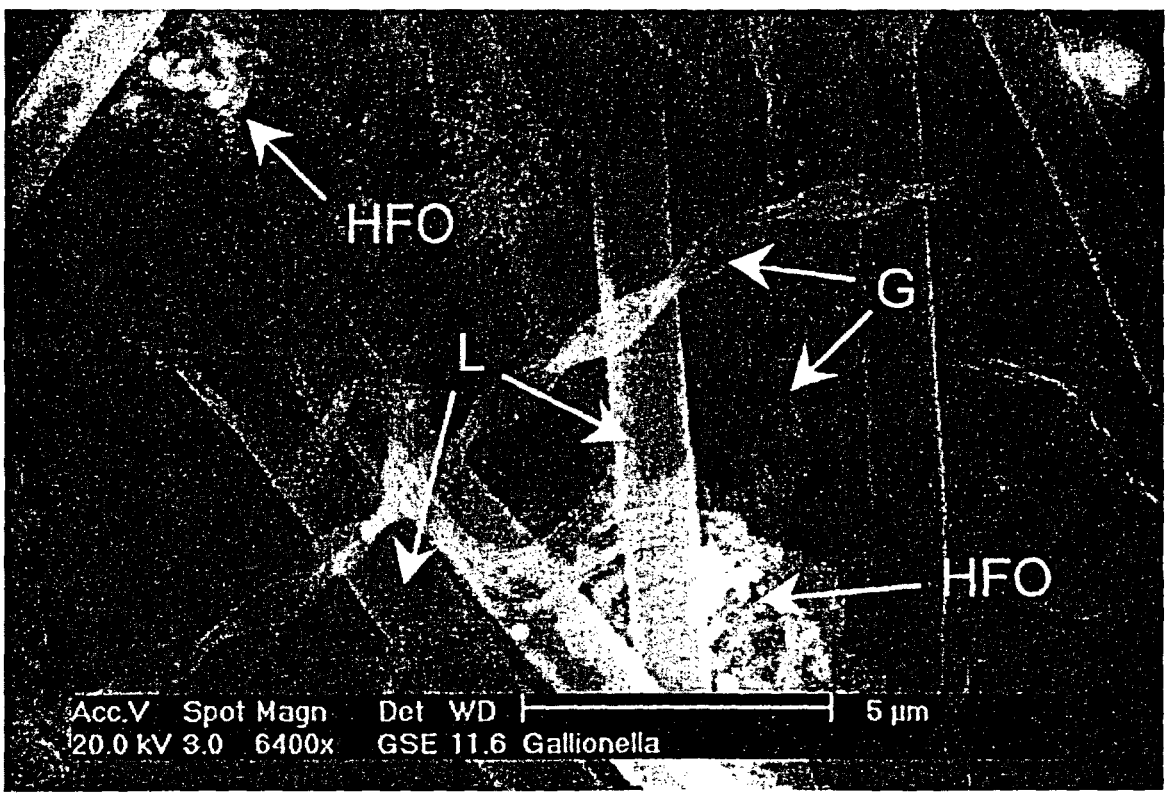

Fig. 1. Environmental scanning electron micrograph showing twisted stalks from *Gallionella ferruginea* (G) and filamentous of sheathed *Leptothrix* species (L) intermixed with fine-grained hydrous Fe oxide mineral precipitates (HFO) in a whole mount specimen from site A2 (scale bar = 5 µm).

Table 1
Total major element concentrations and percentage of the total concentration recovered in the reducible oxide fraction from hydroxylamine extractions of the Strássa bacteriogenic Fe oxides[a]

	Concentration (mmol/kg (percent of total concentration))				
Site	Na	Al	Ca	Mn	Fe
A1	3.5 (100)	12.0 (100)	651.6 (100)	702.9 (100)	6626.7 (100)
A2	158.8 (42)	322.2 (100)	1495.9 (100)	1542.9 (100)	3918.8 (100)
B1	36.9 (100)	7.2 (100)	1193.2 (100)	1377.8 (100)	5290.8 (100)
B2	61.9 (23)	39.2 (44)	1019.2 (100)	329.6 (100)	7636.9 (100)

[a] The standard deviations for duplicate measurements of individual metal concentrations were less than ±10% of the reported values.

largely from bacterial organic matter, in accordance with ESEM observations, as well as powder X-ray diffraction results (Table 2).

The dissolved concentrations of Sr, Cs, Pb and U in the water samples ranged from 0.002 to 1.8 μM range (Table 3). Strontium concentrations were the highest of the measured dissolved heavy metals, followed by U, Cs and Pb. The variation in dissolved heavy metal concentrations and pH between the two sample sites was quite low, as Table 3 shows.

The solid phase metal concentrations of Sr, Cs, Pb and U in the BIOS are shown in Table 4. In comparison to the water samples (Table 3), the metal concentrations in the BIOS were relatively high, implying that the dissolved metals had been sorbed and retained by the solid phase accumulates. To assess the solid phase partitioning of the heavy metals, distribution coefficients (K_d) were calculated following the conventional operational definition as the ratio between solid (Me_{BIOS}) and dissolved ($Me_{Dissolved}$) metal concentrations (Stumm and Morgan, 1996):

$$K_d = [Me_{BIOS}]/[Me_{Dissolved}] \quad (1)$$

The highest K_d values (ca. $10^{3.9}$–$10^{4.7}$) were obtained for Pb partitioning into the BIOS (Fig. 2). Conversely, Sr yielded the lowest K_d values (ca. $10^{3.0}$–$10^{3.1}$) among the heavy metals. Differences in K_d values for an individual metal between samples ranged from a factor of less than 1.25 in the case of Sr to around one order of magnitude for Cs, Pb and U.

A strong inverse linear relationship between log K_d and reducible Fe oxide content was evident for each of the heavy metals (Fig. 2). The decrease in log K_d with increasing reducible oxide content of the BIOS can be inferred from the equilibrium mass action expression describing the interaction and sorption of a dissolved metal at protonated surface sites (SH):

$$K_S \exp(-zF\Psi_P) = [Me_{BIOS}][H^+]/[Me_{Dissolved}][SH] \quad (2)$$

This expression assumes surface site activities are equivalent to their actual concentrations and that the activity of dissolved aqueous species correspond to analytical concentrations, as is expected for low ionic

Table 2
Bulk composition of the Strássa Mine bacteriogenic iron oxides

	Percent by weight[a]			
Site	MnO_2[b]	$Fe(OH)_3$[b]	Total Oxide[c]	Organic[d]
A1	6.1	70.8	76.9	43.9
A2	13.4	41.8	55.2	53.5
B1	12.0	56.5	68.5	24.5
B2	2.9	81.6	84.5	6.2

[a] Total mass balances sum to 100% within the cumulative standard deviations of ±10% associated with the measurements of each individual component.

[b] Calculated using a formula weight of 86.94 for manganese oxide (MnO_2) and 106.85 for hydrous ferric oxide, $Fe(OH)_3$.

[c] Calculated as the sum of manganese and iron oxides.

[d] Calculated based on the measured carbon content of the samples assuming a general formula of CH_2O for organic matter. Environmental scanning electron microscopy indicated that the organic fraction was comprised of biomass derived principally from the Fe(II)-oxidizing bacteria *Leptothrix* sp. and *Gallionella ferruginea*.

Table 3
Dissolved heavy metal concentrations and pH of the Strássa Mine water samples[a]

		Concentration (μM)			
Site	pH	Sr	Cs	Pb	U
A	8.3	1.804	0.005	0.002	0.060
B	8.3	1.632	0.004	0.002	0.045

[a] The relative standard deviations for duplicate measurements of individual metal concentrations were less than ±10% of the reported values.

Table 4
Total concentration of heavy metals in the Strássa bacteriogenic iron oxides[a]

	Concentration (mmol/kg solid)			
Site	Sr	Cs	Pb	U
A1	1.814	0.012	0.024	0.124
A2	2.228	0.058	0.104	0.331
B1	1.780	0.027	0.033	0.200
B2	1.700	0.004	0.014	0.081

[a] The relative standard deviations for duplicate measurements of individual metal concentrations were less than ±10% of the reported values.

strength natural waters (Stumm and Morgan, 1996). In accordance with surface complexation theory, the conventional reference state for the sorption constant (K_S) is zero mean particle surface potential (Ψ_P) (Dzombak and Morel, 1990). The exponential term included in the mass action relationship thus corrects for non-ideal behavior that arises from electrostatic work associated with the transport of ions of charge z through an interfacial potential gradient on sorbent solids; F is the Faraday constant, R is the gas constant and T is absolute temperature. Because the BIOS are comprised principally of reducible oxides and bacterial biomass, the weighted mean surface potential can be formulated as:

$$\Psi_P = \Psi_{ox} f_{ox} + \Psi_{bac} f_{bac} = f_{ox}(\Psi_{ox} - \Psi_{bac}) + \Psi_{bac} \quad (3)$$

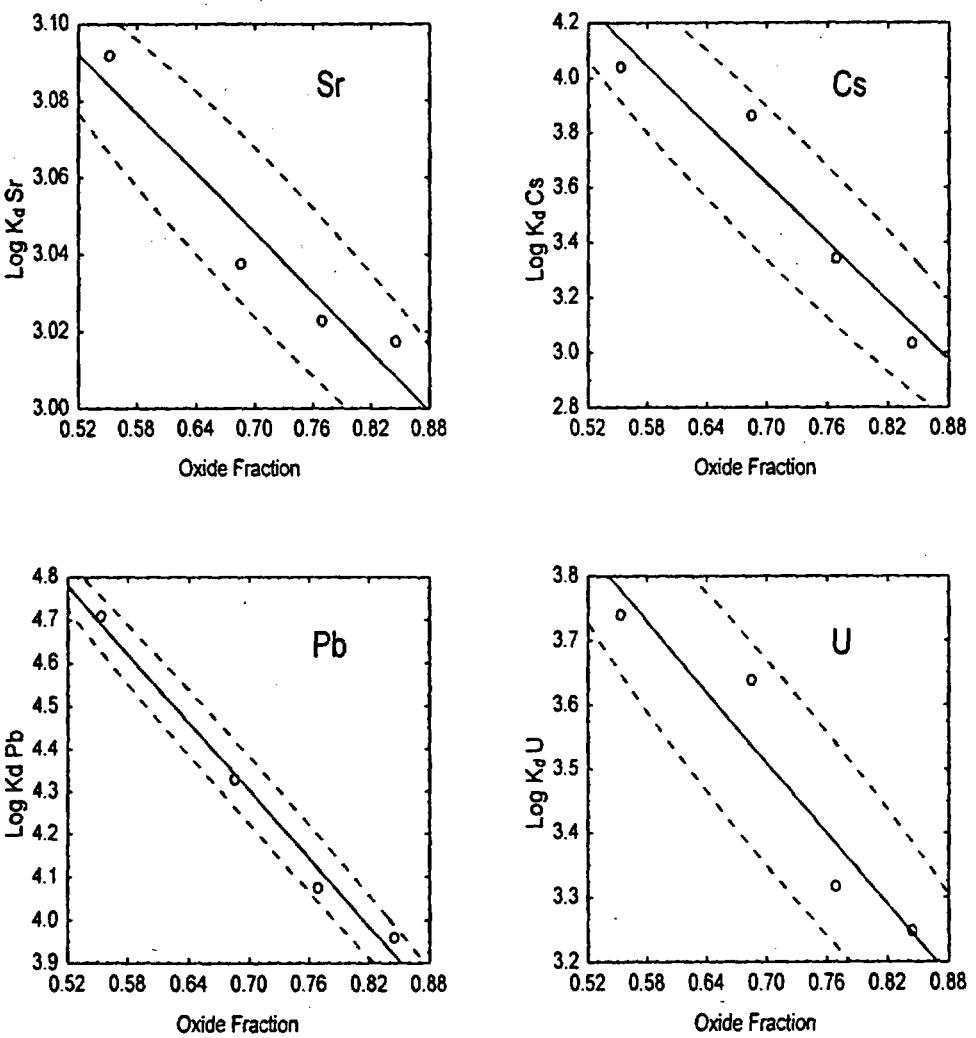

Fig. 2. Plot of log K_d as a function of the mass fraction of reducible oxides in the bacteriogenic Fe oxides. Dashed lines correspond to 90% elliptical confidence intervals for bivariate normal probability distributions of values along the (solid) regression line (STATISTICA v. 5.0). Regression coefficients are given in Table 5.

where f_{ox} and f_{bac} are the reducible oxide and bacterial mass fractions, respectively, and Ψ_{ox} and Ψ_{bac} are the corresponding surface potentials. Combining Eqs.(1)–(3) in logarithmic form yields:

$$\log K_d = \log(K_S[SH]/[H^+]) - 2.303\, z F\Psi_{bac}/RT - f_{ox}2.303zF(\Psi_{ox} - \Psi_{bac})/RT \quad (4)$$

This relationship indicates that, under equilibrium conditions at constant pH, the observed log K_d values of the BIOS should be inversely proportional to the reducible oxide mass fraction, as illustrated in Fig. 2. Further inspection reveals that at the boundary condition of $f_{ox} = 0$, log K_d = log $K_{d\ bacteria}$, while at $f_{ox} = 1$, log K_d = log $K_{d\ oxide}$. These boundary condition values are given in Table 5. Similarly, the slope given in Eq. (4) $[-2.303\ zF(\Psi_{ox}-\Psi_{bac})/RT]$ can be recognized as the logarithm of the ratio between the sorption constants of the oxide and bacteria, respectively (Table 5).

As the regression coefficients given in Table 5 indicate, over 90% of the variance in the heavy metal log K_d values of the BIOS can be attributed directly to differences in the mass fraction of reducible oxides. At the same time, the estimated log K_d values for the oxide fraction are lower than those of the bacterial fraction. These differences are, in turn, reflected in the $\log(K_{S\ oxide}/K_{S\ bacteria})$ values which indicate that sorption affinities of the oxide fraction are, depending on the metal, anywhere from $10^{-0.26}$ to $10^{-3.56}$ times lower than those of the bacterial fraction. The trend among the measured oxide and bacterial K_d values of Pb > U > Sr follows the same order reported for corresponding sorption constants on hydrous Fe(III) oxide (Dzombak and Morel, 1990). A value for the sorption constant of Cs could not be found for comparison; however, the bacterial K_d for Cs is quite large relative to the corresponding oxide K_d. This suggests that the Cs sorption affinity of bacterial-derived organic matter is rather high.

Table 5
Regression coefficients, K_d values and sorption constant ratios obtained from plots of heavy metal partitioning as a function of the mass fraction of reducible oxides in the Strässa bacteriogenic Fe oxides (Fig. 2)

Metal	r^2	log $K_{d\ bacteria}$	log $K_{d\ oxide}$	$\log[K_{S\ oxide}/K_{S\ bacterial}]$
Sr	0.91	3.23	2.97	−0.26
Cs	0.92	6.11	2.55	−3.56
Pb	0.99	6.16	3.51	−2.65
U	0.90	4.79	2.96	−1.83

4. Discussion

In low permeability bodies of hard rock, the major structural features that control the movement of groundwater are hydraulically conductive fracture zones (Gascoyne et al., 1995). Marked redox and O_2 gradients often develop in these systems as meteoric or surface waters recharge the subterranean environment, or when groundwater discharges into excavated tunnels and vaults. Such gradients provide ideal habitats for Fe(II)-oxidizing bacteria like *G. ferruginea* and *Leptothrix* sp. (Ghiorse, 1984; Hallbeck and Pedersen, 1991, 1995). The oxidized Fe(III) generated by these bacteria is commonly subjected to hydrolysis and precipitation at the pH of most natural groundwaters (Stumm and Morgan, 1996). As the bulk compositional analyses on the Strässa BIOS confirm, this contributes to a varying degree of intermixing of Fe oxides and bacterial cell-derived organic matter (Pedersen, 1997; Ferris et al., 1999).

Many studies have shown that the solid phase partitioning of dissolved metals and associated K_d values are quite sensitive to the composition of reactive particulate materials (Warren and Zimmerman, 1994b; Radovanovic and Koelmans, 1998). Because of this sensitivity, reported K_d values for individual metals on natural solids often show considerable divergence, even in systems characterized by relatively constant aqueous geochemical conditions (Ingri and Widerlund, 1994; Warren and Zimmerman, 1994a). As such, the different K_d values obtained for Sr, Cs, Pb and U in the Strässa BIOS are not unusual, but rather illustrate the inherent variability that can be anticipated for metal uptake and retention by heterogeneous solid materials.

Many studies have noted that the incorporation of organic matter into inorganic particulate solids can have a significant impact on metal partitioning and sustain large increases in K_d values (Zachara et al., 1994; Payne et al., 1996). This kind of behavior was observed with the Strässa BIOS and has been noted with similar samples collected 100–400 m underground at the Äspö Hard Rock Laboratory in Sweden (Ferris et al., 1999). For some metals, like Cu for example, enhanced partitioning can be traced qualitatively by way of selective chemical extractions to a very high and specific affinity for the organic fraction of composite sorbents (Warren and Zimmerman, 1994a; Lin and Chen, 1998; Ferris et al., 1999). However, other metals are apt to be released in a non-specific manner (i.e. simultaneously) from organic and inorganic phases in composite solids, particularly at the low pH of reagents commonly used in selective chemical extractions. This serves to confound inferences concerning sorption affinities, making it difficult to use data from selective chemical extractions to interpret variations in

K_d values with respect to changes in solid phase composition.

The utility of surface complexation theory to describe quantitatively the sorptive properties of natural particulate solids has received considerable recent attention (Fein et al., 1997; Warren and Ferris, 1998; Wen et al., 1998). A major guiding postulate in surface complexation theory is the assumption of zero mean surface potential as the reference state for determination of equilibrium sorption constants (Dzombak and Morel, 1990). The implicit corollary is that changes in surface potential, which are known to arise from the incorporation of organic matter into Fe oxides (Day et al., 1994), serve to systematically alter the sorptive properties of particulate solids. In more practical terms, the decrease in heavy metal K_d values with increasing reducible oxide content in BIOS follows a pattern consistent with the fundamental principles of surface complexation theory.

The importance of bacterial derived organic matter in determining the K_d values of heterogenous solids like BIOS has been difficult to assess in a quantitative way, particularly as few intrinsic equilibrium sorption constants have ever been determined for bacteria. Those that do exist suggest that bacteria are very potent sorbents of dissolved metals with sorption affinities that often exceed inorganic solids like hydrous Fe(III) oxides (Dzombak and Morel, 1990; Fein et al., 1997). This perception is strengthened considerably by the low oxide-bacteria intrinsic sorption constant ratios obtained for the retention of Sr, Cs, Pb and U. The implication is that an important role can be inferred for the intermixing of bacterial organic matter with Fe oxides in the transport and fate of dissolved metals in groundwater systems.

The influence of solid phase reactivity and hydraulic conductivity on the dispersion of dissolved metals in groundwater systems, while substantial, have been shown in computer modeling studies to be less exacting parameters than the abundance and spatial distribution of reactive solids, such as hydrous Fe oxides (Thompson et al., 1996). Instead, a high degree of importance can be inferred for multicomponent interactions that are apt to exert concomitant control over the extent and spatial pattern of solid phase metal partitioning. Within this evolving conceptual model, the accumulation of BIOS is of great interest as bacterial-induced mineral precipitation reactions serve to localize Fe oxide deposition in places where bacteria are growing and bacterial cell-derived organic matter enhances solid phase metal retention. Certainly, understanding coupled interactions between bacterial and geochemical processes has emerged as a new focal point for hydrogeochemistry (Warren and Ferris, 1998), especially as computer modeling efforts strive towards accommodating the intrinsic physical, chemical and biological heterogeneity of natural systems in a realistic manner (Thompson et al., 1996)

Acknowledgements

This work was supported by the Natural Science and Engineering Research Council of Canada, The Swedish Institute and The Swedish Foundation for International Cooperation in Research and Higher Education.

References

Day, G.M., Hart, B.T., McKelvie, I.D., Beckett, R., 1994. Adsorption of natural organic-matter onto goethite. Colloids Surf A Physicochem. Eng Aspects 89, 1–13.

Dzombak, D.A., Morel, F.M.M., 1990. Surface Complexation Modeling: Hydrous Ferric Oxide. John Wiley and Sons, New York.

Fein, J.B., Daughney, C.J., Yee, N., Davis, T.A., 1997. A chemical equilibrium model for metal sorption onto bacterial surfaces. Geochim. Cosmochim. Acta 61, 3319.

Ferris, F.G., Schultze, S., Witten, T.C., Fyfe, W.S., Beveridge, T.J., 1989. Metal interactions with microbial biofilms in acidic and neutral pH environments. Appl. Environ. Microbiol. 55, 1249–1257.

Ferris, F.G., Konhauser, K.O., Lyvén, B., Pedersen, K., 1999. Accumulation of metals by bacteriogenic iron oxides in a subterranean environment. Geomicrobiol. J. 16, 181–192.

Filella, M., Buffle, J., Leppard, G.C., 1993. Characterization of submicrometer colloids in fresh-waters: evidence for their bridging by organic structures. Water Sci. Technol. 27, 91–102.

Fortin, D., Leppard, G.C., Tessier, A., 1993. Characteristics of lacustrine diagenetic iron oxyhydroxides. Geochim. Cosmochim. Acta 57, 4391–4404.

Gascoyne, M., Stroes-Gascoyne, S., Sargent, F.P., 1995. Geochemical influences on the design, construction and operation of a nuclear waste vault. Appl. Geochem. 10, 657–672.

Ghiorse, W.C., 1984. Biology of iron- and manganese-depositing bacteria. Ann. Rev. Microbiol. 38, 515–550.

Hallbeck, L., Pedersen, K., 1991. Autotrophic and mixotrophic growth of *Gallionella ferruginea*. J. Gen. Microbiol. 138, 2657–2661.

Hallbeck, L., Pedersen, K., 1995. Biofilm development by the stalk-forming and iron-oxidizing bacterium *Gallionella ferruginea* and evaluation of the benefits associated with the stalk. Microb. Ecol. 30, 257–269.

Ingri, J., Widerlund, A., 1994. Uptake of alkali and alkaline-earth elements on suspended iron and manganese in the Kalix River, northern Sweden. Geochim. Cosmochim. Acta 58, 5433–5442.

Konhauser, K.O., 1997. Bacterial iron biomineralization in nature. FEMS Microbiol. Rev. 20, 315–326.

Konhauser, K.O., Ferris, F.G., 1996. Diversity of iron and silica precipitation by microbial mats in hydrothermal

waters, Iceland: implications for Precambrian iron formations. Geology 24, 323–326.

Landström, O., Tullborg, E.-L., 1995. Interactions of trace metals with fracture filling minerals from the Äspö Hard Rock Laboratory. SKB Technical Report 95-13, Svensk Kärnbränslehantering AB, Stockholm, Sweden.

Lin, J.-G., Chen, S.-Y., 1998. The relationship between adsorption of heavy metals and organic matter in river sediments. Environ. Int. 24, 345–352.

Payne, T.E., Davis, J.A., Waite, T.D., 1996. Uranium adsorption on ferrihydrite: effects of phosphate and humic acid. Radiochim. Acta 74, 239–243.

Pedersen, K., 1997. Microbial life in deep granitic rock. FEMS Microbiol. Rev. 20, 399–414.

Pedersen, K., Karlsson, F., 1995. Investigations of subterranean microorganisms. SKB Technical Report 95-10, Svensk Kärnbränslehantering AB, Stockholm, Sweden.

Nelson, Y.M., Waihung, L., Lion, L.W., Shuler, M.L., Ghiorse, W.C., 1995. Lead distribution in a simulated aquatic environment: effects of bacterial biofilms and iron oxide. Water Res. 29, 1934–1944.

Radovanovic, H., Koelmans, A.A., 1998. Prediction of in situ trace metal distribution coefficients for suspended solids in natural waters. Environ. Sci. Technol. 32, 753–759.

Stumm, W., Morgan, J.J., 1996. Aquatic Chemistry, 3rd ed. John Wiley, New York.

Sundblad, K., 1994. A genetic reinterpretation of the Falun and Ammeberg ore types, Bergslagen, Sweden. Miner. Deposita 29, 170–179.

Tessier, A., Fortin, D., Belzile, N., DeVitre, R.R., Leppard, G.C., 1996. Metal sorption to diagenetic iron and manganese oxyhydroxides and associated organic matter: narrowing the gap between field and laboratory measurements. Geochim. Cosmochim. Acta 60, 387–404.

Thompson, A.F.G., Schafer, A.L., Smith, R.W., 1996. Impacts of physical and chemical heterogeneity on cocontaminant transport in a sandy porous medium. Water Resource Res. 32, 801–818.

Warren, L.A., Ferris, F.G., 1998. Continuum between sorption and precipitation of Fe(III) on microbial surfaces. Environ. Sci. Technol. 32, 2331–2337.

Warren, L.A., Zimmerman, A.P., 1994a. The influence of temperature and NaCl on cadmium, copper and zinc partitioning among suspended particulate and dissolved phases in an urban river. Water Res. 28, 1921–1931.

Warren, L.A., Zimmerman, A.P., 1994b. The importance of surface-area in metal sorption by oxides and organic-matter in a heterogenous natural sediment. Appl. Geochem. 9, 245–254.

Wen, X., Du, Q., Tang, H., 1998. Surface complexation model for the heavy metal adsorption on natural sediment. Environ. Sci. Technol. 32, 870–875.

Zachara, J.M., Resch, C.T., Smith, S.C., 1994. Influence of humic substances on Co2+ sorption by a sursurface mineral separate and its mineralogical components. Geochim. Cosmochim. Acta 58, 553–566.

Creation of a Subsurface Permeable Treatment Zone for Aqueous Chromate Contamination Using In Situ Redox Manipulation

by J.S. Fruchter, C.R. Cole, M.D. Williams, V.R. Vermeul, J.E. Amonette, J.E. Szecsody, J.D. Istok, and M.D. Humphrey

Abstract

An in situ redox manipulation (ISRM) method for creating a permeable treatment zone in the subsurface has been developed at the laboratory bench and intermediate scales and deployed at the field scale for reduction/immobilization of chromate contamination. At other sites, the same redox technology is currently being tested for dechlorination of TCE. The reduced zone is created by injected reagents that reduce iron naturally present in the aquifer sediments from Fe(III) to surface-bound and structural Fe(II) species. Standard ground water wells are used, allowing treatment of contaminants too deep below the ground surface for conventional trench-and-fill technologies.

A proof-of-principle field experiment was conducted in September 1995 at a chromate (hexavalent chromium) contaminated ground water site on the Hanford Site in Washington. The test created a 15 m (~50 feet) diameter cylindrical treatment zone. The three phases of the test consisted of (1) injection of 77,000 L (20,500 gallons) of buffered sodium dithionite solution in 17.1 hours, (2) reaction for 18.5 hours, and (3) withdrawal of 375,000 L (99,600 gallons) in 83 hours. The withdrawal phase recovered 87% to 90% of the reaction products. Analysis of post-experimental sediment cores indicated that 60% to 100% of the available reactive iron in the treated zone was reduced. The longevity of the reduced zone is estimated between seven and 12 years based on the post-experiment core samples. Three and half years after the field test, the treatment zone remains anoxic, and hexavalent chromium levels have been reduced from 0.060 mg/L to below detection limits (0.008 mg/L). Additionally, no significant permeability changes have been detected during any phase of the experiment.

Introduction

The goal of the in situ redox manipulation (ISRM) method is to create a permeable treatment zone in the subsurface to remediate redox-sensitive mobile contaminants (Figure 1). As illustrated, redox sensitive contaminants in the plume are immobilized or destroyed as they migrate through the manipulated zone. The permeable treatment zone is created by injecting appropriate reagents and buffers (e.g., sodium dithionite, potassium carbonate, and potassium bicarbonate) to chemically reduce the ferric iron in the sediments to ferrous iron. The ISRM approach extends the permeable iron redox treatment zone concept to sites where the ground water contaminant plumes are too deep (tens of meters below the ground surface) to be treated by excavation or by trench-emplaced zero-valent iron barriers (Borden et al. 1997; Matheson and Tratnyek 1993; Blowes and Ptacek 1992; Xu and Schwartz 1992). The ISRM approach also provides an alternative to pump and treat, especially for those plumes that require extended treatment times.

A proof-of-principle field test using the ISRM approach was conducted at the 100 H area of the Hanford Site (Figure 2) in September 1995 in an initially aerobic unconfined aquifer with low levels of hexavalent chromium contamination. The field experiment involved the injection and withdrawal of a reagent (sodium dithionite with potassium carbonate/bicarbonate pH buffers) through a standard ground water well into an aquifer to create a reduced

Pages 66–77

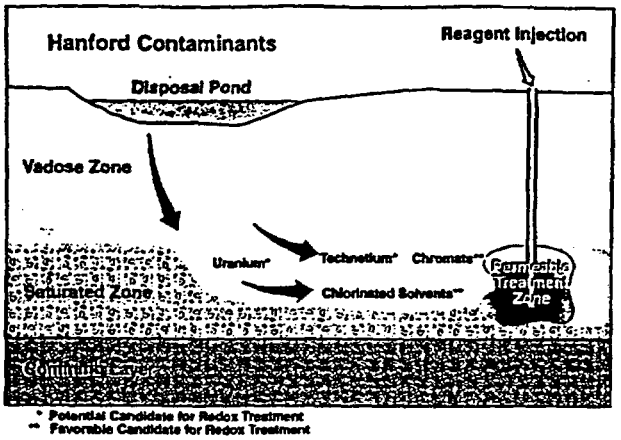

Figure 1. In situ permeable treatment zone concept.

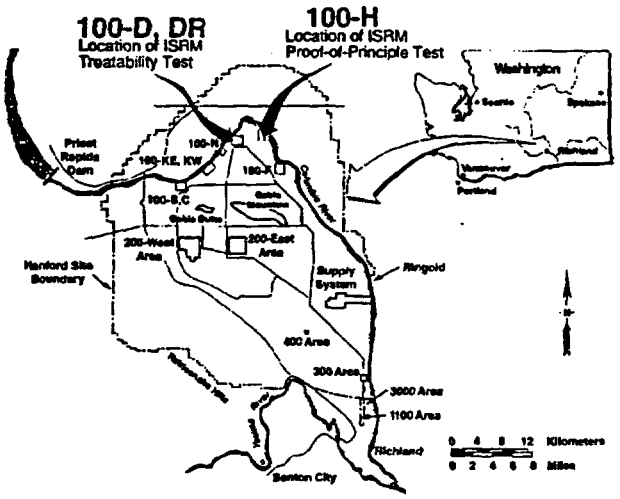

Figure 2. Map of Department of Energy's Hanford site, Washington, showing the location of the 100 H Area ISRM proof-of-principle test site and the 100 D area ISRM treatability test site.

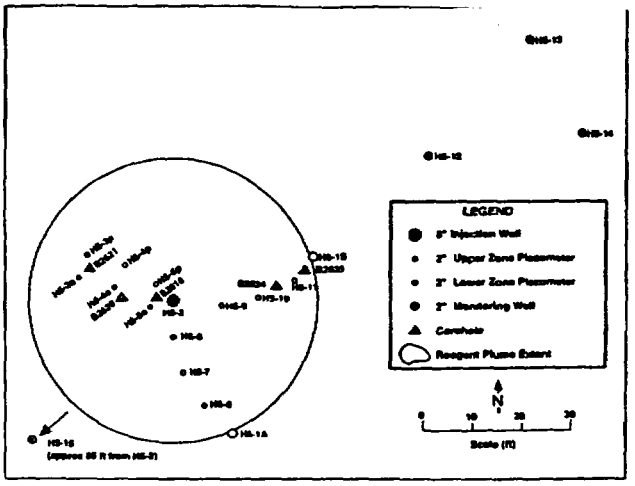

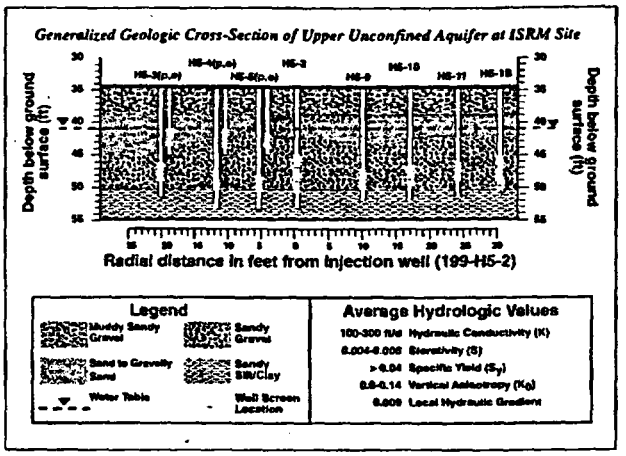

Figure 3. (a) Well layout and corehole locations–100 H area ISRM site. (b) Cross section of aquifer/wells at 100 H. Wells outside the treatment zone (H5-1A, H5-12, H5-13, H5-14, and H5-15) are screened across the entire unconfined aquifer.

zone approximately 15 m (50 feet) in diameter (Figure 3). Three and a half years following the dithionite injection/withdrawal test the treatment zone within the aquifer remains anoxic and hexavalent chromium is below detection limits. This ISRM proof-of-principle field test is the focus of this paper. Laboratory studies and numerical modeling conducted prior to the field test to aid design are discussed briefly below.

Relevant Chemistry of Chromium and Iron in the Subsurface

The target contaminant for this study is chromium in its hexavalent form. In dilute, near neutral aqueous solutions, hexavalent chromium is generally present as the highly soluble and mobile chromate anion $HCrO_4^-$. Its concentration in ground water and surface water in the United States is regulated under the Safe Drinking Water Act (maximum contaminant level [MCL]= 0.100 mg/L as Cr) and the Clean Water Act (ambient water quality criteria [AWQC] = 0.011 mg/L as Cr). The trivalent form of chromium is much less toxic and mobile in the environment. Upon reduction to Cr(III), Cr^{3+} in solution readily hydrolyzes and precipitates as $Cr(OH)_3(s)$ (Rai et al. 1989). Under most ground water conditions the solubility of $Cr(OH)_3(s)$ is well below the 0.100 mg/L MCL. When Cr(III) is precipitated in soils containing ferric iron, solid solutions with ferric iron can also form, resulting in (Cr, Fe) $(OH)_3(s)$. The aqueous Cr(III) concentrations in equilibrium with this phase are even lower than that of the pure $Cr(OH)_3(s)$ phase (Sass and Rai 1987; Patterson et al. 1997).

Once the $Cr(OH)_3(s)$ or $(Cr,Fe)(OH)_3$ phase is formed, it is not readily reoxidized back to chromate. Available information indicates that the rate of oxidation of Cr(III) by oxygen is slow if it occurs at all (Schroeder and Lee 1974; van der Weijden and Reith 1982; Eary and Rai 1987). Manganese oxides are the only other known naturally occurring oxidants capable of oxidizing Cr(III) (Eary and Rai 1987). Although Cr(III) oxidation readily occurs on Mn oxides, a number of factors have been found that greatly limit the progress of this reaction in the subsurface environment (Fendorf et al. 1992, 1993; Fendorf and Zasoski 1992; Manceau and Charlet 1992; Johnson and Xyla 1991; Eary and Rai 1987; Amacher and Baker 1982). Therefore, a method that reduces hexavalent chromium to the trivalent form in ground water should be effective as an aquifer restoration

method.

The most abundant potential inorganic reductant in most ground water aquifers is iron, which occurs naturally in minerals and oxide coatings in aquifer sediments in both the divalent (ferrous) and trivalent (ferric) oxidation states. Although a number of common minerals contain ferrous iron in their internal structure, in oxidizing aquifers, the minerals and soil particles are often coated with ferric iron containing products of weathering such as oxides and oxyhydroxides. It is this surface ferric iron, along with the ferric iron in certain clay minerals, that is chemically reactive and available for use in forming a reductive treatment zone to react with dissolved chromate and other oxidized species. The reaction is illustrated in Equation 1.

$$HCrO_4^-(aq) + 3Fe^{2+}(s) + 8H_2O \rightarrow Fe_3Cr(OH)_{12}(s) + 5H^+ \quad (1)$$

Laboratory Experiments

Initial bench-scale batch and column experiments conducted on Hanford sediments evaluated potential reducing reagents, including sodium dithionite, dissolved sulfur dioxide, and hydroxylamine hydrochloride. Of the reagents tested, only sodium dithionite exhibited substantial reaction rates for reduction of iron in the sediments at ambient temperatures (Fruchter et al. 1992, 1994). Once sodium dithionite was selected as the preferred reagent, a variety of batch and column experiments with sediment and dithionite were performed by Amonette et al. (1994). These bench-scale studies were used to develop an understanding of the important reactions, final reaction products (i.e., residuals), and nature and fate of any ions released from the sediments and sediment surface coatings under reducing conditions (e.g., mobilization of trace metals).

Amonette et al. (1994) indicate that, within the aquifer, the injected dithionite reacts with structural iron in oxyhydroxide and iron-bearing layer silicate mineral phases, reducing Fe(III) to Fe(II) according to the overall reaction described by Equation 2.

$$S_2O_4^{2-}(aq) + 2Fe(III)(s) + 2H_2O \rightarrow 2SO_3^{2-}(aq) + 2Fe(II)(s) + 4H^+ \quad (2)$$

The reduced sediments in the treatment zone can remove dissolved oxygen and redox-sensitive contaminants from ground water flowing through the zone. Within the zone of dithionite-reduced sediments, aqueous chromate reacts with Fe(II) produced by the dithionite reaction (Equation 2) and is precipitated as a solid hydroxide (e.g., $Cr(OH)_3$) according to the example reaction described in Equation 1. Similar precipitation reactions will occur for other oxidized redox-sensitive metal species.

Sodium dithionite is unstable in aqueous solution at neutral pH and can undergo a number of homogeneous and heterogeneous disproportionation reactions that can reduce dithionite concentrations and, as a result, the quantity of Fe(II) produced (Equation 3).

$$S_2O_4^{2-} + \tfrac{1}{2}H_2O \rightarrow SO_3^{2-} + \tfrac{1}{2}S_2O_3^{2-} + H^+ \quad (3)$$

Because stability is greatly enhanced at high pH, the reagent consisted of sodium dithionite in a potassium carbonate/potassium bicarbonate buffer (pH 11). As the solution is injected, the pH drops rapidly to below 9.5 due to reaction with the acidity produced by the oxidation of the sulfur species (dithionite and reaction products). The potassium-based buffer was chosen over its less expensive sodium-based counterpart to reduce the possibility of clay mobilization and flocculation during the emplacement process.

The bench-scale laboratory experiments were followed by a series of intermediate-scale experiments conducted at Oregon State University (Istok et al. 1999). These experiments mimicked the radial flow field planned for the proof-of-principle field test.

Mathematical models were developed to integrate the results from the bench-scale experiments with the site characterization information in order to define nominal specifications for the field experiments (Williams et al. 1994). This process then proceeded in an iterative fashion with designs being checked against experiments at the intermediate scale and improved as necessary before they were carried out in the field. Important design factors include well and corehole placement, reagent and buffer concentrations, injection and withdrawal rates, and the duration of each stage of the experiment (injection, reaction, and withdrawal). Reactive transport numerical models were also used to interpret the results of these experiments to determine reaction kinetics at larger scales (i.e., intermediate and field).

Proof-of-Principle Field Experiment

The discussed laboratory experiments culminated in a full-scale, proof-of-principle ISRM field experiment conducted in September 1995 at the Hanford 100 H area (Figure 2) southwest of the 100 H reactor and about 730 m (2400 feet) from the Columbia River. While the scale of the field test was much larger than the laboratory experiments (Figure 3a), the small size of this field test made it difficult to evaluate downgradient effects due to uncertainties in the ground water flow direction.

The unconfined aquifer at the test site is approximately 12.5 m (41 feet) below the surface and 3 m (9 feet) thick. It is composed of glaciofluvial sands and sandy gravels of the Hanford formation (Figure 3b) and is bounded below by a sandy clay to clayey silt (Ringold lower mud unit). The site is relatively uncontaminated, with only low levels (< 0.100 mg/L) of hexavalent chromium in the ground water. Sixteen wells were drilled and completed, including a central injection/withdrawal well, upper and lower zone monitoring wells within the radial extent of the treatment zone, and four fully screened monitoring wells outside the treatment zone (Figures 3a and 3b). The central injection/withdrawal well and primary monitoring wells within the treatment zone were completed across the lower half of the aquifer to target the

dithionite treatment within this zone. This test design was selected to simplify the experiment by minimizing effects associated with reoxygenation at the water table surface and transient effects associated with the formation of an injection mound.

Prior to conducting the full-scale dithionite injection/withdrawal experiment, a series of site characterization activities were completed. These included hydraulic tests, a full-scale bromide tracer injection/withdrawal test that mimicked all three phases planned for the full-scale dithionite injection/withdrawal experiment, and a "mini" dithionite injection/withdrawal test. These activities are fully described in Fruchter et al. (1996) and Vermeul et al. (1995).

Objectives of the Field Study

The primary objective of the ISRM proof-of-principle field experiment was to determine the feasibility of creating a reduced zone in an aquifer using the ISRM method that could treat hexavalent chromium. Secondary objectives of this test were to evaluate potential side effects of the process (e.g., reagent recovery and residual chemicals in the aquifer, trace metal mobilization, and effects on aquifer permeability). A successful demonstration of the ability to manipulate the redox conditions in the subsurface in a controllable fashion should lead to a viable remediation method for dissolved chromate and other redox sensitive contaminants.

Methods and Materials

This section describes the methods and materials used to conduct the ISRM proof-of-principle field injection/withdrawal test and the activities used to assess the performance. It describes the operation and equipment used in conducting the injection/withdrawal test along with sampling and analysis used in collecting and measuring ground water samples. This section also describes the methods used to collect and measure the reductive capacity of sediment from the reduced zone following the injection/withdrawal test. Finally, the methods used for the hydraulic tests to assess changes in aquifer permeability are also described.

Injection/Withdrawal Test

The dithionite injection/withdrawal field experiment was designed to produce an approximately 15 m (50 foot) diameter reduced zone over the lower portion of the aquifer around the central injection/withdrawal well (H5-2, Figure 3a). The single well dithionite injection/withdrawal test had three distinct phases:

- Injection phase–77,000 L (20,500 gallons) of reagent were injected into the central injection/withdrawal well at a rate of 75 Lpm (20 gpm) for 17.1 hours
- Reaction (or residence) phase–18.5 hour period following the injection stage to provide time for the injected reagent to react with the iron within the sediments
- Withdrawal phase–4.9 injection volumes (375,000 L [99,600 gallons]) were withdrawn from the injection/withdrawal well at a rate of 75 Lpm (20 gpm) to remove any unreacted reagent and pH buffer, reaction products (e.g., thiosulfate, sulfate, sulfite), and mobilized metals.

Table 1
Reagent Concentrations Used During Injection

	Sodium Dithionite	Potassium Carbonate	Potassium Bicarbonate	Sodium Bromide
Tank A	0.1M	0.4 M	0.04 M	90 ppm
Tank B	0.065 M	0.26 M	0.026 M	90 ppm
Tank C	0.033 M	0.13 M	0.013 M	90 ppm

This approach was chosen for emplacement of the reduced zone because it provides for a relatively simple operation and better recovery of injected chemicals than any other technique.

The injection design incorporated injection of three successively lower concentrations of reagent (Table 1) to minimize cost and to decrease the amount of derived waste and aquifer residuals. Time-dependent changes in the injection concentration of sodium dithionite and pH buffers were used to compensate for differences in average residence times and reaction path lengths that occur during the radial injection. The reagent was injected from three 27,000 L (7100 gallon) mixing tanks. These tanks were prefilled to an appropriate level with site ground water supplied by the central injection/withdrawal well. Concentrated liquid reagent consisting of sodium dithionite (Clariant Corp.) and potassium carbonate/bicarbonate buffers were delivered to the site in a tanker truck. The concentrated reagent was added to each tank to achieve the desired injection concentrations and volumes.

Following the residence stage, 4.9 injection volumes were withdrawn from the aquifer through the central injection/withdrawal well and stored in a 380,000 L (100,000 gallon) Modutank installed at the site for analysis prior to disposal. A volume of water larger than that injected was withdrawn to account for dispersive effects and ground water drift.

Ground Water Sampling and Analysis

Ground water samples were collected and analyzed to determine baseline chemistry of the site for operational monitoring of the injection/withdrawal experiment and for post-test performance assessment monitoring. Baseline ground water chemistry samples were collected and analyzed from wells at the site prior to dithionite injection. Dithionite movement and reactivity during the injection, residence, and withdrawal phases of the field test were characterized by monitoring geochemical changes in the ground water (oxygen, pH, and electrical conductivity) and by direct measurement of dithionite. During the injection/withdrawal test, ground water samples and geochemical measurements were taken at intervals ranging from 0.25 to 6.0 hours from the injection/withdrawal well and 12 monitoring wells, resulting in the collection of

approximately 2500 water samples. Following the field test, ground water was monitored to assess the performance of the emplaced treatment zone. The monitoring was initially performed biweekly. After approximately six months the monitoring frequency was reduced to monthly, followed by a quarterly frequency in 1997 and then annually afterwards.

During each phase of the injection/withdrawal experiment, ground water samples were collected using dedicated variable speed submersible pumps installed in all of the monitoring wells. The pumps were controlled from a central location using sampling pump controllers and sampling manifolds. Each sampling manifold was equipped with a flow-through assembly with geochemical field parameter monitoring probes for measurement of dissolved oxygen, electrical conductivity, pH, and temperature. Purge times were determined by monitoring stabilization of field parameters. This sampling protocol resulted in the generation of approximately 20 L (~5 gallons) of purge water during the collection of samples from primary monitoring wells. In addition to field measurements, samples were collected for analysis of hexavalent chromium, major anions, trace metals, and dithionite. Ground water samples collected for trace metal analysis were filtered (0.45 micron) and 10 mL of the sample were preserved with 2 mL of ultra-pure nitric acid.

Trace metals were analyzed using inductively coupled plasma/mass spectrometry (ICP/MS) (U.S. EPA method 6020 ([SW-846]). Anions were analyzed by ion chromatography using U.S. EPA method 300.1. Hexavalent chromium concentrations were measured in a mobile field laboratory at the site using a Hach DR-2000 spectrophotometer and Accuvac Chromaver 3 ampules. The detection limit of this method is 0.008 mg/L and the method is EPA approved. Samples were filtered using a 0.45 micron filter prior to hexavalent chromium analysis.

Dithionite measurements were also made on site during the dithionite injection/withdrawal tests. Due to the instability of dithionite and its reactivity with oxygen, these analyses must be conducted immediately following sample collection. An automated system was developed using syringe pumps for sample dilution and a High-Performance Liquid Chromatography (HPLC). The dilution water was sparged with nitrogen gas to be completely free of dissolved oxygen due to the high dilution factors required for this method (500 to 700 times).

Sediment Sampling and Analysis

Direct evidence of reduction of aquifer sediment was achieved through analysis of sediment samples collected from the treatment zone at the ISRM field experiment site following the dithionite injection/withdrawal experiment (Figure 3a). To minimize contact with atmospheric oxygen, the sediment samples were collected in precut lexan liners, capped, quickly placed in argon-filled bags, and stored in a cooler for transport to the laboratory from the field site. All sample handling in the laboratory was done in an anaerobic glovebox. Thirteen sediment samples and one duplicate were analyzed for reductive capacity.

The primary methodology for determining the reductive capacity of core samples collected from the treatment zone following the ISRM field experiment was to determine the oxygen reducing capacity (ORC) of the samples. Samples were packed in columns, and the ORC of the sediment in the column was then measured by flowing a solution of oxygen-saturated water (~8 mg/L) through the column until effluent dissolved oxygen concentrations approached influent concentrations. Integration of the effluent oxygen breakthrough curve provided a measure of the amount of reductive capacity of the sediment sample. The O_2 reoxidation method was selected because the processes involved in the methodology were similar to oxidizing conditions in the field and were easily automated. The oxygen measurement system was automated using a computer-driven syringe pump and oxygen electrode (YSI Model 5331). This system analyzed water samples from the influent reservoir (air saturated water) prior to each effluent measurement for calculation of the percentage oxygen saturation in the effluent. Automation significantly increased the measurement reliability and number of core samples that could be analyzed due to the reduced labor costs. Time constraints and the asymptotic nature of the oxygen breakthrough curves resulted in the discontinuation of the reoxidation experiments when the dissolved oxygen concentrations in the column effluent exceeded 85% of the dissolved oxygen concentration of the synthetic ground water in the supply reservoir. Total capacity was calculated by linear extrapolation of the late-time slope to 100% breakthrough. ORC was computed by dividing the total mass of oxygen removed by the sediment's dry weight and the equivalent weight of oxygen (8 g/eq).

Another measure of the effectiveness of treatment zone emplacement that better accounts for the heterogeneity of the system is a comparison of the reductive capacity of a sample achieved in the field test with the sample's maximum possible reductive capacity. This comparison provides a percentage estimate of the available Fe(III) that was reduced by the field dithionite injection/withdrawal test. To obtain this information, the sediments in the columns were re-reduced to the maximum capacity of the sample by pumping a prepared dithionite solution through the columns continuously for 24 hours followed by a 24 hour reaction period (no flow). Following the reaction period, three pore volumes of anoxic water were run through the column to flush out the dithionite solution. The ORCs of these fully reduced samples were then determined using the method previously discussed. The percentage of reduction in the field was calculated as a ratio of the ORC measurement achieved in the field test and the maximum ORC measurement of the sediment sample.

Hydraulic Tests

Hydraulic testing of the aquifer at the 100 H area site was conducted as part of the site characterization activities prior to the dithionite injection/withdrawal test to aid in the test design (i.e., determining feasible injection and withdrawal rates) and to establish baseline site condi-

Table 2

Chromium and Dissolved Oxygen Summary of Baseline and Selected Post ISRM Injection/Withdrawal Experiment Measurements at Wells at 100 H Area
(Well locations are shown in Figure 3a.)

Well ID	Baseline–August 1995 Dissolved Oxygen ppm	Baseline–August 1995 Chromium (ICP/MS) ppb	Post Test–November 1997 Dissolved Oxygen ppm	Post Test–November 1997 Chromium (ICP/MS) ppb	Post Test–November 1997 Hexavalent Chromium ppb	Post Test–April 1999 Dissolved Oxygen ppm	Post Test–April 1999 Chromium (ICP/MS)* ppb	Post Test–April 1999 Hexavalent Chromium* ppb
Wells Within Treatment Zone								
H5-2	—	—	0.00	13.2	< 8	0.17	<1	< 8
H5-3p	4.40	50.8	3.50	37.0	30	6.00	13.2	10
H5-3o	5.70	71.0	11.47	35.0	30	9.74	6.0	< 8
H5-4p	2.39	47.1	0.00	3.4	< 8	0.00	1 ± 0.2	< 8
H5-4o	6.07	68.9	8.41	12.6	10	8.80	5.5	< 8
H5-5p	4.27	64.8	0.00	< 3	< 8	0.00	1.6	< 8
H5-5o	5.95	67.4	0.00	< 3	< 8	5.68	2.7	< 8
H5-6	5.36	60.1	0.00	4.1	< 8	0.00	<1	< 8
H5-7	5.14	67.4	0.00	4.5	< 8	0.00	1.5	< 8
H5-8	3.90	61.5	0.00	4.1	< 8	1.92	8.9	10
H5-9	6.93	59.8	0.00	< 3	< 8	0.00	<1	< 8
H5-10	5.57	45.8	0.00	3.4	< 8	0.00	<1	< 8
H5-11	6.61	59.5	0.00	< 3	< 8	0.00	<1	< 8
Wells Outside Treatment Zone								
H5-12	1.88	12.9	6.46	33.0	30	3.18	9.5	10
H5-13	3.48	34.0	8.31	59.4	50	8.17	16.7	10
H5-14	—	—	6.89	53.1	60	6.50	13.3	10
H5-15	Not drilled	Not drilled	9.20	46.5	40	8.74	9.5	10

*Note: Chromium concentrations within the plume in the area of the ISRM test site were significantly lower by the 1999 sampling event due to the injection of large volumes of treated ground water nearby from a pump and treat system that started in mid-1997.

tions. Hydraulic tests were also conducted at the site following the dithionite injection/withdrawal experiment. Pre- and post-experiment hydraulic test responses were compared for the injection/withdrawal well and selected observation wells at the ISRM test site to assess the impact of the field experiment on existing in situ hydraulic properties. Hydraulic tests conducted at the site consisted of both constant-rate discharge and slug interference tests that included continuous pressure response monitoring in most site monitoring wells. Pressure response was monitored using 10 and 20 psi Keller Series 173 pressure transducers and data were recorded on a Campbell Scientific CR10 data logger. Pressure responses were also monitored during both the tracer and dithionite injection/withdrawal tests to monitor the formation of the injection mound, pumping cone of depression, and recovery following the tests.

Results and Discussion

Two different methods were used to measure the performance of the ISRM proof-of-principle field test. The first method involved monitoring oxidized species (i.e., hexavalent chromium and dissolved oxygen) in the ground water from the wells at the site. The second, more direct, method involved collecting and analyzing sediment samples from the unconfined aquifer following the injection/withdrawal test. Sediment analysis also provided for estimates of the longevity of the reduced zone. The success of the ISRM technology for hexavalent chromium treatment was assessed from a comparison of post-injection chromium concentrations with the baseline measurements at the site. The results of these analyses and the evaluation of the data collected for assessing any negative impacts to the aquifer from this ISRM proof-of-principle experiment are discussed in the following sections.

Chromium Immobilization

Baseline and selected post-injection chromium measurements from the wells at the 100 H area ISRM site are provided in Table 2, and in a generally west to east transect of wells screened in the lower portion of the aquifer (i.e., the targeted treatment zone) in Figure 4. Total chromium concentrations before the experiment ranged from 12.9 to 64.8 µg/L at the site. Following the dithionite injection/withdrawal experiment, total chromium concentrations declined to near the detection limit of the analytical method (ICP/MS; 1 to 3 µg/L) in most wells located within the reduced zone in the lower portion of the aquifer. Hexavalent chromium concentrations within the reduced zone following the injection/ withdrawal experiment are mostly below the detection limit of the field measurement method (8 µg/L). Hexavalent chromium was not analyzed before the field experiment, but the total chromium measurements after the experiment had concentrations and trends similar to the post-experiment hexavalent chromium measurements (Table 2). Hexavalent chromium concentrations within the reduced zone also remain below detection limits during the most recent sampling event (April 1999 in Table 2),

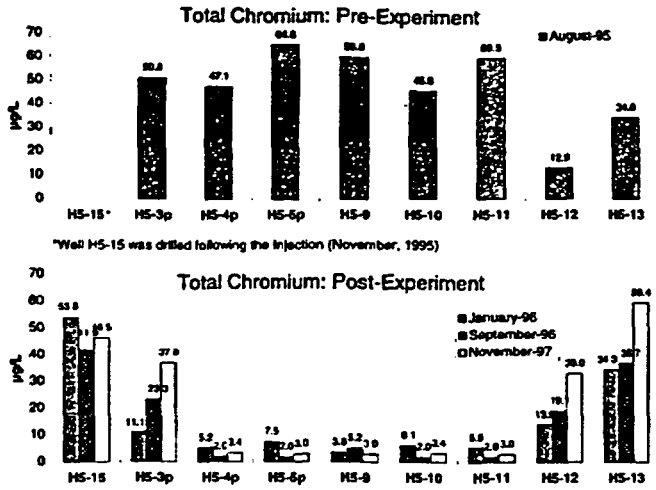

Figure 4. ICP/MS total chromium measurements along a west to east transect showing baseline (a) and selected post-ISRM injection/withdrawal test (b) values.

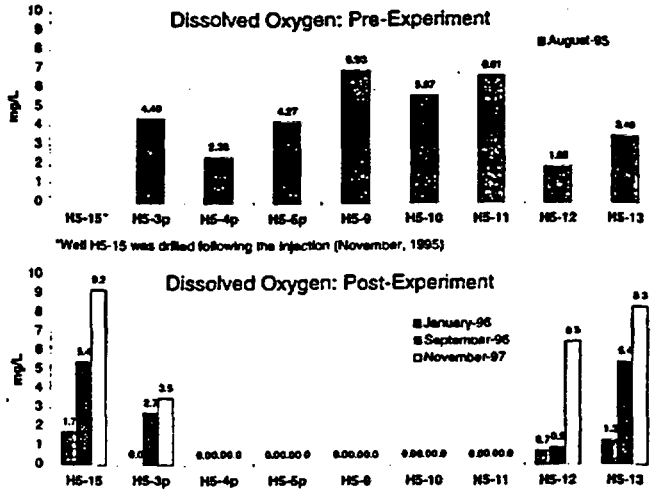

Figure 5. Dissolved oxygen measurements along a west to east transect showing baseline data (a) and selected post-ISRM dithionite injection/withdrawal test data (b).

3.5 years after the injection/withdrawal test. Wells outside the reduced zone also showed significantly lower chromium concentrations in the 1999 sampling event, but the concentrations in the plume around the test site have been impacted from the injection of treated ground water from a pump-and-treat system that began operation in mid-1997.

Chromium concentrations for the wells located on the edges of the reduced zone (e.g., H5-3p and H5-8) and upper portions of the aquifer (H5-3o, H5-4o, and H5-3o) have been increasing since the early times after the test. Being on the outer fringes of the reduced zone, these wells had lower concentrations of dithionite during the injection/withdrawal test and are in the areas expected to oxidize first from the regional generally east-northeast ground water flow direction.

Dissolved Oxygen Behavior

Selected dissolved oxygen concentrations measured at the site are shown in Table 2 and Figure 5. The trends seen in dissolved oxygen are similar to those discussed in the previous section on chromium. Dissolved oxygen concentrations at the site measured in the wells before the injection/ withdrawal experiment ranged between 1.88 to 6.93 mg/L. Following the injection/withdrawal test, the dissolved oxygen concentrations in most of the wells within the reduced zone were approximately 0.00 mg/L, as shown in Figure 5b. With the exception of the wells on the fringes of the reduced zone, the treatment zone remains anoxic 3.5 years after the test.

Reductive Capacity and Barrier Longevity

Table 3 summarizes the results of the ORC analysis of the 13 sediment core samples collected from the treatment zone following the dithionite injection/withdrawal test. These data show that significant treatment capacity was created by the test and a high percentage of reduction of the available Fe(III) (i.e., Fe(III) reducible by dithionite) was achieved within the treatment zone. The ORC measurements on core samples that were fully reduced by dithionite in the laboratory resulted in an average value of Fe(III) of 0.059% by weight for Hanford formation sediments. Estimates for the lifetime of the treatment zone were calculated using the results of ORC analyses of these core samples. The treatment capacity of the bottom 1.5 m (5 feet) of the aquifer was estimated to be between 51 and 85 pore volumes based on (1) the average Fe(III) measured in the Hanford Formation sediments; (2) bulk density and effective porosity estimates of 1.9 g/cm^3 and 0.2, respectively, and assumed dissolved oxygen and hexavalent chromium concentrations of 9 mg/L and 1 mg/L, respectively; and (3) core data indicating that 60% to 100% of the available reactive iron (from core samples collected up to a 7.6 m [25 feet] radial distance) was reduced during the dithionite injection/withdrawal experiment. Assuming a 15.2-m (50 foot) wide treatment zone and a ground water velocity of 0.3 m/day (1 foot/day) (typical of this area of the Hanford site), the estimated longevity of the ISRM treatment zone at 100 H area is between seven and 12 years.

Spatial trends in the effectiveness of the treatment zone emplacement are evident when comparisons of the percentage of available Fe(III) that was reduced by the treatment are made between core samples (Figure 6). There is a general trend of increasing percent reduced with depth; this is consistent with the experimental design, which targeted the bottom 1.5 m (5 feet) of the aquifer. There is also a general trend of decreasing percent reduction with increasing radial distance from the injection/withdrawal well. This trend is also expected since the dithionite concentrations measured in the wells during the injection/withdrawal test were lower in the wells at greater radial distances due to reaction losses along the longer path lengths and from dispersion.

Assessment of Negative Aquifer Impacts

A secondary objective of the test was to assess any negative impacts to the aquifer from the creation of an ISRM treatment zone. These effects include aquifer plugging, residual chemicals, and enhanced mobility of naturally

Table 3

ORC Measurements of Core Samples Collected from the Treatment Zone Following the ISRM Injection/Withdrawal Test
(Borehole locations are shown in Figure 3a.)

Boring ID	Average Depth in m (feet)		Radial Distance in m (feet)		% of Sample < 4.75	Sample ORC (meq/kg)	Pore Volumes of Treatment*	Maximum Sample (meq/kg)	% of Available Fe(III) Reduced
B2618	12.0	(39-40)	1.2	(4)	79	9.9	63	23.4	42
B2618	13.0	(42-43)	1.2	(4)	37	12.6	38	22.4	56
B2618	14.2	(46-47)	1.2	(4)	51	42.7	176	39.1	100
B2618	14.9	(48.5-49.5)	1.2	(4)	43	6.5	22	35.9	18
B2620	13.0	(42-43)	3.0	(10)	79	1.0	6	18.5	5
B2620	14.5	(47-48)	3.0	(10)	34	10.0	28	19.6	51
B2620	15.1	(49-50)	3.0	(10)	30	32.5	78	32.4	100
B2621	15.1	(49-50)	5.8	(19)	29	10.7	25	17.8	60
B2624	12.6	(41-42)	6.4	(21)	79	13.9	88	39.8	35
B2624	13.6	(44-45)	6.4	(21)	42	25.1	85	32.9	76
B2624	14.8	(48-49)	6.4	(21)	38	21.0	64	37.1	57
B2624	14.5	(47-48 [int])	6.4	(21)	60	17.9	86	21.5	83
	14.5	47-48 [ext])	6.4	(21)	60	13.8	66	35.9	38
B2625	14.6	(47.5-48.5)	8.2	(27)	21	1.3	2	16.5	8

*Assumes: bulk density = 1.9 g/cm; porosity = 20%; 9 mg/L dissolved oxygen; 1 mg/L hexavalent chromium.

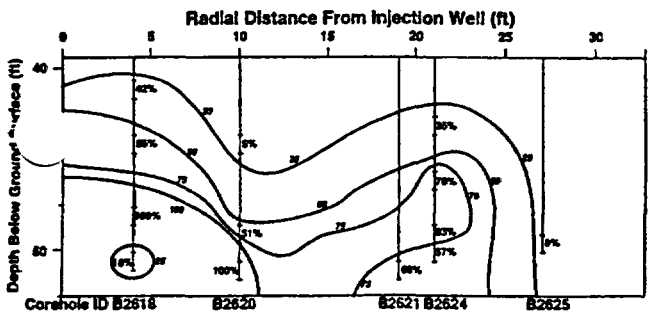

Figure 6. Contour plot of % Fe reduced based on ORC measurements of core samples collected after the 100 H area ISRM proof-of-principle test. Corehole locations are shown as radial distance from the injection/withdrawal well (H5-2). ORC data are from Table 3. See Figure 3a for plan-view locations of coreholes.

occurring metals from altered Eh/pH conditions. These effects are discussed next.

Pre- and post-experiment hydraulic test responses were compared for selected observation well sites at the ISRM demonstration site to assess the impact of the field experiment on existing in situ hydraulic properties. A direct comparison of hydraulic responses was not possible since the aquifer thickness increased from 3 to 4 m for the pre- and post-experiment tests, respectively, due to aquifer response to high water levels in the Columbia River in 1996 and 1997. However, analysis of the available data using methods to account for these differences indicated that the dithionite injection did not result in any measurable degradation in formation permeability. The hydraulic test comparison did indicate a near-well decrease in permeability at the injection/withdrawal well following the injection. This small zone of reduced permeability (i.e., skin effect) may be attributed to entrapment of suspended or colloidal material in the sandpack zone immediately outside the well screen during the withdrawal phase. This near-well reduction in permeability caused no adverse effects during the injection or withdrawal phases of the demonstration and is not expected to result in any significant degradation in the overall hydraulic performance of the treatment zone. A complete description of the hydraulic analysis methods used is included in Fruchter et al. (1996).

Potentially adverse impacts to ground water quality include residual chemicals (i.e., injected reagent or reaction products that were not recovered during the withdrawal) and naturally occurring trace metals mobilized under changing Eh/pH conditions or from dissolution by the reagent during injection. Residual chemicals in the aquifer were potassium, sodium, sulfur species (which eventually oxidize to sulfate), and carbonate. The residuals also affect the pH and electrical conductivity within the treatment zone. Mass balance calculations compared the masses of injected constituents with the masses of withdrawn constituents to determine what percentage of reagents and reaction products were recovered during the withdrawal phase. Samples collected from the extraction stream during the withdrawal phase of the experiment were analyzed for thiosulfate, sulfate, sulfite, and bromide using ion chromatography (IC). Integration of IC measurements from 30 samples collected from the extraction stream during the withdrawal period resulted in an estimate of 87% recovery of the injected sulfur mass during the withdrawal phase and 90% recovery of the injected bromide.

One year after the injection/withdrawal test, wells

Table 4
Residual Chemicals (Na, K SO_4), pH, and Electrical Conductivity

			Pre-Experiment (August 1995) All Wells		Post-Experiment (August 1996) Treatment Zone		Post-Experiment (August 1996) H5-12, H5-13, H5-14	
Quality Parameter	Secondary Standard	Units	Mean	Standard Deviation	Mean	Standard Deviation	Mean	Standard Deviation
K^+	none	ppm	6	1	116	71	7	0.4
Na^+	none	ppm	25	3	55	19	35	7
SO_4^{2-}	250	ppm	—	—	324	213	95	23
pH	—	pH	7.55	0.12	8.19	0.49	7.51	0.01
Conductivity	—	µS/cm	452	42	871	302	559	32

Table 5
Trace Metals with Primary Drinking Water Standards

			Pre-Experiment (August 1995) All Wells		Post-Experiment (August 1996) Treatment Zone		Post-Experiment (August 1996) H5-12, H5-13, H5-14	
Quality Parameter	Secondary Standard	Units	Mean	Standard Deviation	Mean	Standard Deviation	Mean	Standard Deviation
Sb	6	ppb	<1	—	<1	—	<1	—
As	50	ppb	<2	—	<1	—	<1	—
Cd	5	ppb	<1	—	<1	—	<1	—
Cu	50	ppb	5	1	8	1	9	2
Pb	15	ppb	0.4	2	<1	—	<1	—
Ni	1000	ppb	4	3	4	3	5	1
Se	50	ppb	0.3	1	<6	—	<6	—

Table 6
Trace Metals with Secondary Drinking Water Standards

			Pre-Experiment (August 1995) All Wells		Post-Experiment (August 1996) Treatment Zone		Post-Experiment (August 1996) H5-12, H5-13, H5-14	
Quality Parameter	Secondary Standard	Units	Mean	Standard Deviation	Mean	Standard Deviation	Mean	Standard Deviation
Al	50-200	ppb	32	13	<10	—	<10	—
Fe	3000	ppb	5	13	132	162	20	34
Mn	50	ppb	32	59	170	237	14	12
Zn	5000	ppb	25	18	51	5	54	11

within the reduced zone remained elevated in K, Na, and sulfate compared with the pre-experiment baseline values (Table 4). Wells outside the treatment zone were not significantly altered from the pre-experiment baseline measurements.

Tables 5 and 6 summarize the baseline trace metals before and one year after the dithionite injection/withdrawal test with comparisons to primary and secondary drinking water standards. Relative to the baseline data, iron and manganese within the reduced zone were significantly elevated. These trace metals are not expected to migrate a significant distance downgradient of the reduced zone because of their high sorption in the reduced oxidation state (Fe^{2+}, Mn^{2+}). These reduced species are also expected to reoxidize into less soluble species (Fe^{3+} Mn^{3+}) when in contact with unreduced sediment downgradient of the treatment zone. Zinc was also slightly elevated above the baseline values one year after the test. Other trace metals within the reduced zone (e.g., As and Pb), although elevated in the withdrawal stream were not above baseline data one year after the experiment. The increase in these trace metals was due to the dissolution of oxides within the sediment by dithionite. The post-experiment trace metals concentrations in the wells outside the treatment zone were similar to baseline values.

Applications to Ground Water Remediation

The 100 H area ISRM proof-of-principle test site was selected for its relatively simplified hydrogeologic setting and low contamination levels. These conditions reduced the cost and complexity of the test operations and interpretation. Additionally, only the lower portion of the aquifer was targeted to minimize influence of the water table. Following the successful completion of this ISRM proof-of-principle test, a larger scale ISRM treatability study is underway at the 100 D area of the Hanford site (Figure 2) for treatment of much higher concentrations of hexavalent chromium (~1 mg/L) over the entire contaminated unconfined aquifer in a dynamic hydrologic setting near the Columbia River. The goal of this treatability study is to create a 46 m (150 feet) long reduced zone by coalescing a number of cylindrically-shaped reduced zones around a series of injection/withdrawal wells. The larger scale of this test will permit adequate hydraulic gradient determination and monitoring to better assess impacts on water quality downgradient from the ISRM treatment zone. The performance and cost data gathered during the 100 D area treatability study will be used to determine if the ISRM techology will be selected for remediation of the entire 600 m (2000 foot) length of the chromate plume at this location. At other sites, the ISRM technology is currently being tested to determine its effectiveness for the remediation of TCE.

Acknowledgments

The authors would like to thank Steven S. Teel for his assistance in the field test. We would also like to thank Dr. Frank A. Spane for his help in interpreting the hydrologic test data, and Dr. Kirk Cantrell for his thoughts on chromium chemistry. We thank the reviewers for numerous suggestions and corrections. Pacific Northwest National Laboratory is operated by Battelle Memorial Institute for the U.S. Department of Energy under Contract DE-AC06-76RLO 1830. This work is funded by the Office of Science and Technology, within the Department of Energy's Office of Environmental Management, under the Subsurface Contaminant Focus Area.

Editor's Note: The use of brand names in peer-reviewed papers is for identification purposes only and does not constitute endorsement by the authors, their employers, or the National Ground Water Association.

References

Amacher, M.C., and D.A. Baker. 1982. Redox reaction involving chromium, plutonium, and manganese in soils. Final Rep. DE-ASO8-77DPO4515. Inst. for Res. on Land and Water Resour., Penn. State Univ.

Amonette, J.E., J.E. Szecsody, H.T. Schaef, J.C. Templeton, Y.A. Gorby, and J.S. Fruchter. 1994. Abiotic reduction of aquifer materials by dithionite: A promising in-situ remediation technology. In *Proceedings of the 33rd Hanford Symposium on Health and the Environment–In Situ Remediation: Scientific Basis for Current and Future Technologies*, ed. G.W. Gee and N.R. Wing, 851–882. Richland, Washington: Pacific Northwest National Laboratory.

Blowes, D.W., and C.J. Ptacek. 1992. Geochemical remediation of groundwater by permeable reaction walls: Removable of chromate by reaction with iron-bearing solids. *Subsurface Restoration Conference, Third International Conference on Groundwater Quality Research*, Dallas: National Center for Ground Water Research.

Borden, R.C,. R.T. Goin, and C.M. Kao. 1997. Control of BTEX Migration using a biologically enhanced permeable barrier. *Ground Water Monitoring & Remediation* 17, no. 1: 70–80.

Burris, D.R., and C.P. Antworth. 1992. In situ modification of an aquifer material in flow-through systems by a cationic surfactant to enhance retardation of organic contaminants. *Journal of Contaminant Hydrology* 10, no. 4: 325–337.

Cummings, M.A., and S.R. Booth. 1997. Cost effectiveness of in situ redox manipulation for remediation of chromium-contaminated groundwater. LA-UR-97-165. Los Alamos, New Mexico: Los Alamos National Laboratory.

Delvin, J.F., and J.F. Barker. 1994. A semipassive nutrient injection scheme for enhanced in situ bioremediation. *Ground Water* 32, no. 3: 374–380.

Eary, L.E., and D. Rai. 1987. Kinetics of chromium (III) oxidation to chromium(VI) by reaction with manganese dioxide. *Environ. Sci. Technol.* 21, no. 8: 1187–1193.

Fendorf, S. E., M. Fendorf, D.L. Sparks, and R. Gonsky. 1992. Inhibitory mechanisms of Cr(III) oxidation by δ-MnO_2. *J. Colloid and Interface Sci.* 153, no. 1: 37–54.

Fendorf, S.E., R.J. Zasoski, and R.G. Burau. 1993. Competing metal ion influences on chromium(III) oxidation by birnessite. *Soil. Sci. Soc. Am. J.* 57, no. 6: 1508–1515.

Fendorf, S.E., and R.J. Zasoski. 1992. Chromium(III) oxidation by δ-MnO_2. *Environ. Sci. Technol.* 26, no. 1: 79–85.

Fruchter, J.S., J.M. Zachara, J.K. Fredrickson, C.R. Cole, J.E. Amonette, T.O. Stevens, D.J. Holford, L.E. Eary, G.D. Black, and V.R. Vermeul. 1992. Manipulation of natural subsurface processes: Field research and validation. Pacific Northwest Laboratory Annual Report for 1991 to the DOE Office of Energy Research, Part 2: Environmental Sciences. PNL-8000 Pt. 2, 88–106. Richland, Washington: Pacific Northwest Laboratory.

Fruchter, J.S., F.A. Spane, J.K. Fredrickson, C.R. Cole, J.E. Amonette, J.C. Templeton, T.O. Stevens, D.J. Holford, L.E. Eary, B.N. Bjornstad, G.D. Black, J.M. Zachara, and V.R. Vermeul. 1994. Manipulation of natural subsurface processes: Field research and validation. PNL-10123. Richland, Washington: Pacific Northwest National Laboratory.

Fruchter, J.S., J.E. Amonette, C.R. Cole, Y.A. Gorby, M.D. Humphrey, J.D. Istok, F.A. Spane, J.E. Szecsody, S.S. Teel, V.R. Vermeul, M.D. Williams, and S.B. Yabusaki. 1996. In situ redox manipulation field injection test report–Hanford 100H area. PNNL-11372. Richland, Washington: Pacific Northwest National Laboratory.

Istok, J.D., M.D. Humphrey, V.R. Vermeul, M.D. Williams, J.S. Fruchter, and J.E. Szecsody. 1999. In situ redox manipulation intermediate scale experiments. *Ground Water* 37, no. 6: 884–889.

Johnson, C.A., and A.G. Xyla. 1991. The oxidation of chromium(III) to chromium(IV) on the surface of manganate (γMnOOH). *Geochim.Cosmochim. Acta* 55, no. 10: 2861–2866.

Mackay, D.M. and J.A. Cherry. 1989. Groundwater contamination: Pump and treat remediation. *Environ. Sci. Technol.* 23, no. 6: 630–636.

Manceau, A.A., and L. Charlet. 1992. X-ray absorption spectroscopic study of the sorption of Cr(III) at the oxide-water interface: II. Adsorption, coprecipitation, and surface precipitation on hydrous ferric oxide. *J. Colloid Interface Sci.* 148, no. 2: 443–458.

Matheson, L.J., and P.G. Traknyek. 1993. Processes affecting reductive dechlorination of chlorinated solvents by zero-valentiron. In *Proceedings of the 205th ACS National Meeting*, vol. 33, 77–81. Washington, D.C.: American Chemical Society.

Michelsen, D.L., and M. Lofti. 1991. Oxygen microbubble injection for in situ bioremediation: Possible field scenario. Innovative Hazardous Waste Treatment Technology Series, ed. J. Freeman and P. Sferra. Lancaster, Pennsylvania.

Nagel, G., W. Kuehn, P. Werner, and H. Sontheimer. 1982. Sanitation of groundwater by infiltration of ozone treated water. *GWF-Wasser/Abwasser* 123, 399.

Patterson, R.R., S. Fendorf, and M. Fendorf. 1997. Reduction of hexavalent chromium by amorphous iron sulfide. *Environ. Sci. Tech.* 31, no. 7: 2039–2044.

Rai, D., L.E. Eary, and J.M. Zachara. 1989. Environmental chemistry of chromium. *Sci. Total Environ.* 86, no. 1: 15–23.

Sass, B.M., and D. Rai. 1987. Solubility of amorphous chromium(III) iron(III) hydroxide solid solutions. *Inorg. Chem.* 26, no. 14: 2228–2232.

Schroeder, D.C., and G.F. Lee. 1974. Potential transformation of chromium in natural waters. *Water Air Soil Pollut.* 4, no. 4: 355–365.

Scott, A.D., and J.E. Amonette. 1988. Role of iron in mica weathering. In *Iron in Soils and Clay Minerals*, ed. J.W. Stucki, B.A. Goodman, and U. Schwertmann. Dordrecht, The Netherlands: D. Reidel.

Stucki, J.W. 1988. Structural iron in smectites. In *Iron in Soils and Clay Minerals*, ed. J.W. Stucki, B.A. Goodman, and U. Schwertmann. Dordrecht, The Netherlands: D. Reidel.

U.S. Environmental Protection Agency. 1994. Drinking water regulations and health advisories. Washington, D.C.: U.S. Government Printing Office.

van der Weijden, C.H., and M. Reith. 1982. Chromium(III)-chromium(VI) interconversions in seawater. *Mar. Chem.* 11, no. 6: 565–572.

Vermeul, V.R., S.S. Teel, J.E. Amonette, C.R. Cole, J.S. Fruchter, Y.A. Gorby, F.A. Spane, J.E. Szecsody, M.D. Williams, and S.B. Yabusaki. 1995. Geologic, geochemical, microbiologic, and hydrologic characterization at the in situ redox manipulation test site. PNL-10633. Richland, Washington: Pacific Northwest Laboratory.

Williams, M.D., S.B. Yabusaki, and C.R. Cole. 1994. In situ redox manipulation field experiment: Design analysis. In *Proceedings of the 33rd Hanford Symposium on Health and the Environment–In Situ Remediation: Scientific Basis for Current and Future Technologies*, ed. G.W. Gee and N.R. Wing. Richland, Washington: Pacific Northwest Laboratory.

Xu, Y., and F.W. Schwartz. 1992. Immobilization of lead in groundwater with a reactive barrier system. *Subsurface Restoration Conference, Third International Conference on Groundwater Quality Research.* Dallas.

Biographical Sketches

***Jonathan S. Fruchter** is a staff scientist at Pacific Northwest National Laboratory (PNNL) (Battelle Northwest, P.O. Box 999, Richland, WA 99352; (509) 376-3937, fax: (509) 372-1704; e-mail: john.fruchter@pnl.gov) with a B.S. in chemistry from the University of Texas-Austin and a Ph.D. in chemistry from the University of California-San Diego. He also performed post-doctoral research in geochemistry at the University of Oregon. His 25 years of experience at PNNL include conducting characterization measurements at nuclear facilities, coal plants, geothermal plants, and oil shale retorts. He has also conducted remedial investigation studies at Department of Energy and Department of Defense CERCLA (Superfund) sites. For the past 10 years, he has worked on developing and deploying innovative ground water contaminant barrier concepts including redox barriers and permeable adsorptive barriers. Dr. Fruchter has been the manager of the In Situ Redox Manipulation Project since 1993.*

***Charles R. Cole** is a staff scientist in the Hydrology Section at Pacific Northwest National Laboratory (PNNL) (Battelle Northwest, P.O. Box 999, Richland, WA 99352; phone: [509] 372-6068 with a B.S. in physics from Kent State University and an M.S. in computer science from Washington State University. In his 34 years at PNNL, Mr. Cole has been involved with the development of one-, two-, and three-dimensional ground water flow and transport models, and with their application to various contaminant transport studies related to waste management at Hanford; the evaluation of safety and design of remedial action alternatives at hazardous waste disposal sites; dewatering-recharge studies; ground water resource management studies; the assessment of the impact of potential contaminant transport from deep geologic and shallow land burial sites for nuclear waste; and the development of in situ reactive barriers.*

***Mark D. Williams** is a senior research scientist at Pacific Northwest National Laboratory (PNNL) (Battelle Northwest, P.O. Box 999, Richland, WA 99352; phone: [509] 372-6069) since 1992, has a B.S. in geosciences from Penn State University and an M.S. in geological sciences from Indiana University. His research has focused on the development of permeable reactive barrier technologies for remediation of chromate, Sr-90, and dissolved TCE contaminated ground water. These studies included CERCLA treatability studies, field testing, multiscale laboratory experiments, and numerical modeling of ground water flow and reactive transport. His research has also included the development of regional, three-dimensional, hydrogeologic models of flow and contaminant transport for U.S. Department of Energy sites and Russian nuclear production facilities in Western Siberia as part of a joint U.S. and Russian team of scientists. Prior to joining PNNL, Mr. Williams was a systems design and analysis computer programming consultant for seven years.*

***Vince R. Vermeul** is a senior research engineer in the Environmental Technology Division at Pacific Northwest National Laboratory (PNNL) (Battelle Northwest, P.O. Box 999, Richland, WA 99352; phone: [509] 376-8316) with a B.S. in agricultural engineering and an M.S. in environmental engineering from Oregon State University. In his 10 years at PNNL, Mr. Vermeul has been involved primarily with hydrologic and geochemical characterization associated with Department of Energy/Department of Defense remedial investigation studies and development/deployment of in situ permeable reactive barrier technology, including ISRM barriers and permeable adsorptive barriers.*

***James E. Amonette** is a senior research scientist in the Environmental Molecular Sciences Laboratory at Pacific Northwest National Laboratory (PNNL) (Battelle Northwest, P.O. Box 999, Richland, WA 99352; phone: [509] 376-5565) with a B.S. in soil science from New Mexico State University and an M.S. and Ph.D. in soil chemistry from Iowa State University. Since joining PNNL in 1986, Dr. Amonette has specialized in the areas of aqueous geochemistry and soil mineralogy. He has a strong*

interest in the structure and chemistry of minerals and in the application of laser photoacoustic (LPAS), proton-induced x-ray emission (PIXE), x-ray diffraction (XRD), infrared (IR), x-ray absorption (XAS) and other spectroscopic techniques to characterize the solid phases and to predict and monitor the reactions associated with the disposal of hazardous wastes in soil environments.

***James E. Szecsody** is a senior research scientist at Pacific Northwest National Laboratory (PNNL) (Battelle Northwest, P.O. Box 999, Richland, WA 99352; phone: [509] 372-6080) with a B.S. in geology from Arizona State University, an M.S. in hydrology from University of Nevada, Reno, and a Ph.D. in hydrology from University of Arizona. At PNNL Dr. Szecsody has conducted research studies quantifying geochemical and microbial mechanisms that occur in porous media during advective transport at different scales. This includes laboratory research and model simulation at the batch scale to identify and parameterize reactions and processes, and one-dimensional flow experiments to address process coupling with advection, two-dimensional laboratory experiments to address the importance of spatial heterogeneities, and field experiments to upscale engineered geochemical remediation methods. This research also involved development of transport codes that incorporate multispecies transport with multiple chemical equilibrium/kinetic and microbial reactions.*

***Jonathan Istok** is a professor of civil engineering at Oregon State University (Corvallis, OR 97331). He has a Ph.D. in civil engineering from Oregon State University and holds B.S. degrees in civil engineering and geology, and an M.S. in soil science from The Ohio State University. Dr. Istok specializes in the development and testing of alternate ground water remediation technololgies.*

***Mark D. Humphrey** is a senior faculty research scientist at Oregon State University (Department of Civil, Construction, and Environmental Engineering, Corvallis, OR 97331) with a B.S. in geology, a B.S. in chemistry, and an M.S. in environmental engineering, all from Oregon State University. His recent work has focused on the use of intermediate-scale physical aquifer models (PAMs) to study remediation of contaminated aquifers. Research using the models has included transport of dissolved gases in aquifer systems, buoyancy induced flow, creation of a reduced zone for immobilization or degradation of redox sensitive contaminants such as chromate or trichloroethylene (TCE), and removal of TCE through chemical oxidation or solubilization. Results of laboratory investigations were used to design and implement full-scale experiments at contaminated field sites.*

Mr. Humphrey has also been involved with the U.S. Geological Survey in geologic unit characterization and development of hydrologic models at Yucca Mountain, Nevada, the nation's first proposed high-level nuclear waste repository. Construction and deployment of automated data collection systems is another ongoing research effort for Mr. Humphrey.

APPLIED AND ENVIRONMENTAL MICROBIOLOGY, Nov. 1997, p. 4385–4391 Vol. 63, No. 11
0099-2240/97/$04.00+0

Reduction of Hexavalent Uranium from Organic Complexes by Sulfate- and Iron-Reducing Bacteria

RAJAGOPALAN GANESH,[1,2]† KEVIN G. ROBINSON,[1,2]* GREGORY D. REED,[1,2] AND GARY S. SAYLER[2,3]

Department of Civil and Environmental Engineering,[1] Department of Microbiology,[2] and Center for Environmental Microbiology,[3] The University of Tennessee, Knoxville, Tennessee 37996

Received 23 December 1996/Accepted 1 September 1997

The influence of organic-hexavalent-uranium [U(VI)] complexation on U(VI) reduction by a sulfate-reducing bacterium (*Desulfovibrio desulfuricans*) and an iron-reducing bacterium (*Shewanella alga*) was evaluated. Four aliphatic ligands (acetate, malonate, oxalate, and citrate) and an aromatic ligand (tiron [4,5-dihydroxy-1,3-benzene disulfonic acid]) were used to study complexed-uranium bioavailability. The trends in uranium reduction varied with the nature and the amount of U(VI)-organic complex formed and the type of bacteria present. *D. desulfuricans* rapidly reduced uranium from a monodentate aliphatic (acetate) complex. However, reduction from multidentate aliphatic complexes (malonate, oxalate, and citrate) was slower. A decrease in the amount of organic-U(VI) complex in solution significantly increased the rate of reduction. *S. alga* reduced uranium more rapidly from multidentate aliphatic complexes than from monodentate aliphatic complexes. The rate of reduction decreased with a decrease in the amount of multidentate complexes present. Uranium from an aromatic (tiron) complex was readily available for reduction by *D. desulfuricans*, while an insignificant level of U(VI) from the tiron complex was reduced by *S. alga*. These results indicate that selection of bacteria for rapid uranium reduction will depend on the organic composition of waste streams.

Microbially mediated precipitation has been proposed as a viable technique for selective uranium removal from aqueous solutions (32). Certain iron- and sulfate-reducing bacteria can enzymatically reduce highly soluble hexavalent uranium [U(VI)] to the sparingly soluble tetravalent form [U(IV)]. Reduced uranium then abiotically precipitates as uraninite ($UO_{2(S)}$) (23, 34). Attempts to develop this process for uranium removal from various waste streams are in progress (33, 41, 44). For example, groundwaters contaminated with uranium have been successfully treated by using this technique (23, 33). A few studies have evaluated the impact of inorganic ions found in wastewaters on uranium removal by this mechanism. In general, high concentrations of bicarbonate, sulfate, and nitrate ions appear to negatively impact enzymatic removal of uranium (41, 44). Phillips et al. (41) found that an increase in bicarbonate ion concentration from ~30 to 100 mM significantly decreased the rate of uranium reduction by microorganisms. Robinson et al. (44) noted that the presence of ~5,000 mg of nitrate or sulfate ions per liter did not appreciably affect uranium reduction; however, these ions at concentrations of 10,000 to 50,000 mg/liter decreased both the rate and extent of U(VI) removal from solution.

In addition to the inorganic ions evaluated, the presence of organic ligands may influence bioreduction of uranium in wastewaters. Waste streams from radionuclide-processing facilities generally contain several simple and complex organic ligands (16, 37). Organic compounds, through carboxyl, hydroxyl, or other functional-group interactions, spontaneously form coordinate-covalent bonds with metal cations, resulting in organic-metal complexes. Several studies relating the impact of organic-metal complexation to microbial degradation indicate that biodegradation of organic ligands by heterotrophic bacteria and metal bioavailability to assimilatory metal-reducing bacteria are often affected by the presence of organic-metal complexes (14, 18, 45). For example, Firestone and Tiedje (15) studied the biodegradation of nitrilotriacetic acid (NTA) complexed to several metals by using a *Pseudomonas* species. The bacteria rapidly degraded NTA from Ca(II), Mg(II), Mn(II), and Na complexes; however, NTA chelated with Ni(II) was not degraded. In a separate study, *Pseudomonas fluorescens* rapidly degraded citrate from Ca(II), Ni(II), and Fe(III) complexes; however, degradation from an Fe(II) complexes was slower (28). Also, enzymes of *Azotobacter vinelandii* were found to reduce Fe(III) from citrate and azotochelin complexes at different rates during iron assimilation (27). In general, the types of complexes formed, their lability, and the functional group(s) involved in complexation have been proposed as parameters of organic-metal complexes affecting biodegradation (5, 17, 18).

Bioavailability of organic ligands and metals from metal-organic complexes appears to depend not only on the nature of the complexes formed but also on the type of bacteria present. Different *Pseudomonas* species degrade citrate from metal complexes at different rates (38). Two assimilatory metal-reducing bacteria, *P. aeruginosa* (13) and *A. vinelandii* (27), were found to reduce ferric iron from citrate complexes at different rates. The relationship between bacterial metabolism and the mechanism(s) of organic or metal utilization from complexes has not been well established. However, inhibition of the transport system which facilitates intracellular metabolism (4, 52) and structural incompatibility of the chelate with the active sites of the target enzymes (28) have been reported as reasons for the observed differences in the bioavailability of organic-metal complexes.

Several strains of metabolically diverse iron- and sulfate-reducing bacteria can reduce U(VI) in organic-free bicarbonate solutions (32, 34). It is not known if the presence of organic ligands can affect U(VI) reduction by these bacteria due to transport limitations, structural incompatibility, or other mech-

* Corresponding author. Mailing address: Department of Civil and Environmental Engineering, 219A Perkins Hall, University of Tennessee, Knoxville, TN 37996-2010. Phone: (423) 974 0722. Fax: (423) 974 2669. E-mail: kgr@utk.edu.

† Present address: Biopraxis, Inc., San Diego, CA 92191-0078.

TABLE 1. Organic ligands used to evaluate U(VI) biotransformation

Ligand	Nature of ligand	Functional group(s) involved in U(VI) complexation	Stability constant (log K)	Reference
Monodentate acetate	Aliphatic	Carboxyl	3.21	1
Bidentate				
Malonate	Aliphatic	Carboxyl	5.6	43
Oxalate	Aliphatic	Carboxyl	6.5	43
Bi- or polynuclear				
Citrate	Aliphatic	2 carboxyl, 1 hydroxyl	18.9	42
Tiron	Aromatic	Hydroxyl	55.0	25

anisms. Uranium in wastewater often is associated with several simple and complex organic compounds (16, 37). Any impact on the rate of U(VI) reduction due to organic complexation will affect treatment system design by this technique. Hence, it is essential to select bacteria which can most efficiently reduce U(VI) in waste streams containing a variety of organic compounds.

This research was performed to evaluate the availability of U(VI) for microbial reduction in solutions containing organic complexants. One aromatic and four aliphatic organic ligands were used to study the impact of metal-ligand binding on enzymatic U(VI) reduction by two metabolically diverse bacteria.

MATERIALS AND METHODS

Organisms and culture conditions. *Desulfovibrio desulfuricans* (ATCC 29577), a sulfate-reducing bacterium, and *Shewanella alga*, a primary iron-reducing bacterium (7), were used to evaluate U(VI) reduction in solution. Both of these organisms, under anaerobic conditions, can enzymatically reduce U(VI) to the tetravalent form in organic-free bicarbonate solutions with lactate or H_2 gas as the sole electron donor (7, 34). *D. desulfuricans* was grown in a well-defined medium (34) containing lactate as the primary carbon-electron source and sulfate as the electron acceptor. *S. alga* was grown in a medium containing lactate as the carbon-electron source and ferric citrate as the sole electron acceptor (7). Standard anaerobic techniques were used to prepare growth medium and for maintenance of culture conditions throughout this research (26). Briefly, the growth medium was heated to near boiling, purged with a high-purity gas mixture (5% H_2, 10% CO_2, 85% N_2) for 10 min to remove dissolved oxygen, anaerobically transferred in 60-ml volumes to 150-ml serum bottles, and autoclaved to ensure sterility prior to inoculation with cells (21, 26, 32).

Ligand concentration and uranyl ion speciation. Five organic ligands which form monodentate, bidentate, or bi- or polynuclear complexes with uranyl ion were selected for study (Table 1). Four of the ligands selected were aliphatics, which complexed with uranyl ion primarily through carboxyl ion interactions. One ligand, 4,5-dihydroxy-1,3-benzene disulfonic acid (tiron), was aromatic and complexed with uranium exclusively through hydroxyl ion interactions. Thermodynamic stability constants were obtained from the literature (39, 40, 49) and from an empirical relationship developed in our laboratory to approximate stability constants for selected $UO_2(OH)$-organic ligand species (21). These constants were used in association with the computer speciation program MINTEQ2A (2) in the selection of test ligand concentrations and prediction of uranyl ion speciation in each experiment. Two concentrations of each aliphatic ligand were chosen such that most (>98%) or one-half (~50%) of the U(VI) initially added directly complexed the target ligand. The remaining U(VI) formed organic [$UO_2(OH)$-organic ligand] and inorganic [$(UO_2)_xOH_y$] uranyl hydroxide species. In the aromatic-ligand (tiron) solutions, greater than 98% of the U(VI) initially formed ternuclear $(UO_2)_3(OH)_2(tiron)_3$ species at the higher tiron dosage. At the lower ligand concentration, ~50% of the U(VI) added formed ternuclear tiron complexes. The concentration of organic ligands and the percent distribution of various uranium species predicted by MINTEQ2A before microbial reduction are shown in Table 2.

Sample preparation. Batch experiments were performed under nongrowth conditions (7, 21, 34) to evaluate bioreduction of uranyl ion complexed to organic ligands. Test solutions contained H_2 gas as the sole electron donor, uranyl ion as the primary electron acceptor, each target ligand as the primary complexing agent, and sodium nitrate as the background electrolyte (ionic strength, 0.17 M). Initially, stock solutions (1 liter) were prepared by adding each test ligand and sodium nitrate to distilled, deionized water. The pH of the stock was then adjusted to 6.0 by using HNO_3 or NaOH (0.1 M). Subsequently, the solutions were filter sterilized (0.2-μm-pore-size filter), deoxygenated by purging with an anaerobic gas mixture (5% H_2, 10% CO_2, 85% N_2), and dispensed in 9-ml volumes into 25-ml anaerobic pressure tubes. Each tube was then closed with a butyl rubber stopper and sealed with an aluminum cap. A 0.5-ml deoxygenated uranyl nitrate solution [~2-g/liter U(VI) stock] was injected into each tube, resulting in an initial U(VI) concentration of ~100 mg/liter. Solutions were then mixed (100 rpm) at a constant temperature (32°C) for 48 h to allow equilibrium speciation to occur. H_2 gas was then added to the headspace of each pressure tube by injecting 20 ml of an 80% H_2–20% CO_2 gas mixture. The samples were then shaken gently but thoroughly by hand for ~1 min at room temperature to

TABLE 2. Ligand concentrations and distribution of various species, as predicted by MINTEQ2A, before microbial inoculation in test solutions[a]

Ligand and concn (M)	UO_2-organic ligand species	$UO_2(OH)$-organic ligand species	UO_2-inorganic species
Acetate			
0.17	$UO_2(CH_3COO)_3^{-1}$ (91.2)[b] $UO_2(CH_3COO)_2$ (5.8)	$UO_2(OH)CH_3COO$ (2.5)	
0.03	$UO_2(OH)CH_3COO^{-1}$ (23.1) $UO_2(OH)CH_3COO_2$ (8.8) $UO_2(OH)CH_3COO^{+1}$ (4.3)	$UO_2(OH)CH_3COO$ (23)	UO_2OH^+ (1.6) $(UO_2)_3(OH)_5^{-1}$ (38)
Malonate			
0.01	$UO_2(C_3H_4O_4)_2$ (98)	$UO_2(OH)(C_3H_4O_4)$ (1.2)	
0.0075	$UO_2(C_3H_4O_4)_2$ (33.9) $UO_2(C_3H_4O_4)$ (5.5)	$UO_2(OH)(C_3H_4O_4)$ (9.3)	UO_2OH^+ (1.7) $(UO_2)_2(OH)_2$ (1.0) $(UO_2)_3(OH)_5^{-1}$ (48.4)
Oxalate			
0.01	$UO_2(C_2H_4O_4)_3$ (22.8) $UO_2(C_2H_4O_4)_2$ (75.2)	$UO_2(OH)(C_2H_4O_4)$ (1.6)	
0.00075	$UO_2(C_2H_4O_4)_2$ (30.7) $UO_2(C_2H_4O_4)$ (11.9)	$UO_2(OH)(C_2H_4O_4)$ (36.5)	UO_2OH^+ (1.2) $(UO_2)_3(OH)_5^{-1}$ (18.8)
Citrate			
0.005	$[UO_2(C_6H_8O_7)]_2$ (100)		
0.0002	$[UO_2(C_6H_8O_7)]_2$ (49.7)		$(UO_2)_3(OH)_5^{-1}$ (49.7)
Tiron			
0.0004		$(UO_2)_3(OH)_2tiron_3$ (100)	
0.0002		$(UO_2)_3(OH)_2tiron_3$ (50)	$(UO_2)_3(OH)_5^{-1}$ (49.7)

[a] The initial pH was 6.0 in all test solutions.
[b] Each value in parentheses is the percent distribution of that uranium species.

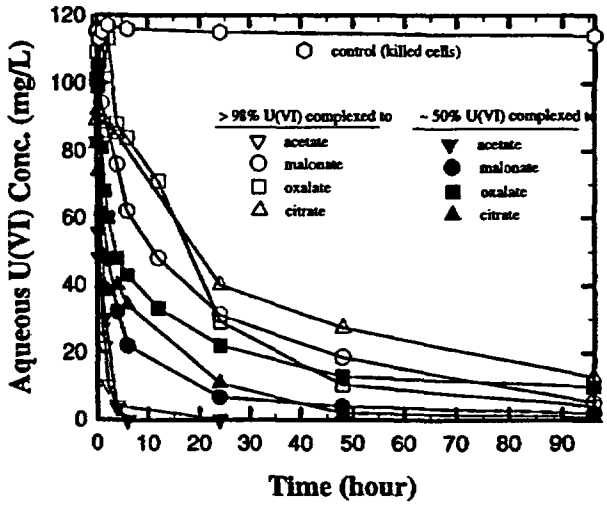

FIG. 1. U(VI) reduction in test solutions containing low and high concentrations (Conc.) of aliphatic organic ligands after inoculation with *D. desulfuricans*.

allow H_2 gas dissolution into each test solution. *D. desulfuricans* or *S. alga* cells grown in nutrient-rich culture medium were collected by centrifugation (7,500 × *g*, 20 min, 4°C), washed twice with a uranium-free anaerobic solution (21), and inoculated into the test samples. Each pressure tube initially contained ~5×10^8 cells/ml of test solution. All samples were then incubated at 32°C, and U(VI) biotransformation was evaluated over time.

Analytical techniques. Uranium levels in test solutions were measured with a kinetic phosphorescence analyzer. This instrument uses a pulsed nitrogen dye laser and a complexing reagent to measure only U(VI) levels in solution (6). Microbial reduction of complexed uranium was evaluated by monitoring the decrease in the U(VI) concentration over time in the unfiltered test solution after cell inoculation. Subsamples (~2 ml) from each pressure tube were collected and appropriately diluted with deoxygenated, deionized water, and the U(VI) level was analyzed under anaerobic conditions (21, 32). Internal standards for calibration were prepared such that the same amounts of organic ligand, sodium nitrate, and other sample constituents were present during uranium analysis (21). Acetate and citrate levels were measured by high-performance liquid chromatography with a Spherisorb C_8 column (21) and an LC90 UV detector set at a 210-nm wavelength. Malonate and oxalate were measured by ion-exchange chromatography with an Ion-Pak AS4A-SC anion-exchange column and an ED40 Dionex conductivity detector. Tiron was measured with a Beckman DU-70 spectrophotometer at a 300-nm wavelength (21).

Statistical analysis. Duplicate measurements of U(VI) concentrations in two tubes for each time period were used for analyses. The U(VI) reduction data were analyzed by using a one-way analysis of variance and a nonparametric Cox and Stuart test (12). The differences in U(VI) reduction rates were determined at a confidence level of 95%.

RESULTS AND DISCUSSION

U(VI) reduction by *D. desulfuricans*. Results indicated that *D. desulfuricans* reduced U(VI) from each of the aliphatic complexes evaluated (Fig. 1). In the higher-concentration acetate, malonate, and oxalate solutions [test ligands initially complexed >98% of the U(VI)], the bacteria reduced more than 95% of the U(VI) initially present after 96 h of incubation. In the higher-concentration citrate solution ~85% of the U(VI) was reduced after 96 h. The trend in uranium reduction for the higher-concentration citrate solution suggested that further reduction can be achieved by extending the incubation period. Significant amounts (>90%) of uranium were also reduced in solutions containing the lower aliphatic ligand concentration [~50% U(VI) initially complexed to the test ligands]. Results suggested that complex formation with aliphatic ligands did not appear to affect the availability of U(VI) as an electron acceptor to the sulfate-reducing bacteria.

TABLE 3. V_i of U(VI) by *D. desulfuricans* in aliphatic solutions

Ligand (concn [M] used)	V_i [mg of U(VI)/mg cell-h]
Acetate (0.17)	1.6×10^{-3}
Acetate (0.003)	1.9×10^{-3}
Malonate (0.01)	9.0×10^{-5}
Malonate (0.00075)	3.4×10^{-4}
Oxalate (0.01)	8.9×10^{-5}
Oxalate (0.00075)	1.8×10^{-4}
Citrate (0.005)	6.0×10^{-5}
Citrate (0.0002)	1.4×10^{-4}

Although a substantial amount of U(VI) was reduced in each test solution, the rate of reduction varied with the type and relative amount of U(VI)-organic complex formed. The differences observed in U(VI) reduction trends were statistically significant ($\alpha = 0.05$). The U(VI) reduction rate kinetic coefficients in the presence of each test ligand were evaluated by using a linearized form of the Michaelis-Menten expression (3, 24, 50). The initial rate of reduction (V_i), which represents the U(VI) reduction rate immediately after cell inoculation, was used to compare the impact of solution constituents (organic complexants) on U(VI) biotransformation (Table 3). The V_i values were normalized to the amount of U(VI) (milligrams) utilized by a unit of cell mass (milligram-cell) by using a conversion of 10^7 cells/mg of biomass (48). It was observed that in solutions containing the higher concentration of aliphatic ligand, the V_i of U(VI) from acetate complexes was ~20-fold higher than that observed in the presence of multidentate aliphatic ligands. This indicated that U(VI) was not as readily available as an electron acceptor from multidentate aliphatic complexes as it was from monodentate (acetate) complexes for *D. desulfuricans*. When the concentrations of multidentate aliphatic ligands were reduced such that ~50% of the U(VI) formed only multidentate complexes, the V_i increased two- to fivefold.

Rapid reduction of U(VI) from selected organic complexes was not due to degradation of these ligands by *D. desulfuricans*. No significant decrease ($\alpha = 0.05$) in organic-ligand concentration was measured, even after 96 h of incubation, in U(VI)-containing solutions (Fig. 2). Note that the bacterium reduced

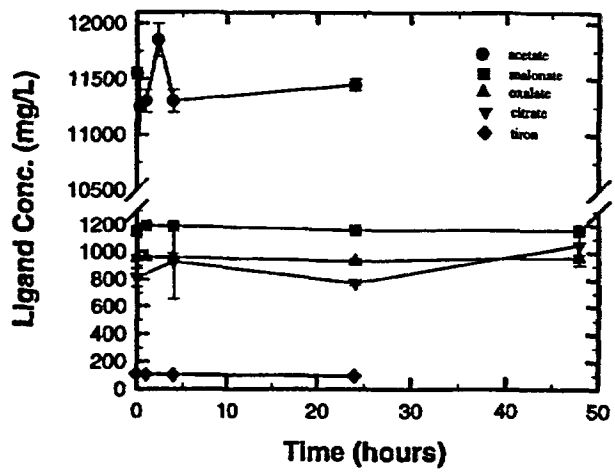

FIG. 2. Concentrations (Conc.) of organic ligands during U(VI) bioreduction by *D. desulfuricans*. Ligands initially complexed >98% of the U(VI).

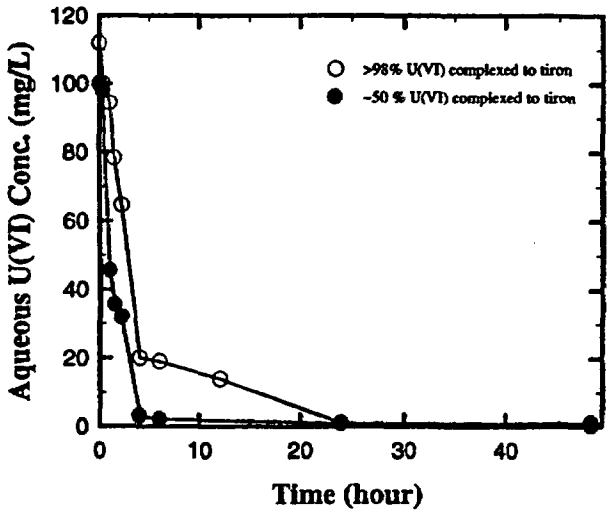

FIG. 3. U(VI) reduction in test solutions containing low and high concentrations (Conc.) of an aromatic organic ligand (tiron) after inoculation with *D. desulfuricans*.

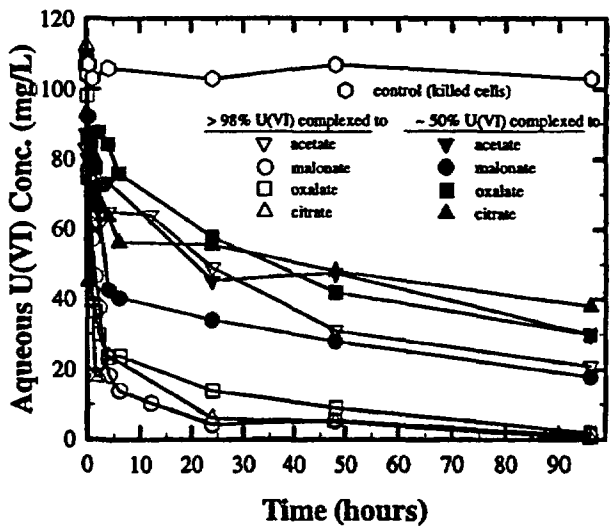

FIG. 4. U(VI) reduction in test solutions containing low and high concentrations (Conc.) of aliphatic organic ligands after inoculation with *S. alga*.

>85% of the U(VI) during this period. The very high concentration of acetate (11,500 mg/liter) utilized in the experiment rendered this ligand analysis difficult. However, evidence in the literature indicates that *D. desulfuricans* does not use acetate as a carbon or electron source (11, 31).

Slower reduction of U(VI) in the presence of multidentate aliphatic ligands was not due to toxicity of these organics to the bacterium. This was verified in a separate experiment in which the bacterium, under resting-cell conditions, readily reduced a poorly complexing compound (thiosulfate) in the presence of each test ligand (21). The results suggested that complexation by multidentate aliphatic ligands was responsible for the slower U(VI) reduction by *D. desulfuricans*, and the extent of impact depended on the amount of U(VI) organically complexed in solution. This impact, however, appeared to differ from that observed during Fe(III) reduction by *D. desulfuricans*. Coleman et al. (10) observed that multidentate aliphatic complexation by NTA did not appreciably affect the trend in Fe(III) reduction by *D. desulfuricans*. The bacteria reduced equal amounts (~3.5 mM) of Fe(III) from poorly crystalline Fe(III)oxide and Fe(III)-NTA complexes after 36 h of incubation. Further investigation is required to better understand the mechanism(s) of metal utilization from aliphatic complexes by the sulfate-reducing bacteria.

The impact of aromatic complexation on U(VI) bioreduction was evaluated by using tiron as the test ligand. Figure 3 shows U(VI) levels in tiron solutions after inoculation with *D. desulfuricans*. The bacteria reduced significant levels of U(VI) (>95%) in solutions containing high, as well as low, concentrations of tiron. Although U(VI) from multidentate aliphatic complexes was not readily available for reduction, *D. desulfuricans* rapidly reduced U(VI) from the multinuclear aromatic complex evaluated. In solutions in which >98% of the U(VI) initially formed ternuclear complexes with tiron, the V_i of U(VI) [5.7×10^{-4} mg of U(VI)/mg cell-h] was approximately 50% lower than that observed in acetate solutions but was more than an order of magnitude higher than that in the presence of multidentate aliphatic ligands. A similar impact on the relative rates of U(VI) reduction was also observed in solutions containing lower concentrations of tiron. The V_i of U(VI) [4.6×10^{-4} mg of U(VI)/mg cell-h] was slightly lower than that observed in solutions containing the lower concentration of acetate but was 1.5- to 3-fold higher than that observed at lower concentrations of multidentate ligands. This suggested that the negative impact on U(VI) reduction due to complexation with the aromatic ligand (tiron) was much less than that observed with multidentate aliphatic ligands.

U(VI) reduction by *S. alga*. Figure 4 shows U(VI) levels in unfiltered aliphatic test solutions after inoculation with *S. alga*. The trends in uranium reduction were very different from those observed when *D. desulfuricans* was used. The extent of U(VI) reduction by *S. alga* in several aliphatic solutions was much lower than that by *D. desulfuricans* observed. When >98% of U(VI) was initially complexed to acetate, approximately 80% of the added U(VI) was reduced after 96 h of incubation. In solutions containing multidentate aliphatics, more than 95% of the U(VI) was reduced during this period. However, in solutions containing lower concentrations of aliphatic ligands, the bacteria reduced only 50 to 80% of the U(VI) initially introduced.

The V_i in test solutions varied with the type and level of U(VI)-aliphatic complexes present (Table 4). When >98% of the U(VI) was complexed to the test organics, the V_i of U(VI) in the presence of multidentate ligands was more than an order of magnitude higher than that observed in monodentate aliphatic (acetate) solutions. The slower reduction from acetate solutions does not appear to be due to toxicity of this ligand,

TABLE 4. V_i of U(VI) by *S. alga* in aliphatic solutions

Ligand (concn [M] used)	V_i [mg U(VI)/mg cell-h]
Acetate (0.17)	2.0×10^{-5}
Acetate (0.003)	1.5×10^{-5}
Malonate (0.01)	1.1×10^{-3}
Malonate (0.00075)	5.7×10^{-5}
Oxalate (0.01)	1.25×10^{-3}
Oxalate (0.00075)	5.2×10^{-5}
Citrate (0.005)	1.3×10^{-3}
Citrate (0.0002)	1.1×10^{-5}

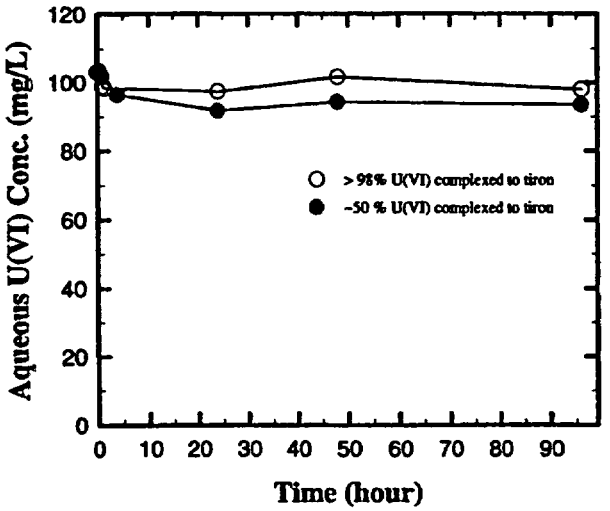

FIG. 5. U(VI) reduction in test solutions containing low and high concentrations (Conc.) of an aromatic organic ligand (tiron) after inoculation with *S. alga*.

since this bacterium was isolated by using a medium containing a high concentration of acetate (7). Furthermore, differences in U(VI) reduction were not due to metabolism of the test ligands by this bacterium. Insignificant amounts of each ligand were utilized by this bacterium during U(VI) reduction (data not shown). Also, *S. alga* does not couple oxidation of acetate and citrate to metal reduction, even under growth conditions (7, 30). It should be noted that, when multidentate ligand levels were lowered such that only ~50% of the U(VI) initially added was complexed, the rate of reduction decreased by more than an order of magnitude (Table 4). This observation suggested that if *S. alga* degraded the test ligands (thereby decreasing their concentration), U(VI) reduction rates would have been retarded rather than enhanced. Therefore, it appears that chemical speciation of uranyl ion in solution rather than inhibition-degradation of organic ligands dictates U(VI) availability to *S. alga*. It has been well documented that the activity of selected yeast cells and *Thiobacillus ferrooxidans* was lower in the presence of uncomplexed uranyl ions (UO_2^{2+}) but was not affected when uranyl ions were complexed to strong complexants such as carbonate or citrate (46–48, 51). In addition, it has been reported that iron-reducing microorganisms from anaerobic sediments reduced Fe(III) from multidentate aliphatic (NTA) complexes more rapidly than from uncomplexed, poorly crystalline Fe(III) oxide (29, 36).

S. alga did not reduce U(VI) from aromatic ternuclear tiron complexes (Fig. 5). Less than 5% of the U(VI) present was reduced in solutions in which the predominant U(VI) species was in the tiron complex (>98%), as well as in solutions containing only ~50% tiron-U(VI) complexes. The reduction trends observed in various experiments indicated that multidentate aliphatic complexes were better sources of the U(VI) electron acceptor for *S. alga* than were monodentate aliphatic complexes (acetate), aromatic complexes (tiron), or uranyl hydroxide species.

It should be noted that tiron formed a polynuclear complex with U(VI) and the stability constant for complexation was higher than values reported for the other organic complexes evaluated (Table 1). However, trends of U(VI) reduction from tiron complexes by either bacterium were more similar to

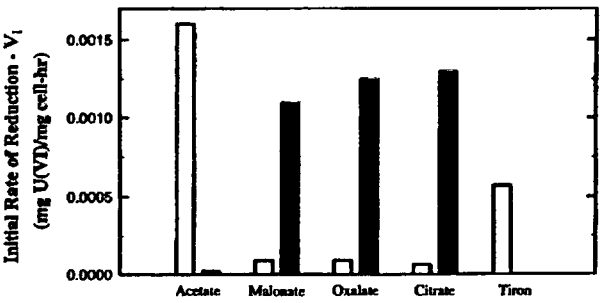

FIG. 6. V_i of U(VI) in test solutions containing organic ligands incubated with *D. desulfuricans* (□) and *S. alga* (■). Ligands initially complexed >98% of the U(VI).

trends observed from the complex with the lowest stability constant (acetate) than from complexes with higher stability constants (multidentate aliphatics). This suggested that reduction of U(VI) from various organic complexes was not primarily related to the respective thermodynamic stability constants. Bolton et al. (5) and Francis et al. (18) have reported that factors such as lability of metal-organic complexes rather than stability constants will dictate the degradation of metal-organic complexes. The functional groups (hydroxyl) involved in U(VI)-tiron complexation and the structural orientation of ternuclear aromatic complexes probably dictated the reduction of U(VI) by microorganisms.

Comparison of U(VI) reduction by *D. desulfuricans* and *S. alga*. A comparison of results indicated that the two bacteria reduced U(VI) very differently from each of the complexes evaluated. *D. desulfuricans* rapidly reduced U(VI) from monodentate aliphatic complexes formed with acetate (Fig. 6). *S. alga* very slowly reduced uranium from this complex. While reduction from multidentate complexes by the sulfate-reducing bacteria was slow, it was rapid in the presence of the iron-reducing bacteria. Rapid reduction of U(VI) by *D. desulfuricans* was also observed in aromatic complexes. Reduction by *S. alga* was slow in these complexes. In addition, a decrease in the amount of organic-U(VI) complex in solution increased the rate of reduction by *D. desulfuricans* and decreased the rate of reduction by *S. alga* (Tables 3 and 4). The vast differences in U(VI) reduction trends observed when the two bacteria were used was due to neither toxicity nor metabolism of organic complexants by either of the bacteria. The results observed may be due to differences in the nature of the enzymes involved in reduction. Sulfate-reducing bacteria have been reported to reduce uranyl ion by using an enzyme (cytochrome c_3) located at the soluble (periplasmic) fraction of the cell (35). This enzyme is not associated with an energy-yielding process leading to growth of the bacteria (34). In contrast, *S. alga* reduced U(VI) by using a multicomponant enzyme system associated with the membrane fraction of the cell (8, 9). The enzyme complex appeared to be involved in phosphorylation–energy-yielding processes of the bacteria (9). Such differences in the location and function of U(VI)-reducing enzymes may have imposed limitations on structural compatibility or transport mechanisms and contributed to the differences in the U(VI) reduction from organic complexes by the two bacteria.

Precipitation of bioreduced uranium. Effective removal of uranium from contaminated water by these microorganisms depends not only on reduction of U(VI) to U(IV) but also on subsequent precipitation of reduced uranium. Precipitation of U(IV), upon microbial reduction, was evaluated by measuring the total dissolved uranium [U(VI) plus U(IV)] in the filtrate

(0.2-μm-pore-size filter) over time. The filtrate (1 ml) was oxidized by using 2 N HNO_3 to convert U(IV) to U(VI) prior to this analysis (21). The results indicated that precipitation of U(IV) depended on the type and concentration of the organic ligand present in solution (data not shown). Briefly, while >95% of the U(IV) precipitated from solutions containing the highest concentrations of acetate and malonate, less than 20% of the U(IV) precipitated in the presence of oxalate and citrate. At the lower concentrations of oxalate and citrate used, >80% of the bioreduced uranium precipitated from solution. However, little (~10%) of the U(IV) precipitated from tiron solutions, even at the lower concentration utilized. A detailed discussion concerning U(IV) precipitation trends in the presence of organic chelating agents is presented elsewhere (19–22).

Implications for wastewater treatment. Results indicated that reduction of U(VI) was affected by various organic compounds when either of the bacteria was evaluated. It appears that ground and surface waters containing uranium but little or no organic matter can be successfully treated by using *D. desulfuricans*. However, experimental results suggest that these aqueous solutions may need to be amended with strong complexants prior to using *S. alga* for uranium reduction. Mixed-process waste streams from industries and leachates produced from environmental restoration operations generally contain complex organic compounds (37). While *S. alga* can rapidly reduce U(VI) from selected multidentate complexes found in such waste streams, reduction by *D. desulfuricans* may be slow. In addition, precipitation of reduced uranium [U(IV)] will depend upon the type and amount of organic ligands present. Hence, it is essential to evaluate the chemical (organic) composition of waste streams prior to selecting the type of bacteria for uranium reduction. Finally, results suggested that the negative impact on biotreatment due to organic-metal complexation can be greatly alleviated by proper selection of bacteria for treatment.

ACKNOWLEDGMENTS

This project was supported by the U.S. Department of Energy (DE-FC05-92-OR-22056) and by the Waste Management Research and Education Institute at the University of Tennessee, Knoxville.

REFERENCES

1. **Ahrland, S.** 1951. On the complex chemistry of the uranyl ion. IV. The complexity of uranyl acetate. Acta Chem. Scand. **5**:199–219.
2. **Allison, J. D., D. S. Brown, and K. J. Vots Gradac.** 1991. MINTEQ2A/PRODEFA2A, a geochemical assessment model for environmental systems. Report EPA-600/3-91-021. U.S. Environmental Protection Agency, Athens, Ga.
3. **Barrio-Lage, G., F. Z. Parsons, and R. S. Nassar.** 1987. Kinetics of depletion of trichloroethene. Environ. Sci. Technol. **21**:366–369.
4. **Bergsma, J., and W. N. Konning.** 1983. The properties of citrate transport in membrane vesicles from *Bacillus subtilis*. Eur. J. Biochem. **1311**:151–156.
5. **Bolton, H., D. C. Girvin, A. E. Plymale, S. D. Harvey, and D. Workman.** 1996. Degradation of metal-nitrilotriacetate complexes by *Chelatobacter heintzii*. Environ. Sci. Technol. **30**:931–938.
6. **Brina, R., and A. G. Miller.** 1992. Direct detection of trace levels of uranium by laser induced kinetic phosphorimeter. Anal. Chem. **64**:1415–1418.
7. **Caccavo, F., Jr., R. P. Blakemore, and D. R. Lovley.** 1992. A hydrogen-oxidizing, Fe(III)-reducing microorganism from the Great Bay estuary, New Hampshire. Appl. Environ. Microbiol. **58**:3211–3216.
8. **Caccavo, F., Jr., Y. A. Gorby, and M. J. McInerney.** 1995. Characterization of a metal reductase complex in the dissimilatory metal-reducing bacterium *Shewanella alga* strain BrY. Poster presented at the 95th General Meeting of the American Society for Microbiology 1995.
9. **Caccavo, F., Jr. (Center for Biofilm Engineering, Montana State University.)** 1995. Personal communication.
10. **Coleman, M. L., D. B. Hedrick, D. R. Lovley, D. C. White, and K. Pye.** 1993. Reduction of Fe(III) in sediments by sulphate-reducing bacteria. Nature **36**:436–438.
11. **Collern, E., S. Fennegan, and P. Lens.** 1995. Anaerobic treatment of sulfate containing waste streams. Antonie van Leeuwenhoek **67**:29–46.
12. **Conover, W. J.** 1980. Practical non-parametric statistics. Wiley science in probability and mathematics. Wiley, Ridge, N.J.
13. **Cox, C. D.** 1980. Iron reductases from *Pseudomonas aeruginosa*. J. Bacteriol. **80**:2121–2128.
14. **Emery, T.** 1976. Fungal ornithine esterases: relationship to iron transport. Biochemistry **15**:2723–2728.
15. **Firestone, M. K., and J. M. Tiedje.** 1975. Biodegradation of metal-nitrilotriacetate complexes by a *Pseudomonas* species: mechanism of reaction. Appl. Microbiol. **29**:758–764.
16. **Francis, A. J., C. R. Iden, B. J. Nine, and C. K. Chang.** 1980. Characterization of organics in leachates from low level radioactive waste disposal sites. Nucl. Technol. **50**:158–163.
17. **Francis, A. J., and C. J. Dodge.** 1993. Influence of complex structure on the biodegradation of iron-citrate complexes. Appl. Environ. Microbiol. **59**:109–113.
18. **Francis, A. J., C. J. Dodge, and J. B. Gillow.** 1992. Biodegradation of metal citrate complexes and implications for toxic-metal mobility. Nature **356**:140–142.
19. **Ganesh, R., K. G. Robinson, and G. D. Reed.** 1995. Biotransformation of uranium complexed to organic ligands by *Desulfovibrio desulfuricans*, abstr. 57, p. 527–534. *In* Proceedings of the 50th Purdue Industrial Waste Conference.
20. **Ganesh, R., K. G. Robinson, G. D. Reed, and M. M. Ghosh.** 1995. Reductive precipitation of organically complexed uranium by bacterial strain BrY, abstr. 1, p. 152–155. *In* Special Symposium on Emerging Technologies in Hazardous Waste Management VII. American Chemical Society, Atlanta, Ga.
21. **Ganesh, R.** 1995. Impact of organic ligands on bioreductive precipitation of hexavalent uranium. Ph.D. thesis. University of Tennessee, Knoxville.
22. **Ganesh, R., K. G. Robinson, G. D. Reed, and G. S. Sayler.** Factors influencing U(VI) reduction from organic complexes by *Shewanella alga*. Submitted for publication.
23. **Gorby, Y. A., and D. R. Lovley.** 1992. Enzymatic uranium precipitation. Environ. Sci. Technol. **26**:205–207.
24. **Goring, A. I., and J. W. Hamaker.** 1972. Organic chemicals in the soil environment. Marcel Dekker, Inc., New York, N.Y.
25. **Gustafson, R. L., C. Richard, and A. E. Martell.** 1960. Polymerization of uranyl-tiron chelates. J. Am. Chem. Soc. **82**:1526–1534.
26. **Hungate, R. E.** 1969. A roll tube method for cultivation of strict anaerobes. Methods Microbiol. **3B**:117–132.
27. **Huyer, M., and W. J. Page.** 1989. Ferric reductase activity in *Azotobacter vinelandii* and its inhibition by Zn^{2+}. J. Bacteriol. **171**:4031–4037.
28. **Joshi-Tope, G., and A. J. Francis.** 1995. Mechanisms of biodegradation of metal-citrate complexes by *Pseudomonas fluorescens*. J. Bacteriol. **177**:8–12. **42**:547–569.
29. **Kelly, W. R., M. P. Saliga, M. L. Machesky, and D. L. Freedman.** 1996. Biodegradation of BTEX under iron-reducing conditions at batch microcosms, abstr. 3, p. 161–172. *In* Proceedings of the 69th Annual Water Environment Federation Conference, Water Environment Federation, Dallas, Tex.
30. **Knight, V., F. Caccavo, S. Wudyka, and R. Blakemore.** 1996. Synergistic iron reduction and citrate dissimilation by *Shewanella alga* and *Aeromonas veronii*. Arch. Microbiol. **166**:269–274.
31. **Krieg, N. R., and J. G. Holt.** 1984. Bergey's manual of systematic bacteriology, vol. 1. p. 663–680. The Williams & Wilkins Co., Baltimore, Md.
32. **Lovley, D. R., E. J. P. Phillips, Y. A. Gorby, and E. R. Landa.** 1991. Biological reduction of uranium. Nature **350**:413–416.
33. **Lovley, D. R., and E. J. P. Phillips.** 1992. Bioremediation of uranium contamination with enzymatic uranium reduction. Environ. Sci. Technol. **26**: 2228–2234.
34. **Lovley, D. R., and E. J. P. Phillips.** 1992. Reduction of uranium by *Desulfovibrio desulfuricans*. Environ. Sci. Technol. **58**:850–856.
35. **Lovley, D. R., P. K. Wideman, J. C. Woodward, and E. J. P. Phillips.** 1993. Reduction of uranium by cytochrome c_3 of *Desulfovibrio vulgaris*. Appl. Environ. Microbiol. **59**:3572–3576.
36. **Lovley, D. R., J. C. Woodward, and F. C. Chapelle.** 1996. Rapid anaerobic benzene oxidation with a variety of chelated Fe(III) forms. Appl. Environ. Microbiol. **62**:288–291.
37. **Macaskie, L. E.** 1991. The application of biotechnology to the treatment of waste produced from the nuclear fuel cycle: biodegradation and bioaccumulation as a means of treating radionuclide containing streams. Crit. Rev. Biotechnol. **11**:41–112.
38. **Madsen, E. L., and M. Alexander.** 1985. Effect of chemical speciation on the mineralization of organic compounds by microorganisms. Appl. Environ. Microbiol. **50**:342–349.
39. **Martell, A. E., and R. M. Smith.** 1977. Critical stability constants—vol. 3. Other organic ligands. Plenum Press, New York, N.Y.
40. **Perrin, D. D.** 1979. Stability constants for metal ion complexes. Part B—organic ligands. Pergamon Press, Oxford, United Kingdom.
41. **Phillips, E. J. P., E. R. Landa, and D. R. Lovley.** 1995. Remediation of uranium contaminated soils with bicarbonate extraction and microbial

U(VI) reduction. J. Ind. Microbiol. 14:203–207.
42. **Rajan, S., and A. E. Martell.** 1965. Equilibrium studies on uranyl complexes. III. Interaction of uranyl ion with citric acid. Inorg. Chem. 4:462–469.
43. **Rajan, S., and A. E. Martell.** 1967. Equilibrium studies on uranyl complexes. IV. Reaction with carboxylic acids. J. Inorg. Nucl. Chem. 29:523–529.
44. **Robinson, K. G., R. Ganesh, G. D. Reed, and D. Kucsmas.** 1994. Biologically mediated removal of uranium in a high nitrate/sulfate wastewater, abstr. 1, p. 199–208. *In* Proceedings of the 67th annual Water Environment Federation Conference. Water Environment Federation, Chicago, Ill.
45. **Roden, E. E., and D. R. Lovley.** 1993. Dissimilatory Fe(III) reduction by the marine microorganism *Desulfuromonas acetoxidans*. Appl. Environ. Microbiol. 59:734–742.
46. **Rothstein, A., and C. Larrabee.** 1948. The relationship of cell surface to metabolism. II. The cell surface of yeast as the site of inhibition of glucose metabolism by uranium. J. Cell. Comp. Physiol. 32:247–259.
47. **Rothstein, A., A. Frankel, and C. Larrabee.** 1948. The relationship of cell surface to metabolism. III. Certain characteristics of the uranium complexation with cell surface groups of yeast. J. Cell Comp. Physiol. 32:247–259.
48. **Rothstein, A., R. C. Meier, and L. Hurwitiz.** 1951. The relationship of cell surface to metabolism. V. The role of uranium complexing loci of yeast metabolism. J. Cell. Comp. Physiol. 37:57–81.
49. **Sillen, L. G., and A. E. Martell.** 1964. Stability constants of metal ion complexes, 2nd ed. Burlington House, London, United Kingdom.
50. **Suflita, J. M., J. A. Robinson, and J. M. Tiedje.** 1983. Kinetics of microbial dehalogenation on haloaromatic substrates in methanogenic environments. Appl. Environ. Microbiol. 45:1466–1473.
51. **Tuovinan, O. H., and D. P. Kelly.** 1974. Studies on the growth of *Thiobacillus ferrooxidans*. II. Toxicity of uranium to growing culture and tolerance conferred by mutation, other metal cations and EDTA. Arch. Microbiol. 95: 153–164.
52. **Van Der Rest, M. E., J. Abee, D. Molenover, and W. N. Konning.** 1991. Mechanism and energetics of a citrate-transport system of *Klebsiella pneumoniae*. Eur. J. Biochem. 195:71–77.

Environ. Sci. Technol. 2001, 35, 3332–3337

Time Scales for Sorption–Desorption and Surface Precipitation of Uranyl on Goethite

DANIEL E. GIAMMAR AND JANET G. HERING*

California Institute of Technology, 1200 East California Boulevard, Environmental Engineering Science (138-78), Pasadena, California 91125

The sorption of uranium on mineral surfaces can significantly influence the fate and transport of uranium contamination in soils and groundwater. The rates of uranium adsorption and desorption on a synthetic goethite have been evaluated in batch experiments conducted at constant pH of 6 and ionic strength of 0.1 M. Adsorption and desorption reactions following the perturbation of initial states were complete within minutes to hours. Surface–solution exchange rates as measured by an isotope exchange method occur on an even shorter time scale. Although the uranium desorption rate was unaffected by the aging of uranium–goethite suspensions, the aging process appears to remove a portion of adsorbed uranium from a readily exchangeable pool. The distinction between sorption control and precipitation control of the dissolved uranium concentration was also investigated. In heterogeneous nucleation experiments, the dissolved uranium concentration was ultimately controlled by the solubility of a precipitated uranyl oxide hydrate. The X-ray diffraction pattern of the precipitate is characteristic of the mineral schoepite. Precipitation is kinetically hindered at low degrees of supersaturation. In one experiment, metastable sorption controlled dissolved uranium concentrations in excess of the solubility limit for more than 30 d.

Introduction

The United States' nuclear weapons program has left a legacy of environmental contamination. Uranium mining, milling, and refining generated the largest volume of weapons waste (*1*), and uranium is a principal contaminant in soils at the Department of Energy weapons processing plants (*2*). The Federal standard for uranium in drinking water, promulgated in December 2000 by the U.S. Environmental Protection Agency, is 30 ppb; the rule will become effective in December 2003 (*3*).

At the Fernald Environmental Management Project (FEMP) in Ohio, high carbonate concentrations have resulted in mobilization of uranium from contaminated soils in the form of uranyl–carbanato complexes and contamination of the underlying aquifer (*4, 5*). At the carbonate-poor Savannah River Site (SRS), colloidal transport of uranium in groundwater has been observed (*6*), and the association of uranium with colloids of kaolinite and iron oxides has been demonstrated by synchrotron X-ray fluorescence (SXRF) measurements (*7*). In SRS surface waters, the transport of uranium during storm events is enhanced by its association with suspended quartz, kaolinite, gibbsite, and goethite solids (*8*).

Because of their high reactive surface areas, iron minerals can strongly influence the fate and transport of uranium. Despite differences in bulk mineralogy, similarities in iron content among Hanford, SRS, and Oak Ridge soils led to similar pH-dependent uranium adsorption (*9*). Sequential extraction of contaminated SRS aquifer solids showed uranium to be associated with amorphous (*10*) and crystalline (*11*) iron oxides, and the association of uranium with zones enriched in iron and manganese was verified by SXRF (*12*). The association of uranium with iron and aluminum oxyhydroxide minerals downgradient of a uranium ore body was suggested by selective extraction (*13, 14*) and has been incorporated into surface complexation models with iron oxides as the dominant sorbent (*15, 16*).

Uranium sorption in single-mineral systems has been investigated for goethite (*17–20*), hematite (*19, 21–23*), and ferrihydrite (*19, 24–26*). Uranium sorption occurs through the formation of inner-sphere surface complexes, which are most likely in bidentate coordination with surface iron centers (*18, 21, 27*). Sorption increases from none at low pH to a maximum at near-neutral pH; in the case of goethite, this sorption edge occurs between pH 5 and pH 6 (*17, 19, 20*). Uranyl complexation by carbonate leads to a significant decrease in sorption, although Bargar et al. (*21, 27*) have presented spectroscopic evidence for ternary uranyl–carbanato surface complexes and have suggested that they could be the dominant species on the surface even at slightly acidic pH.

Uranium uptake (*28*) and release (*29, 30*) from heterogeneous soils is often kinetically controlled. Uranium uptake on hematite (*27*) and ferrihydrite (*26*) exhibited a rapid phase of 30 min to several hours and a longer phase extending for tens and hundreds of hours. Slow sorption has been attributed to interparticle or intraparticle diffusion in pores (*31–33*), sites of low reactivity, and surface precipitation (*34*).

Surface precipitation is a consideration under conditions near or exceeding the solubility of uranyl minerals. Uranium uptake by ferrihydrite has been interpreted as coprecipitation (*35*). Uranyl phosphate microprecipitates identified downgradient of a uranium ore deposit are thought to have nucleated on the surfaces of iron oxyhydroxides at sites of uranium adsorption (*36, 37*). As dissolved uranium concentrations increase, monomeric surface complexes may convert to polymeric surface complexes and ultimately to oligomeric clusters and surface precipitates (*38*).

The objectives of this work were to determine the partitioning of uranium between the solution and the goethite surface and to measure the rates of adsorption and desorption at constant pH and ionic strength. Partitioning experiments were conducted to define a sorption isotherm and to determine conditions necessary for heterogeneous nucleation of a uranium-containing precipitate. Sorption rates were investigated following perturbation of equilibrium states and by isotope exchange.

Materials and Methods

Materials. Goethite was synthesized by heating freshly precipitated ferrihydrite (*39*). The resulting solid was washed by dialysis and then freeze-dried. X-ray diffraction (XRD) and diffuse reflectance Fourier-transform infrared spectroscopy confirmed the identity of the solid as goethite. The surface area of the goethite was measured as 42.2 $m^2 g^{-1}$ by the BET method with nitrogen adsorption using a Micromeritics Gemini surface area analyzer.

* Corresponding author telephone: (626)395-3644; fax: (626)395-2940; e-mail: jhering@caltech.edu.

10.1021/es0019981 CCC: $20.00
Published on Web 07/12/2001

TABLE 1. Relevant Uranyl Complexation and Precipitation Reactions

reaction	log K	ref
$UO_2^{2+} + H_2O = UO_2OH^+ + H^+$	−5.20	*42*
$UO_2^{2+} + 2H_2O = UO_2(OH)_2 + 2H^+$	−11.50[a]	*46*
$2UO_2^{2+} + 2H_2O = (UO_2)_2(OH)_2^{2+} + 2H^+$	−5.62	*42*
$3UO_2^{2+} + 5H_2O = (UO_2)_3(OH)_5^+ + 5H^+$	−15.55	*42*
$4UO_2^{2+} + 7H_2O = (UO_2)_4(OH)_7^+ + 7H^+$	−21.90	*42*
$UO_2^{2+} + CO_3^{2-} = UO_2CO_3(aq)$	9.68	*42*
$UO_2^{2+} + F^- = UO_2F^+$	5.09	*42*
$UO_2^{2+} + 2F^- = UO_2F_2(aq)$	8.62	*42*
$UO_2^{2+} + 3F^- = UO_2F_3^-$	10.90	*42*
$UO_2^{2+} + 4F^- = UO_2F_4^{2-}$	11.70	*42*
$UO_2^{2+} + 3H_2O = UO_32H_2O(s) + 2H^+$	−4.70	*45*
$UO_2^{2+} + 3H_2O = UO_32H_2O(s) + 2H^+$	−5.20	*46*

[a] Used instead of the value given by Grenthe et al. (*42*), which is only a limit of log $K \leq -10.3$.

Stock solutions of uranium for all experiments were prepared by dissolution of $UO_2(NO_3)_2{\cdot}6H_2O$ (Alfa Aesar) in Milli-Q water. A ^{235}U spike of 99% purity in 5% HNO_3 was obtained from L. Silver (Caltech). The pH was buffered with 5 mM 2-(*N*-morpholino)ethanesulfonic acid (MES) and adjusted to pH 6.00 with NaOH. MES was chosen as a pH buffer because of its lack of metal complexation, first demonstrated by Good et al. (*40*) for copper and recently for cadmium and lead (*41*). The ionic strength was fixed at 0.1 M with $NaNO_3$. Calibration standards for inductively coupled plasma–mass spectrometry (ICP–MS) analysis were prepared from a 1000 ppm standard solution (Alfa Aesar).

Experimental Methods. All experiments were conducted at pH 6 and an ionic strength of 0.1 M, were open to the atmosphere, and were at the ambient laboratory temperature (22 ± 2 °C). In partitioning experiments, uranyl nitrate solution was added to 0.1–0.5 g L^{-1} goethite suspensions in both batch and titration modes. A 48-h contact time was used in initial batch experiments with 2–42 μM total uranium. In titration mode, increments of uranyl nitrate solution were added to a 0.1 g L^{-1} goethite suspension at intervals greater than 4 h to final total uranium concentrations up to 46 μM. After the specified contact time, 10-mL samples of suspension were filtered through 0.22-μm cellulose nitrate (Millipore) or 0.2-μm polycarbonate membranes (Millipore), and the last 5 mL was collected and acidified. Data were fit to a Langmuir isotherm by a nonlinear fitting procedure with least-squares optimization using the software application Scientist (MicroMath).

In kinetics experiments, pre-equilibrated suspensions were perturbed, and the time required to re-establish equilibrium was measured. Kinetics experiments were initiated for adsorption by addition of uranium to a goethite suspension and for desorption either by dilution of a uranium-loaded goethite suspension into uranium-free solution or by addition of fluoride as a complexing ligand to a pre-equilibrated uranium–goethite suspension. Fluoride was used because it forms strong dissolved complexes with uranium(VI) (Table 1) even at pH 6. Collected samples were filtered and acidified prior to analysis for dissolved uranium. Sorbed uranium concentrations were calculated as the difference between known total and measured dissolved concentrations. Samples of whole suspension were periodically acidified and filtered to determine if the total uranium concentration was affected by sorption to reactor walls.

The effect of pre-equilibration time (i.e., aging) on the rate of desorption was investigated in a set of dilution-induced desorption experiments initiated from the same uranium–goethite suspension after 1 d, 1 month, and 6 months of mixing. Following the 6-month experiment, a 50-mL portion of the remaining suspension was put through a sequential extraction procedure. In each extraction cycle, the solid was vigorously mixed with 50 mL of extractant for 30 min at a solid to solution ratio of 0.03 g L^{-1}, goethite–extractant suspensions were centrifuged, a filtered supernatant sample was collected, the supernatant was decanted, and fresh extractant was added. The complete extraction process consisted of three cycles with deionized water, three with 1 M acetic acid at pH 5, and three with 1% HNO_3.

An isotope-exchange experiment was used to examine the rate of solution–surface exchange in a system with minimal equilibrium perturbation. After 4 d of equilibration with uranium depleted in ^{235}U, goethite suspensions (total volume = 250 mL) were spiked with 1 mL of 0.252 μM ^{235}U solution adjusted to the same pH and ionic strength. The addition of the ^{235}U significantly decreased the $^{238}U/^{235}U$ isotope ratio in the dissolved phase but did not appreciably change the dissolved uranium concentration. As the dissolved uranium exchanged with the surface, the isotope ratio in solution evolved to match the isotope ratio in the suspension (i.e., solution plus solid). Samples for dissolved and total uranium were taken following the same procedure used in batch equilibrium and equilibrium-perturbation experiments.

A series of experiments was performed to determine the conditions necessary for the heterogeneous nucleation of uranium surface precipitates on goethite. Uranyl nitrate was added incrementally to 0.23 g L^{-1} goethite suspensions to achieve final total uranium concentrations ranging from 20 to 1000 μM. The incremental addition process lasted from a few hours for low total uranium concentrations to 8 d for the maximum addition. At each point of addition, the pH was measured and adjusted as necessary with NaOH. Throughout the experiment, the suspensions were mixed on an orbital shaker. Samples were taken at specific intervals after the completion of the incremental uranium addition (i.e., at nominal $t = 0$) for determination of dissolved and total uranium; suspended solids were collected on the membrane filter used to process each dissolved sample, and the water remaining in the filter holder was removed by displacement with air. The membrane filters were then removed from the holders, mounted on glass slides, air-dried at room temperature, and analyzed by XRD.

Dissolved uranium and iron concentrations were determined by ICP-MS on either a Perkin-Elmer ELAN 5000 or a Hewlett-Packard 4500 instrument. Uranium isotope ratio measurement was performed with a Finnigan Element ICP-MS. XRD patterns were obtained with a Scintag Pad V instrument with a Cu Kα X-ray source and germanium detector.

Results and Discussion

Metastable Sorption. The metastable partitioning of uranium to the goethite surface displays a pattern corresponding to a Langmuir isotherm (Figure 1), in which sorbed uranium is plotted as a function of the total dissolved uranium concentration without distinguishing among dissolved species. At pH 6 and total uranium concentrations between 2 and 40 μM, $(UO_2)_3(OH)_5^+$ is the dominant dissolved species as calculated using critically evaluated stability constants (Table 1). The speciation of uranyl in solution should not however be taken as an indication of the stoichiometry of the surface complex(es). The data were fit to a Langmuir isotherm (eq 1) to obtain parameter values for the sorption constant K_L of 0.653 μM^{-1} and the maximum sorbed density Γ_{max} of 114.4 μmol g^{-1} or 2.71 μmol m^{-2} normalized to surface area:

$$\Gamma = \frac{\Gamma_{max} K_L C}{1 + K_L C} \quad (1)$$

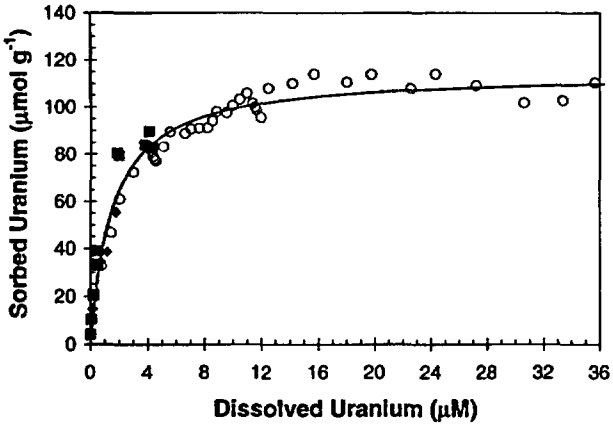

FIGURE 1. Metastable sorption of uranyl on goethite at pH 6 and $I = 0.1$ M. Symbols: data from (■) batch equilibration (0.1–0.5 g L^{-1} goethite), (◆) end points of kinetics experiments (0.010–0.035 g L^{-1} goethite), and (○) incremental loading experiments (0.10 g L^{-1} goethite); (–) Langmuir isotherm.

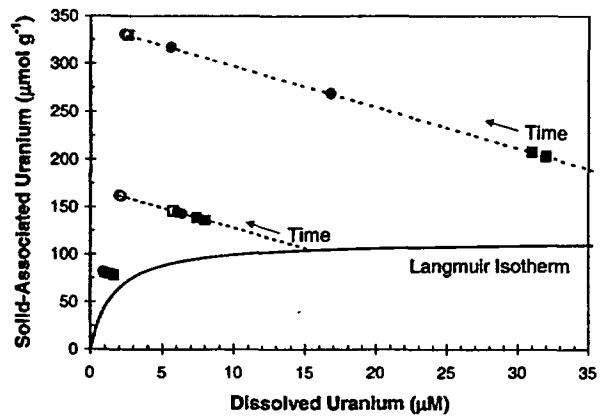

FIGURE 2. Time dependence of uranium partitioning between dissolved and solid-associated phases in a suspension of 0.23 g L^{-1} goethite at pH 6 and $I = 0.1$ M. Symbols: (■) 1, (●) 3, (□) 7, and (○) 32 and 96 d after completion of incremental uranium addition.

where C and Γ are the dissolved and sorbed uranium concentrations, respectively. Note that all of the data with dissolved concentrations greater than 5 μM are from the titration-mode sorption experiments. Under the admittedly simple assumption of monodentate sorption, the value of 2.71 μmol m^{-2} corresponds to 1.63 sorption sites nm^{-2}. This value is comparable to the estimate of 2.3 sites nm^{-2} suggested by Davis and Kent (*43*) as a uniform standard for oxide minerals.

Surface Precipitation. With increasing uranium concentration and sufficient equilibration time, the dissolved uranium concentration will ultimately be controlled by the solubility of a uranyl oxide hydrate precipitate. In a set of experiments specifically designed to be supersaturated with respect to a uranyl oxide hydrate, the formation of surface precipitates was monitored. For systems with 20–80 μM total uranium, the change in solid–solution partitioning over time is plotted together with the Langmuir isotherm in Figure 2. The dissolved concentration was observed to decrease over as long as 32 d; this corresponds to an increase in the solid-associated (i.e., sorbed and precipitated) concentration. After 96 d, the dissolved uranium concentration was 1.9–2.8 μM for experiments with total uranium concentrations 40 μM or greater, a strong indication that a solubility-controlling solid had formed. The experiment with 20 μM total uranium had a lower final dissolved concentration, suggesting that in this experiment the dissolved concentration was still controlled

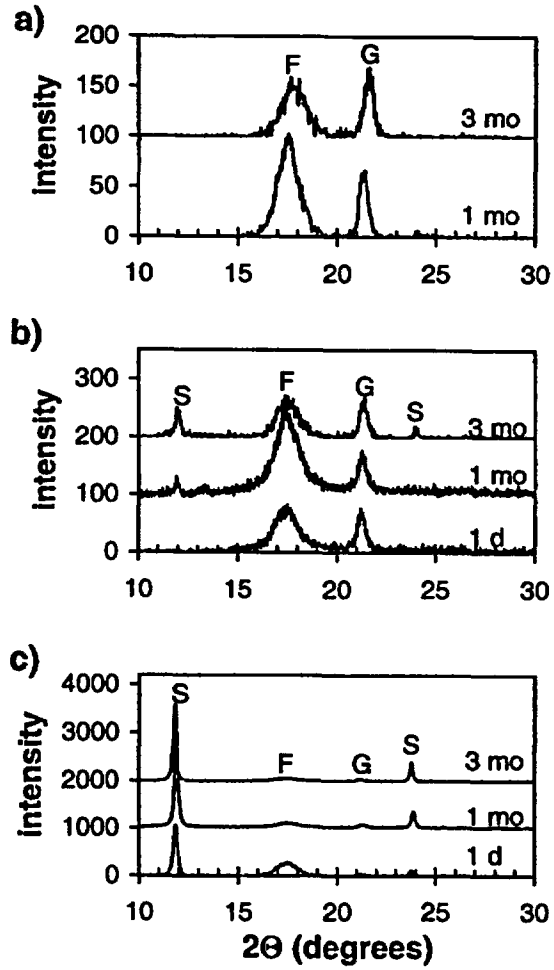

FIGURE 3. X-ray diffraction pattern of solids from a suspension of 0.22–0.23 g L^{-1} goethite with $[U]_T = 20$ (a), 40 (b), and 500 μM (c). $I = 0.1$ M, pH 6. Peaks are present for goethite (G), schoepite (S), and the polycarbonate filter membranes (F).

by sorption. Sorption partitioning experiments with dissolved concentrations above 2.8 μM are supersaturated with respect to the surface precipitate. Dissolved concentrations above this value in the Langmuir isotherm (Figure 1) represent metastable partitioning of uranium between the surface and the aqueous phase before the onset of precipitation. Supersaturated conditions may persist for considerable periods of time at low degrees of supersaturation; the data in Figure 1 correspond to contact times as long as 30 d.

Uranium-loaded goethite samples from the surface-precipitation experiments were analyzed by XRD to probe for crystalline uranyl-containing precipitates. The XRD pattern of the system with 20 μM total uranium (Figure 3a) contains only the peaks for goethite (21.5°) and the polycarbonate filter membrane (16–19°) even after 96 d. For the experiments with 40 and 80 μM total uranium, the XRD patterns of the solids have only goethite and filter peaks for the 1-d sample, but then peaks at 12° and 24° grow in for the 1- and 3-month samples (40 μM in Figure 3b). These peaks are characteristic of the uranyl oxide hydrate minerals schoepite $[(UO_2)_8O_8(OH)_{12}\cdot 12H_2O]$ or metaschoepite $[(UO_2)_8O_8(OH)_{12}\cdot 10H_2O]$, and a search of the International Centre for Diffraction Data database found no other phases consistent with both the reactor contents and the observed diffraction peaks (*44*). For the systems with 140 and 500 μM total uranium, the schoepite peaks are the dominant peaks after only 1 d and, over time, increase relative to the goethite peak (500 μM in Figure 3c). Calculations of the solubility

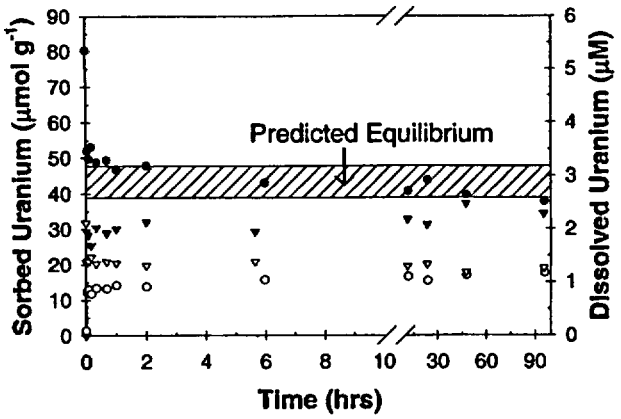

FIGURE 4. Dissolved (open) and sorbed (closed) uranium concentrations in complementary adsorption (triangles) and desorption (circles) experiments of uranyl on goethite for $[U]_T = 2\ \mu M$, 0.025 g L^{-1} goethite, pH 6, and $I = 0.1$ M. Predicted equilibrium range of the sorbed concentration calculated using the Langmuir isotherm with isotherm parameters at 95% confidence values.

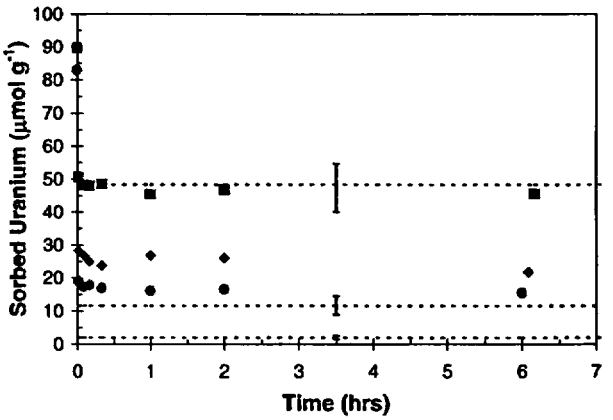

FIGURE 5. Kinetics of desorption following the addition of sodium fluoride to pre-equilibrated uranium–goethite suspensions at pH 6 and $I = 0.1$ M. The pre-equilibrated suspension contained $[U]_T =$ 12.5–13.1 μM, 0.10 g L^{-1} goethite, and $[U]_{sorbed} =$ 82.6–89.7 μmol g^{-1}. Data are shown for 0.62 (■), 1.85 (◆), and 4.05 mM (●) fluoride additions together with predicted sorbed concentrations (lines). Predicted concentrations calculated using the Langmuir isotherm and the assumption that only the uranyl ion and uranyl hydrolysis species can sorb; range based on the 95% confidence values of the isotherm parameters.

of uranium in equilibrium with schoepite are complicated by the significant variability in the published values of the solubility product and the stability constants for uranyl hydrolysis species (Table 1). At pH 6 and 0.1 M ionic strength, a reasonable range for the concentration of dissolved uranium in equilibrium with schoepite is 0.9 (*45*) to 7.5 μM (*46*), which is consistent with our measurements.

Sorption Kinetics. Complementary adsorption and desorption experiments with the same total uranium and goethite concentrations exhibit rapid kinetics in both directions (Figure 4). The reactions proceed to 75% completion within only 2–5 min and reach equilibrium on a time scale of hours. The convergence of the sorbed uranium concentration in adsorption and desorption experiments indicates reversibility, and the final sorbed concentration falls within the predicted range. The range was determined using the Langmuir isotherm with isotherm parameters at their 95% confidence values. Note that these and the following experiments were conducted at conditions undersaturated with respect to schoepite.

As with dilution-induced desorption, fluoride-induced desorption proceeds rapidly (Figure 5). The predicted equilibrium lines in Figure 5 were calculated by assuming that only the uranyl hydrolysis species adsorb to the goethite (*20*). Dissolved uranium speciation in the presence of fluoride was calculated using critically evaluated stability constants (*42*) (Table 1). During fluoride-induced desorption with 0.62 mM sodium fluoride, the experimental data match the predicted equilibrium remarkably well; however, for the higher fluoride additions, the measured extent of desorption is less than predicted. This discrepancy could be explained by a distribution in the binding strengths of sites on the goethite surface. In this case, the fraction of the sorbed uranium that was expected but not observed to desorb may be coordinated at strong sites that are energetically more favorable than fluoride for binding uranyl. The distinction of strong and weak sites on the goethite surface has been employed previously in surface complexation models of uranium on iron oxyhydroxides (*18, 26, 47*).

Results of a duplicate set of solution–surface isotope exchange experiments are displayed in Figure 6. The $^{238}U/^{235}U$ isotope ratio of the depleted uranium used for suspension pre-equilibration was 433.9 and that of the ^{235}U spike was 0.0117. The pH was unaffected by the spike addition, and the total and dissolved uranium concentrations also varied by less than 10% over the course of the experiment. Addition of the ^{235}U spike yielded an instantaneous $^{238}U/^{235}U$ ratio of

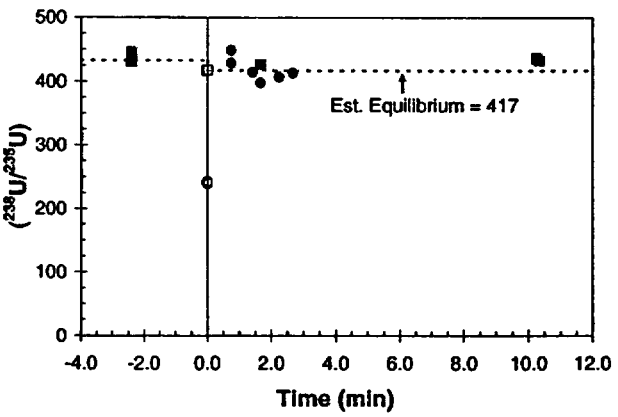

FIGURE 6. Isotope ratio of the total uranium (■, □) and dissolved uranium (●, ○) during isotope exchange between the dissolved and the sorbed phases. Closed symbols indicate measured values, and open symbols indicate calculated values. ^{235}U spike introduced at $t = 0$ to 0.33 g L^{-1} goethite suspension pre-equilibrated with depleted uranium at pH 6 and $I = 0.1$ M.

239–242 for dissolved uranium and 417 for total uranium. The isotope ratio for the dissolved phase increased from its initial value to match that of the total uranium within the 45 s between spike addition and collection of the first sample. As validated by analysis of goethite-free solutions, isotope ratios of 200–300 can be measured by the technique used but were not observed in this work because exchange occurred so rapidly.

In the present work, adsorption of uranium on goethite occurs in a single rapid step reaching completion within a few minutes. In a previous study, Hsi and Langmuir (*19*) noted biphasic adsorption kinetics with a rapid first step completed within minutes and a second step continuing for several days. Gabriel et al. (*18*) determined a first-order rate constant of 1.7 h^{-1} for the adsorption of uranium on goethite in column experiments with goethite-coated cristobalite sand. The rapid nature of the uranium release during desorption experiments suggests that desorption is being controlled by the rate of chemical detachment from the surface and not by diffusion from the interior of the solids. It is not surprising that the desorption is free of the effects of diffusion, because

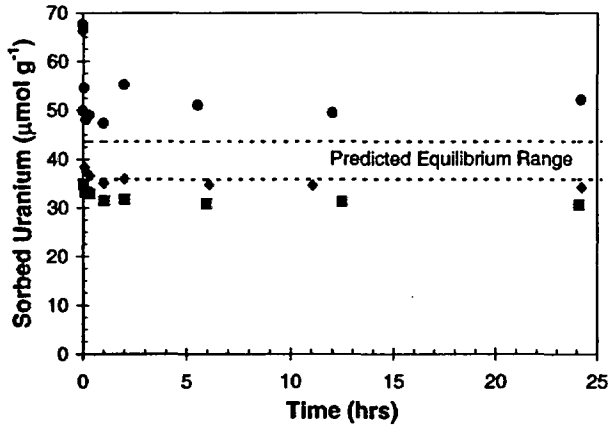

FIGURE 7. Effects of aging time on desorption following a 1:100 dilution of a pre-equilibrated suspension. The pre-equilibrated suspension contained $[U]_T = 200\ \mu M$, 2.94 g L^{-1} goethite, and $[U]_{sorbed} = 66.2-67.7\ \mu mol\ g^{-1}$ at pH 6 and $I = 0.1$ M. Suspension aged for (■) 1 d, (◆) 1 month, and (●) 6.5 months.

a synthetic goethite prepared under controlled laboratory conditions should have minimal microporosity.

Effect of Suspension Aging on Desorption. A single uranium–goethite suspension was prepared with sorbent and uranium concentrations that correspond to sorption and not to surface precipitation. Aliquots of this suspension were used to initiate dilution-induced desorption experiments after 1 d, 1 month, and 6.5 month of aging. For all three aging times, constant sorbed uranium concentrations were established within 1 h of the initiation of desorption (Figure 7). Experiments initiated after 1 d and 1 month of contact both have final sorbed concentrations that agree with the predicted equilibrium value of 38.3 $\mu mol\ g^{-1}$. Desorption initiated after 6.5 months is as rapid as for the earlier times, but the final sorbed uranium concentration is substantially higher than in the other cases and persists to the end of the experiment at nearly 1500 h (data not shown). During sequential extraction of the solids remaining at the end of the 6.5-month experiment, nearly all (90%) of the uranium was extracted with acetic acid and coincided with a substantial release of iron (~25% of the total). The complete digestion of the remaining material contained the majority of the iron but almost no uranium. These results suggest that, during the aging process, a portion of the readily exchangeable uranium may have diffused into the solid or been occluded within an amorphous iron oxide phase that coats the goethite particles. Ohnuki et al. (*25*) found that, during the crystallization process, a portion of the uranium sorbed to amorphous ferric hydroxide was fixed to the crystalline minerals and was not easily removed.

Environmental Implications. The desorption reactions measured in this work occur on time scales much shorter than those of environmental processes such as the flow of groundwater. Rapid partitioning of uranium between solution and surfaces and rapid release of sorbed uranium in response to changing solution conditions are expected. Diffusion in the solid phase may still kinetically limit rates of uptake and release in environmental settings. In an environmental setting, the long residence of uranium in contact with iron oxyhydroxide minerals may lead to partial sequestration of uranium in the structure of surface coatings and micropores.

As long as dissolved uranium concentrations are low, sorption will dominate uranium mobility, but elevated dissolved concentrations will initiate surface precipitation and may actually decrease the dissolved concentration. Elevated concentrations may be found in highly contaminated systems and also during the evaporative concentration of uranium in the pore water of unsaturated soils. The heterogeneous nucleation of a uranyl precipitate may be kinetically limited, and metastable sorption may control the dissolved concentration even when the dissolved concentration exceeds the solubility limit. The mobility of uranium in response to changes in solution conditions may be affected by the distribution of solid-associated uranium between adsorbed and precipitated phases.

Acknowledgments

Lee Silver generously provided the ^{235}U spike. Ken Farley provided time and assistance in the operation of his laboratory's Finnigan Element ICP-MS. Funding was provided to D.G. through a National Science Foundation Graduate Fellowship.

Literature Cited

(1) *Linking Legacies: Connecting Cold War Nuclear Weapons Processes to Their Environmental Consequences*; U.S. Department of Energy, Office of Environmental Management: Washington, DC, 1997.
(2) Riley, R. G.; Zachara, J. M. *Chemical Contaminants on DOE Lands and Selection of Contaminant Mixtures for Subsurface Science Research*; DOE/ER-0547T; U.S. Department of Energy, Office of Energy Research: Washington, DC, 1992.
(3) National Primary Drinking Water Regulations; Radionuclides; Final Rule. *Fed. Regist.* **2000**, *65*, 76707–76753.
(4) Elless, M. P.; Lee, S. Y. *Water, Air, Soil Pollut.* **1998**, *107*, 147–162.
(5) Sidle, W. C.; Lee, P. Y. *Ground Water* **1996**, *5*, 876–882.
(6) Kaplan, D. I.; Bertsch, P. M.; Adriano, D. C.; Orlandini, K. A. *Radiochim. Acta* **1994**, *66/67*, 181–187.
(7) Kaplan, D. I.; Hunter, D. B.; Bertsch, P. M.; Bajt, S.; Adriano, D. C. *Environ. Sci. Technol.* **1994**, *28*, 1186–1189.
(8) Batson, V. L.; Bertsch, P. M.; Herbert, B. E. *J. Environ. Qual.* **1996**, *25*, 1129–1137.
(9) Barnett, M. O.; Jardine, P. M.; Brooks, S. C.; Selim, H. M. *Soil Sci. Soc. Am. J.* **2000**, *64*, 908–917.
(10) Hunter, D. B.; Bertsch, P. M. *J. Radioanal. Nucl. Chem.* **1998**, *234*, 237–242.
(11) Clark, S. B.; Johnson, W. H.; Malek, M. A.; Serkiz, S. M.; Hinton, T. G. *Radiochim. Acta* **1996**, *74*, 173–179.
(12) Bertsch, P. M.; Hunter, D. B.; Sutton, S. R.; Bajt, S.; Rivers, M. L. *Environ. Sci. Technol.* **1994**, *28*, 980–984.
(13) Fenton, B. R.; Waite, T. D. *Radiochim. Acta* **1996**, *74*, 251–256.
(14) Yanase, N.; Nightingale, T.; Payne, T.; Duerden, P. *Radiochim. Acta* **1991**, *52/53*, 387–393.
(15) Jung, J.; Hyun, S. P.; Lee, J. K.; Cho, Y. H.; Hahn, P. S. *J. Radioanal. Nucl. Chem.* **1999**, *242*, 405–412.
(16) Payne, T. E.; Waite, T. D. *Radiochim. Acta* **1991**, *52/53*, 487–493.
(17) Duff, M. C.; Amrhein, C. *Soil Sci. Soc. Am. J.* **1996**, *60*, 1393–1400.
(18) Gabriel, U.; Gaudet, J.-P.; Spadini, L.; Charlet, L. *Chem. Geol.* **1998**, *151*, 107–128.
(19) Hsi, C.-K. D.; Langmuir, D. *Geochim. Cosmochim. Acta* **1985**, *49*, 1931–1941.
(20) Tripathi, V. S. Ph.D. Dissertation, Stanford University, 1984.
(21) Bargar, J. R.; Reitmeyer, R.; Lenhart, J. J.; Davis, J. A. *Geochim. Cosmochim. Acta* **2000**, *64*, 2737–2749.
(22) Ho, C. H.; Miller, N. H. *J. Colloid Interface Sci.* **1986**, *110*, 165–170.
(23) Liger, E.; Charlet, L.; Van Cappellen, P. *Geochim. Cosmochim. Acta* **1999**, *63*, 2939–2955.
(24) Morrison, S. J.; Spangler, R. R.; Tripathi, V. S. *J. Contam. Hydrol.* **1995**, *17*, 333–346.
(25) Ohnuki, T.; Isobe, H.; Yanase, N.; Nagano, T.; Sakamoto, Y.; Sekine, K. *J. Nucl. Sci. Technol.* **1997**, *34*, 1153–1158.
(26) Waite, T. D.; Davis, J. A.; Payne, T. E.; Waychunas, G. A.; Xu, N. *Geochim. Cosmochim. Acta* **1994**, *58*, 5465–5478.
(27) Bargar, J. R.; Reitmeyer, R.; Davis, J. A. *Environ. Sci. Technol.* **1999**, *33*, 2481–2484.
(28) Braithwaite, A.; Richardson, S.; Moyes, L. N.; Livens, F. R.; Bunker, D. J.; Hughes, C. R.; Smith, J. T.; Hilton, J. *Czech. J. Phys.* **2000**, *50*, 265–269.
(29) Braithwaite, A.; Livens, F. R.; Richardson, S.; Howe, M. T.; Goulding, K. W. T. *Eur. J. Soil Sci.* **1997**, *48*, 661–673.
(30) Mason, C. F. V.; Turney, W. R. J. R.; Thomson, B. M.; Lu, N.; Longmire, P. A.; Chisholm-Brause, C. J. *Environ. Sci. Technol.* **1997**, *31*, 2707–2711.

(31) Barrow, N. J.; Gerth, J.; Brümmer, G. W. *J. Soil Sci.* **1989**, *40*, 437−450.
(32) Brümmer, G. W.; Gerth, J.; Tiller, K. G. *J. Soil Sci.* **1988**, *39*, 23−28.
(33) Trivedi, P.; Axe, L. *Environ. Sci. Technol.* **2000**, *34*, 2215−2223.
(34) Sparks, D. L. In *Soil Physical Chemistry*; Sparks, D. L., Ed.; CRC Press: New York, 1999; Chapter 4.
(35) Bruno, J.; de Pablo, J.; Duro, L.; Figuerola, E. *Geochim. Cosmochim. Acta* **1995**, *59*, 4113−4123.
(36) Murakami, T.; Ohnuki, T.; Isobe, H.; Sato, T. *Am. Mineral.* **1997**, *82*, 888−8999.
(37) Sato, T.; Murakami, T.; Yanase, N.; Isobe, H.; Payne, T. E.; Airey, P. L. *Environ. Sci. Technol.* **1997**, *31*, 2854−2858.
(38) Chisholm-Brause, C. J.; Berg, J. M.; Matzner, R. A.; Morris, D. E. *J. Colloid Interface Sci.* **2001**, *233*, 38−49.
(39) Schwertmann, U.; Cornell, R. M. *Iron Oxides in the Laboratory*; VCH: New York, 1991.
(40) Good, N. E.; Winget, G. D.; Winter, W.; Connolly, T. N.; Izawa, S.; Singh, R. M. M. *Biochemistry* **1966**, *5*, 467−477.
(41) Soares, H. M. V. M.; Conde, P. C. F. L.; Almeida, A. A. N.; Vasconcelos, M. T. S. D. *Anal. Chim. Acta* **1999**, *394*, 325−335.
(42) Grenthe, I.; Fuger, J.; Konings, R. J. M.; Lemire, R. J.; Mueller, A. B.; Nguyen-Trung, C.; Wanner, H. *Chemical Thermodynamics of Uranium*; Elsevier: Amsterdam, 1992.
(43) Davis, J. A.; Kent, D. B. In *Mineral−Water Interface Geochemistry*; Hochella, M. F., White, A. F., Eds.; Mineralogical Society of America: Washington, DC, 1990; Chapter 5.
(44) ICDD. *Powder Diffraction File*; International Centre for Diffraction Data: Newtown Square, PA, 1999.
(45) Díaz Arocas, P.; Grambow, B. *Geochim. Cosmochim. Acta* **1998**, *62*, 245−263.
(46) Silva, R. J. *Mater. Res. Soc. Symp. Proc.* **1992**, *257*, 323−330.
(47) Lenhart, J. J.; Honeyman, B. D. *Geochim. Cosmochim. Acta* **1999**, *63*, 2891−2901.

Received for review December 20, 2000. Revised manuscript received May 30, 2001. Accepted May 30, 2001.

ES0019981

Tailings and Mine Waste '02, © 2002 Swets & Zeitlinger, ISBN 90 5809 353 0

In situ treatment of metals in mine workings and materials

J.M. Harrington

ABSTRACT: Contact of oxygen contained in air and water with mining materials can increase the solubility of metals. In heaps leached by cyanide, metals can also be made soluble through complexation with cyanide. During closure, water in heaps, and water collected in mine workings and pit lakes may require treatment to remove these metals. In situ microbiological treatment to create reductive conditions and to precipitate metals as sulfides or elemental metal has been applied at several sites with good success. Treatment by adding organic carbon to stimulate in situ microbial reduction has been successful in removing arsenic, cadmium, chromium, copper, iron, lead, manganese, mercury, nickel, selenium, silver, tin, uranium, and zinc to a solid phase. Closure practices can affect the success of in situ treatment at mining sites, and affect the stability of treated materials. This paper defines factors that determine the cost and permanence of in situ treatment.

1 INTRODUCTION

1.1 *Problem description*

Most mining operations remove materials from the ground that were, prior to being mined, in a chemically reduced state. The processing operation in many cases directly oxidizes the materials (such as in gold and copper leaching); in other cases, the materials are contained in waste piles in a manner that allow oxidation reactions to occur over time. In an oxidized state, many metals are soluble in water that travels through these materials, and these metals will as a consequence be present in seeps from the materials. The oxidation of elements in mined materials and the movement of water through these materials is the cause of acid rock drainage (ARD) and can also be the cause of the release of such elements as arsenic, chromium, selenium, and uranium in neutral pH drainage. The closure of mining operations may require the chemical stabilization of these mined materials to prevent these materials from being a source of environmental contamination. Returning the mined materials to the reduced state that they were in prior to mining makes sense as the method that will leave these materials in a form most chemically similar to the form they were prior to being mined.

1.2 *Green World Science® process*

The Green World Science® (GWS) process is defined by the addition of a reductant into metal-containing materials to prevent metals and other constituents from becoming mobile, and to remove from solution constituents that are already soluble. The reductant may chemically react with the mine materials to remove oxygen and reduce oxidized materials, or the reduced compounds may be added that are microbially oxidized, and the mine materials reduced, by microbial enzymes. (GWS currently owns several patents on this process including US 6,196,765, US 5,710,361, and US 5,362,715 and others allowed and pending.) Organic carbon is the typical reductant utilized in this process; however, the addition of reduced gases into vadose materials is also proposed.

This paper presents data from six applications of the GWS process. The applications include two gold heap leach facilities (Yankee Mine and Coeur Rochester Mine), mine workings in an adit (Mike Horse Mine), a backfilled pit (Beal Mountain Mine), a pit lake (Sweetwater Uranium Mine), and groundwater beneath a test gypsum impoundment (J.R. Simplot phosphate plant). Except for the tailings impoundment, all data presented are for full-scale in situ treatment. There have been more than 20 other applications of the GWS process.

2 IN-PAD HEAP LEACH TREATMENT

2.1 *Yankee mine*

The Yankee mine is a gold heap leach operation. The heap contains approximately 7 million tons of leached ore on one pad. At the close of leaching, GWS added over 185 tons of organic carbon and other nutrients into the barren pond during solution recycle and evaporation. The primary constituents

that required treatment were WAD cyanide, nitrate, aluminum, copper, mercury, silver, selenium, and zinc. Figure 1 shows results from a meteoric water mobility procedure (MWMP) test performed on leached materials prior to treatment, and compares these with results from MWMP on samples removed after treatment. (The MWMP procedure mixes an equal weight of synthetic rainwater with the mine materials for 24 hours; afterwards the water is extracted and the constituent concentrations in the water are reported.) The results of the MWMP prior to treatment are an average of five samples, and post-treatment results are an average from six samples.

The concentrations of constituents of concern in MWMP extracted solution all decreased in the treated samples. The concentration of WAD cyanide and cyanide-complexed metals Cu, Hg, Ni, and Zn all decreased by several orders of magnitude. Section 2.3 discusses the mechanisms that account for these changes.

2.2 *Coeur Rochester mine*

Coeur Rochester mine is located in Nevada and has several heaps on separate pads each with contained solutions ponds. The heap leach operations primarily recover silver and some gold. GWS added 2,100 tons of organic carbon and other nutrients through trenches located on the Stage 1 pad; no prior rinsing of this pad had occurred. The constituents being treated included pH, nitrate, sulfate, and WAD cyanide, arsenic, copper, mercury, nickel, and zinc. Figure 2 compares the MWMP results from untreated and treated areas of the pad. The treated areas were tested after 1 year of treatment; however, the results shown are partial treatment results, as the process will require close to two years to complete.

2.3 *In situ treatment processes in gold and silver heap leach facilities*

The processes that account for the decrease of soluble constituents in heap leach pads are described below:
1) Off-gassing of dissolved constituents: In the treatment process, the added organic carbon is converted to carbon dioxide, which partitions between the gas phase and the interstitial water depending on the interstitial solution pH. Nitrate is converted to nitrogen gas; an organic carbon-dependent process termed denitrification (Narkis *et al*, 1979).
2) Degradation of weak acid dissociable (WAD) cyanide complexes: Two primary mechanisms account for the microbial removal of cyanide. Detoxification—Cyanide is an inhibitor of metabolic processes, and to prevent this inhibition, cells have specific enzymes capable of converting cyanide to less toxic forms, including cyanate and ammonia. Example enzymes are *cyanidase* and *cyanide hydratase* (Raybuck, 1992). Nitrogen Assimilation—Cyanide is also a good nitrogen source for cellular growth, and for this reason is incorporated into biomass during the growth phase of microorganisms (Raef *et al*, 1977). The removal of free cyanide from solution and the degradation of cyanide complexes with relatively low dissociation constants (which includes most of the WAD cyanide forms) occur because of these two cellular processes.

The removal of copper, mercury, nickel, silver, and zinc from solution is caused by the degradation of cyanide, and the consequent removal of this complexing agent that had maintained these metals in solution. In many instances, the degradation of cyanide is not itself sufficient to meet water quality standards for heap leach or tailings drainage, to allow discharge off containment, and further metal removal

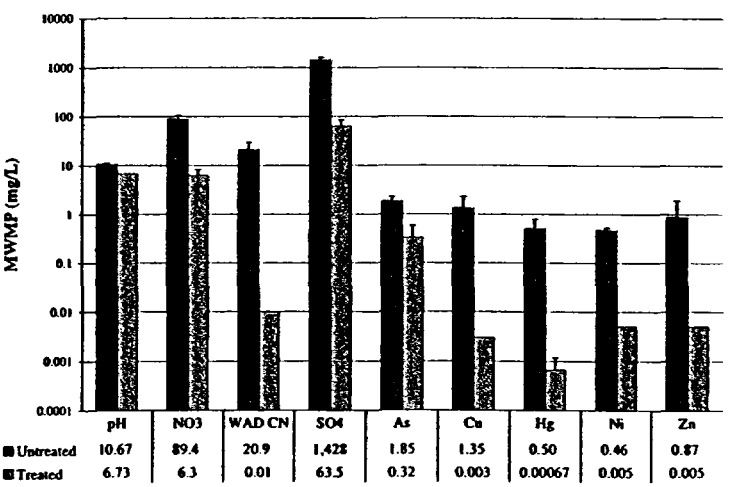

Figure 1. Yankee heap leach prior to and after treatment MWMP comparison.

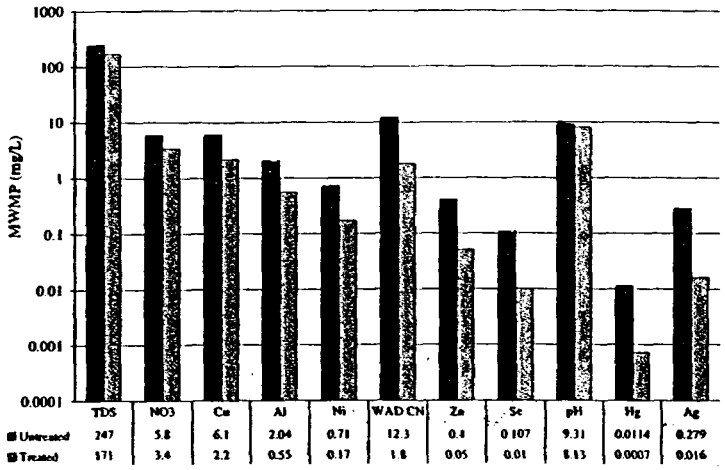

Figure 2. Coeur Rochester Pad 1 treated and untreated MWMP comparison.

by other processes may be required. This can be performed by in situ microbial treatment such as sulfate and metal reduction (see items 3 and 4 below). In other instances, the high pH of the interstitial solutions, created by lime addition prior to leaching, will be sufficient to remove the metals by precipitation in the form of metal hydroxides.

3) Metal Reduction: Several metals are less soluble in their reduced forms. Examples of this are selenium, which is quite insoluble in its elemental form Se^0 and soluble in its oxidized selenate (Se VI) form; chromium, which is quite insoluble as $Cr(OH)_3$ (Cr III) and soluble in the oxidized Cr (VI) form; and uranium, which is quite insoluble in its UO_2 (U (IV)) form and soluble in its oxidized U (VI) form. Cellular metabolic processes oxidize the added organic carbon and enzymatically reduce these metals (Oremland *et al*, 1999). These metals may also be indirectly reduced by contact with other reduced ions that were created by microbial reduction such as ferrous iron and sulfide (Wielinga *et al*, 2001).

4) Sulfate Reduction: The oxidation of organic carbon and the reduction of sulfate is a coupled metabolic process that is performed by microorganisms. Sulfide is a strong reductant, and reacts with both soluble metal and metals in minerals. In some instances, this reaction leads to the formation of insoluble metal sulfide precipitates (including sulfides of As, Cd, Cu, Fe, Hg, Ni, and Zn). In other instances, the presence of sulfide can lead to a temporary increase in metal concentrations (such as the release of iron and manganese into solution from the reductive dissolution of oxide minerals). The amount of metal release can be controlled by managing such parameters as the application rate of organic carbon, providing sufficient time for reactions to come to completion, and by controlling the pH of the treatment solutions. Sulfide is also an efficient reductant of oxidized chromium, selenium, and uranium; the reaction of sulfide with these elements can lead to their immobilization in a sulfide phase.

5) Adjustment of the pH: The microbial oxidation of organic carbon leads to changes in the solution pH by creating carbon dioxide and bicarbonate. In low pH solutions, the pH increases as a result of acidity consumption during iron and sulfate reduction and the formation of bicarbonate (see reactions listed in Table 1). In high-pH solutions, the creation of carbon dioxide leads to the consumption of hydroxide, which results in lower interstitial solution pH. The change of solution pH affects several metals and metalloids whose solubility is pH sensitive. For example, in oxidized conditions, iron, when present, is principally responsible for removing arsenic from solution, and iron-arsenic compounds are least soluble around pH 7.5. In reduced conditions, sulfide can form arsenic sulfides, and arsenic sulfides are least soluble below pH 7. In high pH solutions, soluble arsenic sulfides (AsS^-) can form and may not precipitate; however, if iron is present in high concentrations arsenopyrite may form even in solutions with pH >7. Thus, if arsenic removal is desired in low pH solutions, the formation of arsenic sulfides should be attempted, and if removal is desired in high pH conditions, formation of iron arsenate compounds should be attempted.

2.4 *Factors that affect the application of in situ treatment in heap closure*

Regulatory Framework: Regulations that control heap closure call for geochemical stabilization of heap materials so that a closed heap does not cause

degradation of waters of the State (*e.g.* Nevada Administrative Code 445A). Some US states classify mine wastes based on extraction tests of the heap materials, allowing far less stringent cover to be placed or unregulated solution discharge for heaps that pass extraction tests. In situ treatment should be considered in cases where heap water quality contains constituents of concern that are amenable to in-heap treatment. In cases where the salt concentration is high, discharge of even treated heap solutions may not be feasible because of TDS restrictions. However, removal of certain constituents within the heap may allow for alternative discharge approaches, such as non-discharging wetlands or infiltration systems, where untreated heap solutions may cause ecological toxicity in the wetland or certain constituents may not otherwise be attenuated.

Timing of Treatment: Microbial treatment of a heap leach facility may begin as soon as cyanide addition ceases. It may be advantageous to utilize the rinse period to enhance treatment coverage, as well as to use this period to achieve water quality goals that will reduce the time required to achieve closure after metal recovery has ceased. While in some situations silver recovery may decrease because silver-cyanide complexes can be degraded by microbial enzymes, gold recovery should not decrease because microorganisms cannot degrade gold-cyanide complexes. Some in situ treatment situations have shown an increase of gold content in the doré because other metal-cyanide complexes have been removed from solution, and hence do not compete with gold sorption to carbon.

The evaporative concentration of salts during leaching is a function of the climate, the solution application method, and the length of time that solutions are recycled. Closure of many heaps now involves the reduction of solution inventories by recycling barren solution over the pad until water concentrations are decreased or the cyanide concentrations decrease by natural oxidation or by solar reactions. The decision to evaporatively concentrate heap solutions in many instances dictates the closure plan, and should not be done without considering the implications to the revegetation of the heaps and the long-term cost of heap water disposal. In situ treatment during the final stage of leaching, *i.e.*, the rinsing residual gold-cyanide complexes, may remove the cyanide and metals so that discharge is possible, or at least there will be a wider range of heap drainage disposal options. As an alternative to evaporation that creates a salty discharge, in situ treatment will leave a relatively fresh water solution suitable for watering vegetation or infiltration.

Factors affecting cost and specificity of treatment: There is a predictable order in which microorganisms will transform constituents present in a heap after organic carbon is added. Table 1 summarizes many of the relevant reactions that may occur in a heap leach pad. These microbial reactions occur in natural systems in a predictable order based on the energy (ΔG) of the reaction (Zehnder and Stumm, 1988). Briefly, the ΔG of these redox reactions is a function of the relative strength of the oxidant (*e.g.* oxygen is a stronger oxidant than is sulfate), and the relative concentration of the oxidants and reductants (Pauling, 1988). For instance, a solution with 1 mg/L nitrate and 100 mg/L selenate may favor selenium reducing organisms over nitrate-reducing organisms even though the ΔG of nitrate reduction is greater than the ΔG of selenium reduction.

These reactions show why, in heap leach closure, much of the oxygen that is present in the heap interstices must be consumed prior to significant amounts of denitrification or sulfate reduction. Thus in a heap in which selenium is the target constituent, the cost of treatment will be a factor of the amount of organic carbon required to 1) reduce all of the oxygen initially present in the heap, 2) reduce the oxygen that will diffuse into the heap during treatment, 3) denitrify the nitrate, and 4) reduce the selenium. The cost of the organic carbon to reduce the selenium alone may be less than 1% of the total organic carbon requirement. Table 1 shows the constituents that must be evaluated to determine the total amount of reductant that must be added to treat water in situ.

For in situ sulfate reductive treatment, the amount of sulfate reduction required to remove a particular metal is a function of the reactivity of sulfide with the metals. For example, in a treatment performed in an adit, nearly complete removal of arsenic (50 mg/L to less than 1 mg/L) and zinc (20 mg/L to less than 1 mg/L) was achieved without affecting the iron in solution (600 mg/L). This occurred because zinc and arsenic sulfides, in the particular pH environment of that adit, were less soluble than iron sulfides. In our experience a typical order of metal sulfide removal has been Pb> Zn> Cu> As> Cd> Fe> Mn. This order may change based on factors such as solution pH or the presence of other complexing agents such as some organics (humics + fulvics) that may also affect the precipitation of metals (Lehman and Mills, 1994).

Table 1. Redox reactions catalyzed by microorganisms.

Oxygen Consumption:	
$O_2 + (CH_2O) \rightarrow CO_2 + H_2O$	(1)
Denitrification:	
$4NO_3^- + 5(CH_2O) + 4\,H^+ \rightarrow 2\,N_2 + 5\,CO_2 + 7\,H_2O$	(2)
Iron Reduction:	
$4\,FeOOH + (CH_2O) + 7H^+ \rightarrow 4\,Fe^{2+} + HCO_3^- + 6\,H_2O$	(3)
Selenium Reduction:	
$2\,HSeO_3^- + 2(CH_2O) + 2H^+ \rightarrow 2\,Se^0 + 2\,CO_2 + 4\,H_2O$	(4)
Uranium Reduction:	
$2(CH_2O) + 2UO_2(CO_3)_2^{2-} + 2H_2O \rightarrow 2UO_2 + 5HCO_3^- + H^+$	(5)
Sulfate Reduction:	
$SO_4^{2-} + 2\,(CH_2O) + H^+ \rightarrow HS^- + 2\,CO_2 + H_2O$	(6)

Note: (CH_2O) is the empirical formula for carbohydrates, e.g. glucose is $C_6H_{12}O_6$.

3 BACKFILLED PIT IN SITU TREATMENT

3.1 *Beal Mountain mine*

Beal Mountain mine is a closed gold mine located in Montana. As part of the closure, the mine pit was backfilled with "clean" rock, and seepage that was expected to fill the pit was routed through the pit and into German Gulch located downgradient of the pit. As the pit was filled with rock, seepage from the pit wall and spring precipitation created a pond in the middle of the pit. The pit pond contained nitrate at concentrations (8.1 mg/L) higher than would be allowed to discharge into the gulch (1.0 mg/L). GWS added approximately 20,000 lbs. of nutrients into the pit pond that was located at the center of the pit. As the water elevation rose in the pit, the nitrate concentration in the pond was monitored until the pit was completely filled. Figure 3 shows nitrate concentrations until the pit pond began to drain out of the pit.

After the pit backfilling was completed, two wells installed in the pit backfill were monitored for a suite of parameters. Nitrate concentrations in the pit wells initially were approximately 2 mg/L and have continued to decrease to less than 1 mg/L, and in one well, to concentrations below detection. In addition to the reduction of nitrate, selenium reduction occurred. The two wells initially contained 42 and 47 ppb selenium. As shown in Figure 4, after two years the concentration of selenium has decreased to between 2.0 and 3.0 ppb. In the same time frame, no decrease has been observed for sulfate and other TDS constituents, making an explanation of washout or dilution improbable.

3.2 *In-pit treatment processes*

The treatment of the Beal Mountain backfilled pit illustrates several factors that affect the success of in situ treatment in mine waste. Wells installed on either side of where the pond was located showed the effect from the biological treatment, even though carbon was added only to the pond at the center of the pit. The organic carbon was effectively distributed into the backfill because the carbon was added while the pit was still filling, allowing the carbon to be distributed with the rising water. In general, addition of the reductant to mine wastes as they are placed enhances the distribution and coverage of the treatment process.

Organic carbon was added at a rate sufficient to reduce only the nitrate calculated to be in all of the water in the pit. This rate was calculated to include dissolved oxygen that, it was assumed, was saturated in all of the pit waters. Selenium was reduced because this assumption caused a slight over-treatment of the pit. No measurable sulfate reduction occurred in the pit because the amount of the over-treatment was sufficient only to treat the selenium, but oxidants below selenium, such as sulfate, were not reduced because the carbon had been used up.

At the Beal Mountain backfilled pit, the addition of organic carbon alone was sufficient to remove all of the oxygen present in the pit waters, to denitrify all of the nitrate present in the pit waters, and then to additionally react with selenium. If additional organic carbon had been added, sulfate reduction would have also occurred. In another backfilled pit, organic carbon has been injected at concentrations sufficient to remove more than 99 percent of the sul-

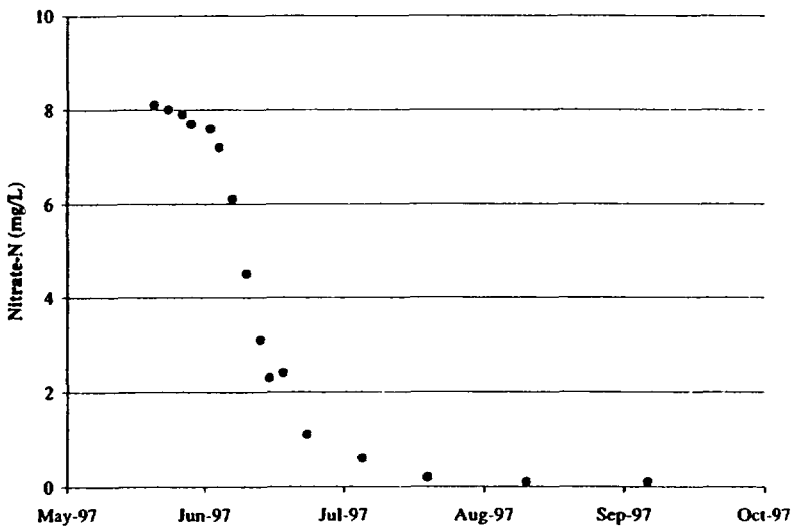

Figure 3. Beal Mountain pit pond nitrate in situ treatment.

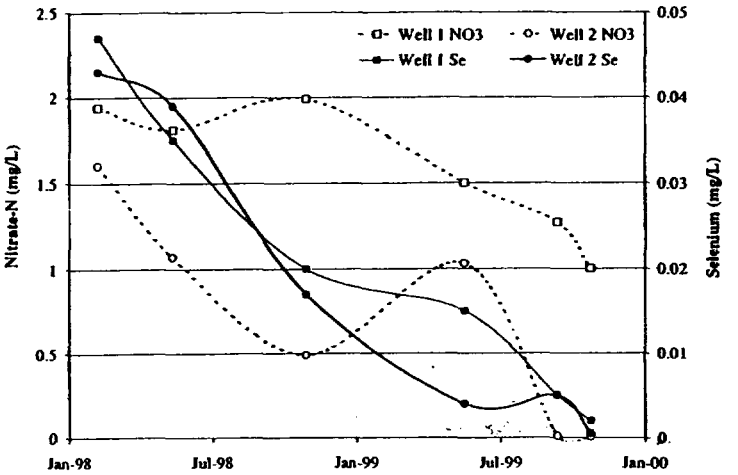

Figure 4. Beal Mountain nitrate and selenium in backfill wells after treatment.

fate, from 1,500 mg/L to less than 1.0 mg/L. In none of these cases was it necessary to inject anything other than organic carbon; rather, injection of organic carbon alone stimulated the organisms naturally present to perform the reaction that was most energetically favorable in that environment. Section 7.2 discusses the abundance and distribution of microbial species that participate in these reactions.

4 PIT LAKE TREATMENT

4.1 *Sweetwater Uranium mine*

Sweetwater Uranium mine is located in Wyoming. Uranium ore and overburden rock had been removed from pits that were dewatered during mining. Approximately 5 million tons of overburden rock was placed back in the pit on one side of the pit. After mining ceased in 1983, the pits were allowed to backfill, and the resultant lake was 125 feet at is deepest, and averaged 65 feet in depth over 60 acres (total volume in the lake was approximately 1.25 billion gallons). After the water level had reached static conditions (with evaporation being the only outflow from the pit) uranium (8.4 mg/L) and selenium (0.45 mg/L) were the only constituents that were present above the site closure standards (5 mg/L and 0.05 mg/L, respectively). GWS added 1.1 million pounds of organic carbon and other nutrients to the pit beginning on October 19, 1999. Figure 5 shows the results of the treatment. In six weeks, the selenium had been precipitated such that the dissolved selenium concentration was less than 0.05 mg/L. In 14 weeks, the uranium had been precipitated such that the dissolved uranium concentration was less than 5.0 mg/L. The lake has now remained below standards for both of these elements for two years.

4.2 *Pit lake treatment processes and issues*

The reactions stimulated in the pit are the same as those stimulated in the heap leach pads and in the backfilled pit. Selenium reduction occurred prior to uranium, consistent with the thermodynamically predicted order described in Section 2.3. There was 1.1 mg/L nitrate in the pit that was removed in the first two weeks of the treatment, also consistent with the energetics of denitrification as compared with selenium reduction.

As with all in situ treatment processes, managing oxygen in the treatment was the highest cost item. More than 80% of the added carbon was consumed in the reduction of oxygen that was present in the pit at the beginning of the treatment, and the oxygen that continued to diffuse into the pit during treatment. For this reason, we chose to perform the treatment of the lake over the wintertime, to take advantage of an ice layer would form over the pit and minimize the mixing and diffusion of oxygen into the lake. While timing the treatment to occur in the winter may have slightly slowed the microbial reaction rate, the organic carbon demand was significantly reduced and strongly reducing conditions were more easily achieved under the ice layer.

A common fallacy believed about microbial treatment is that microorganisms cannot function in cold water at high rates. The water temperature in the Sweetwater pit at the beginning of the treatment was 9°C, and all of the uranium precipitation occurred when the bulk of the pit was approximately 3°C. We have treated other sites when the water temperature was 0.5°C. Microorganisms that are specifically adapted to function in cold temperatures (psychrophilic or psychrotrophic organisms) can function at metabolic rates at near freezing temperatures at least half as fast as as other microbes

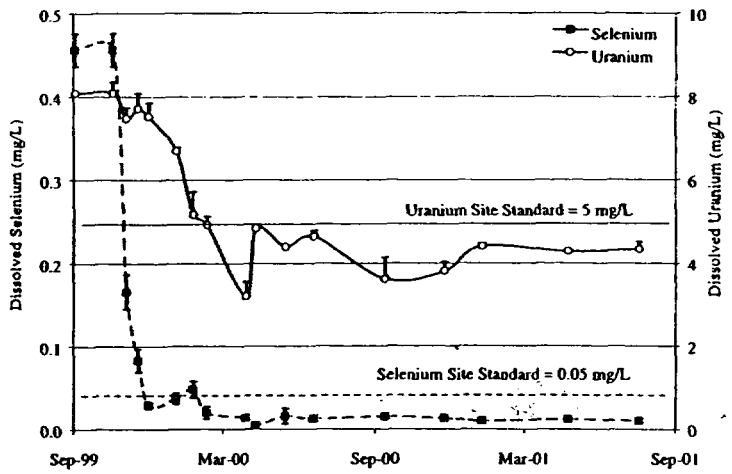

Figure 5. Sweetwater pit lake dissolved selenium and uranium after in situ treatment.

function at 10°C (Knoblauch *et al*, 1999). Psychrophilic cells have a lipid bylayer that allows transport across the cell membrane at cold temperatures, and enzymes with a specific structure to remain flexible in near-freezing water. Our experience is that cold environments do not lack microbes capable of performing the desired metabolic functions at sufficient rates, but rather that the reactants (specifically organic carbon or other reductants) are not present in the cold environments, and must be supplied to allow microbes to be active. The treatment at Sweetwater shows that effective in situ treatment can be achieved in the wintertime. It also illustrates one of the benefits of using organisms that are already present in that system. The fact that the bottom of the lake is 4°C all year means that the lake had 15 years of selection for psychrotrophic organisms that had been exposed to selenium and uranium.

5 UNDERGROUND MINE WORKINGS

5.1 *Mike Horse mine*

The Mike Horse mine is located in Montana. Mike Horse mine is part of a complex of mine workings that together are called the Upper Blackfoot Mining Complex (Anderson and Hansen, 1999). The main Mike Horse adit was plugged and water allowed to pool in the workings in 1996. The average residence time in the pit is 3 months. The fluctuation of the water level in the adit behind the bulkhead on an annual basis is tied to the spring snowmelt. With each rise in water level, additional metals are released, making the flow and loading from the mine workings greatest in the spring and early summer. GWS added 18,000 lbs. of organic carbon and nutrients to the mine workings in October 1996, and added another 40,000 lbs. of organic carbon and nutrients in July 1997.

With each addition of organic carbon, the redox potential in the mine workings decreased down to −100 mV. The ferrous iron ratio to total iron started at approximately 0.50 (equal concentration) and went to close to 1.0 (only ferrous iron). During this stage of iron reduction, the pH of the mine pool increased and the total iron concentration rose. After iron reduction was complete, metals began to precipitate. Figure 6 shows the results for cadmium and copper. The concentration of both of these metals rapidly decreased, reaching 0.018-mg/L copper and 0.006-mg/L cadmium. At the beginning of treatment, copper was 3.0 mg/L and cadmium was 0.25 mg/L.

The spring flush brought a load of new metals into the mine workings, overcoming the reducing conditions in the mine. However, the reducing conditions and metal removal was rapidly achieved again when new organic carbon was added. It may be possible to build up sufficient "buffering" capacity of reduced compounds (specifically sulfide) to prevent the mine workings from becoming oxidized in the spring and early summer.

5.2 *In-mine treatment processes*

The collection of water behind bulkheads is a common practice in the closure of mine workings. The collected water may then be treated in wetlands or other passive treatment system, or in active water treatment plants. The pre-treatment of water behind the bulkhead offers several advantages to treatment outside of the mine. First, the mine workings offer residence time in which reactions can occur. Second, treatment outside of the mine will ultimately necessitate sludge disposal, while in situ treatment can use the mine workings as the repository of the treatment sludge. Third, treatment in the mine can

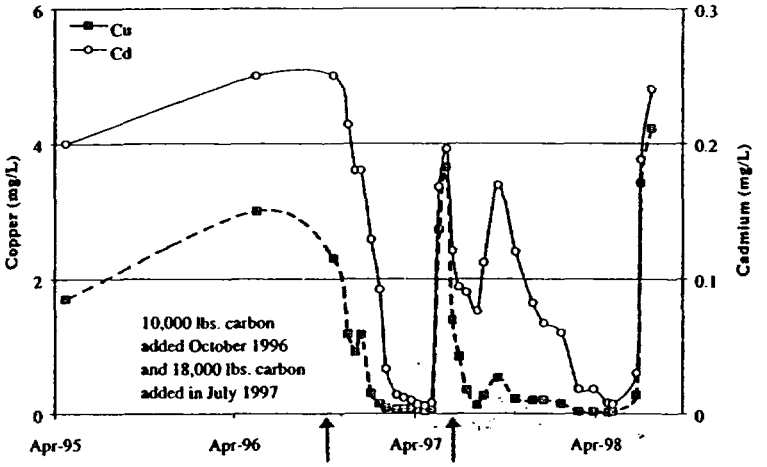

Figure 6. Mike Horse in situ adit treatment results for cadmium and copper.

sludge. Third, treatment in the mine can reduce the leaching of ores that contain sulfide by removing ferric iron from solution. The leaching of sulfides present in rubblized rock in the mine workings and the wall rock by ferric iron can be a significant part of the overall metal load generated in the mine. Removal of ferric iron, both by iron reduction and by precipitation of iron by sulfide, will remove the possibility of leaching reactions from occurring in the mine workings.

The principal reactions that will be useful in the treatment of mine workings are iron reduction and sulfate reduction. Iron reduction raises the pH by consuming acidity during the reaction (reaction 3 in Table 1), and converts ferric iron to ferrous iron, which removes the possibility of additional sulfide oxidation by ferric iron. Sulfate reduction also can reduce ferric iron to ferrous iron by the chemical reaction of aqueous sulfide with ferric iron, producing ferrous iron and elemental sulfur. Sulfate reduction is primarily useful because it can be used to remove metals by the precipitation of metal sulfides. Metals sulfides are often insoluble compounds. The combination of preventing ferric iron leaching in the mine workings, and the in situ precipitation of metals provides significant cost savings compared to any treatment outside of the mine workings.

6 IN SITU GROUNDWATER TREATMENT BENEATH TAILINGS IMPOUNDMENTS

6.1 *J. R. Simplot don plant tailings*

The J. R. Simplot phosphogypsum tailings impoundment is located in Idaho. The reaction of sulfuric acid with phosphate ore produces a tailing solution that is very low pH and typically contains high concentrations of soluble metals. The Simplot tailings contained arsenic that was the most mobile of all the metals in the tailings (least attenuated by the soils beneath the tailings). A test tailings impoundment (1.5 acres) was constructed with a subsoil layer, and a drainage layer beneath the subsoil. Tailings solution was then placed on the subsoil and the arsenic and phosphate concentrations in the drain were monitored. When the arsenic concentration in the drain layer exceeded the arsenic standard (0.05 mg/L) organic carbon began to be added to the tailings solution. This continued for over 400 days, and the drain concentrations of both arsenic and phosphate were monitored. Figure 7 shows these data.

Arsenic was removed from solution within one pore volume after carbon began to be added. This continued for more than ten additional pore volumes. This occurred even though phosphate concentrations continued to rise throughout the experiment, which indicated that arsenic was not being removed because of a sorption reaction. The redox potential after carbon was added dropped from +415 to –280 mV, and stayed at that potential for as long as organic carbon continued to be added. Aqueous sulfide was measured in the drain at approximately 0.3 mg/L for much of the study, indicating that the sulfide was reacting with the arsenic, precipitating arsenic sulfides. That sulfide was the cause of the arsenic removal was confirmed by the post-experimental soil extraction tests, which showed approximately 90% of the arsenic to be bound up in an operationally-defined arsenic sulfide phase.

7 IN SITU TREATMENT APPLICATION NOTES

7.1 *Complementary closure practices*

The range of sites that can be effectively treated by in situ microbial treatment include underground

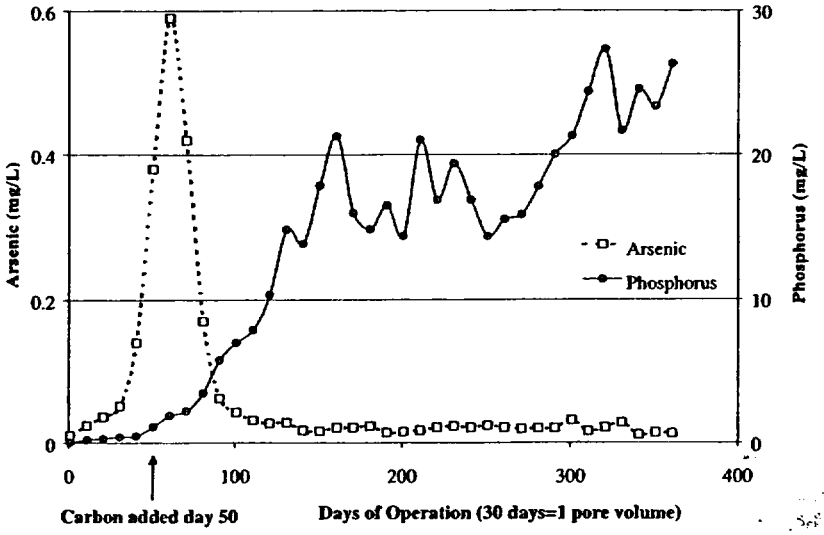

Figure 7. Simplot test gypsum tailings impoundment drain concentrations of arsenic and phosphate.

mine workings, mine pit lakes, backfilled mine pits, heap leach facilities, tailings impoundment ponds, groundwater beneath tailing impoundments, and waste rock facilities. Because oxygen must be removed prior to the treatment of most other constituents, any closure practice that limits the amount of oxygen contact with the mine workings or materials will decrease the cost and increase the effectiveness of the in situ treatment. The installation of a soil cover on a heap, a bulkhead in a mine adit, or the flooding of a mine pit all will reduce the oxygen contact with mining materials. There are two fundamental ways that oxygen contact is minimized: replacement of a gas phase with water (relative oxygen content of oxygen saturated water *vs.* air is 4 x 10^{-5}), and reduction of gas flux through vadose materials by reduction in permeability, typically by installation of a cover.

The effect of a cover on in situ treatment of vadose materials is dual: by limiting recharge, movement of water is deceased, and by limiting oxygen diffusion into the soil. All covers are meant to reduce water infiltration, but not all covers equally reduce gas diffusion. Reduction of gas movement through covers can be achieved by increasing the saturation of a particular layer, or by providing a layer with reduced permeability. Reduction of water infiltration, however, can affect the treatment by reducing the movement of treatment solutions. Thus the timing of the cover placement, after the treatment solutions are adequately applied, is important to increase the coverage and decrease the time for the overall treatment to occur.

Flooding of mine workings or materials is widely practices as an approach to limit the oxidation of sulfides. In some cases, it would not be feasible to keep mine workings dewatered. As noted above, it is better to add the organic carbon to the mine pool prior to flooding to get better coverage of the treatment solution. However, it is our experience that recirculation of organic carbon in a mine pool is possible and that these reactions can be stimulated in a uniform manner using this approach.

The amount of treatment that will be required can also be affected by how rapid the flooding is allowed to occur. The oxidation of sulfides can be slowed or prevented by flooding, and so the sooner after exposure the mine workings or materials are flooded, the lower the constituent load will be that may require treatment. We have proposed filling mine workings with an oxygen-excluding gas such as carbon dioxide to prevent sulfide oxidation reactions when water filling is occurring, or in instances where filling with water is not possible.

7.2 *Microbial versatility, diversity and distribution*

Many microorganisms can utilize a variety of oxidants in the metabolism of organic carbon. Thus, one organism stimulated to perform denitrification by the addition of organic carbon will utilize selenium after the removal of nitrate from solution (reference). In some cases, this metabolic versatility for a single organism covers almost every oxidant listed in Table 1 (Knight and Blakemore, 1998). In other cases, after nitrate has been denitrified, other organisms capable of selenium reduction grow and, from a metabolic perspective, become the dominant organism. The diversity of microorganisms in natural systems is such that in no case that we have yet encoun-

tered have the target organisms not been already present and capable to perform the desired reaction (reference). Even in systems where there have been extreme pH conditions, or where toxic constituents have been present, microorganisms have been present that are capable of performing any of the reactions shown in Table 1. The only cases where adding microorganisms proved desirable was when the time necessary to grow the microbes in situ was longer than was available, such as when a pond had to be treated and drained in a short period of time. It is important to remember that microbial growth times in natural systems may be in the order of days or weeks for one single cell to double (references).

7.3 *Treatment permanence*

In the same way that flooding and covers minimize the potential for sulfide oxidation in untreated mine materials and workings, these same approaches will act to enhance the longevity of an in situ treated mine facility. As can be seen in Figure 6, the Mike Horse mine workings could be easily treated during periods of low recharge, and the treatment effectiveness was lost during periods of high recharge. Slowing recharge will increase the residence time for the microbial reactions to occur.

Maintenance doses of organic carbon can be added to systems to maintain them in a reduced condition. In a reduced state, materials removed during in situ treatment (e.g. metal sulfides, elemental selenium) will remain stable (references). This organic carbon addition can be automated by coupling the addition rate of organic carbon to a redox potential probe.

Removal of metals by sulfate reduction often requires only a small amount of organic carbon, far less than the amount necessary to reduce the total sulfate in solution. However, treatment of such systems can be performed so that excess organic carbon is added, and excess sulfide is created. This excess sulfide may stay in solution as aqueous sulfide, or may precipitate as elemental sulfur. The "bank" of reduced sulfur compounds created can act to maintain the mine materials and workings in a reduced state far after the organic carbon is used up. Elemental sulfur can be microbially disproportionated to produce 3 moles of sulfide and 1 mole of sulfate from 4 moles of elemental sulfur. The sulfide thus produced will react with oxidized metals and precipitate them just as would microbially-produced sulfides from sulfate reduction.

In systems open to the sun, organic carbon can be produced and added to the system through photosynthesis. In the Sweetwater pit, algae were stimulated to create approximately 60,000 lbs. of organic carbon per year. This rate of organic carbon production is sufficient to maintain the reduced selenium and uranium in their insoluble reduced form. Vegetation also produces organic carbon that is deposited to the soil in two forms, through "leakage" of photosynthetic sugars from the roots, to decomposition of dead plant material (roots, stems, leaves). A well-vegetated cover can reduce the oxygen diffusion into the covered materials by consuming oxygen by the decomposition of organic matter.

The burial of constituents removed by in situ treatment will act to minimize the potential for remobilization. In the Sweetwater pit, for instance, the burial of the selenium and uranium removed in one season occurs at a rate of ½ cm/annual lake cycle. This burial though sedimentation is the equivalent of adding a cover layer, because oxygen or oxygenated compounds must diffuse through this layer to react with the reduced compounds removed in the treatment.

The aging of reduced precipitates also acts to minimize the potential for remobilization. Elemental selenium, for instance, when newly formed can be oxidized much more easily than after the precipitate is aged (reference). Pyritized metals are also considered to not be easily mobilized as compared with amorphous sulfide precipitates (reference). The burial and aging of precipitates together reduce the potential for remobilization of metals in many in situ treated mine workings.

7.4 *Conclusions*

The examples presented in this paper illustrate that the in situ treatment of mine materials and workings is a technology with a strong base of application experiences. The range of sites treated show that there is potential for this technology to be applied at a wide variety of sites. The scientific basis for the technology is now understood to a level that allows a good understanding of the application potential at a particular site, and so that potential pitfalls may be avoided.

REFERENCES

Anderson, R., and B. Hansen. 1999. Mine waste and water management at the Upper Blackfoot Mining Complex. In *Tailings and Mine Waste '99*: 715-723 Rotterdam: Balkema.

Knight, V., and R. Blakemore. 1998. Reduction of diverse electron acceptors by Aeromonas hydrophilia. *Archives of Microbiology*, 169: 239-248.

Knoblauch, C., B. Jorgensen, and J. Harder. 1999. Community size and metabolic rates of psychrophilic sulfate-reducing bacteria in arctic marine sediments. *Applied and Environmental Microbiology*, 65: 4230-4233.

Lehman, R.M. and A. Mills. 1994. Field evidence for copper mobilization by dissolved organic matter. *Water Research*, 28: 2487-2497.

Narkis, N., M. Rebhun, and C. Sheindorf. 1979. Denitrification at various carbon to nitrogen ratios. *Water Research*, 13: 91-98.

Oremland, R., J. Blum, A. Bindi, P. Dowdle, M. Herbel, and J. Stolz. 1999. Simultaneous reduction of nitrate and selenate by cell suspensions of selenium-respiring bacteria. *Applied and Environmental Microbiology*, 65: 4385-4392.

Pauling, L. 1988. General Chemistry. New York: Dover Publications.

Raybuck, S. 1992. Microbes and microbial enzymes for cyanide degradation. *Biodegradation* 3: 3-18.

Raef, S., W. Characklis, M. Kessick, and C. Ward. 1977. Fate of cyanide and related compounds in aerobic microbial systems—II, microbial degradation. *Water Research* 11: 485-492.

Wielinga, B., M. Mizuba, C. Hansel, and S. Fendorf. 2001. Iron promoted reduction of chromate by dissimilatory iron-reducing bacteria. *Environmental Science and Technology*, 35: 522-527.

Impact of Human Activity on Groundwater Dynamics (Proceedings of a symposium held during the Sixth IAHS Scientific Assembly at Maastricht, The Netherlands, July 2001). IAHS Publ. no. 269, 2001.

Determining the reactivity of reduced components in Dutch aquifer sediments

NIELS HARTOG
Department of Earth Sciences, Utrecht University, PO Box 80021, 3508 TA Utrecht, The Netherlands
e-mail: nhartog@geo.uu.nl

JASPER GRIFFIOEN
TNO Netherlands Institute of Applied Geosciences, PO Box 6012, 2600 JA Delft, The Netherlands

PIM F. VAN BERGEN & CORNELIS H. VAN DER WEIJDEN
Department of Earth Sciences, Utrecht University, PO Box 80021, 3508 TA Utrecht, The Netherlands

Abstract Sediments from a single aquifer were incubated under atmospheric conditions for 54 days to determine the reactivity of reductants present. The stoichiometric relationships between O_2 consumption and CO_2 production were used to evaluate the relative importance of ongoing redox processes. Respiration of bulk organic matter (BOM) and pyrite oxidation were the major processes occurring, but there was also evidence of siderite oxidation. The rates of BOM oxidation decreased continuously during the experiment. Pyrite oxidation had a maximum in its oxidation rate during the acidification process. When the acidification was buffered by carbonate dissolution, the pyrite oxidation rates decreased continuously. More than one reductant in a sample could be oxidized simultaneously.

Keywords aquifer sediment; organic matter oxidation; pyrite oxidation; reduction reactivity; redox processes; siderite oxidation

INTRODUCTION

Obtaining a detailed insight into the natural reduction capacity of aquifers has become increasingly important over recent decades. This mainly reflects the need to assess the deterioration of groundwater quality by agricultural activities (Goodrich *et al.*, 1991) and the suitability of *in situ* (bio)remediation technologies at contaminated sites (Barcelona & Holm, 1991). In the context of reaching the European objective for nitrate produced from agricultural activities (EU, 1991), recent discussions on the capacity of Dutch aquifers to reduce nitrate, have emphasized the role of pyrite and to a lesser extent that of bulk organic matter in aquifer sediments. The purpose of the present study was to assess the variability in reduction capacity of aquifer sediment by experimentally determining the relative importance of the reactive reductants present.

EXPERIMENTAL PROCEDURES

Sample collection and processing

Six core samples were taken from a borehole in a calcareous aquifer at the De Steeg drinking water production site near Langerak, The Netherlands (Table 1). This unit is

Table 1 Short description of the aquifer samples used in the incubation experiment.

Depth* (m)	<63 μm (wt. %)	63–2000 μm (wt. %)	<2 mm (wt. %)	>2 mm (wt.%)	C_{org} (wt.%)	S (wt. %)	Carbonate (wt.%)	Geological formation†
15.00	0.63	99.37	83.78	16.22	0.06	0.01	2.04	Kreftenheye
20.00	0.39	99.61	99.79	0.21	0.05	0.01	4.32	Kreftenheye
25.00	0.69	99.32	99.57	0.43	0.05	0.12	1.00	Urk
30.00	0.77	99.23	99.93	0.07	0.07	0.15	0.79	Urk
35.00	1.83	98.18	98.84	1.16	0.06	0.10	1.30	Sterksel/Kedichem
39.60	7.41	92.59	99.83	0.17	0.09	0.06	8.68	Sterksel/Kedichem

*Depth below surface level.

†Kreftenheye Formation = fluvio-glacial deposit, Urk Formation = fluvial deposit, Sterksel/Kedichem Formation = fluvial deposits.

confined by Lower Pleistocene clays at the bottom and Holocene clays and peats at the top. Sample depths ranged from 15 to 40 m below the surface. The samples were stored under a nitrogen atmosphere at 8°C directly after collection in the field. The sediments were separated into three particle size fractions: 0–63 μm (fine fraction), 63–2000 μm (coarse fraction) and 0–2000 μm (total fraction).

Sediment incubations

Samples were incubated under dark conditions. Twenty-five millilitres of vitamin and trace element solution were added in order to prevent inhibition due to nutrient limitation. Sample weight ranged from a few grammes for the fine fraction to 100 g for the total fraction. The reaction chambers (Duran 100 ml-bottle) were connected to the closed circuit of a respirometer (Micro-Oxymax™, Columbus Instruments). Carbon dioxide (CO_2) and oxygen (O_2) levels in the headspaces of the reaction chambers were kept at atmospheric conditions at 25°C (± 1°C). The O_2 and CO_2 concentrations were measured every 3 h for 54 days, using an infrared sensor and an oxygen battery (fuel cell), respectively. The reaction chambers were gently shaken (100 rpm) to ensure a well-mixed chemical system.

Directly after the end of the experiment, the pH and the alkalinity of the water in the reaction chambers were measured using a standard field set. Dissolved cations and sulphate were analysed using ICP-MS. X-ray fluorescence (XRF) was used to study the bulk chemistry of the sediments. Mineralogical composition was examined by differential thermal analysis (DTA), thermogravimetry (TG) and X-ray diffraction (XRD). Carbonate and pyrite contents were determined by wet chemical analyses. The organic carbon content was determined using a C/N elemental analyser, while the particle size distribution was obtained by laser diffraction.

RESULTS AND DISCUSSION

Total reduction capacity

The cumulative O_2 consumption after 54 days (Fig. 1) can be taken as a measure of the total reduction capacity (TRC) of the samples, because the final O_2 consumption rates

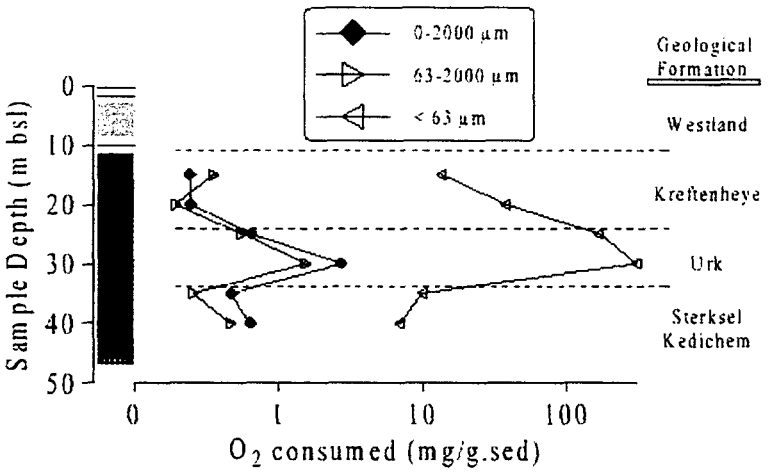

Fig. 1 Depth profile of total O_2 consumption of the different size fractions.

approached zero. This O_2 consumption of the total fractions is lowest in the samples taken from the Kreftenheye Formation, intermediate in those taken from the Sterksel/Kedichem Formation and highest in those taken from the Urk Formation. This trend is also reflected in the total O_2 consumption of the coarse and fine fractions (Fig. 1). Furthermore, the O_2 consumption of the fine fractions is up to 100 times higher than that of the corresponding total fractions. However, in this study, the absolute importance of the fine fraction is limited because it constitutes less than 2% of the total grain size distribution, except for the deepest sample (Table 1). The coarse fraction mainly acts as a dilutant of the reduction activity of the fine fraction.

Contribution of siderite, bulk organic matter and pyrite to the TRC.

Siderite, bulk organic matter (BOM) and pyrite are potentially important O_2 consumers in the aquifer samples studied. The following redox reactions for these components are considered:

siderite

(a) $FeCO_3 + ¼\ O_2 + 1½\ H_2O \rightarrow Fe(OH)_3 + CO_2$

bulk organic matter simplified as CH_2O

(b) $CH_2O + O_2 \rightarrow CO_2 + H_2O$

pyrite

(c) $FeS_2 + 3¾\ O_2 + 3½\ H_2O \rightarrow Fe(OH)_3 + 2\ SO_4^{2-} + 4H^+$

and if proton generation in (c) *is buffered by maintaining calcite equilibrium,*

(d) $FeS_2 + 3¾\ O_2 + 1½\ H_2O + 2\ CaCO_3 \rightarrow Fe(OH)_3 + 2\ Ca^{2+} + 2\ SO_4^{2-} + 2\ CO_2$

It should be noted that the molar ratios of CO_2 produced to O_2 consumed are distinctly different for reactions (a–d). Siderite, BOM, pyrite and buffered pyrite oxidation yield a CO_2 to O_2 ratio of 4, 1, 0 and 8/15 respectively. The relative contribution of the components considered to the total O_2 consumption can be estimated using these ratios.

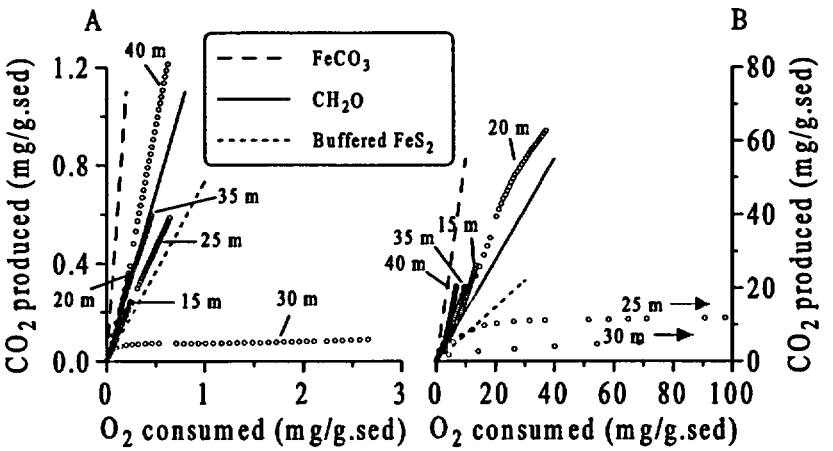

Fig. 2. Oxidation experiments. (a) Cumulative O_2 consumption *vs* cumulative CO_2 production during 54 days of incubation of the total fraction (0–2000 μm) samples. For reasons of clarity, the data plotted are every tenth data point available. Stoichiometric lines are plotted according to reaction (a, b and d) (see text for explanation). (b) same as (a) except for the fine fraction (0–63 μm) total O_2 consumption for 25 m: 167 mg g^{-1} sediment, for 30 m: 299 mg g^{-1} sediment.

Figure 2(a) shows the O_2 consumption versus the CO_2 production in the total fractions. The slopes of the cumulative O_2/CO_2 fall in the range of stoichiometries for the reactions (a–d). The O_2/CO_2 of the total fractions from 20 and 35 m depth only suggest the oxidation of BOM, i.e. reaction (b), while the total fractions from 15 and 25 m depth indicate the oxidation of both BOM and pyrite, i.e. reactions (b) and (d). The total fraction sample from 30 m deep initially shows pyrite oxidation with CO_2 production and O_2 consumption according to reaction (d), and subsequently O_2 consumption without CO_2 production, according to reaction (c). This indicates that the carbonate buffering is limited. The total fraction sample from 40 m deep shows a CO_2/O_2 ratio higher than that for BOM oxidation, thus part of the O_2 consumption must be caused by the oxidation of siderite. The presence of siderite in this sediment was later confirmed by DTA.

Significant differences occur between oxidation reactions in the total (Fig. 2(a)) and fine (Fig. 2(b)) fractions. For example, the CO_2/O_2 ratios of the oxidation reactions in the fine fractions (Fig. 2(b)) from 15, 20, 35 and 40 m depth are closer to the stoichiometric line for siderite oxidation than the corresponding total fractions, suggesting a greater importance of siderite oxidation in these fine fractions. Furthermore, when excluding the total fraction samples that show pyrite oxidation, the sample from 40 m depth consumed most O_2, while of the corresponding fine fractions, the sample from 20 m depth is most reactive. Finally, the pyrite oxidation in the fine fraction from 25 m depth is largely unbuffered by carbonate dissolution, while the corresponding total fraction shows buffered pyrite oxidation. This indicates that the carbonate buffer is largely contained in the coarse fraction.

The relative contribution of the different components was calculated from the resulting CO_2/O_2 ratio at the end of the incubation (Table 2). The interpretations based on the CO_2/O_2 ratios are confirmed by the pH and sulphate measurements in the water

Table 2 Measured CO_2/O_2 ratios, pH and sulphate (NA = not analysed) concentrations and calculated relative contributions of reactions (a–d) to the total O_2 consumption of the total fraction samples.

Depth (m)	$(CO_2/O_2)_{end}$ (molar)	Relative contribution of oxidation reactions (a–d) (a)	(b)	(c)	(d)	pH_{end}	$sulphate_{end}$ (mmol l^{-1})
15.00	0.75		0.46		0.54	7.2	4.4
20.00	1.06	0.02	0.98			7.5	1.7
25.00	0.66		0.27		0.73	6.3	12.7
30.00	0.02			0.96	0.04	2.1	34.0
35.00	0.94		0.87		0.13	6.8	NA
39.60	1.41	0.14	0.86			7.1	5.0

at the end of the incubations. The samples that show pyrite oxidation have high sulphate concentrations. The final pH of the sample from 30 m depth, which shows unbuffered pyrite oxidation, was 2.1. The final pH values of the other sediment incubations were near neutral (Table 2).

Kinetics and oxidation rates of the reducing components

Figure 3(a) shows the difference in the typical evolution of O_2 consumption rates between BOM and pyrite oxidation without carbonate buffering. The rates of BOM and buffered pyrite oxidation decreased continuously during the experiment. Decreasing rates for BOM oxidation are often observed (e.g. Kristensen *et al.*, 1995) and can be explained by an increasing stability of the organic compounds remaining (Cowie *et al.*, 1992; Hulthe *et al.*, 1998). Iron hydroxides, produced during buffered pyrite oxidation, may precipitate as a diffusion layer on the pyrite surfaces, slowing its oxidation (e.g. Nicholson *et al.*, 1990). The rates of unbuffered pyrite oxidation started to increase after one week, following cessation of CO_2 production once the carbonate

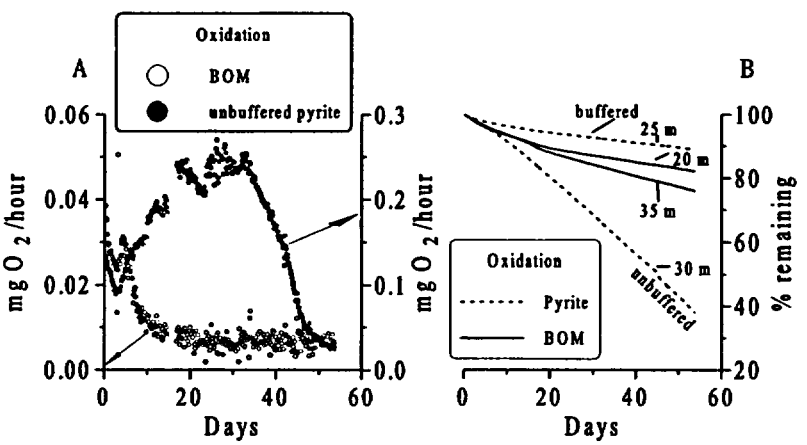

Fig. 3 Kinetics. (a) Oxygen consumption rate for the fine fractions from 20 and 25 m depth. All data points are shown. (b) Oxidation rates of selected components in four total fractions. Initial contents: 15 m: 0.06 C%, 25 m: 4272 ppm FeS_2, 30 m: 4350 ppm FeS_2, 35 m: 0.06 C%.

buffer had been consumed. Then the rates dropped off until the end of the experiment when the samples had acidified to a pH <2. Since only the samples that showed unbuffered pyrite oxidation exhibit this typical sequence, we interpret this maximum in the O_2 consumption rate to be a pH effect. The dissolution of an inhibiting iron hydroxide coating on the pyritic surface at low pH and the subsequent release of ferric ions, that are important intermediates in the oxidation of pyrite by O_2 (Moses *et al.*, 1987), are probable causes for the increased rates. We suggest that the subsequent decrease in rates at lower pH is due to the decreasing rate of the of ferrous iron oxidation, which is the overall controlling process (Moses *et al.*, 1991)

The oxidative loss of reductants in four samples is shown in Fig. 3(b). In these samples, there was a main oxidative process (reactions a–d) responsible for the observed O_2 consumption (Table 2). The relative amounts of reductant from the sediment analyses and the cumulative O_2 consumption were calculated. The samples from 20 and 35 m depth showed oxidation of BOM. Assuming no inert organic fraction, a first order degradation model can be used:

$$\mathrm{dBOM}/\mathrm{d}t = -k \times \mathrm{BOM}$$

half-lives for the BOM present were estimated to be 214 and 141 days. These oxidation rates were higher than the buffered but lower than the unbuffered pyrite oxidation rates in the samples from 25 and 30 m depth, respectively. Clearly, the buffered oxidation of pyrite in the sample from 25 m depth is slower than the oxidation of the pyrite in the sample from 30 m depth, in which half of the pyrite was oxidized in 45 days. The difference in rate between buffered and unbuffered pyrite oxidation is probably due to the precipitation of iron hydroxides on the pyrite surfaces during buffered pyrite oxidation (Nicholson *et al.*, 1990). The effect of the precipitation of an iron hydroxide coating on the oxidation of pyrite can be described (results not shown) by a shrinking core model (cf. Nicholson *et al.*, 1990). During unbuffered pyrite oxidation, however, these precipitated iron hydroxides may re-dissolve again during acidification and thus facilitate enhanced pyrite oxidation.

CONCLUSIONS

Our oxidation experiments showed the presence of BOM, pyrite and siderite as reactive reductants within a single hydrological unit. Our results clearly show that, if present, these reductants can be oxidized simultaneously. Both the TRC and the reductants that are responsible for the O_2 consumption seem to be related to the geological provenance and/or history of the sediment. The TRC of the total fractions (0–2000 μm) taken from this single aquifer unit varies by about 10 times. In these sediments, the fine fraction (0–63 μm) is about 100 times more reactive than the coarse fraction (63–2000 μm), but, because of the small amount of the fine fraction present, this has a limited effect on the reactivity of the total fraction. The coarse fraction mostly dilutes the reactivity of the fine fraction, but seems to be important in providing acid buffering capacity. This spatial heterogeneity in reactivity complicates hydrogeochemical modelling of the oxidation in a single aquifer system, since different reactions happen concurrently.

REFERENCES

Barcelona, M. J. & Holm, R. T. (1991) Oxidation-reduction capacities of aquifer solids. *Environ. Sci. Technol.* **25**, 1565–1572.

Cowie, G. L., Hedges, J. I. & Calvert, S. E. (1992) Sources and relative reactivities of amino acids, neutral sugars, and lignin in an intermittently anoxic marine environment. *Geochimica et Cosmochimica Acta* **56**, 1963–1978.

European Union (EU) (1991) *Council Directive* 91/676/EEC of 12 December 1991.

Goodrich, J. A., Lykins, Jr., B. W. & Clark, R. M. (1999) Drinking water from agriculturally contaminated groundwater. *J. Environ. Qual.* **91**, 217–235.

Hulthe, G., Hulth, S. & Hall, P. O. J. (1998) Effect of oxygen on degradation rate of refractory and labile organic matter in continental margin sediments. *Geochimica et Cosmochimica Acta* **62**(8), 1319–1328.

Kristensen, E., Ahmed, S. I. & Devol, A. H. (1995) Aerobic and anaerobic decomposition of organic matter in marine sediments: which is fastest? *Limnol. Oceanogr.* **40**(8), 1430–1437.

Moses, C. O., Nordstrom, D. K., Herman, J. S. & Mills, A. L. (1987) Aqueous pyrite oxidation by dissolved oxygen and by ferric iron. *Geochimica et Cosmochimica Acta* **51**, 1561–1571.

Moses, C. O. & Herman, J. S (1991) Pyrite oxidation at circumneutral pH. *Geochimica et Cosmochimica Acta* **55**, 474–482.

Nicholson, R. V., Gillham, R. W. & Reardon, E. J. (1990) Pyrite oxidation in carbonate-buffered solution: 2. Rate control by oxide coatings. *Geochimica et Cosmochimica Acta* **54**, 395–402.

Waterloo

- Earth Sci Home
- People
- Undergraduate
- Information
- Graduate
- Information
- Courses
- Research
- Thesis titles
- Resources
- Links
- News & Events
- Contact Info

- CGC
- GEOSCIED IV

QSI

WATERLOO Science

Earth Sciences

HEAGLE, Dru

Nitrate concentrations in the Thornton Well Field near Woodstock, Ontario, have been steadily increasing since 1980. This study was undertaken to determine the source and behaviour of nitrate in the regional aquifer. The investigation is a part of a major research project involving hydrogeology and the use of dating techniques to evaluate the long-term water quality of the Thorton Well Field. Geochemical and hydrogeological tools were used to ascertain the source and location of the elevated nitrate concentration and to determine the factors that control nitrate concentrations in the groundwater flow system from the recharge area to the production wells.

A complex two aquifer, three aquitard geologic system has been delineated. Discontinuous layers of sand, till and gravel comprise the geology allow local recharge water to penetrate deep into the aquifer system. Land use in the surrounding area is primarily agricultural.

Three geochemical regions were found in the area surrounding the Thorton Well Field. The north region is characterized by low NO_3^-N (<0.05 to 0.5 mg/l) and high sulphate values (11-94 mg/l) with varying levels of dissolved oxygen (<0.05 to 12 mg/l). Nitrate fertilizer applied to the fields in the north region was not found in the shallow groundwater suggesting that nitrate attenuation is occurring before the water reaches the saturated zone.

In the east region, reducing conditions in the saturated zone are responsible for the geochemistry of the groundwater. The

reducing conditions are due to the shallow depth to the water table and higher concentrations of DOC (3 to 11 mg/l).

The region west of the well field appears to be responsible for most of the nitrate reaching the well field. Land use is dominantly agricultural with fertilizer applications at approximately 450 kg-N/ha. NO_3^-N concentrations are found above 10 mg/l in the area. Point sources of focused recharge (drainage tile discharges; and depression-focused recharge) and broad-scale diffuse recharge allow nitrate to impact the shallow aquifer. Nitrate levels, sulphate concentration, $\delta^{15}N$ in nitrate, and $\delta^{34}S$ in sulphate from this region are very similar to the values at the production wells. High dissolved oxygen concentrations inhibit denitrification. NO_3^-N concentration in the unsaturated zone beneath an agricultural field in this area was 8 mg/l. discharge from a tile drain in this area had NO_3^- N concentrations as high as 17 mg/l. this drainage water was directly recharging the shallow aquifer.

Denitrification in the study site appears to be controlled by sulphide bearing minerals in surficial till and unweathered aquifer sediments. An increase in sulphate concentration, depletion of $\delta^{34}S$ in sulphate, and the decrease in NO_3^-N levels suggests that denitrification by pyrite oxidation is occurring in the surficial till of the north region and in the shallow aquifer of the east region.

This study highlights the complexity of regional recharge and the variability in the distribution of controls on nitrate geochemistry. Recharge of elevated nitrate groundwater occurs through broad-scale diffuse recharge but also from point sources (tile drains) at locations where the shallow aquifer is near the surface. Factors that control the distribution of nitrate are regional groundwater flow direction and redox conditions. The variability of redox conditions in an aquifer affects the viability of denitrification, and therefore, nitrate distribution.

Last revised May, 2001.

APPLIED AND ENVIRONMENTAL MICROBIOLOGY, June 2002, p. 2704–2710 Vol. 68, No. 6
0099-2240/02/$04.00+0 DOI: 10.1128/AEM.68.6.2704–2710.2002

Immobilization of Radionuclides and Heavy Metals through Anaerobic Bio-Oxidation of Fe(II)

Joseph G. Lack,[1] Swades K. Chaudhuri,[1] Shelly D. Kelly,[2] Kenneth M. Kemner,[2] Susan M. O'Connor,[1] and John D. Coates[1]*

Department of Microbiology, Southern Illinois University, Carbondale, Illinois 62901,[1] and Environmental Research Division, Argonne National Laboratory, Argonne, Illinois 60439[2]

Received 17 October 2001/Accepted 13 March 2002

Adsorption of heavy metals and radionuclides (HMR) onto iron and manganese oxides has long been recognized as an important reaction for the immobilization of these compounds. However, in environments containing elevated concentrations of these HMR the adsorptive capacity of the iron and manganese oxides may well be exceeded, and the HMR can migrate as soluble compounds in aqueous systems. Here we demonstrate the potential of a bioremediative strategy for HMR stabilization in reducing environments based on the recently described anaerobic nitrate-dependent Fe(II) oxidation by *Dechlorosoma* species. Bio-oxidation of 10 mM Fe(II) and precipitation of Fe(III) oxides by these organisms resulted in rapid adsorption and removal of 55 μM uranium and 81 μM cobalt from solution. The adsorptive capacity of the biogenic Fe(III) oxides was lower than that of abiotically produced Fe(III) oxides (100 μM for both metals), which may have been a result of steric hindrance by the microbial cells on the iron oxide surfaces. The binding capacity of the biogenic oxides for different heavy metals was indirectly correlated to the atomic radius of the bound element. X-ray absorption spectroscopy indicated that the uranium was bound to the biogenically produced Fe(III) oxides as U(VI) and that the U(VI) formed bidentate and tridentate inner-sphere complexes with the Fe(III) oxide surfaces. *Dechlorosoma suillum* oxidation was specific for Fe(II), and the organism did not enzymatically oxidize U(IV) or Co(II). Small amounts (less than 2.5 μM) of Cr(III) were reoxidized by *D. suillum*; however, this appeared to be inversely dependent on the initial concentration of the Cr(III). The results of this study demonstrate the potential of this novel approach for stabilization and immobilization of HMR in the environment.

The mobility of trace metals and radionuclides released into aquatic and terrestrial environments by mining, industrial processes, and municipal waste disposal practices is an area that deserves significant scientific, public health, and regulatory attention. The U.S. Environmental Protection Agency includes cadmium, chromium, copper, lead, mercury, nickel, silver, and zinc on its priority pollutant list for waste effluents. Geochemical controls that regulate the trace element concentrations in oxic natural waters include adsorption and coprecipitation by hydrous oxides of iron and manganese. These hydrous oxides occur as discrete grains and as coatings on aquifer materials. They have been shown to be the major host minerals for many trace elements in soils and for ^{60}Co and isotopes of plutonium and americium in soils and sediments of a disposal area at Oak Ridge National Laboratory (27).

Adsorption of heavy metals and radionuclides (HMR) onto iron and manganese oxides has long been recognized as an important reaction for immobilization of these compounds (2, 4, 28, 33, 45, 46, 47, 51, 52). However, the adsorptive capacity of the hydrous oxides in some environments may not be sufficient to immobilize all of the HMR present. Many studies have investigated the bioremediative potential of stimulating reducing bacteria to use some of the soluble HMR as electron acceptors and thus precipitate them out of solution (10, 35, 42, 43). However, there are many unknowns and potential limitations for this technique, including (i) the fate of the reduced immobilized HMR once the bioremediative process is complete and the environment reverts back to an oxic state; (ii) the potential for bio-oxidation and subsequent resolubilization of the reduced immobilized HMR; (iii) the fact that reductive remediation may not be suitable for low-level, long-term contamination as there may be insufficient HMR contaminants available to support a metal-reducing microbial community; and (iv) the fact that many metals are bound and solubilized by natural and anthropogenic organic matter present in most environments regardless of their valence state (12, 16, 50, 59).

An alternative to bioreduction is selective anaerobic bio-oxidation of added Fe(II) under anoxic conditions. This technique, if successful, should result in immobilization of contaminating HMR on newly formed Fe(III) oxides. Anaerobic bio-oxidation of Fe(II) was only recently identified, and very little is known regarding the ubiquity and diversity of organisms capable of this metabolism. Previous studies have shown that Fe(II) oxidation is mediated by anoxygenic phototrophs (32, 61), as well as various nitrate-respiring organisms (8) and perchlorate-respiring organisms (11, 15, 20, 38, 48). The end product of this metabolism is generally amorphous Fe(III) oxide (8, 11, 57, 61). Amorphous Fe(III) oxide [$Fe_2O_3 \cdot H_2O(am)$], or ferrihydrite, has often been used for studies of adsorption of trace metals because it is a uniform material with well-known surface properties that is easily reproduced (2). It is also representative of metal oxides in the natural environment and is a

* Corresponding author. Mailing address: Department of Microbiology, Southern Illinois University, Carbondale, IL 62901. Phone: (618) 453-6132. Fax: (618) 453-8036. E-mail: jcoates@micro.siu.edu.

precursor of many natural forms of crystalline Fe(III) oxides, such as goethite and hematite (22, 53, 63). Previous studies have shown that metals such as cobalt, chromium, cadmium, lead, uranium, and radium are rapidly adsorbed by this iron form (2, 4, 44, 51), and some of these metals with lower ionic radii (e.g., Co^{2+} and Cd^{2+}) are incorporated into the Fe(III) oxide structure as the amorphous Fe(III) oxides begin to recrystallize with age. Under these conditions these trace metals become tightly bound in the Fe(III) oxide crystals (2) and are thus immobilized.

As part of a study on the metabolic diversity of organisms capable of growth by anaerobic respiration of perchlorate, we isolated a novel organism, *Dechlorosoma suillum* strain PS, from a swine waste lagoon (1, 20, 48). Physiological characterization revealed that *D. suillum* rapidly oxidized Fe(II) with nitrate or chlorate as the electron acceptor under strictly anaerobic conditions (15, 38, 48). Recently, we demonstrated that Fe(II) oxidation by *D. suillum* resulted in the formation of different end products depending on the rate of Fe(II) oxidation (15, 38). In cell suspension experiments, Fe(II) was rapidly oxidized to an amorphous ferrihydrite similar to that formed by other previously described nitrate-dependent Fe(II) oxidizers (38); however, under growth conditions with acetate as a cosubstrate and nitrate as the electron acceptor, Fe(II) oxidation resulted in the production of a broad range of crystalline iron minerals, including magnetite, which accounted for as much as 25% of the original Fe(II) in the culture under the growth conditions tested (15). Here we report on the bioremediation potential of this metabolism for immobilization of HMR in reducing environments as a result of engineered anaerobic bio-oxidation.

MATERIALS AND METHODS

Medium and culture conditions. *D. suillum* strain PS was maintained in an anoxic, defined freshwater medium described previously (11) with acetate (10 mM) as the sole electron donor and chlorate (10 mM) or nitrate (10 mM) as the sole electron acceptor. Standard anaerobic techniques were used throughout this study (34). Anoxic medium (pH 6.8) was prepared by boiling the medium to remove dissolved O_2 before it was dispensed under an N_2-CO_2 (80:20, vol/vol) gas phase into anaerobic pressure tubes or serum bottles that were sealed with thick butyl rubber stoppers.

Alternative electron donors and acceptors were added from sterile stock solutions. Chloride salts of the metals cadmium ($CdCl_2$), cobalt ($CoCl_2$), and uranium (UCl_2O_2) were also added from sterile stock solutions. Reduced U(IV) was produced in culture medium by amending freshly prepared anoxic basal medium with an anoxic uranyl chloride stock to give the desired final U(IV) concentration. The medium was further amended with palladium-coated aluminum chips and gassed out with H_2 to abiotically reduce the UO_2Cl_2. Once the uranium was reduced, the headspace gas was replaced with N_2-CO_2 and the aluminum chips were removed by decantation.

Cell suspension preparation. Cells of *D. suillum* strain PS were grown anaerobically in 500-ml volumes of medium with acetate (10 mM) as the electron donor and chlorate or nitrate (10 mM) as the electron acceptor. After dense growth of *D. suillum*, cells were harvested by centrifugation at 4°C under an N_2-CO_2 headspace. The cell pellets were each washed twice and resuspended in 1 ml of anoxic bicarbonate buffer (2.5 g $liter^{-1}$, pH 6.8) and sealed in a 10-ml serum vial with a thick butyl rubber stopper under an N_2-CO_2 headspace.

Analytical techniques. Acetate concentrations were analyzed by high-performance liquid chromatography with UV detection at 210 nm (model SPD-10A; Shimadzu Scientific Instruments, Columbia, Md.) by using an HL-75H$^+$ cation-exchange column (catalog no. 79476; Hamilton Company, Reno, Nev.). The eluent was 0.016 N H_2SO_4 at a flow rate of 0.4 ml min^{-1}. Chlorate, chloride, nitrate, and nitrite concentrations were analyzed by ion chromatography with conductivity detection (model CDD-6A; Shimadzu Scientific Instruments) by using IonPac AS9-HC with suppressed conductivity by ASRS-II in a recycle mode (catalog no. 51786; Dionex Corporation, Sunnyvale, Calif.). The eluent was 9 mM sodium carbonate at a flow rate of 1.0 ml min^{-1}. Growth of cultures on soluble electron acceptors was determined by direct cell counting and by monitoring the increase in optical density at 600 nm. Concentrations of HCl-extractable Fe(II) were determined colorimetrically by the ferrozine assay at 562 nm (41). For insoluble Fe(II) minerals, the total Fe(II) content was determined by extraction for 24 h in 5 N HCl prior to analysis with the ferrozine assay.

Soluble concentrations of U(VI) were determined by using reverse-phase chromatography coupled to postcolumn derivatization with the dye Arsenazo III. This method is a modification of the method first described by Barkley et al. (7). A detection limit of 0.50 μM can be achieved with this technique. A Dionex DX500 instrument equipped with a Supelcosil LC-18 column (150 by 450 mm), an absorbance detector set to a wavelength of 658 nm, and a pneumatic unit for delivery of the postcolumn reagent was used. The chromatographic conditions included a mobile phase of 85% 0.20 M hydroxyisobutyric acid (pH 4.0) and 15% methanol at a flow rate of 1.4 ml · min^{-1} and 0.125 mM Arsenazo III as a postcolumn reagent at a flow rate of 0.60 ml·min^{-1}.

X-ray absorption spectroscopy. The biogenic Fe(III) oxides containing uranium were centrifuged, and the resulting wet paste was mounted in a hollowed-out Plexiglas (thickness, 1.5 mm) sample holder. Kapton film was used to contain the sample within the hollowed-out region of the Plexiglas holder and to allow penetration of the synchrotron radiation. The centrifuge tube was opened, and the material was mounted in the Plexiglas holder in an anaerobic glove box (Coy Laboratories) to maintain anoxic conditions. Uranium L-III edge fluorescence X-ray absorption fine-structure (XAFS) spectroscopy (37) measurements were obtained for the wet homogeneous paste. All XAFS measurements were made at the Materials Research Collaborative Access Team insertion device beamline (54) at the Advanced Photon Source, Argonne National Laboratories, Argonne, Ill. The energy of the incident X rays was selected by using Bragg reflection from two Si(111) crystals from the third harmonic of the beamline undulator. Higher-order harmonics were rejected by using an Rh mirror. The incident X-ray intensity was sampled by using an ion chamber filled with nitrogen gas, and the fluorescent X-ray intensity was sampled by using a Stern-Heald detector filled with free-flowing Ar gas at atmospheric pressure. An Sr filter of six absorption lengths was used to reduce the elastically scattered radiation contributing to the background signal. Linearity tests (36) indicated that there was less than 0.38% nonlinearity in the experimental setup for a 50% decrease in incident X-ray intensity. The incident X-ray intensity varied by less than 15% throughout the energy range of the XAFS measurements. The transmission XAFS signal of an yttrium-containing X-ray filter was used as an energy reference to accurately align the edge-energy positions of all data, as described elsewhere (23). Three energy scans were collected at six different locations on the sample to reduce radiation-induced chemical effects on the sample. The sample was exposed for approximately 1 min for each of the three measurements at each location. Measuring several spectra at each of the six sample locations allowed determination of radiation-induced chemical effects at the 1-min time scale. No time-dependent change was observed in the X-ray absorption near-edge spectra (XANES) data for any of the samples.

Three experimental U extended X-ray absorption fine-structure standards were measured: hydrated uranium ([U] = 500 ppm in double-distilled deionized water, pH 0.96), uranium in an acetic acid solution ([U] = 500 ppm in acetic acid [ratio of U to acetic acid, 1:100], pH 4.4), and a uranium phosphate solution ([U] = 500 ppm [ratio of U to P, 1:100], pH 1.5). In addition, to determine the average valence state of the U in a bio-oxidized sample, two U XANES powder standards (UO_2 and UO_3) were measured. The theoretical codes contained in the UWXAFS package (55) were used to analyze all data. The program FEFF7 (62) was used to construct the theoretical XAFS data on the basis of uranyl crystal structures, and the results are presented in Table 1. The results of a best-fit analysis of the experimentally obtained data with theoretically generated data indicated that the S02 best-fit values were 1.0 ± 0.2. The value for E0 was determined in the fit. For the standards, two different E0 values were used. The structural parameters determined in a fit to the U-containing biogenic Fe(III) oxide XAFS data included N_{degen} (coordination number), R (distance to the neighboring atoms for a single scattering path), and σ^2 (relative mean square displacement between the absorbing U atom and the neighboring atoms for a single scattering path). Fitting of the XAFS data for the U-containing biogenic Fe(III) oxides had three independent points and 12 variables. Error analysis and goodness-of-fit parameters were calculated with the fitting routine FEFFIT.

RESULTS AND DISCUSSION

Abiotic adsorption of HMR onto ferrihydrite. When the Fe(II) content of anoxic uninoculated basal culture medium

TABLE 1. Best-fit values for the XAFS data for the uranium-containing biogenic iron oxide sample[a]

Path	N_{degen}	R (Å)	σ^2 (10^{-3} Å^2)
U-Oax	2.0	1.797 ± 0.015	0.0 ± 0.2
U-Oeq	4.7 ± 4.5	2.379 ± 0.045	5.1 ± 15.3
U-Oeq	1.7 ± 0.7	2.161 ± 0.143	5.1 ± 15.3
U-Oax1–U-Oax1	2.0	3.594 ± 0.029	0.0 ± 0.7
U-Oax1–U-Oax2	2.0	3.594 ± 0.029	0.0 ± 0.7
U-Oax1–U-Oax2	2.0	3.594 ± 0.029	0.0 ± 0.7
U-Fe1	0.7 ± 0.2	2.921 ± 0.033	0.0 ± 15.4
U-Fe2	0.5 ± 0.4	3.521 ± 0.061	0.0 ± 15.4

[a] Path indicates the atom types in the scattering paths of the photoelectron that are included in the model of the experimental XAFS data. For example, U-Oax represents a single scattering path from a uranium atom to an axial oxygen atom and then back to the original uranium atom. U-Fe1 and U-Fe2 represent two unique single scattering paths with different distances between the U atom and the Fe1 or Fe2 atom. N_{degen} is the degeneracy of the specific path. For single scattering paths, the degeneracy is equal to the average number of atoms at the same average distance from the U atom, commonly referred to as the XAFS coordination number. R is one-half of the photoelectron path length described by the path. The R for a single scattering path is the average distance between the uranium atom and the backscattering atom. σ^2 is the relative mean square displacement about the equilibrium half-path length. σ^2 is commonly referred to as the XAFS Debye-Waller factor.

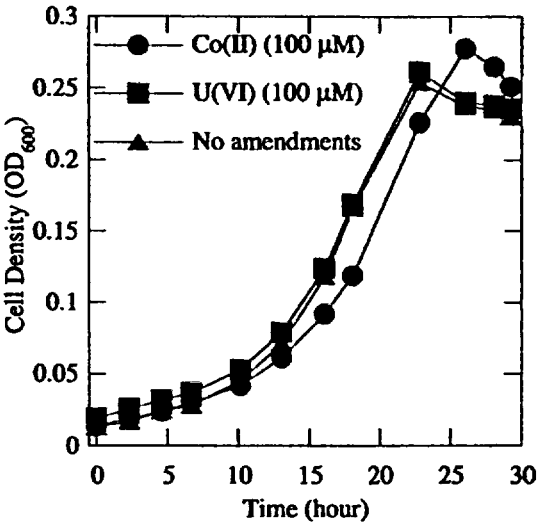

FIG. 2. Growth of *D. suillum* in the absence and in the presence of soluble uranium and cobalt. OD_{600}, optical density at 600 nm.

(11) was abiotically oxidized by a brief (1-min) exposure to air, an orange-brown precipitate, presumably amorphous ferric oxyhydroxide, rapidly formed within 1 h. Addition of Co(III) or U(VI) (100 μM) to the air-treated medium resulted in slow removal of the soluble metals from solution over a period of 120 days (Fig. 1). In contrast, if the anoxic Fe(II)-containing medium was exposed to oxygen after addition of the uranium or cobalt, the HMR were rapidly removed from solution, and complete removal was observed within 2 h (Fig. 1). Previous studies have similarly shown that metals such as cobalt, cadmium, lead, uranium, and radium are rapidly adsorbed by ferric iron mineral phases, especially amorphous ferric oxyhydroxide, and pulled from solution over time (2, 4, 51). In addition, some metals with lower ionic radii (e.g., Co^{2+} and Cd^{2+}) may be incorporated into the Fe(III) oxide structure as the amorphous Fe(III) oxides crystallize with age. These trace metals can become tightly bound into the Fe(III) oxide crystals (2) and thus become immobilized.

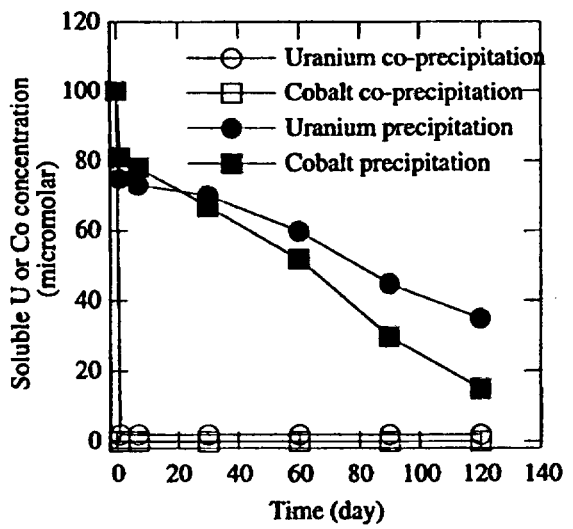

FIG. 1. Adsorption and precipitation of uranium and cobalt by Fe(III) oxides abiotically formed prior to and after addition of soluble U(VI) and Co(III).

Anoxic biological HMR immobilization. Addition of soluble U(VI) or Co(III) at a concentration of 100 μM had no effect on growth or on nitrate-dependent Fe(II) oxidation by *D. suillum* (Fig. 2). Similar to what was observed for abiotic oxidation of the Fe(II)-containing medium (see above), anaerobic biological oxidation of the Fe(II) by *D. suillum* in the presence of either Co(III) or U(VI) also resulted in rapid removal of the HMR from solution (Fig. 3). Interestingly, the removal of the U(VI) or Co(III) by the biogenically produced oxides was not as complete as the removal observed in the abiotic experiments, and only 55% of the initial 100 μM uranium was removed from solution. This difference in binding capacity between the abiotically produced Fe(III) oxides and the biogenic Fe(III) oxides may be the result of microbial cells bound to the reactive surfaces of the biogenically produced Fe(III) oxides, resulting in a decrease in available binding sites for HMR.

More cobalt (81% of the initial 100 μM) than uranium was removed from solution as a result of biological Fe(II) oxidation. When a similar experiment was performed with cadmium, 69% of the initial 100 μM was bound by the biogenically formed iron minerals. Comparison of the atomic radii of these ions (R_U = 1.75 Å, R_{Cd} = 1.55 Å, R_{Co} = 1.35 Å) to the atomic radius of Fe (1.4 Å) suggests that the amounts of U, Cd, and Co removed from solution are inversely related to the similarity of their sizes to the size of Fe.

Valence state and local chemical environment of uranium bound to the biogenic iron oxides. XANES is a useful technique for determination of the average valence state of uranium in samples (3, 9, 24, 37) as the energy position of the edge step (i.e., the increase in adsorption) is directly related to the valence state of the uranium. Comparison of the energy-

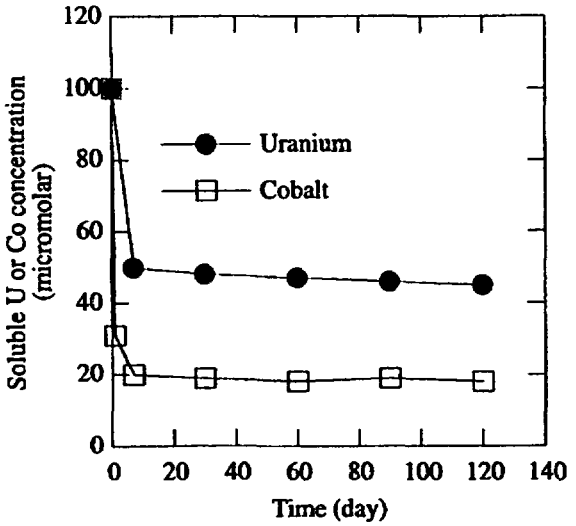

FIG. 3. Adsorption and precipitation of soluble uranium and cobalt by Fe(III) oxides biogenically formed after addition of U(VI) and Co(III).

aligned and step-height-normalized XANES data from the uranium content of the biogenically formed iron oxides produced by *D. suillum* with the data obtained with UO_2 [U(IV)] and UO_3 [U(VI)] standards indicated that the uranium was present only in the oxidized U(VI) state (Fig. 4A).

Theoretical models based on the crystal structure of hydrogen uranyl phosphate tetrahydrate (49) and sodium uranyl(VI) triacetate (58) were generated with the FEFF7 theoretical codes and used as preliminary models for the experimental XAFS data for uranium acetate, uranium phosphate, and hydrated uranyl solutions. The fit to the hydrated uranyl standard showed the importance of multiple scattering paths from the two closely bound axial oxygen atoms of the uranyl. Therefore, these multiple scattering paths were included in the fitting of the XAFS data for the bio-oxidized sample. Two distinct equatorial oxygen paths improved the quality of the fit for the biogenic sample, decreasing the reduced chi-square value by a factor of 2.6. The results of the best fit of the XAFS data indicated that two different equatorial oxygen groups were present in the biogenic uranium-iron oxide solids with approximately 4.7 oxygen atoms at 2.2 Å and 1.7 oxygen atoms at 2.4 Å (Table 1). The data in the Fourier transform region from 2 to 3.5 Å were modeled with two higher coordination shells containing all possible combinations of C, P, U, or Fe at ~2.9 and ~3.5 Å. The model that included two Fe shells was statistically better than any other model, reducing the reduced chi-square value by a factor of 3 to 7. Results of the fit to the experimental magnitude and real part of the Fourier transformed data are shown in Fig. 4B. The sum of the average numbers of Fe atoms in both higher coordination shells is consistent with one, indicating that uranyl was associated with the surface of the iron (hydr)oxides in two different geometries. A U-Fe distance of approximately 3.5 Å is consistent with U(VI) forming bidentate inner-sphere complexes with iron (hydr)oxide surfaces.

Similar uranium XAFS studies of uranium-iron (hydr)oxide

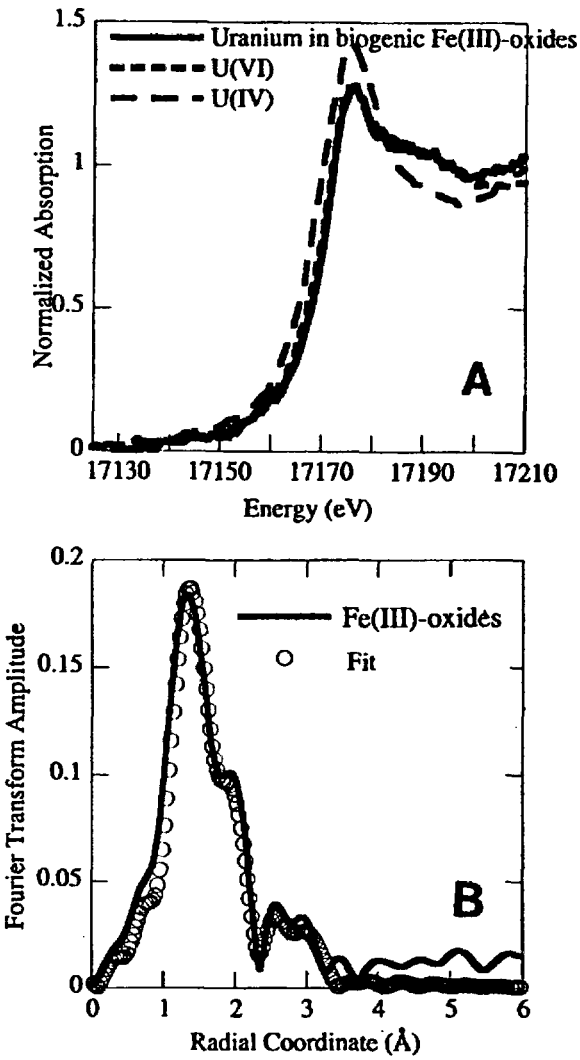

FIG. 4. (A) Energy-aligned and step-height-normalized XANES data from the UO_2 [U(IV)] and UO_3 [U(VI)] standards compared with data from the uranium content of biogenically formed iron oxides. (B) Magnitude and real part of the Fourier transformed $\chi(k)*k$ best-fit model and data from biogenic solids.

interactions have been described previously (6, 44, 60). Although U-C distances of ~2.9 Å have been reported in a previous study (6), the results from the fitting of our experimental data are better described with a U-Fe correlation of ~2.9 Å than with a U-C correlation at ~2.9 Å. It is important that in our experimental system there are a large number of crystallographic iron (hydr)oxide phases. Therefore, the shorter U-Fe distance reported here (to our knowledge, the first observation of its kind) may be due to an as-yet-unknown interaction between uranium and iron (hydr)oxide.

Potential remobilization of uranium as a result of biological Fe(II) oxidation. With a reduction potential (E'_0) of approximately −0.07 V at pH 7.0 for the U(VI)-U(IV) couple (26), it is possible that any insoluble U(IV) in the environment abiotically could react with biogenically produced Fe(III) to form

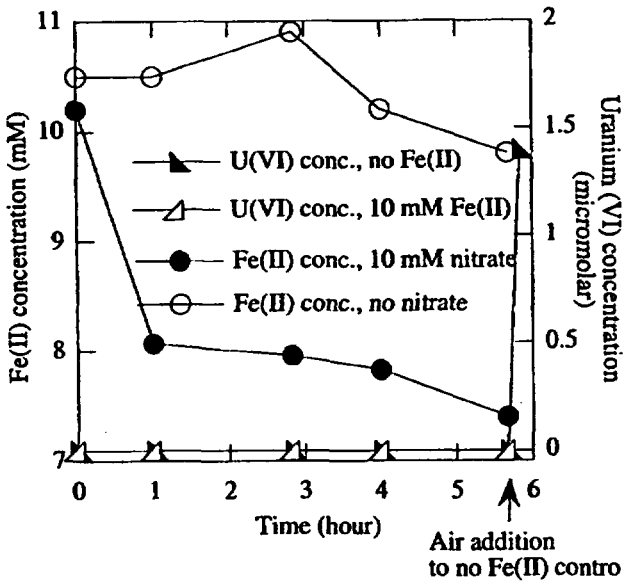

FIG. 5. Fe(II) bio-oxidation and uranium solubilization by an active culture of *D. suillum* with nitrate as the sole electron acceptor. conc., concentration.

soluble U(VI) and Fe(II). If anaerobic biogenically formed Fe(III) (hyd)oxides are to be utilized as a way to attenuate radionuclides in reducing environments, it is very important to ensure that metals such as uranium are not abiotically reoxidized and solubilized by these iron (hydr)oxides. To ensure that the bio-oxidation of Fe(II) did not result in resolubilization of any previously reduced and immobilized U(IV), an anaerobic washed cell suspension of *D. suillum* was amended with insoluble U(IV) and 10 mM $FeCl_2$ and with nitrate (10 mM) as the sole electron acceptor. Cation chromatography analysis indicated that in the absence of Fe(II), no U(VI) was present in solution, demonstrating that *D. suillum* cannot use reduced uranium as an electron donor (Fig. 5). If O_2 was added to the headspace of the control culture that was not amended with Fe(II), the uranium rapidly appeared in solution as U(VI), demonstrating that in the absence of the biogenically produced Fe(III) (hydr)oxides the U(IV) in this system was unstable and could readily be reoxidized and solubilized (Fig. 5). This was expected as U(IV) is notoriously unstable in the presence of oxygen (26). In samples amended with Fe(II), the uranium did not come back into solution during the incubation, although nitrate-dependent Fe(II) oxidation occurred rapidly, indicating that the insoluble uranium remained in an insoluble form regardless of its valence state in the presence of the biogenically formed Fe(III) (hydr)oxides (Fig. 5).

Oxidation of other metals. Many of the organisms known to be capable of dissimilatory Fe(III) reduction have also been shown to be capable of utilizing the oxidized forms of several other transition metals as alternative electron acceptors in place of Fe(III) (13, 14, 17, 18, 19, 21, 39, 40). It is currently not known if nitrate-dependent Fe(II) oxidizers can similarly utilize the reduced forms of other transition metals as surrogates for Fe(II). As outlined above, the results shown in Fig. 5 indicated that U(IV) was not oxidized by *D. suillum* with nitrate as the sole electron acceptor. Similar to the results observed for U(IV) (see above), when an anaerobic washed cell suspension of *D. suillum* in bicarbonate buffer was amended with 100 μM Co(II) as a potential electron donor and nitrate as the sole electron acceptor, no Co(III) was produced during incubation. In contrast, however, when a similar experiment was performed with Cr(III), small amounts of Cr(VI) were produced during the 4-h incubation, and a total of 2.5% of the initial Cr(III) was oxidized (data not shown). No Cr(III) oxidation occurred if the cells or the nitrate was omitted. If the initial Cr(III) concentration was increased to 500 μM, only 0.24% of the Cr(III) was oxidized (data not shown), suggesting that chromium toxicity may have affected enzymatic oxidation of the Cr(III) by the cells.

Significance. Anaerobic bio-oxidation of Fe(II) was only recently identified, and very little is known regarding the ubiquity and diversity of organisms capable of this metabolism. Previous studies have shown that Fe(II) oxidation is mediated by anoxygenic phototrophs (32, 61), as well as by various nitrate-respiring organisms (8, 29, 56, 57). Recent studies have also demonstrated that members of the newly described genera *Dechloromonas* and *Dechlorosoma* (1), isolated for their ability to grow by dissimilatory perchlorate reduction, also oxidize Fe(II) anaerobically with chlorate or nitrate as an alternative electron acceptor (11, 15, 20, 38, 48). Previous investigations demonstrated that nitrate-dependent Fe(II) oxidation by *D. suillum* was not limited to soluble Fe^{2+} ions and that insoluble Fe(II) bound up in mineral matrices was also available for these organisms (15). In addition, these studies also demonstrated that the oxidized iron end product formed [amorphous Fe(III) (hydr)oxide or carbonate-containing green rusts] was dependent on the rate of Fe(II) oxidation by this organism (15, 38). Both of these forms of iron are known to be unstable in the environment and are strong adsorbents for HMR (4, 5, 25, 30, 31).

The results of this study demonstrate that this metabolism offers a unique alternative for immobilization of toxic HMR in affected environments. Thus, selective anaerobic bio-oxidation of Fe(II) added to the environment may be an effective means of capping off and completing the attenuation of HMR in a reducing environment, allowing the system to naturally revert to an oxic state while preventing remobilization of previously reduced and immobilized HMR. This bio-oxidation process may be applied in two ways: (i) by precipitating Fe(III) (hydr)oxides over immobilized HMR in situ, forming an insoluble barrier that crystallizes with time, inhibiting future bioreduction, and adsorbing any leached HMR locally, or (ii) by engineering an Fe(III) oxide wall in situ, downstream of the immobilized HMR, which catches and adsorbs any HMR that may be solubilized and remobilized as a result of environmental fluxes, such as reoxidation (biotically or abiotically) or ligation.

ACKNOWLEDGMENTS

We thank L. A. Achenbach for a critical review of the manuscript.

Support for this research was provided by grant DE-FG02-98ER62689 from the Department of Energy NABIR Program. Use of the Advanced Photon Source was supported by the U.S. Department of Energy Basic Energy Sciences Office of Science under contract W-31-109-Eng-38. Work performed at the Materials Research Collaborative Access Team beamline is supported in part by the Department of Energy under grant DE-FG02-000ER45811.

REFERENCES

1. **Achenbach, L. A., R. A. Bruce, U. Michaelidou, and J. D. Coates.** 2001. *Dechloromonas agitata* gen. nov., sp. nov. and *Dechlorosoma suillum* gen. nov., sp. nov., two novel environmentally dominant (per)chlorate-reducing bacteria and their phylogenetic position. Int. J. Syst. Evol. Microbiol. **51:** 527–533.
2. **Ainsworth, C., J. Pilon, P. Gassman, and W. Van der Sluys.** 1994. Cobalt, cadmium, and lead sorption to hydrous iron oxide: residence time effect. Soil Sci. Soc. Am. J. **58:**1615–1623.
3. **Allen, P. G., D. K. Shuh, J. J. Bucher, N. M. Edelstein, T. Reich, M. A. Denecke, and H. Nitsche.** 1996. EXAFS determinations of uranium structures: the uranyl ion complexed with tartaric, citric, and malic acids. Inorg. Chem. **35:**784–787.
4. **Ames, L., J. McGarrah, B. Walker, and P. Salter.** 1983. Uranium and radium sorption on amorphous ferric oxyhydroxide. Chem. Geol. **40:**135–148.
5. **Ames, L. L., J. E. McGarrah, and B. A. Walker.** 1983. Sorption of uranium and radium by biotite, muscovite, and phlogopite. Clay Miner. **31:**343–351.
6. **Bargar, J. R., R. Reitmeyer, J. J. Lenhart, and J. A. Davis.** 2000. Characterization of U(VI)-carbonato ternary complexes on hematite: EXAFS and electrophoretic mobility measurements. Geochim. Cosmochim. Acta **64:** 2737–2749.
7. **Barkley, D. J., L. A. Bennett, J. R. Charbonneau, and L. A. Pokrajac.** 1992. Applications of high performance ion chromatography in the mineral processing industry. J. Chromatogr. **606:**195–201.
8. **Benz, M., A. Brune, and B. Schink.** 1998. Anaerobic and aerobic oxidation of ferrous iron at neutral pH by chemoheterotrophic nitrate-reducing bacteria. Arch. Microbiol. **169:**159–165.
9. **Bertsch, P. M., D. B. Hunter, S. R. Sutton, S. Bajt, and M. L. Rivers.** 1994. In situ chemical speciation of uranium in soils and sediments by micro X-ray absorption spectroscopy. Environ. Sci. Technol. **28:**980.
10. **Bopp, L. H., and H. L. Ehrlich.** 1988. Chromate resistance and reduction in *Pseudomonas fluorescens* strain LB300. Arch. Microbiol. **150:**426–431.
11. **Bruce, R. A., L. A. Achenbach, J. D. Coates.** 1999. Reduction of (per)chlorate by a novel organism isolated from a paper mill waste. Environ. Microbiol. **1:**319–331.
12. **Buffle, J.** 1988. Complexation reactions in aquatic systems. Wiley, New York, N.Y.
13. **Caccavo, F., J. D. Coates, R. A. Rossello-Mora, W. Ludwig, K. H. Schleifer, D. R. Lovley, and M. J. McInerney.** 1996. *Geovibrio ferrireducens*, a phylogenetically distinct dissimilatory Fe(III)-reducing bacterium. Arch. Microbiol. **165:**370–376.
14. **Caccavo, F., D. J. Lonergan, D. R. Lovley, M. Davis, J. F. Stolz, and M. J. McInerney.** 1994. *Geobacter sulfurreducens* sp. nov., a hydrogen- and acetate-oxidizing dissimilatory metal-reducing microorganism. Appl. Environ. Microbiol. **60:**3752–3759.
15. **Chaudhuri, S. K., J. G. Lack, and J. D. Coates.** 2001. Biogenic magnetite formation through anaerobic biooxidation of Fe(II). Appl. Environ. Microbiol. **67:**2844–2848.
16. **Coates, J. D., R. Chakraborty, S. M. O'Connor, C. Schmidt, and J. Thieme.** 2001. The geochemical effects of microbial humic substances reduction. Acta Hydrochim. Hydrobiol. **28:**420–427.
17. **Coates, J. D., T. Councell, D. R. Lovley, and D. J. Lonergan.** 1998. Carbohydrate-oxidation coupled to Fe(III) reduction, a novel form of anaerobic metabolism. Anaerobe **4:**277–282.
18. **Coates, J. D., D. J. Lonergan, and D. R. Lovley.** 1995. *Desulfuromonas palmitatis* sp. nov., a long-chain fatty acid oxidizing Fe(III) reducer from marine sediments. Arch. Microbiol. **164:**406–413.
19. **Coates, J. D., and D. R. Lovley.** Genus *Geobacter*. *In* G. M. Garrity (ed.), Bergey's manual of systematic bacteriology, 2nd ed., vol. 2, in press. Springer-Verlag, New York, N.Y.
20. **Coates, J. D., U. Michaelidou, R. A. Bruce, S. M. O'Connor, J. N. Crespi, and L. A. Achenbach.** 1999. Ubiquity and diversity of dissimilatory (per)chlorate-reducing bacteria. Appl. Environ. Microbiol. **65:**5234–5241.
21. **Coates, J. D., E. J. P. Phillips, D. J. Lonergan, H. Jenter, and D. R. Lovley.** 1996. Isolation of *Geobacter* species from a variety of sedimentary environments. Appl. Environ. Microbiol. **62:**1531–1536.
22. **Cowan, C. E., J. M. Zachara, and C. T. Resch.** 1991. Cadmium adsorption on iron oxides in the presence of alkaline-earth elements. Environ. Sci. Technol. **25:**437–446.
23. **Cross, J. L., and A. L. Frenkel.** 1998. Use of scattered radiation for absolute X-ray energy calibration. Rev. Sci. Instrum. **70:**38–40.
24. **Dent, A. J., J. D. F. Ramsay, and S. W. Swanton.** 1992. An EXAFS study of uranyl ion in solution and sorbed onto silica and montmorillonite clay colloids. J. Colloid Interface Sci. **150:**45.
25. **Domingo, C., R. Rodriguez-Clemente, and M. Blesa.** 1994. Morphological properties of alpha-FeOOH, gamma-FeOOH obtained by oxidation of aqueous Fe(II) solutions. J. Colloid Interface Sci. **165:**244–252.
26. **Dounce, A. L., and J. F. Flagg.** 1949. The chemistry of uranium compounds, p. 55–145. *In* C. Voegtlin and H. C. Hodge (ed.), Pharmacology and toxicology of uranium compounds. McGraw-Hill, New York, N.Y.
27. **Drever, J. I.** 1997. The geochemistry of natural waters. Prentice Hall, Upper Saddle River, N.J.
28. **Dzombak, D. A., and F. M. M. Morel.** 1990. Surface complexation modeling: hydrous ferric oxide. John Wiley and Sons, New York, N.Y.
29. **Hafenbradl, D., M. Keller, R. Dirmeier, R. Rachel, P. Rossnagel, S. Burggraf, H. Huber, and K. O. Stetter.** 1996. *Ferroglobus placidus* gen. nov., sp. nov., a novel hyperthermophilic archaeum that oxidizes Fe^{2+} at neutral pH under anoxic conditions. Arch. Microbiol. **166:**308–314.
30. **Hansen, H. C. B., and C. B. Koch.** 1998. Reduction of nitrate to ammonium by sulfate green rust—activation energy and reaction mechanism. Clay Miner. **33:**87–101.
31. **Hansen, H. C. B., C. B. Koch, H. Nancke-Krogh, O. K. Borggaard, and J. Sorensen.** 1996. Abiotic nitrate reduction to ammonium: key role of green rust. Environ. Sci. Technol. **30:**2053–2056.
32. **Heising, S., and B. Schink.** 1998. Phototrophic oxidation of ferrous iron by a *Rhodomicrobium vannielii* strain. Microbiology **144:**2263–2269.
33. **Hohl, H., and W. Stumm.** 1976. Interaction of Pb^{2+} with hydrous Al_2O_3. J. Colloid Interface Sci. **55:**281–288.
34. **Hungate, R. E.** 1969. A roll tube method for cultivation of strict anaerobes. Methods Microbiol. **3B:**117–132.
35. **Ishibashi, Y., C. Cervantes, and S. Silver.** 1990. Chromium reduction in *Pseudomonas putida*. Appl. Environ. Microbiol. **56:**2268–2270.
36. **Kemner, K. M., A. J. Kropf, and B. A. Bunker.** 1994. A low-temperature total electron yield detector for X-ray absorption fine structure spectra. Rev. Sci. Instrum. **65:**3667–3669.
37. **Koningsberger, D. C., and R. Prins.** 1988. X-ray absorption: principles, applications, techniques of EXAFS, SEXAFS, and XANES. Wiley, New York, N.Y.
38. **Lack, J. G., S. K. Chaudhuri, R. Chakraborty, L. A. Achenbach, and J. D. Coates.** Anaerobic bio-oxidation of Fe(II) by *Dechlorosoma suillum*. Microb. Ecol., in press.
39. **Lovley, D. R., and J. D. Coates.** 2000. Novel forms of anaerobic respiration of environmental relevance. Curr. Opin. Microbiol. **3:**252–256.
40. **Lovley, D. R., S. J. Giovannoni, D. C. White, J. E. Champine, E. J. P. Phillips, Y. A. Gorby, and S. Goodwin.** 1993. *Geobacter metallireducens* gen. nov. sp. nov., a microorganism capable of coupling the complete oxidation of organic compounds to the reduction of iron and other metals. Arch. Microbiol. **159:**336–344.
41. **Lovley, D. R., and E. J. P. Phillips.** 1988. Novel mode of microbial energy metabolism: organic carbon oxidation coupled to dissimilatory reduction of iron or manganese. Appl. Environ. Microbiol. **54:**1472–1480.
42. **Lovley, D. R., and E. J. P. Phillips.** 1992. Bioremediation of uranium contamination with enzymatic uranium reduction. Environ. Sci. Technol. **26:** 2228–2234.
43. **Lovley, D. R., E. J. P. Phillips, Y. A. Gorby, and E. R. Landa.** 1991. Microbial reduction of uranium. Nature **350:**413–416.
44. **Manceau, A., L. Charlet, M. C. Boisset, B. Didier, and L. Spadini.** 1992. Sorption and speciation of heavy metals on hydrous iron and manganese oxides. From microscopic to macroscopic. Appl. Clay Sci. **7:**201–230.
45. **Means, J. A., and D. A. Crerar.** 1978. Migration of radioactive wastes: radionuclide mobilization by complexing agents. Science **200:**1477–1481.
46. **Means, J. L., D. A. Crerar, and M. P. Borcsik.** 1978. Adsorption of Co and selected actinides by Mn and Fe oxides in soils and sediments. Geochim. Cosmochim. Acta **42:**1763–1773.
47. **Means, J. L., D. A. Crerar, M. P. Borcsik, and M. P. Duguid.** 1978. Radionuclide adsorption by manganese oxides and implications for radioactive waste disposal. Nature **274:**44–47.
48. **Michaelidou, U., L. A. Achenbach, and J. D. Coates.** 2000. Isolation and characterization of two novel (per)chlorate-reducing bacteria from swine waste lagoons, p. 271–283. *In* E. D. Urbansky (ed.), Perchlorate in the environment. Kluwer Academic/Plenum, New York, N.Y.
49. **Morosin, B.** 1978. Hydrogen uranyl phosphate tetrahydrate, a hydrogen ion solid electrolyte. Acta Crystallogr. Sect. B Struct. Crystallogr. Cryst. Chem. **34:**3732–3834.
50. **Moulin, V., and C. Moulin.** 1995. Fate of actinides in the presence of humic substances under conditions relevant to nuclear waste disposal. Appl. Geochem. **10:**573–580.
51. **Salomons, W., and U. Forstner.** 1984. Metals in the hydrocycle. Springer-Verlag, New York, N.Y.
52. **Saunders, J. A., M. A. Pritchett, and R. B. Cook.** 1997. Geochemistry of biogenic pyrite and ferromanganese coatings from a small watershed: a bacterial connection. Geomicrobiol. J. **14:**203–217.
53. **Schwertmann, U., and R. M. Taylor.** 1989. Iron oxides, p. 379–438. *In* J. B. Dixon and S. B. Weed (ed.), Minerals in the soil environment. Soil Science Society of America, Madison, Wis.
54. **Segre, C. U., N. E. Leyarovska, L. D. Chapman, W. M. Lavender, P. W. Plag, A. S. King, A. J. Kropf, B. A. Bunker, K. M. Kemner, P. Dutta, R. S. Duran, and J. Kaduk.** 2000. Synchrotron radiation instrumentation: eleventh U. S. conference, p. 419–422. American Institute of Physics, College Park, Md.
55. **Stern, E. A., M. Newville, B. Ravel, Y. Yacoby, and D. Haskel.** 1995. The UWXAFS analysis package: philosophy and details. Physica B **208–209:**117–120.

56. **Straub, K. L., M. Benz, and B. Schink.** 2001. Iron metabolism in anoxic environments at near neutral pH. FEMS Microbiol. Ecol. 34:181–186.
57. **Straub, K. L., M. Benz, B. Schink, and F. Widdel.** 1996. Anaerobic, nitrate-dependent microbial oxidation of ferrous iron. Appl. Environ. Microbiol. 62:1458–1460.
58. **Templeton, D. H., A. Zalkin, H. Ruben, and L. K. Templeton.** 1985. Redetermination and absolute configuration of sodium uranyl(VI) triacetate. Acta Crystallogr. Sect. C 41:1439–1441.
59. **Thurman, E. M.** 1985. Organic chemistry of natural waters. Martinus Nijhoff/Dr W. Junk Publishers, Boston, Mass.
60. **Waite, T. D., J. A. Davis, T. E. Payne, G. A. Waychunas, and N. Xu.** 1994. Uranium(IV) adsorption to ferrihydrite: application of a surface complexation model. Geochim. Cosmochim. Acta 58:5465–5478.
61. **Widdel, F., S. Schnell, S. Heising, A. Ehrenreich, B. Assmus, and B. Schink.** 1993. Ferrous iron oxidation by anoxygenic phototrophic bacteria. Nature 362:834–835.
62. **Zabinski, S. I., J. J. Rehr, A. Ankudinov, R. C. Albers, and M. J. Eller.** 1995. Multiple-scattering calculations of X-ray-absorption spectra. Phys. Rev. B 52:2995–3009.
63. **Zachara, J. M., R. L. Girvin, R. L. Schmidt, and C. T. Resch.** 1987. Chromate adsorption on amorphous iron oxyhydroxide in the presence of major groundwater ions. Environ. Sci. Technol. 21:589–594.

UNITED STATES DEPARTMENT OF THE INTERIOR
GEOLOGICAL SURVEY

Relative importance of organic carbon and sulfide sulfur in a Wyoming roll-type uranium deposit

by

Joel S. Leventhal and Elmer S. Santos

Open File Report 81-580
1981

Contents

Illustrations

Table

Abstract

Organic carbon, sulfide sulfur and uranium content in samples from the Highland uranium mine, Powder River Basin, Wyoming are presented. These data show strong statistical correlation between organic C and S and U and S, but not between U and organic C. This is interpreted to mean that sulfide is the concentrating agent for the uranium in this roll-type deposit. However, organic carbon (possibly introduced) is the energy source for sulfate-reducing bacteria.

Introduction

Organic carbon and sulfide sulfur are common constituents in many roll-type uranium deposits but their exact roles in ore-forming processes is not completely understood. In the primary uranium deposits of the Ambrosia Lake district in New Mexico, the organic matter obviously plays a major role as a concentrator of uranium (by chelation and ion exchange). In the south Texas deposits, many of which contain little or no organic matter, sulfur is the reductant and concentrator of uranium. In the Wyoming roll-type deposits, both organic carbon and sulfide sulfur are present, usually in small amounts (<1 percent).

Harshman (1974, p. 177) suggested that since "there was no direct correlation between uranium and organic content".... there is "considerable doubt on the belief that organic carbon was directly involved" for five roll-type deposits he studied. King and Austin (1966) give results for a series of samples collected an oxidized, ore and reduced rock from the Gas Hills. Their plots show increased organic C, S, and U in the ore zone. The ore-zone U and S are several percent, whereas the organic carbon is about 0.5 percent.

In this paper we report the results of a statistical analysis involving uranium, organic carbon, and sulfide sulfur in samples collected from a roll-type deposit in Wyoming, and we discuss the relative importance of organic carbon and sulfur as concentrators of uranium. Our interpretation of the statistical data gives conclusions that are similar to the model proposed by Langen and Kidwell (1974) and Dahl and Hagmaier (1974) and provides data for the models proposed by Rackley (1972) and Granger and Warren (1974).

Acknowledgements

We thank the officials of Exxon, USA for permission to sample their property, particularly W. C. Duke who made us aware of the unique exposure of the roll geometry on the floor of the open pit which enabled us to obtain clear samples of both oxidized and reduced rock adjacent to the roll. We also wish to thank Van Shaw, and Paul Briggs and Hugh Millard, U.S. Geological Survey, for the analytical work. We also thank Charles Pierson (USGS) for helping us with the multiple regression analysis and use of partial correlation coefficients.

Samples and Analyses

The samples were collected in 1978 at the Highland open pit mine situated in the southern part of the Powder River Basin, Wyoming (fig. 1). Our samples are from the uppermost of three ore bodies in three successive sand units. Drill hole 47-45 (fig. 1). 77 m (250 ft) N.45°W. of sample OX-1-2[illegible] encounters 4.6 m (15 ft) of ore in the lower part of a 8.4-m (36-ft)-thick sand. We believe our samples are from a plane through the nose of the roll (as opposed to the limb). The samples were collected from the floor of the pit

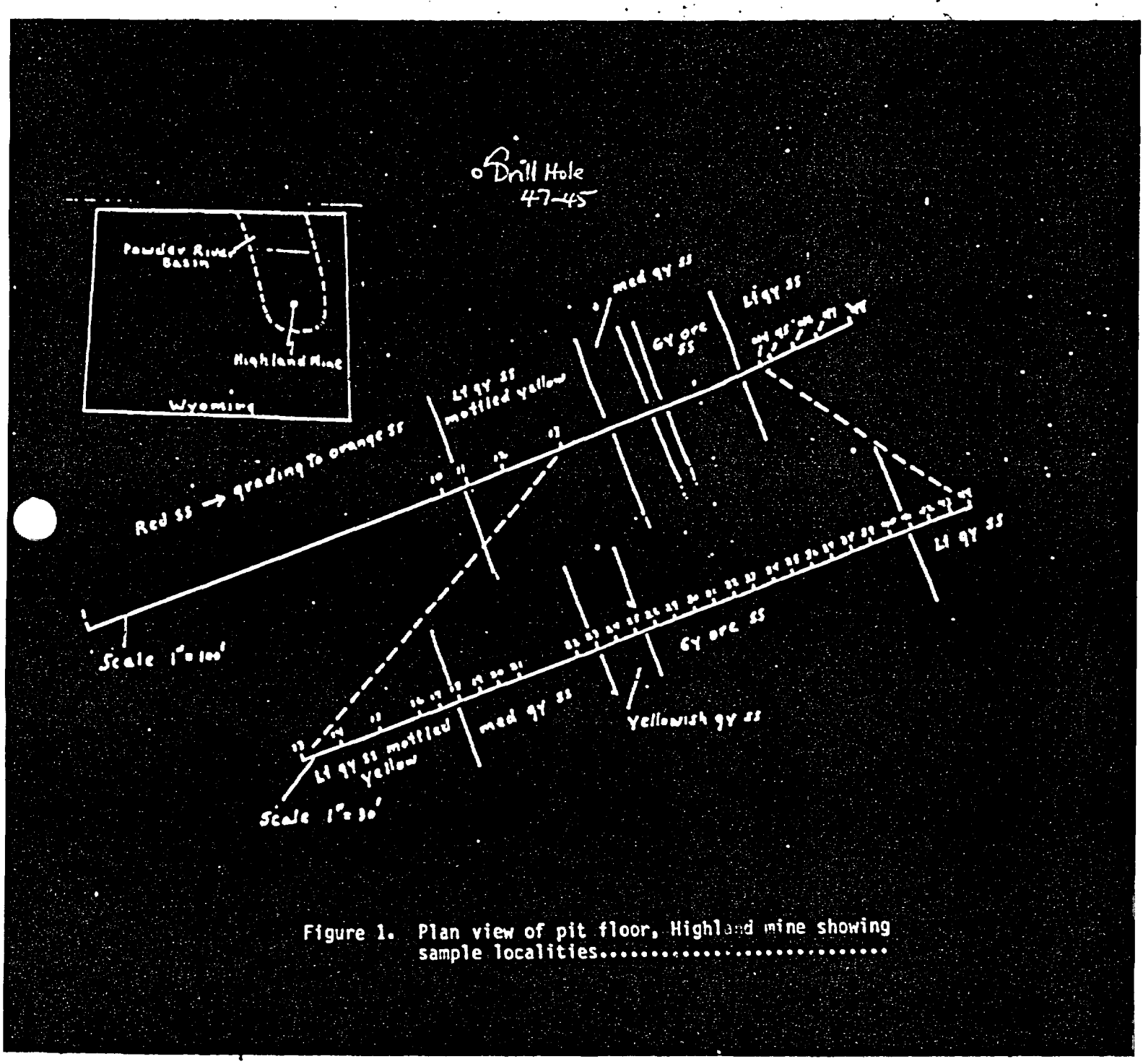

Figure 1. Plan view of pit floor, Highland mine showing sample localities.....

immediately after a swath of fresh rock, oriented perpendicular to the ore zone boundaries, had been exposed by a bulldozer cut. Samples were collected at 6- to 15-m (20- to 50-ft) intervals in oxidized rock remote from the ore zone, and at 1.5-m (5-ft) intervals through the ore zone as well as near its boundaries. Figure 1 shows the locality and spacing of samples. Santos (1981) gives a complete description and chemical analyses of the samples.

The samples were analysed by the usual methods (Leventhal and others, 1978; Leventhal and Shaw, 1980) which include total carbon by LECO combustion, carbonate carbon by titration, and organic carbon by difference. Sulfide sulfur was measured by LECO combustion after removal of sulfate sulfur. Uranium was measured by the delayed neutron method (Millard, 1976). The results of analyses are shown in table 1. Samples 1-15 are on the oxidized side of the roll, samples 16-22 and 25-41 are in ore, samples 23 and 24 are in a slightly oxidized bleached zone, and samples 42-48 are on the reduced side of the ore zone.

Statistical

Results from samples 16-41 were treated statistically for linear-least-squares fit to the equation $y=mx + b$, where y is the dependent variable, x is the independent variable, m is the slope, and b is the intercept. This was done in three ways: with uranium as y and sulfur as x; with uranium as y and organic carbon as x; and with sulfur as y and organic carbon as x. In each case, that removing one to four samples changed the correlation coefficient (r). The significance of the fit to the linear equation was judged by the r value and number of pairs of data values based on standard statistical

Table 1.--Analyses of 38 samples from the Highland mine

Sample No.	U (ppm)		Organic Carbon (percent)	Sulfide Sulfur (percent)
OX-1-1	5.5		0.04	<.01
10	12.0		.03	<.01
11	4.18	oxidized	.05	<.01
12	17.3	zone	.02	<.01
13	11.0		.03	<.01
14	392		.08	<.01
15	23.2		.04	<.01
16	625		.05	.01
17	603		.13	.01
18	5370		.14	.13
19	3450		.08	.01
20	1260		.09	.04
21	2380		.12	.03
22	832		.15	.01
23	28		.04	<.01
24	2000		.07	.02
25	1070		.18	.02
26	5620	ore	1.22	.51
29	2230	zone	.16	.07
30	5950		.28	.11
31	9600		.26	.17
32	2340		.59	.04
33	5580		.09	.07
34	1590		.03	.02
35	698		.13	.04
36	996		<.01	.02
37	1080		.21	.02
38	1130		.01	.01
39	659		.38	.04
40	621		.18	.01
41	1130		.10	<.01
42	135		.63	.09
43	120		.19	.01
44	271	reduced-	.26	.03
45	96.3	barren	.25	.06
46	83.9	zone	.18	.01
47	150		1.97	.09
48	24.7		.07	.04

tables. Multiple regression analysis was also run for the equation U=i + jC + kS, where i is a constant, j and k are slopes, C and S are carbon and sulfur, the independent variable, and U is uranium, the dependent variable. Partial correlation coefficients were also calculated for

$$r_{ij \cdot k} = \frac{r_{ij} - r_{ik} r_{jk}}{\sqrt{(1 - r_{ik}^2)(1 - r_{jk}^2)}}$$

(Krumbein and Graybill, 1965).

Discussion

Table 1 shows that, in many samples, the weight-percent of uranium exceeds that of sulfide-sulfur and organic carbon, but this low concentration of S and C relative to U does not violate the ideas presented here. As uranium was reduced, sulfide and organic C (if organic C was a reductant) were oxidized. Some organic carbon may also have been consumed by bacteria that reduced sulfate to sulfide. The reducing power of sulfide, when it is oxidized to sulfate, is such that about 25 times its weight of uranium can be converted from U^{+6} to U^{+4}. In the oxidation of sulfide to sulfate, 7 electrons per atom of sulfur (atomic wt. = 32) become available for the reduction of 3.5 atoms of uranium (atomic wt. = 238). Thus, 0.02 percent sulfide will reduce about 0.5 percent uranium. If the oxidation of sulfide is incomplete and stops at an intermediate stage, as when sulfide oxidizes to thiosulfate, about 10 times its weight of uranium could be reduced. Although greatly simplified here, the calculations involving the reduction of U that can be attributed to the complete or partial oxidation of sulfide are given by Warren and Granger (1973).

Figures 2, 3, and 4 show plots of the data for organic carbon versus sulfur, organic carbon versus uranium, and sulfur versus uranium. A rough increase of sulfur with increase of organic carbon (fig. 2), was observed in these samples. This increase may be similar to the covariance of C and S which has been observed in many recent and ancient sediments (Goldhaber and Kaplan, 1974, for review; Leventhal and Goldhaber, 1978; Leventhal, 1979) which is due to micro-organisms that utilize organic matter and sulfate to produce CO_2 and sulfide. This reaction does not go to completion, so the sediments contain the residual organic material and sulfide in a relatively constant proportion; hence the covariance of carbon and sulfur. This relation holds for in-situ (syngenetic or epigenetic) reactions but does not apply to migrated sulfides such as H_2S moving up faults (Goldhaber and others, 1979).

A statistical treatment involving carbon and sulfur was performed on samples 16 through 41, samples mostly in the ore zone (sample 23, not mineralized, was excluded in this and subsequent operations). Table 1 and figure 2 show that sample 26 is anomalous in that it contains much more of both carbon and sulfur than do the other samples in the group. When sample 26 is included, the statistical treatment yields an r value of 0.85, which is significant at the 99.9-percent level. When sample 26 is omitted, an r value of 0.32 is obtained, which is not statistically significant. Thus, one unusual (outlier) sample can change the statistical conclusions. For this reason we have done our statistics in several ways to see this effect. Inspection of the data reveals that samples 32 and 39 are also somewhat anomalous in that they have a higher carbon content than do the other samples in the group, coupled with a low sulfur content. Omission of samples 26, 32, and 39 yields an r value of 0.59, which is significant at the

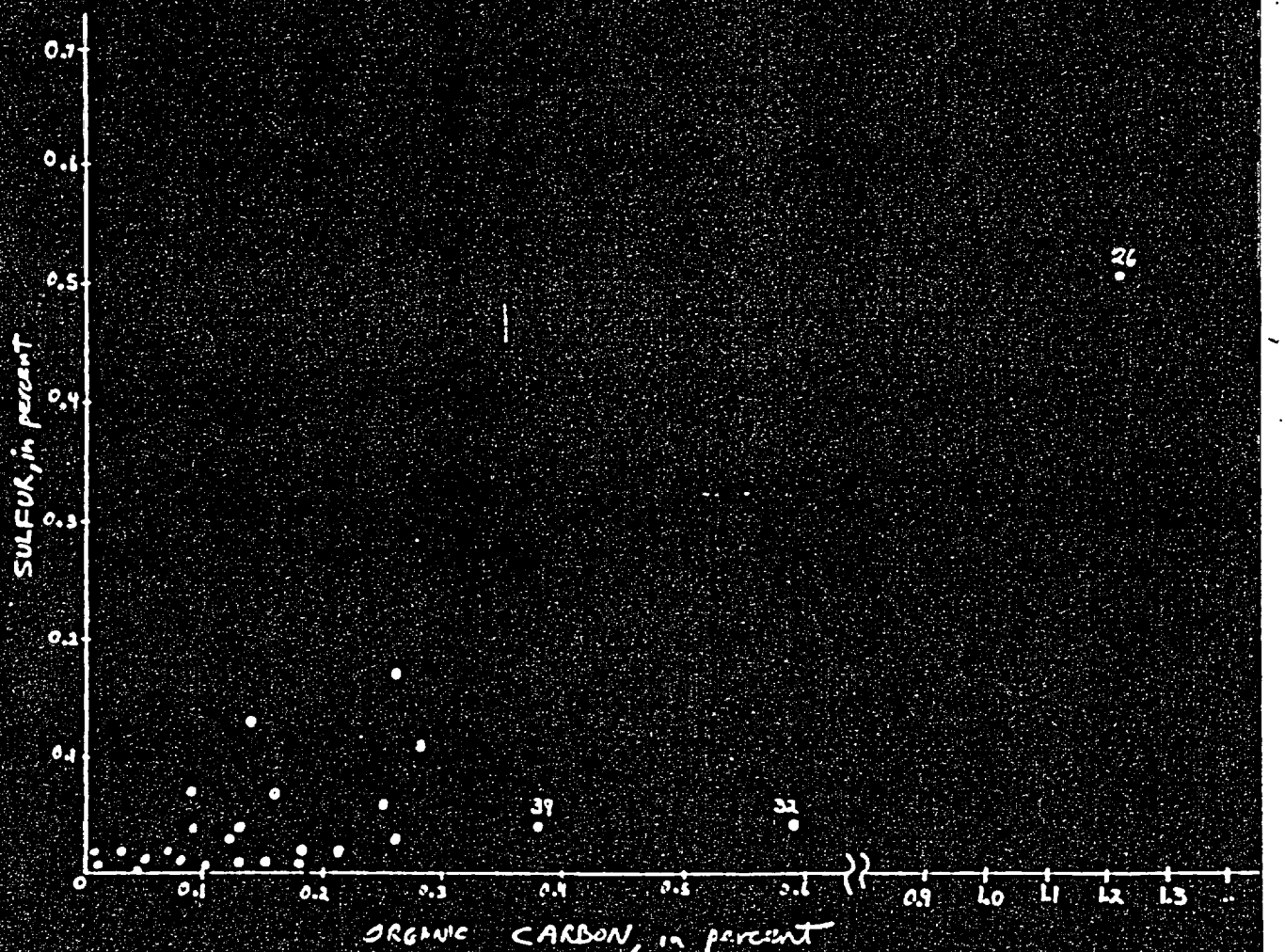

Figure 2. Plot of organic carbon versus sulfur
Numbers refer to sample number on table 1.

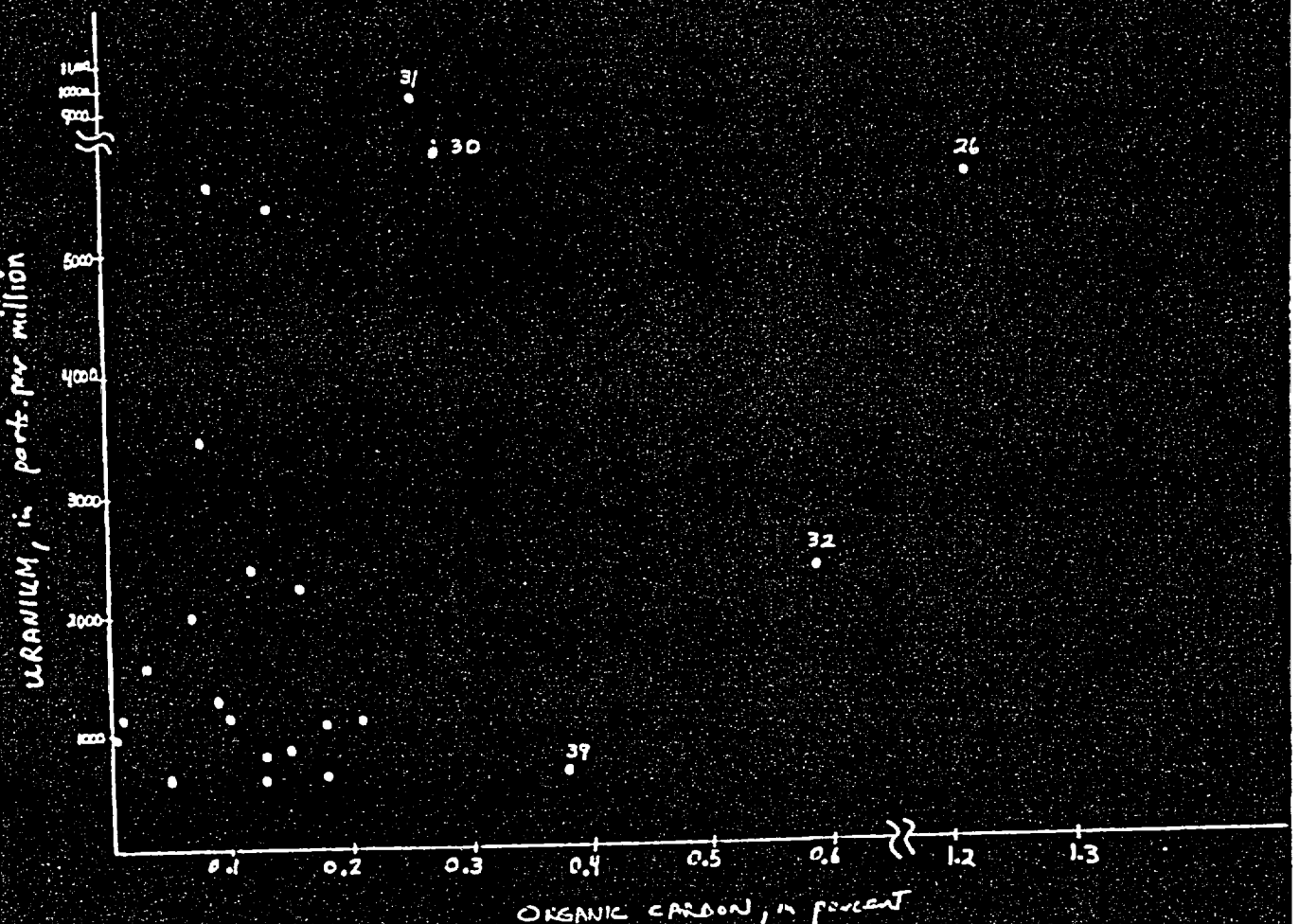

Figure 3. Plot of organic carbon versus uranium. Numbers refer to sample number on table 1.

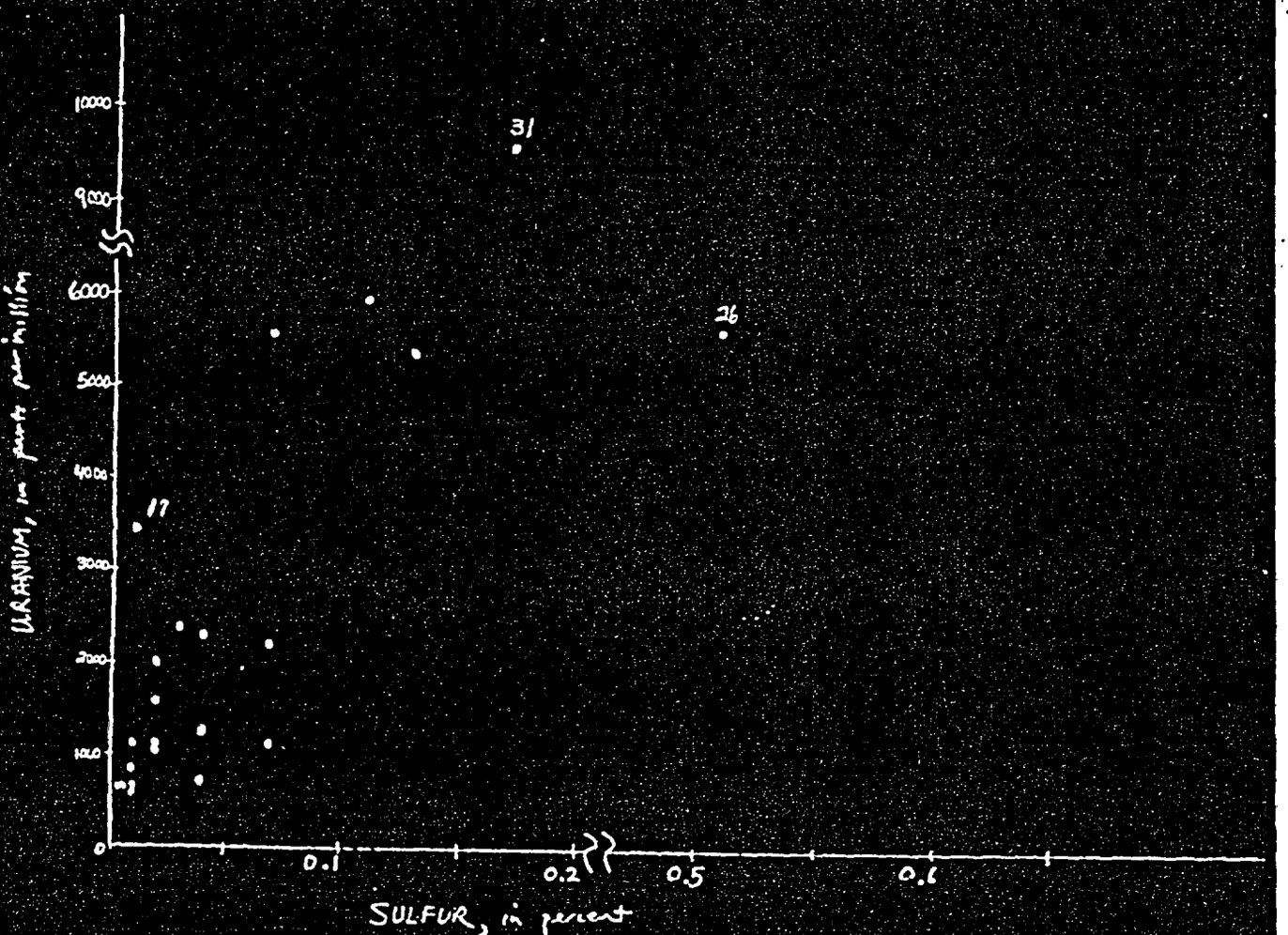

Figure 4. Plot of sulfur versus uranium. Numbers refer to sample number on table 1.

99 percent level. The correlation of carbon and sulfur, when the three samples mentioned are disregarded, suggests that *in situ* sulfate reduction may be the origin of the sulfide in the ore zone.

Linear-least-squares computation involving uranium and organic carbon yields an r value of 0.36 for all samples 16 through 41. In an analogous fashion to C and S data treatment, above, we find r values of 0.25, 0.32, 0.15, and 0.33 when various samples that might be considered anomalous (samples 26, 26 + 32, 26 + 32 + 31, and 26 + 32 + 31 + 39, respectively) are omitted singly or collectively (fig. 3). All these r values are less than 0.39, which is the value required for statistical significance (even) at the 90-percent level.

Linear-least-squares computation involving sulfur and uranium (fig. 4) yields an r value of 0.61 for all samples 16 through 41, which is significant at the 99-percent level. Omission of samples that might be considered anomalous (samples 26, 31, and 19), either singly or collectively, yields r values of 0.89, 0.81, and 0.87, which are all significant at the 99.9-percent level. The linear regression of U versus C, C versus S or U versus S on this small number of samples yields results that depend somewhat on choice of samples. However, the statistical significance seems to have only one interpretation (see Conclusions).

The complex geologic samples can be examined another way. Multiple regression analysis and partial correlation coefficients were calculated by C. T. Pierson (U.S. Geological Survey). The results show the following: For all 3 variables (C and S as independent), the equation is $U = 4.28 - 0.062\,C + 0.766S$. The correlation coefficients are $r_{UC} = .352$, $r_{US} = .688$, $r_{CS} = .569$. The partial correlation coefficient is $r_{UC.S} = -.067$, which is not

significant (0.35 is needed for even 90-percent significance), where $r_{UC.S}$, is the correlation coefficent for U and C with variable S is held fixed. Conversely, the $r_{US.C} = 0.634$, which is significant at the 99-percent level.

Conclusions

The results of these statistical analyses indicate that sulfur is much more closely related to uranium than is organic carbon for this roll-type deposit. Two related explanations are given: (1) The organic matter is not of primary importance as an agent to localize uranium in this particular roll-type deposit, but the sulfide is. (2) The fact that the organic matter and sulfide are genetically related is not violated: the sulfide migrates after formation and the residual organic matter is immobile; or perhaps mobile organic matter of external source was the energy source for sulfate reduction. Thus, carbon and sulfur both play essential, but distinct, roles in formation of this type of deposit.

References

Dahl, A. R., and Hagmaier, J. L., 1974, Genesis and characteristics of southern Powder River basin uranium deposits, Wyoming, USA, in Formation of uranium ore deposits; Internat. Atomic Energy Agency Proc., Vienna, p. 182.

Goldhaber, M. B., and Kaplan, I. R., 1974, The sulfur cycle, in E. D. Goldberg, ed., The Sea, v. 5, Marine Chemistry, Goldberg, ed., New York, John Wiley, p. 569-655.

Goldhaber, M. B., Reynolds, R. L., and Rye, R. O., 1978, Origin of a south Texas roll-type uranium deposit: Econ. Geol., v. 73, p. 1690-1705.

Granger, H. C., and Warren, C. G., 1974, Zoning in the altered tongue associated with roll type uranium deposits, in Formation of uranium ore deposits: Internat. Atomic Energy Agency; Proc., Vienna, p. 185-199.

Harshman, E. N., 1974, Distribution of elements in some roll-type uranium deposits, in Formation of uranium ore deposits; Internat. Atomic Energy Agency Proc., Vienna, p. 169-181.

King, J. W., and Austin, S. R., 1966, Some characteristics of roll-type uranium deposits at Gas Hills, Wyoming: Mining Engineering, v. 18, no. 5, p. 73-80.

Krumbein, W. C., and Graybill, F. A., 1965, Introduction to statistical models in geology: New York, McGraw Hill, p. 297-299.

Langen, R. E., and Kidwell, A. L., 1974, Geology and geochemistry of the Highland uranium deposit, Converse County, Wyoming: Mountain Geologist, v. 11, no. 2, p. 85-93.

Leventhal, J. S., 1979, The relationship between organic carbon and sulfide sulfur in recent and ancient marine and euxinic sediments [abs.]: Trans. Am. Geophys. Union, v. 60, p. 282.

Leventhal, J. S., and Goldhaber, M. B., 1978, New data for uranium, thorium, carbon, and sulfur in Devonian black shale, from West Virginia, Kentucky and New York: First Eastern Gas Shales Symposium (Oct. 17-19, 1977), Morgantown, MERC/SP-77-5 p. 183-221.

Leventhal, J. S., and Shaw, V. E., 1980, Organic matter in Appalachian Devonian black shale: Jour. Sed. Petrol., v. 50, p. 77-81.

Leventhal, J. S., Crock, J. G., Mountjoy, W., Thomas, J. A., Shaw, V. E., Briggs, P. H., Wahlberg, J. S., and Malcolm, M. J., 1978, Preliminary analytical results for a new U.S. Geological Survey Devonian Ohio shale standard, SDO-1: U.S. Geological Survey Open-File Report 78-447, 11 p.

Millard, H. T., Jr., 1976, Determination of uranium and thorium in USGS standard rock, in U.S. Geol. Survey Prof. Paper 840, p. 61-65.

Rackley, R. I., 1972, Environment of Wyoming Tertiary uranium deposits: Bull. Amer. Assoc. Petrol. Geol., v. 56, p. 755-774.

Santos, E. S., 1981, Analytical data on samples collected in the southern part of Powder River Basin, Wyoming, 1972-79: U.S. Geological Survey Open-File Report 81-83, 68 pp.

Warren, C. G., and Granger, H. C., 1973, Concept of growth and maturity of ore stage pyrite in roll-type uranium deposits: Jour. Research, U.S. Geol. Survey, v. 1, p. 151-155.

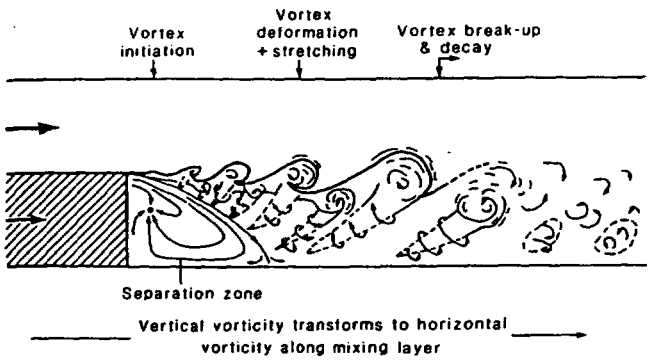

FIG. 3 A schematic model of mixing-layer distortion at the confluence of two flows of different depth. This planform diagram illustrates that deformation of the vertical mixing-layer vortices leads to the production of horizontal vorticity, enhanced mixing and fluid upwelling downstream of the confluence.

3). In Fig. 3 we illustrate a schematic model of this process of vortex and mixing-layer distortion.

Such complex three-dimensional deformation of the mixing layer is characteristic of all the unequal-depth mixing flows that we have studied. Although we have examined only zero degree confluence angles, mixing-layer distortion such as that described here can be expected at any junction in which the confluent channels are of different depths. The orientation of the separation zone is controlled by the planform geometry of the negative step, which in natural channels is formed by avalanche faces of tributary mouth bars which dip into the central confluence scour[1,5,6]. Consequently, the degree of entrainment of deeper-channel fluid into the separation zone and the position of the zone of upwelling will be dependent on the position of the tributary mouth bars, this itself being controlled by the junction angle and the ratio of discharges between the confluent channels[2,5,18]. This process of mixing-layer distortion and fluid upwelling may be invoked to explain patterns of fluid mixing at natural river junctions[22,23] where fluid from one channel is observed to upwell within the body of the other tributary flow downstream from the confluence.

The process we have outlined here has many implications. The dispersal of sediment at junctions across channel towards the shallower tributary may be greatly enhanced by such a depth differential between the confluent channels. This may influence erosion, through the position of the mixing layer and its associated higher Reynolds stresses, and deposition through control of the location of both zones of upwelling and the principal sediment transport pathways. Helical flow cells, which have been described at river channel confluences[1,20], may also originate from such depth-differential-controlled processes and not from any inherent helical flow where flows of equal depth combine. Attempts at modelling the near-field of side discharges in effluent dispersal[24] must also account for this mixing-layer distortion, which may significantly increase the potential for mixing across the shallower channel at a junction while simultaneously decreasing the rate of mixing across the deeper channel. Thus, effluents suspended in a deep channel may be rapidly transferred across the flow of a shallower channel when the two flows merge. □

Received 19 November 1990; accepted 18 February 1991.

1. Mosley, M. P. *J. Geol.* **84**, 535-562 (1976).
2. Ashmore, P. E. & Parker, G. *Water Resour. Res.* **19**, 342-402 (1983).
3. Roy, A. G. & Bergeron, N. *Geomorphology* **3**, 99-112 (1990).
4. Klassen, G. J. & Vermeer, K. *Proc. Int. Conf. Fluvial Hydraul.* Budapest, 1-14 (1988).
5. Best, J. L. *Sedimentology* **35**, 481-498 (1988).
6. Mosley, M. P. & Schumm, S. A. *Econ. Geol.* **72**, 691-694 (1977).
7. Reid, I., Best, J. L. & Frostick, L. E. in *Floods: Hydrological, Sedimentological and Geomorphological Implications* (eds Beven, K. & Carling, P.) 135-150 (Wiley, Chichester, 1989).
8. Bryant, I. D., Holyoak, D. T. & Mosely, K. A. *Proc. Geol. Ass.* **94(4)**, 321-343 (1983).
9. Best, J. L. & Brayshaw, A. C. *J. geol. Soc. Lond.* **142**, 747-755 (1985).
10. Soong, H. K. thesis, Univ. Connecticut (1976).
11. Hager, W. H. *J. hydraul. Engng* **115**, 243-259 (1989).
12. Sutherland, A. J. in *Proc. 9th Aus. Fluid Mech. Conf.* 259-263 (Univ. of Auckland, 1986).
13. Chu, V. H. & Babarutsi, S. *J. hydraul. Engng* **114**, 1257-1274 (1988).
14. Richards, K. S. *Water Resour. Res.* **16**, 241-244 (1980).
15. Best, J. L. & Reid, I. *J. hydraul. Engng* **110**, 1588-1594 (1984).
16. Roy, A. G. & Woldenberg, M. J. *J. Geol.* **94**, 401-411 (1986).
17. Roy, A. G. & Roy, R. *Earth Surf. Proc. Landf.* **13**, 77-84 (1988).
18. Best, J. L. *Soc. Econ. Palaeontologists and Mineralogists spec. Publ.* **39**, 27-35 (1987).
19. Kennedy, B. A. *Earth Surf. Proc. Landf.* **9**, 153-173 (1984).
20. Ashmore, P. E. *Earth Surf. Proc. Landf.* **7**, 201-225 (1982).
21. Winant, C. D. & Browand, F. K. *J. Fluid Mech.* **63**, 237-255 (1974).
22. Sternberg, H. O. *The Amazon River of Brazil* 74 (Steiner, Weisbader, 1975).
23. Roy, A. G. & De Serres, B. *Bull. Soc. Géog. Liège* **25**, 113-127 (1989).
24. McGuirk, J. J. & Rodi, W. *J. Fluid Mech.* **86**, 761-781 (1978).

ACKNOWLEDGEMENTS. We thank the Earth Sciences workshop at Leeds for construction of the mixing-flow apparatus. Travel for A.G.R. was made possible through a grant from FCAR; this paper was prepared while J.L.B. held a Royal Society/NSERC Anglo-Canadian Scientific Exchange Scheme Fellowship at the Université de Montréal that was also supported by the Foundation for Canadian Studies. We are grateful for the thoughtful comments of Jim Pizzuto.

Microbial reduction of uranium

Derek R. Lovley, Elizabeth J. P. Phillips, Yuri A. Gorby & Edward R. Landa

Water Resources Division, 430 National Center, US Geological Survey, Reston, Virginia 22092, USA

REDUCTION of the soluble, oxidized form of uranium, U(VI), to insoluble U(IV) is an important mechanism for the immobilization of uranium in aquatic sediments and for the formation of some uranium ores[1-10]. U(VI) reduction has generally been regarded as an abiological reaction in which sulphide, molecular hydrogen or organic compounds function as the reductant[1,2,5,11]. Microbial involvement in U(VI) reduction has been considered to be limited to indirect effects, such as microbial metabolism providing the reduced compounds for abiological U(VI) reduction and microbial cell walls providing a surface to stimulate abiological U(VI) reduction[1,12,13]. We report here, however, that dissimilatory Fe(III)-reducing microorganisms can obtain energy for growth by electron transport to U(VI). This novel form of microbial metabolism can be much faster than commonly cited abiological mechanisms for U(VI) reduction. Not only do these findings expand the known potential terminal electron acceptors for microbial energy transduction, they offer a likely explanation for the deposition of uranium in aquatic sediments and aquifers, and suggest a method for biological remediation of environments contaminated with uranium.

It is becoming increasingly clear that the reduction of metals in anaerobic environments is often the result of the direct enzymatic reduction by bacteria[14,15]. For example, the Fe(III)-reducing microorganism, strain GS-15, grows under anaerobic conditions by enzymatically coupling the oxidation of acetate to carbon dioxide with the reduction of Fe(III) to Fe(II)[16,17] according to:

$$CH_3COO^- + 8Fe(III) + 4H_2O \rightarrow 8Fe(II) + 2HCO_3^- + 9H^+$$

Thermodynamic calculations have indicated that, per electron transferred, acetate oxidation coupled to U(VI) reduction has the potential to yield more than twice the energy that is available from Fe(III) reduction[8]. When GS-15, grown on acetate and Fe(III), was inoculated into an anaerobic medium with acetate as the sole electron donor and U(VI) as the potential electron acceptor, U(VI) was reduced to U(IV) over time (Fig. 1*a*). Growth coincided with U(VI) reduction and stopped as U(VI) became depleted. When [2-^{14}C]-acetate was incorporated into the medium, $^{14}CO_2$ was generated in direct proportion to U(VI) reduction (Fig. 1*b*). In a separate experiment in which acetate concentrations were measured in cultures growing with U(VI) reduction, U(VI) and acetate loss over time were linearly related (correlation coefficient $r = 0.9$) with a U(VI)/acetate ratio of

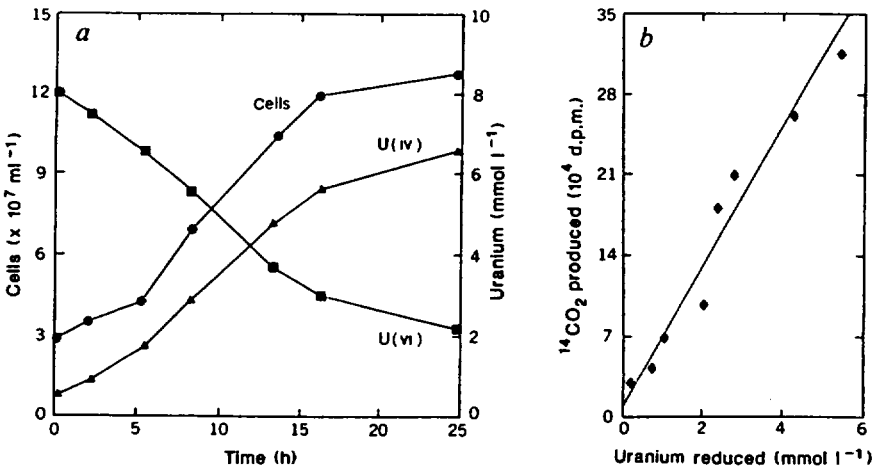

FIG. 1 Cell numbers, and U(VI) and U(IV) concentrations over time (*a*), and relationship between $^{14}CO_2$ production from [2-^{14}C]-acetate and U(VI) reduction (*b*) when GS-15 was inoculated into a medium with acetate as the electron donor and U(VI) as the electron acceptor. GS-15 obtained energy to support growth by reducing U(VI) to U(IV) while oxidizing acetate to carbon dioxide.
METHODS. Cells grown anaerobically at 30 °C in an acetate-Fe(III)-citrate medium[17] were inoculated into a similar medium but with Fe(III) replaced with 10 mmol l^{-1} uranyl chloride. Acetate concentrations were: 10 mmol l^{-1} (*a*) and 3.5 mmol l^{-1} (including 0.5 μCi of [2-^{14}C]-acetate (53 mCi/mmol)) (*b*). Cell numbers[17] and $^{14}CO_2$ produced[29] were determined as previously described. All manipulations for the determination of U(VI) and U(IV) concentrations were carried out in an anaerobic chamber. Subsamples were acidified with 12 N HCL to provide a final concentration of 4 N HCL. In (*a*), 2 ml of each acidified subsample were immediately added to a glass column (10-cm length, 1-cm inner diameter) containing Dowex AG1X8. As previously determined[8], on this column U(VI) is retained in 4 N HCl whereas U(IV) is not. The column was washed with 20 ml of 4 N HCL to collect the U(IV) and then washed with 20 ml of 0.1 N HCL to elute the U(VI). The concentrations of uranium in the U(VI) and U(IV) fractions were determined by directly aspirating the samples into a directly coupled plasma spectrometer and monitoring absorption at 424.167 nm. In (*b*), U(VI) in the anaerobic, acidified samples was analysed with a kinetic phosphorescence analyser (KPA-10, Chemchek Instruments), which uses a pulsed nitrogen dye laser and a complexing agent to measure U(VI) in solution. The loss of U(VI) as measured by this method could be accounted for by the production of U(IV) when samples were also analysed by the method used in (*a*).

3.6:1. Given that a small proportion of the acetate metabolized would be incorporated into cells, these results indicate that GS-15 can obtain energy for growth by oxidizing acetate with the reduction of U(VI) to U(IV) according to:

$$CH_3COO^- + 4U(VI) + 4H_2O \rightarrow 4U(IV) + 2HCO_3^- + 9H^+$$

Energy conservation from acetate oxidation coupled to U(VI) reduction should be through electron-transport and oxidative phosphorylation, because there is no known mechanism to generate net ATP through substrate level phosphorylation with acetate as the substrate. Subsequent studies have indicated that, in GS-15, electron transport to U(VI) proceeds through a respiratory chain containing cytochrome b_{558} (Y.G., manuscript in preparation). GS-15 is considered to reduce U(VI) directly rather than indirectly through reduction of Fe(III) with subsequent reduction of U(VI) by Fe(II), because Fe(II) did not reduce U(VI) in the growth medium and U(VI) was rapidly reduced in cell suspensions that had been repeatedly washed and resuspended in iron-free buffer.

One other organism, *Alteromonas putrefaciens*, is known to obtain energy for growth from electron transport to Fe(III)[18,19]. *A. putrefaciens* grew with H_2 as the sole electron donor and U(VI) as the electron acceptor (Fig. 2). In parallel studies, the stoichiometry of H_2 consumption and U(VI) reduction was consistent with the reaction:

$$H_2 + U(VI) \rightarrow U(IV) + 2H^+$$

Other electron donors for Fe(III) reduction by *A. putrefaciens* (formate, lactate, pyruvate) also supported U(VI) reduction.

Neither H_2 nor any of the organic electron donors for U(VI) reduction by GS-15 or *A. putrefaciens* reduced U(VI) in the absence of the organisms (Fig. 3 and data not shown). Furthermore, reduction of U(VI) in washed cell suspensions of GS-15 or *A. putrefaciens* was much faster than the reduction of U(VI) in the presence of a high concentration (1 mmol l^{-1}) of sulphide (Fig. 3). With extended incubation, cell suspensions of GS-15 reduced U(VI) concentrations below 0.4 μmol l^{-1}.

These results demonstrate that, although abiological reduction of U(VI) by sulphide, H_2 or organic compounds is typically considered to be the mechanism for U(VI) reduction in sedimentary environments[1,2,5,11], enzymatic reduction of U(VI) by microorganisms using U(VI) as a terminal electron acceptor is also possible. Furthermore, microbial reduction of U(VI) has the potential to proceed much more rapidly than abiological U(VI) reduction. Previous evidence for the potential of microorganisms to reduce U(VI) was the report that, in the presence of U(VI), crude cell-free extracts of *Micrococcus lactilyticus* consumed H_2 in quantities that were consistent with U(VI) reduction to U(IV)[20]. But these extracts reduced a wide range of metals with no evidence that the metal reduction was an enzymatic reaction or had any physiological significance in whole cells[15].

To evaluate more fully the relative potential for microbiological and abiological U(VI) reduction in reduced sediments, U(VI) was added to highly reduced methane-producing, sulphide-containing sediments of the Potomac River (Fig. 4). U(VI) reduction was much more rapid and extensive in the biologically

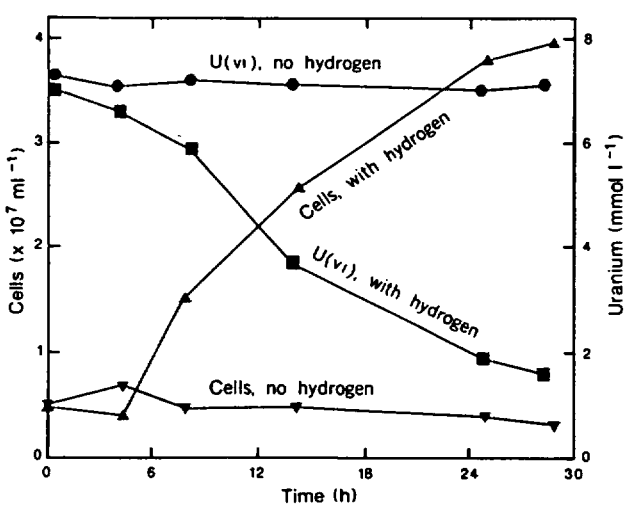

FIG. 2 Cell numbers and U(VI) and U(IV) concentrations over time when *Alteromonas putrefaciens* was inoculated into a U(VI)-containing medium with or without H_2. *A. putrefaciens* grew with the reduction of U(VI) to U(IV) in the presence of H_2, but not with H_2 omitted.
METHODS. Cells grown anaerobically at 30 °C with H_2 (60 kPa) as the electron donor and Fe(III)-citrate as the electron acceptor[18] were inoculated into a similar medium but with Fe(III) replaced with 10 mmol l^{-1} uranyl acetate. Controls had no added H_2. U(VI) was determined as in Fig. 1*b*.

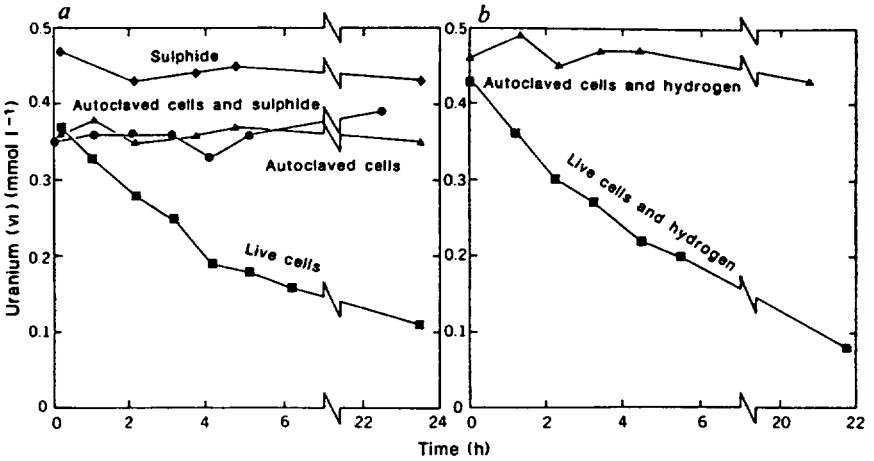

FIG. 3 U(VI) concentrations over time in the presence of various combinations of potential U(VI) reductants and cells of GS-15 (*a*) or *Alteromonas putrefaciens* (*b*). U(VI) was only reduced in the presence of actively metabolizing cells.
METHODS. Washed cells of Fe(III)-grown GS-15 (*a*) or *A. putrefaciens* (*b*) were suspended at 30 °C under N_2–CO_2 (80:20) in 10 ml of bicarbonate buffer ($NaHCO_3$, 0.025g; pH 6.7) containing uranyl acetate (0.4 mmol l^{-1}) to provide ~100 ng of cell protein per ml. Sodium sulphide (1 mmol l^{-1}) or H_2 (56 kPa) were added as noted. Aliquots were removed over time, flushed with N_2–CO_2 to remove sulphide if necessary, and U(VI) was determined as in Fig. 1*b*.

active sediments than in sediments in which the microorganisms were inactivated with heat. The microorganisms responsible for the U(VI) reduction were not identified, but these sediments do contain Fe(III)-reducing microorganisms which rapidly become active when an electron acceptor is added[21]. These results further suggest that models for U(IV) deposition in sedimentary environments should consider the possibility that microbial populations that have grown up with Fe(III), or possibly other electron acceptors, can reduce U(VI) entering these environments.

Geochemical evidence from a number of environments is consistent with U(VI) reduction by Fe(III)-reducing microorganisms leading to U(IV) deposition. For example, in marine sediments, deposition of U(IV) typically takes place within the sediment zone in which microorganisms oxidize organic matter with the reduction of Fe(III)[4–8,10]. Sulphide is unlikely to be the U(VI) reductant in these instances as sulphide does not accumulate in the Fe(III)-reducing zone of marine sediments. Furthermore, sulphide does not appear to reduce U(VI) in marine waters[9,22,23]. Abiological reduction of U(VI) by organic matter or H_2 in the Fe(III)-reducing zone of sediments also seems unlikely because organic-matter reduction of U(VI) is restricted to high temperature (>120 °C)[24,25] and, as shown above, at low temperatures, H_2 does not readily reduce U(VI) in the absence of microbial activity.

The common observation of U(IV) accumulations in the bleached 'reduction spots' of otherwise red, Fe(III)-rich rocks[26,27] provides another example in which uranium deposition is likely to be associated with the activity of Fe(III)-reducing bacteria. The lack of red colour in the reduction spots is due to localized reduction of Fe(III) which, recent evidence suggests, is the result of microbial Fe(III) reduction[26,28]. Even for environments such as sandstone- or roll-type uranium deposits, in which there is a co-accumulation of sulphide and U(IV) minerals, there is no direct evidence for sulphide reduction of U(VI) and other reduction mechanisms cannot be ruled out[12].

The potential for uranium contamination of surface and ground waters through uranium mining activities, irrigation of agricultural lands and disposal of nuclear wastes is an environmental concern. The results presented here suggest that, in many instances, it may be possible to immobilize uranium contamination by stimulating microbial U(VI) reduction in aquatic sediments or ground water. GS-15 and other Fe(III)-reducing microorganisms can oxidize important organic contaminants with Fe(III) as the electron acceptor[29,30]. Thus, in the case of 'mixed wastes', which contain both organic contaminants and radioactive metals, the activity of U(VI)-reducing bacteria might be able to couple the decomposition of toxic organic compounds with the immobilization of uranium. Other radioactive metals, such as plutonium and technetium, which have multiple redox states and are insoluble in the reduced form, could potentially be treated in a similar manner. □

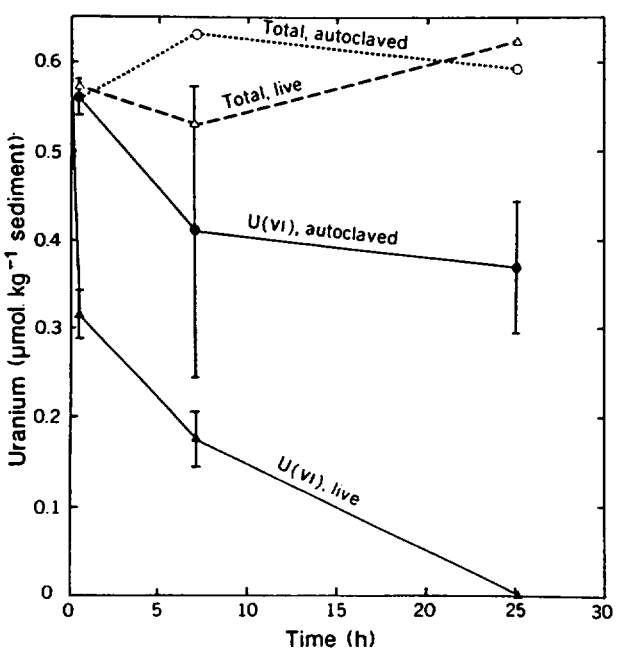

FIG. 4 Concentrations of U(VI) and total uranium over time in live and sterilized sediments. U(VI) was reduced much faster and more completely in live sediments, which reduced U(VI) below the detection limit of 2 nmol l^{-1} within 25 h.
METHODS. Uranyl acetate was added to anaerobically incubated, methane-producing sediments from the Potomac River in which sulphate had already been reduced to sulphide[21]. Sediments were autoclaved four times (121 °C, 1 h) for abiotic controls. Over time, subsamples (~0.3 g) were removed and extracted under anaerobic conditions in 5 ml of 100 mmol l^{-1} bicarbonate for 30 min. U(VI) was measured as in Fig. 1*b*. To determine total uranium in the extracts, U(IV) was first oxidized to U(VI) by bubbling the extract in air for 5 min.

Received 8 November 1990; accepted 15 January 1991.

1. Jensen, M. L. *Econ. Geol.* **53**, 598–616 (1958).
2. Hostetler, P. B. & Garrels, R. M. *Econ. Geol.* **57**, 137–167 (1962).
3. Turekian, K. K. & Bertine, K. K. *Nature* **229**, 250–251 (1971).
4. Bonatti, E., Fisher, D. E., Joensuu, O. & Rydell, H. S. *Geochim. cosmochim. Acta* **35**, 189–201 (1971).
5. Langmuir, D. *Geochim. cosmochim. Acta* **42**, 547–569 (1978).
6. Kadko, D. *Earth planet. Sci. Lett.* **51**, 115–131 (1980).
7. Colley, S. & Thomson, J. *Geochim. cosmochim. Acta* **49**, 2339–2348 (1985).
8. Cochran, J. K., Carey, A. E., Sholkovitz, E. R. & Surprenant, L. D. *Geochim. cosmochim. Acta* **50**, 663–680 (1986).
9. Anderson, R. F., LeHuray, A. P., Fleisher, M. Q. & Murray, J. W. *Geochim. cosmochim. Acta* **53**, 2205–2213 (1989).
10. Wallace, H. E. *et al. Geochim. cosmochim. Acta* **52**, 1557–1569 (1988).
11. Maynard, J. B. *Geochemistry of Sedimentary Ore Deposits* (Springer, New York, 1983).

12. Taylor, G. H. in *Biogeochemical Cycling of Mineral-Forming Elements* (eds Trudinger, P. A. & Swaine, D. J.) 485–514 (Elsevier, New York, 1979).
13. Mohagheghi, A., Updegraff, D. M. & Goldhaber, M. B. *Geomicrobiol. J.* **4**, 153–173 (1985).
14. Ehrlich, H. L. *Geomicrobiology* (Marcel Dekker, New York, 1990).
15. Ghiorse, W. C. in *Biology of Anaerobic Microorganisms* (ed. Zehnder, A. J. B.) 305–331 (Wiley, New York, 1988).
16. Lovley, D. R., Stolz, J. F., Nord, G. L. & Phillips, E. J. P. *Nature* **330**, 252–254 (1987).
17. Lovley, D. R. & Phillips, E. J. P. *Appl. environ. Microbiol.* **54**, 1471–1480 (1988).
18. Lovley, D. R., Phillips, E. J. P. & Lonergan, D. J. *Appl. environ. Microbiol.* **55**, 700–706 (1989).
19. Myers, C. R. & Nealson, K. H. *Science* **240**, 1319–1321 (1988).
20. Woolfolk, C. A. & Whiteley, H. R. *J. Bacteriol.* **84**, 647–658 (1962).
21. Lovley, D. R. & Phillips, E. J. P. *Appl. environ. Microbiol.* **53**, 2636–2641 (1987).
22. Anderson, R. F., Fleisher, M. Q. & LeHuray, A. P. *Geochim. cosmochim. Acta* **53**, 2215–2224 (1989).
23. Anderson, R. F. *Uranium* **3**, 145–164 (1987).
24. Breger, I. A. in *Formation of Uranium Ore Deposits* 99–124 (International Atomic Energy Agency, Vienna, 1974).
25. Nakashima, S., Disnar, J. R., Perruchot, A. & Trichet, J. *Geochim. cosmochim. Acta* **48**, 2321–2329 (1984).
26. Hoffman, B. A. *Chem. Geol.* **81**, 55–81 (1990).
27. Harrison, R. K. *G.B. geol. Surv. Bull.* **52**, 1–26 (1975).
28. Lovley, D. R., Chapelle, F. H. & Phillips, E. J. P. *Geology* **18**, 954–957 (1990).
29. Lovley, D. R. *et al. Nature* **339**, 297–299 (1989).
30. Lovley, D. R. & Lonergan, D. J. *Appl. environ. Microbiol.* **56**, 1858–1864 (1990).

ACKNOWLEDGEMENTS. We thank Ruth Smith and Ray Van Hoven for technical assistance and Ron Oremland, Tom Kraemer, Marty Goldhaber, Rich Reynolds and Richard Smith for helpful discussions. This study was supported by the US Geological Survey Toxic Waste/Groundwater Contamination Programme.

Evidence for volcanic eruption on the southern Juan de Fuca ridge between 1981 and 1987

William W. Chadwick Jr*, Robert W. Embley† & Christopher G. Fox†

* OSU/CIMRS, Hatfield Marine Science Center, Newport, Oregon 97365, USA
† PMEL/NOAA, Hatfield Marine Science Center, Newport, Oregon 97365, USA

THE formation of new ocean crust at mid-ocean ridges is known to be a discontinuous process in both space and time, but little is known about the frequency and duration of eruptions along an active ridge segment. Here we present evidence, from Sea Beam surveys and underwater photography, for the eruption of lavas along a segment of the Juan de Fuca ridge between 1981 and 1987. Although previous studies have inferred volcanic activity on ridges in areas where recent seismicity or young lava flows have been observed[1–4], none has yet had direct evidence to date such a recent submarine eruption. The temporal coincidence between this eruptive episode and the megaplumes (huge, sudden emissions of hot mineral-laden water) observed over this part of the ridge[5,6] in 1986 and 1987 supports previous suggestions[5–10] that megaplumes are caused by sea-floor spreading events.

The lavas that were erupted during the 1980s occur as a series of pillow mounds and ridges between 45°00.5′ N and 45°09.5′ N along the northern Cleft segment (Fig. 1). The evidence for the recent eruption of these lavas was first discovered through a discrepancy between microbathymetry derived from a towed camera system and bathymetric charts based on Sea Beam surveys. Three camera tows (collected in 1989 from the National Oceanic Atmospheric Administration (NOAA) ship *Discoverer*) over the southernmost pillow mound (mound 1, Fig. 1) showed glassy lava flows forming a 35-m-high hill, ~1 km in diameter. Earlier Sea Beam bathymetry (based on data collected in May 1981 from the NOAA ship *Surveyor*) shows no such hill, but instead a gentle slope to the east (Fig. 2*a*). The Sea Beam and camera-tow bathymetry correspond closely in other areas.

Other surveys confirm the recent appearance of mound 1. Bathymetry from Sea Beam surveys conducted over the same area by the research vessel *Atlantis II* in September 1987 and by the *Discoverer* in August 1990 shows a 25-m-high mound in the exact location of the glassy lavas delineated by the camera tows (Fig. 2*b*). Mound 1 was also imaged by a SeaMARC I sidescan survey in August 1987 from the *Discoverer*, and appears as an unfractured positive relief feature which covers pre-existing fractures (Fig. 3). The date of eruption of mound 1 is further restricted by a single Sea Beam swath collected during a camera tow by the *Surveyor* in June 1983. Although the data only sample the western edge of mound 1, the coverage is adequate to show that the 1983 swath has the same pre-eruption depth contours as the 1981 Sea Beam survey, and does not show the contours of the new lava mound. These Sea Beam surveys definitely constrain the time of the eruption of mound 1 to between 1981–1987, and probably to between 1983–1987.

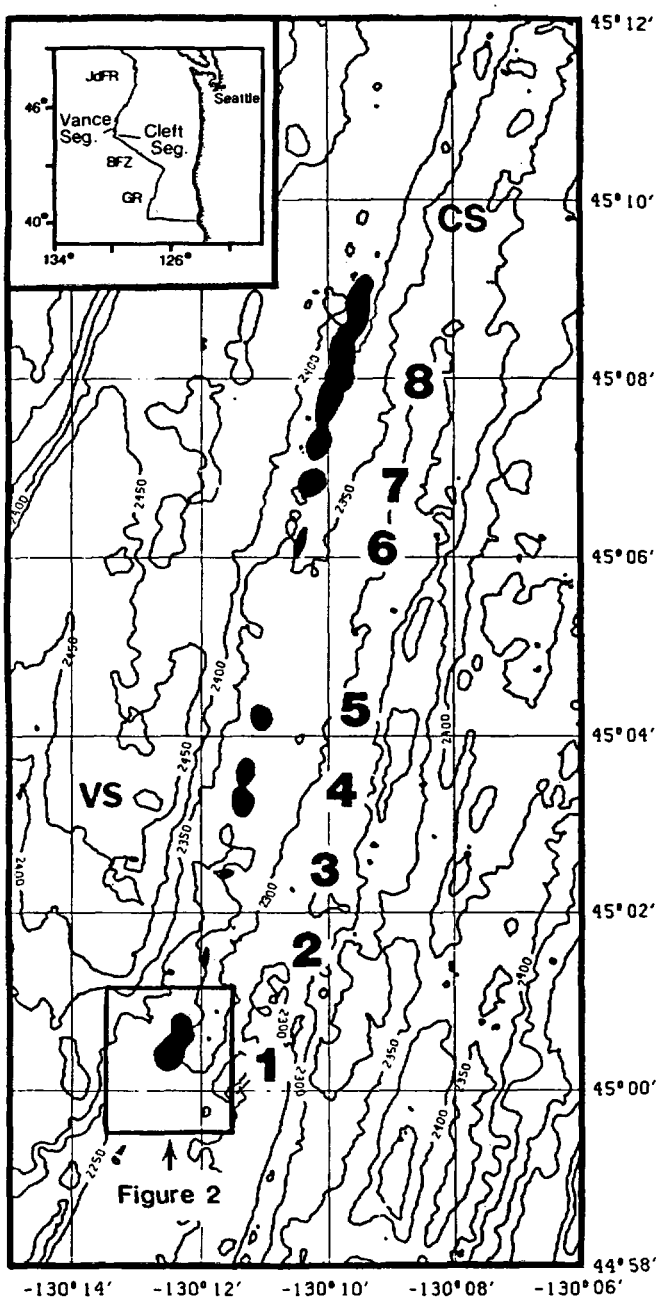

FIG. 1 Sea Beam bathymetric map of overlap region between Cleft and Vance segments, southern Juan de Fuca ridge (50-m contours); CS is northern end of Cleft segment, VS is southern end of Vance segment. Solid black areas show locations of new pillow lava mounds. Numbers to right of each mound are for identification in text. Box around mound 1 shows outline of Fig. 2. On inset map, GR is Gorda ridge, BFZ is Blanco Fracture Zone, and JdFR is Juan de Fuca ridge.

Environ. Sci. Technol. 2000, 34, 3229–3234

In Situ Stabilization of Metal-Contaminated Groundwater by Hydrous Ferric Oxide: An Experimental and Modeling Investigation

TODD A. MARTIN* AND
J. HOUSTON KEMPTON
Exponent, 4940 Pearl East Circle, Suite 300, Boulder, Colorado 80301

A potential method is investigated for remediation of metal-contaminated groundwater by in-situ emplacement of an adsorptive coating on the aquifer matrix. The coating is emplaced by sequentially injecting solutes that react as they mix in the aquifer to form a sparingly soluble solid with a high metal-adsorption capacity. Dissolved metals are removed passively as groundwater flows through the treated aquifer. The potential effectiveness of this method was demonstrated by sequentially injecting first ferrous sulfate and then oxygen solutions into a column of unconsolidated sand, producing a coating of hydrous ferric oxide (HFO) as the unretarded oxygen reacted with Fe(II) bound to the sand. The HFO delayed the breakthrough of Cr(VI) and As(V) by 8 and 30 pore volumes, respectively, relative to the unamended material. Attenuation of solutes by the unamended sand was reaction-rate limited, but coupled transport/equilibrium geochemical modeling matched well with the increased metal attenuation by the coating. Potential advantages of this method include the following: (1) coatings are emplaced preferentially in high-conductivity zones, reducing problems caused by aquifer heterogeneity; (2) surface disturbance is minimal; (3) regeneration of the coating is straightforward; (4) no hazardous material is generated; and (5) existing geochemical models can help extrapolate to larger scales.

Introduction

Remediation of contaminated groundwater remains one of the most intractable problems of environmental restoration. Contaminants typically enter groundwater at concentrations that are thousands or even millions of times above risk-based action levels and then disperse as they are carried through aquifers in flowing groundwater. The typical result is a large volume of groundwater with contaminant concentrations that exceed regulatory standards. Remediation is complicated by a combination of physical limits, such as incomplete delineation of source areas and plume extent, restricted access to the subsurface, differential solute transport due to subsurface heterogeneity, and contaminant diffusion out of low-permeability zones. Chemical phenomena, such as slow dissolution of contaminant sources or slow desorption from the aquifer matrix, further limit the success of remedial efforts.

* Corresponding author phone: (303) 444-7270; fax: (303) 444-7528; e-mail: martint@exponent.com.

The magnitude of the groundwater contamination problem is immense: 300 000–400 000 sites nationwide contain contaminated soil and/or groundwater (*1*). Of the Superfund sites for which Records of Decision have been issued, 75% contained some form of metals contamination (*2*). Federal expenditures on cleanup of contaminated sites are expected to be between $234 and $389 billion over the next 75 years, with combined expenditures for cleanup of all private and public U.S. sites projected to be between $500 billion and $1 trillion (*3*). The high cost of restoring these sites is related, in part, to the difficulty of remediating groundwater using existing technologies. There is thus a clear need for alternative technologies to clean up contaminated groundwater. In this paper, we investigate a potential new in-situ method for remediating metal-contaminated groundwater by coating contaminated aquifers with an adsorptive substrate, which then passively removes metals from solution.

Available Groundwater Remediation Technologies

Although available techniques for cleanup of metals-contaminated groundwater can be highly effective, all have cost or practicability considerations that limit their utility for specific applications. For example, pump-and-treat technology—flushing water from an aquifer until contaminant concentrations drop below target cleanup levels—is effective at containing groundwater plumes. However, posttreatment audits of field-scale systems have demonstrated that this technology has high short- and long-term operating costs (*4*, *5*), and a recent evaluation of 77 pump-and-treat systems found that regulatory standards had been achieved at only about 10% of the sites evaluated (*1*). The failure of pump-and-treat remediation to meet cleanup goals can be attributed to ineffective containment of point sources, or to the slow release of contaminants from the aquifer itself by desorption, diffusion out of dead-end pore spaces, or diffusion from macro-scale low-conductivity zones.

In-situ technologies have the potential to provide passive or semipassive treatment with minimal long-term operational requirements and site disturbance but often suffer from chemical or physical limitations. Electrokinetic separation techniques, which induce the migration and recovery of ions in groundwater using electrical currents (*3*), have limited effectiveness due to production of H^+, which has high ionic mobility relative to most metals (*6*). Permeable reactive subsurface walls, often used with impermeable walls to focus the flow of contaminated groundwater, are becoming an accepted technology (*1*, *7*) and have been used to achieve in-situ immobilization of U, Mo, Cr(VI), Sr, Tc, and Ni using various adsorption, reduction, and precipitation reactions (*8*–*13*). While these technologies operate passively after installation, few of the reactive wall materials currently used in practice (*14*) can be cost-effectively regenerated in place, and thus they may require periodic excavation and renewal. Furthermore, reactive subsurface walls are less practical where plumes are large, groundwater is deep, or surface features complicate excavation. Newly developed techniques for containing contamination through in-situ aquifer permeability reduction, such as grouting with supersaturated gypsum solutions (*15*) or microbially produced polysaccharides (*16*), seem promising for controlling point sources but are less practical for dispersed plumes.

In-situ geochemical stabilization techniques, of which the method presented in this paper is one, reduce contaminant mobility by decreasing its solubility (*3*). In-situ metal sulfide precipitation has been achieved by direct injection of calcium polysulfide (*17*) and by passive sulfide leaching from a peat

10.1021/es980861w CCC: $19.00
Published on Web 06/23/2000

and gypsum substrate (*18*), although permanent stability presumably would require continued exclusion of oxygen to avoid oxidation and remobilization of metals. Laboratory tests indicate that injection of zeolites, immobilized organic chelates, and microbes can reduce metal solubility in situ (*6*). Ferrous iron injection has been shown to be a potentially effective approach to immobilizing Cr(VI) by inducing its reduction to less soluble Cr(III) (*19*). Laboratory tests have demonstrated that in-situ emplacement of HFO in aquifers—apparently by injecting an acidic Fe(III) solution (*6*) or by simple oxygen injection alone (*20*)—produces an adsorptive substrate with minimal decrease in aquifer permeability (*3*).

In Situ Remediation by Emplacing an Adsorptive Coating

The conceptual remedial method presented in this investigation involves injecting a series of soluble components into the aquifer, where they react and precipitate as they mix in situ, coating the aquifer with an insoluble, nontoxic substrate that has a high affinity for trace-metal contaminants. This substrate produces a passive treatment zone in the aquifer, which provides long-term remediation of metals-contaminated groundwater.

Inducing in-situ precipitation reactions to form an adsorptive substrate requires that the sequentially injected reactants mix completely within the aquifer. Field-scale tests have demonstrated that dispersion can provide for microscale in-situ mixing of sequentially injected solutes at distance from injection wells (*21*). However, aquifer dispersivity is generally scale dependent—an artifact of variable solute transport rates in the different strata, rather than true dispersion (*22*), and standard aquifer dispersivity calculations may significantly overestimate actual subsurface solute mixing. We have thus assumed that substrate precipitation reactions would be more complete if mixing occurred by differential transport rates rather than by physical dispersion. Differential solute transport rates are more easily quantified than microscale dispersion, allowing more control over the location of substrate emplacement. In practice, in-situ mixing is achieved by sequentially injecting soluble reactants, slowest-migrating component first, so that precipitation reactions occur as faster-moving solutes overtake slower ones in the aquifer, coating the aquifer matrix with the adsorptive substrate.

Ideal substrates should precipitate from a mixture of reactants that have high solubility, low toxicity, differential retardation in the aquifer, and rapid (or at least accurately known), homogeneous reaction kinetics. The resulting substrate should be chemically stable and should have a large surface area and high affinity for metals, and ideally, accurate thermodynamic adsorption parameters should be available to allow modeling of adsorptive attenuation of dissolved metals. For this bench-scale testing, hydrous ferric oxide (HFO), typically reported as FeOOH or $Fe(OH)_3$, was selected as a substrate that met these criteria. HFO is sparingly soluble at groundwater pH greater than 4−5 s.u. ($K_{sp} = 10^{-38}$), provided that conditions remain sufficiently oxidizing to prevent reduction of Fe^{3+} back to Fe^{2+}. HFO has a large surface area (~600 m^2/g), a strong affinity for many dissolved metals (*23*), and fast metal adsorption kinetics (e.g., typically equilibrating in a few hours) (*24*). The adsorption of metals by HFO is pH dependent, and the effects of pH vary between metals, so groundwater pH is an important consideration in evaluating the efficacy of the use of HFO as an in-situ adsorptive substrate. Parameters for diffuse-layer adsorption to HFO have been compiled for most metals and common anions (*23*) and incorporated into geochemical models (*25*), allowing for prediction of metal removal efficiency by the HFO coating.

Precipitation of HFO in the test column was achieved by sequentially injecting an anoxic $Fe(SO_4)$ solution, followed by oxygenated water. The HFO precipitation proceeded in two steps—oxidation of Fe(II) by

$$Fe^{2+} + H^+ + \frac{1}{4}O_2 \rightarrow Fe^{3+} \frac{1}{2}H_2O \qquad (1)$$

then precipitation of HFO by

$$Fe^{3+} + 3H_2O \rightarrow Fe(OH)_{3(s)} + 3H^+ \qquad (2)$$

$FeSO_4$ is highly soluble ($K_{sp} = 10^{0.46}$) under near-neutral pH conditions; dissolved oxygen concentrations approaching 44 mg/L can be achieved by purging with purified oxygen gas (PO_2 = 1 atm; T = 20 °C; $H = 10^{4.6}$ atm) or much higher if added as H_2O_2. Dissolved oxygen injected into the subsurface can be consumed by reduced minerals or by microbial respiration, restricting the feasibility of reaction 1 under highly reducing conditions. In general, however, oxygen is not significantly retarded in oxic, sandy aquifers, such as that simulated in this study, and greater retardation of Fe^{2+} can be expected, either by adsorption to mineral surfaces or by chemical precipitation, such as reaction with calcite to form siderite ($FeCO_3$). The homogeneous oxidation reaction (reaction 1) is second order with respect to $[OH^-]$ and is essentially complete in a few hours under neutral pH conditions (*26*). Once Fe^{3+} is produced, precipitation of HFO (reaction 2) is nearly instantaneous.

Experimental Design

Laboratory experiments were conducted in two phases, first to emplace the in-situ HFO coating on aquifer material and second, to measure the resulting increase in metal attenuation produced by the coating. All experimental work was performed at Exponent's Boulder, Colorado laboratory. All analyses for dissolved metals were conducted by the University of Colorado, Boulder, Department of Geological Sciences. X-ray diffraction (XRD) analyses of the sand were conducted at the Colorado School of Mines, Department of Geological Sciences.

Materials. The simulated aquifer matrix was a well-sorted, medium sand, with median grain size of 0.6 mm, >99% finer than 2 mm, and <1% finer than 0.063 mm (by weight). XRD analyses coupled with visual point-count inspection found that the sand consisted of 75% quartz and 20% feldspar, with trace amounts of plagioclase, muscovite, hornblende, calcite, and ferroan dolomite. Tests were conducted in Plexiglas columns filled with sand in 5-cm lifts, compacted between each lift. Ferrous iron and oxygen retardation were determined in an 8-cm (inner diameter), 0.3-m-long column packed with sand, and the HFO emplacement and metal attenuation measurements were conducted using a 10-cm (inner diameter) column with a length of 0.75 m.

Three solutions were used to emplace the HFO coating on the simulated aquifer matrix, each starting with 0.6 M $NaHCO_3$ in deionized (DI) water: an anoxic solution with an equilibrated concentration of 1.3 or 3.6 mM ferrous iron added as $FeSO_4 \cdot 7H_2O$ (referred to hereafter as the iron solution), an anoxic solution without iron (referred to hereafter as the anoxic solution), and an oxic solution with 1.3 mM O_2 (PO_2 = 1 atm) (referred to hereafter as the oxygen solution).

The anoxic solution and the oxygen solution had a pH of 7.5 s.u. and an alkalinity of 80 mg/L as $CaCO_3$. The pH and alkalinity of the iron solution were lower (5 s.u. and 20 mg/L as $CaCO_3$, respectively), likely due to the precipitation of siderite. Oxygen content was maintained by continuously sparging the solution in air-lock vessels with purified oxygen gas, and anoxia was maintained by sparging with purified argon gas. Attenuation of As(V) and Cr(VI) was evaluated using DI water mixed to an alkalinity of 20 mg/L as $CaCO_3$

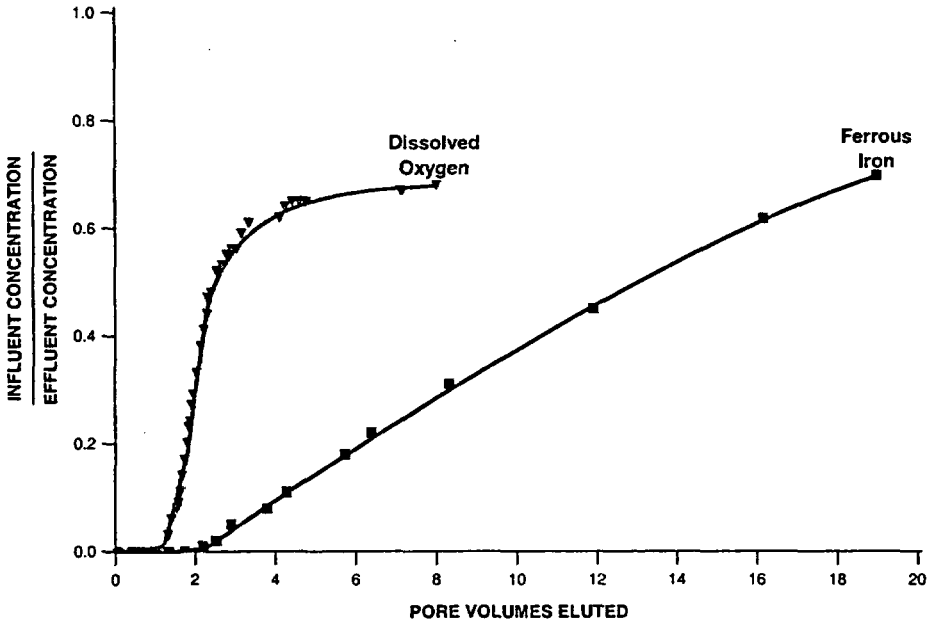

FIGURE 1. Breakthrough of iron and oxygen from sand column.

(added as $NaHCO_3$) and a pH of 7.0, with 0.01 mM As(V) (added as $Na_2HAsO_4 \cdot 7H_2O$) and 0.01 M Cr(VI) (added as $K_2Cr_2O_7$). These metals concentrations were selected to be representative of concentrations at the leading edge of a groundwater plume. The solution was also amended with 0.15 mM NaCl to provide a chloride tracer. The solution, hereafter referred to as the metals solution, was equilibrated with the atmosphere prior to injection.

Methods. Both sand-packed columns were purged for 10 min with $CO_{2(g)}$ before wetting and then flushed immediately with the anoxic solution in an upflow direction. The $CO_{2(g)}$ displaced the oxygen entrained in the pores, and subsequent dissolution of the $CO_{2(g)}$ reduced the gas volume in the pores. Flushing with anoxic solution continued for each column until the pH (as determined by an Orion gel epoxy electrode) and alkalinity (measured by a Hach digital titrator) of the column effluent were equal to those of the influent, and the effluent dissolved oxygen (DO; measured using an Orion 820 electrode) was below detection (0.01 mg/L). The pore volume of each column was determined by comparing the column weight before and after saturation and was confirmed to the measured volume of water added to just saturate the column. The measured pore volumes of the 8-cm and 10-cm columns were 0.6 and 1.9 L, respectively, corresponding to porosities of 0.39 and 0.33, respectively. The difference in porosity between the two columns (relative percent difference = 8.3%) likely reflects variable packing efficiencies during column construction and measurement error.

Oxygen attenuation was determined by injecting the oxygen solution at 7.5 ± 2.5 mL/min into the 8-cm column filled with anoxic water and monitoring the effluent oxygen concentration. Ferrous iron attenuation was measured in the same column by injecting the 1.3-mM iron solution at 7.5 ± 2.5 mL/min into the column filled with anoxic water and monitoring the column effluent ferrous iron concentration using the Hach spectrophotometer phenanthroline method.

The HFO coating was created by injecting one pore volume of the 1.3-mM iron solution into the 10-cm column, followed by 0.25 pore volume of the anoxic solution (a spacer to avoid precipitation at the injection port). The oxygen solution was then injected until breakthrough occurred. The column was then flushed with anoxic groundwater until column effluent DO concentrations were below detection. The coating emplacement process was then repeated following the same procedures, except that a 3.6-mM iron solution was used. Dissolved and total ferrous and ferric iron concentrations in the effluent demonstrated that more than 95% of the injected iron reacted in situ, which corresponds to 520 mg of HFO, or an average HFO coating concentration of 50-mg/kg HFO (as Fe), assuming that the HFO was evenly distributed across the column sand matrix. (The actual distribution of the HFO coating was not measured, and the HFO concentrations likely varied across the column.)

The attenuation of As(V) and Cr(VI) was determined by injecting the metals solution into the 10-cm sand-packed column at 7.5 ± 2.5 mL/min for a total of 100 pore volumes. The As and Cr concentrations in the outflow were measured at 1- to 5-pore-volume increments using inductively coupled plasma (ICP) spectroscopy (U.S. EPA Method 6010A). The baseline metal attenuation was determined by injecting the metals solution into the uncoated sand, and attenuation in the treated sand was measured by injecting the metals solution into the HFO-coated sand. Effluent pH and iron and chloride concentrations were monitored throughout the course of the metals attenuation experiments.

Results

Breakthrough curves show that the sand slightly retarded oxygen migration (retardation factor ~ 2; Figure 1). Dissolved oxygen was first detected in the column effluent at 1.3 pore volumes, with $C/C_o = 0.5$ at 2.5 pore volumes and $C/C_o \cong 0.7$ at 5 pore volumes. Oxygen breakthrough then leveled off, remaining at C/C_o of 0.7 through 8 pore volumes, when the experiment was terminated. Ferrous iron in the 1.3-mM solution was retarded to a much greater degree, with effluent ferrous and ferric iron below 0.02 mM until 2.5 pore volumes, $C/C_o \cong 0.5$ at 13 pore volumes, and a $C/C_o \cong 0.7$ when the experiment was terminated at 19 pore volumes. Although the transport of oxygen and iron appeared to be rate-limited, it is apparent that dissolved oxygen migrated faster than iron through the sand matrix. The differential attenuation of the two solutes allowed for their mixing in situ to create the HFO coating on the aquifer materials, by sequentially injecting first iron and then oxygen into the column (see Methods).

The measured breakthrough curves for As(V) and Cr(VI) from the columns of HFO-coated and unamended sand are shown in Figure 2. These results demonstrate that the 50-

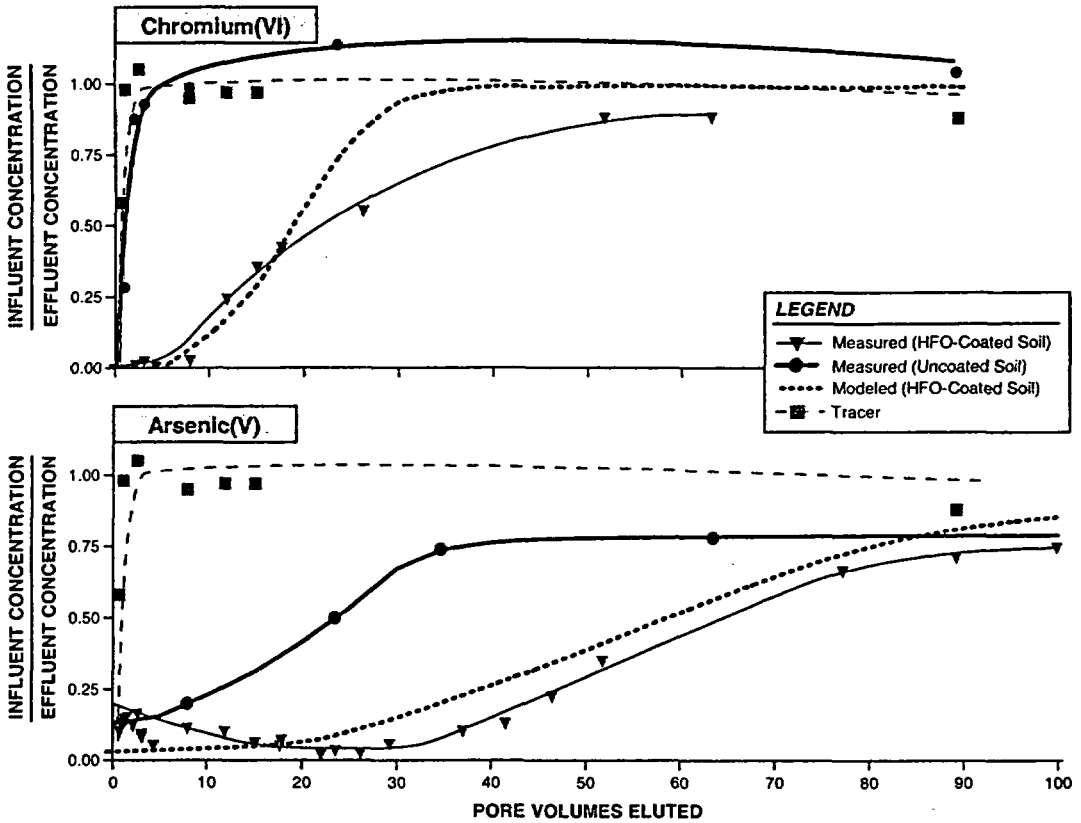

FIGURE 2. Measured and modeled breakthrough curves for chromium(VI) and arsenic(V) in sand column before and after application of 50-mg/kg HFO substrate.

mg/kg HFO coating (as Fe) slowed Cr(VI) breakthrough by 8 pore volumes, and As(V) breakthrough by 30 pore volumes, relative to their breakthrough from the unamended sand. At a $C/C_o = 0.5$, the HFO-coated sand had removed from solution more than 80% of the total dissolved load of arsenic and chromium introduced to the column.

The breakthrough of all of the solutes [Fe, DO, As(V), and Cr(VI)], with the exception of Cr(VI) from the unamended sand, occurred over several pore volumes. Breakthrough of the conservative chloride tracer was rapid, indicating that dispersion was small and that the slow breakthrough of the solutes was the result of unknown rate-limited processes—probably a combination of adsorption, precipitation, and diffusion to low-permeability zones—that were slow relative to the column residence time (approximately 4 h). In particular, iron may have precipitated as siderite ($FeCO_3$) around calcite in the sand matrix. Furthermore, 100% breakthrough was not achieved in most cases, indicating that these rate-limited processes were not carried to completion over the experiment's duration. The shape of the As(V) breakthrough curve from the unamended sand was similar to that from the coated sand, indicating that, although the attenuation of As(V) by the sand matrix itself was rate limited, the additional adsorptive attenuation of As(V) by the HFO coating was not. In contrast, Cr(VI) was only slightly retarded by the unamended sand, but the tail in the breakthrough curve from the HFO-coated sand suggests that Cr(VI) adsorption to HFO may have been rate limited.

The U.S. Geological Survey's geochemical transport code, PHREEQC (*25*), was used to simulate the observed attenuation of As(V) and Cr(VI) by the HFO coating. PHREEQC incorporates thermodynamic equilibrium and diffuse-layer adsorption into a one-dimensional transport model. The column experiments were simulated using 10 evenly spaced model cells, with equilibrium reactions calculated within each cell. The HFO substrate (not measured) was assumed to be evenly distributed within the column. Predictions of the As(V) and Cr(VI) breakthroughs were corrected for the background attenuation of the aquifer material by simple linear addition to the breakthrough from the unamended sand. Because the attenuation mechanism of the metals by the unamended sand was unknown, and because the observed As(V) transport in these materials was rate limited, PHREEQC was not used to simulate the background attenuation of the metals by the unamended sand. The only calibration of modeled to observed breakthrough was achieved by adjusting the weak adsorption-site density. A site density of 0.3 mol/mol—a value near the middle of the 0.05–0.91 mol/mol range summarized by Dzombak and Morel (*23*)—provided the best match to observed As(V) and Cr(VI) breakthrough (Figure 2).

The results of the modeling effort indicate that coupled transport/geochemical equilibrium models can potentially be applied as predictive tools in evaluating the effectiveness of the proposed in-situ remedial method under a variety of groundwater environments. Disequilibrium processes, such as the observed attenuation of Fe(II), limit extrapolation to field-scale conditions using equilibrium models such as PHREEQC, and geochemical processes within an aquifer, such as solute attenuation to the aquifer matrix itself, are often difficult to quantify. As a result, model predictions of natural systems will likely require supplementation with bench- and pilot-scale studies to derive reasonable estimates of substrate effectiveness under field conditions. However, the accuracy of PHREEQC at predicting the incremental attenuation from the HFO substrate indicates that such equilibrium models can be used to evaluate the efficacy of the remedial method for other metal contaminants—such as cadmium, copper, lead, mercury, nickel, radium, uranium, and zinc—that also have a high affinity for HFO (*27–29*) and well-characterized DLM adsorption parameters.

Discussion: Potential Application

Because in-situ approaches "bring the remediation to the contaminant," factors that limit most treatment technologies—aquifer heterogeneity, limited access to the subsurface, and slow dispersed contaminant release—are potentially less problematic. While pump-and-treat systems require long-term continuous operation, in-situ remediation requires additional action only when solutes break through the treated zone. And while many reactive walls require excavation of trenches to the base of the treated aquifer, adsorptive substrates can be emplaced using only injection wells, reducing surface disturbance and costs and avoiding the limitation of trench depth.

Successful in-situ emplacement of adsorptive substrates for groundwater remediation relies on the ability to disperse and mix the reactive solutes throughout a given zone of the aquifer to precipitate the adsorptive substrate. Our research has shown that the substrate can be applied via sequential injection of differentially attenuated solutes. Testing at a larger scale would be required to determine whether sufficient substrate dispersal can be achieved in a field-scale application. Furthermore, the rate-limited transport of the dissolved oxygen and iron during the substrate emplacement step suggests that existing equilibrium models may not be effective at simulating the substrate emplacement process.

Once a coating is in place, inefficiencies caused by aquifer heterogeneity are addressed implicitly with in-situ chemical precipitation. Injected solutes follow natural flow paths, so as long as the injection wells penetrate the major strata, the adsorptive substrate is emplaced preferentially in the most permeable zones, ensuring that most of the water flowing through the treated aquifer zone encounters the substrate. Aquifer heterogeneity can actually be an advantage—the fact that flow bypasses low-conductivity zones reduces the apparent aquifer porosity (*30*) and thus reduces the volume of aquifer material that requires treatment with the substrate. Perhaps most important, an in-situ adsorptive substrate reduces the need for complete source removal. All contaminant sources—incompletely removed point sources as well as releases by slow desorption and dispersion out of low-permeability strata—can be treated passively when contaminated groundwater enters the substrate-coated aquifer zone. Long-term geochemical model simulations during this investigation indicate that the ultimate fate of adsorbed metals in the treated aquifer zone will be slow desorption to groundwater at relatively low concentrations (in this case, below 0.02 mg/L), consistent with observed Cr breakthrough from HFO-bearing aquifer matierals during a recent laboratory study (*19*).

Pore plugging and associated reduction in permeability from adsorptive substrates may be a concern, and highly concentrated iron solutions have even been designed to grout aquifers (*31*). But the metal retardation reported in our study was achieved with only 50 mg of Fe per kg, which at an HFO density of 3.5 g/cm^3 (*23*), a porosity of 0.36, and assumed even distribution of HFO across the sand matrix (the actual distribution of the HFO coating in the column was not measured) would have decreased porosity by less than 0.1%. Thus, while porosity reduction has the potential to restrict permeability in coated aquifers, this potential problem is probably limited to treatment of highly concentrated metals plumes (e.g., hundreds to thousands ppm of metals).

Substrate stability can also impart important limits on this method. For example, HFO will redissolve at low pH or under conditions that reduce Fe^{3+} back to the more soluble Fe^{2+} (i.e., low-Eh groundwater). As a result, in situ application of an HFO coating will be limited in such systems. If chemically stable, the effectiveness of in-situ treatment would depend, at a minimum, on the mass of added substrate, the groundwater flow rate, and the contaminant concentrations. The substrate life may be predictable based on calibration of computational models to bench-scale tests.

If necessary, the attenuation capacity of the treated aquifer could be regenerated by reapplying the adsorptive substrate. An additional benefit of retreatment is that subsequent injection of the substrate using the original wells should emplace the new substrate in the previously treated zones, partially encapsulating and further stabilizing the previously adsorbed metals.

Costs of treatment using in-situ adsorptive coatings are likely to compare favorably to pump-and-treat. Both approaches incur initial capital costs for well installation, pumps, piping, instrument control, and water treatment systems. Application of in-situ coatings would require additional capital costs for reagents, storage tanks, and related control systems, but water treatment would be required only during the emplacement of the reactive coating—allowing for use of less expensive water treatment alternatives (e.g., leasing). More significantly, the long-term operation requirements of pump-and-treat would incur significantly larger operations and maintenance costs, relative to the semipassive in-situ coatings approach. Finally, at sites where pump-and-treat systems are already in place, emplacement of in-situ adsorptive coatings could potentially be applied to eliminate the need for (and the associated cost of) long-term operation of the pump-and-treat system.

Additional Research Needs

The clearest research need is for field-scale testing of in-situ HFO emplacement and resulting metal stabilization to determine the effectiveness in large-scale heterogeneous media. Such testing should focus on measuring the distribution and chemical stability of the substrate and calibrating computational chemical transport models to measured substrate emplacement and metal attenuation. Analysis should focus on measuring technical effectiveness and eventually estimating the practical application costs using standard matrics (e.g., per m^3 water treated, to facilitate comparison across technologies). Finally, parallel work should evaluate the feasibility of in-situ emplacement of various other adsorptive substrates and their effectiveness at stabilizing metals. Two potential substrates include gibbsite [$Al(OH)_3$] and hausmanite [MnOOH]—both of which are commonly occurring oxide minerals known to be strong metal sorbents (*28, 32*).

Literature Cited

(1) NRC. *Alternatives for groundwater cleanup*; National Research Council; National Academy Press: Washington, DC, 1994.

(2) Evanko, C. R.; Dzombak, D. A. Technology Evaluation Report No. TE-97-01; Groundwater Remediation Technologies Analysis Center: Pittsburgh, PA, 1997.

(3) NRC. *Innovations in groundwater and soil cleanup: from concept to commercialization*; National Research Council; National Academy Press: Washington, DC, 1997.

(4) *General Methods for Remedial Operations Performance Evaluations*; U.S. Environmental Protection Agency, Office of Research and Development, Environmental Research Laboratory: Athens, GA, 1992a.

(5) *Evaluation of Groundwater Extraction Remedies: Phase II*; U.S. Environmental Protection Agency, Office of Emergency and Remedial Response: Washington, DC, 1992b.

(6) Chemical Barriers to Feasibility and Field Demonstration. In *In Situ Remediation Integrated Program*; Technology Summary No. DOE/EO134P; U.S. Department of Energy: Springfield, VA, 1994.

(7) Morrison, S. J.; Spangler, R. R. *Environ. Progress* **1993**, *12*, 175–181.

(8) Blowes, D. W.; Ptacek, C. J.; Jambor, J. L. *Environ. Sci. Technol.* **1997**, *31* (12), 3348–3357.

(9) Vance, D. B. *Environ. Technol.* **1997** (July–August).

(10) Morrison, S. J.; Tripathi, V.S.; Spangler, R. R. *J. Contamin. Hydrol.* **1995**, *17*, 347–363.

(11) Lee, S. Y.; Francis, C. W.; Timpson, M. E.; Elles, M. P. *Radionuclide Containment in Soil by Phosphate Treatment*; Contract AC05-84OR21400; Oak Ridge National Laboratory: Oak Ridge, TN, 1995; 4 pp.
(12) Cantrell, K. J.; Kaplan, D. I.; Wietsma, T. W. *J. Haz. Mater.* **1995**, *42*(2), 201−212.
(13) Benner, S. G.; Blowes, D. W.; Ptacek, C. J. *Ground Water Monit. Rem.* **1997**, *17*(4), 99−107.
(14) Vidic, R. D.; Pohland, F. G. *Treatment walls*; Technology Evaluation Report TE-96-01; Groundwater Remediation Technologies Analysis Center: Pittsburgh, PA, 1996.
(15) Ziegenbalg, G.; Crosby, K. S. *Mineral Resources Eng.* **1997**, *6*(4), 173−186.
(16) Johnston, C. D.; Rayner, J. L.; DeSoysa, D. S.; Ragusa, S. R.; Trefry, M. G.; Davis, G. B. *In Situ On Site Bioremediation Symposium (4th)*; New Orleans, LA, 1997; Vol. 4, pp 241−246.
(17) Pyrih, R. Z.; Krauth, P.; Hardison, R. L. *In Situ Geochemical Fixation of Uranium and Molybdenum Using Calcium Polysulfide*; Preprint No. 98-138 from the Society for Mining, Metallurgy, and Exploration annual meeting; Orlando, FL, 1998.
(18) Lolcama, J. L. *Toxic Substance Hydrol. Sci., Sel. Pap. Conference*; Dutton, A. R., Ed.; 1994; pp 684−697
(19) Seaman, J. C.; Bertsch, P. M.; Schwallie, L. *Environ. Sci. Technol.* **1999**, *33*, 938−944.
(20) Rott, U.; Friedle, M. *In Situ Treatment of Arsenic in Groundwater*; International Conference on Arsenic Exposure and Health Effects (3rd); San Diego, CA, 1998.
(21) Devlin, J. F.; Barker, J. F. *Can. Water Resour. Res.* **1996**, *32*(9), 2869−2877.
(22) Gelhar, L. W.; Montoglou, A.; Welty, C.; Rehfeldt, K. R. *A Review of Field Scale Subsurface Solute Transport Processes Under Saturated and Unsaturated Conditions. Electric Power Research Institute*; Palo Alto, CA, 1985; 107 pp.
(23) Dzombak, D. A.; Morel, F. M. M. *Surface Complexation Modeling: Hydrous Ferric Oxide*; John Wiley and Sons: New York, 1990.
(24) Klaus, P. R.; Jain, A.; Loeppert, R. H. *Environ. Sci. Technol.* **1998**, *23*(3), 344−349.
(25) Parkhurst, D. L. *PHREEQC. A computer program for speciation, reaction-path, advective transport, and inverse geochemical calculations*; International Groundwater Modeling Center, FOS 87; Golden, CO, 1997.
(26) Sung, W.; Morgan, J. J. *Environ. Sci. Technol.* **1980**, *15*(5), 561−568.
(27) Allison, J. D.; Brown, D. S.; Novo-Gradac, K. J. *MINTEQA2/PRODEFA2, A Geochemical Assessment Model for Environmental Systems: Version 3.0 User's Manual: 1991*; EPA/600/3-91/021; U.S. Environmental Protection Agency, Office of Research and Development, Environmental Research Laboratory: Athens, GA, 1991.
(28) Leckie, J. O.; Benjamin, M. M.; Hayes, K.; Kaufman, G.; Altman, S. *Adsorption-Coprecipitation of Trace Metals from Water with Iron Hydroxide*; Document 910-1; Electric Power Research Institute: 1980.
(29) *Chemical Attenuation Rates, Coefficients and Constants in Leachate Migration. Volume 1: A Critical Review*; EPRI EA-3356; Prepared for the Electric Power Research Institute by Battelle Pacific Northwest Laboratories: Richland, WA, 1984.
(30) Williams, M. D.; Yabusaki, S. B.; Cole, C. R.; Vermeul, V. R. In Situ Redox Manipulation Field Experiment: Design Analysis; In *In Situ Remediation: Sci. Basis Curr. Future Technol., Hanford Symposium Health Environment*, 33rd ed.; Gee, G. W., Wing, R. N., Eds.; Battelle Press: Columbus, OH, 1994; Vol. 2, pp 1131−1153.
(31) Hapka, A. M.; Whang, J. M. In Situ Precipitation of an Iron Based Grout; In *Environ. Technol., Proc. Int. Symp., (3rd)*; Hsai, F., Inyang, H. I., Eds.; 1996; Vol. 1, pp 375−378.
(32) Stumm, W. *Chemistry of the Solid-Water Interface*; John Wiley & Sons: New York, 1992.

Received for review August 20, 1998. Revised manuscript received May 2, 2000. Accepted May 2, 2000.

ES980861W

Environ. Sci. Technol. 2000, 34, 1062–1068

Uranium Uptake from Aqueous Solution by Interaction with Goethite, Lepidocrocite, Muscovite, and Mackinawite: An X-ray Absorption Spectroscopy Study

LESLEY N. MOYES,*,† RICHARD H. PARKMAN,†,‡ JOHN M. CHARNOCK,†,‡,§ DAVID J. VAUGHAN,† FRANCIS R. LIVENS,† COLIN R. HUGHES,‡ AND ANNA BRAITHWAITE||

Department of Chemistry and Department of Earth Sciences, University of Manchester, Manchester M13 9PL, U.K., CLRC Daresbury Synchrotron Laboratory, Warrington, WA4 4AD, U.K., and BNFL plc., Sellafield, Seascale, Cumbria, CA20 1PG, U.K.

The retention of radionuclides by interaction with mineral phases has significant consequences for the planning of their short- and long-term disposal to geological systems. An understanding of binding mechanisms is important in determining the ultimate fate of radionuclides following release into natural systems and will give increased confidence in predictive models. X-ray absorption spectroscopy (XAS) has been used to study the local environment of uranium taken up from aqueous solution by the surfaces of goethite, lepidocrocite, muscovite, and mackinawite. On both iron hydroxides uranium uptake occurs by surface complexation and ceases when the surface is saturated. The muscovite surface does not become saturated and uptake increases linearly suggesting formation of a uranium phase on the surface. Uranium uptake on mackinawite also suggests a replacement or precipitation process. XAS indicates that bidentate inner-sphere surface complexes are formed on the iron hydroxides by coordination of two surface oxygens from an iron octahedron in the equatorial plane of the complex. Uranium uptake on muscovite may occur through surface precipitation, the first layer of uranium atoms binding through equatorial coordination of two adjacent surface oxygens from a silicate tetrahedron, with the axial oxygens of the uranyl unit aligned across the hexagonal "cavities" created by the rings of tetrahedra. At low concentrations, uptake on mackinawite occurs at locally oxidized regions on the surface via a similar mechanism to that on iron hydroxides. At the highest concentrations, equatorial oxygen bond distances around 2.0–2.1 Å are observed, inconsistent with the presence of uranyl species. The average number of axial oxygens also decreases with increasing concentration, and these results suggest partial reduction of uranium. The nature of these different surface reactions plays an important role in assessing the geochemical behavior of uranium in natural systems, particularly under reducing conditions.

Introduction

The uptake of uranium on soil and sediment components has been extensively studied (*1–11*). Many of these studies have been concerned with the binding mechanisms of the uranyl ion (UO_2^{2+}) under oxic conditions.

Morris et al. (*7*) used Raman spectroscopy to identify distinct binding sites on a smectite clay. At low and intermediate loadings of uranium, uptake occurs at pH-dependent amphoteric edge sites, and, at higher loadings, binding occurs at fixed charge (exchange) surface sites. Further studies on clay minerals have shown that as surface coverage increases, the number of equatorial oxygens around the uranyl unit increases, as does the U–O bond distance (*6*). This suggests that initial uptake to the most energetically favorable sites allows a close approach of the uranyl unit and an inner-sphere reaction with the surface. After this, uptake is on to less favorable sites, so that the U–O distance increases with uptake. At high surface coverage, the binding complex appears to be similar to that in the aqueous phase, implying unselective and weak binding.

Uranium binding by iron oxide minerals also appears to be by inner-sphere surface complex formation involving two oxygens of the FeO_6 octahedron (*8*). Surface complexation modeling of uranyl species in carbonate-free solution at pH > 5 suggests that mono-, bi-, and tridentate uranyl–hydroxy complexes are responsible for uptake on ferric hydroxides (*2*). Uranium uptake on calcite is a complex combination of processes depending on pH and on CO_2 and U concentrations; under some conditions uranium is weakly adsorbed as a monolayer, while under others formation of a precipitate on the calcite surface is observed (*12*). Sulfide minerals also take up uranium (*5, 13, 14*), and reduction of trace metals in solution by sulfide minerals has been observed (*9, 15*).

Uptake studies which rely on bulk measurements (sorption isotherms, distribution coefficients) are essential to understand the behavior of uranium under different pH, temperature, and concentration conditions. However, to give increased confidence, they need to be combined with direct observation of species coordination at the mineral/water interface. X-ray absorption spectroscopy (XAS) is the most effective way of analyzing the local environment of uranium species bound to a fine particle mineral phase and has the ability to distinguish between various adsorption and surface precipitation processes (*16*). For these reasons, this study concentrates on the XAS analysis of uranium taken up on several mineral phases and compares the different coordination behavior observed. The current work supports and extends previously reported experiments on iron oxides/hydroxides under a variety of conditions (*1, 2, 8*) and reports, for comparison, new studies involving muscovite and mackinawite.

Experimental Section

In this work, powdered samples of the mineral phases were reacted with solutions of the uranyl ion (as nitrate) at increasing concentrations, and the uranium uptake measured. The form in which the uranium was taken up by each mineral was then investigated using X-ray absorption spectroscopy.

* Corresponding author phone: +44(161)-275-4647; fax: +44(161)-275-4598; e-mail: Lesley.Moyes@man.ac.uk.
† Department of Chemistry, University of Manchester.
‡ Department of Earth Sciences, University of Manchester.
§ CLRC Daresbury Synchrotron Laboratory.
|| BNFL plc., Sellafield, Seascale, Cumbria, CA20 1PG, U.K.

10.1021/es990703k CCC: $19.00
Published on Web 02/18/2000

Mineral Preparation. Goethite and lepidocrocite were synthesized according to Schwertmann and Cornell (*17*), and the purity and homogeneity were confirmed by powder X-ray diffraction (XRD). Goethite and lepidocrocite prepared by this method typically have surface areas of 20 and 70–80 $m^2 g^{-1}$, respectively. A natural muscovite sample was ground with acetone in a planetary ball mill. The surface area (BET isotherm method) of the powdered material was 39.8 $m^2 g^{-1}$. Mackinawite (tetragonal FeS_{1-x}) was obtained by precipitation from an aqueous Fe(II) solution by addition of aqueous Na_2S at controlled pH, as described by Lennie et al. (*18*) and Lennie and Vaughan (*19*). This procedure was carried out using deaerated deionized water under an oxygen-free nitrogen atmosphere. The freeze-dried precipitate was stored under nitrogen. The sample was amorphous when examined by X-ray powder diffraction; however, extended absorption fine structure spectroscopy (EXAFS) analysis of the Fe K-edge gave coordination numbers and interatomic distances (four S atoms at 2.20 Å and four Fe atoms at 2.5–2.6 Å) consistent with mackinawite as described by Lennie et al. (*18*) and Lennie and Vaughan (*19*). The material is prone to oxidation, making surface area measurements difficult.

Batch Experiments. In the batch uptake experiments, a solid/solution ratio of 0.1 g/10 mL was used for the goethite and mackinawite, while 0.3 g/30 mL was used for the lepidocrocite and muscovite. With the exception of mackinawite (see below), the samples of solid material were rewet overnight in deionized water (10 or 30 mL as appropriate) in 50 mL capped polyethylene centrifuge tubes. Uranyl nitrate in aqueous solution was added to give initial uranium solution concentrations of 0.025, 0.05, 0.1, 0.2, 0.5, and 1.0 mM. Spike volumes did not exceed 100 μL, to avoid significantly affecting the solid/solution ratio. In all cases, three identical samples were prepared for each concentration. The uranium solution was kept in contact with the solid material for 24 h and agitated. Final pH values were 3.6–4.8 for lepidocrocite; 3.7 (high $[U]_{soln}$) – 7.0 (low $[U]_{soln}$) for goethite; and 4.6 (high $[U]_{soln}$) – 8.1 (low $[U]_{soln}$) for muscovite. The implications of these variations in pH are discussed later. After centrifuging (6000 rpm; 30 min), the supernatants were removed and filtered (0.45 μm), and a known aliquot was diluted appropriately with 2% (v/v) HNO_3 (Aristar) for analysis by inductively coupled plasma mass spectrometry (ICPMS). The remaining slurry of solid material was sealed in the centrifuge tube and frozen in liquid nitrogen to minimize further reaction before X-ray absorption analysis.

The mackinawite samples were treated similarly, except all manipulations were carried out in a glovebag under an oxygen-free nitrogen atmosphere and using degassed deionized water. Initial solution concentrations ranged from 0.5 to 5.0 mM. The remaining slurry was carefully inserted into polyethylene tubing (ca. 5 mm diameter), sealed, and frozen in liquid nitrogen. At all concentrations of uranium in solution the pH equilibrated between pH 6.7 and 7.0, suggesting that addition of the uranium did not significantly affect the pH of the system.

X-ray Absorption Spectroscopy. The local environment of the uranium taken up by the solid minerals was investigated by both X-ray absorption near edge structure (XANES) and extended X-ray absorption fine structure (EXAFS) spectroscopies. The general principles of XAS and its applications to mineral systems have been comprehensively reviewed elsewhere (*20, 21*).

Uranium L(III)-edge X-ray absorption spectra were collected on Station 9.2 at the CLRC Daresbury Synchrotron Radiation Source, operating at 2 GeV with a typical beam current of 150 mA. A double crystal Si (*220*) monochromator was used and detuned to 50% of maximum intensity to minimize high energy harmonic contamination. A frozen slurry sample, prepared as described above, was mounted in an aluminum sample holder and kept at liquid nitrogen temperature. The monochromator was calibrated using a crystalline UO_3 standard sample (edge position 17 169 eV). Fluorescence spectra were collected over an energy range of ~16 900 eV to ~18 050 eV using a 13-element Ge detector. The signal from each element was collected and examined separately before being added to the total. A minimum of four scans per sample were collected, and the data summed to improve data quality. An aqueous solution of uranyl nitrate (50 mM) and solid samples of U_3O_8 and UO_2 (diluted with boron nitride) were also analyzed. Background subtracted spectra were analyzed in EXCURV97 (*22*) using full curved wave theory, including multiple scattering from the uranyl group where necessary (*23–25*). Phase shifts were derived in the programs from ab initio calculations using Hedin-Lundqvist potentials and von Barth ground states (*26*). Fourier transforms of the EXAFS spectra were used to obtain an approximate radial distribution function around the central uranium atom (the absorber atom); the peaks of the Fourier transform can be related to "shells" of surrounding backscattering atoms characterized by atom type, number of atoms in the shell, the absorber-scatterer distance, and a Debye–Waller factor, $2\sigma^2$ (a measure of both the thermal motion between the absorber and scatterer and of the static disorder or range of absorber-scatterer distances, which may be viewed as an index of uncertainty in an individual shell). The data were fitted for each sample by defining a theoretical model and comparing the calculated EXAFS spectrum with the experimental data. Shells of backscatterers were added around the uranium and by refining an energy correction E_f (the Fermi energy), the absorber-scatterer distance, and the Debye–Waller factor for each shell, a least squares residual (the *R*-factor (*27*)) was minimized. For each shell of scatterers around the uranium, the number of atoms in the shell was chosen to give the best fit but not refined. Additional shells of scatterers beyond the first were only included in the final fit if they made an improvement in the *R*-factor (at least 4%). Multiple scattering was included in the theoretical model, where necessary, by defining the geometry of the model and calculating all the multiple scattering pathways during refinement, using small atom theory (*28*) to minimize computation time.

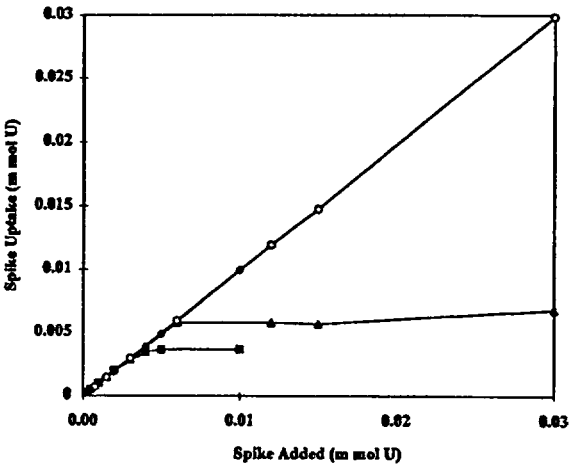

FIGURE 1. Uptake of uranium from solution as a function of initial uranium solution concentration: (▲) on lepidocrocite; (■) on goethite; (○) on muscovite; and (◇) on mackinawite.

Results and Discussion

Batch Experiments. The uptake of uranium as a function of initial solution concentration is shown for each of the minerals in Figure 1, although it is difficult to interpret these

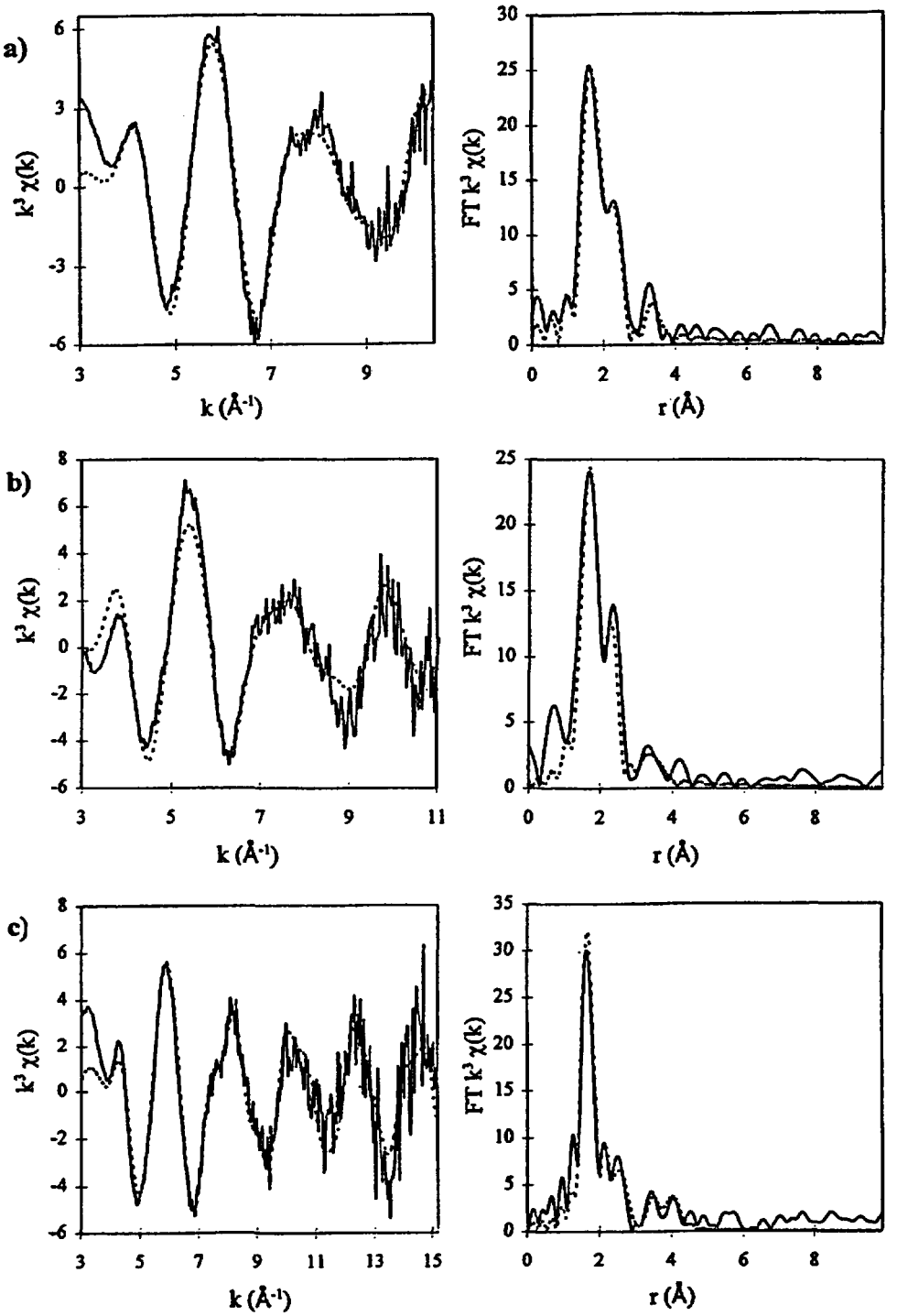

FIGURE 2. k^3-weighted EXAFS and Fourier transforms for U on (a) lepidocrocite (from 0.5 mM U solution); (b) goethite (from 0.2 mM U solution); and (c) muscovite (from 0.4 mM U solution). Solid lines represent experimental data and dashed lines the best fit.

in detail due to the variability in pH. However, at the pH conditions employed uranyl hydroxy solution species are dominant in all systems (*1, 29*). Uptake on lepidocrocite and goethite follow very similar patterns, flattening off at higher concentrations. Uranium solution concentration has been shown to have a significant effect on sorption energetics (*6, 7, 30*), and these results indicate saturation of the available surface sites in support of previous work (*3, 31*). Uptake of uranium on muscovite and mackinawite is very different, increasing linearly with concentration and exceeding 99% at each concentration. In effect, uranium is quantitatively removed from solution at all concentrations. In the case of muscovite, the surface loadings greatly exceed the cation exchange capacity of 18.8 ± 3.4 cmol/kg. This behavior suggests formation of a new phase at the surface (*32*). The continued uptake of uranium with increasing concentration on both muscovite and mackinawite may be due to the formation of a new uranium-containing phase on the surface. This hypothesis is examined in more detail in the following sections.

TABLE 1. Parameters Obtained from EXAFS Data Fitting of U L(III)-Edge Spectra for Lepidocrocite, Goethite, and Muscovite[a]

sample (initial soln concn)	shell no.	atom type	N	r (Å)	$2\sigma^2$ (Å^2)	R
U on lepidocrocite	1	O	2.0	1.81	0.003	25.9
(0.5 mM)	2	O	4.0	2.40	0.015	
	3	Fe	1.0	3.45	0.017	
U on goethite	1	O	2.0	1.80	0.006	38.9
(0.2 mM)	2	O	5.0	2.40	0.024	
	3	Fe	1.0	3.47	0.015	
U on muscovite	1	O	2.0	1.80	0.003	40.1
(0.4 mM)	2	O	4.0	2.35	0.028	
	3	Si	1.0	2.75	0.011	
	4	Si	2.0	3.66	0.010	
	5	U	1.0	3.86	0.010	

[a] N is the coordination number (±1), r is the interatomic distance (±0.02 Å), $2\sigma^2$ is the Debye–Waller factor, and R is the overall goodness of fit.

Analysis of EXAFS Spectra. For lepidocrocite, goethite, and muscovite all the XAS spectra were very similar, regardless of uranium concentration. The results for one representative sample of each of these are therefore discussed in detail. The EXAFS spectra and corresponding Fourier transforms for these samples are shown in Figure 2a–c. Corresponding parameters obtained from analysis of the spectra are summarized in Table 1.

U on Fe Hydroxides. For both lepidocrocite and goethite (Figure 2a,b), the best fit was achieved with two axial uranyl oxygens at ~1.80 Å and five oxygen atoms at ~2.40 Å. These distances suggest uptake of the uranyl ion, coordinated in the equatorial plane by 4–6 ligands. In each case the fit is improved by a third shell containing at least one Fe atom at ~3.50 Å. This is also consistent with results of Waite et al. (*8*), whose study of uranyl ion uptake on ferrihydrite surfaces also suggested that the equatorial oxygens could be separated into two groups, with 3 O at 2.35 Å and 2 O at 2.52 Å. In the present study, the resolution of the data was such that no improvement in fit was found on fitting with the equatorial oxygens as two shells. Uranyl carbonato complexes have been proposed on iron oxide surfaces from XAS analysis (*33*), but attempts to fit our data with carbonate ligands gave no improvement in fit.

Our EXAFS data suggest one environment for the equatorial oxygens. However, as Waite et al. (*8*) proposed there may be more than one type of equatorial U–O environment, with the U–O distances to the surface O atoms being longer than those to the water ligands. If this is the case, then for the U–Fe distance obtained experimentally in our work, the distance between U and surface O would have to be ~2.50 Å, close to that found by Waite et al. (*8*). If the equatorial oxygens atoms are at two distinct distances, then given the experimental average equatorial U–O distance of ~2.40 Å, the remaining three equatorial O atoms would be at 2.33 Å which is very similar to the distance observed by Waite et al. (*8*).

U on Muscovite. In common with the results for U on the iron hydroxides, the best fit to the EXAFS data for U on muscovite (Figure 2c) also shows two uranyl oxygens at 1.80 Å and at least four equatorial oxygen ligands at a shorter distance of 2.35 Å. Fitting the equatorial oxygens at two different distances did not improve the fit, but the high Debye–Waller factor (Table 1) may signify slight differences in U–O distances in the second shell. An improved fit is obtained when silicon atoms are fitted in third and fourth shells, with a best model fit obtained with one silicon at 2.75 Å and two at 3.66 Å. However, a U–Si distance of 2.75 Å is short, giving a U–O–Si angle of less than 90°, which would suggest a significant amount of distortion of the surface on binding. Replacement of Si with O at this distance did not improve the fit significantly and multiple backscattering analysis also showed no improvement in fit. The peak at 3.66 Å can be fitted with two Si atoms, although inclusion of multiple backscattering further improves the fit. The feature at 3.86 Å can be fitted with four Si atoms, although a U atom at this distance gives a slightly better fit. A uranium atom at this distance could be due to formation of a uranium-(hydr)oxide precipitate which is consistent with the uptake curve (Figure 1), although it may reflect the presence of a neighboring uranyl complex on the muscovite surface.

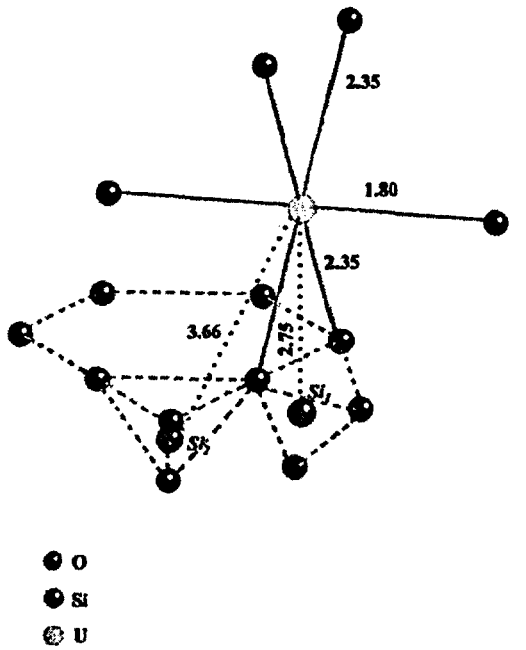

FIGURE 3. Proposed binding mechanism for uranyl species on muscovite surface (distances, in Å, are experimentally derived). Solid lines depict discrete bonds between uranium and oxygen atoms. Dashed lines indicate "through-space" distances in muscovite tetrahedral plane. Dotted lines indicate "through-space" U–Si distances. Si–O bonds in individual tetrahedra have been omitted for clarity.

An idealized model for coordination of a single uranyl ion on the muscovite surface is illustrated in Figure 3. Two equatorial coordination positions are filled by two corner oxygens of an $[SiO_4]^{4-}$ tetrahedron. This tetrahedron forms part of one of the hexagonal rings of silicate tetrahedra which make up the tetrahedral layer in the muscovite structure, so the Si atoms of two adjacent tetrahedra are observed at a distance of 3.66 Å. In this model, the axial oxygen atoms of the uranyl unit are aligned across the hexagonal cavities at the centers of the rings of tetrahedra. In the absence of distortion, the model-derived U- - -Si_1 distance is 2.57 Å compared with 2.75 Å from experiment, and the U- - -Si_2 distance is 4.03 Å compared to 3.66 Å from experiment. The experimental and calculated distances differ by up to 0.4 Å, but the calculations assume that the geometry of the tetrahedron remains undistorted on uranium coordination to the surface, and also that the bonding and nonbonding equatorial oxygens are all at equal distances from the uranium center. The discrepancies between calculation and experiment suggest that the system is significantly distorted.

Other EXAFS studies of uranium sorption on phyllosilicates have been interpreted in terms of surface complex

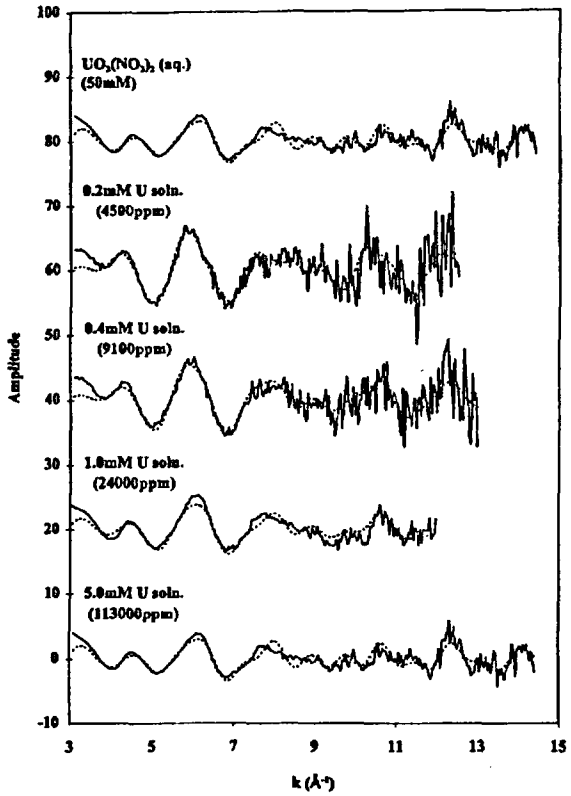

FIGURE 4. EXAFS spectra for U on mackinawite and for UO_2^{2+} in aqueous solution. For mackinawite samples original solution concentrations (mM) are given, with mass of U sorbed (μg) per g of sorbent in parentheses. Solid lines represent experimental data and dashed lines the best fit.

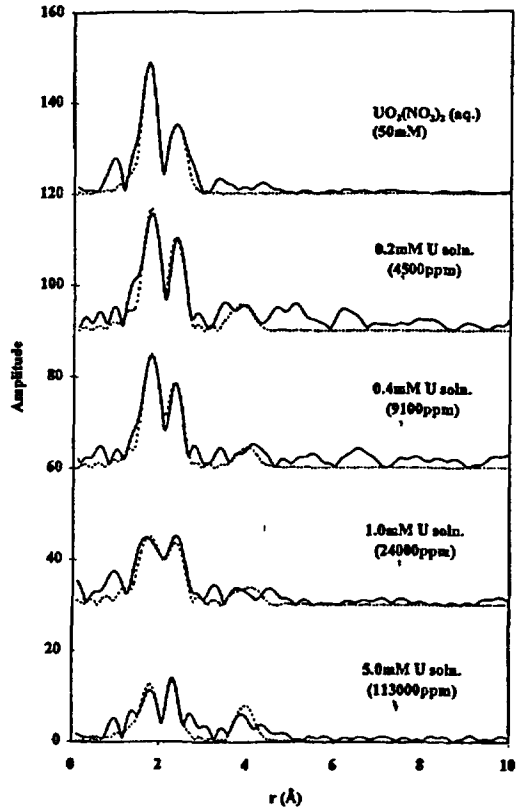

FIGURE 5. Fourier transforms for U on mackinawite and for UO_2^{2+} in aqueous solution. For mackinawite samples original solution concentrations (mM) are given, with mass of U sorbed (μg) per g of sorbent in parentheses. Solid lines represent experimental data and dashed lines the best fit.

formation. Chisholm-Brause et al. (*6*) suggested that there are three distinct environments for oxygen atoms in the equatorial plane of the uranyl species sorbed on to the surface of montmorillonite. As surface coverage increases, there is an increase in both the number of equatorial oxygen atoms and the U–O distance. This implies that energetically more favorable surface sites are filled first. Thereafter, less favorable sites are filled as coverage increases, resulting in longer U–O distances but higher equatorial coordination numbers. Similarly, Dent et al. (*30*) have also shown that the EXAFS spectra of uranyl species sorbed onto montmorillonite at pH 5, closely resemble those of hydrolyzed species in solution; in other words, the uranyl structure is largely retained on sorption. Unlike muscovite, the interlayer of montmorillonite can expand to ~8 Å, allowing a hydrated uranyl complex to enter between the layers and presenting additional sites for uranium uptake.

In the present study, the best fit is obtained with 4 ± 1 oxygen atoms in the equatorial plane. However, the comparatively high Debye–Waller factor for this shell may reflect some disorder, such as would arise given a mixture of four- and five-coordinate species. First and second shell distances in the present study agree well with those found by other workers (*6, 30*); however, third and fourth shell data for U–Si distances are not available for comparison.

U on Mackinawite. The variation in uranium uptake on mackinawite with initial concentration in solution (Figure 1) suggests formation of a new phase on the surface (*32*). The EXAFS spectra (Figure 4) and their Fourier transforms (Figure 5) for four samples of increasing uranium concentration are displayed along with those for the uranyl ion in aqueous solution. It is clear that there are substantial differences between the Fourier transforms for different concentrations. The parameters (Table 2) indicate that at the two lower concentrations, the best fit is given by two axial oxygen and four equatorial oxygen atoms, with an additional Fe shell as in the inner-sphere surface complexes proposed for the hydrous iron oxide system. At higher concentrations, the best fits are obtained by splitting the second shell into two separate subshells containing oxygen atoms at 2.07–2.14 and 2.31–2.36 Å. The ~2.1 Å distances are too short for

TABLE 2. Parameters Obtained from EXAFS Data Fitting of U L(III)-Edge Spectra for Mackinawite[a]

initial U soln concn (concn on mineral)	shell no.	atom type	*N*	*r* (Å)	$2\sigma^2$ (Å^2)	*R*
0.2 mM	1	O	2	1.81	0.005	53.7
(4500 ppm)	2	O	4	2.40	0.009	
	3	Fe	2	3.83	0.013	
0.4 mM	1	O	2	1.82	0.006	57.0
(9100 ppm)	2	O	4	2.38	0.011	
	3	Fe	2	3.96	0.016	
1.0 mM	1	O	2	1.81	0.012	46.0
(24 000 ppm)	2	O	2	2.14	0.022	
	3	O	4	2.36	0.012	
	4	Fe	2	3.97	0.015	
5.0 mM	1	O	2	1.83	0.014	53.4
(113 000 ppm)	2	O	1	2.07	0.003	
	3	O	5	2.31	0.020	
	4	Fe	2	3.97	0.008	

[a] *N* is the coordination number (±1), *r* is the interatomic distance (±0.02 Å), $2\sigma^2$ is the Debye–Waller factor (Å^2), and *R* is the overall goodness of fit.

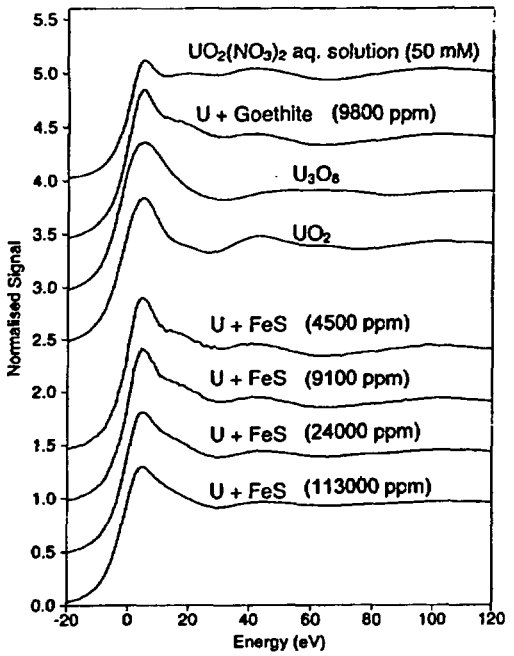

FIGURE 6. Uranium L(III)-edge XANES spectra. Mass of U sorbed (μg) per g of sorbent in parentheses.

equatorially bound oxygens, so binding cannot be explained solely in terms of a simple uranyl complex at higher concentrations. In addition, the Fourier transforms (Figure 5) show that the intensities of the first and second shell peaks vary greatly over the concentration range. The amplitude of a peak in the Fourier transform is a function of N and the Debye–Waller factor, so decreasing the coordination number and/or increasing the Debye–Waller factor will result in a lower amplitude. In addition, significant increases in the Debye–Waller factor of first shell data are observed with increased loading, which will also affect amplitude. However, larger Debye–Waller factors do suggest disorder which is consistent with the presence of mixed uranium species. This suggests partial reduction of uranium, leading to an increased average coordination number and a range of U–O distances between 2.07 and 2.36 Å, as found in the data fitting at higher concentrations (Table 2). Fitting the spectra with only one oxygen atom in the first shell gave higher R-factors, suggesting that there is a significant uranyl contribution even at higher surface concentrations.

The binding mechanisms in this system are obviously more complex than those of uranium on the iron hydroxide and silicate surfaces. At low surface concentrations, sorption apparently occurs in a similar way to that described for the iron hydroxide surfaces. Although mackinawite is a sulfide mineral, oxidized regions of the surface may be present, and the uranyl ion may form surface complexes in these areas (*34*). Once these sites are saturated, uptake may continue by coupled reduction of uranium and surface oxidation. As solution concentrations increase, a greater proportion of the uranium would be reduced, so the average number of axial oxygens would decrease and U–O distances around 2 Å, characteristic of oxide phases containing at least some U(IV) centers, e.g. U_3O_8 (*35*) would be observed. We may then expect a uranium atom to provide the best fit in the fourth shell at higher concentrations (Table 2), although iron gives a slightly lower R-factor in both cases. Thus, at high U loadings the precipitation of a discrete uranium oxide phase containing both U(VI) and U(IV) centers, e.g. U_3O_8 or U_4O_9 may occur. This is consistent with the findings of Wersin et al. (*9*) who reported uptake of uranyl on pyrite and galena surfaces associated with precipitation of a uranium oxide of mixed oxidation state.

The suggestion of phase formation is supported by the XANES data. Figure 6 shows the U L(III)-edge XANES spectra of the mackinawite samples along with spectra for U_3O_8, UO_2, uranyl on goethite, and aqueous uranyl nitrate. At low uranium loadings, the mackinawite XANES strongly resembles that of U on goethite, but as the U concentrations on the mackinawite surface increase, the XANES changes. The peak at 3–5 eV becomes less pronounced, while the region from 8 to 20 eV becomes more smoothly curved. At the highest surface concentration, the XANES most closely resembles that of U_3O_8, consistent with the EXAFS data.

Acknowledgments

The support of the Natural Environment Research Council (Grant GR3/9690) and of BNFL plc. is acknowledged. Thanks are due to CLRC Daresbury Laboratory for the provision of beamtime and support in carrying out the experiments.

Literature Cited

(1) Ho, C. H.; Doern, D. C. *Can. J. Chem.* **1985**, *63*, 1100.
(2) Hsi, C.-K. D.; Langmuir, D. *Geochim. Cosmochim. Acta* **1985**, *49*, 1931.
(3) Borovec, Z. *Chem. Geol.* **1981**, *32*, 45.
(4) Payne, T. E.; Waite, T. D. *Radiochim. Acta* **1991**, *52/53*, 487.
(5) Morse, J. W.; Arakaki, T. *Geochim. Cosmochim. Acta* **1993**, *57*, 3635.
(6) Chisholm-Brause, C. J.; Conradson, S. D.; Buscher, C. T.; Eller, P. G.; Morris, D. E. *Geochim. Cosmochim. Acta* **1994**, *58*, 3625.
(7) Morris, D. E.; Chisholm-Brause, C. J.; Barr, M. E.; Conradson, S. D.; Eller, P. G. *Geochim. Cosmochim. Acta* **1994**, *58*, 3613.
(8) Waite, T. D.; Davis, J. A.; Payne, T. E.; Waychunas, G. A.; Xu, N. *Geochim. Cosmochim. Acta* **1994**, *58*, 5465.
(9) Wersin, P.; Hochella, M. F., Jr.; Persson, P.; Redden, G.; Leckie, J. O.; Harris, D. W. *Geochim. Cosmochim. Acta* **1994**, *58*, 2829.
(10) Duff, M. C.; Amrhein, C. *Soil Sci. Soc. Am. J.* **1996**, *60*, 1393.
(11) Turner, G. D.; Zachara, J. M.; McKinley, J. P.; Smith, S. C. *Geochim. Cosmochim. Acta* **1996**, *60*, 3399.
(12) Carroll, S. A.; Bruno, J. *Radiochim. Acta* **1991**, *52/53*, 187.
(13) Kornicker, W. A.; Morse, J. W. *Geochim. Cosmochim. Acta* **1991**, *55*, 2159.
(14) Watson, J. H. P.; Ellwood, D. C. *Miner. Eng.* **1994**, *7*, 1017.
(15) Bancroft, G. M.; Hyland, M. M. *Rev. Mineral.* **1990**, *23*, 511.
(16) Charlet, L.; Manceau, A. *J. Colloid Interface Sci.* **1992**, *148*, 443.
(17) Schwertmann, U.; Cornell, R. M. *Iron Oxides in the Laboratory – Preparation and Characterisation*; VCH: New York, 1991; Chapters 5–6, pp 61–84.
(18) Lennie, A. R.; Redfern, S. A.; Schofield, P. F.; Vaughan, D. J. *Miner. Mag.* **1995**, *59*, 677.
(19) Lennie, A. R.; Vaughan, D. J. In *Mineral Spectroscopy: A Tribute to Roger G. Burns*; Dyar, M. D., McCammon, C., Schaefer, M. W., Eds.; The Geochemical Society Special Publication No. 5, 1996; p 117.
(20) Calas, G.; Bassett, W. A.; Petiau, J.; Steinberg, D.; Tchoubar, D.; Zarka, A. *Phys. Chem. Miner.* **1984**, *11*, 17.
(21) Brown, G. E., Jr.; Calas, G.; Waychunas, G. A.; Petiau, J. *Rev. Mineral.* **1988**, *18*, 431.
(22) Binsted, N. *CLRC Daresbury Laboratory EXCURV97 program*; CLRC Daresbury Laboratory: Warrington, 1997.
(23) Lee, P. A.; Pendry, J. B. *Phys. Rev. B* **1975**, *11*, 2795.
(24) Gurman, S. J.; Binsted, N.; Ross, I. *J. Phys. C: Solid State Physics* **1984**, *17*, 143.
(25) Gurman, S. J.; Binsted, N.; Ross, I. *J. Phys. C: Solid State Physics* **1986**, *19*, 1845.
(26) Hedin, L.; Lundqvist, S. *Solid State Phys.* **1969**, *23*, 1.
(27) Binsted, N.; Strange, R. W.; Hasnain, S. S. *Biochemistry* **1992**, *31*, 12117.
(28) Rehr, J. J.; Albers, R. C. *Phys. Rev. B: Condensed Matter* **1990**, *41*, 8139.
(29) Langmuir, D. *Geochim. Cosmochim. Acta* **1978**, *42*, 547.
(30) Dent, A. J.; Ramsay, J. D. F.; Swanton, S. W. *J. Colloid Interface Sci.* **1992**, *150*, 45.

(31) Tsunashima, A.; Brindley, G. W.; Bastovanov, M. *Clays Clay Miner.* **1981**, *29*, 10.
(32) Parkman, R. H.; Charnock, J. M.; Bryan, N. D.; Livens, F. R.; Vaughan, D. J. *Am. Miner.* **1999**, *84*, 407.
(33) Bargar, J. R.; Reitmeyer, R. L.; Davis, J. A. *Environ. Sci. Technol.* **1999**, *33* (14), 2481.
(34) McIntyre, N. S.; Zetaruk, D. G. *Anal. Chem.* **1977**, *49*, 521.
(35) Wells, A. F. *Structural Inorganic Chemistry*, 4th ed.; Clarendon: Oxford, 1975.

Received for review June 28, 1999. Revised manuscript received December 20, 1999. Accepted December 20, 1999.

ES990703K

Environ. Sci. Technol. 1997, 31, 2039–2044

Reduction of Hexavalent Chromium by Amorphous Iron Sulfide

RONALD R. PATTERSON AND SCOTT FENDORF*
Soil Science Division, University of Idaho, Moscow, Idaho 83844-2339

MARK FENDORF
National Center for Electron Microscopy, Lawrence Berkeley Laboratory, 1 Cyclotron Road, Berkeley, California 94720

The reduction of Cr(VI) to Cr(III) decreases the toxicity and mobility of chromium contaminants in soils and water. In addition, the formation of a highly insoluble Cr(III) product would decrease the likelihood of future Cr(III) re-oxidation. Amorphous iron sulfide minerals like mackinawite (FeS_{1-x}) have the potential to reduce large quantities of Cr(VI) and in the process form very stable [Cr, Fe]$(OH)_3$ solids. In this study, we examine the effectiveness of amorphous FeS as a reductant of Cr(VI) by identifying the solution and solid-phase products of the reaction between FeS suspensions and chromate. Iron sulfide suspensions at pH 5.0, 7.0, and 8.0 were reacted with a range of Cr(VI) solutions from 50 to 5000 μM in a N_2 atmosphere glovebox for 3 d. Solutions were analyzed using ICP–AES, IC, and colorimetric methods; solids were analyzed using XRD, TEM, EDS, and XANES spectroscopy. Iron sulfide removed all of the added Cr(VI) from solution for the reaction conditions studied and reduced between 85% and 100% of the Cr(VI) to Cr(III). Chromate reduction occurred dominantly at the FeS surface and resulted in $[Cr_{0.75},Fe_{0.25}](OH)_3$; while less extensive, reduction of Cr(VI) by Fe(II) (aq) was noted and produced a solid with the opposite Cr:Fe ratio, $[Cr_{0.25},Fe_{0.75}](OH)_3$.

Introduction

The widespread use of chromium in industrial applications such as tanning, metallurgy, and plating has lead to its introduction into soils and waters. The reduction of Cr(VI) to Cr(III) and the formation of insoluble chromium precipitates are essential steps in the remediation of chromium-contaminated sites (*1*). Once chromium enters the environment, its most stable oxidation states are Cr(III) and Cr(VI). While trivalent chromium is relatively innocuous and immobile, Cr(VI) moves readily through soils and aquatic environments and is a strong oxidizing agent capable of being absorbed through the skin (*2*). Hexavalent chromium is an irritant of plant and animal tissues and is a carcinogen (*3*). Because of these toxic effects, the U.S. EPA Drinking Water Regulations limit total chromium in drinking water to less than or equal to 0.1 mg/L (*4*).

Predicted speciation of chromium based on redox potentials and pH often differs appreciably from the measured species (*5, 6*). For Cr(VI) reduction to occur, a suitable redox couple having a compatible electron symmetry to allow electron exchange must be present. Several effective Cr(VI) reducing agents are commonly found in soils, including ferrous iron (*7*), sulfide (*6*), and organic complexes (*8–11*). Additionally, direct enzymatic reduction of chromate has been demonstrated for a number of soil microorganisms (*12, 13*). Bartlett and Kimball (*14*) found that soils high in organic matter reduced Cr(VI) to Cr(III) rapidly over a pH range of 4.4–7.6. However, later work by James and Bartlett (*15*) showed that Cr(III) may form soluble chelated complexes with organic reductants. This greatly increases the chance for Cr(III) to eventually oxidize again and become remobilized.

Aqueous ferrous iron and sulfide have been demonstrated to effectively reduce Cr(VI) (*1, 6, 7*). The reduction of Cr(VI) to Cr(III) by ferrous iron is very rapid and is described by the following general reaction:

$$Cr(VI)(aq) + 3Fe(II)(aq) \rightarrow Cr(III)(aq) + 3Fe(III)(aq) \quad (1)$$

At pH values greater than 4, brown precipitates were observed by Eary and Rai (*6*) and were hypothesized to form via the following reaction

$$xCr(III) + (1-x)Fe(III) + 3H_2O \leftrightarrow (Cr_xFe_{1-x})(OH)_3(s) + 3H^+ \quad (2)$$

where x can vary from 0 to 1. The precipitate formed was thought to be $Cr_{0.25}Fe_{0.75}(OH)_3$, but was not conclusively identified.

Several other studies have shown the effectiveness of Fe(II) in chromium reduction. Under reduced conditions, Fe(II) is a major reductant of Cr(VI) in forested wetland soils (*16*) and in the sand and gravel of a suboxic aquifer (*17*). In fact, the rate of chromate reduction by Fe(II) is very rapid and proceeds even in the presence of dissolved O_2 at pH $\leq$ 8.0 (*18*). Eary and Rai (*19*) found that ferrous iron-bearing minerals such as hematite and biotite reduced hexavalent chromium as the minerals underwent dissolution. The rate of reduction was limited by the rate of Fe(II) release from the minerals, indicating that Cr(VI) was not reduced at the solid–water interface.

Iron sulfides can be a ubiquitous component of reduced soil and sediments. Some iron sulfide minerals, e.g., pyrite, are also found under oxidized conditions. Because Fe(II) and sulfide have both demonstrated the ability to reduce Cr(VI), the combination of these species in FeS should make it an effective reductant of Cr(VI). Our experiments were designed to test this premise. We characterized the solution and solid-phase products of reactions between iron sulfide suspensions and Cr(VI) to determine the fate of chromium, iron, and sulfur. By knowing how these elements partition themselves throughout the solid and solution phases, the extent of actual reduction and potential re-oxidation of Cr can be more accurately predicted.

Materials and Methods

The redox activity of the reagents used in the following procedure required that great care be taken to minimize oxygen exposure. Accordingly, all reagents were prepared using distilled and de-ionized water that had been thoroughly purged (~15 min/L) with 99.99% pure nitrogen gas. The synthesis of the reagents and all subsequent handling of the samples used during the experiment were conducted in a nitrogen-purged Labconco controlled atmosphere glovebox. Ambient O_2(g) inside the glovebox was measured using gas chromatography (GC) and ranged between 50 and 80 ppm throughout the experiment.

A stock FeS suspension with a density of 10.0 g/L FeS was prepared for all experiments. The suspension was made by mixing equal volumes of 1.0 M $FeCl_2$ and 1.0 M Na_2S solution at a constant rate of 0.50 L/min into a 2.0-L reaction vessel.

* Corresponding author e-mail:Fendorf@uidaho.edu.

S0013-936X(96)00836-X CCC: $14.00

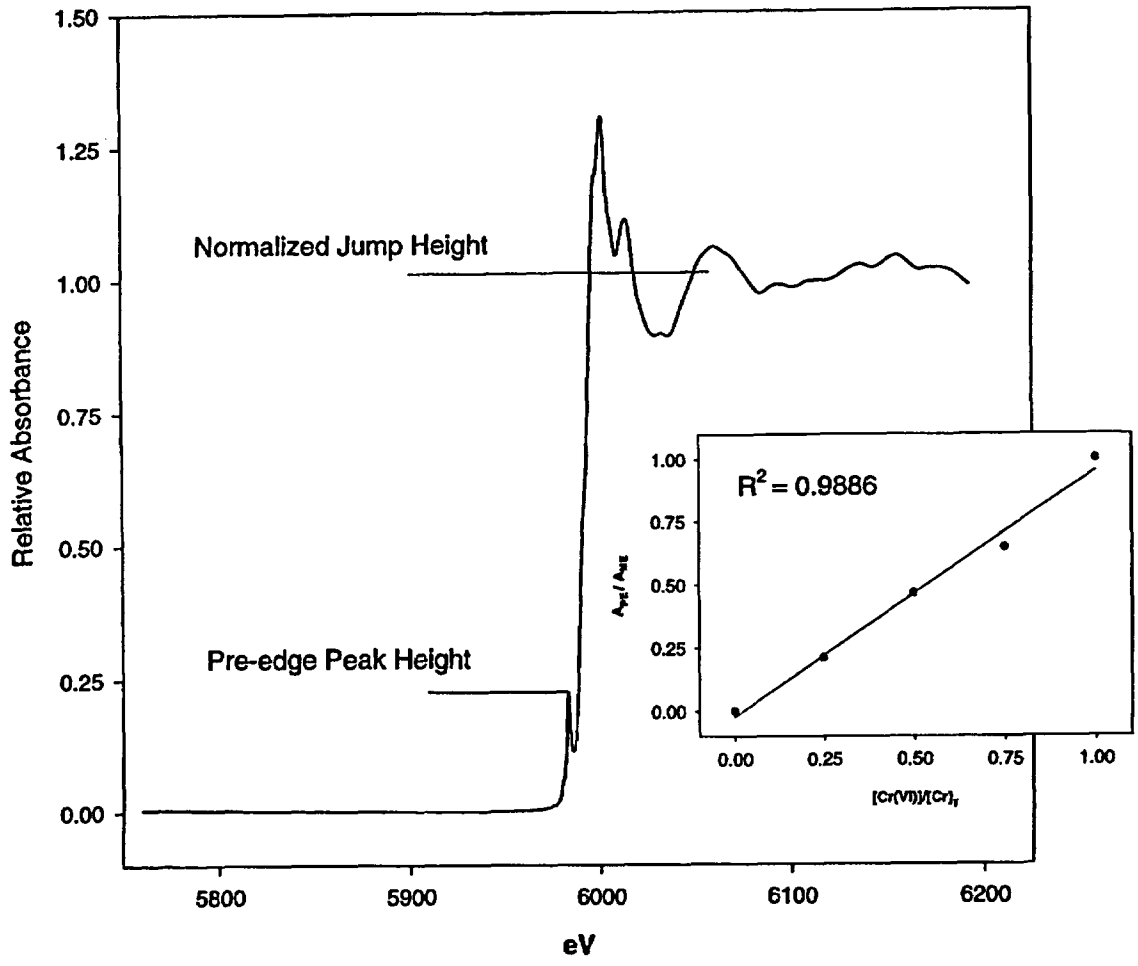

FIGURE 1. XANES spectra of a chromium standard [Cr(VI):Cr(III); 1:3]. The ratio of the Cr(VI) pre-edge peak was divided by the normalized jump height to calculate points for a standard curve. Inset: Standard curve of the pre-edge (PE) to main-edge (ME) amplitude for a series of [Cr(VI)]/[Cr]T).

TABLE 1. Solution Species and Proportion of Cr(VI) in Solids from Reaction of FeS with Cr(VI)[a]

sample	sulfite[b]	sulfate[b]	thiosulfate[b]	Fe(II)[b,d]	[Cr(VI)] / [Cr]T[c]
			pH 5.0		
blank	2.075	15.178	15.430	770.1	0
50	2.84 (± 1.05)	8.32 (± 1.21)	13.85 (± 2.65)	1460	12
100	2.83 (± 0.69)	8.85 (± 2.47)	25.30 (± 3.95)	1010	6.8
500	3.90(± 1.84)	6.95 (± 1.04)	46.39 (± 8.26)	1780	2.9
5000	2.27 (± 2.05)	4.50 (0.92)	0.11 (± 0.14)	1040	0
			pH 7.0		
blank	3.510	28.587	51.803	49.8	0
50	3.13 (± 0.93)	32.08 (± 0.87)	46.41 (± 0.57)	30.1	16
100	4.02 (± 0.66)	24.12 (± 2.25)	47.66 (± 1.50)	50.3	2.6
500	9.58 (± 9.14)	20.66 (± 2.88)	40.89 (± 12.25)	39.7	0
5000 μM	5.62 (± 4.01)	14.38 (± 2.18)	240.2 (± 39.86)	30.0	0
			pH 8.0		
blank	0.00	11.92	3.35	0.00	0
50	1.77 (± 0.56)	12.20 (± 0.21)	0.61 (± 0.08)	0.00	0
100	1.44 (± 0.21)	10.46 (± 1.15)	0.51 (± 0.03)	0.00	0
500	1.20 (± 0.15)	10.15 (± 0.93)	1.38 (± 0.19)	0.00	0
5000	1.26 (± 0.49)	18.33 (± 1.56)	5.13 (± 1.13)	0.00	0

[a] Trace amounts of polythionates were also found but are not reported. [b] Solution species, μM. [c] Solid-phase ratio. [d] Fe(II) = [Fe]T(aq).

Both reagents were in a 0.10 M NaCl matrix. Rapid mixing of the reagents produced very fine, highly reactive iron sulfide particles. After the particles settled to the bottom of the reaction vessel, the supernatant was removed and the precipitate was washed with 0.1 M NaCl solution. This procedure was repeated until Fe(II) concentrations in the supernatant were below 10.0 μM.

A Siemens powder X-ray diffractometer (XRD) used to analyze the precipitate indicated that the solid was dominantly amorphous. Slight ordering of the sample produced broad diffraction peaks characteristic of mackinawite (FeS_{1-x}) (*20*), a metastable, tetragonal iron sulfide mineral that commonly

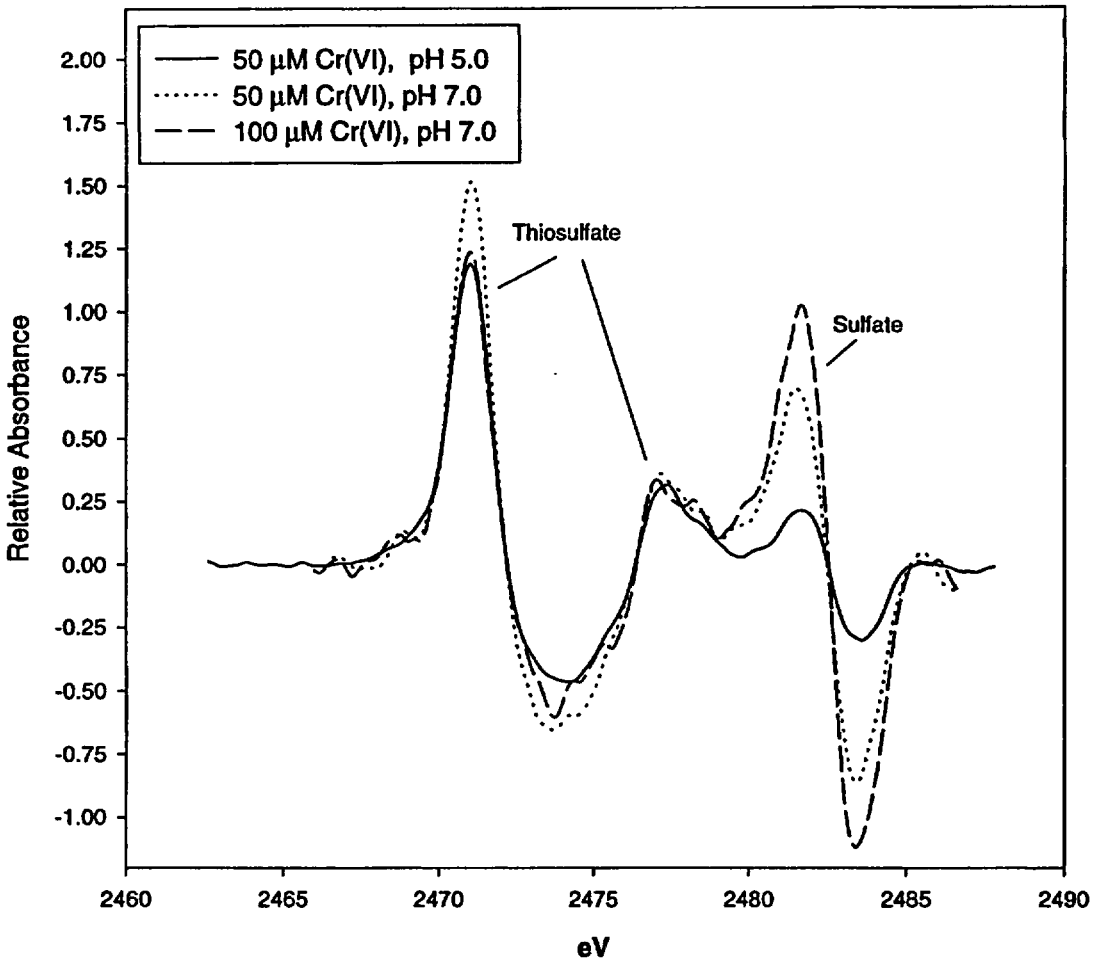

FIGURE 2. Derivative sulfur XANES spectra for a pH 5.0 sample with 50 μM initial Cr(VI) and 50 and 100 μM Cr(VI) samples at pH 7.0. Peak positions for thiosulfate and sulfate were determined by comparison to standard compounds.

occurs in reduced environments (*21*). Oxidation of FeS by exposure to air for 24 h formed lepidocrocite (γ-FeOOH).

Iron Sulfide Reactions with Cr(VI). The iron sulfide suspension was reacted with four concentrations of Cr(VI): 50, 100, 500, and 5000 μM. The Cr(VI) stock solution was 100.0 mM K_2CrO_4, and all reactions were carried out in a 0.1 M NaCl matrix. The total volume of the samples was 100 mL with an iron sulfide suspension density of 0.5 g/L. Samples were prepared at pH values of 5.0, 7.0, and 8.0 to determine the effect of pH on the reaction for each of the Cr(VI) concentrations. All experiments were performed in triplicate with one control (100 mL of 0.5 g/L FeS suspension without the addition of Cr) at each pH. The samples were reacted in 125-mL Nalgene plastic bottles with screw-on plastic lids. After Cr(VI) was added to the FeS suspensions and the pH was adjusted, the reaction vessels were capped and placed on a reciprocating shaker inside of the glovebox for 72 h. A preliminary study, as well as kinetics research of Cr(VI) reduction by Fe(II) (*18, 19*), indicated that Cr was completely removed from solution within 1 h. To ensure that the reactions reached a steady state, they were continued for 3 d with pH adjustments daily; only minimal changes in pH were noted after the first day of reaction. After the 3-d reaction period, the samples were filtered through 0.22-μm membrane filters. The resulting solutions and precipitates were saved in N_2-purged containers and stored in the glovebox until analysis.

Solution Analysis. Colorimetric methods were used to analyze solution samples for Cr(VI) (*22*), Fe(II) (*23*), and sulfide (S^{2-}) (*24*) using a Bausch and Lomb Spectronic 501 spectrometer. Total S, Fe, and Cr in solution were measured using a Thermo Jarrell Ash IRIS inductively coupled plasma (ICP) spectrometer. Speciation of sulfur products in solution was accomplished using ion chromatography (IC). A Dionex Advanced Gradient Pump (AGP) with a CDM-3 conductivity detector and an Ion Pac AS11 analytical column were used for all IC experiments. A gradient elution using 5.0 and 100 mM NaOH eluents was found to separate and detect S^{2-}, $S_2O_3^{2-}$, SCN^-, SO_3^{2-}, and SO_4^{2-} standards within 25 min. We started our gradient method with 5.0 mM NaOH for the first 3 min. The sample (in a 10.0-μL sample loop) was injected into the column 2 min after the start of the run. After the first 3 min, 100 mM NaOH was slowly added into the eluent until the final proportions of the two eluents at the end of the run was 60% 5.0 mM and 40% 100 mM NaOH.

A method for preserving reactive sulfur species for IC analysis was adapted from Moses et al. (25). Two 5.0-mL aliquots were taken from each sample and filtered through 0.22-μm membrane filters. Immediately after filtration, 0.1 g of Na Amberlite cation exchange resin (100 mesh) was added to ensure the complete removal of Fe(II) from the samples, thus preserving thiosulfate. Sulfite oxidation was inhibited by the addition of 50.0 μL of 37% aqueous formaldehyde to one of the aliquots (aliquot 1). The other aliquot (aliquot 2) preserved polythionate for analysis by adding 1.0 mL of 0.1 M KCN. The reaction of polythionate ($S_nO_6^{2-}$, $n = 4-6$) ions with cyanide (CN^-) produces $n - 3$ thiocyanate (SCN^-) ions. Thiocyanate is more resistant to degradation than poly-

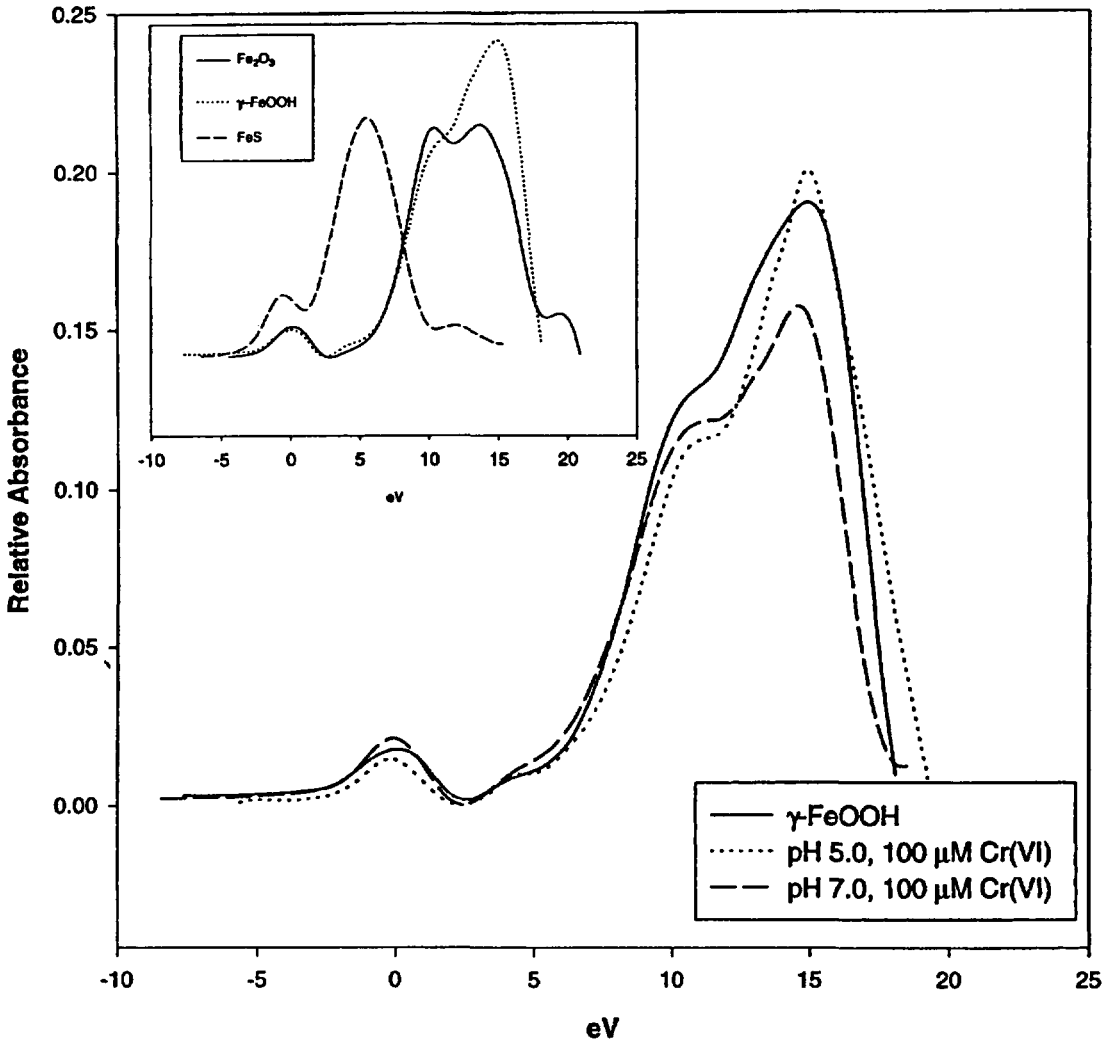

FIGURE 3. First derivative Fe XANES spectra of FeS reacted with 100 μM initial Cr(VI) at pH 5.0 and 7.0 showing similarity to the FeOOH standard. Iron standards of FeS, FeOOH, and Fe_2O_3 are shown for comparison in the inset.

thionates and is easily measured using IC. Thiosulfate is also produced from this reaction and can be easily measured using IC as well. Concentrations of SO_4^{2-}, SO_3^{2-}, and $S_2O_3^{2-}$ are determined in aliquot 1. Analysis of aliquot 2 allows the concentrations of polythionate to be calculated. During IC analysis, large chloride peaks from the salt matrix of our samples had identical retention times as those observed for sulfide standards, making detection of sulfide in our samples using IC impossible. For this reason, sulfide was analyzed colorimetrically with a separate 8.0-mL aliquot. No sulfide was detected in any of the reacted samples. Using ICP data for total sulfur, a comparison was made to the totals obtained from IC analysis to ensure that the majority of sulfur in our samples was speciated.

Solid-Phase Analysis. X-ray absorption near edge spectroscopy (XANES) was conducted at the Stanford Synchrotron Radiation Laboratory (SSRL) on beam line 4-1 using a Si (111) monochromator. Data were collected through the K-edge regions of S, Fe, and Cr. Sulfur and iron speciation in solids was done by comparing first derivatives of the sample spectra to first derivative spectra of standard compounds (*26–29*). Chromium was also speciated using XANES spectroscopy. A series of Cr(III):Cr(VI) standards were made by adding Cr_2O_3 and Na_2CrO_4 powders at Cr molar ratios of 0:1, 1:3, 1:1, 3:1, and 1:0. The powders were then ground and mixed using a corundum mortar and pestle. An estimate of the percentage of Cr(VI) in the solid can be calculated by dividing the height of the Cr(VI) pre-edge peak by the total atomic absorption (Figure 1); the height of the Cr(VI) pre-edge peak is proportional to the concentration of Cr(VI), while the height of the total jump is proportional to the total amount of chromium. Good agreement ($r^2 \geq 0.988$) was found between the known and calculated amounts of Cr(VI) in standards (inset, Figure 1), which was then used to calculate the Cr(VI) to Cr(III) ratio in the solids.

To explore the solid-phase products and alterations evident at the highest Cr(VI) concentrations, transmission electron microscopy (TEM) imaging and energy dispersive spectroscopy (EDS) analysis of the solid products was performed. TEM imaging was done at the National Center for Electron Microscopy (NCEM), at the Lawrence Berkeley National Laboratory using a TopCon 002B high-resolution TEM. The combination of the TEM and EDS techniques allows both the exploration of a sample's morphology (using TEM) as well as the identification of elemental composition.

Results and Discussion

Iron sulfide is extremely effective at removing chromate from solution through the pH range of 5.0–8.0 and through a range of initial Cr(VI) concentrations from 50 to 5000 μM. Under the conditions of this experiment, FeS removed all of the added hexavalent chromium from solution, and all of the

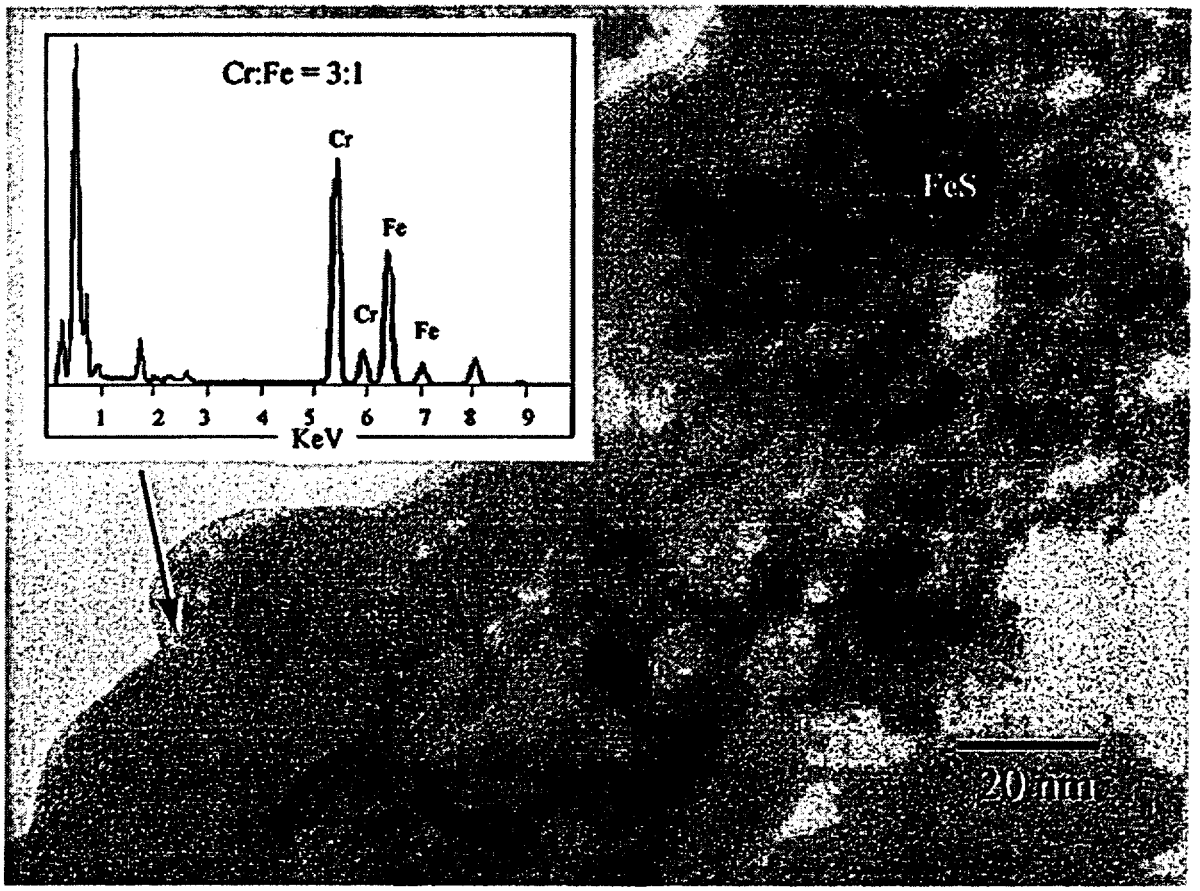

FIGURE 4. High-resolution TEM image of FeS reacted with 5000 μM Cr(VI) at pH 7.0. The darker, unreacted FeS particles can be seen beneath a "rind-like" Fe-Cr-S product. The relative proportion of Cr to Fe in the reaction product was determined by EDS spectroscopy (inset), which indicates a ratio of 3:1 in the solid. Smaller portions of the solid showed an opposite Cr:Fe ratio of 1:3 thought to be formed by solution reaction between Fe(II) and chromate.

chromium (trivalent or hexavalent) was partitioned into the solid phase.

Total iron in solution after the reaction period was extremely low or below detection limits at pH 7.0 and pH 8.0. However, significant amounts of Fe(II) were measured in solution at pH 5.0, ranging from 0.97 to 1.90 mM (Table 1). Iron sulfide suspensions at pH 5.0 and pH 7.0 before the addition of Cr(VI) had Fe(II) concentrations of 0.77 and 0.050 mM, respectively. This increase in Fe(II) at low pH can be explained by an increase in solubility of FeS, which increases drastically at low pH. Morse et al. (*30*) report a K_{sp} of 2.86 $\times$ 10^{-4} for the dissolution of mackinawite by the following reaction:

$$H^+ + FeS \rightarrow Fe^{2+} + HS^- \quad (3)$$

Our 0.5 g/L suspensions underwent complete mineral dissolution at pH < 4.0. Although the levels are low, O_2 inside the glovebox would also contribute to the oxidative dissolution of FeS.

Thiosulfate is the dominant S phase in solution resulting from FeS reacting with Cr(VI), with smaller amounts of sulfate produced (Table 1); trace amounts of sulfite and polythionates were also observed. Total S in solution was generally highest at pH 7.0 and lowest at pH 8.0 for samples with initial Cr(VI) concentrations between 0 and 500 μM (Table 1). The pH 7.0 sulfur data most likely reflect the resistance of thiosulfate decomposition in solutions at neutral pH (*25*). The small amount of S remaining in solution at pH 8.0 is likely a consequence of a decrease in the Cr(VI) reduction rate by sulfide at high pH (*6*). At pH 5.0, solution S increases with initial Cr(VI) through the 50–500 μM range but decreases at 5000 μM Cr(VI) (see Table 1). A possible explanation for this result is that the oxidized S products have a low affinity for the FeS surface but have a high affinity for the surface of ferric (and chromic) oxyhydroxides formed from the oxidation of FeS. Furthermore, the oxidized solid product [$Cr_xFe_{1-x}(OH)_3 \cdot nH_2O$] appears to form in amounts significant enough to affect S sorption at the highest initial Cr(VI) concentration. The oxidized surface seems to have little affinity for S products at pH 7.0 and pH 8.0, which is in agreement with expected anion adsorption trends.

Solid-Phase Products. XANES spectroscopy was conducted to determine the solid-phase speciation of Cr, Fe, and S. Of particular significance were the levels of Cr(VI) in the solids that might be released back to solution. XANES spectroscopy was performed on samples reacted at pH 5.0, pH 7.0, and pH 8.0 with initial Cr(VI) concentrations of 50, 100, 500, and 5000 μM. As initial Cr(VI) concentrations increase, a greater percentage of the total chromium is reduced. This may result because of an increase in oxidative dissolution of the FeS particles associated with higher initial chromate concentrations. The dissolution of the FeS would release highly reactive Fe(II) and S^{2-} ions into solution. Sulfide has been shown directly reduce Cr(VI) (*6*) and to catalyze the reduction of Cr(VI) by ferrous iron (*1*); these two processes may account for the increased reduction of chromium at high initial Cr(VI) concentrations.

Qualitative sulfur speciation of solid products formed under conditions similar to those found in reduced soils (neutral to low pH, with low metal concentrations) was done

by comparing the first derivative XANES spectra of sulfur standards to the unknowns. This technique allows subtleties in the data caused by changes in oxidation state or local structural environment to be amplified and easier comparisons between standards and unknowns (*26*). Figure 2 shows that the primary sulfur species found in the solids at pH 5.0 and pH 7.0 are thiosulfate and sulfate, the same species observed in solution. The positions of the inflection points in the data matched peaks produced by Na_2SO_4 and $Na_2S_2O_3$ standards.

A similar technique was used for solid-phase iron analysis. Figure 3 shows first derivative spectra of several common Fe minerals. By comparing the derivative spectra for reacted samples with standards, the Fe oxidation state was determined. A close match between the derivative spectra of γ-FeOOH and reacted FeS was observed, in agreement with XRD data that indicated γ-FeOOH to be the dominant crystalline phase in FeS oxidized by oxygen rather than chromate.

In an effort to identify the Fe-Cr solid product, TEM imaging with EDS analysis was performed on FeS reacted with 5000 μM Cr(VI) at pH 7.0 (Figure 4); this pH was chosen based on the solution data results, which indicated that S oxyanions were not sorbed appreciably. EDS spectroscopy was performed over several locations on the particle surface including edge regions without substrate FeS. Through most of the sample, a 3:1 ratio of Cr to Fe was observed. This ratio is indicative of Cr(VI) reacting with the FeS solid and supports the XANES data; increasing amounts of Cr(VI) are reduced as the solubility of FeS decreases with increased pH. If the reduction of Cr(VI) was dominated by reactions between Fe(II) and HS^- ions in solution, the opposite result would be expected due to the greater dissolution of FeS with decreasing pH.

The solution- and solid-phase data as well as the observation that the reaction consistently raised the pH of the solutions allow a possible overall reaction to be hypothesized:

$$3CrO_4^{2-} + 2FeS + 9H_2O \rightarrow 4[Cr_{0.75},Fe_{0.25}](OH)_3 + Fe^{2+} + S_2O_3^{2-} + 6OH^- \quad (4)$$

Interestingly, small "pockets" of the opposite ratio (3:1 Fe to Cr) were also observed. We believe this to be the product formed by the reaction between Cr(VI) and aqueous Fe(II):

$$3Fe^{2+} + HCrO_4^- + 8H_2O \rightarrow 4[Cr_{0.25},Fe_{0.75}](OH)_3 + 5H^+ \quad (5)$$

While the proposed dominant product of Cr(VI) reduction by FeS, $[Cr_{0.75},Fe_{0.25}](OH)_3 \cdot nH_2O$ (eq 4), seems conclusive, the complete sulfur reaction mechanism is complicated and unresolved. The $S_2O_3^{2-}$ and SO_4^{2-} products found in solution indicate a complex reaction mechanism involving several sulfur intermediates.

The large concentrations of Cr(VI) that can be reduced by FeS over the period of a few hours lead us to believe that the dissolution of Fe(II) does not have to occur before chromium can be reduced. It appears that reduction is taking place at the solid–solution interface, making these materials far more efficient reductants than iron-bearing oxide minerals such as biotite. Regardless of whether the reaction occurs at the FeS surface or in solution with a dissolution product, systems containing FeS appear to be very effective reductants of Cr(VI). Only small amounts of Cr(VI) were detected in solid products at the end of the reaction period, and no chromium remained in solution. In addition to the reduction of chromium, the formation of $[Cr_{0.75},Fe_{0.25}](OH)_3 \cdot nH_2O$ solids should greatly decrease the chance of chromium reoxidation.

Acknowledgments

We thank Drs. M. Morra, P. Brown, and S. Wood at the University of Idaho for their assistance on this project. Special thanks are given to the staff of SSRL and NCEM for their help in this study. Funding for this research was provided by the NSF-Idaho EPSCoR program and the National Science Foundation (Grant OSR-930539). Electron microscopy was performed at the National Center for Electron Microscopy, Lawrence Berkeley Laboratory, a facility funded by the Director, Office of Energy Research, Office of Basic Energy Sciences, Material Science Division of the U.S. Department of Energy under Contract DE-AC03-76F00098. XANES analyses were performed at SSRL, which is operated by the Department of Energy, Office of Basic Energy Sciences.

Literature Cited

(1) *Control and treatment technology for the metal finishing industry. Sulfide precipitation*; U.S. Environmental Protection Agency, Technology Transfer Summary Report; U.S. Government Printing Office: Washington, DC, 1980; EPA 625/8-80-003.
(2) Nriagu, J. O.; Nieboer, E. *Chromium in the natural and human environments*; John Wiley and Sons: New York, 1988.
(3) *Medical and biological effects of environmental pollutants: Chromium*; National Research Council, Printing and Publishing Office, National Academy of Science: Washington, DC, 1974.
(4) *Drinking water regulations and health advisories* U.S. Environmental Protection Agency, Office of Water; U.S. Government Printing Office: Washington, DC, 1994.
(5) Fendorf, S. E. *Geoderma* **1995**, *67*, 55.
(6) Pettine, M.; Millero, F. J.; Passino, R. *Mar. Chem.* **1994**, 335.
(7) Eary, L. E.; Rai, D. *Environ. Sci. Technol.* **1988**, *22*, 972.
(8) Deng, B.; Stone, A. T. *Environ. Sci. Technol.* **1996**, *30*, 463.
(9) Wittbrodt, P. R.; Palmer, C. D. *Environ. Sci. Technol.* **1995**, *29*, 255.
(10) Elovitz, M. S.; Fish, W. *Environ. Sci. Technol.* **1995**, *29*, 1933.
(11) Lay, P. A.; Levina, A. *Inorg. Chem.* **1996**, *35*, 7709.
(12) Bonet, R.; Simon-Pujol, M. D. *Appl. Environ. Microbiol.* **1993**, *59*, 3516.
(13) Ishibashi, Y.; Cerantes, C.; Silver, S. *Appl. Environ. Microbiol.* **1990**, *56*, 2268.
(14) Bartlett, R. J.; Kimble, J. M. *J. Environ. Qual.* **1976**, *5*, 83.
(15) James, B. R.; Bartlett, R. J. *J. Environ. Qual.* **1983**, *12*, 169.
(16) Masscheleyn, P. H.; Pardue, J. H.; DeLaune, R. D.; Patrick, W. H., Jr. *Environ. Sci. Technol.* **1992**, *26*, 1217.
(17) Anderson, L. D.; Kent, D. B.; Davis, J. A. *Environ. Sci. Technol.* **1994**, *28*, 178.
(18) Fendorf, S. E.; Li, G. *Environ. Sci. Technol.* **1996**, *30*, 1614.
(19) Eary, L. E.; Rai, D. *Am. J. Sci.* **1989**, *289*, 180.
(20) Vaughan, D. J.; Craig, J. R. *Mineral chemistry of metal sulfide*; Cambridge University Press: London, 1978; pp 53–54.
(21) Arakaki, T.; Morse, J. W. *Geochim. Cosmochim. Acta* **1993**, *57*, 9.
(22) Bartlett, R. J.; James, B. R. *J. Environ. Qual.* **1979**, *8*, 31.
(23) Gibbs, M. M. *Water Res.* **1979**, *13*, 295.
(24) Cline, I. D. *Limnol. Oceanogr.* **1969**, *14*, 454.
(25) Moses, C. O.; Nordstrom, D. K.; Mills, A. L. *Talanta* **1984**, *31*, 331.
(26) Vairavamurthy, A.; Zhou, W.; Eglinton, T.; Manowitz, B. *Geochim. Cosmochim. Acta* **1994**, *58*, 4681.
(27) Frank, P.; Hedman, B.; Carlson, R. M. K.; Hodgson, K. O. *Inorg. Chem.* **1994**, *33*, 3794.
(28) Waldo, G. S.; Carlson, R. M. K.; Moldowan, J. M.; Peters, K. E.; Penner-Hahn, J. E. *Geochim. Cosmochim. Acta* **1991**, *55*, 801.
(29) George, G. N.; Gorbaty, M. L.; Kelemen, S. R.; Sansone, M. *Energy Fuels* **1991**, *5*, 93.
(30) Morse, J. W.; Millero, F. J.; Cornwell, J. C.; Rickard, D. *Earth Sci. Rev.* **1987**, *24*, 1.

Received for review September 27, 1996. Revised manuscript received February 25, 1997. Accepted March 4, 1997.[•]

ES960836V

[•] Abstract published in *Advance ACS Abstracts*, May 1, 1997.

Pergamon

PII: S0883-2927(98)00003-1

Applied Geochemistry, Vol. 13, No. 6, pp. 767–778, 1998

0883-2927/98 $ - see front matter

Field tracer test for denitrification in a pyrite-bearing schist aquifer

Hélène Pauwels*, Wolfram Kloppmann, Jean-Claude Foucher, Anne Martelat and Valérie Fritsche

BRGM Research Division, Avenue Claude Guillemin, B.P. 6009, 45060 Orleans, France

(Received 22 May 1997; accepted in revised form 15 December 1997)

Abstract—A small-scale artificial tracer test performed on a schist aquifer in Brittany has helped clarify mechanisms and kinetics of *in situ* autotrophic denitrification. NO_3 was injected as a pulse simultaneously with a conservative tracer -Br^-. During the test, which lasted 210 h, 73% of the injected Br^- was recovered, as against only 47% of the NO_3. The 26% difference in the recovery of the two injected species is interpreted as being the result of denitrification, in part due to the direct oxidation of pyrite present in the solid aquifer according to the reaction: $5FeS_2 + 14NO_3^- + 4H^+ \rightarrow 7N_2 + 10SO_4^{2-} + 5Fe^{2+} + 2H_2O$, and in part due to subsequent iron oxidation according to the reaction: $NO_3^- + 5Fe^{2+} + 6H^+ \rightarrow 1/2N_2 + 5Fe^{3+} + 3H_2O$. Despite the potential increase in SO_4 and Fe resulting from denitrification through pyrite oxidation, the concentrations of these elements in the groundwater remain moderate due to the precipitation of minerals such as jarosite and/or natroalunite. Tracer transfer takes place in a heterogeneous medium which, according to the breakthrough curves, can be simplified to a dual-porosity aquifer comprising a high-permeability (fractures or large fissures) medium of low porosity from which only minor denitrification of circulating NO_3-bearing water was observed and a low-permeability (small fissures) medium of high porosity which induces a higher denitrification rate in the circulating NO_3-bearing water. The kinetics of the denitrification reaction are high compared with results obtained for other environments and can be described by a first-order model with a half life of 7.9 days for the low-porosity medium and only 2.1 days for the high-porosity medium.

INTRODUCTION

Nitrate contamination in agricultural regions results largely from the use of chemical fertilizers and animal manure; when surface application exceeds plant requirements, the highly soluble and mobile NO_3 is leached into the underlying groundwater. Nitrate pollution, which is on the increase, poses a serious threat to drinking water supplies and currently represents one of the major problems related to groundwater quality in Europe and America where the maximum admissible concentration of NO_3 permitted in drinking water is 0.80 mmol·l^{-1} (50 mg NO_3 l^{-1}) and 0.72 mmol l^{-1} (45 mg NO_3 l^{-1}), respectively.

The only way of removing NO_3 from groundwater so as to improve water quality is by denitrification (Edmunds and Walton, 1983, Trudell *et al.*, 1986; Mariotti *et al.*, 1988), i.e. the transformation of NO_3 into gaseous N_2 or N_2O, which involves several steps ($NO_3 \Rightarrow NO_2 \Rightarrow NO \Rightarrow N_2O \Rightarrow N_2$). Several electron donors for denitrification are present both in groundwater and in the solid aquifer, for example, CH_4, Fe^{2+}, H_2, H_2S and dissolved organic C in the groundwater and organic C, Fe–silicate and sulphide minerals in the solid phase (Postma, 1990; Hiscock *et al.*, 1991; Korom, 1992). The reactions are generally biologically mediated by either autotrophic or heterotrophic bacteria that derive their respective energy requirements from the oxidation of inorganic and organic material. However, even though the reactions may be thermodynamically favoured, kinetic limitations are to be expected.

Recent work has been directed towards developing numerical models to help understand and predict contaminant transport in aquifers. Denitrification is a relatively common process which has been considered in several NO_3-transport models (Frind *et al.*, 1990; Kinzelbach *et al.*, 1991; Postma *et al.*, 1991; Engesgaard and Kipp, 1992). Denitrification kinetics is *a priori* one of the modelling parameters, despite the fact that when groundwater flowrates are sufficiently low, equilibrium can be expected (Postma *et al.*, 1991). However, flowrates increase when groundwater moves through fractures and the denitrification rate can no longer be neglected. Several factors, such as water pH, temperature, electron-donor availability and metal concentration, influence the denitrification rate (Knowles, 1982; Bradley and Chapelle, 1993). Several orders of magnitude are reported in the literature for *in situ* denitrification rates, varying from less than 1 μmol l^{-1} d^{-1} (and probably far lower) to 0.22 mmol l^{-1} d^{-1} (Korom, 1992).

*Corresponding author.

Artificial tracer testing is a common method for determining transport parameters of a compound, namely a pollutant, and its interaction with the solid matrix. The purpose of this paper is to discuss denitrification and NO_3-transport parameters in an aquifer within an agricultural catchment where denitrification has been demonstrated (Pauwels, 1994). It concerns more specifically the denitrification kinetics and is based on the results obtained from an artificial tracer test.

LOCATION AND DESCRIPTION OF THE SITE

The Coët-Dan drainage basin, approximately 70 km SW of Rennes in Brittany, France (Fig. 1), is underlain by fissured and fractured Brioverian schist (530 Ma), with local facies variations dominated by silt, clay or sandstone (Pellerin and Van Vliet-Lanoe, 1994). Intensive agricultural activity in the catchment is dominated by corn and wheat farming, temporary pastures for dairy production and a high level of indoor pig-stock breeding. This activity has caused high concentrations of NO_3 in the surface waters, which have been monitored since 1972 by CEMAGREF (Centre nationale du Machinisme Agricole, du Génie Rural, des Eaux et Forêts) to investigate the effects of modern agriculture on surface-water resources (Cann, 1990); since 1989, mean annual concentrations at the basin outlet have commonly exceeded 1 mmol $NO_3\,l^{-1}$ (Cann, 1996).

The investigation of groundwater quality in the basin is more recent (Pauwels *et al.*, 1996). Results have shown that, in general, the hydrogeological configuration of the basin is based on the presence of two aquifer compartments; an upper compartment of sedimentary cover with interstitial porosity that has a captive role and a lower compartment made up of schist with fissure and fracture porosity that has a transmissive role (Martelat and Lachassagne, 1995). The chemical composition of the groundwater in the first few metres below the water table, where schist and sandstone are highly weathered, reveals high NO_3 contamination with concentrations as much as 3.2 mmol $NO_3\,l^{-1}$. At deeper levels, where the water moves through fractures in the solid rock, NO_3 concentrations decrease to below the detection limit. Part of this decrease is interpreted as being due to denitrification, i.e. the biological transformation of NO_3 into gaseous N_2 or N_2O. Pauwels (1994) demonstrated the occurrence of two denitrifying processes, heterotrophic and autotrophic. With the heterotrophic process, the oxidation of organic matter, catalysed by heterotrophic bacteria, contributes to the production of CO_2 as follows:

$$CH_2O + 4/5NO_3^- + 4/5H^+ \longrightarrow 2/5N_2 + CO_2 + 7/5H_2O \quad (1)$$

where CH_2O is a simplified formula for organic matter.

As pyrite is present in the aquifer rock, the denitrification reaction, mediated by the autotrophic bacteria *Thiobacillus denitrificans* (Kölle *et al.*, 1985), also occurs by the oxidation of S compounds:

$$5FeS_2 + 14NO_3^- + 4H^+ \longrightarrow 7N_2 + 10SO_4^{2-} + 5Fe^{2+} + 2H_2O \quad (2)$$

Pumping tests and monitoring of piezometric levels at the test site close to the outlet of the basin, revealed that although hydraulic connection between the two aquifer compartments is rather poor, the vertical flow component cannot be neglected. During the high-water period, ascending flow contributes to the recharge of the shallow aquifer and the river, whereas at low water the flux is inverted and shallow groundwater penetrates into the underlying aquifer.

Variations in NO_3 concentration with time have been observed in the deeper part of the aquifer (Pauwels, 1996), with concentrations ranging from the detection limit to more than 0.15 mmol $NO_3\,l^{-1}$. Variations in denitrification products (SO_4 and CO_2) have also been observed, suggesting rapid transfer of contaminated waters and a high denitrification rate (Pauwels, 1996). A small-scale tracer experiment was performed between two wells (F1 and DNS1; Figs 1 and 2) so as to further our understanding of the NO_3-transfer process and the denitrification rate.

The mineralogy of the schist was determined from DNS1 drill cuttings and through examination of cores from nearby shallow wells. The schist contains mainly quartz, muscovite and chlorite and, to a lesser extent, K-feldspar and plagioclase. Pyrite is present as the main accessory mineral below 7 m depth and, as determined from F1 cuttings, varies between 0.3 and 5‰ of the dry rock weight. Secondary solid phases include illite, smectite and Fe(II) hydroxides. Two secondary SO_4 minerals were also identified by X-ray diffraction on samples

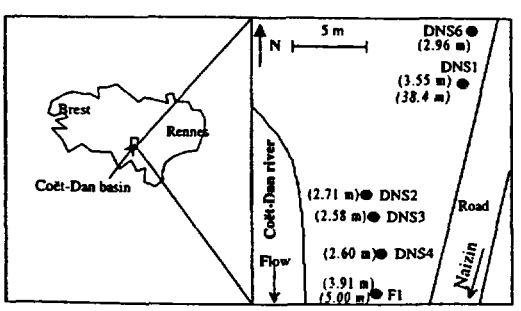

Fig. 1. Location of the test site in the Coët-Dan basin, Brittany, France, showing piezometric heads determined with respect to ground level at DNS1 (data in italics are the drawdown levels measured during pumping).

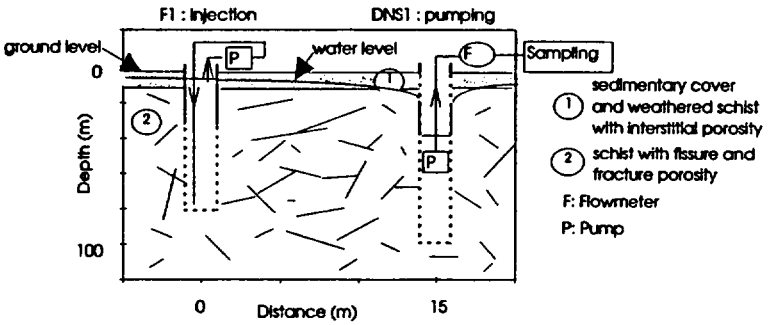

Fig. 2. Cross section illustrating the injection and pumping wells during the tracer test.

from several depths: jarosite ($KFe_3(SO_4)_2(OH)_6$) and natroalunite ($NaAl_3(SO_4)_2(OH)_6$).

METHODOLOGY

The test site near the basin outlet includes 6 cased wells (4 to 97 m deep) drilled along a profile of about 20 m near the Coët-Dan river, with screened intervals giving access to various parts of the aquifer. The tracer test was carried out between two wells, an "upstream" well (F1) for pulse injection and a "downstream" well (DNS1) for pumping (Fig. 1). F1 is slotted between 32 and 82 m depth, and DNS1, 15.2 m farther N, is slotted between 1 and 97 m depth (Fig. 2).

Pumping in DNS1 began on 30 August 1995 with a flowrate of 1.4 $m^3 h^{-1}$. As a result of pumping, the dynamic level of DNS1 decreased by 35 m due to important losses in hydraulic head (quadratic terms); true drawdown was determined at 10 m. After 2 days of pumping, a first test was run by injecting only the conservative tracer Br^- (3 kg of $NaBr^-$) into F1. Two days later, pumping was suspended for 10 h and water samples were taken at selected levels using a down-hole sampler comprising 3 distinct chambers separated by packers that allows precise sampling of the water from a chosen level of the aquifer by aspiration from the surface (Foucher *et al.*, 1995).

In order to study denitrification, a tracer mixture of Br^- (3 kg of $NaBr^-$) and NO_3 (5 kg of $NaNO_3$) was prepared in a 50-l container before being injected on 12 September 1995 through a tube leading to the bottom of well F1 (Fig. 2). The water column in F1 was continuously mixed by recirculation (extraction near the water surface, reinjection at the bottom) so as to obtain a homogenous concentration of the tracer throughout.

Because the injection well F1 is only slotted below 32 m depth, the tracer test concerned the unweathered zone of the aquifer. Nevertheless, pumping in DNS1 enhances vertical flux which allows mixing between a shallow groundwater component and the produced deep groundwater.

Sampling and measurements

Before starting the test, water samples were collected from the different wells at the site, including those concerned by the present experiment (F1 and DNS1). During the test, which continued until 21 September 1995, samples were collected at the DNS1 well head (after flowrate measurement) by an operator during the day and by an automatic sampler at night; samples were also taken in F1 so as to monitor the loss of tracers from the well. The samples were filtered after determining pH and E_h.

Alkalinity was measured on site by titration with HCl and the equivalent point determined according to Gran (1952). The solutions were also analysed immediately after recovery for Fe^{2+} using the "Merck Spectroquant Fe" spectrometric measuring method.

Anion (Br^-, NO_3, NO_2, Cl and SO_4) concentrations were determined in the laboratory by capillary electrophoresis (CIA Waters), with precision ranging from 5% for concentrations over 0.03 mmol l^{-1}, to 10% for concentrations between 0.01 and 0.03 mmol l^{-1}. NH_4 was determined colorimetrically with a precision of 5% and a detection limit of 0.005 mmol l^{-1}. Only the waters collected in the wells before tracer injection were analysed for cations (Na, K, Ca and Mg [HPLC, Dionex; precision greater than 5%]) and for dissolved organic C (by pyrolysis at 680°C and CO_2 infrared detection [TOC 5000 Shimadzu]).

Five samples for bacteriological determination were also collected in sterile plastic containers before and during the test and stored at 4°C before analysis in the GRAM company laboratories.

RESULTS

Analytical results

The chemical composition of the waters from F1, DNS1 and the other neighbouring wells before tracer injection is shown in Table 1 and the evolution

Table 1. Chemical composition of the samples from the injection (F1), pumping (DNS1) and neighbouring (DNS2, DNS3, DNS4, DNS6) wells before tracer injection. Concentrations are expressed in mmol l^{-1}, except alkalinity which is in meq l^{-1}

Well	Slotted depth (m)	Sampling date	pH	T (°C)	Alk	Na	K	Ca	Mg	Cl	NO_3	SO_4	Fe	DOC
F1	32–81	29-08-95	6.67	12.5	1.02	0.80	0.033	0.36	0.38	0.67	<0.002	0.24	0.059	0.042
DNS1	1–97	01-09-95	6.36	14.1	0.69	n.d.	n.d.	n.d.	n.d.	0.77	0.026	0.24	0.038	n.d.
DNS4	1–4	29-08-95	6.47	21.1	1.95	1.30	0.11	0.90	1.20	1.56	2.54	0.04	0.064	0.77
DNS6	1–5	29-08-95	5.17	16.9	0.051	1.27	0.077	0.51	1.14	1.61	1.50	0.18	0.002	n.d.
DNS2	14–21	28-08-95	6.68	12.9	1.0	0.86	0.059	0.44	0.38	0.79	0.011	0.32	0.082	0.058
DNS3	7–15	28-08-95	6.06	13.3	0.44	0.94	0.046	0.31	0.31	0.97	<0.002	0.36	0.032	0.058

of the chemical composition of the groundwaters in the injection and pumping wells is illustrated by Figs 3–6. Before the mixed NO_3–Br^- tracer test started, the NO_3 concentration in F1 was below the detection limit (Table 1). In DNS1, as this well also taps water rich in NO_3's from the upper part of the aquifer, NO_3's were detected in the water at concentrations of around 0.025 mmol l^{-1} after 2 days of pumping (when the first samples were taken), following which the waters showed a rapid decrease in NO_3 concentration to below the detection limit (Fig. 3), where it remained during the following 10 days of pumping before NO_3 injection.

The Br^- concentration versus depth in DNS1 (Fig. 4), recorded during the first step of the present test on 3 September 1995 when pumping had been suspended and Br^- concentrations were 60% of the maximum concentration of the breakthrough curve, indicates that Br reached the pumping well mainly through the aquifer below 50 m depth. This result also indicated that the NO_3's would be transferred between the injection and pumping wells exclusively in the lower part of the aquifer where natural NO_3 concentrations are below the limit of detection as a result of denitrification.

Monitoring the tracer concentrations in F1 after the mixed Br–NO_3 tracer injection showed that half of the injected compounds had left the well less than $5\frac{1}{2}$ h after injection [Fig. 5(a)]. The amount of tracer left in well F1 was less than 20% after 1 day, less than 10% after 2 days and only 2% after 5 days (17 September 1995). During this time, the NO_3/Br ratio in the F1 groundwater remained stable [Fig. 5(b)] and it can therefore be concluded that no denitrification took place in the injection well before the departure of the NO_3 into the reservoir.

The Cl concentration in the pumped DNS1 waters [Fig. 6(a)] increased steadily during the test. Although this can be explained by the observed variations in Cl with time and space in the lower compartment of the aquifer, the curve on Fig. 6(a) could also indicate an increasing contribution of shallow groundwater; heavy rains that fell during the testing may have recharged the upper part of the aquifer and hence increased the contribution of this level in the pumped DNS1 waters. If such were

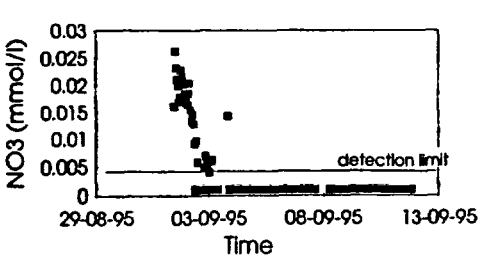

Fig. 3. Evolution of NO_3 concentration in the pumping well DNS1 before NO_3 injection in F1.

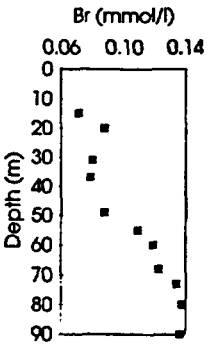

Fig. 4. Bromide concentrations as a function of depth in the pumping well DNS1 two days after the first injection of NaBr in F1.

the case, one would expect the NO_3 concentration in the upper compartment of the aquifer (measured at 1.5 mmol l^{-1}; Table 1) to have contributed to the NO_3 concentration measured in the pumped waters. However, as NO_3 concentration in DNS1 water was below the detection limit at the end of the test, we conclude that contribution of shallow groundwater to the deeper groundwater pumped by DNS1 could not have been significant, unless denitrification occurred during the transfer of the shallow groundwater to the pumping well. Even were one to accept this explanation, the denitrification of the shallow groundwater would be unrelated to the reduction of the NO_3's injected into F1 for the purpose of the test because this occurs only below a depth of 50 m.

The samples collected for biological determination showed that denitrifying bacteria, both heterotrophic (which reduce NO_3^- to NO_2^- alone or to gaseous species) and autotrophic (*Thiobacillus denitrificans*), were present in the waters before NO_3 injection, despite the lack of NO_3 in the samples

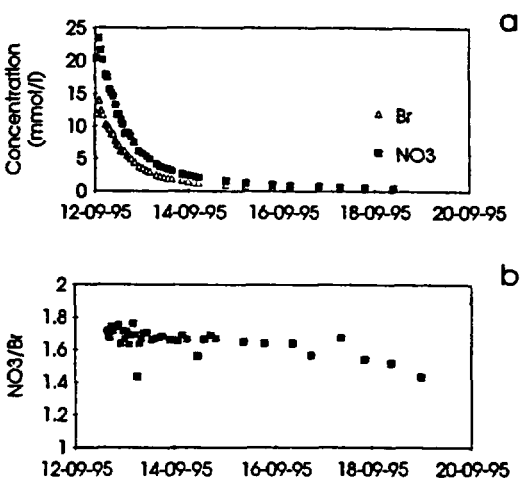

Fig. 5. (a) Evolution of the mixed tracer concentrations in the injection well F1 as a function of time. (b) Evolution of the NO_3/Br ratio in the injection well F1 as a function of time.

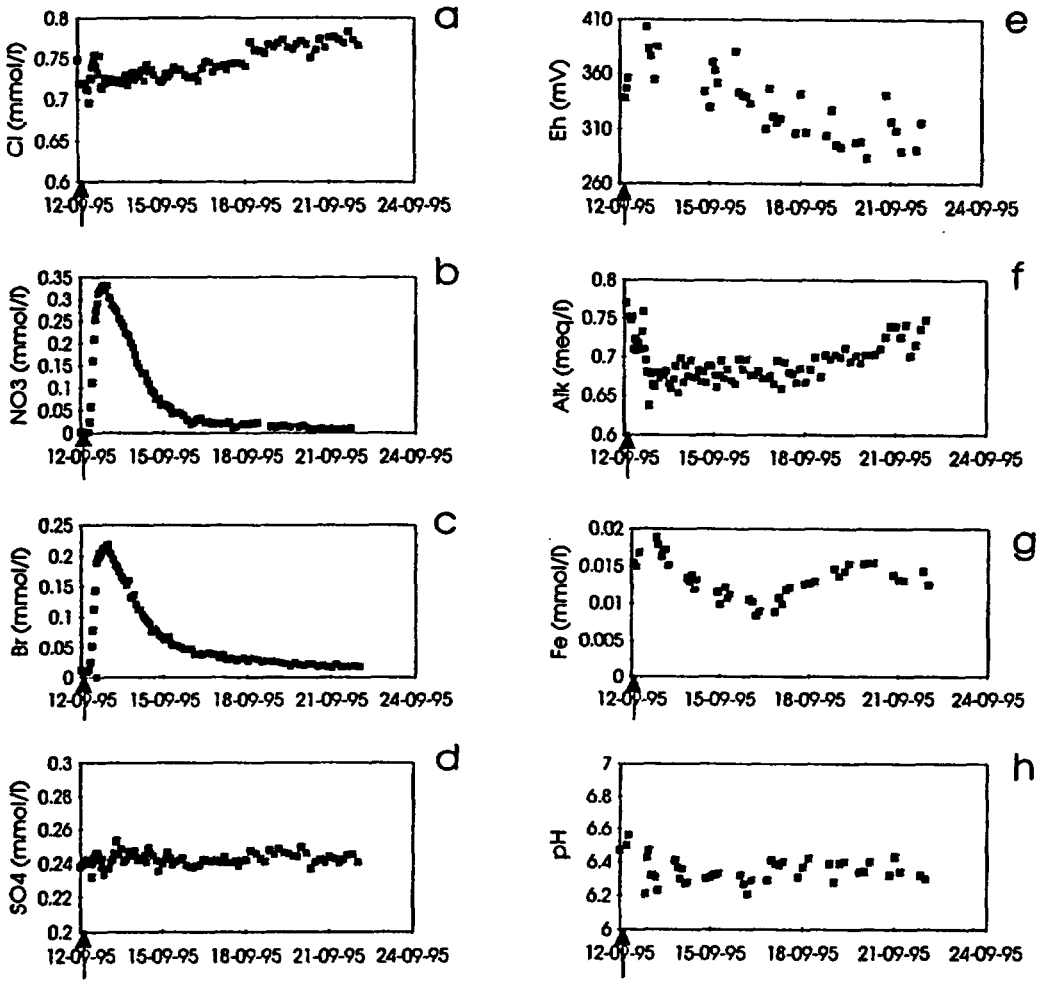

Fig. 6. Chemical composition of the water from the pumping well DNS1 as a function of time. The arrows indicate the moment of tracer injection in F1. (a) Cl^-, (b) NO_3^-, (c) Br^-, (d) S^{2-}, (e) E_h, (f) alkalinity, (g) Fe and (h) pH.

(Table 2). This presence indicates that if denitrification occurred after NO_3 injection, the possible lag period for biodegradation cannot be due to the lack of micro-organisms. The data on Table 2 only reflect the presence or lack of denitrifying bacteria and not a quantification of them; considering that most may be related to the aquifer matrix (Korom, 1992).

The evolution of tracer concentrations in the pumping well [Fig. 6(b) and (c)] indicates that breakthrough, and hence transfer between the two wells, is very rapid. NO_3 and Br appeared in the pumped water only $5\frac{1}{2}$ h after injection in F1. Other chemical variations were also observed during the test (Fig. 6), some of which must be due to interaction between the reactive tracer (NO_3) and the rock reservoir: for example, with appearance of the NO_3 in DNS1, E_h increased (NO_3 being an oxidant) and total alkalinity and Fe concentration decreased, whereas SO_4 concentration remained fairly stable throughout the test. NO_2 and NH_4 were almost absent during the test, suggesting that if NO_3 reduction does occur, the dominant products are gaseous species such as N_2 or N_2O.

Table 2. Quantity of denitrifying bacteria recorded in samples during the artificial tracer test on 12 and 13 September 1995

Denitrifying bacteria	Sampled 12-9-95	Sampled 13-9-95
Thiobacillus ferroxidans (nb/ml)	<0.5	0.6
Thiobacillus denitrificans (nb/ml)	200000	25000
Heterotrophic bacteria able to reduce NO_3 to gaseous N_2 (nb/ml)	13000	600
Heterotrophic bacteria able to reduce NO_3 to N_2 (nb/ml)	13000	25000

Evidence for denitrification

Assuming a conservative behaviour for Br and similar transport mechanisms for NO_3 and Br, the comparison between Br and NO_3 concentrations makes it possible to estimate the quantity of NO_3 removed by denitrification. If no NO_3 loss occurs in the system, then the $[NO_3]/[Br]$ ratio would remain constant throughout the duration of the test. The ratio would be equal to that measured in the injected water {1.69 in present case [Fig. 5(b)]} and NO_3 concentration would be expressed by:

$$[NO_3]_{cons.} = [Br] \times 1.69$$

where $[NO_3]$cons. is the NO_3 concentration determined if it were a conservative tracer and [Br] is the Br concentration in each sample.

The difference between this value and that measured during pumping would correspond to the missing NO_3, i.e. the quantity of NO_3 reduced.

The test results clearly show that significant amounts of NO_3 disappeared during the short circulation between the injection and pumping wells [Fig. 7(a)]. The amount of reduced NO_3 increased sharply during the first few hours of pumping then stabilized about 20 h after injection at between 0.03 and 0.05 mmol l^{-1}. After 100 h, the absolute amount of NO_3 reduced in each litre of pumped water decreased due to continued dilution of the tracer pulse, as shown on the Br breakthrough curve [Fig. 6(c)]. Nevertheless, the relative amount of reduced NO_3 can be expressed by:

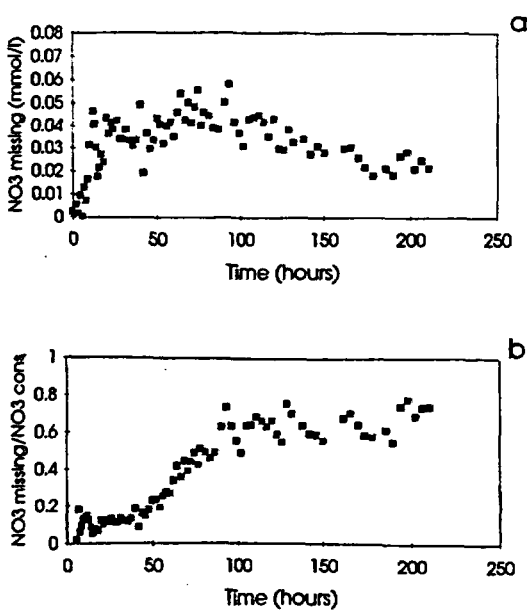

Fig. 7. (a) Concentration of missing NO_3 in the pumped DNS1 waters, calculated from Br-concentrations. ($[NO_3]_{missing} = [Br]_{meas} * 1.69 - [NO_3]_{meas}$). (b) Evolution of the $[NO_3]_{missing}/[NO_3]_{const}$ ratio in the pumped water as a function of time. ($[NO3]_{const} = [Br]_{meas} * 1.69$).

$$1 - \frac{[NO_3]_{meas.}}{[Br]_{meas.} \times 1.69}$$

which increased during the course of the test [Fig. 7(b)].

Breakthrough curve modelling

Interpretation of the results of pumping tests carried out on well DNS1 (Martelat and Lachassagne, 1995) showed that, as a first approximation, the fissured schist of the Coët-Dan site can be regarded as a homogeneous porous aquifer. It therefore seemed appropriate to use the CATTI two-dimensional dispersion model (Sauty *et al.*, 1989), which is based on the concept of a porous homogeneous and isotropic aquifer with infinite lateral extension, for the hydrodynamic interpretation of the tracer-test results.

Pumping in DNS1 created a cone of depression about 10 m deep for a pumping rate of 1.4 $m^3 h^{-1}$. As the injection well F1 is situated only 15.2 m from DNS1, it is assumed that the tracer propagated under the predominant influence of the hydraulic gradient imposed by DNS1. Radial convergent flow conditions were assumed during modelling. The observed input function [injected tracer mass in F1 as a function of time, Fig. 5(a)] was used for the modelling, making use of a convolution procedure. The aquifer thickness was fixed at 50 m (the length of the slotted casing in F1) which also corresponds to the observations of tracer breakthrough in DNS1 shown in Fig. 4; changing this value would only influence the calculated porosity. The pumping rate can be taken as being approximately constant throughout the tracer test with a mean value of 3.9×10^{-4} $m^3 s^{-1}$.

Calibration of the breakthrough curve of the conservative tracer Br^- using an equivalent unimodal porous-aquifer model was not satisfactory because the peak and tail of the tracer breakthrough cannot be correctly fitted simultaneously: for example, fitting the peak of the breakthrough curve induces an underestimate of the tail with respect to the actual data. We therefore turned to a different conceptual model to represent the fissured aquifer by considering an equivalent dual-porosity aquifer to calibrate the breakthrough curve (Fig. 8). Figure 9 illustrates the schematic model, which can be justified by geological observations at the test site where there is evidence for two generations of fissures in the Paleozoic schists (Legendre, personal communication). In the high-permeability medium, transport takes place along the large fissures (or open fractures), the volume of which is small compared to the total volume of the aquifer which means that equivalent porosities are low and that transport is relatively rapid; transport paths are probably fairly

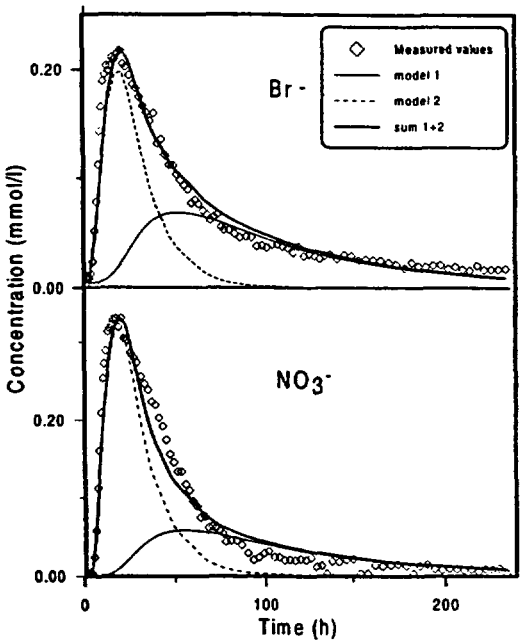

Fig. 8. Tracer breakthrough curves for Br^- and NO_3^- in DNS1 and analytical curves modelled with CATTI.

direct and hydrodynamic dispersion low. However, this high-permeability medium overlaps with a low-permeability medium in which the major part of the total fissure volume is represented by a network of smaller fissures and where equivalent porosity and kinematic dispersion are expected to be higher. The transport is therefore slowed down by interchanges between the two media. It is considered that the first tracer-bearing waters to reach DNS1 derive mainly from the rapid transport through the large fissures, whereas the later the sample is collected the greater the time spent by the tracers in the low-permeability medium.

The evolution of the overall tracer transport during the test is represented on the breakthrough curve (Fig. 8) by a superposition of transport through the low- and high-permeability media. For the low-permeability medium, the porosity of an equivalent porous medium (reflecting the volume of fissures relative to the total rock volume) and the longitudinal dispersivity are respectively about 8 and 2 times higher than for the high-permeability medium. When the tracer transport occurred mainly through the high-permeability medium similar amounts of Br^- and NO_3^- were recovered, respectively, 28 and 25% of the total injected mass. When time is spent by the tracers in the low-permeability medium the NO_3 loss increases; recovery of the remaining tracer is only 22% of the total injected mass for NO_3 compared to 45% for Br. We can thus state that:

— According to the global recovery of NO_3 (47%) and Br (73%), 26% of the injected NO_3 is missing, probably due to a denitrification process.

— The main loss of NO_3 seems to take place in the low-permeability medium.

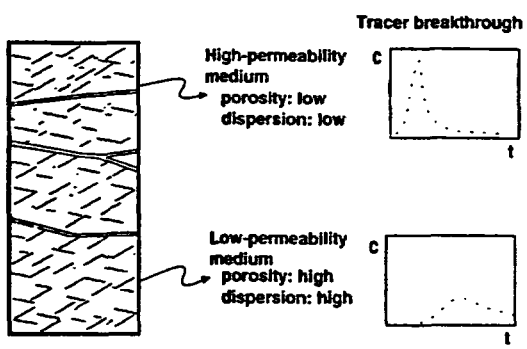

Fig. 9. Schematic representation of the conceptual model used for calibrating the tracer breakthrough curves.

Heterotrophic or autotrophic denitrification?

The chemical composition of the groundwater pumped from DNS1 should reflect the process by which injected NO_3 is reduced, i.e. autotrophic or heterotrophic denitrification. As the dissolved organic C content in the injection well fluid is relatively low (0.04 mmol l^{-1}), and since no organic matter was detected in the rock matrix, only a very small quantity of NO_3 should be reduced by heterotrophic denitrification. With 0.04 mmol l^{-1} of organic C, it is possible to reduce 0.03 mmol l^{-1} of NO_3^- according to equation 1. The water analysed at the DNS1 well head corresponds to a mixing in the well between the partly denitrified injected pulse of tracer, diluted during its transport from injection to pumping well, and a large amount of water from the vicinity of the pumping well. Therefore, the *in situ* concentrations of tracer and of reduced NO_3 along the flow path will be much higher than those observed or calculated from the breakthrough curves, which means that the main denitrification process cannot be a heterotrophic reaction. Consequently, an autotrophic reaction is considered to play the important role.

Simple calculations were carried out to evaluate whether sufficient pyrite is present in the matrix of the aquifer section concerned by the present test to account for the 26% loss of injected NO_3, i.e. that denitrification is not electron-donor limited. The mean content of pyrite in F1 below a depth of 50 m is 2.8‰ of the dry weight of the rock. According to reaction (2), the reduction of 1 kg of injected NO_3 (26% of the total injected mass) would require 685 g of pyrite. Assuming a density of 2.3 g cm^{-3} for the schist, this amount of pyrite would be contained in 0.1 m^3 of schist. Hence, a comparatively small amount of pyrite relative to pyrite availability (which does not seem to be a limiting factor here) is involved in the denitrification of the present test.

The results of the tracer experiment were then used to evaluate the rate of denitrification. Field estimates of heterotrophic denitrification rates are generally reported as zero-order reactions (Korom, 1992), whereas field studies in the Fuhrberg aquifer near Hanover revealed that autotrophic denitrification has a first-order kinetic rate constant (Frind *et al.*, 1990). In the present case, reaction rates (whether zero-order or second-order) cannot be tested by a simple graphical method because of continuous dilution of the tracer pulse during its transfer through the aquifer, but a first order can be graphically represented even in the case of dilution. The NO_3 concentrations were therefore plotted as $\ln(C/C_0)$ vs time, where C is the NO_3 concentration at time t and C_0 the concentration measured if NO_3 reduction does not occur: a first-order model represented by such a diagram would give a straight line. In the present case, two fairly linear segments can be observed [Fig. 10(a)]; before 14 September 1995 (first 40 h), the gradient is low compared to that between 14 and 17 September (40–120 h), indicating that the denitrification rate increased with time. From 17 September onwards, no correlation is observed with time. The rate coefficient, k, deduced from the plot for before 14 September is approximately $0.00365\ h^{-1}$ (correlation coefficient = 0.82) [Fig. 10(b)], which is equivalent to a half life, $t_{1/2}$, of 7.9 days. Between 14 and 17 September, the denitrification rate increased, with an apparent k of approximately $0.01352\ h^{-1}$ (correlation coefficient = 0.94) [Fig. 10(c)] and a $t_{1/2}$ of 2.1 days. As departure of the tracer from the injection well is not immediate, the transfer time of the tracers between the two wells is slightly overestimated and denitrification is in reality probably even more rapid than calculated. After 16 September, data on the plot are scattered, which may partly be due to an increase in analytical uncertainties related to the lower concentrations of both Br and NO_3.

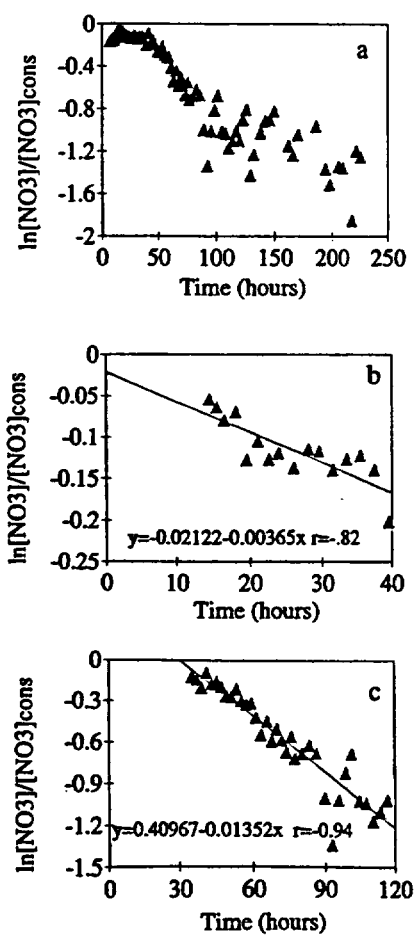

Fig. 10. Plot of the logarithm of NO_3^- concentration over expected NO_3^- concentration assuming no denitrification versus time. The solid lines are the regressions.

DISCUSSION

Relationship between denitrification kinetics and fluid path

An evolution in the kinetic rate with time has been demonstrated by the half life ranging from 7.9 to 2.1 days, which could be explained by several processes. One of these is microbial metabolic lag, which is defined as the delay that would occur before a change in the metabolic state of the microbial components in response to the injection of NO_3 (Bartford *et al.*, 1982). Since microbial metabolic lag may result in significantly less degradation of the substrate than might be otherwise expected (Wood and Dawson, 1992) and not necessarily in a lack of degradation, it could explain the evolution in the kinetic rate. In porous media, lag times of days to weeks have already been observed for the degradation of certain compounds (Bouwer and McCarty, 1983; Truex *et al.*, 1992). In the present case, the chemical composition of the groundwaters a few months before the test revealed the presence of NO_3 in the medium. However, contact between bacteria and NO_3 is not necessarily sufficient to suppress lag time because lag associated with a loss of the microbial component's ability to degrade a substrate has been observed even when a compound has been depleted for times as little as a few minutes (Pickett *et al.*, 1979, 1980). Based on these considerations and even though rapid denitrification processes were actually observed (depletion of NO_3's demonstrated in the first Br-bearing samples), we cannot definitively dismiss the fact that microbial metabolic lag may occur. Two different denitrification kinetics could also be related to fluid transport rather than to metabolic lag. By comparing Figs 8 and 10, the lower kinetic rate corresponds to the part of the breakthrough curve (Fig. 8) which could be explained by the rapid

transport preferentially through the high-permeability medium, whereas from 14 September, the produced fluids contain mainly tracers which would have diffused to the lower-permeability medium and been denitrified to a greater extent. The test has therefore shown that denitrification during transport occurs preferentially through the interchanges of NO_3 between the high-permeability (larger fissures) and the low-permeability media. Moreover, these results may also indicate that denitrification occurs without any, or with very little, microbial metabolic lag, since a first-order kinetic law can be applied to the early produced waters.

Denitrification kinetics

Autotrophic denitrification kinetics observed in other studies are lower than in the present case where half lives of 7.9 and 2.1 days were obtained relative to the high and low permeability of the medium respectively. In the Fuhrberg field near Hanover, the half life for microbial denitrification with pyrite was found to be in the range of 1 to 2.3 a (Frind *et al.*, 1990). At the Beuxes site, France, Le Bideau and Dudoignon (1996) also recorded microbial denitrification with pyrite and they estimated the denitrification rate to be in the range of 0.014 to 0.028 mmol $NO_3\,l^{-1}\,d^{-1}$, values that are higher than those of the Fuhrberg field, but lower than those estimated in the present study. For the Beuxes site, Le Bideau and Dudoignon (1996) estimated their values from a fluid containing 1.6 mmol l^{-1} of NO_3 which had been completely depleted in NO_3 during its circulation through the aquifer. So as to be able to compare the two data sets, the present estimated kinetic rates were expressed as the amount of NO_3 reduced per day in a 1.6 mmol l^{-1} NO_3 fluid. So that NO_3 concentration decreases to 0.0016 mmol l^{-1}, transport exclusively through the large fissures of the high-permeability medium, where the denitrification rate is lower, should last 79 days (denitrification of 0.02 mmol $NO_3\,l^{-1}\,d^{-1}$), whereas if tracer-bearing water remains mainly in the low-permeability medium, denitrification will induce the same concentration decrease in only 21 days (denitrification of 0.076 mmol $NO_3\,l^{-1}\,d^{-1}$). When modelling NO_3 reduction at the Rabis aquifer in Denmark, Postma *et al.* (1991) used a chemical-equilibrium model because the denitrification rate was high compared to the water transport rate. According to ^3H dating, the vertical-transport rate of water was only 0.75 m a^{-1}. The kinetics of autotrophic denitrification estimated during the present test are thus comparatively high; in fact they are amongst the highest recorded in the literature to date. As mentioned above, the denitrification rate depends on several parameters and these results confirm the necessity of experimentally evaluating the denitrification rates for a specific aquifer before modelling NO_3 transfer or reactions; data must not be extrapolated from one aquifer to another.

During a tracer test, denitrification kinetics may be disturbed with respect to natural conditions due to the injection of other tracers with NO_3. The effects of some tracers on microbial processes can be important, particularly through the inhibition of microbial activity; for example, Cl^- has been found to be an inhibitor of nitrification (Roseberg *et al.*, 1986). The effect of Br on denitrification was evaluated by Groffman *et al.* (1995) who conducted experiments using 1.25 mmol l^{-1} Br solution. The authors did not observe any effect on the denitrification rate, whereas Cl^- at the same concentration caused a decrease in denitrifying activity. In the present study, the Br concentrations in the F1 water just after tracer injection reached 21.3 mmol l^{-1}, which is much higher than in Groffman's experiments, although these fluids are rapidly diluted and the breakthrough peak in DNS1 attained 0.22 mmol l^{-1}. As the tracer propagates through a fissured medium, the concentration is not homogenous and may therefore be far higher locally. In view of the higher concentration, an effect of the Br concentration on denitrification kinetics cannot be completely dismissed. Furthermore, the conditions of the present test are different to those of Groffman *et al.* (1995) considering that denitrification is autotrophic in the former and heterotrophic in the latter. Nevertheless, if Br affects microbial processes, its presence could inhibit activity, resulting in the denitrification kinetics for the present test being underestimated with respect to the actual denitrification rate occurring naturally in the aquifer.

Precipitation of secondary sulphate minerals

According to equation 2, autotrophic denitrification should induce an increase in SO_4 concentration: a reduction of 0.05 mmol l^{-1} of NO_3 should increase SO_4 concentration by 0.036 mmol l^{-1}, which is theoretically observable for a background concentration of around 0.24 mmol l^{-1}. In other environments, the release of SO_4 involves high concentrations (> 1–2 mmol l^{-1}) (Frind *et al.*, 1990; Postma *et al.*, 1991; Le Bideau and Dudoignon, 1996) although in some cases the produced SO_4 is reduced back to sulphide with organic C serving as the electron donor (Frind *et al.*, 1990). Such a reaction has not been observed in the Coët-Dan aquifer and no sulphide was detected during the present test. The removal of SO_4 could occur through mineral precipitation. Moreover, an iron decrease observed a few hours after NO_3 injection, albeit that the oxi-

dation of pyrite liberates Fe, indicates that Fe is also removed from solution by precipitation.

Study of the rock matrix revealed the presence of two SO_4 minerals, natroalunite and jarosite, which are assumed to be responsible for SO_4 removal in the present case. Equilibrium calculations using EQ3 software (Wolery *et al.*, 1990) were performed to test the validity of this assumption. The chemical composition of the water sample used for the calculations (Table 3) corresponds to the concentration of some elements in DNS1 water a few moments after the maximum tracer concentration; the composition was also partly derived from that of the F1 water before injection since a complete analysis of DNS1 water before and during the test is not available. Sodium concentration was calculated from the Na concentration in F1, and Br and NO_3 concentrations in DNS1 since tracers were added as $NaNO_3$ and $NaBr^-$. Although original Al data were not available, Al concentrations in the waters were determined a few months after the test; therefore two data were retained for the calculations: $3.3 \cdot 10^{-8}$ mol l^{-1}, which was the concentration in F1 and $1.74 \cdot 10^{-7}$ mol l^{-1} which was the concentration in DNS2. Calculations performed with EQ3 show that water is undersaturated with respect to jarosite. However, in a recent experimental study, Baron and Palmer (1996) report a solubility product of jarosite significantly lower than in previous studies, which indicates that this mineral is more stable and can occur at higher pH than was generally assumed. Applying the data of Baron and Palmer (1996) at 12.2°C leads to a saturation index $(\log(\text{I.A.P.})/K_s)$ of −0.1, which indicates that the water is close to saturation with respect to jarosite. To calculate the saturation state with respect to natroalunite, it was necessary to have the solubility product (K_s) of natroalunite. Since jarosite and alunite belong to a group of isostructural minerals described by the general formula $AB_3(SO_4)_2(OH)_6$, the Gibbs free energy of natroalunite was calculated from those of jarosite, Na–jarosite and alunite and those of Na_2O, K_2O, Al_2O_3 and Fe_2O_3 according to the method developed for the enthalpy of formation (Vieillard, 1994). The calculated saturation index for natroalunite (−1.51 with Al concentration = $1.74 \cdot 10^{-7}$ mol l^{-1}) indicates that the water is undersaturated with respect to this mineral. However, the published Gibbs free energies of Na–Jarosite and alunite may not be sufficiently precise to derive that of natroalunite without error. Moreover, during transfer between the two wells (F1 and DNS1) the water probably underwent several mixings that would have modified its chemical composition, the last one being mixing in the pumping well. In other words, the chemical composition of the water pumped by DNS1 is probably not representative of that of the water in all the parts of the aquifer. For this reason, oversaturation of the groundwater with respect to natroalunite could be attained in some micro-environments and could induce precipitation, although this process is not expected from the chemical composition of the pumped waters.

Table 3. Chemical composition of water used for thermodynamic calculations

pH	6.3
E_h (mV)	+360
Alkalinity (meq l^{-1})	0.68
Na (mmol l^{-1})	12.0
K (mmol l^{-1})	0.033
Ca (mmol l^{-1})	0.36
Mg (mmol l^{-1})	0.38
Cl (mmol l^{-1})	0.67
NO_3 (mmol l^{-1})	0.26
SO_4 (mmol l^{-1})	0.24
Br (mmol l^{-1})	0.15
Fe (μmol l^{-1})	14.3
Al (μmol l^{-1})	0.033
	0.174

The chemical evolution between the water injected in F1 and the water pumped from DNS1 shows that the injection of NO_3 and subsequent denitrification induces chemical reactions in the aquifer, which include mineral oxidation (pyrite) as well as precipitation (Fe, SO_4). Both autotrophic and heterotrophic denitrification theoretically involves an increase in total alkalinity. According to equation 2, the reduction of 0.05 mmol l^{-1} of NO_3^- to gaseous N_2 should increase total alkalinity by 0.014 meq l^{-1}, whereas the test showed a decrease of about 0.07 meq l^{-1} (Fig. 6(f)). Similarly, iron concentration should increase by 0.018 mmol l^{-1}, whereas the test showed an iron depletion [Fig. 6(g)]. As the dissolution–precipitation reaction of jarosite is written as:

$$KFe_3(SO_4)_2(OH)_6 + 6H^+ \leftrightarrow K^+ + 3Fe^{3+} + 2SO_4^{2-} + 6H_2O \quad (3)$$

the precipitation of jarosite implies oxidation of Fe^{2+} to Fe^{3+}. In this case, NO_3^- is the only available electron donor and hence Fe participates in the denitrification, the reaction of which can be written as:

$$NO_3^- + 5Fe^{2+} + 6H^+ \longrightarrow 1/2N_2 + 5Fe^{3+} + 3H_2O \quad (4)$$

By combining equations 2)–(4, the following equation is obtained:

$$3FeS_2 + 9NO_3^- + K^+ + 3H_2O \longrightarrow 9/2N_2 + 4SO_4^{2-} + KFe_3(SO_4)_2(OH)_6 \quad (5)$$

which indicates that all Fe produced during denitrification is involved in jarosite precipitation. This

reaction does not, however, explain Fe depletion, alkalinity decrease or SO_4 stability.

Sulphate could be involved in the precipitation of another mineral, natroalunite, for which the dissolution–precipitation is written as:

$$NaAl_3(SO_4)_2(OH)_6 + 6H_2O \leftrightarrow Na^+ + 3Al(OH)_4^- + 2SO_4^{2-} + 6H^+ \quad (6)$$

The alkalinity decrease noted during the present test was probably the result of a combination of several processes. For example:

(a) Alkalinity decrease may be partly due to an analytical artefact if oxidation of Fe^{2+} occurred before or during alkalinity titration and was followed by Fe^{3+} precipitation according to the reaction below:

$$Fe^{2+} + 1/4O_2 + 2OH^- + 1/2H_2O \longrightarrow Fe(OH)_3 \quad (7)$$

As Fe concentration is of the order of 12.5 μmol l^{-1}, such a reaction would cause an alkalinity decrease of only 0.025 meq l^{-1} rather than 0.07 meq l^{-1}, suggesting that at least one other process is involved.

(b) A more rapid transfer of the injected anions (Br and NO_3^-) than of Na injected at the same time could also contribute to the alkalinity decrease if the cation deficit were compensated by an increase of protons. Cation retardation with respect to anion transport is a well-known process (Leblanc *et al.*, 1991). The Na might also exchange for surface-bound Ca^{2+}, inducing calcite precipitation and then alkalinity decrease. Nevertheless, these processes cannot be assessed here as Na concentrations are not available.

(c) The decreased Fe concentration in the pumping well is not explained by equation 5 and is probably due to mineral precipitation, possibly jarosite. Such a reaction would take up the excess SO_4 produced by the reaction in equation 5. By combining equations 3) and (4, we obtain the following reaction that could explain the Fe depletion:

$$NO_3^- + 5Fe^{2+} + 5/3K^+ + 10/3SO_4^{2-} + 7H_2O \longrightarrow 5/3KFe_3(SO_4)_2(OH)_6 + 4H^+ + 1/2N_2 \quad (8)$$

According to equation 8, a consumption of 7.2 μmol l^{-1} of Fe^{2+} produces an alkalinity decrease of 0.006 meq l^{-1}. Although probably a contributing factor, this is insufficient to account for the whole of the observed decrease.

CONCLUSIONS

A small-scale tracer test using NO_3 has improved our knowledge of denitrification processes in the schist aquifer of the Coët-Dan drainage basin. High denitrification rates have been demonstrated which vary depending on the medium permeability; first-order denitrification rates in the high-permeability medium (large fissures) have an estimated half life of around 7.9 days whereas those in the low-permeability medium have an estimated half life of 2.1 days, i.e. the faster the flow the slower the denitrification rate. These rates are higher than those previously determined for other environments, showing that each environment has its specific rates that depend on several parameters. Great care must therefore be taken in extrapolating denitrification rates from one data set to another for a different environment.

Two denitrification processes have previously been demonstrated in aquifers, a heterotrophic process with oxidation of organic matter, and an autotrophic process due to oxidation of pyrite. Interpretation of the present tracer test results has demonstrated another process, the reduction of NO_3 through oxidation of Fe^{2+}.

Several processes may be responsible for denitrification in an aquifer due to the presence of several electron donors. In the present case, denitrification is accompanied by the precipitation of SO_4- and Fe-bearing minerals, probably jarosite, which prevents the accumulation of Fe^{2+} and SO_4^{2-} in the groundwaters. The lack of high SO_4 and Fe concentrations is very beneficial to water quality.

The high denitrification rates estimated here could be used in modelling NO_3 transfer and denitrification in the Coët-Dan drainage basin in order to evaluate the evolution of NO_3 contamination in the aquifer. The high denitrification rate also means that it is possible to envisage using the denitrifying properties of the aquifer matrix to decontaminate surface waters through forced underground circulation.

Acknowledgements—This is BRGM contribution No. 97013. Technical equipment on site was funded by CST-BVRE. The geochemical study was partly funded by BRGM and the French Ministry of the Environment. The authors acknowledge Dr Ph. Vieillard (Poitiers University) for the discussion about Natroalunite Gibbs free energy calculation and Dr J-P. Sauty for its help on CATTI utilisation. Thanks are due to Dr R. Jakobsen and an anonymous reviewer, whose comments greatly improved the manuscript The authors would like also to thank Rowena Stead and Patrick Skipwith for editing the English.

Editorial handling:—A. Appelo

REFERENCES

Baron D. and Palmer C. D. (1996) Solubility of jarosite at 4–35 °C. *Geochim. Cosmochim. Acta* **60**, 185–195.

Bartford J. P., Pamment N. B. and Hall R. J. (1982) Lag phases and transients. In *Microbial Population*

Dynamics, ed. M. J. Bazin, pp. 55–90. CRC Press, Boca Raton, FL.

Bouwer E. J. and McCarty P. (1983) Transformations of 1- and 2-carbon halogenated aliphatic organic compounds under methanogenic conditions. *Appl. Environ. Microbiol.* **45**, 1286–1294.

Bradley P. M. and Chapelle F. H. (1993) Arsenate inhibition of denitrification in NO_3 contaminated sediments. *Soil. Biol. Biochem.* **25**, 1459–1462.

Cann Ch. (1990) Transfer of nutrients in a region of intensive farming. In *Hydrological Research Basins and the Environment, Proceedings and Information. TNO Commitee on Hydrological Research*, Vol. 44, pp. 311–318. The Hague, The Netherlands.

Cann Ch. (1996) Variations des teneurs en azote dans quelques cours d'eau bretons. In *Hydrologie dans les pays celtiques*, eds. P. Mérot and A. Jigorel, les Colloques 79, pp. 193–201. INRA, Paris.

Edmunds W. M. and Walton N. R. G. (1983) The Lincolshire limestone: Hydrogeochemical evolution over a ten-year period. *J. Hydrol.* **61**, 201–211.

Engesgaard P. and Kipp K. L. (1992) A geochemical transport model for redox-controlled movement of mineral fronts in groundwater flow systems: A case of NO_3 removal by oxidation of pyrite. *Water Resour. Res.* **28**, 2829–2843.

Foucher J.-C., Brach M. and Pauwels H. (1995) Préleveur Multi-entrées. Patent No. 95.15366 registered on 22/12/95.

Frind E. O., Duynisveld W. H. M., Strebel O. and Boettcher J. (1990) Modeling of multicomponent transport with microbial transformation in groundwater: The Fuhrberg case. *Water Resour. Res.* **26**, 1707–1719.

Gran G. (1952) Determination of the equivalence point in potentiometric titrations. Part II. *Analyst* **77**, 661–671.

Groffman P. M., Gold A. J. and Howard G. (1995) Hydrologic tracer effects on soil microbial activities. *Soil Sci. Soc. Am. J.* **59**, 478–481.

Hiscock K. M., Lloyd J. W. and Lerner D. N. (1991) Review of natural and artificial denitrification of groundwater. *Wat. Res.* **25**, 1099–1111.

Kinzelbach W., Schäfer W. and Herzer J. (1991) Numerical modeling of natural and enhanced denitrification processes in aquifers. *Water Resour. Res.* **27**, 1123–1135.

Knowles R. (1982) Denitrification. *Microbiol. Rev.* **46**, 43–70.

Kölle W., Strebel O. and Böttcher J. (1985) Formation of sulfate by microbial denitrification in a reducing aquifer. *Wat. Supply* **3**, 35–40.

Korom S. F. (1992) Natural denitrification in the saturated zone: A review. *Wat. Resour. Res.* **28**, 1657–1668.

Le Bideau L. and Dudoignon P. (1996) Mise en évidence de mécanisme de dénitrification naturelle sur substrat sulfuré sur le site de Beuxes (Vienne France). *C. R. Acad. Sci. Paris* **322**(IIa), 555–562.

Leblanc R. D., Garabedian P. S., Hess M. K., Gelhar W. L., Quadri D. R., Stollenwerk G. K. and Wood W. W. (1991) Large-scale natural gradient tracer test in sand and gravel, Cape Cod, Massachusetts. 1. Experimental design and observed tracer movement. *Wat. Resour. Res.* **27**, 895–910.

Mariotti A., Landreau A. and Simon B. (1988) 15N isotope biogeochemistry and natural denitrification process in groundwater: Application to the chalk aquifer of northern France. *Geochim. Cosmochim. Acta* **52**, 1869–1878.

Martelat A. and Lachassagne P. (1995) Bassin versant représentatif du Coët Dan (Naizin Morbihan), hydrologie: Détermination des caractéristiques hydrodynamiques du système aquifère au lieu-dit Le Stimoes. Unpublished BRGM Report No. R38474DR/HYT95, 54 pp.

Pauwels H. (1994) Natural denitrification in groundwater in the presence of pyrite: Preliminary results obtained at Naizin (Brittany, France). *Mineral. Mag.* **58A**, 696–697.

Pauwels H. (1996) Preliminary results on chemical variations in a schist aquifer: Implications for NO_3 transport and denitrification. In *Hydrologie and les pays celtiques*, eds. P. Mérot and A. Jigorel, les Colloques 79, pp. 111–117. INRA, Paris.

Pauwels H., Martelat A., Lachassagne P., Foucher J.-C. and Legendre O. (1996) Evolution des teneurs en NO_3's dans l'aquifère du bassin versant du Coët Dan (Naizin, Morbihan). *ESRA'96 l'eau Souterraine en Région Agricole*. pp. S4–81. Poitiers, Sept. 9–12.

Pellerin J. and Van Vliet-Lanoe B. (1994) Cadre géomorphologique du bassin du Coët Dan et du Haut Evel (Morbihan): Rapport sur les travaux de cartographie et de stratigraphie. Unpublished report, University of Brest.

Pickett A. M., Bazin M. J. and Topiwala H. H. (1979) Growth and composition of *Escherichia coli* subjected to square-wave perturbation in nutrient supply: Effect of varying frequencies. *Biotechnol. Bioeng.* **21**, 1043–1055.

Pickett A. M., Bazin M. J. and Topiwala H. H. (1980) Growth and composition of *Escherichia coli* subjected to square-wave perturbation in nutrient supply: Effect of varying amplitudes. *Biotechnol. Bioeng.* **22**, 1213–1224.

Postma D. (1990) Kinetics of NO_3 reduction by detrital Fe(II)-silicates. *Geochim. Cosmochim. Acta* **54**, 903–908.

Postma D., Boesen C., Kristiansen H. and Larsen F. (1991) NO_3 reduction in an unconfined sandy aquifer: Water chemistry, reduction processes, and geochemical modeling. *Water Resour. Res.* **27**, 2027–2045.

Roseberg R. J., Christensen N. W. and Jackson T. L. (1986) Chloride, soil solution osmotic potential and soil pH effects on nitrification. *Soil Sci. Soc. Am. J.* **50**, 941–945.

Sauty J. P., Kinzelbach W. and Voss A. (1989) Computer aided tracer test interpretation. BRGM Report No. 89 SGN 217 EEE, 72 pp.

Trudell M. R., Gillham R. W. and Cherry S. A. (1986) An in-situ study of the occurrence and rate of denitrification in a shallow unconfined sand aquifer. *J. Hydrol.* **83**, 251–268.

Truex M. J., Brockman F. J., Johnstone D. L. and Fredrickson J. K. (1992) Effect of starvation on induction of quinoline degradation for a subsurface bacterium in a continous-flow column. *Appl. Environ. Microbiol.* **58**, 2386–2392.

Vieillard Ph. (1994) Prediction of enthalpy of formation based on refined crystal structures of multisite compounds: Part 1. Theories and examples. *Geochim. Cosmochim. Acta* **19**, 4049–4063.

Wolery T. J., Jackson K. J., Bourcier W. L., Bruton C. J., Viani B. E., Knauss K. G. and Delany J. M. (1990) Current status of the EQ3/6 software package for geochemical modeling. In *Chemical Modeling of Aqueous Systems II*, eds. D. C. Melchior and R. L. Basset, American Society Symposium Series 416, pp. 104–116. American Chemical Society.

Wood B. D., and Dawson C. N. (1992) Effects of lag and maximum growth in contaminant transport and biodegradation modeling. In *Mathematical modeling in water resources*, ed. T. F. Russel, Vol. 2, pp. 317–324. Elsevier Applied Science, New York.

APPLIED AND ENVIRONMENTAL MICROBIOLOGY, Sept. 2000, p. 3711–3721 Vol. 66, No. 9
0099-2240/00/$04.00+0

Modeling Reduction of Uranium U(VI) under Variable Sulfate Concentrations by Sulfate-Reducing Bacteria

JOHN R. SPEAR,* LINDA A. FIGUEROA, AND BRUCE D. HONEYMAN

Division of Environmental Science and Engineering, Colorado School of Mines, Golden, Colorado 80401

Received 4 February 2000/Accepted 22 June 2000

The kinetics for the reduction of sulfate alone and for concurrent uranium [U(VI)] and sulfate reduction, by mixed and pure cultures of sulfate-reducing bacteria (SRB) at 21 ± 3°C were studied. The mixed culture contained the SRB *Desulfovibrio vulgaris* along with a *Clostridium* sp. determined via 16S ribosomal DNA analysis. The pure culture was *Desulfovibrio desulfuricans* (ATCC 7757). A zero-order model best fit the data for the reduction of sulfate from 0.1 to 10 mM. A lag time occurred below cell concentrations of 0.1 mg (dry weight) of cells/ml. For the mixed culture, average values for the maximum specific reaction rate, V_{max}, ranged from 2.4 ± 0.2 μmol of sulfate/mg (dry weight) of SRB · h^{-1}) at 0.25 mM sulfate to 5.0 ± 1.1 μmol of sulfate/mg (dry weight) of SRB · h^{-1} at 10 mM sulfate (average cell concentration, 0.52 mg [dry weight]/ml). For the pure culture, V_{max} was 1.6 ± 0.2 μmol of sulfate/mg (dry weight) of SRB · h^{-1} at 1 mM sulfate (0.29 mg [dry weight] of cells/ml). When both electron acceptors were present, sulfate reduction remained zero order for both cultures, while uranium reduction was first order, with rate constants of 0.071 ± 0.003 mg (dry weight) of cells/ml · min^{-1} for the mixed culture and 0.137 ± 0.016 mg (dry weight) of cells/ml · min^{-1} (U_0 = 1 mM) for the *D. desulfuricans* culture. Both cultures exhibited a faster rate of uranium reduction in the presence of sulfate and no lag time until the onset of U reduction in contrast to U alone. This kinetics information can be used to design an SRB-dominated biotreatment scheme for the removal of U(VI) from an aqueous source.

Sulfate-reducing bacteria (SRB) are important in the mobility of sulfur in the environment (32, 36). Both higher plants and animals depend upon microbially produced reduced sulfur for acquisition in their own metabolism. SRB use sulfate as an oxidizing agent for the dissimilation of an organic substance (herein, lactate). Several species of SRB have been described for their ability to reduce inorganic aqueous ions in solution. SRB have been shown to metabolize iron [Fe(III)], chromium [Cr(VI)], uranium [U(VI)], manganese [Mn(IV)], and technetium [Tc(VII)], among others (20, 21, 22, 23, 26, 39). Models for the SRB reduction of these metals and radionuclides can be used to develop and design treatment systems employing SRB for bioremediation. For example, bioreduction of soluble hexavalent uranium [U(VI)] to insoluble tetravalent uranium [U(IV)] can be utilized to remove soluble uranium from groundwaters, mine waters, or secondary waste streams.

In addition to SRB, a number of bacterial species have been described as capable of reducing U(VI) to U(IV), including *Geobacter metallireducens* (25) (previously reported as GS-15 [11]), *Shewanella putrefaciens* (25), and *Shewanella alga* strain BrY (previously reported as BrY, or *Shewanella halotolerans* strain BrY [3]). A kinetic study for the reduction of U(VI) has been described for the iron-reducing *S. alga* strain BrY (40) but not for SRB. Before a biotreatment scheme can be designed and implemented, studies must go beyond the identification of novel processes, to quantifying the kinetics of such a process. Because of the metabolic diversity of the SRB, it is important to identify the species involved in the processes studied. Since sulfate reduction rates depend upon the species used and experimental conditions, it is important to characterize sulfate reduction for the mixed culture used in previous uranium reduction experiments (38) that were performed under repeatable, uniform conditions.

The goals of this study were to characterize the mixed SRB culture previously isolated (38) and to develop models to describe sulfate reduction alone and sulfate reduction with concurrent uranium reduction. Utilizing a mixed cell culture was viewed as an advantage in that in an operational biotreatment scheme, purity of culture in treating large volumes of water will be difficult to maintain. Understanding U(VI) reduction by SRB in a consortium is more likely to be relevant for an operational condition. The nature of the mixed SRB culture was examined via 16S ribosomal DNA (rDNA) analysis. Models for separate sulfate reduction and concurrent sulfate and uranium reduction were fit to data generated by both a mixed and a pure culture of SRB. Sulfate and cell concentrations were varied during these experiments, which were conducted at room temperature, 21 ± 3°C. This is at the upper end of temperatures expected in natural waters that could be treated. Sulfate concentration is expected to be a variable in the treatment of uranium-contaminated waters, and cell concentration is an operational variable for treatment design. These kinetic determinations were made under conditions of insignificant growth (in the absence of nutrients other than a lactate carbon source; the sulfate concentrations present could facilitate growth, but experimental time courses were too short), and under anaerobic batch conditions, to isolate the enzymatic reductive processes of both electron acceptors from those of cellular growth processes. Quantification with modeling of the sulfate reduction rate alone and the uranium reduction rate in the presence of sulfate is important for the design of a treatment system employing SRB to remove metals and radionuclides, likely to be operational under dynamic, nonstatic conditions.

* Corresponding author. Present address: Department of Molecular, Cellular, and Developmental Biology, Campus Box 347, University of Colorado, Boulder, Boulder, CO 80309. Phone: (303) 735-1808. Fax: (303) 492-7744. E-mail: spearj@colorado.edu.

MATERIALS AND METHODS

Bacterial cultures. The mixed culture of SRB was obtained as previously described (38). All chemicals utilized for these studies were reagent grade or

better and were used without further purification. Continuous cultivation of SRB cells in a chemostat was carried out on an insulated magnetic stirrer in an anaerobic chamber (Bactron II, Sheldon Manufacturing, Cornelius, Oreg.) fed with anaerobic mixed gas (AMG) containing 90% N_2, 5% H_2, and 5% CO_2. The growth medium used was a modified Postgate C medium (36) containing potassium phosphate (mono) at 0.5 g/liter, ammonium chloride at 1.0 g/liter, sodium sulfate at 2.0 g/liter, calcium chloride at 0.06 g/liter, magnesium chloride at 0.06 g/liter, iron sulfate at 0.005 g/liter, sodium citrate at 0.3 g/liter, yeast extract at 0.1 g/liter, and sodium lactate (60% syrup) at 15 ml/liter. Cell concentrations ranged from 0.1 to 0.15 mg (dry weight)/ml of growth medium from the 250- or 500-ml square polycarbonate chemostats with a hydraulic residence time of 8 to 12 h. The average temperature during growth in the chemostat on the chamber stage was 21 ± 3°C. The *Desulfovibrio desulfuricans* (ATCC 7757) culture was grown in continuous fashion with an 8-h hydraulic residence time as described for the mixed culture above. Refrigerated stocks of both cultures were transferred to freshly prepared media approximately every 2 weeks.

To facilitate comparison of the mixed cell culture used in these studies with data by other investigators, the biomass equivalents were determined. By using a Petroff-Hausser counting chamber, the average cell count was 1.5×10^9 cells/ml from a growth chemostat, for an average of 3 mg of cells (wet weight)/ml and 0.148 mg of cells (dry weight)/ml as determined by a standard dry weight analysis (10). The values reported for dry weights of SRB cells per milliliter reflect the cell concentration per milliliter of medium used for the actual batch experimental conditions, not those of growth.

Molecular characterization. For molecular characterization of the mixed cell culture used in this and a previous study (38), the methods of Hugenholtz et al. were followed (12). Bead beating for cellular disruption and DNA extraction was followed by PCR with the primers 8F universal forward and 1492R universal reverse (18). *Taq* polymerase-amplified PCR products were directly inserted into a PCR4-TOPO vector, followed by reaction with One Shot Competent Cells in a TOPO TA Cloning Kit (Invitrogen, Carlsbad, Calif.). Restriction fragment length polymorphism (RFLP) analysis was carried out on a mini-prepped, T3–T7 primer-amplified PCR (Invitrogen) clone colony DNA product, using the restriction enzymes *Hin*PI and *Msp*I (New England Biolabs, Beverly, Mass.). After bead beating, all steps were performed using a 96-well format.

After determination of nonidentical banding patterns of PCR-amplified positive clones on an RFLP gel, the amplified DNA fragments were sent to the Forsythe Dental Center in Boston, Mass., for sequence analysis. Purified DNA from PCR was sequenced using an ABI prism cycle-sequencing kit (dRhodamine Terminator Cycle Sequencing kit with AmpliTaq DNA polymerase FS; Perkin-Elmer). The manufacturer's protocol was followed. Sequencing was performed using an ABI 377 DNA sequencer. DNA sequences were identified by using the BLAST (basic local alignment search tool) server of the National Center for Biotechnology Information over the World Wide Web (1). The 16S rRNA gene sequences were manually aligned with other sequences by using the Ribosomal Database Project (27; http://www.cme.msu.edu/RDP/) and the ARB database (http://pop.mikro.biologie.tu-muenchen.de/pub/ARB/) taxonomic listings. Percent identity was calculated by using the Lane mask (17) with no right correction.

Kinetics studies. As described elsewhere, a method was developed to examine the enzymatic reduction kinetic of U(VI) to U(IV) by SRB using the radionuclide ^{233}U as a tracer (38). For sulfate reduction experiments, this method, in combination with the methods of Ingvorsen and colleagues (13, 14) was applied by substituting $Na_2{}^{35}SO_4$ as the radionuclide tracer. Briefly, a selected amount of the SRB cell mass (0.2 to 1.3 mg [dry weight]/ml per experiment) was obtained from a growth chemostat, washed in a sulfate-free sodium bicarbonate (2.5 g/liter) buffer, and then suspended anaerobically in a sterile medium (10 mM lactate–20 mM sodium bicarbonate) with a small magnetic stir bar, in sterile 30-ml polycarbonate septum flasks sealed with Teflon-lined butyl rubber stoppers (38). The headspace in these sealed reaction vessels contained ~10 ml of the anaerobic chamber's AMG. The turbid culture was in contact with the buffered carbon source/electron donor for ≤15 min prior to the addition of sulfate. Sulfate was added from a 10 mM stock solution spiked with $Na_2{}^{35}SO_4$ as a tracer, typically 25 μl of a 45,000-dpm/ml stock $Na_2{}^{35}SO_4$ solution (purchased from Isotope Products Laboratory, Burbank, Calif.). The Na_2SO_4 electron acceptor was mixed with the $Na_2{}^{35}SO_4$ spike in a syringe and fed to the cells by injection through the septum. For experiments with both electron acceptors, U(VI) was added as uranyl acetate, $UO_2(CH_3COO)_2 \cdot 2H_2O$, from a 10 mM stock solution spiked with $^{233}U(VI)$, typically 200 μl of a 23,670-dpm/ml stock $^{233}U(VI)$ solution (purchased from Isotope Products Laboratory). The U(VI) electron acceptor was mixed with the $^{233}U(VI)$ spike in a syringe and fed to the cells by the same method as the sulfate. The injection of electron acceptors set the time at $t = 0$ and marked the start of the kinetic experiment. The initial pH of these kinetics experiments was 7.2 ± 0.2.

The anaerobic polycarbonate flasks were stirred on insulated magnetic stir motors at ambient room conditions (21 ± 3°C). Samples (1 1/2 ml) were removed by syringe at times of interest. The removed aliquot of the solution was then placed in a 1.5-ml polystyrene microcentrifuge tube containing zinc acetate to give a final concentration of 6 mM (100 μl of a 0.1 M solution), capped tightly, and spun at 16,000 × *g* for 3 min. The zinc acetate immediately preserves produced ^{35}S sulfides (14), forming a precipitating $Zn^{35}S$. Zn is not known to complex with sulfate in solution, and this was experimentally validated. Almost 1.5 ml (cell suspension less pellet volume [~50 μl]) of supernatant solution was collected by pipette and added to 20-ml plastic scintillation vials containing 10 ml of Ultima Gold scintillation cocktail (Packard Instrument, Meriden, Conn.). The cell pellet was suspended in 0.5 ml of deionized water and transferred to a scintillation vial, and 1 ml of deionized water was added for volume equalization.

The mass balance of uranium and/or sulfate was checked at least three times per experiment. The soluble and the precipitated isotope in one of duplicate samples were separated and prepared as described, and the other sample was blended directly with scintillation cocktail. Over the course of an experiment, some sulfides accumulated in the anaerobic headspace of the reaction vessel, a portion of which contain ^{35}S. To account for this mass, any remaining cells in media at the end of an experiment were removed via syringe. Six milliliters of 2% (wt/vol) zinc acetate was then added through the septum to precipitate the gaseous sulfides, which were then removed in 2-ml aliquots, blended with scintillation cocktail, and counted. This additional sulfide activity was added to the total activity, and balanced the mass between the beginning and the end of the experiment. Vials were analyzed on either a model 1600TR or a model 2500TR Packard Tri-Carb Liquid Scintillation Analyzer for 10 min/vial. Separation of activity was easily accomplished by taking advantage of the β emission of ^{35}S at 167 keV and the α emission of ^{233}U at 4.824 and 4.783 MeV. This allows for tracking of the uranium and sulfate reduction in the pellet and supernatant samples. Typical counting errors were 5% or less. Sulfide determinations were made using a method developed by Updegraff and Wren (41) with 0.01 M silver nitrate as a titrant.

A test was conducted to determine how much sulfate adsorbs to the walls of the experimental reaction vessel, i.e., the Teflon-coated butyl rubber-sealed 30-ml polycarbonate septum flask. Using $Na_2{}^{35}SO_4$ as a tracer for sodium sulfate sorption, we found that 4.7% of the sulfate adsorbs to the walls of the vessel over 4 h. Using the same method, sulfate sorption to the walls of 100-ml glass serum bottles was found to be 9.5%. Spear et al. (38) found that 15% of the initial U concentration sorbed to the walls of traditional glass serum bottles, and that was reduced to 4% in polycarbonate. Because of these adsorptive effects, glass vessels were not used in these studies.

Control experiments were performed by the same method with the addition of 10 mM sodium molybdate, a sulfate analog (36) for the enzyme cytochrome c_3, one of the enzymes responsible for the reduction of both sulfate and uranium (21) prior to the addition of Na_2SO_4 or uranyl acetate. In the presence of the sodium molybdate, no sulfate or uranium reduction by the SRB was observed. Data analysis and kinetic modeling were conducted with the data from the scintillation method on Microsoft EXCEL spreadsheets.

RESULTS

16S rRNA sequence. Cells from the isolated mixed culture initially appeared to be all of vibrio shape, all stained gram negative, and exhibited an active production of sulfide. With time (months), small gram-positive rods were observed and spores were periodically present. At any one time the gram-positive species represented 0 to 10% of the total cells present. For these reasons molecular characterization was needed to define the culture. The decision to sequence 500 bp of the 16S rRNA gene fragments from clones of this mixed culture was made because of differences in banding patterns on RFLP gels. Two hundred twenty clones were subjected to RFLP analysis, and there appeared to be two distinct banding patterns, with one pattern far more prevalent than the other, by a ratio of 10:1. The most prevalent pattern was found to be 99% identical to that of a *Desulfovibrio vulgaris* strain (PT-2; accession number M98496 as described by Kane et al. [16]). The other pattern was found to be similar to that of a unique, low-G+C, gram-positive, anaerobic genus (94% identical to *Clostridium butyricum* over 500 bp considered; accession number M59085 as described by C. R. Woese, D. Yang, and L. Mandelco [unpublished data]). Sequences were manually aligned with similar sequences using the BLAST server. RFLP analysis performed on the culture 1 year earlier yielded the same patterns, indicating no change in culture constituents. The SRB culture was initially isolated by picking one colony from an agar deep tube method (36) at a high dilution; with time, the culture came to be contaminated by the spore-forming *Clostridium* sp. This was viewed as an advantage because such a contaminant would likely come to be present in a bioremediation treatment scheme. This mixed cell culture was stable over a period of 5 years and showed little variability.

TABLE 1. Maximum specific reaction rate coefficients for the mixed cell culture reducing sulfate

Initial sulfate concn (mM)	Initial cell concn (mg [dry wt]/ml)	k_0 (μM SO_4^{2-}/mg [dry wt] of SRB/ml · min^{-1})	V_{max} (μmol SO_4^{2-}/mg [dry wt] of SRB · h^{-1})
0.1	0.07 ± 0.01[a]	31 ± 6	1.9 ± 0.4
0.1	0.10 ± 0.02[a]	51 ± 1	3.1 ± 0.1
0.25	0.57 ± 0.01	40 ± 3	2.4 ± 0.2
1.0	0.56 ± 0.01	33 ± 1	2.0 ± 0.1
10	0.46 ± 0.01	83 ± 19	5.0 ± 1.1
100	0.47 ± 0.01	ND[b]	ND

[a] For 0.1 mM sulfate, the cell concentration is lower because at higher cell concentrations the reduction of the sulfate is too rapid to determine experimentally.
[b] ND, not determined because of insignificant sulfate reduction.

Sulfate reduction kinetics. The reduction of sulfate concentrations ranging from 0.1 to 100 mM was examined for the mixed cell culture. Cell concentrations were similar for all sulfate concentrations except 0.1 mM, where the cell concentration was approximately 1/10 of that in the other sulfate reduction experiments (Table 1). For an initial sulfate concentration (S_0) of 100 mM, there was no measurable reduction over 3 h. For an S_0 of 10 mM, 45% of the sulfate was reduced in 3 h by a similar cell concentration. There was 100% removal of sulfate when S_0 was 1.0, 0.25, or 0.1 mM, as shown in Fig. 1.

Modeling of sulfate reduction. A zero-order model, with respect to sulfate concentration, best fit the experimental data where

$$S = S_0 - k_0 X(t - t_L) \quad (1)$$

and S is the model predicted millimolar concentration of sulfate, S_0 is the initial millimolar concentration of sulfate, k_0 is the maximum specific reaction rate coefficient expressed as the millimolar concentration of SO_4^{2-} per milligram (dry weight) of cells per milliliter per minute, X is the bacterial cell concentration in milligrams (dry weight) per milliliter, t is time in minutes, and t_L is the lag time until the onset of sulfate reduction. A 30-min lag time was observed only with a low bacterial cell concentration (0.07 mg [dry weight] of cells/ml or lower) and an S_0 of 0.1 mM sulfate, as shown in Fig. 2. For an S_0 of 0.1 mM and an X_0 of 0.1 mg (dry weight) of cells/ml, there was no lag time. Reduction of sulfate alone proceeded without a lag for initial sulfate concentrations of 1 to 10 mM. The zero-order model is a simplification of Michaelis-Menten and Monod type kinetics at high substrate concentrations. Parameter equivalence between models can be given by

$$k_0 \equiv \frac{\mu_m}{Y} \equiv V_{max} \quad (2)$$

where k_0 is defined, μ_m is the Monod maximum specific growth rate constant in units of 1 h^{-1}, Y represents cell yield, expressed as mass of cells in milligrams per milligram of substrate used, and V_{max} is the Michaelis-Menten maximum substrate utilization rate constant, expressed as the millimolar concentration of SO_4^{2-} per milligram (dry weight) of cells per milliliter per minute. Zero-order model fits to sulfate reduction data are shown in Fig. 1, 2, and 3; correlation coefficients, r^2, were ≥0.92.

Figure 4 shows the reduction of 1 mM sulfate by both the mixed and pure cell cultures. The maximum specific rate coefficients are estimated to be the same when normalized to cell mass, where 33 ± 1 μM SO_4^{2-}/mg (dry weight) of SRB/ml · min^{-1}, with an r^2 of 0.99 for the mixed culture, and 26 ± 2 μM SO_4^{2-}/mg (dry weight) of SRB/ml · min^{-1}, with an r^2 of 0.96 (V_{max} = 1.6 μmol of SO_4^{2-}/mg [dry weight] · h^{-1}) for the pure culture, were calculated. The data indicate that *D. desulfuricans* (ATCC 7757) behaves much like *Desulfobacter postgatei* at 21 ± 3°C (13).

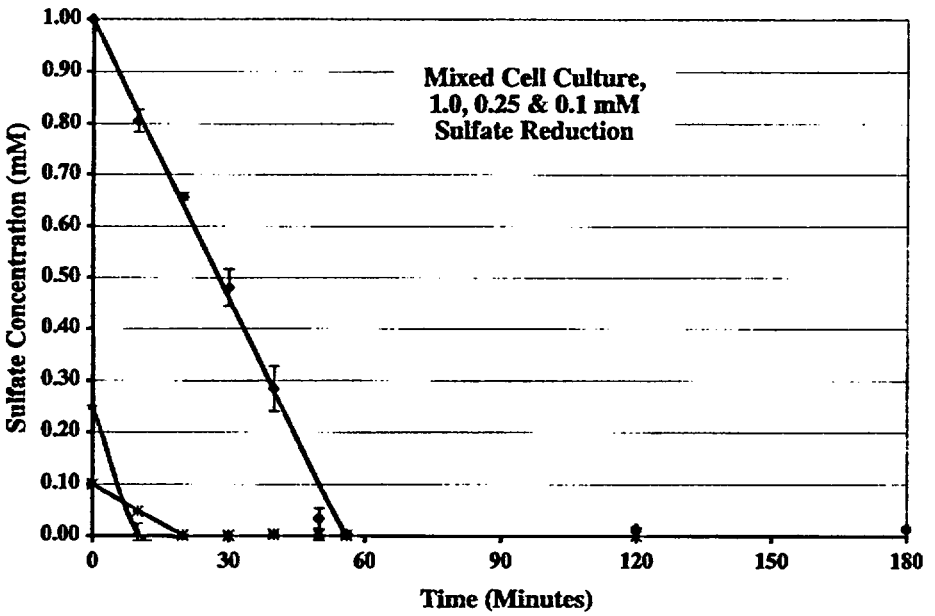

FIG. 1. Time course of sulfate reduction by the mixed cell culture fit with a zero-order model. Model lines are based on the coefficients of Table 1. Each set of data points represents an average of at least two experiments with the same mixed cell culture. ◆, S_0 = 1.0 mM and X_0 = 0.53 mg (dry weight) of cells/ml; ▲, S_0 = 0.25 mM and X_0 = 0.57 mg (dry weight) of cells/ml; ✱, S_0 = 0.1 mM and X_0 = 0.1 mg (dry weight) of cells/ml. Error bars, standard errors.

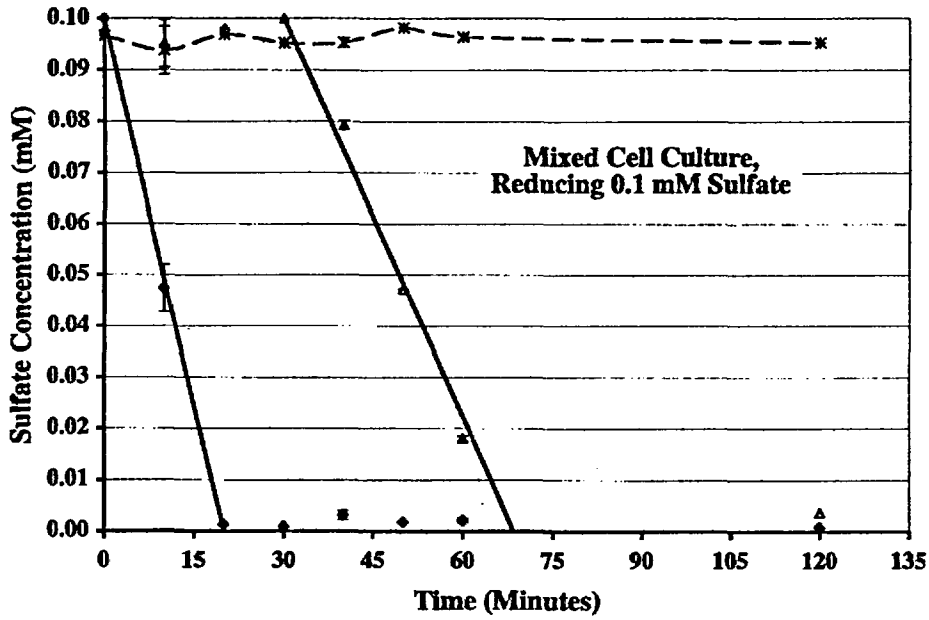

FIG. 2. Reduction of 0.1 mM sulfate by low mixed-cell concentrations. ◆, 0.1 mg (dry weight) of cells/ml (no lag time); △, 0.07 mg (dry weight) of cells/ml (30-min lag time); ✳, 0.06 mg (dry weight) of cells/ml (no sulfate reduction). Zero-order model lines are fit through the 0.1- and 0.07-mg (dry weight)/ml data points, representing model values given in Table 1. Each data set represents averages from two experiments. Error bars, standard errors.

Uranium and sulfate reduction. Time courses for the reduction of soluble U(VI) to insoluble U(IV) and for the reduction of soluble sulfate to sulfide for a typical experiment are shown in Fig. 5. Rate constants were determined only for the removal of the U(VI) and sulfate. Uranium reduction was more rapid in the presence of sulfate than in its absence for both the mixed and pure cell cultures. Figure 6 shows data for the reduction of U(VI) alone (38) and for uranium reduction with sulfate [at electron equivalent amounts of U(VI) and sulfate] for the mixed cell culture. Because the reduction of sulfate to sulfide is an 8-electron transfer and the reduction of U(VI) to U(IV) is a 2-electron transfer, the sulfate concentration used was equivalent to 25% of the uranium concentration. A 90-minute lag time for the reduction of U(VI) only was decreased to 5 ±

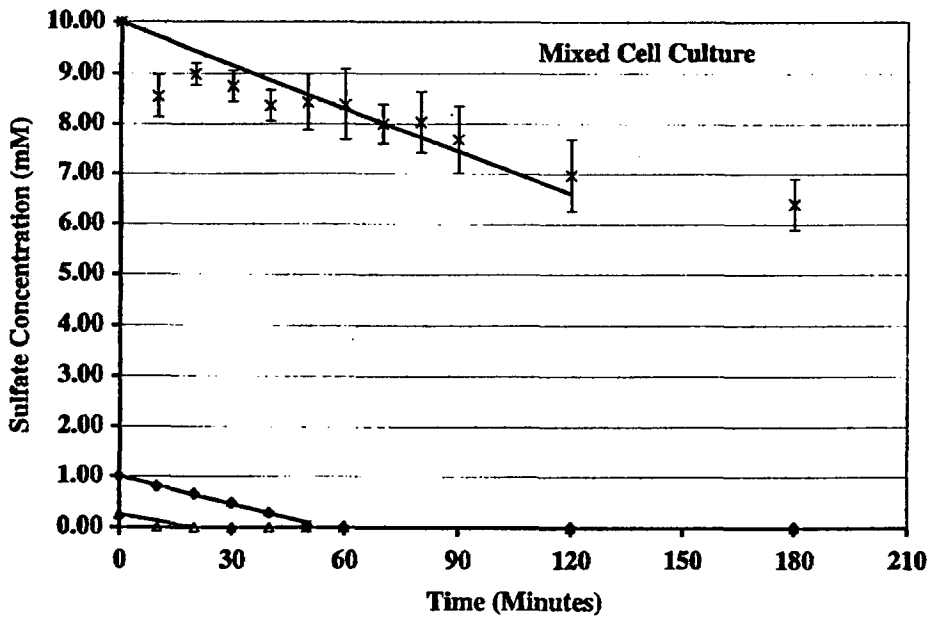

FIG. 3. Model simulations of variable sulfate concentration with approximately equal cell concentrations. ✳, S_0 = 10 mM and X_0 = 0.49 mg (dry weight) of cells/ml; ◆, S_0 = 1.0 mM and X_0 = 0.53 mg (dry weight) of cells/ml; △, S_0 = 0.25 mM and X_0 = 0.57 mg (dry weight) of cells/ml. Error bars, standard errors.

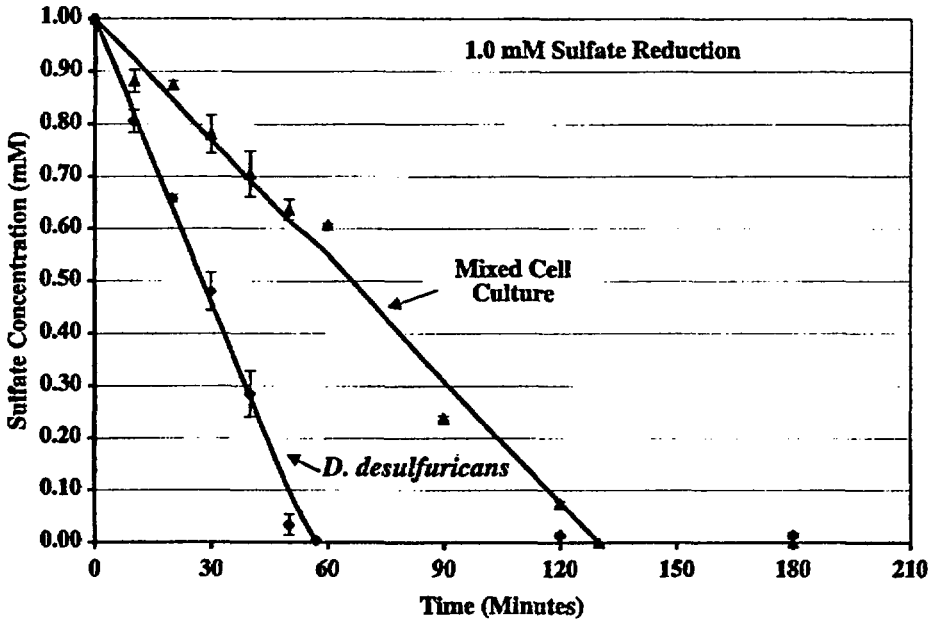

FIG. 4. Reduction of 1 mM sulfate by the mixed cell culture and by the pure culture of *D. desulfuricans*. ◆, 323.0 mg (wet weight) of cell mass, which is equivalent to 0.53 mg (dry weight)/ml of medium used in the batch experiment, for the mixed cell culture; ▲, 298.0 mg (wet weight) of cell mass, which is equivalent to 0.30 mg (dry weight)/ml of medium used in the batch experiment for the pure culture of *D. desulfuricans* (ATCC 7757). Zero-order model lines are fit to the plotted data. Error bars, standard errors.

5 min for U(VI) in the presence of sulfate for an initial U(VI) concentration (U_0) of 1 mM, an S_0 of 0.25 mM, and an X_0 of ≈0.5 mg (dry weight) of cells/ml.

Modeling of uranium and sulfate reduction. Under all experimental conditions tested, sulfate reduction was best fit by a zero-order model (equation 1), and uranium reduction was best fit by a first-order model. The first-order model fit to the U(VI) reduction data was

$$U = U_0 e^{-k_1 X t} \quad (3)$$

where U is the model predicted millimolar concentration of uranium, U_0 is the initial millimolar concentration of uranium, k_1 is the first-order rate constant, expressed as milligrams (dry weight) of cells per milliliter per minute, and X and t are as defined above. A linearized form of equation 3 was fit to the data to determine the rate constant k_1,

$$\ln U = \ln U_0 - k_1 X t \quad (4)$$

with units and terms as defined above. The model fits using average coefficients, and the data are shown in Fig. 7A for the mixed cell culture and in Fig. 7B for *D. desulfuricans* (ATCC 7757). In all cases the models fit the data with coefficients of determination, r^2, of 0.96 or higher. Figure 8 shows the respective model fits for uranium reduction in the presence of a sulfate concentration that might be found in freshwater. Figure 9 shows the uranium reduction kinetics in the presence of a higher, 10 mM sulfate concentration relevant for high-sulfate natural waters containing uranium.

DISCUSSION

Various aspects of the SRB reduction of U(VI) to U(IV) have been studied. Lovley and Phillips (21) found that *D. desulfuricans* was capable of uranium reduction. They later demonstrated that cytochrome c_3 was an essential component of uranium reduction by *D. desulfuricans* (22). Ganesh et al. (9) considered the SRB reduction of U(VI) in organic complexes. Tebo and Obraztsova (39) identified an SRB capable of growth with U(VI) as an electron acceptor. Spear et al. (38) established the rate constants for uranium reduction by a mixed SRB culture and by *D. desulfuricans*. In all cases U(IV) was precipitated from solution as the mineral uraninite, UO_2. Three studies have considered the reduction of U in the presence of the native sulfate electron acceptor, and that was for a pure culture of *D. desulfuricans* (21, 30, 31, 40a). These studies however, have not modeled the kinetics involved across a range of solution conditions. A few reports have described the kinetics for the enzymatic reduction of sulfate alone under various conditions (8, 13, 14, 21, 28, 29, 33, 34, 37). Ingvorsen and Jørgensen (14) provided kinetics information for four SRB pure cultures at 20°C; Ingvorsen et al. (13) provided the kinetics for both batch and chemostat cultures at 30°C; and Sonne-Hansen et al. (37) provided the kinetics for sulfate reduction by two species of thermophilic SRB at 70°C.

Sulfate reduction. For *Desulfovibrio vulgaris* (Hildenborough), Ingvorsen and Jørgensen (14), found a V_{max} of 1.1 μmol of SO_4^{2-}/mg (dry weight) · h^{-1}. For *D. postgatei*, Ingvorsen et al. obtained a V_{max} of 4.2 μmol of SO_4^{2-}/mg (dry weight) · h^{-1} (13). The *Desulfovibrio* sp. identified in the mixed cell culture for this report has a V_{max} range of 2 to 5 μmol of SO_4^{2-}/mg (dry weight) · h^{-1} (Table 1), similar to the V_{max} for *D. postgatei* and for *D. vulgaris* (Hildenborough) at 21 ± 3°C (13, 14). Vester and Ingvorsen report that 4.1 × 10^{-14} mol of SO_4^{2-}/cell · day^{-1} could be reduced by a pure culture of *Desulfobulbus propionicus* by using a direct cell count method, and a value of 2.43 × 10^{-13} using a T-MPN (tracer most-probable-number) method to calculate cell number (42). The range in this study was 0.73 × 10^{-14} to 1.2 × 10^{-14} mol of SO_4^{2-}/cell ·

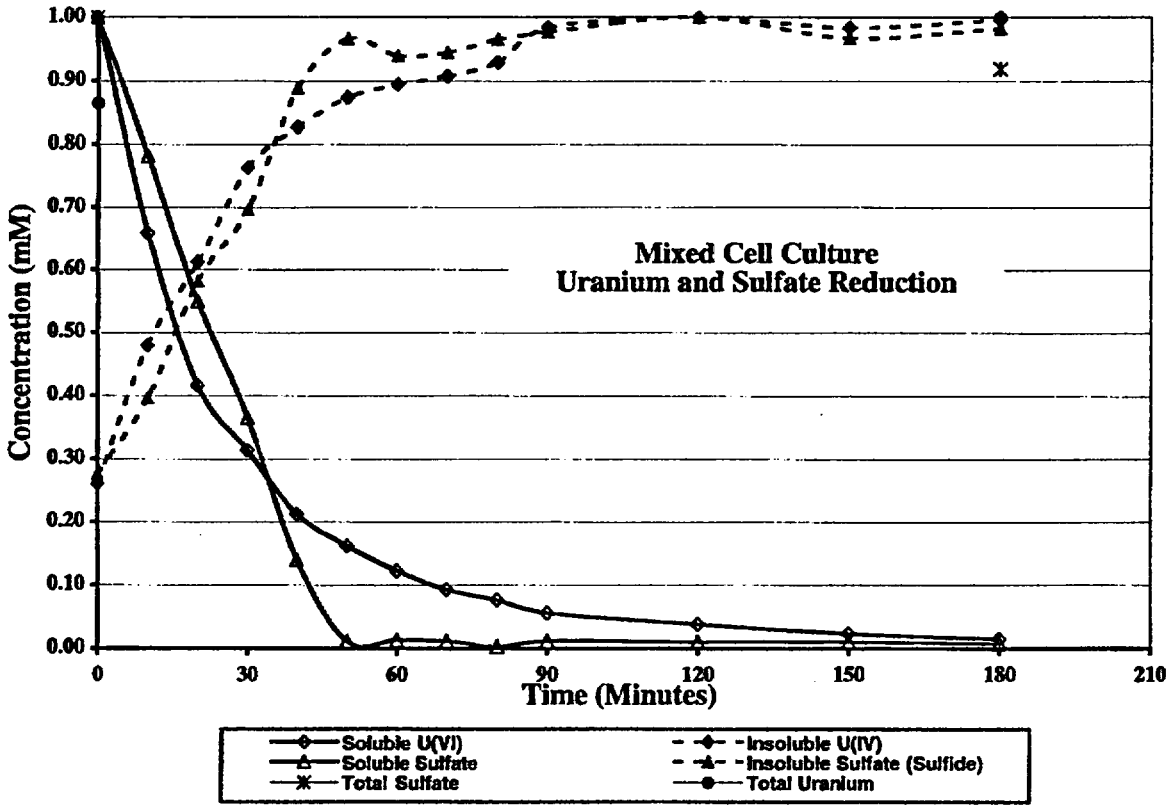

FIG. 5. Time course of 1 mM uranium and sulfate reduction by the mixed cell culture dominated by a *Desulfovibrio* sp. Insoluble U(IV) (as uraninite [38]) was collected in pellet fractions of sample aliquots, and insoluble ^{35}S was collected as insoluble sulfides after reacting with zinc acetate in sample aliquots. Solid circles at time zero and 180 min represent total activity of uranium, ^{233}U [U(VI) plus U(IV)], for mass balance accountability; starbursts at the same time points show total activity for ^{35}S ($^{35}SO_4^{2-}$ plus un-ionized sulfides [$^{35}S^{2-}$]) for mass balance. Data are for one experiment with 0.51 mg (dry weight) of cells/ml.

day^{-1}, consistent with those of Vester and Ingvorsen and others (13, 15).

A lag time until the onset of U(VI) reduction was previously observed for the mixed cell culture used here (38). This lag time was dependent upon cell concentration and ranged from 30 min at a cell concentration of 1.27 mg (dry weight) of cells/ml to 3 h at a low cell concentration of 0.18 mg (dry weight) of cells/ml. A lag time was also present for the pure culture of *D. desulfuricans* (ATCC 7757) that was approximately 30 min less than that of the mixed cell culture for the same cell concentration. Figure 2 shows a similar lag time for sulfate at low cell concentrations. Thus, for the mixed cell culture, a reproducible and predictable lag time until the onset of reduction for both the native electron acceptor and U(VI) is possible. The *D. desulfuricans* (ATCC 7757) culture was not tested at these low cell concentrations for the possibility of a lag time for sulfate reduction.

Ingvorsen et al. (13) observed a sulfate concentration-based threshold, whereby when sulfate concentration decreased low enough in their batch experimental system with both batch- and chemostat-grown cells, no reduction was evident. Figure 2 shows a cell concentration-based threshold, which could be analogous to the sulfate concentration threshold, by which the physiological state of the cells determines the amount of sulfate reduction possible (13).

Concurrent uranium and sulfate reduction. The design of a uranium removal biotreatment system employing SRB requires a knowledge of the individual and concurrent rates of U(VI) and sulfate reduction. Bioreactor systems can be designed for sequential growth and U(VI) reduction or for concurrent growth and U(VI) reduction, depending upon the system layout and the SRB employed. Rate information is needed to design a growth reactor that integrates into its design the potential for the competitive effects of concurrent U(VI) and SO_4^{2-} reduction in a combined growth and U(VI) reduction system.

The fact that sulfate reduction and uranium reduction were best fit by different models suggests that the rate-limiting step for sulfate and U(VI) reduction is not the same. Sulfate reduction has been hypothesized to occur within the cytoplasmic membrane (35), while uranium reduction has been hypothesized to occur in the periplasmic space (outside of the cytoplasmic membrane) (24). Since these two reductions physically take place in different locations, a difference in the rate-limiting step is feasible even though cytochrome c_3 has been identified as a critical component for both. In addition, the pathway for sulfate reduction involves multiple cytoplasmic enzymes (e.g., adenylyl sulfate reductase [19, 35]) which are probably not used for uranium reduction. One of the enzymatic components that is not common between the two pathways may be rate-limiting for sulfate. Thus, the observation of different rates of sulfate and uranium reduction by the same organism is reasonable. Though the data were not modeled, experimentation performed on a pure culture of *D. vulgaris* (Hildenborough) (ATCC 29579) showed that cytochrome c_3 was the enzyme responsible for U reduction via a first-order process

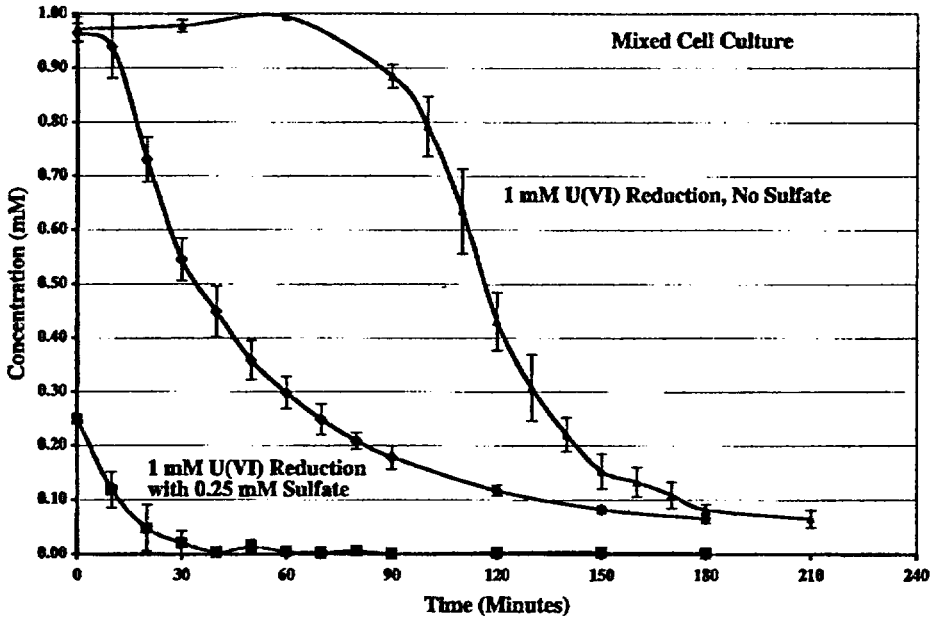

FIG. 6. Time course of uranium and sulfate reduction by the *Desulfovibrio* sp.-dominated mixed culture, with a U_0 of 1.0 mM and an S_0 of 0.25 mM. ▲, U(VI) reduction in the absence of sulfate, with a U_0 of 1.0 mM and an X_0 of 0.46 mg (dry weight) of cells/ml (38); ◆, U(VI) reduction (U_0 = 1.0 mM) in the presence of 0.25 mM sulfate; ■, X_0 = 0.48 mg (dry weight) of cells/ml. Each data set is an average from three experiments with the mixed cell culture. Error bars, standard errors.

nearly identical to that described for the mixed cell culture here (24).

Since the mixed cell culture contains two species, it was not possible to distinguish the contribution of each to the reduction of uranium. The mixed cell culture described here, however, does contain a *Clostridium* sp., and *Clostridium* is another bacterial genus described as being capable of uranium reduction (5, 6, 7). However, the fraction of biomass associated with the *Clostridium* sp. was no more than 10%. This was observed both by Gram staining of the culture and visualization and by the presence of a 10-to-1 *Desulfovibrio* sp.-to-*Clostridium* sp. banding pattern on a 100-clone RFLP gel. As a genus, *Clostridium* does not dissimilatorily reduce sulfate to sulfide; thus, the sulfate reduction described for the mixed culture is expected to be due to the presence of the *Desulfovibrio* sp. (4). By considering the reduction of both electron acceptors by the pure culture of *D. desulfuricans* (Fig. 7B) under the same experimental conditions as the mixed cell culture (Fig. 7A), a contrast can be made. The rate constant for uranium reduction by the *D. desulfuricans* culture was two to three times higher than that for the mixed cell culture (Table 2), while the rate of sulfate reduction rate was about the same. If both genera were reducing U(VI), the mixed cell culture's kinetics would likely be high, higher than that of the pure culture. In addition, the dry weight of *D. desulfuricans* cells present in the pure culture was 58% of that used for the mixed culture, because experiments were carried out by wet weight cell mass comparisons that were nearly identical (the difference comes from water content and other factors contributing to mass [10]).

Both the mixed and pure cell cultures exhibited lag times of ≥90 min for U(VI) reduction in the absence of sulfate (Fig. 7); in the presence of sulfate these were reduced to near zero. For both cultures, the presence of sulfate aided the reduction of uranium, bringing it to a first-order rate of reduction from a Monod non-growth-based rate with a long lag time (38). However, once the lag phase was over, the amount of time required to remove 90% of the uranium was about the same. From the kinetics coefficients determined for these two cultures, it appears that the *Clostridium* sp. of the mixed cell culture is not contributing significantly to U(VI) reduction. The rate constants for sulfate reduction were unchanged in the presence and absence of uranium for both cultures.

Further analysis indicates that as the sulfate concentration increases in the medium from 0.25 to 10 mM, the rate of sulfate reduction by the mixed culture doubles. Over the same sulfate concentrations, the mixed culture shows an optimum rate of uranium reduction occurring at a sulfate concentration of 1 mM. The pure culture experiments were done at 1 mM sulfate and uranium concentrations based on the optimum seen for U(VI) removal by the mixed culture.

Lovley and Phillips (21) examined uranium reduction in the presence of sulfate by *D. desulfuricans* (ATCC 29577) in glass serum bottles at 35°C. L-Cysteine was added as a reductant to a bicarbonate-buffered medium for experiments exploring U(VI) reduction in the presence of sulfate, because it yielded higher rates of sulfate reduction. This was not done in our studies. Their results show that for the pure *D. desulfuricans* (ATCC 29577) culture, the presence of sulfate had no significant effect on U(VI) reduction. Our data, for both the mixed and pure *D. desulfuricans* (ATCC 7757) cultures, indicate otherwise, as shown in Fig. 7. The presence of an electron equivalent amount of sulfate, 0.25 mM sulfate, up to 10 mM sulfate (40 times the electron equivalents) removed the lag time for U(VI) reduction and enhanced the overall rate of U(VI) reduction. Lovley and Phillips (21) also suggest that U(VI) reduction did not influence the rate of sulfate reduction by *D. desulfuricans* (ATCC 29577). This was also observed for both the mixed and pure cultures in this study (Tables 1 and 2). Lovley and Phillips showed that *D. desulfuricans* (ATCC 29577) could reduce an initial 0.35 mM U(VI) concentration down to 0.09 mM with concurrent reduction of 2.0 mM sulfate down to 1.1 mM in 4 h, with an initial biomass concentration of

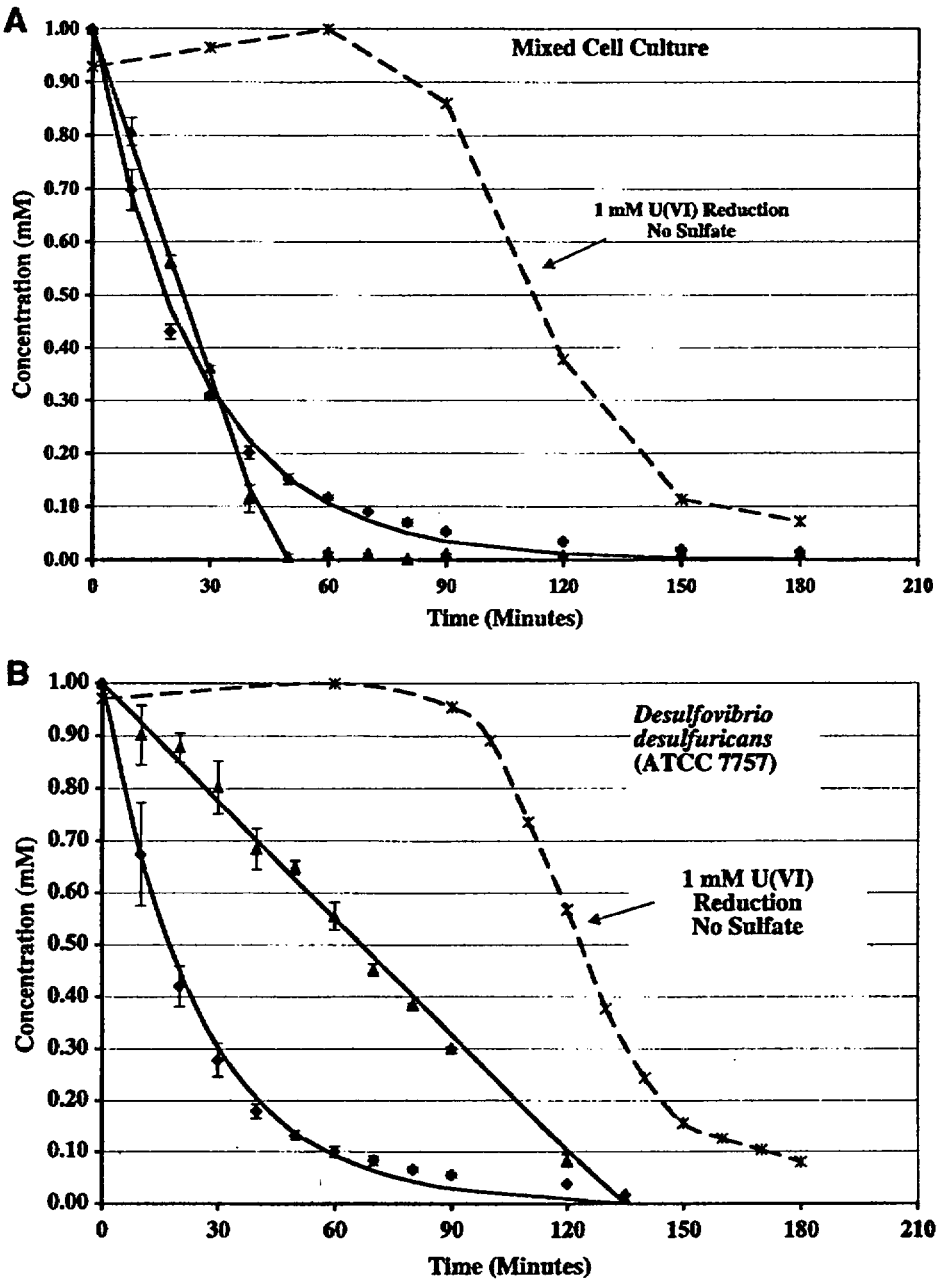

FIG. 7. (A) Time course of concurrent uranium and sulfate reduction for a U_0 of 1.0 mM and an S_0 of 1.0 mM by the mixed cell culture. ▲, sulfate concentration; ◆, U(VI) concentration. Lines represent zero-order and first-order models fit to sulfate and uranium reduction data, respectively. Data points are average values from two separate experiments. Average X_0 = 0.51 mg (dry weight) of cells/ml. ✱, reduction of 1 mM U(VI) alone by 0.50 mg (dry weight) of cells/ml by the same mixed cell culture (38). Error bars, standard errors. (B) Time course of concurrent uranium and sulfate reduction for a U_0 of 1.0 mM and an S_0 of 1.0 mM by the pure culture *D. desulfuricans* (ATCC 7757). Symbols are as described for panel A. Data points are average values from two separate experiments. Average X_0 = 0.29 mg (dry weight) of cells/ml. ✱, reduction of 1 mM U(VI) alone by 0.32 mg (dry weight) of cells/ml (38). A model for this reduction is reported elsewhere (38). Error bars, standard errors.

approximately 0.2 to 1.0 mg (dry weight) of cells/ml (0.5 mg of protein/mg [dry weight] conversion assumed per Bailey and Ollis [2]) at 35°C (18). A decrease in the reaction temperature from 35 to 20°C would produce at least a 50% decrease in the reaction rate (2). Thus, at a temperature comparable to that used in this study, U(VI) and sulfate reduction by *D. desulfuricans* (ATCC 29577) would be expected to take 6 to 8 h. If the experiment is conducted in glass serum bottles, a 15% sorptive effect of uranium and a 10% sorptive effect for sulfate may be present, though the overall reduction trend is the same. Both cultures utilized in this study showed a higher rate of reduction as described; this, however, may be a function of the cell concentrations used.

For the concurrent reduction of sulfate and uranium by

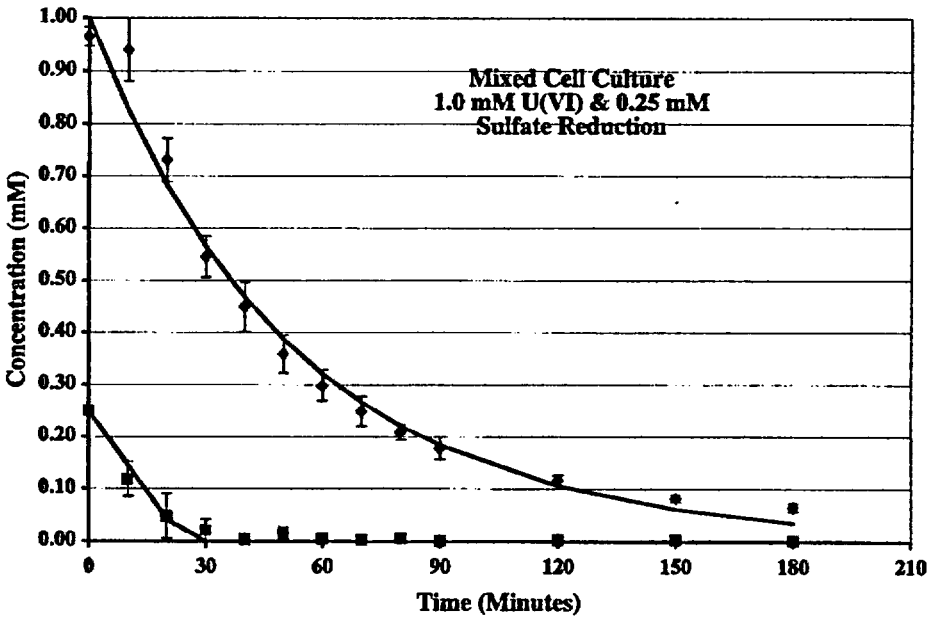

FIG. 8. Zero- and first-order models applied to the enzymatic reduction of 0.25 mM sulfate and 1 mM uranium by the mixed cell culture, respectively. Each set of data points is an average from three experiments with the same mixed cell culture. Models are fit to plotted data with values given in Table 2. X_0 = 0.48 mg (dry weight) of cells/ml. Error bars, standard errors.

SRB, two reductive processes for U(VI) are possible: enzymatic reduction as described above and chemical reduction by SRB-produced sulfides. Originally, this was thought to be the dominant mechanism, as it is thermodynamically feasible (30, 31). Lovley and Phillips (21) found that the enzymatic reduction was significantly faster than the nonenzymatic, sulfide reduction of U(VI), even in the presence of catalytic SRB cell surfaces, as the temperature optimum for U(VI) reduction is consistent with enzymatic reduction. Based on Lovley and Phillips' conclusions, we did not test for any sulfide effects in the combined reduction experiments. Considering the relatively short time courses of our experiments, the temperature of our experiments, and the kinetics coefficients described in Table 2, the sulfides produced may have had a role in the fact that the

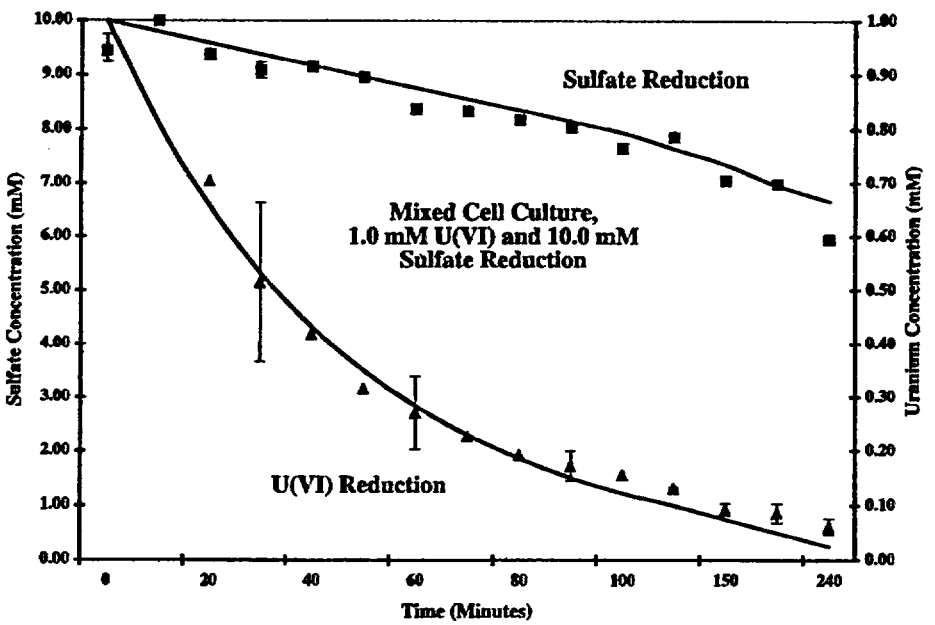

FIG. 9. Zero- and first-order models applied to the enzymatic reduction of 10 mM sulfate and 1 mM uranium by the mixed cell culture, respectively. The average X_0 for the three experiments with the same mixed cell culture represented is 0.46 mg (dry weight) of cells/ml. Error bars, standard errors.

TABLE 2. Zero- and first-order model kinetics coefficients determined for both the mixed and pure cell cultures

Culture	Initial cell concn (mg [dry wt] of cells/ml)	Initial sulfate concn (mM)	Initial uranium concn (mM)	k_0 (μM SO_4^{2-}/(mg [dry wt] of SRB/ml) · min^{-1})	k_1 (mg [dry wt] of SRB/ml) · min^{-1})
Mixed cell	0.47 ± 0.01	0.25	1.0	20 ± 4	0.041 ± 0.004
	0.50 ± 0.01	1.0	1.0	36 ± 7	0.071 ± 0.003
	0.46 ± 0.01	10	1.0	41 ± 6	0.039 ± 0.009
D. desulfuricans (ATCC 7757)	0.29 ± 0.004	1.0	1.0	26 ± 2	0.137 ± 0.016

lag time seen with reduction of U(VI) only was minimized when sulfate was also present for reduction. This effect, however, is likely to be minor.

Conclusion. For the mixed cell culture, a reproducible and predictable lag time until the onset of reduction for both the native electron acceptor, sulfate and U(VI) is possible. A cell concentration-based threshold until the onset of sulfate reduction can begin was reproducibly found for the mixed cell culture, resulting in a described lag time. This culture exhibited a similar lag time in reducing U(VI) alone, though at a higher cell concentration. Zero- and first-order models best fit the data for the concurrent removal of sulfate and uranium, respectively, suggesting that the rate-limiting step for each electron acceptor's reduction is not the same. These studies were performed at room temperature for both cultures, the upper-end temperature of natural waters. For a bio-based treatment system this is important, as U(VI)-containing waters are naturally cool. For the cultures tested herein, reduction of aqueous U(VI) was enhanced by the presence of aqueous sulfate. The presence of sulfate both minimizes the lag time and increases the overall rate.

ACKNOWLEDGMENTS

Support for this work was provided by the National Science Foundation (BES-9410343) and an Environmental Protection Agency STAR graduate fellowship (U-914935-01-0).

We thank Abigail Salyers, University of Illinois, Urbana, and Edward Leadbetter, University of Connecticut, co-leaders of the 1998 Microbial Diversity Course at the Marine Biological Laboratory, Woods Hole, Mass., for providing the opportunity to molecularly characterize the mixed culture presented. We also thank Bruce Paster of the Forsythe Dental Center in Boston, Mass., for sequencing our 16S rRNA gene fragments, Norman Pace, University of Colorado, Boulder, for the opportunity to fully characterize the mixed cell culture, and J. Kirk Harris of the University of California, Berkeley, for training with the 96-well clone/PCR/RFLP format. Frequent consultations with Dave Updegraff, retired professor of chemistry and microbiology at the Colorado School of Mines, were very helpful.

REFERENCES

1. **Altschul, S. F., W. Gish, W. Miller, E. W. Myers, and D. J. Lipman.** 1990. Basic local alignment search tool. J. Mol. Biol. 215:403–410.
2. **Bailey, J. E., and D. F. Ollis.** 1986. Biochemical engineering fundamentals, 2nd ed. McGraw-Hill, New York, N.Y.
3. **Caccavo, F., Jr., R. P. Blakemore, and D. R. Lovley.** 1992. A hydrogen-oxidizing, Fe(III)-reducing microorganism from the Great Bay Estuary, New Hampshire. Appl. Environ. Microbiol. 58:3211–3216.
4. **Cato, E. L., W. L. George, and S. M. Finegold.** 1986. Genus *Clostridium* p. 1141. *In* N. R. Krieg and J. G. Holt (ed.), Bergey's manual of systematic bacteriology, vol. 2. Baltimore: Williams and Wilkins, Baltimore, Md.
5. **Francis, A. J., C. J. Dodge, F. Lu, G. P. Halada, and C. R. Clayton.** 1994. XPS and XANES studies of uranium reduction by *Clostridium* sp. *Environ. Sci. Technol.* 28:636–639.
6. **Francis, A. J., C. J. Dodge, and J. B. Gillow.** September 1991. U.S. Patent 5,047,152.
7. **Francis, A. J., C. J. Dodge, J. B. Gillow, and J. E. Cline.** 1991. Microbial transformations of uranium in wastes. Radiochim. Acta 52/53:311–316.
8. **Fukui, M., and S. Takii.** 1994. Kinetics of sulfate respiration by free-living and particle-associated sulfate-reducing bacteria. FEMS Microb. Ecol. 13: 241–248.
9. **Ganesh, R., K. G. Robinson, G. D. Reed, and G. S. Sayler.** 1997. Reduction of hexavalent uranium from organic complexes by sulfate- and iron-reducing bacteria. Appl. Environ. Microbiol. 63:4385–4391.
10. **Gerhardt, P., et al. (ed.).** 1981. *Manual of methods for general bacteriology*, p. 505. American Society for Microbiology, Washington, D.C.
11. **Gorby, Y. A., and D. R. Lovley.** 1992. Enzymatic uranium precipitation. Environ. Sci. Technol. 26:205–207.
12. **Hugenholtz, P., C. Pitulle, K. L. Hershberger, and N. R. Pace.** 1998. Novel division level bacterial diversity in a Yellowstone hot spring. J. Bacteriol. 180:366–376.
13. **Ingvorsen, K., A. J. B. Zehnder, and B. B. Jørgensen.** 1984. Kinetics of sulfate and acetate uptake by *Desulfobacter postgatei*. Appl. Environ. Microbiol. 47:403–408.
14. **Ingvorsen, K., and B. B. Jørgensen.** 1984. Kinetics of sulfate uptake by freshwater and marine species of *Desulfovibrio*. Arch. Microbiol. 139:61–66.
15. **Jørgensen, B. B.** 1978. A comparison of methods for the quantification of bacterial sulfate reduction in coastal marine sediments. III. Estimation from chemical and bacteriological field data. Geomicrobiology 1:49–64.
16. **Kane, M. D., L. K. Poulsen, and D. A. Stahl.** 1993. Monitoring the enrichment and isolation of sulfate-reducing bacteria by using oligonucleotide hybridization probes designed from environmentally derived 16S rRNA sequences. Appl. Environ. Microbiol. 59:682–686.
17. **Lane, D. J., B. Pace, G. J. Olsen, D. A. Stahl, M. L. Sogin, and N. R. Pace.** 1985. Rapid determination of 16S ribosomal RNA sequences for phylogenetic analyses. Proc. Natl. Acad. Sci. USA 82:6955–6959.
18. **Lane, D. J.** 1991. 16S/23S rRNA sequencing, p. 115–175. *In* E. Stackebrandt and M. Goodfellow (ed.), Nucleic acid techniques in bacterial systematics. John Wiley and Sons, New York, N.Y.
19. **LeGall, J., D. V. DerVartanian, and H. D. Peck, Jr.** 1979. Flavoproteins, iron proteins, and hemoproteins as electron-transfer components of the sulfate-reducing bacteria. Curr. Top. Bioenerg. 9:237–265.
20. **Lloyd, J. R., H. F. Noling, V. A. Sole, K. Bosecker, and L. E. Macaskie.** 1998. Technetium reduction and precipitation by sulfate-reducing bacteria. Geomicrobiol. J. 15:45–58.
21. **Lovley, D. R., and E. J. P. Phillips.** 1992. Reduction of uranium by *Desulfovibrio desulfuricans*. Appl. Environ. Microbiol. 58:850–856.
22. **Lovley, D. R., and E. J. P. Phillips.** 1994. Reduction of chromate by *Desulfovibrio vulgaris* and its c_3 cytochrome. Appl. Environ. Microbiol. 60:726–728.
23. **Lovley, D. R., E. E. Roden, E. J. P. Phillips, and J. C. Woodward.** 1993. Enzymatic iron and uranium reduction by sulfate reducing bacteria. Mar. Geol. 113:41–53.
24. **Lovley, D. R., P. K. Widman, J. C. Woodward, and E. J. P. Phillips.** 1993. Reduction of uranium by cytochrome c_3 of *Desulfovibrio vulgaris*. Appl. Environ. Microbiol. 59:3572–3576.
25. **Lovley, D. R., E. J. P. Phillips, Y. A. Gorby, and E. R. Landa.** 1991. Microbial uranium reduction. Nature 350:413–416.
26. **Madigan, M. T., J. M. Martinko, and J. Parker (ed.).** 2000. Brock: biology of microorganisms, 9th ed., p. 498–502. Prentice-Hall, Upper Saddle River, N.J.
27. **Maidak, B. L., N. Larson, M. J. McCaughey, R. Overbeek, G. J. Olsen, K. Fogel, J. Blandy, and C. R. Woese.** 1994. The Ribosomal Database Project. Nucleic Acids Res. 22:3485–3487.
28. **Marschall, C., P. Frenzel, and H. Cypionka.** 1993. Influence of oxygen on sulfate reduction and growth of sulfate-reducing bacteria. Arch. Microbiol. 159:168–173.
29. **Middleton, A. C., and A. W. Lawrence.** 1977. Kinetics of microbial sulfate reduction. J. Water Pollut. Control Fed. 1977:1659–1670.
30. **Mohagheghi, A.** 1985. The role of aqueous sulfide and sulfate-reducing bacteria in the kinetics and mechanisms of the reduction of uranyl ion. Ph.D. thesis T-3029. Colorado School of Mines, Golden.
31. **Mohagheghi, A., D. M. Updegraff, and M. B. Goldhaber.** 1985. The role of sulfate reducing bacteria in the deposition of sedimentary uranium ores. Geomicrobiol. J. 4:153–173.
32. **Odom, J. M., and R. Singleton (ed.).** 1993. The sulfate-reducing bacteria: contemporary perspectives. Springer-Verlag, New York, N.Y.
33. **Okabe, S., and W. G. Characklis.** 1992. Effects of temperature and phosphorous concentration on microbial sulfate reduction by *Desulfovibrio desulfuricans*. Biotechnol. Bioeng. 39:1031–1042.
34. **Okabe, S., P. H. Nielsen, and W. G. Characklis.** 1992. Factors affecting

microbial sulfate reduction by *Desulfovibrio desulfuricans* in continuous culture: limiting nutrients and sulfide concentration. Biotechnol. Bioeng. **40:** 725–734.

35. **Peck, H. D., Jr., and J. LeGall.** 1982. Biochemistry of dissimilatory sulphate reduction. Philos. Trans. R. Soc. Lond. Ser. B. **298**:443–466.
36. **Postgate, J. R.** 1984. The sulphate-reducing bacteria, 2nd ed. Cambridge University Press. Cambridge, United Kingdom.
37. **Sonne-Hansen, J., P. Westermann, and B. K. Ahring.** 1999. Kinetics of sulfate and hydrogen uptake by the thermophilic sulfate-reducing bacteria *Thermodesulfobacterium* sp. strain JSP and *Thermodesulfovibrio* sp. strain R1Ha3. Appl. Environ. Microbiol. **65**:1304–1307.
38. **Spear, J. R., L. A. Figueroa, and B. D. Honeyman.** 1999. Modeling the removal of uranium U(VI) from aqueous solutions in the presence of sulfate-reducing bacteria. Environ. Sci. Technol. **33**:2667–2675.
39. **Tebo, B. M., and A. Y. Obraztsova.** 1998. Sulfate-reducing bacterium grows with Cr(VI), U(VI), Mn(IV), and Fe(III) as electron acceptors. FEMS Microbiol. Lett. **162**:193–198.
40. **Truex, M. J., B. M. Peyton, N. B. Valentine, and Y. A. Gorby.** 1997. Kinetics of U(VI) reduction by a dissimilatory Fe(III)-reducing bacterium under non-growth conditions. Biotechnol. Bioeng. **55**:490–496.

40a. **Tucker, M. D., L. L. Barton, and B. M. Thomson.** 1996. Kinetic coefficients for simultaneous reduction of sulfate and uranium by *Desulfovibrio desulfuricans*. Appl. Microbiol. Biotechnol. **46**:74–77.

41. **Updegraff, D. M., and G. B. Wren.** 1954. The release of oil from petroleum-bearing materials by sulfate-reducing bacteria. Appl. Microbiol. **2**:309–322.
42. **Vester, F., and K. Ingvorsen.** 1998. Improved most-probable-number method to detect sulfate-reducing bacteria with natural media and a radiotracer. Appl. Environ. Microbiol. **64**:1700–1707.

Pergamon

Geochimica et Cosmochimica Acta, Vol. 58, No. 13, pp. 2829–2843, 1994

0016-7037/94 $6.00 + .00

0016-7037(94)00081-6

Interaction between aqueous uranium (VI) and sulfide minerals: Spectroscopic evidence for sorption and reduction

PAUL WERSIN,[1,*] MICHAEL F. HOCHELLA JR.,[1,†] PER PERSSON,[1,‡] GEORGE REDDEN,[2] JAMES O. LECKIE,[2] and DAVID W. HARRIS[3]

[1]Department of Geology, Stanford University, Stanford, CA 94305, USA
[2]Department of Civil Engineering, Stanford University, Stanford, CA 94305, USA
[3]Charles Evans and Associates, 301 Chesapeake Drive, Redwood City, CA 94063, USA

(*Received April* 20, 1993; *accepted in revised form February* 25, 1994)

Abstract—The interaction of aqueous U(VI) with galena and pyrite surfaces under anoxic conditions has been studied by solution analysis and by spectroscopic methods. The solution data indicate that uranyl uptake is strongly dependent on pH; maximum uptake (>98%) occurs above a pH range of between 4.8 and 5.5, depending on experimental conditions. Increasing the sorbate/sorbent ratio results in a relative decrease in uptake of uranyl and in slower sorption kinetics.

Auger electron spectroscopy (AES) analysis indicates an inhomogeneous distribution of sorbed uranium at the surface. In the case of galena, formation of small precipitates (~40 nm wide needles) of a uranium oxide compound are found. Pyrite shows a patchy distribution of uranium, mainly associated with oxidized surface species of sulfur and iron. X-ray photoelectron spectroscopy (XPS) yields insight into possible redox processes indicating, for both sulfides, the concomitant formation of polysulfides and a uranium oxide compound with a mixed oxidation state at a U(VI)/U(IV) ratio of ~2. Furthermore, in the case of pyrite, at pH above 6 increased oxidation of sulfur and iron and higher relative amounts of unreduced surface-uranyl are observed. Fourier Transformed Infrared (FTIR) analysis of surface-bound uranyl shows a significant shift of the asymmetric stretching frequency to lower wavenumbers which is consistent with the formation of a U_3O_8-type compound and thus, independently, confirms the partial reduction of uranyl at the sulfide surface.

The combination of AES, XPS, and FTIR provides a powerful approach for identifying mechanisms that govern the interaction of redox sensitive compounds in aqueous systems. Our overall results indicate that sulfide minerals are efficient scavengers of soluble uranyl. Comparing our results with recent field observations, we suggest that thermodynamically metastable U_3O_8 controls uranium concentrations in many anoxic groundwaters.

INTRODUCTION

THE MOBILITY OF URANYL, U(VI), in groundwater plays an important role in (1) ore deposit formation and (2) assessment of radioactive waste disposal. It has been shown that the mobility of uranium critically depends on immobilization processes such as sorption to solid particles and reduction of U(VI) to U(IV) (e.g., MORSE and CHOPPIN, 1991). Also, sorption onto ferric oxides and clays, which is prevalent in natural groundwater, has been investigated in detail (HO and DOERN, 1985; HO and MILLER, 1986; HSI and LANGMUIR, 1985; JAMES et al., 1983; GIBLIN et al., 1981; KOSS, 1988; TSAI and WAITE, 1991).

Immobilization of U(VI) by reduction to U(IV), although considered one of the dominant processes in low-temperature uranium deposit formation (WARREN and GRANGER, 1973; HARSHMAN, 1976), has received relatively little attention in the literature. Field observations from marine systems indicate that reduction of U(VI) is primarily controlled by kinetic, not thermodynamic factors (ANDERSON, 1987; KLINKHAMMER and PALMER, 1991). In fact, in a study by ANDERSON et al. (1989), no reduction of U(VI) was observed in anoxic, H_2S-bearing bottomwaters, whereas reduction to U(IV) was shown to occur in the underlying sediment at similar redox conditions. Supportive evidence for the inert properties of uranyl in H_2S-bearing homogeneous solutions is given by KOCHENOV et al. (1977); however, these authors also found that the addition of mineral particles (e.g., phosphate minerals) to the solutions resulted in reduction of uranyl. Certain bacteria have also been found to be highly efficient reducers of U(VI) (LOVELY and PHILLIPS, 1992; LOVLEY et al., 1991).

In inorganic systems, sulfide minerals are expected to be efficient reducing agents judging from the structure of a number of ore deposits. Observations of uranium deposits formed in a groundwater environment, e.g., a sandstone-type deposits (LANGMUIR and CHATAM, 1980), reveal association of U(IV) minerals with sulfide minerals (mainly pyrite). Experimental studies have also shown sulfide minerals to have the capacity to reduce trace metals such as Au(III), Pd(II), Ag(I), and Cr(VI) (BANCROFT and HYLAND, 1990; BUCKLEY et al., 1989; HISKEY et al., 1987; PERRY et al., 1984). However, for uranyl, no such experimental work is available.

This has lead us to investigate the interaction of uranyl with two sulfide surfaces (galena and pyrite) under conditions relevant to anoxic groundwaters. From equilibrium calcu-

* *Present address:* MBT Tecnología Ambiental, Parc Tecnològic ... es, 08290 Cerdanyola, Spain.
† *Present address:* Department of Geological Sciences, Virginia ... nic Institute and State University, Blacksburg, VA 24061.
‡ *Present address:* Department of Chemistry, Swedish University ... gricultural Sciences, 75007 Uppsala, Sweden.

Pergamon

Geochimica et Cosmochimica Acta, Vol. 58, No. 13, pp. 2829–2843, 1994

0016-7037/94 $6.00 + .00

0016-7037(94)00081-6

Interaction between aqueous uranium (VI) and sulfide minerals: Spectroscopic evidence for sorption and reduction

PAUL WERSIN,[1,*] MICHAEL F. HOCHELLA JR.,[1,†] PER PERSSON,[1,‡] GEORGE REDDEN,[2] JAMES O. LECKIE,[2] and DAVID W. HARRIS[3]

[1]Department of Geology, Stanford University, Stanford, CA 94305, USA
[2]Department of Civil Engineering, Stanford University, Stanford, CA 94305, USA
[3]Charles Evans and Associates, 301 Chesapeake Drive, Redwood City, CA 94063, USA

(*Received April* 20, 1993; *accepted in revised form February* 25, 1994)

Abstract—The interaction of aqueous U(VI) with galena and pyrite surfaces under anoxic conditions has been studied by solution analysis and by spectroscopic methods. The solution data indicate that uranyl uptake is strongly dependent on pH; maximum uptake (>98%) occurs above a pH range of between 4.8 and 5.5, depending on experimental conditions. Increasing the sorbate/sorbent ratio results in a relative decrease in uptake of uranyl and in slower sorption kinetics.

Auger electron spectroscopy (AES) analysis indicates an inhomogeneous distribution of sorbed uranium at the surface. In the case of galena, formation of small precipitates (~40 nm wide needles) of a uranium oxide compound are found. Pyrite shows a patchy distribution of uranium, mainly associated with oxidized surface species of sulfur and iron. X-ray photoelectron spectroscopy (XPS) yields insight into possible redox processes indicating, for both sulfides, the concomitant formation of polysulfides and a uranium oxide compound with a mixed oxidation state at a U(VI)/U(IV) ratio of ~2. Furthermore, in the case of pyrite, at pH above 6 increased oxidation of sulfur and iron and higher relative amounts of unreduced surface-uranyl are observed. Fourier Transformed Infrared (FTIR) analysis of surface-bound uranyl shows a significant shift of the asymmetric stretching frequency to lower wavenumbers which is consistent with the formation of a U_3O_8-type compound and thus, independently, confirms the partial reduction of uranyl at the sulfide surface.

The combination of AES, XPS, and FTIR provides a powerful approach for identifying mechanisms that govern the interaction of redox sensitive compounds in aqueous systems. Our overall results indicate that sulfide minerals are efficient scavengers of soluble uranyl. Comparing our results with recent field observations, we suggest that thermodynamically metastable U_3O_8 controls uranium concentrations in many anoxic groundwaters.

INTRODUCTION

THE MOBILITY OF URANYL, U(VI), in groundwater plays an important role in (1) ore deposit formation and (2) assessment of radioactive waste disposal. It has been shown that the mobility of uranium critically depends on immobilization processes such as sorption to solid particles and reduction of U(VI) to U(IV) (e.g., MORSE and CHOPPIN, 1991). Also, sorption onto ferric oxides and clays, which is prevalent in oxic groundwater, has been investigated in detail (HO and DOERN, 1985; HO and MILLER, 1986; HSI and LANGMUIR, 1985; AMES et al., 1983; GIBLIN et al., 1981; KOSS, 1988; PAYNE and WAITE, 1991).

Immobilization of U(VI) by reduction to U(IV), although considered one of the dominant processes in low-temperature ore deposit formation (WARREN and GRANGER, 1973; BROOKINS, 1976), has received relatively little attention in the literature. Field observations from marine systems indicate that reduction of U(VI) is primarily controlled by kinetic, not thermodynamic factors (ANDERSON, 1987; KLINKHAMMER and PALMER, 1991). In fact, in a study by ANDERSON et al. (1989), no reduction of U(VI) was observed in anoxic, H_2S-bearing bottomwaters, whereas reduction to U(IV) was shown to occur in the underlying sediment at similar redox conditions. Supportive evidence for the inert properties of uranyl in H_2S-bearing homogeneous solutions is given by KOCHENOV et al. (1977); however, these authors also found that the addition of mineral particles (e.g., phosphate minerals) to the solutions resulted in reduction of uranyl. Certain bacteria have also been found to be highly efficient reducers of U(VI) (LOVELY and PHILLIPS, 1992; LOVLEY et al., 1991).

In inorganic systems, sulfide minerals are expected to be efficient reducing agents judging from the structure of a number of ore deposits. Observations of uranium deposits formed in a groundwater environment, e.g., a sandstone-type deposits (LANGMUIR and CHATAM, 1980), reveal association of U(IV) minerals with sulfide minerals (mainly pyrite). Experimental studies have also shown sulfide minerals to have the capacity to reduce trace metals such as Au(III), Pd(II), Ag(I), and Cr(VI) (BANCROFT and HYLAND, 1990; BUCKLEY et al., 1989; HISKEY et al., 1987; PERRY et al., 1984). However, for uranyl, no such experimental work is available.

This has lead us to investigate the interaction of uranyl with two sulfide surfaces (galena and pyrite) under conditions relevant to anoxic groundwaters. From equilibrium calcu-

* *Present address:* MBT Tecnología Ambiental, Parc Tecnològic del Vallès, 08290 Cerdanyola, Spain.
† *Present address:* Department of Geological Sciences, Virginia Polytechnic Institute and State University, Blacksburg, VA 24061, USA.
‡ *Present address:* Department of Chemistry, Swedish University of Agricultural Sciences, 75007 Uppsala, Sweden.

lations (neglecting surface effects), such an interaction should involve reduction of uranyl to crystalline UO_2 and oxidation of sulfide to sulfate (LISITSIN, 1962; LANGMUIR, 1978). From field observations, however, naturally occurring uraninite formed in low-temperature environments commonly has compositions within the UO_2-U_3O_8 solid solution series, usually ranging from U_2O_5 to U_3O_8 (LANGMUIR, 1978).

It is well known that the kinetics of redox reactions occurring at mineral/water interfaces often critically depend on the reactivity of surface sites (cf., e.g., WEHRLI, 1991). Therefore, in addition to solution analysis, spectroscopic analysis of the mineral surface is becoming a prerequisite for studying complex sorption processes. For example, spectroscopic evidence is vital for unequivocal distinction between adsorption and surface precipitation (SPOSITO, 1986; CHARLET and MANCEAU, 1992) as the principal sorption process. Thus, the term sorption, as used in this study, does not imply any mechanistic interpretation.

Recently, much progress has been made in applying spectroscopic methods to geochemical systems at interfaces (e.g., BROWN, 1990; HOCHELLA, 1990, and references therein). The usefulness of X-ray photoelectron spectroscopy (XPS) for studying metal sorption including redox reactions has been shown for oxide, clay, and sulfide systems (e.g., BANCROFT and HYLAND, 1990; DILLARD et al., 1981). Valuable information on the spatial distribution of sorbed metals can be obtained by application of Auger electron spectroscopy (AES) coupled with scanning electron microscopy (SEM) (e.g., HOCHELLA, 1988). The use of high resolution AES allows distinction between uniform sorption and cluster formation at the surface down to a scale of a few hundred ångstroms. In this study, we have used both XPS and AES to gain insight into redox chemistry and distribution of sorbed species and surface alterations. Furthermore, we have used Fourier Transformed Infrared (FTIR) spectroscopy to investigate the effect of sorption on the U-O bond. We have interpreted the results of these spectroscopic techniques in the light of monitoring pH, redox conditions, and dissolved metal concentrations.

EXPERIMENTAL METHODS

Materials

Galena (Joplin, Missouri, USA) and pyrite (unknown locality in Peru) were obtained from the Stanford mineral collection. In addition, the following solids were used as standard materials: specular hematite (Minas Gerais, Brazil), synthetic hematite prepared by the method of MATIJEVIC and SCHEINER (1978), uraninite (Mitchell County, North Carolina, USA), uranyl nitrate from Baker Corp., and X-ray amorphous UO_3 prepared by heating uranyl nitrate to 480°C for 12 h (WHEELER et al., 1964).

Powders and larger fragments of galena and pyrite were prepared in a glove bag which was thoroughly purged with argon (five cycles of evacuation and refilling) to minimize oxygen concentrations. The minerals were cleaved with a hammer and chisel to obtain fresh surfaces. Powders were prepared by grinding in an agate mortar. In most cases the powder was sieved through a 45 μm copper sieve. The prepared solids were stored in glass vials filled with argon, sealed with a rubber septum, held in place with a brass ring. Storage time prior to exposure to uranyl solutions ranged from hours to a maximum of 2 days.

Characterization of the starting material included X-ray diffraction, SEM, AES, XPS, and FTIR. In addition, Krypton BET analysis was performed for the crushed powder. The surface area of the crushed powder was found to be 0.6 ± 0.1 and 0.7 ± 0.1 m^2/g for galena and pyrite, respectively. X-ray diffraction of the powders indicated good crystallinity with no secondary phases. Surface analysis by XPS of galena indicated an essentially pure material with no evidence of surface oxidation products. In the case of pyrite, no oxidation products were detected, but, occasionally, minor impurities of Si, Hg, Cu, and Ag were detected and estimated to be below 1 mol%.

Other starting materials included standardized uranyl nitrate solutions at 1000 ppm U at pH = 3.4, as well as NaOH, HNO_3, and $HClO_4$ standard solutions all from Baker Corp. For all experiments, double deionized water was used. Nitrogen and argon gases were 99.9% pure.

Sorption Experiments

All sorption experiments were performed at room temperature (20 ± 2°C) under nitrogen or argon atmospheres. The equilibration time was 6 to 9 days except for experiments where the kinetics of uptake were studied. The pH was varied in some cases by addition of NaOH or HNO_3 to test the effect of pH, and in the majority of the experiments pH was maintained between 5 and 6. The possible effect of laboratory light was checked by running some experiments in the dark. No differences between these experiments and experiments run in laboratory light were observed. Since pyrite shows much higher reactivity for molecular oxygen compared to galena (e.g., BRION, 1980; TOSSELL and VAUGHAN, 1987), we used a slightly different procedure for each system as follows.

Galena

All experiments were performed under an argon atmosphere. Uranyl nitrate solutions were prepared by diluting standard solutions with water and then adjusting the pH to the desired value with 0.1 M (M = mol/dm^3) NaOH and 0.1 M HNO_3. All reagents had previously been purged with argon. The resulting solution was added with a syringe (previously purged with Ar) to the galena solid (single crystal or powder) in a glass vial capped with a rubber septum. In the case of solid suspensions (10 to 40 g/L) the vials were put onto a lab shaker for equilibration. At the end of the experiment, further treatment was performed in a glove bag purged with argon to ensure anoxic conditions. After removing the rubber septum, the pH of the solution was measured, then an aliquot was passed through a 0.2 μm disposable filter into a vacuum flask containing one drop of concentrated HNO_3 for uranium and lead analysis. The remaining material was collected on a 0.2 μm nylon filter, rinsed with Ar-purged H_2O, and dried under low vacuum in a desiccator. In the case of single crystals, samples were either blow dried or dipped into water before drying and prior to analysis. No difference between these two drying methods was observed.

Pyrite

All experiments were performed in a glove box (Labconco #50600). To remove oxygen, the glove box was purged for 2–3 days with nitrogen which was passed through two wash bottles filled with a reduced vanadeous chloride solution ("Jones reductor") followed by a basic solution to trap acidic vapors. The entering gas stream did not produce a color change in either the methylene blue test strip or a saphranine-O solution at pH 9. At this pH, the theoretical P_{O_2} is around 10^{-20} atm. The desiccator containing the pyrite starting material (single crystals and powder) was introduced via the prep chamber into the main chamber of the glove box which was then swept with nitrogen for one additional day prior to the start of an experiment. All solutions were boiled and transferred to the glove box. The uranyl nitrate solutions were prepared in the glove box under a continuous stream of the entering gas in the same manner as the galena samples. Pyrite powder was washed under slightly acidic conditions (pH = 4 adjusted with $HClO_4$), filtered in a vacuum flask, and rinsed with H_2O in order to remove impurities at the surface. This washing procedure was repeated three times. Thereafter, the uranyl nitrate solution was added, either as described for galena, in which case the vials remained sealed, or the vials were opened and continually monitored with a pH electrode, while a continuous stream of N_2 was passed over the solution. In the case of powder suspensions, stirring was ensured by a small

rotator (sealed vials) or by a magnetic stirrer (open vials). The filtering and drying procedure was the same as for the galena samples, except that it was performed in the glove box.

Solution Analysis

pH measurement

The pH was monitored using an Orion Ross combination glass electrode (part no. 8103). The electrode was calibrated with standard buffer solutions (4 and 7) before and after each experiment. The pH of the solutions were measured before addition of the solid and after the reaction period.

Uranium analysis

Dissolved uranium (that which passed through a 0.2 μm pore-size filter) was analyzed by liquid scintillation counting using a Packard Model (model no. 2500) instrument. The filtrate (2–4 mL) was mixed with 15 mL of EcoLite #882475 (ICN Biomedicals, Inc.) solution. Standard solutions which were prepared from uranyl nitrate (1000 ppm U) stock solutions (Baker Corp.) were used for calibration. Counting times were 2–4 h per sample. The sensitivity limit was found to be approximately 2–3 μM U. The amount of sorbed uranium was determined by the difference between total added U and the measured concentration in solution.

Atomic absorption analysis

Total dissolved metal (lead and iron) in the suspensions was occasionally analyzed by atomic absorption using a Perkin-Elmer model 403 spectrometer configured in the graphite furnace mode.

Auger Electron Spectroscopy (AES) and Scanning Electron Microscopy (SEM)

AES is a surface sensitive spectroscopic technique for measuring atomic composition with high lateral resolution. The applications of this method for geochemical purposes has been extensively reviewed in HOCHELLA (1988). In this study AES and SEM analyses were performed using a Perkin Elmer 670 Nanoprobe. The same electron beam used to excite the Auger electrons of the sample is used to generate SEM images via a secondary electron detector attachement. Beam conditions used were between 3 and 5 kV accelerating voltage, and 5 to 20 nA beam current. The spatial resolution of AES with this instrument under these conditions ranges from 500 to 1000 Å, and the depth of analysis is about 10 Å. Galena and pyrite standards for AES reference spectra were analyzed before and after immersion in pure deoxygenated water. In order to identify Auger electron lines for uranium unambiguously (cf. BASTASZ and FELTER, 1982), standards including uraninite and uranyl sorbed onto a single hematite crystal were also analyzed. Samples analyzed by AES and SEM were in contact with air for less than 2 min prior to transfer to the ultra-high vacuum of the instrument.

X-Ray Photoelectron Spectroscopy (XPS)

XPS, like AES, is a surface sensitive spectroscopic technique. However, its strength lies in the determination of chemical states at a surface rather than lateral resolution. The applications of this method for geochemical purposes have been extensively reviewed in HOCHELLA (1988) and BANCROFT and HYLAND (1990). XPS analysis was done using a VG ESCALAB MkII. Experimental conditions were vacuums in the range of 5×10^{-7} to 10^{-9} Torr, nonmonochromatic Al X-rays (about 200 watts), and pass energies between 20 and 50 eV. Semiquantitative chemical analysis was carried out by determining experimental photoionization cross-sections for the Pb4*f*, S2*p*, and Fe2*p* lines of galena and pyrite standards. For U4*f*, a theoretical photoionization cross-section (σ) (SCOFIELD, 1976) was used. From these cross-sections the effective intensity ratios were calculated. For example, the elemental ratio of U/Pb in the near-surface is

$$\frac{U}{Pb} = \frac{I_{U4f}}{I_{Pb4f}} \cdot \frac{\sigma_{Pb4f}}{\sigma_{U4f}}, \quad (1)$$

where I designates peak intensities.

Using the approximation of HOCHELLA and CARIM (1988), under the assumption of a uniform layer, the thickness of sorbed material (x) on the surface can be estimated:

$$x = -\lambda \cdot \cos\theta \cdot \ln\left(1 - \frac{\frac{I_{U4f}}{\sigma_{U4f}}}{\frac{I_{U4f}}{\sigma_{U4f}} + \frac{I_{Pb4f}}{\sigma_{Pb4f}}}\right), \quad (2)$$

where θ is the angle between the sample normal and the direction of the detector and λ is the attenuation length (SEAH and DENCH, 1979).

The absolute electron binding energies were determined using the gold dot method outlined by STIPP and HOCHELLA (1991). Curve fitting was performed with a least-squares Gaussian-Lorentzian fitting routine after the background was subtracted using a Shirley-type algorithm. Also, in the case of U4$f_{7/2}$ lines, interfering X-ray satellites associated with U4$f_{5/2}$ lines were subtracted.

Fourier Transformed Infrared (FTIR) Spectroscopy

In addition to XPS and AES we employed diffuse reflectance FTIR spectroscopy, which is a nonvacuum technique. Depending on the nature of the absorber, this technique can show high sensitivity for surface compounds/complexes on powdered samples. Galena and pyrite have no infrared active vibrations in the mid-infrared region. This property makes it favorable to conduct IR spectroscopic studies of IR active species sorbed on the surfaces of these minerals. Consequently, if an absorption band is observed in the spectra of galena or pyrite it must originate from a sorbed species, from oxidation products, or from some other type of surface contamination. The free uranyl ion has three fundamental vibrational modes: symmetric stretching (ν_1), bending (ν_2), and asymmetric stretching (ν_3). In a linear and symmetric ion only ν_2 and ν_3 modes are infrared active. All three modes will be infrared active if uranyl is coordinated in such a way that it does not have a center of symmetry. In any case, ν_1 and ν_2 will give rise to relatively weak bands. We will therefore discuss the more intense asymmetric stretching vibration, ν_3. To be able to qualitatively interpret the spectra of uranyl sorbed on galena and pyrite we have made comparisons with the spectra of selected model compounds.

All IR spectra were recorded using a Mattson Cygnus 100 FTIR spectrometer equipped with a diffuse reflectance unit (Harrick Scientific Corp.). The diffusely reflected radiation was registered with a wide range mercury cadmium telluride detector. The sample compartment was purged with air which was previously dried and CO_2-scrubbed. KBr (IR quality, Fluka Corp.) was used as a non-absorbing matrix and background. The diffuse reflectance spectra were obtained from 20 mg of the sample mixed with 0.5 g KBr powder. All spectra were recorded by averaging 128 scans at a resolution of 4 cm^{-1}.

RESULTS

We studied the sorption of uranyl to galena and pyrite powder suspensions and single crystals at room temperature, under anoxic conditions by (1) correlating the solution pH with dissolved metal concentrations (U, Pb, Fe) and (2) analyzing the solid surface by three independent spectroscopic methods; AES/SEM, XPS, and FTIR. A summary of the experimental conditions and methods applied to the presented experimental data is given in Table 1.

Metal Uptake from Solution

Galena

High uptake of uranium above pH = 4.7 is observed for the galena suspensions. This pH-dependent sorption is shown for total uranium (U_t) of 0.2 mM in Fig. 1 which indicates constant high uptake up to pH 8. Monitoring the pH of initial solutions (before addition of the solid) and final solutions

Table 1
Overview of representative uranyl sorption experiments with galena and pyrite substrates. Equilibration times = 6-8 days (except no. 6 and 7), pH corresponds to value (± 0.1) measured after equilibration, U_t is total U added, p: powder, c: single crystals.

run no.	type	U_t mM	pH	XPS	FTIR	SEM/ AES	Comments
galena							
1	p	4.00	4.4	+	+	-	no. 1-3 have same surface areas
2	p	1.00	5.0	+	+	-	
3	p	0.24	5.2	+	+	-	
4	p	0.50	5.2	-	+	-	
5	p	0.50	5.0	-	-	-	pretreated surface (oxidized)
6	p	0.20	5.1	+	-	-	samples taken at diff. equilib. times
7	p	0.20	5.2	+	-	-	pretreated surf., diff. equilib. times
8	c	2.50	5.0	+	-	-	
9	c	0.20	6.5	+	-	-	
10	c	0.04	5.5	+	-	-	
11	c	0.02	5.3	+	-	-	
12	c	0.02	5.3	+	-	-	
13	c	0.20	5.0	-	-	+	
pyrite							
20	p	0.20	5.1	+	-	-	
21	p	0.24	5.2	-	-	-	
22	p	0.24	6.3	+	+	-	
23	p	0.20		+	+	-	pH stat used
24	c	0.20	5.1	+	-	+	
25	c	0.20	5.8	+	-	+	
26	c	0.20	6.3	+	-	-	

(after reaction with the solid) usually shows little change (within 0.2 pH units) for a large range of U_t (0.1–1 mM). However, in experiments which were characterized by high solid/solution ratio and unbuffered initial conditions (pH $\approx$ 5.5), an increase of 2 to 3 pH units was noted.

We further investigated the effect of uranyl concentration on the sorption process and ran experiments at different U_t. Blank runs (without adding the solid) at high concentrations of U_t (1 and 4 mM) were also performed to reassure the absence of precipitation from homogeneous solution (see also KOCHENOV et al., 1977). As shown in Table 2, the amount of uptake shows a gradual increase from 90% uranium for the highest concentration of uranyl added (4 mM) up to 99% uranium for U_t = 0.2 mM. Using the crystallographic site density on (001)-type faces (5.6 sites/nm^2) and the surface area of our samples the amount of uranium sorbed (U_{sorb})

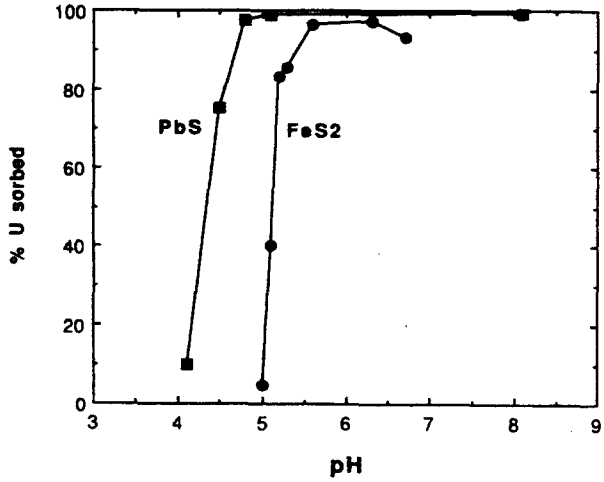

FIG. 1. Sorption isotherm of uranyl sorbed as a function of pH; U_t = 0.2 mM, surface area = 50 m^2 dm^{-3}. Squares: galena sorbent; circles: pyrite sorbent.

Table 2
Influence of uranyl concentration on galena sorption data. Equilibration time = 7 days, surface area = 50m^2 dm^{-3}, U_t (total added U), U_{sorb} (U on surface), S_t (crystallographic surface sites); see also XPS and IR data. Subscript "diss" refers to total concentration in solution.

run no.	U_t µM	U_{diss} µM	U_{sorb} %	U_{sorb}/S_t -	Pb_{diss} µM
1	4000	400	90.0	8.7	68.8
2	1000	12	98.8	2.4	3.3
3	244	2	99.2	0.6	0.6

with respect to total surface sulfur sites (S_t) can be estimated. For the reacted suspensions this computation indicates (1) a high U_{sorb}/S_t ratio (0.6–10) at the surface and (2) a gradual decrease in the percent uranyl removed from solution with an increase of this ratio.

Uptake of uranium from solution follows relatively slow kinetics and suggests a two-step process, i.e., a relatively fast initial uptake within the first hour of reaction and a subsequent slower uptake which proceeds for days (Fig. 2). Moreover, the rate of uptake is dependent on the amount of uranium added with higher concentrations showing slower uptake kinetics.

The evolution of dissolved lead follows trends parallel to the sorption of uranium. A gradual increase in the lead concentration with time is noted upon addition of uranyl (Table 3). Furthermore, the released lead concentrations are proportional to the added uranyl concentrations, as shown from the experimental series in Table 2. In one set of experiments (#5; Table 3) an oxidized galena surface, which was prepared by heating galena powder for 24 h at 100°C, was exposed to the same conditions as a parallel experiment using unoxidized material (#4, Table 3). The kinetic behavior of both experiments exhibits similar trends in terms of uranium uptake. The oxidized sample shows one to two orders of magnitude higher concentrations of released lead. Also, the data suggest an increase of released lead with time.

Pyrite

Like galena, uranium uptake by pyrite is pH dependent (Fig. 1). In this case maximum uptake occurs above pH = 5.5.

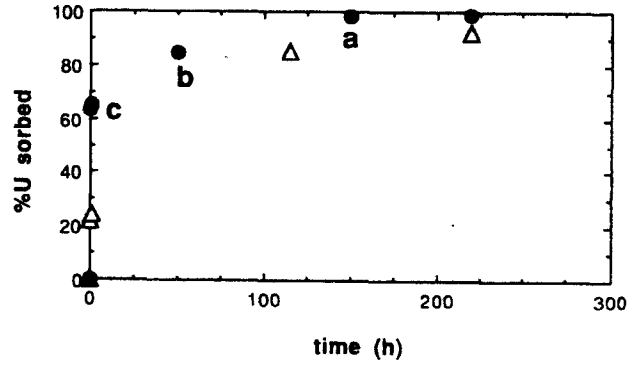

FIG. 2. Kinetics of uranyl sorption on galena, pH = 5.2 ± 0.3, surface area = 10 m^2 dm^{-3}. Circles: U_t = 0.2 mM; triangles: U_t = 0.5 mM. Compare samples a, b, c with corresponding XPS data in Fig. 7.

Table 3
Influence of kinetics on U sorption on galena for two different surfaces: no. 4 non-oxidized surface, no. 5 previously oxidized surface in air at 100 °C. Otherwise same conditions for both experiments: surface area = 10m² dm⁻³, pH = 5.0 ± 0.2, U_t = 500 μM.

run no.	time hours	U_{diss} μM	Pb_{diss} μM
4	1.5	392	8.7
	40	378	24.6
	2000	39.2	56.9
control*	2000	-	17.7
5	1.5	379	214
	25	364	202
	2000	77	304
control*	2000	-	195

* refers to control experiment where only water at pH = 5 was added.

Preliminary experiments indicated that maximum uptake depends on the U_{sorb}/S_t ratio and the sorption edge is shifted to lower pH (down to pH = 5.0) for lower ratios. It appears that above pH 6 there is a slight decrease in the percent uranium removed from solution (Fig. 1), although there is insufficient data to establish a definite trend. In our experiments, pH was not controlled, except for one set of experiments where pH was kept relatively constant with a pH stat (Table 4). At pH values higher than 6 a significant drop in pH during reaction with uranyl is noted in contrast to the galena system. Also, the dissolved iron concentration is lowered by addition of uranyl compared to pure pyrite suspensions in the absence of added uranium.

Due to the different experimental procedure (see Experimental Section) compared to galena, no short time kinetic data are available. However, our results indicate that uranium uptake at the pyrite surface is completed within two days for U_t between 0.1–0.5 mM.

AES/SEM

The combination of AES and SEM analysis used in this study provides information on the spatial distribution (down to a lateral resolution of 500 Å) for elements within approximately the top 10 Å of the surface. In particular, we focused on the spatial distribution of sorbed uranium and on possible reaction products resulting from the interaction of uranium with the sulfide surface. Auger reference spectra taken for sulfide standards before and after immersion in pure deoxygenated water showed no noteable differences.

Table 4
Representative pyrite sorption data.
Equilibration time 6 to 8 days, surface area = 40 - 50 m² dm⁻³.

run no.	pH	U_t μM	$\%U_{sorb}$	Fe_{diss} μM
20	5.1	200	34.6	3.5
21	5.2	236	98.8	2.6
22	6.3	236	97.2	1.1
23*	5.8	200	97.2	1.5

* pH stat used

Galena

Figure 3a depicts a SEM micrograph of a galena crystal surface after reaction in a uranyl solution (0.2 mM) at pH 5.0. AES analysis was performed both on the flat (001) plane (area 1 in Fig. 3a) and on the rough surface containing small galena crystallites (area 2). The Auger spectra for the same regions (Fig. 4a) display a significant difference of chemical composition between the two areas. Whereas the flat surface exhibits very little uranium (<1/10 monolayer based on uniform coverage), the rough surface shows a significant enrichment of uranium and oxygen, and a decrease in carbon, lead, and sulfur. The flat surface showed very similar Auger spectra to those obtained for the galena standards.

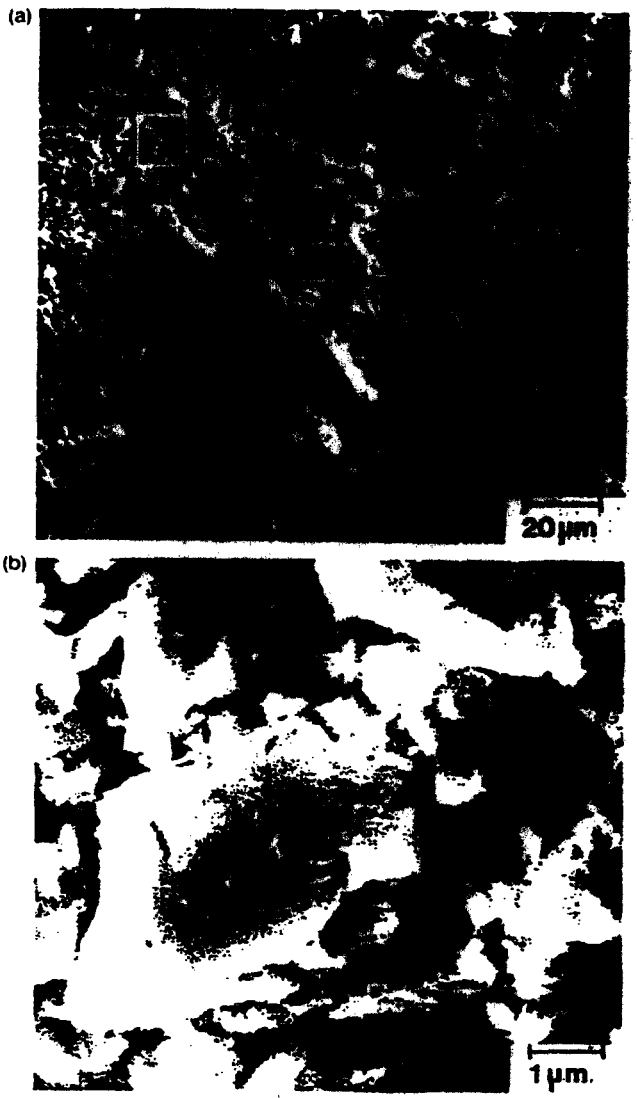

FIG. 3. SEM image of freshly cleaved galena single crystal exposed to 0.2 mM uranyl nitrate solutions at pH = 4.8 for 5 days. (a) rectangular boxes (area 1 and 2) indicate areas of AES analysis given in Fig. 4a. (b) High magnification of area 2 shows aggregation of galena particles. Note occurrence of small needle-shaped particles visible on galena substrate: AES analyses of small particle located just to the left of the center of the image and of adjacent flat substrate are given in Fig. 4b.

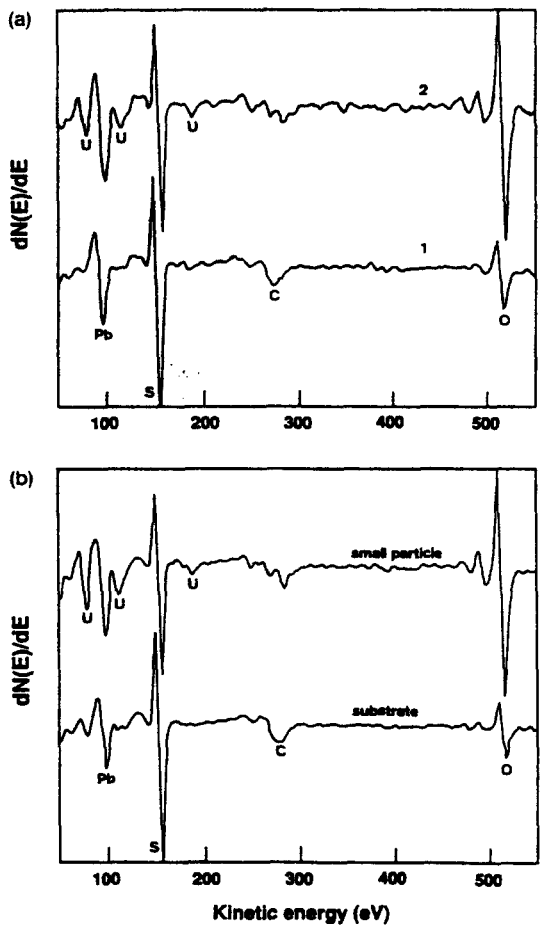

FIG. 4. Differentiated Auger spectra of galena sample exposed to uranyl nitrate solution. (a) areas 1 and 2 respectively illustrated in Fig. 3a. (b) small needle-shaped particle and adjacent flat surface illustrated in Fig. 3b.

The rough surface was examined in more detail. This area shows an aggregation of relatively small, irregularly shaped particles (Fig. 3b). However, relatively flat surfaces are also present. As illustrated in this figure, very small needle-like particles (500 Å in width) occur both on the flat surfaces and on the irregular edges. Using high-resolution AES, it was possible to determine the elemental composition of the small particles and the adjacent flat surfaces (Fig. 4b). Again, a significant difference is observed in the resulting Auger spectra. The Auger spectra obtained with a beam on a small particle shows major uranium and oxygen lines, in addition to lead and sulfur lines. The substrate shows little to no uranium, very weak oxygen, and major lead and sulfur. Analysis of other needle-like particles and adjacent substrate yields similar results. The lead and sulfur signals in the particle spectrum are most likely due to the forward scattering of the electron beam onto the substrate from these exceptionally narrow needles. These particles probably only contain uranium and oxygen and their formation is presumably favored in regions of high surface area. Moreover, these precipitates appear to have formed along crystallographically preferred directions since, in many cases, they are found to be oriented in a parallel arrangement.

Pyrite

We present the SEM and AES analysis of two pyrite surfaces exposed to 0.2 mM uranyl nitrate solutions at pH 5.2 and 5.6 (runs no. 24 and 25, Table 1). SEM analysis of freshly broken pyrite crystal samples reveal, as expected, poor cleavage and concoidal fracture (in contrast to galena). AES analysis of uranium for both samples shows a more uniform distribution of uranium relative to galena and no evidence for small U-rich particles. However, distinct spatial heterogeneities of uranium are still found. In fact, both samples show discrete patches of oxidized reaction products within a matrix of FeS_2, the latter which does not show an AES spectrum significantly different from unreacted pyrite. The formation of these oxidized zones is found to be far more extensive for the higher pH sample. The oxidized zones are identified by the increased relative intensity of the oxygen lines compared to reference pyrite surfaces. Two chemically distinct oxidized zones are found (Figs. 5 and 6), one characterized by low sulfur, high iron and oxygen (area 1) and the other by relatively high sulfur, iron, and oxygen (area 2). The former suggests a Fe(III) oxide-rich area and the latter an oxidized S-rich area. Uranium is consistently associated with these oxidized areas whereas it occurs at much lower levels in the unoxidized areas (area 3). The sample equilibrated at lower pH does not show such variability in chemical composition and reveals a high, more uniform, uptake of uranium (data not shown). Nevertheless, occasional distinct zones of very low sulfur, high iron and oxygen suggest the presence of Fe(III) oxide containing similar amounts of uranium as the S-rich zones.

In summary, AES/SEM analysis suggests a pH-dependent redox process where a U-O compound is correlated with areas of surface oxidation.

XPS

In contrast to AES, XPS data reflects the average surface composition over a relatively large area (2–5 mm^2 as used in this study), but this technique yields more information on

FIG. 5. SEM image of freshly cleaved pyrite single crystal exposed to 0.2 mM uranyl nitrate solution at pH = 6.5 for 6 days. Areas 1, 2, and 3 are analyzed by AES as shown in Fig. 6.

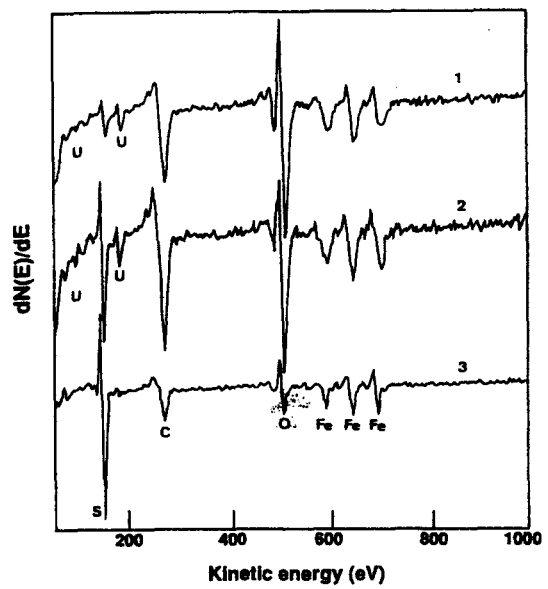

FIG. 6. Differentiated Auger spectra of pyrite sample exposed to uranyl nitrate solution. Labels 1, 2, and 3 correspond to spectra of areas illustrated in Fig. 5.

chemical states of near-surface elements. XPS analysis focused on redox processes involving uranyl and sulfide. In the case of galena, semiquantitative XPS analysis of surface uranium is compared to sorbed uranium concentrations derived from solution analysis.

Analysis of standards and photopeak energy calibration

Table 5 shows binding energies of the main uranium photopeak, U4$f_{7/2}$, for U(VI) and U(IV) compounds used as standards in this study and from data found in the literature. Our analysis of the U(VI) materials (sorbed uranyl on hematite, UO_3, and $UO_2(NO_3)_2$) show similar U4$f_{7/2}$ binding energies (±0.3 eV) whereas a shift of 1.2–1.5 eV to lower binding energies is observed for U(IV) oxide. This agrees with previous XPS studies of uranium oxide compounds (CHADWICK, 1973; ALLEN et al., 1974; SUNDER et al., 1981; VEAL and LAM, 1982). This shift has been established to be characteristic of the oxidation state for a given uranium oxide (Table 5). Changes in coordination of uranium, as shown for various UO_3 oxides (ALLEN and HOLMES, 1987) have no discernable effect on U4$f_{7/2}$ peak energies.

Interestingly, for all analyzed U(VI) compounds, a slight shift (0.2–0.4 eV) of the U4$f_{7/2}$ photopeak to lower binding energy and line broadening is observed upon continued exposure to the ultra-high vacuum (UHV) of the spectrometer (i.e., over several hours). This change is most significant for low surface concentrations of uranium on Fe_2O_3. Similar observations for UO_3 exposed to UHV were made by ALLEN and HOLMES (1987) and interpreted as a gradual reduction of U(VI). Therefore, for calibration purposes and to be consistent throughout our study, we analyzed all samples within 1 h of UHV exposure at similar base pressures (see Experimental Section).

Shake-up lines for both U(IV) and U(VI) on the high binding energy side of the main peaks have been identified by ALLEN et al. (1987) who studied oxidation of crystalline UO_2. In our samples, however, perhaps in part due to relatively weak uranium signal intensities, no shake-up features are observed.

XPS analysis of all galena single crystals and powder reference samples do not exhibit any noteable differences in their spectra. The analyzed standards include samples which were either directly measured after cleavage, stored in air for several hours, or immersed in deoxygenated water. In all cases there is no indication of polysulfide or S-O compounds at the surface. However, for the preoxidized surfaces before immersion (see run no. 7, Tables 1 and 6), a minor peak at ~168 eV on the high binding energy side of the S2*p* line is revealed which is characteristic of surface-bound sulfate (e.g., BALTRUS and PROCTOR, 1990). For pyrite standards, the XPS data also indicate the absence of surface oxidation for powder and single crystal samples prepared under controlled atmosphere conditions (see Experimental Section) before and after immersion in water. This is reflected in the Fe2*p* and the S2*p* lines which do not indicate any contribution from oxidized compounds. However, for samples exposed to air, the S2*p* line indicates surface oxidation by the presence of a S-O compound.

Galena

The intensity of the U4f line for reacted galena samples is compared to the concentrations of sorbed uranium (Table 6). To normalize the XPS data for each sample, we calculated the U4*f*/Pb4*f* line intensity ratio. Figure 7 illustrates the increase of the relative intensity of U4*f* with increasing equilibration time. This corresponds to the same experiments depicted in Fig. 2. The increase agrees with the increase of surface uranium determined by solution analysis within 15%. This demonstrates the usefulness of XPS as a semiquantitative analytical tool for measurement of sorbed uranium. Furthermore, if uniform coverage is assumed, we have estimated the equivalent number of monolayers sorbed using Eqn. 2. The result is between 1 and 2, and is in agreement with results from solution analysis.

The line shapes of U4*f* are not affected by an increase in equilibration time (Fig. 7 and Table 6) or by increase in pH. However, the concentration of added uranium does have a

Table 5
XPS absolute binding energies for U4$f_{7/2}$ line determined for various uranium oxide compounds.

sample	U4$f_{7/2}$ (eV)	reference
UO_2 powder	380.8 ± 0.1	this
UO_2 crystal	380.8 ± 0.1	"
UO_3 (amorph)	382.4 ± 0.2	"
uranyl on Fe_2O_3	382.2 ± 0.25	"
UO_2	380.1	1
U_4O_9	380.8	1
U_3O_8	381.1	1
UO_3	381.9	1
UO_2	380.7	2
U_3O_8	381.1	2
UO_3	381.9	2

1: Allen et al. (1974), 2: Chadwick (1973)

Table 6
XPS data for galena samples; t refers to equilibration time of experiment, FWHM refers to full width at half maximum for $U4f_{7/2}$ line. The elemental ratio is calculated according to Eq. 1 (text).

sample/ run no.	equilibration time	U_t (mM)	$U4f_{7/2}$ (eV)	FWHM (eV)	U/Pb %(atom)	S/Pb %(atom)
	powders					
1	t = 7 days	4	381.9	2.3	2.46	0.8
2	t = 7 days	1	382.0	2.9	1.04	1.0
3	t = 7 days	0.2	381.5	2.8	0.47	1.1
6	t = 2 min.	0.2	381.4	2.4	0.03	1.0
	t = 1 hours	"	381.6	2.5	0.04	1.0
	t = 2 days	"	381.5	2.5	0.15	0.9
	t = 9 days	"	381.4	2.4	0.21	0.9
7	t = 7 days, ox. surf.	0.2	381.5	2.5	0.17	0.9
	crystals					
8	t = 1 day	2.5	382.1	2.5	0.31	0.9
9	t = 7 days	0.2	381.6	2.7	1.83	0.7
10	t = 7 days	0.04	381.4	3.1	0.05	0.9
11	t = 7 days	0.02	381.2	3.1	0.02	1.2
12	t = 7 days	0.02	381.5	2.9	0.09	1.0

significant effect on the U4*f* binding energies and peak shape. At high concentration of added uranyl (≥1 mM), the lines observed correspond to the ones found for uranyl-type compounds (Table 5). In other words, these lines are identical to the one found for uranyl sorbed on hematite. At low concentrations of added uranyl (≤0.5 mM), lines are found to be broadened and separated by 0.5–0.9 eV to lower binding energies, to a position between those for pure U(IV) and U(VI) compounds. In fact, these lines can be adequately fit with two lines corresponding to tetravalent and hexavalent states, respectively (Fig. 8). This systematic change in U4*f* line shape relative to the one noted at high U_t is observed for both powder suspensions and for single crystals (Table 6). It is also interesting to note that the same U4*f* line positions and shapes are seen for powders where the surface of galena was previously oxidized by heating at 100°C under air and subsequently exposed to the same experimental conditions (compare exp. #6 and #7, Table 6).

Analysis of the S2p line of the galena surface indicates a slight broadening to higher binding energies upon increasing reaction time with uranium (Fig. 9). This shift is characteristic of polysulfide formation. The S2p line for this compound is centered between 161.5 and 163.5 eV (HYLAND and BANCROFT, 1989; BUCKLEY and WOODS, 1984; BRION, 1980). However, none of our S2p spectra taken from reacted solids indicates the presence of S-O species (sulfate) which have a characteristic peak at about 168 eV.

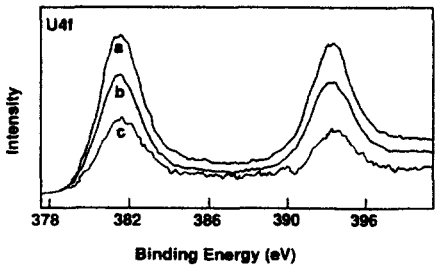

FIG. 7. U4*f* spectra of galena powders exposed to uranyl nitrate solutions. Samples a, b, c correspond to experiments depicted in Fig. 2.

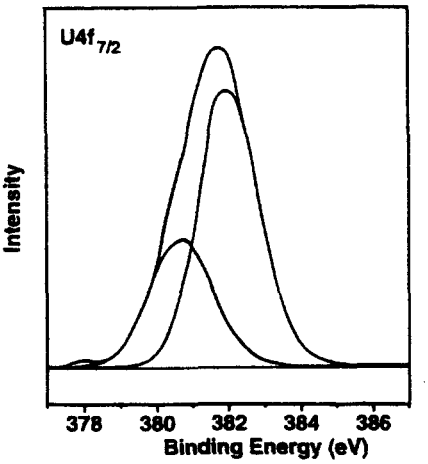

FIG. 8. Typical smoothed $U4f_{7/2}$ spectrum of galena sample exposed to 0.2 mM uranyl nitrate solution. Spectral envelope represents the measured spectrum (background subtracted and smoothed) and the sum of the two component curves; peak components are for U(IV) (lower binding energy) and U(VI) (higher binding energy), respectively.

The S/Pb intensity ratio shows a certain variation for reference samples (0.9–1.1) and for reacted galena (0.7–1.2, Table 6). This ratio, which may be affected by heterogeneously distributed impurities on these surface (see Experimental Section), shows no clear-cut effect with regard to sorbed uranium except in the case of very high concentrations. Thus, comparison of experiments #1, #2, and #3 which were performed at the same conditions with regard to surface area suggests a decrease of the S/Pb intensity ratio at highest uranium loadings (Table 6). This suggests a slight depletion of sulfur at the surface for very high uranium loadings. Furthermore, at these surface loadings we observed broadening of the Pb4*f* lines towards higher binding energies. These lines can be fit with two peaks shifted by 0.9 eV (data not shown). This indicates two different environments for surface lead. The high binding energy line is consistent with that of a lead hydroxide (BUCKLEY and WOODS, 1984).

Pyrite

In contrast to galena, XPS data for pyrite indicates a significant effect of pH on the reaction products at the sulfide surface (Table 7). In the pH range of 5.1–5.3, the U4*f* lines

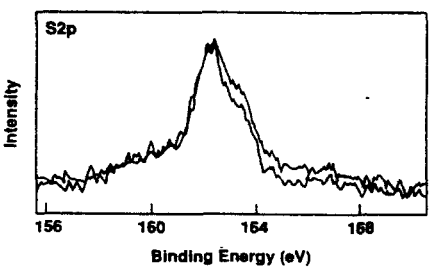

FIG. 9. S2*p* spectra of unreacted galena sample (lower curve) and galena sample reacted with uranyl nitrate solutions (upper curve). Spectra are not background subtracted.

are found to be very similar to those observed for galena in the same U_t concentration range (0.2 mM), thus indicating the formation of a mixed U(IV)-U(VI) oxide. The corresponding S2*p* line shows a very slight broadening towards higher binding energies which is compatible with polysulfide formation observed in the pyrite system (e.g., HYLAND and BANCROFT, 1989; MYCROFT et al., 1990). The Fe2*p* lines, however, show no noticeable difference compared to the unreacted samples and therefore no indication of Fe(III) at the surface.

At higher pH (>5.5), the U4*f*, S2*p*, and Fe2*p* lines show considerable broadening towards higher binding energies (Table 7, Fig. 10), a feature which increases with increasing pH. A significant Fe(III) component is exhibited by the Fe2*p* spectrum at pH > 6 (Fig. 10a) in contrast to the lower pH samples. Analysis of the corresponding S2*p* line indicates significantly increased amounts of polysulfide at the surface compared to the lower pH sample (Fig. 10b). The slight broadening of the U4*f* line to higher binding energies (Fig. 10c) is interpreted in terms of a higher U(VI) component as discussed previously. Moreover, in one experiment (exp. #22) with relatively high concentrations of uranium (0.5 mM) at a pH of 7.5, we observed a great degree of broadening of the S2*p* lines, which can be attributed to relatively high amounts of polysulfide and elemental sulfur, and extremely broad U4*f* lines (Table 7). These broad U4*f* lines, which were not observed in any other experiment or standard, are presumably caused by (1) contribution of U(IV) and U(VI) components and (2) charge shifting due to extensive coverage of insulating oxidized products.

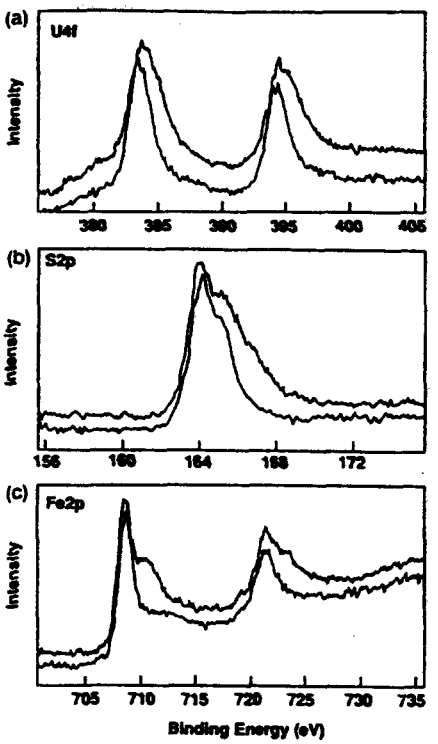

FIG. 10. Narrow scan XPS spectra of pyrite samples exposed to uranyl nitrate solutions. Lower spectrum corresponds to pH = 5.0–5.1, higher spectrum corresponds to pH = 6.5–5.5 (#24 and #26, Table 6). (a) U4*f* spectra (not charge shifted); (b) S2*p* spectra (not charge shifted), high amount of polysulfide for upper spectrum. (c) Fe2*p* spectra, shoulders at ~711 eV and ~724 eV correspond to Fe(III) oxide species.

FTIR

IR spectra of uranium and sulfide model compounds

The uranyl ion in aqueous solution, coordinated to water molecules, displays an asymmetric stretching frequency of ~950 cm^{-1} (HOEKSTRA, 1982, and references therein). Frequencies around this value are also found when uranyl is coordinated to other hard type ligands. When the uranyl ion is coordinated to oxide mineral surfaces, a decrease in the ν_3 frequency has been observed (HO and MILLER, 1986; this study). This downward shift of ν_3 shows that the uranyl moiety is distorted upon coordination to the surface. This is in agreement with solution chemical data which suggests that uranyl is coordinated as an inner-sphere complex (HSI and LANGMUIR, 1985). If it were coordinated as an outer-sphere complex, we would expect a ν_3 frequency close to the one found in water, ~950 cm^{-1}.

Coordination by very soft ligands, i.e., those with high electron donating capacity to uranyl, results in a lowering of the ν_3 frequency (BULLOCK, 1967). Values below 900 cm^{-1} are commonly found. Changes in the oxidation state of U(VI) strongly affect the IR spectroscopic features of the U-O entity. The compounds U_2O_5 and U_3O_8, and oxides of higher formal oxidation states of uranium, show absorption bands between ~700 and ~900 cm^{-1} (SIEGEL and HOEKSTRA, 1971). For example, U_3O_8 has a broad intense band centered around 750 cm^{-1}. As has been pointed out previously, no isolated uranyl groups exist in these types of compounds (HOEKSTRA and SIEGEL, 1961). Consequently, their IR spectra cannot be discussed in terms of pure ν_1, ν_2, ν_3 vibrational modes. Instead the bands in this region are thought to originate from U-O-U-O-U chains (HOEKSTRA, 1982). Note that although the position of these bands are rather variable, they always occur at lower frequency than ν_3 of uranyl adsorbed on oxide minerals (Table 8). Uranium oxides where uranium has a formal oxidation state lower than in U_2O_5 do not show any bands in the region discussed above (HOEKSTRA, 1982).

The IR spectra of the galena and pyrite standard powders included the starting material for all experimental runs presented below (Tables 9 and 10), immersed and not immersed

Table 7
XPS data for pyrite samples; equilibration time 6-8 days

sample/ run no.	pH initial	pH final	U_t mM	U4$f_{7/2}$ eV	FWHM eV	U/Fe %(atom)	S/Fe %(atom)
powders							
20	5.0	5.1	0.20	381.5	2.5	2.21	1.9
23	5.8	5.8	0.20	381.8	3.3	2.51	1.7
22	8.1	6.3	0.24	382.0*	4.7*	3.32*	2.4
crystals							
24	5.2	5.2	0.20	381.5	2.2	2.77	2.3
25	5.6	5.2	"	381.8	2.4	1.83	1.4
26	6.5	5.5	"	381.8	2.4	0.57	1.4

* line shape influenced by presence of oxidized products (see text)

in deoxygenated water. For all standards, the complete absence of IR active vibrations in the mid-infrared region was noted which indicates the absence of S-O species at the surface.

Galena

The IR spectra obtained for galena powders are summarized in Table 9. The IR bands reported occur consistently at lower wavenumbers than the ν_3 mode of uranyl sorbed on hematite (Tables 8 and 9). Furthermore, the results in Table 9 and Fig. 11 show that the position of the bands depends on the amount of uranium sorbed to the sulfide surface. At high surface concentrations, the observed band is shifted by $\sim 30\ cm^{-1}$ with respect to uranyl coordinated to the hematite surface. At the lowest surface concentration, this band is shifted as much as $90\ cm^{-1}$. This shift, which is indicative of a considerable change in the uranium-oxygen bonding, is compatible with a partial reduction of U(VI) at the lead sulfide surface, as outlined above. Although the absorption maximum is shifted to slightly higher wavenumbers, the IR spectrum of the low surface concentration sample is similar to the spectrum of U_3O_8. It is therefore tentatively suggested that this surface phase has a composition similar to U_3O_8.

Pyrite

The absorption band in the IR spectrum of the uranium species sorbed on pyrite displays an even more pronounced shift than was found for the galena samples, compared to the ν_3 frequency of unreduced uranyl on hematite (Tables 8 and 9). Interestingly, in addition to the main band, a shoulder at lower wavenumber is observed (Fig. 12). This might suggest reduction to a lower formal oxidation state on pyrite. Figure 12 also illustrates that an increase in pH results in two distinct band or groups of bands, one centered around $800\ cm^{-1}$, thus corresponding to a mixed U(VI)-U(IV) compound, and the other centered around $915\ cm^{-1}$, which is in the range of unreduced uranyl.

DISCUSSION

Redox Process

Under the assumption of a homogeneous distribution of uranium, both solution and XPS data independently yield estimates of 1–2 monolayers of uranium coverage in the pH range of maximum uptake. However, AES/SEM results show that the coverage is actually quite inhomogeneous. In the case of galena, small discrete uranium oxide needle-like particles (~50 nm wide) are observed on 'rough' surfaces, whereas the majority of the flat PbS (001) cleavage surfaces contains little or no evidence of uranium (i.e., below detection limits). In the case of pyrite, AES/SEM results give no evidence for the formation of small U-rich particles, but they also indicate an inhomogeneous distribution of uranium with enrichment occurring in the oxidized zones of the pyrite surface.

IR data indicate that the asymmetric stretching frequency of aqueous uranyl, ν_3, is significantly lowered (by 120–160 cm^{-1}) upon interaction with sulfide surfaces. Based on this data alone, this could be due to possible U-S bonding which could account for a significant lowering of the ν_3 frequency of unreduced uranyl ions, given the soft character of the sulfide ligand. This, however, would involve a nearly uniform distribution of uranyl on the galena surface for these relatively high concentrations of surface uranium. This can be ruled out on the basis of the AES/SEM results. Instead, the IR data support the XPS results which indicate partial reduction of U(VI) to U(IV) resulting from the formation of a mixed U(VI)-U(IV) oxide compound. In fact, overall results of all the analytical methods applied indicate a similar sorption process for both sulfides in that (1) both minerals show similar scavenging capacity for aqueous uranyl, and (2) XPS and IR data reveal similar results for both galena and pyrite. In both cases, the core level electrons of uranium and the vibrational frequencies of the uranyl bond observed are consistent with a mixed U(VI)-U(IV) oxide compound (Table 10). However, spectroscopic results also indicate that, in the case of pyrite, at higher pH conditions (pH > 6.3), an additional U(VI) component is observed from the analysis of the IR and XPS

Table 8
FTIR uranyl stretching frequency data for some standards

sample	exp. conditions	ν_3 (cm^{-1})	ref.
U(VI) on Fe_2O_3	U_t = 0.5 mM	925	this
"	U_t = 0.1 mM	919	this
U(VI) on Fe_2O_3	not specified	910	1
U(VI) in water	H_2O (ClO_4^-)	958-974	2
U_3O_8	solid	750	3

References- 1: Ho and Miller (1986) 2: Siegel and Hoekstra (1971) 3: Hoekstra (1982)

Table 9
FTIR uranyl stretching frequency data for galena and pyrite samples

sample run no	exp. conditions	U_t mM	ν_3 cm^{-1}
PbS			
4	40 min., cf. Tables 1, 3	0.5	872
	8 days, "	0.5	856
1	cf. Tables 1, 2, 6	4	893
2	"	1	870
3	"	0.2	839
FeS_2			
23	cf. Tables 1, 4, 7	0.2	800
22	"	0.2	805, 913

Table 10
Comparison between XPS and FTIR data for uranium oxide compounds. Sulfide samples taken for U_t = 0.2 mM.

sample	$U4f_{7/2}$ eV	ν_3 cm^{-1}	ref.
UO_{2+x}	380.8	-	this, 1
U on Fe_2O_3	382.2	919-925	this
U_3O_8	381.1	700-800	1, 2, 3
U on PbS	381.4	840	this
U on FeS_2	381.5	805	this

1: Allen et al. (1974); 2: Chadwick (1973); 3: Siegel and Hoekstra (1971)

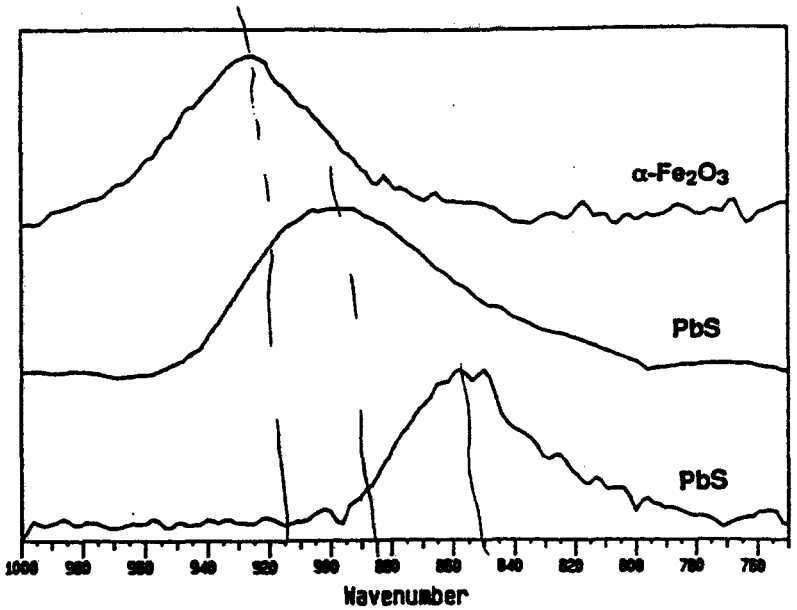

FIG. 11. FTIR spectra given as relative intensities in diffuse reflectance mode showing ν_3 vibration of uranyl. Upper spectrum: Uranyl sorbed on hematite. Middle spectrum: Uranyl sorbed on galena for U_t = 4 mM (#1). Lower spectrum: Uranyl sorbed on galena for U_t = 0.2 mM (#3).

spectra. This result is discussed in the section "Effects of pH in the pyrite system" below.

Table 10 illustrates that this mixed U(VI)-U(IV) oxide is compatible with a U_3O_8-type compound. From the XPS/IR data we cannot unambiguously determine the exact stoichiometry of this uranium oxide. However, from curve fitting computations of the U4$f_{7/2}$ line (Fig. 8) an estimate for the U(VI)/U(IV) ratio can be made. This ratio ranges from 2 to 1.5 which is similar to a U_3O_8 stoichiometry (ratio of 2). We also have performed equilibrium calculations with the HYDRAQL code (PAPELIS et al., 1988) using the NEA Database for uranium (GRENTHE et al., 1992) to test saturation conditions of our reacted suspensions with respect to crystalline U_3O_8. In doing these calculations, we have assumed that equilibrium has been reached within 6–9 days resulting in a total concentration of uranium in the range of 1 to 3 μM in solution (cf. Fig. 1). We make the further assumption that the E_h is fixed by the U(VI)/U(IV) couple in the pH range of interest (pH 5.5–8). Our results indicate supersaturation with respect to U_3O_8 by 2–3 orders of magnitude. Further, the possible effect of particle size on solubility has been checked by using the relationship between particle size

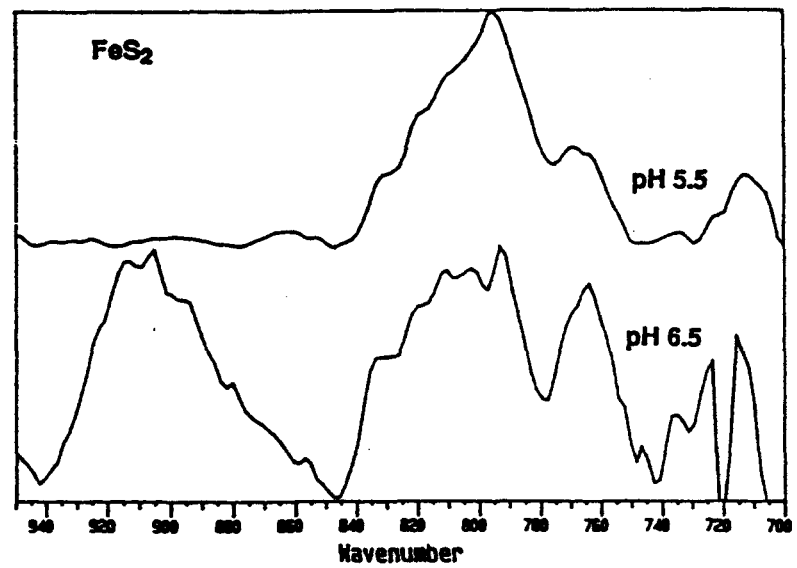

FIG. 12. FTIR spectra given as relative intensities in diffuse reflectance mode of pyrite samples after exposure to 0.2 mM uranyl nitrate solutions. Upper spectrum: pH = 5.5; lower spectrum: pH = 6.5.

and solubility, as given by SCHINDLER (1967). On the basis of an estimated particle size of 100 nm (as observed from AES/SEM analysis) and an estimated interfacial energy for U_3O_8 of ~200 mJ/m^2 (SOEHNEL, 1982), an increase of about one order of magnitude in solubility with respect to crystalline U_3O_8 is obtained. These results suggest that our system is not in equilibrium with crystalline U_3O_8. This can be explained either by the fact that sorption equilibrium has not been reached during the equilibration time of 6–9 days or by the presence of a metastable, poorly crystalline U(VI)/U(IV) phase whose precipitation is kinetically favored over U_3O_8.

Broadening of the S2*p* photolines relative to those measured on the unreacted surfaces indicates oxidation of both sulfide surfaces which is concurrent with uranyl uptake. However, a significant difference between pyrite and galena is noted with regard to pH. The pyrite system clearly shows a pH effect on the redox process where increasing pH leads to enhanced oxidation. For galena, this effect is not observed.

Kinetic Considerations

The sorption kinetics observed for the galena system, as derived from solution analysis combined with XPS information on the corresponding solid phase, yields insight into processes governing the formation of a uranium oxide precipitate. The U4*f* spectra from the galena, after exposure to a uranyl nitrate solution for 1 min, 60 min, 50 h, and 9 days show identical line shapes in spite of increasing percent in uptake. This indicates that a uranium oxide species in a mixed oxidation state is formed regardless of equilibration time. Consequently, the slow sorption kinetics observed (see above) are not noticeably affected by the reduction of uranyl.

On the other hand sorption kinetics are significantly affected by the U_{sorb}/S_t ratio, where higher ratios yield slower relative rates for the percent uranium sorbed. Slower kinetics have been observed for metal sorption to oxide surfaces at higher sorbate/sorbent ratios before (e.g., DZOMBAK and MOREL, 1986; EARY and RAI, 1989). DZOMBAK and MOREL (1986) explained this decrease by the dominance of precipitation over adsorption in the sorption process. From this combined kinetic information we deduce that the observed slow sorption process is critically dependent on the sorbate/sorbent ratio. Our data suggest that adsorption and reduction of U(VI) are fast relative to precipitation.

It is interesting to note that oxidation of the PbS surface prior to uranyl exposure in one set of experiments (exp. #5, see Results Section) does not have any significant effect on the sorption kinetics of uranyl (compare with exp. #4). This strongly suggests that the rapid dissolution of the oxidized surface layer does not affect the sorption process which proceeds at a much lower rate. In effect, the uranyl dominantly "sees" the freshly generated nonoxidized sulfide surface.

These kinetic effects, which have been discussed for sorbed uranium concentrations corresponding to U_{sorb}/S_t ratios ranging from 1–2, are altered at even higher ratios. In these cases reduction is clearly inhibited during the sorption process by the precipitation of U(VI) at the surface.

Effect of Uranyl Concentration in the Galena System

The effect of uranyl concentration in the galena system is manifested by all analytical techniques. An increase from 0.2 mM to 4 mM uranyl results in a decrease of the sorption from 99–90% U at constant sorbent surface area. Furthermore, this increase of U_t at the surface yields a gradual increase of the U(VI) component, as evidenced by XPS and IR results. In other words, higher surface loading leads to higher amounts of unreduced uranyl.

Simultaneously, the PbS surface is significantly affected by higher uranium loadings, as indicated by the dissolution of Pb(II) from the surface. The enhanced release of Pb(II) at higher U_t is accompanied by a change of the structural environment of surface Pb(II) which is shown from the broadening of the Pb4*f* line and appearance of a second peak shifted by 1.0 eV to higher binding energies. In addition, the Pb/S ratio increases from 1 to 1.2. Both results suggest formation of a S-deficient Pb-O–rich surface layer. In fact, the position of the second peak of the Pb4*f* line (data not shown) is in agreement with the peak measured for $Pb(OH)_2$ (BUCKLEY and WOODS, 1984). Thus, our data suggest the formation of a hydrous lead oxide phase at high loadings of uranium. However, the increased Pb(II) concentrations in solution are far too low (~1000 times) to show equilibrium with a pure $Pb(OH)_2$ solid phase. The possibility exists that, for high U_t, a coprecipitation reaction of uranyl and Pb(II) resulting in a relatively insoluble $(Pb\text{-}UO_2)_x(OH)_y$ surface compound could occur.

Analysis of the S2*p* line indicates polysulfide formation for all concentrations of sorbed uranium. The increase in U_t has no significant effect on the line shapes. Furthermore, the occurrence of S-O compounds is not supported by XPS or by IR analysis. Previous XPS results on galena oxidation in aqueous solution (BUCKLEY and WOODS, 1984; BRION, 1980) show agreement with this finding. However, recent work of Bancroft and coworkers (BANCROFT and HYLAND, 1990; MYCROFT et al., 1990) involving, e.g., Au(III) reduction on sulfide surfaces, has emphasized the high solubility of sulfates forming on surfaces. In our system, oxidation of galena to soluble sulfate would involve the release of Pb^{2+} and the production of protons. This is illustrated for neutral solutions where the dominant hydrolyzed uranyl species is a 3:5 complex (GRENTHE et al., 1992), by the following overall redox reaction:

$$(UO_2)_3(OH)_5^+ + PbS(s) = U_3O_8(s) + SO_4^{2-} + Pb^{2+} + 3H_2O + H^+.$$

Our results do show an enhanced release of Pb^{2+} relative to PbS reacted only with water, but they do not show a decrease of pH except for very high U_t (as discussed below). To the contrary, in the case of unbuffered initial conditions, i.e., pH 5.5 and high solid/solution ratio, we noticed an increase in pH (see Results Section). This suggests a sink for protons during the redox process. A possibility for this lies in the formation of soluble polysulfides. According to CHEN and GUPTA (1973) and others, the dominant polysulfide in the neutral pH range is S_4^{2-}. Hence, this can be illustrated by

$$3[(UO_2)_3(OH)_5^+] + 4PbS(s) + 3H^+ = 3U_3O_8(s) + S_4^{2-} + 4Pb^{2+} + 9H_2O.$$

In summary, our results for galena indicate oxidation of surface S^{2-} to polysulfide upon interaction with uranyl. In

addition, we suggest that direct oxidation to sulfate is of minor importance compared to soluble polysulfide formation. At very high U_{sorb}/S_t ratios (>5), further sorption of uranyl may result in a coprecipitation reaction which can be schematically written as

$$(UO_2)_3(OH)_5^+ + 3Pb^{2+} + 7H_2O = 3[(UO_2, Pb)(OH)_4] + 7H^+.$$

The resulting release of protons is in fact observed at very high U_t.

Effect of pH in the Pyrite System

The effect of pH on the sorption process is noted for the pyrite system in contrast to the galena system. In the pyrite system, at lower pH (5.2 to 5.5) the reaction products observed at the surface are very similar to the ones observed for galena. Thus, the redox process involves reduction of uranyl giving rise to a mixed U(VI)-U(IV)-oxide and the oxidation of sulfide to polysulfide. The effect of iron in the redox process in this lower pH range cannot be unequivocally evaluated from our data. XPS results show no evidence of Fe(II) oxidation at the near-surface. However, Auger spot analysis of a single crystal surface does suggest the occurrence of some minor Fe(III) (see Results Section). On the other hand, small amounts of oxidized iron on the initially fractured surface prior to exposure to uranyl could have caused this effect.

At higher pH, i.e., pH > 6.0, a considerable drop in pH upon addition of uranyl is noted and a significant change in the reaction products is observed. XPS and AES both point to an increase in reaction products at the surface of FeS_2. In fact, increased formation of both polysulfide and Fe(III) oxide is indicated by XPS and supported by AES. In addition, XPS and FTIR indicate a higher U(VI) component compared to lower pH samples.

Oxidation of FeS_2 in neutral to alkaline solution has been shown to be a rather complicated process that can involve many elementary reactions depending on a number of variables (e.g., surface area, pH, concentration of oxidant; NORDSTROM, 1982). The identification of the final reaction products occurring at the solid surface limits the possibilities for rate-determining redox reactions. Thus, from observed sulfate formation in solution, implications for the oxidation of the FeS_2 surface have been made. From our surface analysis, however, the near-surface shows a significant amount of polysulfide composition. This observation is compatible with the decreased solubility of polysulfides at higher pH (CHEN and GUPTA, 1973). Since in this work we have not measured sulfate in solution, no quantitative statement of the relative importance of oxidized sulfur species can be made. Despite the uncertainty in the oxidation products of sulfur, the observed increase of Fe(III) at the surface of pyrite with increasing pH is well established and arises from the decreased solubility of Fe(III) oxides with increasing pH. This effect has been observed in a number of pyrite oxidation studies (e.g., NICHOLSON et al., 1990; BALTRUS and PROCTOR, 1990). The formation of a Fe(III) oxide at the pyrite surface has also been shown to strongly affect oxidation rates. In agreement with the pyrite oxidation model of SINGER and STUMM (1970a,b), NICHOLSON et al. (1990) observed a significant decrease in oxidation rates upon formation of a Fe(III) oxide layer. In our system, the precipitation of a Fe(III) oxide could also have a significant effect on the redox process resulting in a decrease of reduction of uranyl.

As mentioned above, in the higher pH region, surface uranium has a higher U(VI)/U(IV) ratio compared to lower pH samples. AES analysis shows that a significant fraction of uranium is associated with oxidized zones which suggest the presence of Fe(III) oxide precipitates, since they are characterized high iron and oxygen and very low sulfur. IR data reveal two separate vibrational frequencies for samples exposed to relatively high uranyl concentrations, one corresponding to the uranyl-type species and the other to a U_3O_8-like phase. This combined set of spectroscopic data suggest that unreduced uranyl is concentrated at the oxidized Fe(III) oxide surface. This hypothesis is supported by a number of studies which show a strong affinity of uranyl for ferric oxide surfaces. In fact, the uranyl moiety shows a favorable structural environment for binding to Fe-OH surface sites (e.g., HO and MILLER, 1986). On the basis of these considerations, we suggest that at circumneutral conditions, the interaction of uranyl with pyrite is strongly influenced by a coprecipitation reaction of ferric oxide and uranyl. This, in turn, decreases the reducing capacity of the pyrite substrate. Support for this reasoning is given by field observations which show intimate association of ferric oxides with uranyl minerals (WABER, 1991).

Geochemical Implications

Our results show that sulfide minerals are efficient scavengers of soluble uranyl. In fact, sulfide surfaces act as reductants resulting in precipitation of insoluble reduced uranium oxide. The extent of this immobilization process in groundwaters is affected by a number of factors (e.g., presence of ligands), many of which have not been investigated in this study. Nevertheless, some implications for groundwaters can be drawn from our results.

(1) We have not observed complete reduction of soluble U(VI) to U(IV) at the sulfide surface, but rather partial reduction and precipitation of an intermediate U(VI)-U(IV) oxide which is thermodynamically metastable with regard to crystalline UO_2 (LANGMUIR, 1978). Similar behavior is observed for many other precipitates formed in low-temperature environments. Thus, iron sulfides, iron oxides, and aluminum oxides show stable intermediate phases and slow conversion to the thermodynamically stable endoproduct. The importance of these precursors in modeling of solute transport has been recently discussed by STEEFEL and VAN CAPPELLEN (1990). As evidenced from high resolution SEM, the uranium oxide particles on galena are exceedingly small even in the case of high concentrations of uranium present in the system. In a groundwater system the possible occurrence of such uranium phases would therefore be difficult to detect by conventional analytical techniques. A recent field study involving the uranium mobility in the Poços de Caldas area, Brazil (WABER, 1991) supports the formation of a U_3O_8 compound and its control on uranium solubility.

(2) Pyrite, by far the most common sulfide mineral, shows a strong pH dependence in terms of its capacity for reducing uranyl. This arises from Fe(III) oxide precipitation at the

pyrite surface under neutral to alkaline conditions: this oxide is also an efficient scavenger of uranyl as shown by this study and previous work. However, the sorption of unreduced uranyl, as opposed to reduced uranyl, has consequences in terms of uranium mobility. Thus, minor changes in pH, carbonate, or E_h in a groundwater are expected to affect surface-bound uranyl to a much greater extent than a reduced U-precipitate because of the much lower solubility of U(IV) compared to U(VI). For example, a decrease in pH of a groundwater would lead to release of surface-bound uranyl but would not strongly affect U_3O_8. Furthermore, the reduction of uranyl at a pyrite-containing redox front is expected to depend on the ratio of Fe(III) oxide/pyrite in terms of exposed surface area. Evidence from field data to support this hypothesis is lacking.

CONCLUSION

The mobility of uranyl is significantly affected by its interaction with sulfide surfaces. The immobilization of soluble uranium arises from the adsorption of uranyl, reduction of sorbed uranyl, and precipitation of a mixed U(VI)-U(IV) oxide. The identification of the individual processes important under natural water conditions is aided by appropriate spectroscopic methods. The use of XPS yields insight into the redox process by its ability to identify the surface reaction products which are U(VI), U(IV), and polysulfide. FTIR data support this result by indicating a change of the uranyl environment consistent with the U_3O_8 structure. AES/SEM analysis gives direct evidence of a precipitation process by revealing discrete uranium oxide precipitates on the galena surface in contrast to a more homogeneous, but patchy precipitates of uranium on the surface of pyrite.

The reduction of U(VI) is affected at high U_t concentrations. Under these conditions, significant amounts of unreduced uranyl precipitate on the sulfide surface. Contrary to the galena data, the pyrite data indicate a strong influence of pH on the redox process. At pH > 6, pyrite oxidation leads to precipitation of Fe(III) which in turn results in decreased reduction of sorbed U(VI).

Relating our results to U-bearing groundwaters, we suggest that reduction of soluble uranyl at the redox front gives rise to a poorly crystalline U_3O_8 phase which exerts control on uranium concentrations under anoxic conditions. This hypothesis is supported by recent field data of the Poços de Caldas site investigation (Waber, 1991).

Acknowledgments—This work was a collaborative effort within the Aqueous and Surface Geochemistry Group at Stanford. Many people within and outside this group have contributed to this work. We would especially like to thank Matthias Kohler, Lambis Papelis, Jodi Junta, Patricia Dove, and Paul Brooks for useful discussions. The comments of Dr. David Vaughan and of an anonymous reviewer have helped to improve this manuscript. This work was made possible by grants from Rotary International (to PW), the Petroleum Research Fund of the American Chemical Society (22892-ACS, 2 to MFH), the National Science Foundation (EAR9105000 to MFH), and the Environmental Protection Agency. We also gratefully acknowledge the Center for Materials Research at Stanford and Prof. Gary Sposito at U.C. Berkeley for the use of his FTIR laboratory.

Editorial handling: T. Pačes

REFERENCES

ALLEN G. C. and HOLMES N. R. (1987) Surface characterization of α, β, γ, and δ-UO_3 using X-ray photoelectron spectroscopy. *J. Chem. Soc. Dalton Trans.* 3009–3015.

ALLEN G. C., CROFTS J. A., CURTIS M. T., TUCKER P. M., CHADWICK D., and HAMPSON P. J. (1974) X-ray photoelectron spectroscopy of some uranium oxide phases. *J. Chem. Soc. Dalton Trans.*, 1296–1301.

ALLEN G. C., TEMPEST P. A., and TYLER W. T. (1987) Oxidation of crystalline UO_2 studied using X-ray photoelectron spectroscopy and X-ray diffraction. *J. Chem. Soc. Faraday Trans.* 1, 83, 925–935.

AMES L. L., MCGARAH J. E., and WALKER B. A. (1983) Sorption of trace constituents from aqueous solution onto secondary minerals. 1. Uranium. *Clays Clay Mineral.* 31, 321–334.

ANDERSON R. F. (1987) Redox behavior of uranium in an anoxic marine basin. *Uranium* 3, 145–164.

ANDERSON R. F., FLEISHER M. Q., and LEHYRAY A. P. (1989) Concentration, oxidation state and particulate flux of uranium in the Black Sea. *Geochim. Cosmochim. Acta* 53, 2215–2224.

BALTRUS J. P. and PROCTOR A. (1990) Composition of overlayers on oxidized pyrite surfaces. *Appl. Surf. Sci.* 44, 147–150.

BANCROFT G. M. and HYLAND M. M. (1990) Spectroscopic studies of adsorption/reduction reactions of aqueous metal complexes on sulphide surfaces. In *Mineral-Water Interface Geochemistry* (ed. M. F. HOCHELLA and A. F. WHITE); *Rev. Mineral.* 23, pp. 511–558.

BASTASZ R. and FELTER T. E. (1982) MNN Auger spectrum of uranium. *Phys. Rev. B*, 26, 3529–3533.

BRION D. (1980) Etude par spectroscopie de photoélectrons de la dégradation superficielle de FeS_2, $CuFeS_2$, ZnS et PbS à l'air et dans l'eau. *Appl. Surf. Sci.* 5, 133–152.

BROOKINS D. G. (1976) Position of uraninite and/or coffinite accumulations to the hematite-pyrite interface in sandstone-type deposits. *Econ. Geol.* 71, 944–948.

BROWN G. E., JR. (1990) Spectroscopic studies of chemisorption reaction mechanisms at oxide-water interfaces. In *Mineral-Water Interface Geochemistry* (ed M. F. HOCHELLA and A. F. WHITE); *Rev. Mineral.* 23, pp. 309–363.

BUCKLEY A. N. and WOODS R. (1984) An X-ray photoelectron spectroscopic study of the oxidation of galena. *Appl. Surf. Sci.* 17, 401–414.

BUCKLEY A. N., WOUTERLOUOOD H. J., CARTWRIGHT P. S., and GILLARD R. D. (1989) The interaction of pyrite with solutions containing silver. *J. Appl. Electrochem.* 19, 744–757.

BULLOCK J. I. (1967) Infrared spectra of some uranyl nitrate complexes. *J. Inorg. Nucl. Chem.* 29, 2257–2264.

CHADWICK D. (1973) Uranium 4f binding energies studied by X-ray photoelectron spectroscopy. *Chem. Phys. Lett.* 21, 291–294.

CHARLET L. and MANCEAU A. (1992) X-ray absorption spectroscopic study of the sorption of Cr(III) at the oxide-water interface. II. Adsorption, coprecipitation and surface precipitation on ferric hydrous oxide. *J. Colloid Interf. Sci.* 148, 443–458.

CHEN K. Y. and GUPTA S. K. (1973) Formation of polysulfides in aqueous solution. *Environ. Lett.* 4, 187–200.

DILLARD J. G., KOPPELMAN M. H., CROWTHER D. L., SCHENCK C. V., MURRAY J. W., and BALISTRIERI L. (1981) X-ray photoelectron spectroscopic (XPS) studies on the chemical nature of metals ions adsorbed on clays and minerals. In *Adsorption From Aqueous Solution* (ed. P. H. TEWARI), pp. 227–241. Plenum Press.

DZOMBAK D. A. and MOREL F. M. M. (1986) Sorption of cadmium on hydrous ferric oxide at high sorbate/sorbent ratios: Equilibrium, kinetics, and modeling. *J. Colloid Interf. Sci.* 112, 588–598.

EARY L. E. and RAI D. (1989) Kinetics of chromate reduction by ferrous ions derived from hematite and biotite at 25°C. *Amer. J. Sci.* 289, 180–213.

GIBLIN A. M., BATTS B. D., and SWAINE D. J. (1981) Laboratory simulation studies of uranium mobility in natural waters. *Geochim. Cosmochim. Acta* 45, 699–709.

GRENTHE I., FUGER J., KONINGS R. J. M., LEMIRE R. J., MULLER A. B., NGUYEN-TRUNG C., and WANNER H. (1992) *Chemical Thermodynamics. Vol. 1. Chemical Thermodynamics of Uranium.* OECD-NEA, Elsevier.

HISKEY J. B., PHULE P. P., and PRITZKER M. D. (1987) Studies on the effect of addition of silver on the direct oxidation of pyrite. *Metallurgical Trans.* **18B**, 641–647.

HO C. H. and DOERN D. C. (1985) The sorption of uranyl species on a hematite sol. *Canadian J. Chem.* **63**, 1100–1105.

HO C. H. and MILLER N. H. (1986) Adsorption of uranyl species from bicarbonate solution onto hematite particles. *J. Colloid Interf. Sci.* **110**, 165–171.

HOCHELLA M. F., JR. (1988) Auger electron and X-ray photoelectron spectroscopy spectroscopies. In *Spectroscopic Methods in Mineralogy and Geology* (ed. F. C. HAWTHORNE); *Rev. Mineral.* **18**, pp. 573–637.

HOCHELLA M. F., JR. (1990) Atomic structure, microtopography, composition, and reactivity of mineral surfaces. In *Mineral-Water Interface Geochemistry* (ed. M. F. HOCHELLA and A. F. WHITE); *Rev. Mineral.* **23**, pp. 87–132.

HOCHELLA M. F., JR. and CARIM A. H. (1988) A reassessment of electron escape depths in silicon and thermally grown silicon dioxide thin films. *Surf. Sci. Lett.* **197**, L260–L268.

HOEKSTRA H. R. (1982) Vibrational spectra. In *Gmelin's Handbook of Inorganic Chemistry. Uranium. Suppl. Vol. A5. Spectra.*, Chap. 5, pp. 211–240. Verlag-Chemie.

HOEKSTRA H. R. and SIEGEL S. (1961) The uranium-oxygen system: U_3O_8-UO_3. *J. Inorg. Nucl. Chem.* **18**, 154–165.

HSI C. D. and LANGMUIR D. (1985) Adsorption of uranyl onto ferric oxyhydroxides: Application of the surface complexation site-binding model. *Geochim. Cosmochim. Acta* **49**, 1931–1941.

HYLAND M. M. and BANCROFT G. M. (1989) An XPS study of gold deposition at low temperatures on sulphide minerals: Reducing agents. *Geochim. Cosmochim. Acta* **53**, 367–372.

KLINKHAMMER G. P. and PALMER M. R. (1991) Uranium in the oceans: Where it goes and why. *Geochim. Cosmochim. Acta* **55**, 1799–1806.

KOCHENOV A. V., KOROLEV K. G., DUBINCHUK V. T., and MEDVEDEV Y. L. (1977) Experimental data on the conditions of precipitation of uranium from aqueous solutions. *Geochem. Intl.* **14**, 82–87.

KOSS V. (1988) Modeling of U(VI) sorption and speciation in a natural sediment—Groundwater system. *Radiochim. Acta* **44/45**, 403–406.

LANGMUIR D. (1978) Uranium solution-mineral equilibria at low temperature with applications to sedimentary ore deposits. *Geochim. Cosmochim. Acta* **42**, 547–569.

LANGMUIR D. and CHATAM J. R. (1980) Groundwater prospecting for sandstone-type uranium deposits: A preliminary comparison of the merits of mineral-solution equilibria and single element tracer methods. *J. Geochem. Explor.* **13**, 201–219.

LISITSIN A. K. (1962) Form of occurrence of uranium in ground waters and conditions of precipitation as UO_2. *Geokhimia* **9**, 763–769.

LOVLEY D. R. and PHILLIPS E. J. P. (1992) Bioremediation of uranium contamination with enzymatic uranium reduction. *Environ. Sci. Technol.*, 2228–2234.

LOVELY D. R., PHILLIPS E. J. P., GORBY Y. A., and LANDA E. R. (1991) Microbial reduction of uranium. *Nature* **350**, 413–416.

MATIJEVIC E. and SCHEINER P. (1978) Ferric hydrous oxide sols III. Preparation of uniform particles by hydrolysis of Fe(III)-chloride, -nitrate, and -perchlorate solutions. *J. Colloid Interf. Sci.* **46**, 13–25.

MORSE J. W. and CHOPPIN G. R. (1991) The chemistry of transuranic elements in natural waters. *Rev. Aquatic Sci.* **4**, 1–22.

MOSES C. O. and HERMAN J. S. (1991) Pyrite oxidation at circumneutral pH. *Geochim. Cosmochim. Acta* **55**, 471–482.

MYCROFT J. R., BANCROFT G. M., MCINTYRE, LORIMER J. W., and HILL I. R. (1990) Detection of sulphur and polysulphides on electrochemically oxidized surfaces by X-ray photoelectron spectroscopy and Raman spectroscopy. *J. Electroanal. Chem.* **292**, 139–152.

NICHOLSON R. V., GILLHAM R. W., and REARDON E. J. (1990) Pyrite oxidation in carbonate-buffered solution: 2. Rate control by oxide coatings. *Geochim. Cosmochim. Acta* **54**, 395–402.

NORDSTROM D. K. (1982) Aqueous pyrite oxidation and the consequent formation of secondary iron minerals. In *Acid Sulfate Weathering* (ed. L. R. HOSSAER et al.), pp. 37–56. *Soil Sci. Soc. Amer.*

PAPELIS C., HAYES K. F., and LECKIE J. O. (1988) HYDRAQL: A program for the computation of chemical equilibrium composition of aqueous batch systems including surface-complexation modeling of ion adsorption at the oxide/solution interface. Technical Report No. 306. Environmental Engineering and Science. Stanford University.

PAYNE T. E. and WAITE T. D. (1991) Surface complexation modelling of uranium sorption data obtained by isotope exchange techniques. *Radiochim. Acta* **52/53**, 487–493.

PERRY D. L., TSAO L., and TAYLOR J. A. (1984) The galena/dichromate solution interaction and the nature of the resulting chromium(III) species. *Inorg. Chim. Acta* **85**, L57–L60.

SCHINDLER P. W. (1967) Heterogeneous equilibria involving oxides, hydroxides, carbonates, and hydroxide carbonates. In *Equilibrium Concepts in Natural Water Systems* (ed. W. STUMM); *ACS Symp. Ser. No. 67*, pp. 196–221.

SCOFIELD J. H. (1976) Hartree-Slater subshell photoionization cross-sections at 1254 and 1487 eV. *J. Electron Spectros. Related Phenom.* **8**, 129–137.

SEAH M. P. and DENCH W. A. (1979) Quantitative electron spectroscopy of surfaces: A standard data base for electron inelastic mean free paths in solids. *Surf. Interf. Anal.* **1**, 2–11.

SIEGEL S. and HOEKSTRA H. R. (1971) An examination of the symmetry of alpha uranium trioxide. *Inorg. Nucl. Chem. Lett.* **7**, 497–504.

SINGER P. C. and STUMM W. (1970a) Acidic mine drainage: The rate-determining step. *Science* **167**, 1121–1123.

SINGER P. C. and STUMM W. (1970b) Oxygenation of ferrous iron. Fed. Water Quality Admin. Rept. No. 14010-06/69.

SOEHNEL O. (1982) Electrolyte crystal-aqueous solution interfacial tensions from crystallization data. *J. Crystal Growth* **57**, 101–108.

SPOSITO G. (1986) Distinguishing adsorption from surface precipitation. In *Geochemical Processes of Mineral Surfaces* (ed. J. A. DAVIS and K. F. HAYES); *ACS Symp. Ser. No. 323*, pp. 217–228.

STEEFEL C. I. and VAN CAPPELLEN P. (1990) A new kinetic approach to modeling water-rock interaction: The role of nucleation, precursors, and Ostwald ripening. *Geochim. Cosmochim. Acta* **54**, 2657–2677.

STIPP S. L. and HOCHELLA M. F., JR. (1991) Structure and bonding environments at the calcite surface as observed with X-ray photoelectron spectroscopy (XPS) and low energy electron diffraction (LEED). *Geochim. Cosmochim. Acta* **55**, 1723–1736.

SUNDER S., SHOESMITH D. W., BAILEY M. G., STANCHELL F. W., and MCINTYRE N. S. (1981) Anodic oxidation of UO_2. Part 1. Electrochemical and X-ray photoelectron spectroscopic studies in neutral solutions. *J. Electroanal. Chem.* **130**, 163–179.

TOSSELL J. A. and VAUGHAN D. J. (1987) Electronic structure and chemical reactivity of the surface of galena. *Canadian Mineral.* **25**, 381–392.

VEAL B. W. and LAM D. J. (1982) Photoemission spectra. In *Gmelin's Handbook of Inorganic Chemistry. Uranium. Suppl. Vol. A5. Spectra.*, Chap. 4, pp. 176–210. Verlag-Chemie.

WABER N. (1991) Mineralogy, petrology and geochemistry of the Poços de Caldas analogue study sites, Minas Gerais, Brazil. II: Morro do Ferro. SKB Technical Report 90-12, Stockholm, Sweden.

WARREN C. G. and GRANGER H. C. (1973) The concept of growth and maturity of ore-stage pyrite in roll-type uranium deposit. *USGS. J. Res.* **1**, 151–155.

WEHRLI B. (1991) Redox reactions of metal ions at mineral surfaces. In *Aquatic Chemical Kinetics* (ed. W. STUMM), pp. 311–336. Wiley.

WHEELER V. J., DELL R. M., and WATT E. (1964) Uranium trioxide and the UO_3 Hydrates. *J. Inorg. Nucl. Chem.* **26**, 1829–1845.

WHITE A. F. (1990) Heterogeneous electrochemical reactions associated with oxidation of ferrous oxides and silicate surfaces. In *Mineral-Water Interface Geochemistry* (ed. M. F. HOCHELLA and A. F. WHITE); *Rev. Mineral.* **23**, pp. 467–510.